Complexity and Robustness Trade-Off for Traditional and Deep Models 2022

Lead Guest Editor: Shahzad Sarfraz
Guest Editors: Muhammad Ahmad, Manuel Mazzara, and Salvatore Distefano

Complexity and Robustness Trade-Off for Traditional and Deep Models 2022

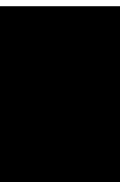# Complexity and Robustness Trade-Off for Traditional and Deep Models 2022

Lead Guest Editor: Shahzad Sarfraz
Guest Editors: Muhammad Ahmad, Manuel Mazzara, and Salvatore Distefano

Chief Editor

Hiroki Sayama (iD), USA

Contents

Contents

WILEY | Hindawi

Research Article

Nonlinear dynamics of the media addiction model using the fractal-fractional derivative technique

Saima Rashid (ID)**,[1] Rehana Ashraf,[2] and Ebenezer Bonyah** (ID)**[3]**

[1]*Department of Mathematics, Government College University, Faisalabad, Pakistan*
[2]*Department of Mathematis, Lahore College for Women University, Lahore, Pakistan*
[3]*Department of Mathematics Education, Akenten Appiah Menka University of Skills Training and entrepreneurial Development, Kumasi, Ghana*

Correspondence should be addressed to Saima Rashid; saimarashid@gcuf.edu.pk and Ebenezer Bonyah; ebbonya@gmail.com

Excessive use of social media is a developing concern in the twenty-first century. This issue needs to be addressed before it has any more significant consequences than what we are currently experiencing. As a preventive technique, advertisements and awareness-raising campaigns about the detrimental impact of digital technologies are used. The application of novel mathematical techniques and terminologies in this field of study will have significant potential to enhance healthy living by preventing certain ailments. This is the most compelling justification for conducting a new study with the most up-to-date techniques at our disposal. This study investigates clear and concise transmission in order to generate a deterministic mathematical model of social media addiction $\mathbb{SMA}$ using the fractal-fractional (FF) derivative operator. Also, the analysis of the $\mathbb{SMA}$ model in terms of the invariant domain, the existence of a positive invariant solution, and equilibria assumptions are stated in a detailed manner. Besides that, the basic reproduction number $\mathbb{R}_0 < 1$ is computed, demonstrating that the proposed methodology is more efficacious. The Atangana-Baleanu FF differential operators are recently defined in FF differential operators that are applied to characterize the $\mathbb{SMA}$ model's mathematical algorithm. We investigated the numerical behaviour of the $\mathbb{SMA}$ in three ways: (i) changing the fractional-order (α) as well as the fractal-dimension ($\wp$); (ii) changing α while keeping $\wp$ constant; and (iii) changing $\wp$ while keeping α constant. Our examined visualizations and simulation studies using MATLAB for the numerical modelling of the aforementioned system showed that the novel developed Atangana-Baleanu FF differential operators produce remarkable results when compared to the classical frame.

1. Introduction

With the popularity of networking communication comes an increase in the psychoactive properties of this technological innovation. Numerous investigations have linked compulsive media platform use to undesirable outcomes, including decreased efficiency, adverse social interactions, and decreased life contentment. The misuse of social networking sites has increased at an alarming rate. For example, Facebook has 68 percent and 73 percent of the adolescent community in the United States, respectively [1]. Over prescription of social media addiction is connected with impaired effectiveness appraisal, problematic interpersonal interactions, insomnia, reduced levels of happiness, and sentiments of hostility, stress, and melancholy, see [2–7]. To be consistent with the preponderance of the research, we included the terms "social media addiction" ($\mathbb{SMA}$) or "addicted social networking usage" (in a non-clinical meaning) in the entirety of that kind of analysis, while acknowledging the concerns surrounding the terminology [8]. Whenever it becomes more appropriate to employ certain concepts, exclusions are created. For the purposes of this evaluation, we characterize excessive social media adoption as becoming extremely apprehensive regarding social media, intrinsically incentivized, and dedicating a significant portion of time and vitality to incorporating social media to the juncture where an individual's group opportunities, intimate communication, surveys, and/or

general well-being and well-being are jeopardized [9].There is now a discrepancy in theorizing $\mathbb{SMA}$, particularly how it progresses. There have been multiple evaluations of conceptualizations to elucidate $\mathbb{SMA}$, but limited research has addressed the mathematical frameworks implemented in actual research on $\mathbb{SMA}$. One evaluation, in particular, barely discussed three extensively acknowledged internet dependency scenarios. One questionnaire range of interventions includes broad scientific viewpoints (for example, neurological aspects and behavioural insights) without addressing relevant paradigms. Although some alternative analyses reviewed various relevant conceptual models, analyzed their flaws, and proposed hypothetical modifications, they did not describe how scientific findings about $\mathbb{SMA}$ implement these conceptualizations and the various attributes in these structures. Furthermore, new scientific findings on $\mathbb{SMA}$ are appearing at an astonishing rate; there is a need for a comprehensive overview of essential mathematical approaches. Alemneh and Alemu [10] constructed and examined a mathematical formulation for the dissemination and prevention of $\mathbb{SMA}$ in global society in 2021, as continues to follow:

$$\begin{cases} \dot{S}(\zeta) = \varsigma + \gamma R(\zeta) - \lambda\theta A(\zeta)S(\zeta) - (\kappa + \nu)S(\zeta), \\ \dot{E}(\zeta) = \lambda\theta A(\zeta)S(\zeta) - (\phi + \nu)E(\zeta), \\ \dot{A}(\zeta) = \beta\phi E(\zeta) - (\nu + \varepsilon + \psi)A(\zeta), \\ \dot{R}(\zeta) = (1 - \beta)\phi E(\zeta) + \varepsilon A - (\nu +)R(\zeta), \\ \dot{Q}(\zeta) = \kappa S(\zeta) + (1 - \gamma)R(\zeta) - \nu Q(\zeta), \end{cases} \quad (1)$$

The current community is categorized into five compartments depending on addiction level in the scheme (1). Compartment 1: individuals that are likely to be exposed are those that are not obsessed but are accessible to $\mathbb{SMA}$ is represented by $\mathbf{S}(\zeta)$. Compartment 2: individuals who utilize SM relatively regularly yet do not become obsessed are referred to as exposed individuals $\mathbf{E}(\zeta)$. Compartment 3: compulsive populace are persons who are obsessed to SM and spend a significant amount of time doing it $\mathbf{A}(\zeta)$. Compartment 4: retrieved individuals are persons who have progressed from $\mathbb{SMA}$, $\mathbf{R}(\zeta)$ is the number of individuals who have benefited from $\mathbb{SMA}$. Compartment 5: $\mathbf{Q}(\zeta)$ represents anyone that doesn't use or stop using SM perpetually. The number of individuals in the community is: $\mathbf{N} = \mathbf{S} + \mathbf{E} + \mathbf{A} + \mathbf{R} + \mathbf{Q}$. The model's suppositions are as follows: the dissemination of the $\mathbb{SMA}$ issue occurs in a confined area and is not reliant on intimate relations, racial group, or sentient socialist system. Representatives combining uniformly, and social networking dependent individuals will convey to non-addictive people when they are in contact with the compression of habit forming. Furthermore, the mathematical expressions of this scheme are amalgamated by employing the social networking addiction process, which begins with the introduction of vulnerable people into the community at a rate of ς. They are prompted to transfer to the revealed condition by addicted humans

having a stress interaction incidence of and a probabilistic transference ratio of θ. At a proportion of κ, certain vulnerable persons migrate to a set of individuals who never access digital platforms. The challenged people are divided into two classes: one that develops obsession and advances to the addictive class at a pace $\beta\phi$, and another that recovers using therapy at a pace $(1 - \beta)\phi$. Many dependent individuals transfer to the recovery class at a pace of or die as a result of the overuse of dependence on social networks at a ratio of ψ. People who have overcome become vulnerable again at a ratio of or eventually discontinue access to digital platforms at a ratio of $(1 - \gamma)\varrho$. Eventually, all of the inhabitants in each group have a spontaneous mortality rate of ν. Alemneh and Alemu [10] further examined the robustness of the equilibria and applied Pontryagin's maximal principle to design the best monitoring mechanism.In past times, fractional calculus has been consistently proven to be an outstanding approach for illustrating the heredity properties of diverse formations. Furthermore, fractional differential operators have been used in a plethora of distinctive manifestations, such as hydroelectricity, fluid dynamics, chromatography, commerce, and viruses, utilising numerous fractional strategies such as Caputo, Hadamard, Riemann-Liouville, Katugumpola, Caputo–Fabrizio, Atangana-Baleanu and fractal–fractional, see [11–13]. This combo has suddenly accumulated a wealth of traction, partly because fractional differential equations have been shown to be superb tools for displaying a few incredibly challenging phenomena in a wide range of various and endless academic disciplines; assessors are encouraged to [14–20]. In 2019, the African mathematician Abdon-Atangana [21] proposed novel differential operators with fractal derivatives based on the combination of index law, modified Mittag-Leffler rule, and exponential decay law. Novel formulations, according to [20], offer additional non-local physical challenges with fractal characteristics simultaneously. Chen et al. [21] investigated the classification of anomalous propagation by deriving the underlying component of the numerical scheme using fractal derivative. For the purpose of evaluating processing performance and dispersion velocity, they compared fractional and fractal derivatives. Wei et al. [22] employed a scalability transformation technique to offer fractal modelling of elastic deformation. Sania et al. [24] introduced differential operators with fractional order and fractal dimension to describe additional chaotic complexity, wherein various kinds of orientations were mentioned: King Cobra, Shilnikov, Thomas cyclically symmetric, Langford, and Rössler. Rashid et al. [25] discussed the complex oscillatory behaviour of a human liver model via FF derivative operator technique. According to current evidence analysis of the data collected for this study, none of the works have addressed the mathematical framework of $\mathbb{SMA}$ involving fractal-fractional derivatives. The novelty of this article is the addition of the FF fractional derivative to the $\mathbb{SMA}$ model. The improved $\mathbb{SMA}$ transmitting system incorporating the fractal-fractional derivative in the Atangana-Baleanu sense is proposed in the following framework:

$$\begin{cases} {}^{\textbf{FF}}\textbf{D}_\zeta^{\alpha,\wp}\textbf{S}(\zeta) = \varsigma + \gamma\varrho\textbf{R}(\zeta) - \lambda\theta\textbf{A}(\zeta)\textbf{S}(\zeta) - (\kappa + \nu)\textbf{S}(\zeta), \\ {}^{\textbf{FF}}\textbf{D}_\zeta^{\alpha,\wp}\textbf{E}(\zeta) = \lambda\theta\textbf{A}(\zeta)\textbf{S}(\zeta) - (\phi + \nu)\textbf{E}(\zeta), \\ {}^{\textbf{FF}}\textbf{D}_\zeta^{\alpha,\wp}\textbf{A}(\zeta) = \beta\phi\textbf{E}(\zeta) - (\nu + \epsilon + \psi)\textbf{A}(\zeta), \\ {}^{\textbf{FF}}\textbf{D}_\zeta^{\alpha,\wp}\textbf{R}(\zeta) = (1 - \beta)\phi\textbf{E}(\zeta) + \epsilon\textbf{A} - (\nu + \varrho)\textbf{R}(\zeta), \\ {}^{\textbf{FF}}\textbf{D}_\zeta^{\alpha,\wp}\textbf{Q}(\zeta) = \kappa\textbf{S}(\zeta) + (1 - \gamma)\varrho\textbf{R}(\zeta) - \nu\textbf{Q}(\zeta). \end{cases}$$

$$\text{(2)}$$

having initial conditions $(\textbf{S}, \textbf{E}, \textbf{A}, \textbf{R}, \textbf{Q}) = (\textbf{S}_0, \textbf{E}_0, \textbf{A}_0, \textbf{R}_0, \textbf{Q}_0)$, where ${}^{\textbf{FF}}\textbf{D}_\zeta^{\alpha,\wp}(.)$ denotes the FF operator in terms of Atangana-Baleanu derivative operator, whilst α presents the fractional-order and $\wp$ denotes the fractal-dimension, respectively. Furthermore, Table 1 contains explanations of all attributes. Recently, Alemneh and Alemu [10] demonstrated the mathematical modeling with optimal control analysis of $\mathbb{SMA}$. Kongson et al. [27] expounded the estimates for $\mathbb{SMA}$ model pertaining to the Atnagana-Baleanu fractional derivative operator in the Caputo context. Leveraging the aforementioned proclivity, we employ a newly formed arbitrary order derivative in the $\mathbb{SMA}$ model. The main purpose of this research is to investigate the $\mathbb{SMA}$ model via a pioneering FF derivative operator in the Atangana-Baleanu sense and to characterize the complexities of the uniqueness and existence of the aforementioned framework response by utilizing the Picard-Lindlöf and contraction mapping techniques. Furthermore, to the best of our knowledge, there is no previous paper related to $\mathbb{SMA}$ qualitative aspects of fractal–fractional derivative based on the Atangana-Baleanu context. As a result, the main objective of this paper is to bridge that gap. Graphical results demonstrate that while fixing and varying fractional-order and fractal-dimension how they affect the model's characterizations. This article's entire tasks are organized into five portions, which are provided as they continue to be implemented: Section 2 summarizes and presents the core notions and relevant formulations of FF derivatives in the Atangana-Baleanu interpretations. Section 3 describes the analysis of the model that corresponds to the positivity, bounded domain, invariant region, and equilibria points via the FF derivative operator technique. Section 4 illustrates and performs a convergence and uniqueness investigation for the above-mentioned $\mathbb{SMA}$ with the aid of the FF derivative operator and the numerical formulation of the Newton polynomial approach. Section 5 deals with the numerical outcomes and description of the suggested $\mathbb{SMA}$ model's solution. The prime focus of the planned study is on which we will exhibit simulation consequences. Ultimately, Section 6 summarizes the remarks and discusses the promising possibilities of the fractal-fractional $\mathbb{SMA}$ model.

2. Preliminaries

In what follows, it is vital to investigate some fundamental FF operator notions prior to continuing on to the formal model. Consider there be a function $\textbf{y}(\zeta)$, which is continuous and fractal differentiable on $[c, d]$ and has fractal-

dimension $\wp$ and fractional-order α, in addition to the specifications in [21, 24].

Definition 2.1 (see [21, 24]). Suppose there be a FF operator of $\textbf{y}(\zeta)$ having power law kernel in terms of Riemann–Liouville (RL) can be expressed in the form:

$$^{FFP}\textbf{D}_{0,\zeta}^{\alpha,\textbf{p}}(\textbf{y}(\zeta)) = \frac{1}{\Gamma(\textbf{r} - \alpha)}\frac{d}{d\zeta^\wp}\int_0^\zeta (\zeta - \varpi)^{\textbf{r} - \alpha - 1}\textbf{y}(\varpi)d\varpi, \quad \text{(3)}$$

where $(d\textbf{y}(\varpi)/d\varpi^\wp) = \lim\limits_{\zeta \mapsto \varpi}(\textbf{y}(\zeta) - \textbf{y}(\varpi)/\zeta^\wp - \varpi^\wp)$ and $\textbf{r} - 1 < \alpha, \wp \le \textbf{r} \in \mathbb{N}$.

Definition 2.2 (see [21, 24]). Suppose there be a FF operator of $\textbf{y}(\zeta)$ having exponential kernel in terms of RL can be expressed in the form:

$$^{FFE}\textbf{D}_{0,\zeta}^{\alpha,\wp}(\textbf{y}(\zeta)) = \frac{\textbf{M}(\alpha)}{1 - \alpha}\frac{d}{d\zeta^\wp}\int_0^\zeta \exp\left(-\frac{\alpha}{1 - \alpha}(\zeta - \varpi)\right)\textbf{y}(\varpi)d\varpi, \quad \text{(4)}$$

such that $\textbf{M}(0) = \textbf{M}(1) = 1$ with $\alpha > 0, \wp \le \textbf{r} \in \mathbb{N}$.

Definition 2.3 (see [21, 24]). Suppose there be a FF operator of $\textbf{y}(\zeta)$ with Mittag-Leffler kernel in terms of RL can be expressed in the form:

$$^{FFE}\textbf{D}_{0,\zeta}^{\alpha,\wp}(\textbf{y}(\zeta)) = \frac{\textbf{ABC}(\alpha)}{1 - \alpha}\frac{d}{d\zeta^\wp}\int_0^\zeta E_\alpha\left(-\frac{\alpha}{1 - \alpha}(\zeta - \varpi)\right)\textbf{y}(\varpi)d\varpi,$$

$$\text{(5)}$$

such that $\textbf{ABC}(\alpha) = 1 - \alpha + (\alpha/\Gamma(\alpha))$ with $\alpha > 0, \wp \le 1 \in \mathbb{N}$.

Definition 2.4 (see [21, 24]). The corresponding FF integral form of (3) is described as:

$$^{FFP}\mathbb{J}_{0,\zeta}^\alpha(\textbf{y}(\zeta)) = \frac{\wp}{\Gamma(\alpha)}\int_0^\zeta (\zeta - \varpi)^{\alpha - 1}\varpi^{\wp - 1}\textbf{y}(\varpi)d\varpi. \quad \text{(6)}$$

Definition 2.5 (see [21, 24]). The corresponding FF integral version of (4) is described as:

$$^{FFP}\mathbb{J}_{0,\zeta}^\alpha(\textbf{y}(\zeta)) = \frac{\alpha\wp}{\textbf{M}(\alpha)}\int_0^\zeta \varpi^{\wp - 1}\textbf{y}(\varpi)d\varpi + \frac{\wp(1 - \alpha)\zeta^{\wp - 1}\textbf{y}(\zeta)}{\textbf{M}(\alpha)}. \quad \text{(7)}$$

Definition 2.6 (see [21, 24]). The corresponding FF integral form of (5) is described as:

$$^{FFP}\mathbb{J}_{0,\zeta}^\alpha(\textbf{y}(\zeta)) = \frac{\alpha\wp}{\textbf{ABC}(\alpha)}\int_0^\zeta \varpi^{\wp - 1}(\zeta - \varpi)^{\alpha - 1}\textbf{y}(\varpi)d\varpi$$

$$\text{(8)}$$

$$+ \frac{\wp(1 - \alpha)\zeta^{\wp - 1}\textbf{y}(\zeta)}{\textbf{ABC}(\alpha)}.$$

Definition 2.7 (see [14]). Let $\textbf{y} \in H^1(\delta, \gamma), \delta < \gamma$ and the Atangana-Baleanu-Caputo derivative operator is defined as:

TABLE 1: Table of specified variables and their descriptions

Parameters	Explanation	Data estimated	References
ς	Acquisition of susceptible people	0.5	Supposed
ν	natural death rate	0.05	[39]
λ	Addiction transfer percentage to vulnerable persons	0.1-0.8	[39]
θ	Interaction proportion of vulnerable people involving addicted people	0.2	[39]
β	Percentage of uncovered persons who get obsessed	0.7	[39]
ψ	induce mortality rate	0.01	Supposed.
ϕ	People who quit the exposed group	0.25	[39].
ϵ	Addicts who enter the rehabilitated group as a result of the therapy	0.7	[40]
κ	Susceptible persons who do not take and/or stop utilizing SM	0.01	Supposed.
γ	The percentage of rehabilitated people susceptible to SMA	0.35	[41]
ϱ	People who depart the rehabilitated category	0.4	[40]

$$
{}_{\mathbf{c}}^{ABC}\mathbf{D}_{\zeta}^{\alpha}(\mathbf{y}(\zeta)) \qquad = \frac{\mathbf{ABC}(\alpha)}{1-\alpha}\int_{\mathbf{c}}^{\zeta} y'(\varpi) \\
\cdot E_{\alpha}\left(-\frac{\alpha(\zeta-\varpi)^{\alpha}}{1-\alpha}\right)d\varpi, \alpha \in [0,1], \tag{9}
$$

where $\mathbf{ABC}(\alpha)$ represents the normalization function.

3. Qualitative analysis of $\mathbb{SMA}$

In this section, we demonstrate that $\mathbb{SMA}$ presented in (1) is epidemiologically viable by ensuring that the system's corresponding model parameters are non-negative for every time-step ζ. This is based on the more straightforward argument that the $\mathbb{SMA}$ model with non-negative ICs becomes non-negative for all $\zeta > 0$. The preceding is a lemma.

Lemma 3.1. *Suppose there be the initial data $\mathscr{G} \geq 0$, where $\mathscr{G}(\zeta) = (\mathbf{S}(\zeta), \mathbf{E}(\zeta), \mathbf{A}(\zeta), \mathbf{R}(\zeta), \mathbf{Q}(\zeta))$. Thus the $\mathbb{SMA}$ system (1) are positive for all $\zeta > 0$. Also, $\lim \mathbf{N}(\zeta) \leq (\varsigma/\nu)$ having $\mathbf{N}(\zeta) = \mathbf{S}(\zeta) + \mathbf{E}(\zeta) \overset{\zeta \mapsto \infty}{+} \mathbf{A}(\zeta) + \mathbf{R}(\zeta) + \mathbf{Q}(\zeta)$.*

Proof. Assume that $\Xi = \sup\{\zeta > 0 \colon \mathscr{G}(\zeta) > 0 \in [0, \zeta]\}$. Therefore, $\Xi > 0$, the first equation of the framework (1) consists of following

$$
\frac{\mathbf{S}(\zeta)}{d\zeta} = \varsigma + \gamma\varrho\mathbf{R}(\zeta) - \lambda\theta\mathbf{A}(\zeta)\mathbf{S}(\zeta) - (\kappa + \nu)\mathbf{S}(\zeta), \tag{10}
$$

with $\eta = \lambda\theta\mathbf{A}(\zeta)$, then (10) diminishes to

$$
\frac{\mathbf{S}(\zeta)}{d\zeta} = \varsigma - \eta\mathbf{S}(\zeta) - (\kappa + \nu)\mathbf{S}(\zeta). \tag{11}
$$

It follows that

$$
\frac{d}{d\zeta}\left\{\mathbf{S}(\zeta)\exp\left((\kappa+\mu)\zeta + \int_0^{\Xi}\eta(\phi_1)d\phi_1\right)\right\} \\
= \varsigma\left((\kappa+\mu)\zeta + \int_0^{\Xi}\eta(\phi_1)d\phi_1\right). \tag{12}
$$

Consequently, we have

$$
\mathbf{S}(\Xi)\exp\left((\kappa+)\mu\Xi + \int_0^{\Xi}\eta(\phi_1)d\phi_1\right) - \mathbf{S}(0) \\
= \varsigma \exp\left((\kappa+\mu)y_1 + \int_0^{\Xi}\eta(\phi_2)d\phi_2\right)dy_1. \tag{13}
$$

Note that

$$
\mathbf{S}(\Xi) = \mathbf{S}(0)\exp\left(-(\kappa+\mu)\Xi - \int_0^{\Xi}\eta(\phi_1)d\phi_1\right) \\
+ \exp\left(-(\kappa+\mu)\Xi - \int_0^{\Xi}\eta(\phi_1)d\phi_1\right) \\
\times \int_0^{\Xi}\varsigma \exp\left((\kappa+\mu)y_1 + \int_0^{\Xi}\eta(\phi_2)d\phi_2\right)dy_1 > 0. \tag{14}
$$

Thus, we can obtain $\mathscr{G}(\zeta) > 0$ for any $\zeta > 0$ by repeating the previous methods for the leftover equations of model (1).

Now adding the $\mathbb{SMA}$ cohorts lead to the subsequent

$$
\frac{d\mathbf{N}}{d\zeta} \leq \varsigma - \nu\mathbf{N} - \psi\mathbf{A}. \tag{15}
$$

If there is no death to the $\mathbb{SMA}$, then

$$
\frac{d\mathbf{N}}{d\zeta} \leq \varsigma - \nu\mathbf{N}. \tag{16}
$$

Therefore, we have

$$
\lim_{\zeta \mapsto \infty} \mathbf{N}(\zeta) \leq \frac{\varsigma}{\nu}, \tag{17}
$$

which is the desired proof.

Further, in order to show the invariant region for the proposed $\mathbb{SMA}$ system (1), suppose

$$
\nabla = \left\{(\mathbf{S}, \mathbf{E}, \mathbf{A}, \mathbf{R}, \mathbf{Q}) \in \mathbb{R}_+^5 \colon 0 < \mathbf{N}(\zeta) \leq \frac{\varsigma}{\nu}\right\}. \tag{18}
$$

□

Lemma 3.2. *The domain represented by ∇ is positively invariant for the $\mathbb{SMA}$ system (1) along with non-negative ICs $\mathbf{S}, \mathbf{E}, \mathbf{A}, \mathbf{R}, \mathbf{Q} > 0$ for all $\zeta \geq 0$.*

Proof. In view of (12), then we have

$$\frac{\mathrm{d}\mathbf{N}}{\mathrm{d}\zeta} = \varsigma - \nu\mathbf{N}. \tag{19}$$

Therefore, we have $(\mathrm{d}\mathbf{N}/\mathrm{d}\zeta) \leq 0$, if $\mathbf{N}(0) \geq (\varsigma/\nu)$. Thus, we have

$$\mathbf{N}(\zeta) \leq \mathbf{N}(0)\exp(-\nu\zeta) + \frac{\varsigma}{\nu}(1 - \exp(-\nu\zeta)), \tag{20}$$

which shows that, the domain presented by ∇ is positively invariant. Moreover, if $\mathbf{N}(0) > (\varsigma/\nu)$ or $\mathbf{N}(\zeta)$ approaches to ς/ν asymptotically. Hence, the domains presented by ∇ capture all of the possibilities in $\mathbb{R}_+^5$. $\square$

3.1. Existence and nonnegativity of the solution.

Further, we investigate the existence and nonnegativity of the $\mathbb{SMA}$ system (2).

Theorem 3.3. *If there be a unique solution of the system (2) and capture the solution in $\mathbb{R}_+^5$.*

Proof. In order to prove the solution of the system (2) is positive, we have

$$\begin{cases} {}^{\mathbf{FF}}\mathbf{D}_{0,\zeta}^{\alpha,\wp}\mathbf{S}(\zeta)|_{\mathbf{S}=0} = \varsigma \geq 0, \\ {}^{\mathbf{FF}}\mathbf{D}_{0,\zeta}^{\alpha,\wp}\mathbf{E}(\zeta)|_{\mathbf{E}=0} = 0, \\ {}^{\mathbf{FF}}\mathbf{D}_{0,\zeta}^{\alpha,\wp}\mathbf{A}(\zeta)|_{\mathbf{A}=0} = \beta\phi\mathbf{E}(\zeta) \geq 0, \\ {}^{\mathbf{FF}}\mathbf{D}_{0,\zeta}^{\alpha,\wp}\mathbf{R}(\zeta)|_{\mathbf{R}=0} = (1-\beta)\phi\mathbf{E} + \epsilon\mathbf{A}(\zeta) \geq 0, \\ {}^{\mathbf{FF}}\mathbf{D}_{0,\zeta}^{\alpha,\wp}\mathbf{Q}(\zeta)|_{\mathbf{Q}=0} = \kappa\mathbf{S}(\zeta) + (1-\gamma)\varrho\mathbf{R}(\zeta) \geq 0, \end{cases} \tag{21}$$

which indicates that the system (2) solution exist in $\mathbb{R}_+^5 \forall \zeta > 0$. Summing up all cohorts in (2), we have

$$^{\mathbf{FF}}\mathbf{D}_{0,\zeta}^{\alpha,\wp}\mathbf{N}(\zeta) = \varsigma - \nu\mathbf{N}. \tag{22}$$

Moreover, we have

$$\lim_{\mathfrak{n}\to\infty} \sup\mathbf{N}(\zeta) \leq \frac{\varsigma}{\nu} \tag{23}$$

and hence, the biologically viable domain for the system (2) can be represented by

$$\nabla^1 = \left\{(\mathbf{S}, \mathbf{E}, \mathbf{A}, \mathbf{R}, \mathbf{Q}) \in \mathbb{R}_+^5 : 0 < \mathbf{N}(\zeta) \leq \frac{\varsigma}{\nu}\right\}. \tag{24}$$

$\square$

The framework for $\mathbb{SMA}$ mentioned-above (2) in the FF operator in the Atangana-Baleanu sense is implemented to provide the outcomes in the next subsection.

3.2. Stability result for disease free case.

The stability outcomes for the $\mathbb{SMA}$ framework introduced by at disease free equilibrium (DFE) E_0 are explored in this section. We can get the respective formulas by changing the right side terms of the $\mathbb{SMA}$ (2) to zero, as

$$\begin{cases} {}^{\mathbf{FF}}\mathbf{D}_{0,\zeta}^{\alpha,\wp}\mathbf{S}(\zeta) = 0, \\ {}^{\mathbf{FF}}\mathbf{D}_{0,\zeta}^{\alpha,\wp}\mathbf{E}(\zeta) = 0, \\ {}^{\mathbf{FF}}\mathbf{D}_{0,\zeta}^{\alpha,\wp}\mathbf{A}(\zeta) = 0, \\ {}^{\mathbf{FF}}\mathbf{D}_{0,\zeta}^{\alpha,\wp}\mathbf{R}(\zeta) = 0, \\ {}^{\mathbf{FF}}\mathbf{D}_{0,\zeta}^{\alpha,\wp}\mathbf{Q}(\zeta) = 0, \end{cases} \tag{25}$$

we have the following *DFE* as follows

$$E_0 = \left(\frac{\varsigma}{\kappa + \nu}, 0, 0, 0, \frac{\kappa\varsigma}{\nu(\nu + \kappa)}\right). \tag{26}$$

Furthermore, the fundamental reproduction number $\mathbb{R}_0$, which may be determined by applying the next generation methodology for the scheme, can be used to examine the robustness of DFE at E_0. The infectious cohorts in the $\mathbb{SMA}$ system (2) are $\mathbf{E}, \mathbf{A}$, and the matrices $\mathbf{F}$ and $\mathbf{V}$ are obtained as follows:

$$\mathbf{F} = \begin{bmatrix} \lambda\theta\mathbf{A}\mathbf{S} \\ 0 \\ 0 \end{bmatrix} \text{and} \mathbf{V} = ((\nu + \phi)\mathbf{E} - \phi\beta\mathbf{E} + (\nu + \epsilon + \psi)\mathbf{A}$$
$$- (1-\beta)\phi\mathbf{E} + (\nu + \varrho)\mathbf{R}). \tag{27}$$

Hence, the fundamental reproductive number can be calculated as

$$\mathbb{R}_0 = \widetilde{\rho}\left(\mathcal{F}\mathcal{V}^{-1}\right) = \frac{\lambda\varsigma\beta\phi\theta}{(\kappa + \nu)(\phi + \nu)(\nu + \epsilon + \psi)}. \tag{28}$$

3.3. Strength number.

Following the work [28], we will present the strength number. In recent years, the concept of reproduction in a specific infectious problem has been extensively used in epidemiology modelling. As predicted by the concept, two components, $\mathbf{F}$ and $\mathbf{V}$, will be identified in (27)

$$\left(\mathbf{F}\mathbf{V}^{-1} - \mu\mathbf{I}\right) = 0 \tag{29}$$

will be employed to generate the reproductive number [29]. The nonlinear portion of the classes that are infected is how the component $\mathbf{F}$, which is quite intriguing, gets derived

$$\frac{\partial}{\partial\mathbf{A}}\left(\frac{\mathbf{A}}{\mathbf{N}}\right) = \frac{[\mathbf{N} - \mathbf{A}]}{\mathbf{N}^2}. \tag{30}$$

Again, we have

$$\frac{\partial^2}{\partial\mathbf{A}^2}\left(\frac{(\mathbf{N}-1)}{\mathbf{N}^3}\right)$$
$$= \frac{-2[\mathbf{N} - \mathbf{A}]}{\mathbf{N}^3}$$
$$= \frac{-2(\varsigma - \nu(\mathbf{S}(\zeta) + \mathbf{E}(\zeta) + \mathbf{R}(\zeta) + \mathbf{Q}(\zeta))) - \beta\phi\mathbf{E}(\zeta) + \epsilon\mathbf{A}(\zeta)}{(\mathbf{S}(\zeta) + \mathbf{E}(\zeta) + \mathbf{A}(\zeta) + \mathbf{R}(\zeta) + \mathbf{Q}(\zeta))^3}. \tag{31}$$

At DFE $E_0 = (\varsigma/\kappa + \nu, 0, 0, 0, \kappa\varsigma/\nu(\nu + \kappa))$, we have

$$\frac{\partial^2}{\partial \mathbf{A}^2}\left(\frac{(\mathbf{N} - 1)}{\mathbf{N}^3}\right) = \frac{-2(\varsigma - \nu(\mathbf{S}_0 + \mathbf{E}_0 + \mathbf{R}_0 + \mathbf{Q}_0)) - \beta\phi\mathbf{E}_0 + \epsilon\mathbf{A}_0}{(\mathbf{S}_0 + \mathbf{E}_0 + \mathbf{A}_0 + \mathbf{R}_0 + \mathbf{Q}_0)^3}$$

$$= \frac{-2(\varsigma - \nu(\mathbf{S}_0 + \mathbf{Q}_0))}{(\mathbf{S}_0 + \mathbf{Q}_0)^3}. \tag{32}$$

In this case, we have the following

$$\mathbf{F}_{\mathbb{A}} = \begin{bmatrix} \dfrac{-2\lambda(\varsigma - \nu(\mathbf{S}_0 + \mathbf{Q}_0))}{(\mathbf{S}_0 + \mathbf{Q}_0)^3} \\ 0 \\ 0 \end{bmatrix}. \tag{33}$$

Then $\det(\mathbf{F}_{\mathbb{A}}\mathbf{V}^{-1} - \mu\mathbf{I}) = 0$ leads to

$$\mathbb{A}_0 = \frac{-2\lambda\nu^3(\kappa + \nu - 1)}{\varsigma^2} < 0. \tag{34}$$

Therefore, the dispersion will have a single magnitude and fade out if there is no regeneration mechanism, which is indicated by a value of $\mathbb{A}_0 = 0$. Furthermore, $\mathbb{A}_0 > 0$ denotes a strength that will trigger a renewing mechanism, indicating that the expansion will contain multiple waves. However, biologists will give a precise explanation of the aforementioned number.

Theorem 3.4. *The DFE at E_0 for $\mathbb{SMA}$ model (2) is locally asymptotically stable when* $\mathbb{R}_0 < 1$ *satisfying the assumption*

$$\left|\arg(\mu_j)\right| > \frac{\varphi\pi}{2}. \tag{35}$$

Proof. To illustrate the provided hypothesis, we must first acquire the Jacobian matrix by evaluating $\mathbb{SMA}$ system (2) at the DFE E_0, we have

$$\mathbb{J}_{E_0} = \begin{bmatrix} -(\kappa + \nu) & 0 & -\dfrac{\lambda\varsigma\theta}{\kappa + \nu} & \gamma\varrho & 0 \\ 0 & -(\phi + \nu) & \dfrac{\lambda\varsigma\theta}{\kappa + \nu} & 0 & 0 \\ 0 & \beta\phi & -(\epsilon + \psi + \nu) & 0 & 0 \\ 0 & (1 - \beta)\phi & \epsilon & -(\varrho + \nu) & 0 \\ \kappa & 0 & 0 & (1 - \gamma)\varrho & -\nu \end{bmatrix}. \tag{36}$$

The negative eigenvalues are $-\nu, -(\nu + \kappa), -(\nu + \varrho), -(\nu + \phi)$ and remaining eigenvalues can be achieved from the following expression $\mu^2 + (\epsilon + \psi + \phi + 2\nu)\mu + (\phi + \nu)(\epsilon + \psi + \nu) - (\lambda\varsigma\beta\phi\theta/\kappa + \nu)$. the coefficients $(\epsilon + \psi + \phi + 2\nu)$ and $(\phi + \nu)(\epsilon + \psi + \nu) - (\lambda\varsigma\beta\phi\theta/\kappa + \nu)$ are positive, for the DFE case, the value of $\mathbb{R}_0$ should be less than 1. So that the Rough-Hurtwiz condition is satisfied for the assumptions presented if and only if $(\epsilon + \psi + \phi + 2\nu) > 0$, $(\phi + \nu)(\epsilon + \psi + \nu) - (\lambda\varsigma\beta\phi\theta/\kappa + \nu) > 0$ and $(\epsilon + \psi + \phi + 2\nu)(\phi + \nu)(\epsilon + \psi + \nu) - (\lambda\varsigma\beta\phi\theta/\kappa + \nu) > 0$. Thus, the Rough-Hurtwiz condition promise the local asymptotic stability of the $\mathbb{SMA}$ system presented (2) at DFE E_0. The aforesaid results were achieved utilizing the FF framework as described and utilized in [30]. □

3.4. Endemic equilibrium and their stability. The endemic equilibria of the $\mathbb{SMA}$ (2) designated by $E_1 = (\mathbf{S}^*, \mathbf{E}^*, \mathbf{A}^*, \mathbf{R}^*, \mathbf{Q}^*)$ and the outcome indicated in (2) are presented in this subsection as

$$\mathbf{S}^* = \frac{(\nu + \epsilon + \psi)(\nu + \phi)}{\lambda\beta\phi\theta},$$

$$\mathbf{E}^* = \frac{(\nu + \epsilon + \psi)\big(\varsigma\beta\phi\lambda\theta(\varrho + \nu) - (\kappa + \nu)(\epsilon\phi(\varrho + \nu) + \epsilon\varrho\nu) - (\psi + \nu)(\kappa + \nu)(\nu + \phi)(\nu + \varrho) - \epsilon\nu^2(\nu + \kappa)\big)}{\lambda\beta\phi\theta(\beta\phi\gamma\varrho(\psi + \nu) - \phi\gamma\varrho(\epsilon + \varrho + \nu) + (\epsilon + \psi + \nu)(\nu + \phi)(\varrho + \nu))},$$

$$\mathbf{A}^* = \frac{\big(\varsigma\beta\phi\lambda\theta(\varrho + \nu) - (\kappa + \nu)(\epsilon\phi(\varrho + \nu) + \epsilon\varrho\nu) - (\psi + \nu)(\kappa + \nu)(\nu + \phi)(\nu + \varrho) - \epsilon\nu^2(\nu + \kappa)\big)}{\lambda\theta(\beta\phi\gamma\varrho(\psi + \nu) - \phi\gamma\varrho(\epsilon + \varrho + \nu) + (\epsilon + \psi + \nu)(\nu + \phi)(\varrho + \nu))}, \tag{37}$$

$$\mathbf{R}^* = \frac{((\alpha - 1)(\nu + \psi) - \epsilon)(\varsigma\beta\lambda\phi\theta - (\nu + \phi)(\kappa + \nu)(\nu + \epsilon + \psi))}{\lambda\beta\theta(\beta\phi\gamma\varrho(\psi + \nu) - \phi\gamma\varrho(\epsilon + \varrho + \nu) + (\epsilon + \psi + \nu)(\nu + \phi)(\varrho + \nu))},$$

$$\mathbf{Q}^* = \frac{\kappa}{\nu}\left(\frac{(\nu + \epsilon + \psi)(\nu + \phi)}{\lambda\beta\phi\theta}\right) + \frac{\varrho(1 - \gamma)}{\nu}\frac{((\alpha - 1)(\nu + \psi) - \epsilon)(\varsigma\beta\lambda\phi\theta - (\nu + \phi)(\kappa + \nu)(\nu + \epsilon + \psi))}{\lambda\beta\theta(\beta\phi\gamma\varrho(\psi + \nu) - \phi\gamma\varrho(\epsilon + \varrho + \nu) + (\epsilon + \psi + \nu)(\nu + \phi)(\varrho + \nu))}.$$

Theorem 3.5. *The $\mathbb{SMA}$ presented by (2) has the following assertions:*

- *(a) if $\mathbb{R}_0 > 1$, then system (2) exhibits unique endemic equilibrium.*
- *(b) if $\mathbb{R}_0 = 1$, then system (2) has forward bifurcation.*
- *(c) if $\mathbb{R}_0 < 1$, then system (2) does not contain the endemic equilibrium point or has backward bifurcation.*

4. The fractal-fractional $\mathbb{SMA}$ model

Here, we used the novel FF methodology in this section to reassemble the classical integer-order $\mathbb{SMA}$ system with a non-singular and nonlocal kernel (2). The $\mathbb{SMA}$ framework that ensues when the FF operator is taken into account is (2).

4.1. Existence-uniqueness outcomes of FF-$\mathbb{SMA}$. Now, the existence-uniqueness of the $\mathbb{SMA}$ obtained in the FF operator are succinctly discussed in (2). To do so, we shall use a FF derivative to generate the generic Cauchy problem:

$$\begin{cases} {}^{FF}\mathbf{D}_{0,\zeta}^{\alpha,\wp}\Lambda(\zeta) = \Upsilon(\zeta,\Lambda(\zeta)), \\ \Lambda(0) = \Lambda_0. \end{cases} \tag{38}$$

In view of Definition (12), the right hand side of (38) yields:

$$\frac{\mathbf{ABC}(\alpha)}{1-\alpha}\frac{d}{d\zeta}\int_0^\zeta \Upsilon(\mathbf{u},\Lambda(\mathbf{u}))\overline{E}_\alpha\left(-\frac{\alpha}{1-\alpha}(\zeta-\mathbf{u})^\alpha\right)d\mathbf{u} \tag{39}$$
$$= \wp\zeta^{\wp-1}\Upsilon(\zeta,\Lambda(\zeta)).$$

Considering the implementation of the appropriate integral, the following conclusions are drawn as:

$$\Lambda(\zeta) = \frac{1-\alpha}{\mathbf{ABC}(\alpha)}\wp\zeta^{\wp-1}\Upsilon(\zeta,\Lambda(\zeta)) + \frac{\wp\alpha}{\mathbf{ABC}(\alpha)\Gamma(\alpha)} \tag{40}$$
$$\int_0^\zeta (\zeta-\mathbf{u})^{\alpha-1}\Upsilon(\mathbf{u},\Lambda(\mathbf{u}))\mathbf{u}^{\wp-1}d\mathbf{u} + \Lambda(0).$$

Employing the Picard-Lindelöf method, we have

$$\prod_{\eta_1}^{\eta_2} = \mathfrak{F}_\mathbf{p}(\zeta_\mathbf{p}) \times \overline{\mathcal{M}_0(\Lambda_0)}, \tag{41}$$

where $\overline{\mathfrak{F}_\mathbf{p}(\zeta_\mathbf{p})} = [\zeta_{\mathbf{p}-\mu_1}, \zeta_{\mathbf{p}+\mu_1}], \overline{\mathcal{M}_0(\Lambda_0)} = [\zeta_0 - \nu_1, \zeta_0 + \nu_1]$.
Accordingly, surmise that

$$\hbar = \sup_{\zeta \in \prod_{\eta_1}^{\eta_2} \|\Upsilon\|} \tag{42}$$

Furthermore, the norm is written as follows:

$$\|\mathfrak{F}\|_\infty = \sup_{\zeta \in \prod_{\eta_1}^{\eta_2} \|\mathfrak{F}\|,} \tag{43}$$

and consider the operations

$$\Theta\big[\mathscr{C}\big[\mathfrak{F}_\mathbf{p}(\zeta_\mathbf{p}), \mathcal{M}_\mathfrak{b}(\zeta_\mathbf{p})\big]\big] \longrightarrow \mathscr{C}\big(\mathfrak{F}_\mathbf{p}(\mathfrak{b}), \mathcal{M}_\mathfrak{b}(\zeta_\mathbf{p})\big), \tag{44}$$

described as

$$\Theta\Upsilon(\zeta) = \Upsilon_0 + \frac{1-\alpha}{\mathbf{ABC}(\alpha)}\wp\zeta^{\wp-1}\Upsilon(\zeta,\Lambda(\zeta)) + \frac{\alpha\wp}{\mathbf{ABC}(\alpha)\Gamma(\alpha)}$$
$$\int_0^\zeta (\zeta-\mathbf{u})^{\alpha-1}\Upsilon(\mathbf{u},\Lambda(\mathbf{u}))\mathbf{u}^{\wp-1}d\mathbf{u}. \tag{45}$$

The essential objective is to illustrate that the aforementioned operator can convert a completely empty metric space onto itself. We also aim to illustrate that it has the potential to map contractions. First and foremost, we show that

$$\|\Theta\Lambda(\zeta) - \Lambda_0\| \le \mathfrak{b},$$
$$\|\Theta\Lambda(\zeta) - \Lambda_0\| \le \frac{1-\alpha}{\mathbf{ABC}(\alpha)}\wp\zeta^{\wp-1}\|\Upsilon(\zeta,\Lambda(\zeta))\|_\infty + \frac{\alpha\wp}{\mathbf{ABC}(\alpha)\Gamma(\alpha)}$$
$$\int_0^\zeta (\zeta-\mathbf{u})^{\alpha-1}\|\Upsilon(\mathbf{u},\Lambda(\mathbf{u}))\|\mathbf{u}^{\wp-1}d\mathbf{u}$$
$$\le \frac{1-\alpha}{\mathbf{ABC}(\alpha)}\wp\zeta^{\wp-1}\mathfrak{F} + \frac{\alpha\wp}{\mathbf{ABC}(\alpha)\Gamma(\alpha)}\mathfrak{F}\int_0^\zeta (\zeta-\mathbf{u})^{\alpha-1}\mathbf{u}^{\wp-1}d\mathbf{u}. \tag{46}$$

Inserting $\mathbf{u} = \zeta\mathbf{x}$, then produces the foregoing

$$\|\Theta\Lambda(\zeta) - \Lambda_0\| \le \frac{1-\alpha}{\mathbf{ABC}(\alpha)}\wp\zeta^{\wp-1}\mathfrak{F} + \frac{\alpha\wp}{\mathbf{ABC}(\alpha)\Gamma(\alpha)}\mathfrak{F}\zeta^{\alpha+\wp-1}\mathfrak{B}_1(\wp,\alpha). \tag{47}$$

Therefore,

$$\|\Theta\Lambda(\zeta) - \Lambda_0\| \le \mathfrak{b} \mapsto \mathfrak{F} <$$
$$\frac{\mathfrak{b}\mathfrak{B}_1(\wp,\alpha)}{(1-\alpha/\mathbf{ABC}(\alpha))\wp\zeta^{\wp-1} + (\alpha\wp/\mathbf{ABC}(\alpha)\Gamma(\alpha))\zeta^{\alpha+\wp-1}}. \tag{48}$$

Then, surmising $\Lambda_1, \Lambda_2 \in \mathscr{C}[\mathfrak{F}_\mathbf{p}(\zeta_\mathbf{p}), \mathcal{M}_\mathfrak{b}(\zeta_\mathbf{p})]$. To obtain at the following result, apply the Banach fixed point theorem:

$$\|\Theta\Lambda_1 - \Theta\Lambda_2\| \le \mathbb{L}_\Omega\|\Lambda - \Lambda_2\|_\infty, \tag{49}$$

where $\mathbb{L}_\Omega < 1$.

$$\|\Theta\Lambda_1 - \Theta\Lambda_2\| \le \frac{1-\alpha}{\mathbf{ABC}(\alpha)}\wp\zeta^{\wp-1}\|\Upsilon(\zeta,\Lambda_1) - \Upsilon(\zeta,\Lambda_2)\|$$
$$+ \frac{\alpha\wp}{\mathbf{ABC}(\alpha)\Gamma(\alpha)}\int_0^\zeta (\zeta-\mathbf{u})^{\alpha-1}\mathbf{u}^{\wp-1}\|\Upsilon(\zeta,\mathbf{u}_1) - \Upsilon(\zeta,s_2)\|d\mathbf{u}, \tag{50}$$

Owing to the contraction mapping Υ, we have

$$\left\|\Theta\Lambda_1 - \Theta\Lambda_2\right\| \leq \frac{1-\alpha}{\mathbf{ABC}(\alpha)}\wp\zeta^{\wp-1}\mathbb{L}_\Lambda\left\|\Lambda_1 - \Lambda_2\right\|_\infty$$

$$+ \frac{\alpha\wp}{\mathbf{ABC}(\alpha)\Gamma(\alpha)}\mathbb{L}_\Lambda\left\|\Lambda_1 - \Lambda_2\right\|_\infty \int_0^\zeta (\zeta - \mathbf{u})^{\alpha-1}\mathbf{u}^{\wp-1}\mathrm{d}\mathbf{u}$$

$$\leq \frac{1-\alpha}{\mathbf{ABC}(\alpha)}\wp\zeta^{\wp-1}\mathbb{L}_\Lambda\left\|\Lambda_1 - \Lambda_2\right\|_\infty$$

$$+ \frac{\alpha\wp}{\mathbf{ABC}(\alpha)\Gamma(\alpha)}\mathbb{L}_\Lambda\left\|\Lambda_1 - \Lambda_2\right\|_\infty\zeta^{\alpha+\wp-3}\mathfrak{B}_1(\wp,\alpha). \tag{51}$$

Consequently, we have

$$\left\|\Theta\Lambda_1 - \Theta\Lambda_2\right\| \leq \left(\frac{1-\alpha}{\mathbf{ABC}(\alpha)}\wp\zeta^{\wp-1}\mathbb{L}_\Lambda + \frac{\alpha\wp}{\mathbf{ABC}(\alpha)\Gamma(\alpha)}\mathbb{L}_\Lambda\zeta^{\alpha+\wp-3}\mathfrak{B}_1(\wp,\alpha)\right)\left\|\Lambda_1 - \Lambda_2\right\|_\infty$$

$$< \left(\frac{1-\alpha}{\mathbf{ABC}(\alpha)}\wp\mathbf{a}^{\wp-1}\mathbb{L}_\Lambda + \frac{\alpha\wp}{\mathbf{ABC}(\alpha)\Gamma(\alpha)}\mathbb{L}_\Lambda\mathbf{a}^{\alpha+\wp-3}\mathfrak{B}_1(\wp,\alpha)\right)\left\|\Lambda_1 - \Lambda_2\right\|_\infty. \tag{52}$$

If the supposition made is correct, then

$$\mathbb{L}_\Lambda < \frac{1-\alpha}{\mathbf{ABC}(\alpha)}\wp\mathbf{a}^{\wp-1}\mathbb{L}_\Lambda + \frac{\alpha\wp}{\mathbf{ABC}(\alpha)\Gamma(\alpha)}\mathbb{L}_\Lambda\mathbf{a}^{\alpha+\wp-3}\mathfrak{B}_1(\wp,\alpha), \tag{53}$$

then the contraction criterion is achieved, i.e.,

$$\left\|\Theta\Lambda_1 - \Theta\Lambda_2\right\| \leq \left\|\Lambda_1 - \Lambda_2\right\|_\infty. \tag{54}$$

In a nutshell, the proof is completed by demonstrating that there is only one solution.

In the next, we describes the numerical solutions for the proposed $\mathbb{SMA}$ system.

4.2. Newton polynomial approach. Here, we configure a comprehensive analysis of the numerical approach, which relies on an efficient Newton polynomial method. This methodology, which was also originally envisioned in [34], is more effective than some of the previous methods available in the analysis. To continue further with the approach, we apply the equation:

$$^{\mathbf{FF}}\mathbf{D}_\zeta^{\alpha,\wp}\Lambda(\zeta) = \Upsilon(\zeta, \Lambda(\zeta)). \tag{55}$$

Integrating (55) with respect to ζ, produces

$$\Lambda(\zeta) - \Lambda(0) = \frac{1-\alpha}{\mathbf{ABC}(\alpha)}\wp\zeta^{\wp-1}\Upsilon(\zeta, \Lambda(\zeta)) + \frac{\alpha\wp}{\mathbf{ABC}(\alpha)\Gamma(\alpha)}$$

$$\int_0^\zeta (\zeta - \mathbf{u})^{\alpha-1}\mathbf{u}^{\wp-1}\Upsilon(\zeta, \Lambda(\zeta))\mathrm{d}\mathbf{u}. \tag{56}$$

Taking $\mathscr{W}(\zeta, \Lambda(\zeta)) = \wp\zeta^{\wp-1}\Upsilon(\zeta, \Lambda(\zeta))$, then (56) reduces to

$$\Lambda(\zeta) - \Lambda(0) = \frac{1-\alpha}{\mathbf{ABC}(\alpha)}\mathscr{W}(\zeta, \Lambda(\zeta)) + \frac{\alpha}{\mathbf{ABC}(\alpha)\Gamma(\alpha)}$$

$$\int_0^\zeta (\zeta - \mathbf{u})^{\alpha-1}\mathscr{W}(\mathbf{u}, \Lambda(\mathbf{u}))\mathrm{d}\mathbf{u}. \tag{57}$$

At $\zeta_{\mathbf{p}+1} = (n+1)\Delta\zeta$, we have

$$\Lambda(\zeta_{\mathbf{p}+1}) - \Lambda(0) = \frac{1-\alpha}{\mathbf{ABC}(\alpha)}\mathscr{W}(\zeta_{\mathbf{p}}, \Lambda(\zeta_{\mathbf{p}})) + \frac{\alpha}{\mathbf{ABC}(\alpha)\Gamma(\alpha)}$$

$$\int_0^{\zeta_{\mathbf{p}+1}} (\zeta_{\mathbf{p}+1} - \mathbf{u})^{\alpha-1}\mathscr{W}(\mathbf{u}, \Lambda(\mathbf{u}))\mathrm{d}\mathbf{u}. \tag{58}$$

Therefore, we have

$$\Lambda(\zeta_{\mathbf{p}+1}) = \Lambda(0) + \frac{1-\alpha}{\mathbf{ABC}(\alpha)}\mathscr{W}(\zeta_{\mathbf{p}}, \Lambda(\zeta_{\mathbf{p}})) + \frac{\alpha}{\mathbf{ABC}(\alpha)\Gamma(\alpha)}\sum_{\iota=2}^{\mathbf{P}}$$

$$\int_{\zeta_\iota}^{\zeta_{\iota+1}} (\zeta_{\mathbf{p}+1} - \mathbf{u})^{\alpha-1}\mathscr{W}(\mathbf{u}, \Lambda(\mathbf{u}))\mathrm{d}\mathbf{u}. \tag{59}$$

To estimate the mapping, employ the Newton polynomial $\mathscr{W}(\zeta, \Lambda(\zeta))$, we have

$$\mathscr{U}_{\mathbf{p}}(\mathbf{u}) = \mathscr{W}(\zeta_{\mathbf{p}-2}, \Lambda(\zeta_{\mathbf{p}-2}))$$

$$+ \frac{\mathscr{W}(\zeta_{\mathbf{p}-1}, \Lambda(\zeta_{\mathbf{p}-1})) - \mathscr{W}(\zeta_{\mathbf{p}-2}, \Lambda(\zeta_{\mathbf{p}-2}))}{\Delta\zeta}(\mathbf{u} - \zeta_{\mathbf{p}-2})$$

$$+ \frac{\mathscr{W}(\zeta_{\mathbf{p}}, \Lambda(\zeta_{\mathbf{p}})) - 2\mathscr{W}(\zeta_{\mathbf{p}-1}, \Lambda(\zeta_{\mathbf{p}-1})) + \mathscr{W}(\zeta_{\mathbf{p}-2}, \Lambda(\zeta_{\mathbf{p}-2}))}{2(\Delta\zeta)^2}$$

$$(\mathbf{u} - \zeta_{\mathbf{p}-2})(\mathbf{u} - \zeta_{\mathbf{p}-1}). \tag{60}$$

Substituting (60) into (57), yields

$$\Lambda^{\mathbf{p}+1} = \Lambda^0 + \frac{1-\alpha}{\mathbf{ABC}(\alpha)}\mathscr{W}(\zeta_{\mathbf{p}}, \Lambda(\zeta_{\mathbf{p}}))$$

$$+ \frac{\alpha}{\mathbf{ABC}(\alpha)\Gamma(\alpha)}\sum_{\iota=2}^{\mathbf{P}}\int_{\zeta_\iota}^{\zeta_{\iota+1}} (\zeta_{\mathbf{p}+1} - \mathbf{u})^{\alpha-1}\left(\mathscr{W}(\zeta_{\ell-2}, \Lambda^{\ell-2})\right.$$

$$+ \frac{\mathscr{W}(\zeta_{\ell-1}, \Lambda^{\ell-1}) - \mathscr{W}(\zeta_{\ell-2}, \Lambda^{\ell-2})}{\Delta\zeta}(\mathbf{u} - \zeta_{\ell-2})$$

$$\left.+ \frac{\mathscr{W}(\zeta_\ell, \Lambda^\ell) - 2\mathscr{W}(\zeta_{\ell-1}, \Lambda^{\ell-1}) + \mathscr{W}(\zeta_{\ell-2}, \Lambda^{\ell-2})}{2(\Delta\zeta)^2}(\mathbf{u} - \zeta_{\ell-2})(\mathbf{u} - \zeta_{\ell-1})\right)\mathrm{d}\mathbf{u}. \tag{61}$$

Simple computations yield
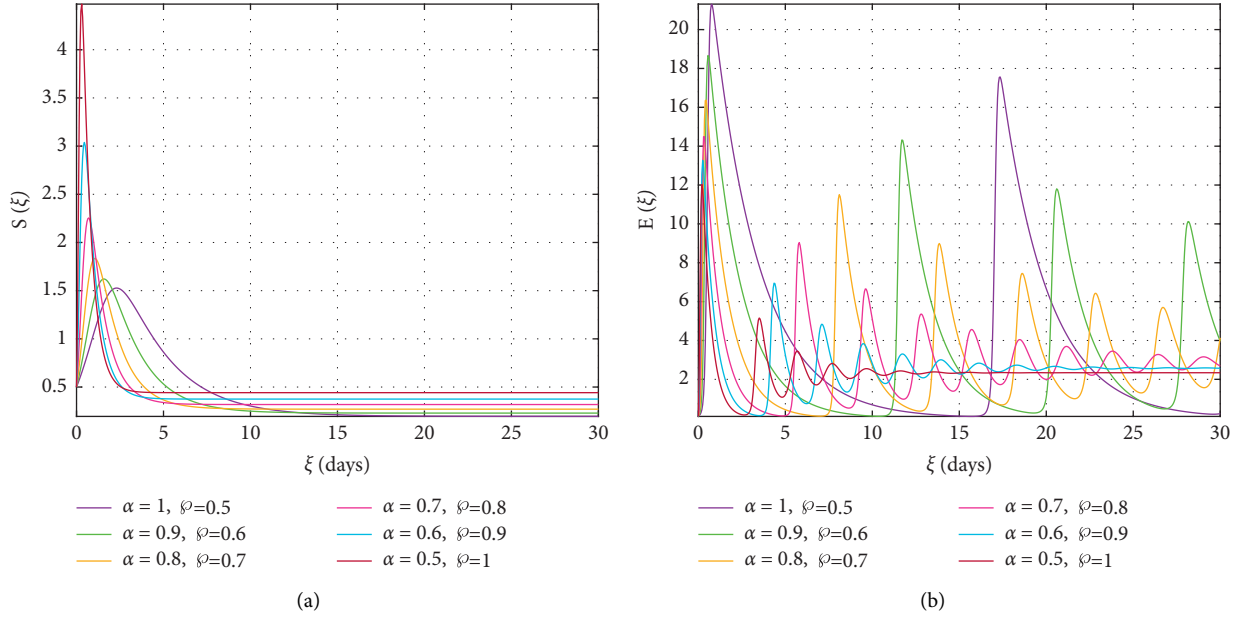
FIGURE 1: (a) Displays of susceptible individuals $\mathbf{S}(\zeta)$ (b) Displays of exposed individuals $\mathbf{E}(\zeta)$ using a Newton polynomial approach for decreasing fractional-order α and increasing fractal-dimension $\wp$.

FIGURE 2: (a) Displays of addicted individuals $\mathbf{A}(\zeta)$ (b) Displays of recovered individuals $\mathbf{R}(\zeta)$ using a Newton polynomial approach for decreasing fractional-order α and increasing fractal-dimension $\wp$.

$$\Lambda^{\mathbf{p}+1} = \Lambda^0 + \frac{1-\alpha}{\mathbf{ABC}(\alpha)} \mathscr{W}\left(\zeta_{\mathbf{p}}, \Lambda\left(\zeta_{\mathbf{p}}\right)\right)$$

$$+ \frac{\alpha}{\mathbf{ABC}(\alpha)\Gamma(\alpha)} \sum_{\iota=2}^{\mathbf{p}} \left\{ \int_{\zeta_\iota}^{\zeta_{\iota+1}} \left(\zeta_{\mathbf{p}+1} - \mathbf{u}\right)^{\alpha-1} \mathscr{W}\left(\zeta_{\ell-2}, \Lambda^{\ell-2}\right) d\mathbf{u} + \int_{\zeta_\iota}^{\zeta_{\iota+1}} \left(\zeta_{\mathbf{p}+1} - \mathbf{u}\right)^{\alpha-1} \frac{\mathscr{W}\left(\zeta_{\ell-1}, \Lambda^{\ell-1}\right) - \mathscr{W}\left(\zeta_{\ell-2}, \Lambda^{\ell-2}\right)}{\Delta\zeta} \left(\mathbf{u} - \zeta_{\ell-2}\right) d\mathbf{u} \right. \tag{62}$$

$$\left. + \int_{\zeta_\iota}^{\zeta_{\iota+1}} \left(\zeta_{\mathbf{p}+1} - \mathbf{u}\right)^{\alpha-1} \frac{\mathscr{W}\left(\zeta_\ell, \Lambda^\ell\right) - 2\mathscr{W}\left(\zeta_{\ell-1}, \Lambda^{\ell-1}\right) + \mathscr{W}\left(\zeta_{\ell-2}, \Lambda^{\ell-2}\right)}{2\left(\Delta\zeta\right)^2} \left(\mathbf{u} - \zeta_{\ell-2}\right)\left(\mathbf{u} - \zeta_{\ell-1}\right) d\mathbf{u} \right\}.$$

Note that

$$\Lambda^{\mathbf{P}+1} = \Lambda^0 + \frac{1-\alpha}{\mathbf{ABC}(\alpha)} \mathscr{W}\big(\zeta_{\mathbf{p}}, \Lambda(\zeta_{\mathbf{p}})\big)$$

$$+ \frac{\alpha}{\mathbf{ABC}(\alpha)\Gamma(\alpha)} \sum_{\iota=2}^{\mathbf{P}} \mathscr{W}\big(\zeta_{\ell-2}, \Lambda^{\ell-2}\big) \int_{\zeta_\iota}^{\zeta_{\iota+1}} \big(\zeta_{\mathbf{p}+1} - \mathbf{u}\big)^{\alpha-1} \mathrm{d}\mathbf{u}$$

$$+ \frac{\alpha}{\mathbf{ABC}(\alpha)\Gamma(\alpha)} \sum_{\iota=2}^{\mathbf{P}} \frac{\mathscr{W}\big(\zeta_{\ell-1}, \Lambda^{\ell-1}\big) - \mathscr{W}\big(\zeta_{\ell-2}, \Lambda^{\ell-2}\big)}{\Delta\zeta}$$

$$\int_{\zeta_\iota}^{\zeta_{\iota+1}} \big(\zeta_{\mathbf{p}+1} - \mathbf{u}\big)^{\alpha-1} (\mathbf{u} - \zeta_{\ell-2})\mathrm{d}\mathbf{u}$$

$$+ \frac{\alpha}{\mathbf{ABC}(\alpha)\Gamma(\alpha)} \sum_{\iota=2}^{\mathbf{P}} \frac{\mathscr{W}\big(\zeta_{\ell}, \Lambda^{\ell}\big) - 2\mathscr{W}\big(\zeta_{\ell-1}, \Lambda^{\ell-1}\big) + \mathscr{W}\big(\zeta_{\ell-2}, \Lambda^{\ell-2}\big)}{2(\Delta\zeta)^2}$$

$$\int_{\zeta_\iota}^{\zeta_{\iota+1}} \big(\zeta_{\mathbf{p}+1} - \mathbf{u}\big)^{\alpha-1} (\mathbf{u} - \zeta_{\ell-2})(\mathbf{u} - \zeta_{\ell-1})\mathrm{d}\mathbf{u}. \tag{63}$$

Using the fact that

FIGURE 3: Displays of individuals who quit or not using $\mathbf{Q}(\zeta)$ social media using a Newton polynomial approach for decreasing fractional-order α and increasing fractal-dimension $\wp$.

$$\int_{\zeta_\iota}^{\zeta_{\iota+1}} \big(\zeta_{\mathbf{p}+1} - \mathbf{u}\big)^{\alpha-1} d\mathbf{u} = \frac{(\Delta\zeta)^\alpha\{(\mathbf{p} - \iota + 1)^\alpha - (\mathbf{p} - \iota)^\alpha\}}{\alpha},$$

$$\int_{\zeta_\iota}^{\zeta_{\iota+1}} (\mathbf{u} - \zeta_{\iota-2})\big(\zeta_{\mathbf{p}+1} - \mathbf{u}\big)^{\alpha-1} d\mathbf{u} = \frac{(\Delta\zeta)^{\alpha+1}\{(\mathbf{p} - \iota + 1)^\alpha(\mathbf{p} - \iota + 2\alpha + 3) - (\mathbf{p} - \iota + 1)^\alpha(\mathbf{p} - \iota + 3\alpha + 3)\}}{\alpha(\alpha + 1)}, \tag{64}$$

$$\int_{\zeta_\iota}^{\zeta_{\iota+1}} \big(\zeta_{\mathbf{p}+1} - \mathbf{u}\big)^{\alpha-1}(\mathbf{u} - \zeta_{\ell-2})(\mathbf{u} - \zeta_{\ell-1}) d\mathbf{u} = \frac{(\Delta\zeta)^{\alpha+2}}{\alpha(\alpha + 1)(\alpha + 2)}$$

$$\times \big\{(\mathbf{p} - \iota + 1)^\alpha\big[2(\mathbf{p} - \iota)^2 + (3\alpha + 10)(\mathbf{p} - \iota) + 2\alpha^2 + 9\alpha + 12\big] - (\mathbf{p} - \iota)^\alpha\big[2(\mathbf{p} - \iota)^2 + (5\alpha + 10)(\mathbf{p} - \iota) + 6\alpha^2 + 18\alpha + 12\big]\big\}.$$

Furthermore, we have

$$\Lambda_{\mathbf{p}+1} = \Lambda_0 + \frac{1-\alpha}{\mathbf{ABC}(\alpha)} \mathscr{W}\big(\zeta_{\mathbf{p}}, \Lambda(\zeta_{\mathbf{p}})\big)$$

$$+ \frac{\alpha(\Delta\zeta)^\alpha}{\mathbf{ABC}(\alpha)\Gamma(\alpha + 1)} \sum_{\iota=2}^{\mathbf{P}} \mathscr{W}\big(\zeta_{\ell-2}, \Lambda^{\ell-2}\big)\{(\mathbf{p} - \iota + 1)^\alpha - (\mathbf{p} - \iota)^\alpha\}$$

$$+ \frac{\alpha(\Delta\zeta)^\alpha}{\mathbf{ABC}(\alpha)\Gamma(\alpha + 2)} \sum_{\iota=2}^{\mathbf{P}} \{\mathscr{W}\big(\zeta_{\ell-1}, \Lambda^{\ell-1}\big) - \mathscr{W}\big(\zeta_{\ell-2}, \Lambda^{\ell-2}\big)\}$$

$$\times \{(\mathbf{p} - \iota + 1)^\alpha(\mathbf{p} - \iota + 2\alpha + 3) - (\mathbf{p} - \iota + 1)^\alpha(\mathbf{p} - \iota + 3\alpha + 3)\} \tag{65}$$

$$+ \frac{\alpha(\Delta\zeta)^\alpha}{2\mathbf{ABC}(\alpha)\Gamma(\alpha + 2)} \sum_{\iota=2}^{\mathbf{P}} \{\mathscr{W}\big(\zeta_{\ell}, \Lambda^{\ell}\big) - 2\mathscr{W}\big(\zeta_{\ell-1}, \Lambda^{\ell-1}\big) + \mathscr{W}\big(\zeta_{\ell-2}, \Lambda^{\ell-2}\big)\}$$

$$\times \big\{(\mathbf{p} - \iota + 1)^\alpha\big[2(\mathbf{p} - \iota)^2 + (3\alpha + 10)(\mathbf{p} - \iota) + 2\alpha^2 + 9\alpha + 12\big]$$

$$- (\mathbf{p} - \iota)^\alpha\big[2(\mathbf{p} - \iota)^2 + (5\alpha + 10)(\mathbf{p} - \iota) + 6\alpha^2 + 18\alpha + 12\big]\big\}.$$

Therefore, a general approximate solution of the $\mathbb{SMA}$ is as follows:
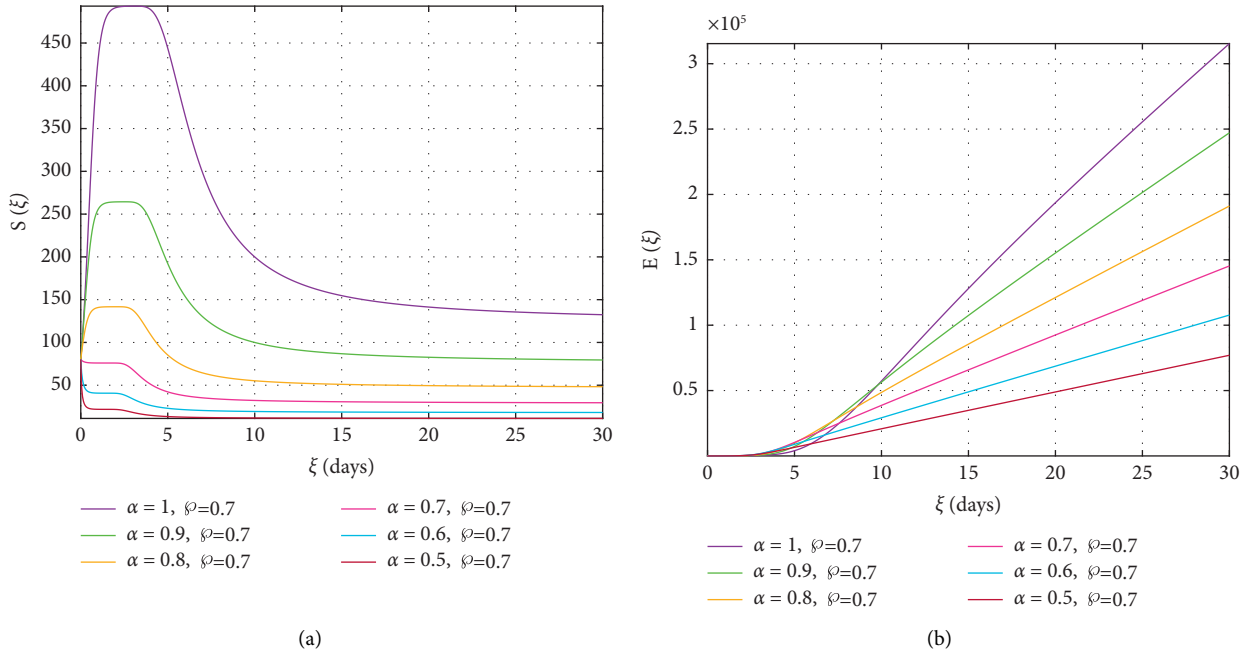
Figure 4: (a) Displays of susceptible individuals $S(\zeta)$ (b) Displays of exposed individuals $E(\zeta)$ using a Newton polynomial approach for decreasing fractional-order α and fractal-dimension $\wp = 0.7$.
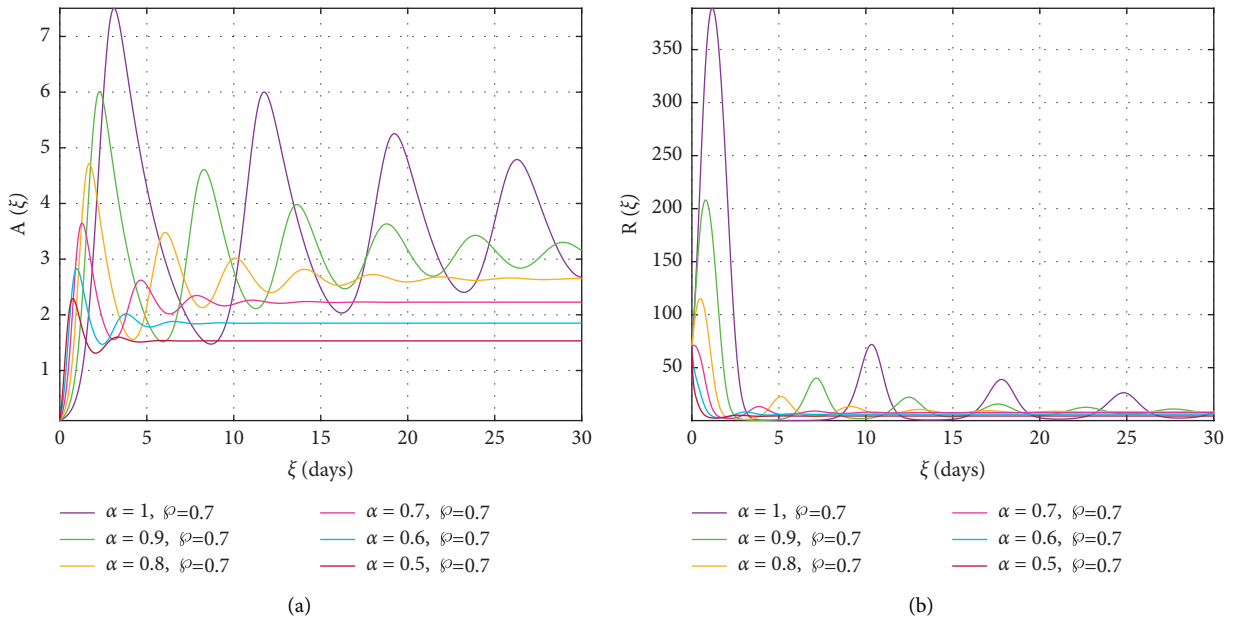
Figure 5: (a) Displays of addicted individuals $A(\zeta)$ (b) Displays of recovered individuals $R(\zeta)$ using a Newton polynomial approach for decreasing fractional-order α and fractal-dimension $\wp = 0.7$.
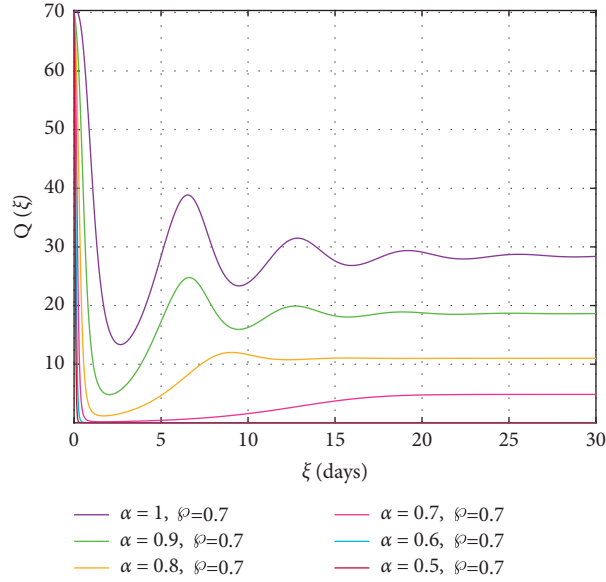
FIGURE 6: Displays of individuals who quit or not using $\mathbf{Q}(\zeta)$ using a Newton polynomial approach for decreasing fractional-order α and fractal-dimension $\wp = 0.7$.

$$\Lambda_{\mathbf{p}+1} = \Lambda_0 + \frac{1-\alpha}{\mathbf{ABC}(\alpha)} \wp \zeta_{\mathbf{p}}^{\wp-1} \mathcal{W}\left(\zeta_{\mathbf{p}}, \Lambda\left(\zeta_{\mathbf{p}}\right)\right)$$

$$+ \frac{\alpha(\Delta\zeta)^\alpha}{\mathbf{ABC}(\alpha)\Gamma(\alpha+1)} \sum_{\iota=2}^{\mathbf{p}} \wp \zeta_{\iota-2}^{\wp-1} \mathcal{W}\left(\zeta_{\ell-2}, \Lambda^{\ell-2}\right) \left\{(\mathbf{p}-\iota+1)^\alpha - (\mathbf{p}-\iota)^\alpha\right\}$$

$$+ \frac{\wp\alpha(\Delta\zeta)^\alpha}{\mathbf{ABC}(\alpha)\Gamma(\alpha+2)} \sum_{\iota=2}^{\mathbf{p}} \left\{\zeta_{\iota-1}^{\wp-1} \mathcal{W}\left(\zeta_{\ell-1}, \Lambda^{\ell-1}\right) - \zeta_{\iota-2}^{\wp-1} \mathcal{W}\left(\zeta_{\ell-2}, \Lambda^{\ell-2}\right)\right\}$$

$$\times \left\{(\mathbf{p}-\iota+1)^\alpha (\mathbf{p}-\iota+2\alpha+3) - (\mathbf{p}-\iota+1)^\alpha (\mathbf{p}-\iota+3\alpha+3)\right\}$$

$$+ \frac{\wp\alpha(\Delta\zeta)^\alpha}{2\mathbf{ABC}(\alpha)\Gamma(\alpha+2)} \sum_{\iota=2}^{\mathbf{p}} \left\{\zeta_{\iota}^{\wp-1} \mathcal{W}\left(\zeta_{\ell}, \Lambda^{\ell}\right) - 2t_{\iota-1}^{\wp-1} \mathcal{W}\left(\zeta_{\ell-1}, \Lambda^{\ell-1}\right) + \zeta_{\iota-2}^{\wp-1} \mathcal{W}\left(\zeta_{\ell-2}, \Lambda^{\ell-2}\right)\right\}$$

$$\times \left\{(\mathbf{p}-\iota+1)^\alpha \left[2(\mathbf{p}-\iota)^2 + (3\alpha+10)(\mathbf{p}-\iota) + 2\alpha^2 + 9\alpha + 12\right] - (\mathbf{p}-\iota)^\alpha \left[2(\mathbf{p}-\iota)^2 + (5\alpha+10)(\mathbf{p}-\iota) + 6\alpha^2 + 18\alpha + 12\right]\right\}.$$

$$(66)$$

4.3. New numerical technique for $\mathbb{SMA}$ FF-AB derivative model.
The objective of this task is to provide a structured approach technique for interacting with the (1) social media framework, using the FF operator in the Atangana-Baleanu context. converting the (2) system to the FF-Atangana-Baleanu derivative configuration as follows:

$$^{ABR}\mathbf{D}_{0,\zeta}^{\alpha,\wp}(\mathbf{S}(\zeta)) = \wp\zeta^{\wp-1}\mathcal{F}_1(\mathbf{S},\mathbf{E},\mathbf{A},\mathbf{R},\mathbf{Q},\zeta), \quad ^{ABR}\mathbf{D}_{0,\zeta}^{\alpha,\wp}(\mathbf{E}(\zeta)) = \wp\zeta^{\wp-1}\mathcal{F}_2(\mathbf{S},\mathbf{E},\mathbf{A},\mathbf{R},\mathbf{Q},\zeta), \quad ^{ABR}\mathbf{D}_{0,\zeta}^{\alpha,\wp}(\mathbf{A}(\zeta)) = \wp\zeta^{\wp-1}\mathcal{F}_3(\mathbf{S},\mathbf{E},\mathbf{A},\mathbf{R},\mathbf{Q},\zeta), \quad ^{ABR}\mathbf{D}_{0,\zeta}^{\alpha,\wp}(\mathbf{R}(\zeta)) = \wp\zeta^{\wp-1}\mathcal{F}_4(\mathbf{S},\mathbf{E},\mathbf{A},\mathbf{R},\mathbf{Q},\zeta),$$

$$^{ABR}\mathbf{D}_{0,\zeta}^{\alpha,\wp}(\mathbf{Q}(\zeta)) = \wp\zeta^{\wp-1}\mathcal{F}_5(\mathbf{S},\mathbf{E},\mathbf{A},\mathbf{R},\mathbf{Q},\zeta).$$

$$(67)$$

Employing the AB fractional integral operator, the preceding conclusions were made as
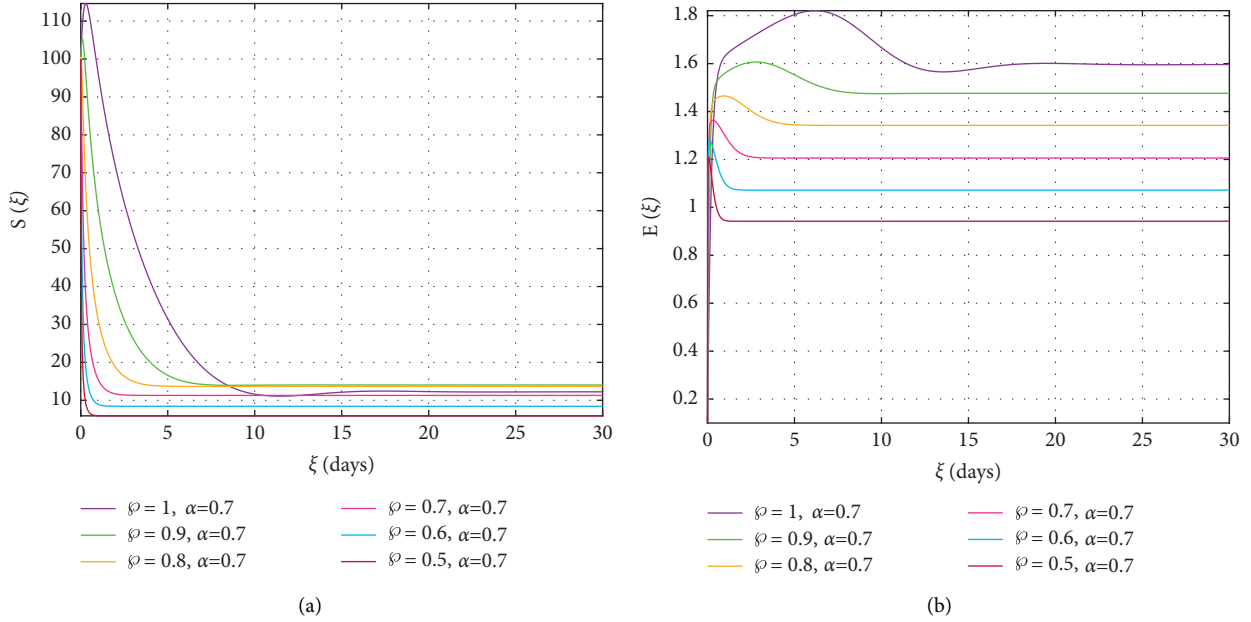
Figure 7: (a) Displays of susceptible individuals $\mathbf{S}(\zeta)$ (b) Displays of exposed individuals $\mathbf{E}(\zeta)$ using a Newton polynomial approach for decreasing fractal-dimension $\wp$ and fixed $\alpha = 0.7$.

$$\mathbf{S}(\zeta) = \mathbf{S}(0) + \frac{\wp\zeta^{\wp-1}(1-\alpha)}{\mathbf{ABC}(\alpha)}\mathscr{F}_1(\mathbf{S},\mathbf{E},\mathbf{A},\mathbf{R},\mathbf{Q},\zeta)$$
$$+\frac{\alpha\wp}{\mathbf{ABC}(\alpha)\Gamma(\alpha)}\int_0^\zeta \xi^{\wp-1}(\zeta-\xi)^{\alpha-1}\mathscr{F}_1(\mathbf{S},\mathbf{E},\mathbf{A},\mathbf{R},\mathbf{Q},\zeta)\mathrm{d}\xi,$$

$$\mathbf{E}(\zeta) = \mathbf{E}(0) + \frac{\wp\zeta^{\wp-1}(1-\alpha)}{\mathbf{ABC}(\alpha)}\mathscr{F}_2(\mathbf{S},\mathbf{E},\mathbf{A},\mathbf{R},\mathbf{Q},\zeta)$$
$$+\frac{\alpha\wp}{\mathbf{ABC}(\alpha)\Gamma(\alpha)}\int_0^\zeta \xi^{\wp-1}(\zeta-\xi)^{\alpha-1}\mathscr{F}_2(\mathbf{S},\mathbf{E},\mathbf{A},\mathbf{R},\mathbf{Q},\zeta)\mathrm{d}\xi,$$

$$\mathbf{A}(\zeta) = \mathbf{A}(0) + \frac{\wp\zeta^{\wp-1}(1-\alpha)}{\mathbf{ABC}(\alpha)}\mathscr{F}_3(\mathbf{S},\mathbf{E},\mathbf{A},\mathbf{R},\mathbf{Q},\zeta)$$
$$+\frac{\alpha\wp}{\mathbf{ABC}(\alpha)\Gamma(\alpha)}\int_0^\zeta \xi^{\wp-1}(\zeta-\xi)^{\alpha-1}\mathscr{F}_3(\mathbf{S},\mathbf{E},\mathbf{A},\mathbf{R},\mathbf{Q},\zeta)\mathrm{d}\xi,$$

$$\mathbf{R}(\zeta) = \mathbf{R}(0) + \frac{\wp\zeta^{\wp-1}(1-\alpha)}{\mathbf{ABC}(\alpha)}\mathscr{F}_4(\mathbf{S},\mathbf{E},\mathbf{A},\mathbf{R},\mathbf{Q},\zeta)$$
$$+\frac{\alpha\wp}{\mathbf{ABC}(\alpha)\Gamma(\alpha)}\int_0^\zeta \xi^{\wp-1}(\zeta-\xi)^{\alpha-1}\mathscr{F}_4(\mathbf{S},\mathbf{E},\mathbf{A},\mathbf{R},\mathbf{Q},\zeta)\mathrm{d}\xi,$$

$$\mathbf{Q}(\zeta) = \mathbf{Q}(0) + \frac{\wp\zeta^{\wp-1}(1-\alpha)}{\mathbf{ABC}(\alpha)}\mathscr{F}_5(\mathbf{S},\mathbf{E},\mathbf{A},\mathbf{R},\mathbf{Q},\zeta)$$
$$+\frac{\alpha\wp}{\mathbf{ABC}(\alpha)\Gamma(\alpha)}\int_0^\zeta \xi^{\wp-1}(\zeta-\xi)^{\alpha-1}\mathscr{F}_5(\mathbf{S},\mathbf{E},\mathbf{A},\mathbf{R},\mathbf{Q},\zeta)\mathrm{d}\xi.$$

$$(68)$$

At ζ_{n+1}, We obtain the below

$$\mathbf{S}^{n+1}(\zeta) = \mathbf{S}(0) + \frac{\wp\zeta^{\wp-1}(1-\alpha)}{\mathbf{ABC}(\alpha)}\mathscr{F}_1(\mathbf{S}^n,\mathbf{E}^n,\mathbf{A}^n,\mathbf{R}^n,\mathbf{Q}^n,\zeta_n)$$
$$+\frac{\alpha\wp}{\mathbf{ABC}(\alpha)\Gamma(\alpha)}\int_0^{\zeta_{n+1}} \xi^{\wp-1}(\zeta_{n+1}-\xi)^{\alpha-1}\mathscr{F}_1(\mathbf{S},\mathbf{E},\mathbf{A},\mathbf{R},\mathbf{Q},\xi)\mathrm{d}\xi,$$

$$\mathbf{E}^{n+1}(\zeta) = \mathbf{E}(0) + \frac{\wp\zeta^{\wp-1}(1-\alpha)}{\mathbf{ABC}(\alpha)}\mathscr{F}_2(\mathbf{S}^n,\mathbf{E}^n,\mathbf{A}^n,\mathbf{R}^n,\mathbf{Q}^n,\zeta_n)$$
$$+\frac{\alpha\wp}{\mathbf{ABC}(\alpha)\Gamma(\alpha)}\int_0^{\zeta_{n+1}} \xi^{\wp-1}(\zeta_{n+1}-\xi)^{\alpha-1}\mathscr{F}_2(\mathbf{S},\mathbf{E},\mathbf{A},\mathbf{R},\mathbf{Q},\xi)\mathrm{d}\xi,$$

$$\mathbf{A}^{n+1}(\zeta) = \mathbf{A}(0) + \frac{\wp\zeta^{\wp-1}(1-\alpha)}{\mathbf{ABC}(\alpha)}\mathscr{F}_3(\mathbf{S}^n,\mathbf{E}^n,\mathbf{A}^n,\mathbf{R}^n,\mathbf{Q}^n,\zeta_n)$$
$$+\frac{\alpha\wp}{\mathbf{ABC}(\alpha)\Gamma(\alpha)}\int_0^{\zeta_{n+1}} \xi^{\wp-1}(\zeta_{n+1}-\xi)^{\alpha-1}\mathscr{F}_3(\mathbf{S},\mathbf{E},\mathbf{A},\mathbf{R},\mathbf{Q},\xi)\mathrm{d}\xi,$$

$$\mathbf{R}^{n+1}(\zeta) = \mathbf{R}(0) + \frac{\wp\zeta^{\wp-1}(1-\alpha)}{\mathbf{ABC}(\alpha)}\mathscr{F}_4(\mathbf{S}^n,\mathbf{E}^n,\mathbf{A}^n,\mathbf{R}^n,\mathbf{Q}^n,\zeta_n)$$
$$+\frac{\alpha\wp}{\mathbf{ABC}(\alpha)\Gamma(\alpha)}\int_0^{\zeta_{n+1}} \xi^{\wp-1}(\zeta_{n+1}-\xi)^{\alpha-1}\mathscr{F}_4(\mathbf{S},\mathbf{E},\mathbf{A},\mathbf{R},\mathbf{Q},\xi)\mathrm{d}\xi,$$

$$\mathbf{Q}^{n+1}(\zeta) = \mathbf{Q}(0) + \frac{\wp\zeta^{\wp-1}(1-\alpha)}{\mathbf{ABC}(\alpha)}\mathscr{F}_5(\mathbf{S}^n,\mathbf{E}^n,\mathbf{A}^n,\mathbf{R}^n,\mathbf{Q}^n,\zeta_n)$$
$$+\frac{\alpha\wp}{\mathbf{ABC}(\alpha)\Gamma(\alpha)}\int_0^{\zeta_{n+1}} \xi^{\wp-1}(\zeta_{n+1}-\xi)^{\alpha-1}\mathscr{F}_5(\mathbf{S},\mathbf{E},\mathbf{A},\mathbf{R},\mathbf{Q},\xi)\mathrm{d}\xi.$$

$$(69)$$

(69) has been modified significantly, yielding the following results:
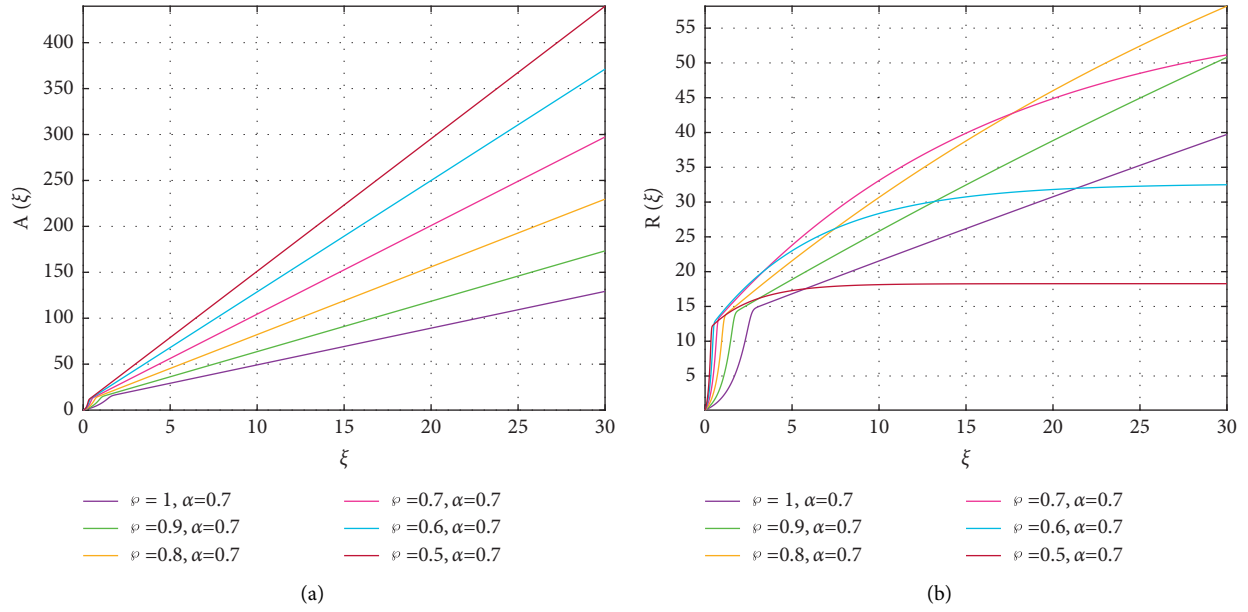
Figure 8: (a) Displays of addicted individuals $\mathbf{S}(\zeta)$ (b) Displays of recovered individuals $\mathbf{E}(\zeta)$ using a Newton polynomial approach for decreasing fractal-dimension $\wp$ and fixed $\alpha = 0.7$.
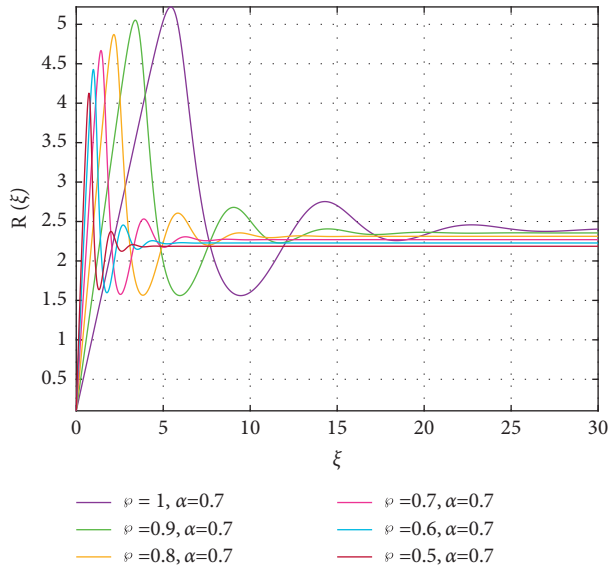
Figure 9: Displays of individuals who quit or not using $\mathbf{Q}(\zeta)$ employing the Newton polynomial approach for decreasing fractal-dimension $\wp$ and fixed $\alpha = 0.7$.

$$
\begin{aligned}
\mathbf{S}^{n+1}(\zeta) &= \mathbf{S}(0) + \frac{\wp\zeta^{\wp-1}(1-\alpha)}{\mathbf{ABC}(\alpha)}\mathcal{F}_1(\mathbf{S}^n, \mathbf{E}^n, \mathbf{A}^n, \mathbf{R}^n, \mathbf{Q}^n, \zeta_n) \\
&\quad + \frac{\alpha\wp}{\mathbf{ABC}(\alpha)\Gamma(\alpha)} \sum_{\ell=0}^{n} \in \zeta_{\zeta_\ell}^{\zeta_{\ell+1}} \xi^{\wp-1}(\zeta_{n+1}-\xi)^{\alpha-1}\mathcal{F}_1(\mathbf{S}, \mathbf{E}, \mathbf{A}, \mathbf{R}, \mathbf{Q}, \xi)d\xi, \\
\mathbf{E}^{n+1}(\zeta) &= \mathbf{E}(0) + \frac{\wp\zeta^{\wp-1}(1-\alpha)}{\mathbf{ABC}(\alpha)}\mathcal{F}_2(\mathbf{S}^n, \mathbf{E}^n, \mathbf{A}^n, \mathbf{R}^n, \mathbf{Q}^n, \zeta_n) \\
&\quad + \frac{\alpha\wp}{\mathbf{ABC}(\alpha)\Gamma(\alpha)} \sum_{\ell=0}^{n} \in \zeta_{\zeta_\ell}^{\zeta_{\ell+1}} \xi^{\wp-1}(\zeta_{n+1}-\xi)^{\alpha-1}\mathcal{F}_2(\mathbf{S}, \mathbf{E}, \mathbf{A}, \mathbf{R}, \mathbf{Q}, \xi)d\xi, \\
\mathbf{A}^{n+1}(\zeta) &= \mathbf{A}(0) + \frac{\wp\zeta^{\wp-1}(1-\alpha)}{\mathbf{ABC}(\alpha)}\mathcal{F}_3(\mathbf{S}^n, \mathbf{E}^n, \mathbf{A}^n, \mathbf{R}^n, \mathbf{Q}^n, \zeta_n) \\
&\quad + \frac{\alpha\wp}{\mathbf{ABC}(\alpha)\Gamma(\alpha)} \sum_{\ell=0}^{n} \in \zeta_{\zeta_\ell}^{\zeta_{\ell+1}} \xi^{\wp-1}(\zeta_{n+1}-\xi)^{\alpha-1}\mathcal{F}_3(\mathbf{S}, \mathbf{E}, \mathbf{A}, \mathbf{R}, \mathbf{Q}, \xi)d\xi, \\
\mathbf{R}^{n+1}(\zeta) &= \mathbf{R}(0) + \frac{\wp\zeta^{\wp-1}(1-\alpha)}{\mathbf{ABC}(\alpha)}\mathcal{F}_4(\mathbf{S}^n, \mathbf{E}^n, \mathbf{A}^n, \mathbf{R}^n, \mathbf{Q}^n, \zeta_n) \\
&\quad + \frac{\alpha\wp}{\mathbf{ABC}(\alpha)\Gamma(\alpha)} \sum_{\ell=0}^{n} \in \zeta_{\zeta_\ell}^{\zeta_{\ell+1}} \xi^{\wp-1}(\zeta_{n+1}-\xi)^{\alpha-1}\mathcal{F}_4(\mathbf{S}, \mathbf{E}, \mathbf{A}, \mathbf{R}, \mathbf{Q}, \xi)d\xi, \\
\mathbf{Q}^{n+1}(\zeta) &= \mathbf{Q}(0) + \frac{\wp\zeta^{\wp-1}(1-\alpha)}{\mathbf{ABC}(\alpha)}\mathcal{F}_5(\mathbf{S}^n, \mathbf{E}^n, \mathbf{A}^n, \mathbf{R}^n, \mathbf{Q}^n, \zeta_n) \\
&\quad + \frac{\alpha\wp}{\mathbf{ABC}(\alpha)\Gamma(\alpha)} \sum_{\ell=0}^{n} \in \zeta_{\zeta_\ell}^{\zeta_{\ell+1}} \xi^{\wp-1}(\zeta_{n+1}-\xi)^{\alpha-1}\mathcal{F}_5(\mathbf{S}, \mathbf{E}, \mathbf{A}, \mathbf{R}, \mathbf{Q}, \xi)d\xi.
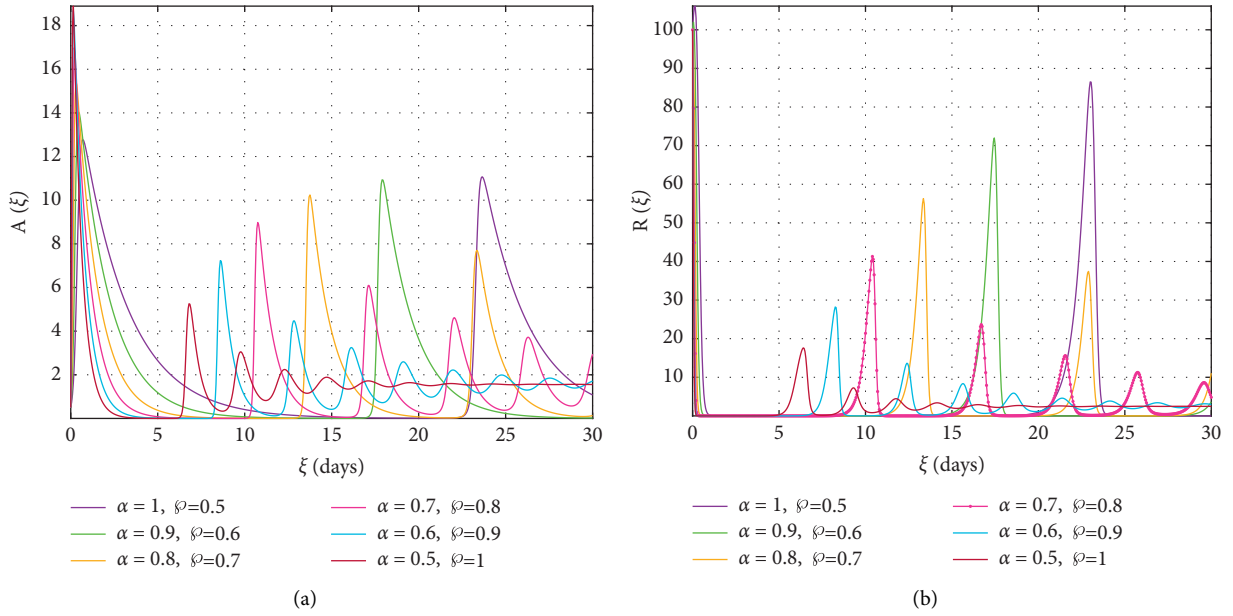\end{aligned}
\tag{70}
$$
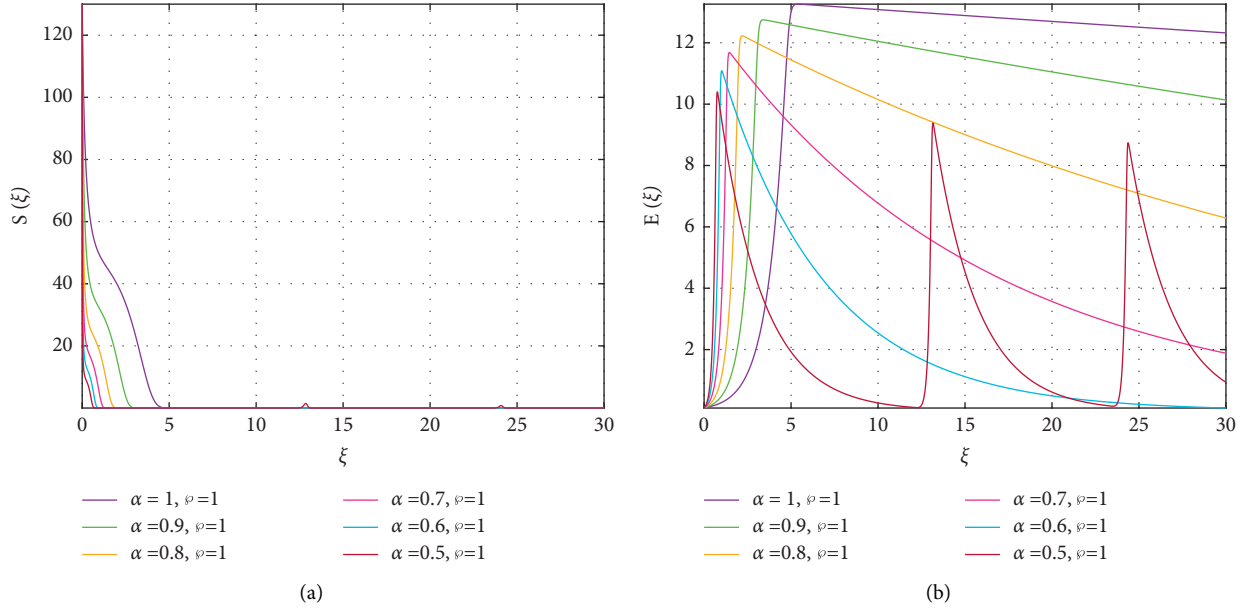
FIGURE 10: (a) Displays of susceptible individuals $\mathbf{S}(\zeta)$ (b) Displays of exposed individuals $\mathbf{E}(\zeta)$ using an another numerical approach for decreasing fractional-order α and fixed fractal-dimension $\wp = 1$.

Moreover, implementing $\xi^{\alpha-1}\mathscr{F}_\iota(\mathbf{S}, \mathbf{E}, \mathbf{A}, \mathbf{R}, \mathbf{Q}, \xi)$ for $\iota = 1, 2, \ldots, 5$ to describe the expressions in (70), in the defined interval $[\zeta_\ell, \zeta_{\ell+1}]$, the relevant numerical strategy is constructed as

$$
\begin{aligned}
\mathbf{S}^{\mathfrak{n}+1}(\zeta) &= \mathbf{S}(0) + \frac{\wp\zeta^{\wp-1}(1-\alpha)}{\mathbf{ABC}(\alpha)}\mathscr{F}_1(\mathbf{S}^{\mathfrak{n}}, \mathbf{E}^{\mathfrak{n}}, \mathbf{A}^{\mathfrak{n}}, \mathbf{R}^{\mathfrak{n}}, \mathbf{Q}^{\mathfrak{n}}, \zeta_{\mathfrak{n}}) \\
&+ \frac{(\Delta\zeta)^\alpha\wp}{\mathbf{ABC}(\alpha)\Gamma(\alpha+2)}\sum_{\ell=0}^{\mathfrak{n}}\left\{\left\{\zeta_\ell^{\alpha-1}\mathscr{F}_1\left(\mathbf{S}^\ell, \mathbf{E}^\ell, \mathbf{A}^\ell, \mathbf{R}^\ell, \mathbf{Q}^\ell, \zeta_\ell\right)\right\} \times \left((\mathfrak{n}+1-\ell)^\alpha(\mathfrak{n}-\ell+2\alpha) - (\mathfrak{n}-\ell)^\alpha(\mathfrak{n}-\ell+2+2\alpha)\right) - \left\{\zeta_{\ell-1}^{\wp-1}\mathscr{F}_1\left(\mathbf{S}^{\ell-1}, \mathbf{E}^{\ell-1}, \mathbf{A}^{\ell-1}, \mathbf{R}^{\ell-1}, \mathbf{Q}^{\ell-1}, \zeta_{\ell-1}\right)\right\} \times \left((\mathfrak{n}+1-\ell)^{\alpha+1} - (\mathfrak{n}-\ell)^\alpha(\mathfrak{n}-\ell+1+\alpha)\right)\right\},
\end{aligned}
$$

$$
\begin{aligned}
\mathbf{E}^{\mathfrak{n}+1}(\zeta) &= \mathbf{E}(0) + \frac{\wp\zeta^{\wp-1}(1-\alpha)}{\mathbf{ABC}(\alpha)}\mathscr{F}_2(\mathbf{S}^{\mathfrak{n}}, \mathbf{E}^{\mathfrak{n}}, \mathbf{A}^{\mathfrak{n}}, \mathbf{R}^{\mathfrak{n}}, \mathbf{Q}^{\mathfrak{n}}, \zeta_{\mathfrak{n}}) \\
&+ \frac{(\Delta\zeta)^\alpha\wp}{\mathbf{ABC}(\alpha)\Gamma(\alpha+2)}\sum_{\ell=0}^{\mathfrak{n}}\left\{\left\{\zeta_\ell^{\alpha-1}\mathscr{F}_2\left(\mathbf{S}^\ell, \mathbf{E}^\ell, \mathbf{A}^\ell, \mathbf{R}^\ell, \mathbf{Q}^\ell, \zeta_\ell\right)\right\} \times \left((\mathfrak{n}+1-\ell)^\alpha(\mathfrak{n}-\ell+2\alpha) - (\mathfrak{n}-\ell)^\alpha(\mathfrak{n}-\ell+2+2\alpha)\right) - \left\{\zeta_{\ell-1}^{\wp-1}\mathscr{F}_2\left(\mathbf{S}^{\ell-1}, \mathbf{E}^{\ell-1}, \mathbf{A}^{\ell-1}, \mathbf{R}^{\ell-1}, \mathbf{Q}^{\ell-1}, \zeta_{\ell-1}\right)\right\} \times \left((\mathfrak{n}-\ell+1)^{\alpha+1} - (\mathfrak{n}-\ell)^\alpha(\mathfrak{n}-\ell+1+\alpha)\right)\right\},
\end{aligned}
$$

$$
\begin{aligned}
\mathbf{A}^{\mathfrak{n}+1}(\zeta) &= \mathbf{A}(0) + \frac{\wp\zeta^{\wp-1}(1-\alpha)}{\mathbf{ABC}(\alpha)}\mathscr{F}_3(\mathbf{S}^{\mathfrak{n}}, \mathbf{E}^{\mathfrak{n}}, \mathbf{A}^{\mathfrak{n}}, \mathbf{R}^{\mathfrak{n}}, \mathbf{Q}^{\mathfrak{n}}, \zeta_{\mathfrak{n}}) \\
&+ \frac{(\Delta\zeta)^\alpha\wp}{\mathbf{ABC}(\alpha)\Gamma(\alpha+2)}\sum_{\ell=0}^{\mathfrak{n}}\left\{\left\{\zeta_\ell^{\alpha-1}\mathscr{F}_3\left(\mathbf{S}^\ell, \mathbf{E}^\ell, \mathbf{A}^\ell, \mathbf{R}^\ell, \mathbf{Q}^\ell, \zeta_\ell\right)\right\} \times \left((\mathfrak{n}+1-\ell)^\alpha(\mathfrak{n}-\ell+2\alpha) - (\mathfrak{n}-\ell)^\alpha(\mathfrak{n}-\ell+2+2\alpha)\right) - \left\{\zeta_{\ell-1}^{\wp-1}\mathscr{F}_3\left(\mathbf{S}^{\ell-1}, \mathbf{E}^{\ell-1}, \mathbf{A}^{\ell-1}, \mathbf{R}^{\ell-1}, \mathbf{Q}^{\ell-1}, \zeta_{\ell-1}\right)\right\} \times \left((\mathfrak{n}-\ell+1)^{\alpha+1} - (\mathfrak{n}-\ell)^\alpha(\mathfrak{n}-\ell+1+\alpha)\right)\right\},
\end{aligned}
$$

$$
\begin{aligned}
\mathbf{R}^{\mathfrak{n}+1}(\zeta) &= \mathbf{R}(0) + \frac{\wp\zeta^{\wp-1}(1-\alpha)}{\mathbf{ABC}(\alpha)}\mathscr{F}_4(\mathbf{S}^{\mathfrak{n}}, \mathbf{E}^{\mathfrak{n}}, \mathbf{A}^{\mathfrak{n}}, \mathbf{R}^{\mathfrak{n}}, \mathbf{Q}^{\mathfrak{n}}, \zeta_{\mathfrak{n}}) \\
&+ \frac{(\Delta\zeta)^\alpha\wp}{\mathbf{ABC}(\alpha)\Gamma(\alpha+2)}\sum_{\ell=0}^{\mathfrak{n}}\left\{\left\{\zeta_\ell^{\alpha-1}\mathscr{F}_4\left(\mathbf{S}^\ell, \mathbf{E}^\ell, \mathbf{A}^\ell, \mathbf{R}^\ell, \mathbf{Q}^\ell, \zeta_\ell\right)\right\} \times \left((\mathfrak{n}+1-\ell)^\alpha(\mathfrak{n}-\ell+2\alpha) - (\mathfrak{n}-\ell)^\alpha(\mathfrak{n}-\ell+2+2\alpha)\right) - \left\{\zeta_{\ell-1}^{\wp-1}\mathscr{F}_4\left(\mathbf{S}^{\ell-1}, \mathbf{E}^{\ell-1}, \mathbf{A}^{\ell-1}, \mathbf{R}^{\ell-1}, \mathbf{Q}^{\ell-1}, \zeta_{\ell-1}\right)\right\} \times \left((\mathfrak{n}-\ell+1)^{\alpha+1} - (\mathfrak{n}-\ell)^\alpha(\mathfrak{n}-\ell+1+\alpha)\right)\right\},
\end{aligned}
$$

$$(71)$$

$$
\begin{aligned}
\mathbf{Q}^{\mathfrak{n}+1}(\zeta) &= \mathbf{Q}(0) + \frac{\wp\zeta^{\wp-1}(1-\alpha)}{\mathbf{ABC}(\alpha)}\mathscr{F}_5(\mathbf{S}^{\mathfrak{n}}, \mathbf{E}^{\mathfrak{n}}, \mathbf{A}^{\mathfrak{n}}, \mathbf{R}^{\mathfrak{n}}, \mathbf{Q}^{\mathfrak{n}}, \zeta_{\mathfrak{n}}) + \frac{(\Delta\zeta)^\alpha\wp}{\mathbf{ABC}(\alpha)\Gamma(\alpha+2)}\sum_{\ell=0}^{\mathfrak{n}}\left\{\left\{\zeta_\ell^{\alpha-1}\mathscr{F}_5\left(\mathbf{S}^\ell, \mathbf{E}^\ell, \mathbf{A}^\ell, \mathbf{R}^\ell, \mathbf{Q}^\ell, \zeta_\ell\right)\right\} \times \left((\mathfrak{n}+1-\ell)^\alpha(\mathfrak{n}-\ell+2\alpha) - (\mathfrak{n}-\ell)^\alpha(\mathfrak{n}-\ell+2+2\alpha)\right) \right. \\
&\left. - \left\{\zeta_{\ell-1}^{\wp-1}\mathscr{F}_5\left(\mathbf{S}^{\ell-1}, \mathbf{E}^{\ell-1}, \mathbf{A}^{\ell-1}, \mathbf{R}^{\ell-1}, \mathbf{Q}^{\ell-1}, \zeta_{\ell-1}\right)\right\} \times \left((\mathfrak{n}-\ell+1)^{\alpha+1} - (\mathfrak{n}-\ell)^\alpha(\mathfrak{n}-\ell+1+\alpha)\right)\right\}.
\end{aligned}
$$

$$(72)$$

5. Numerical results and description

In this part, we exhibit simulation results for the FF derivative operator for the $\mathbb{SMA}$ model (2) assuming the numerical methods proposed by [34], as mentioned previously. Such numeric findings are obtained using non-negative factors, as indicated in Table 1. We examine a FF $\mathbb{SMA}$ model, including the Atangana-Baleanu approach in the Caputo context, to demonstrate the reliability and usefulness of the new efficient and Newton polynomial approach. We can effortlessly acquire approximate methods
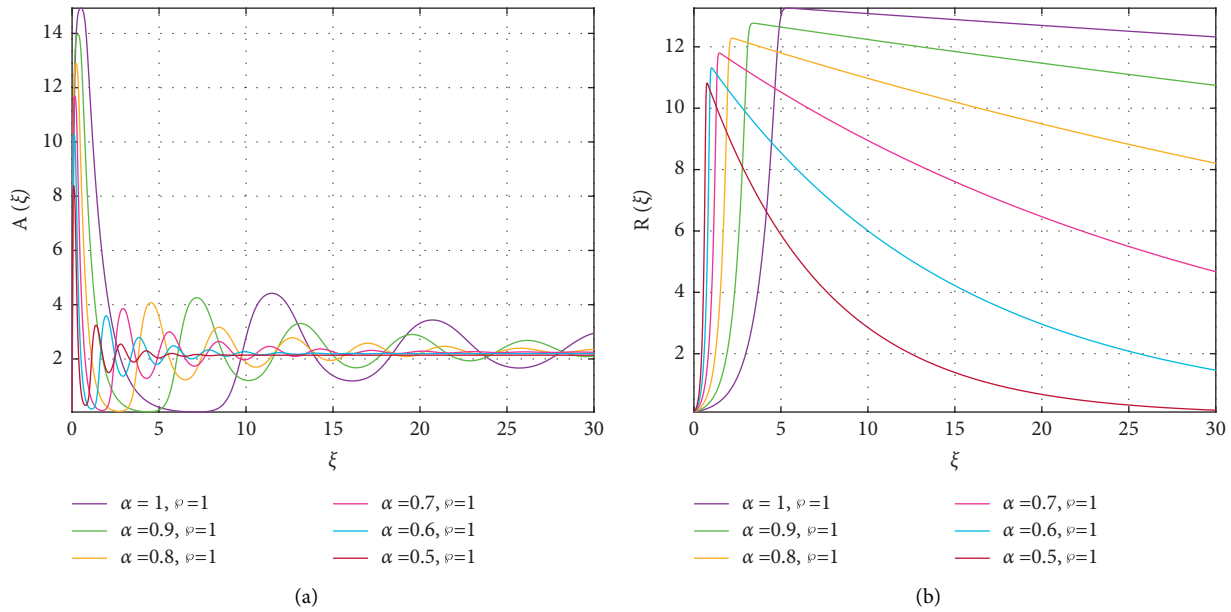
FIGURE 11: (a) Displays of addicted individuals $\mathbf{S}(\zeta)$ (b) Displays of recovered individuals $\mathbf{E}(\zeta)$ using a another numerical approach for decreasing fractional-order α and fixed fractal-dimension $\wp = 1$.
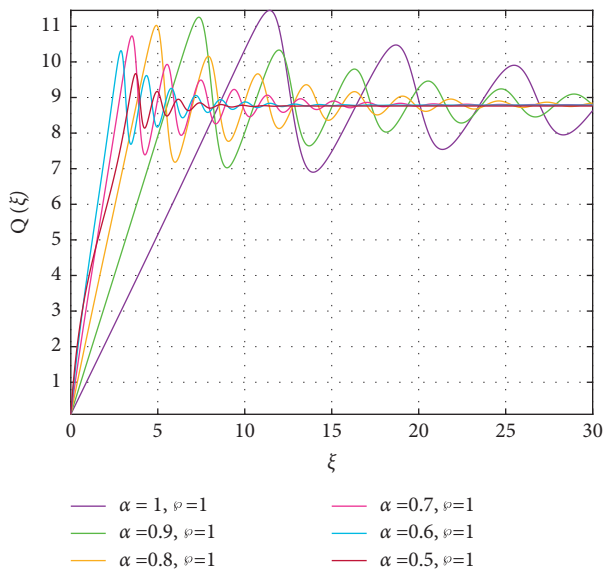
FIGURE 12: Displays of individuals who quit or not using $\mathbf{Q}(\zeta)$ applying an another numerical approach for decreasing fractional-order α and fixed fractal-dimension $\wp = 1$.

for it using new efficient and Newton polynomial approach. The primary goal of this review is to identify individuals who are vulnerable and exposed to various fractional Brownian patterns as well as classical motion. The simulation results of the scheme (2) for various Brownian motions are $\alpha = 1.0, 0.9, 0.8, 0.7, 0.6, 0.5$ are presented in Figure11(a)-1(b), Figure 2(a)-2(b) and Figure 3(a)-3(b). As seen in Figure 1(a), the susceptible group diminishes as fractional orders increase and reach 1 while increasing the fractal-dimension $\wp$, and finally remains consistent including all Brownian motion at $\mathbf{S} = 8.1212$. Furthermore, when $\mathbf{E} =$

0.0450 and $\mathbf{A} = 0.0104$, Figure 1(b) and Figure 2(a) illustrate that the unprotected and addictive groups rise dramatically and decline, respectively, exhibiting behaviour of different fractional orders eventually reaching 1. When $\mathbf{R} = 0.0236$ and $\mathbf{Q} = 1.7517$, Figure 2(b) and Figure 3 indicate that the community of individuals who are rehabilitated and consistently do not utilize and discontinue using SM significantly improves and drops, respectively, using multiple fractional-orders changes, reaching 1.

In a similar way, we can discuss the behaviour of Figure 4(a)-4(b), Figure 5(a)-5(b) and Figure 6(a)-6(b), by incorporating the values of $\lambda = 0.5$, the induced mortality rate of 0.05 and $\kappa = 0.06$ via the FF operator in the Atangana-Baleanu sense. In this case, the graphical representation has a lower fractional-order α while keeping the fractal-dimension $\wp = 0.7$ constant. The fundamental target of this article is that subtle improvements in the fractional derivative order have no impact on the general behaviour of the consequent structures; simply simulation studies are altered.

Figure 7(a)-7(b), Figure 8(a)-8(b) and Figure 9(a)-9(b) demonstrates that the percentage of unprotected people appears to have decreased in the first two years, but affected people revert to utilizing social platforms owing to the scheme's ineffectiveness via FF derivative operator in the Atangana-Baleanu sense. In this case, the graphical representation has a lower fractal-dimension $\wp$ while retaining a constant fractional-order $\alpha = 0.7$. As a result, fighting $\mathbb{SMA}$ in the community is ineffective.

As shown in Figure 10(a)-10(b), Figure 11(a)-11(b) and Figure 12(a)-12(b), the proportion of affected and intoxicated people was diminished when the method was used against no approach within the FF derivative operator in the Atangana-Baleanu sense. The graphical illustration in this approach has a lower fractional-order α while maintaining a

constant fractal-dimension $\wp = 1$. The proposed technique appears to be efficacious in diminishing dependency load during the implementation, and hence can be considered an ideal contender for managing the stress of $\mathbb{SMA}$.

6. Conclusion

In this investigation, we presented a mathematical framework for the prevalence and distribution of the $\mathbb{SMA}$ model, including the fractal-fractional derivative operator in the Atangana-Baleanu sense. According to the analysis, the system's disease-free equilibrium is locally asymptotically stable when the $\mathbb{R}_0 < 1$, but generally unstable. The stability of equilibria points was explored utilizing $\mathbb{R}_0$. Bifurcation investigation shows that the model demonstrates forward bifurcation at $\mathbb{R}_0 = 1$. Furthermore, this study proposes two effective mathematical approaches for numerically solving a fractional SMA model in the fractal-fractional derivatives perspective. One initial approach relies on product integration formulation, while the other is focused on the numeric Newton polynomial approach. When the obtained simulations from the two methodologies are compared, it is clear that their respective behaviour in fixing the challenges is remarkably analogous. The findings demonstrate that our generated results are in close harmony with the precise outcomes. In a simulation study, the responses from the two different techniques exhibit the same behaviour for fractional order and fractal-dimension. Such mathematical approaches can also be leveraged to generate analytical results for other complex scientific systems of any complexity. The numerical behaviours produced by the aforesaid approaches are perfectly compatible with the model's projected rational behaviour. [30–34].

Data Availability

No data were used to support this study.

Conflicts of Interest

The authors declare that they have no competing interests.

Authors' Contributions

S. Rashid provided the main ideas of the article, constructed the main algorithm and proved the convergence, also submitted the article. R. Ashraf drafted the manuscript and provided qualitative analysis. E. Bonyah provided the solution and illustrations of the final revision. All authors read and approved the final manuscript.

References

[1] A. Smith and M. Anderson, "Social media Use 2018: Demographics and Statistics," 2018, http://www.pewinternet.org/2018/03/01/social-media-use-in-2018.

[2] D. J. Kuss, M. D. Griffiths, L. Karila, and J. Billieux, "Internet addiction: a systematic review of epidemiological research for the last decade," *Current Pharmaceutical Design*, vol. 20, no. 25, pp. 4026–4052, 2014.

[3] J. Fox and J. J. Moreland, "The dark side of social networking sites: an exploration of the relational and psychological stressors associated with Facebook use and affordances," *Computers in Human Behavior*, vol. 45, pp. 168–176, 2015.

[4] K. W. Müller, M. Dreier, M. E. Beutel, E. Duven, S. Giralt, and K. Wölfling, "A hidden type of internet addiction? Intense and addictive use of social networking sites in adolescents," *Computers in Human Behavior*, vol. 55, pp. 172–177, 2016.

[5] V. Gupta, N. Jain, P. Katariya et al., "An emotion care model using multimodal textual analysis on COVID-19, " chaos, solit," *Fract*, vol. 144, pp. 0960–0779, 2021.

[6] K. Shah, M. Arfan, I. Mahariq, A. Ahmadian, S. Salahshour, and M. Ferrara, "Fractal-fractional mathematical model addressing the situation of corona virus in Pakistan," *Results in Physics*, vol. 19, p. 103560, 2020.

[7] S. Salahshour, A. Ahmadian, B. A. Pansera, and M. Ferrara, "Uncertain inverse problem for fractional dynamical systems using perturbed collage theorem," *Communications in Nonlinear Science and Numerical Simulation*, vol. 94, p. 105553, 2021.

[8] C. Andreassen and S. Pallesen, "Social network site addiction - an overview," *Current Pharmaceutical Design*, vol. 20, no. 25, pp. 4053–4061, 2014.

[9] E. W. J. J. Lee, S. S. Ho, and M. O. Lwin, "Explicating problematic social network sites use: a review of concepts, theoretical frameworks, and future directions for communication theorizing," *Explicating problematic social network sites use: A review of concepts, theoretical frameworks, and future directions for communication theorizing New Media & Society*, vol. 19, no. 2, pp. 308–326, 2017.

[10] H. T. Alemneh and N. Y. Alemu, "Mathematical modeling with optimal control analysis of social media addiction," *Infectious Disease Modelling*, vol. 6, pp. 405–419, 2021.

[11] R. Hilfer, *Applications of Fractional Calculus in Physics*, Word Scientific, Singapore, 2000.

[12] A. Kilbas, H. M. Srivastava, and J. J. Trujillo, *Theory and Application of Fractional Differential Equations*, Math Stud, North Holland, 2006.

[13] A. Atangana, A. Akgül, and K. M. Owolabi, "Analysis of fractal fractional differential equations," *Alexandria Engineering Journal*, vol. 59, no. 3, pp. 1117–1134, 2020.

[14] M. Caputo and M. Fabrizio, "A new definition of fractional derivative without singular kernel," *Prog. Fract. Differ. Appl.* vol. 73, no. 1–13, 2015.

[15] R. Scherer, S. L. Kalla, Y. Tang, and J. Huang, "The Grünwald-Letnikov method for fractional differential equations," *Computers & Mathematics with Applications*, vol. 62, no. 3, pp. 902–917, 2011.

[16] I. Podlubny, *Fractional Differential Equations*, Academic Press, San Diego, 1999.

[17] A. Atangana and D. Baleanu, "New fractional derivatives with nonlocal and non-singular kernel: theory and application to heat transfer model," *Thermal Science*, vol. 20, no. 2, pp. 763–769, 2016.

[18] A. Atangana and S. Qureshi, "Modeling attractors of chaotic dynamical systems with fractal-fractional operators," *Chaos, Solitons & Fractals*, vol. 123, pp. 320–337, 2019.

[19] A. Raza, A. Ahmadian, M. Rafiq, S. Salahshour, and M. Ferrara, "An analysis of a nonlinear susceptible-exposed-infected-quarantine-recovered pandemic model of a novel coronavirus with delay effect," *Results in Physics*, vol. 21, Article ID 103771, 2021.

[20] S. Ahmad, A. Ullah, K. Shah, and T. SalahshourAhmadianCiano, "Fuzzy fractional-order model of the novel coronavirus," *Advances in Difference Equations*, vol. 2020, no. 1, p. 472, 2020.

[21] A. Atangana, "Fractal-fractional differentiation and integration: connecting fractal calculus and fractional calculus to predict complex system," *Chaos, Solitons & Fractals*, vol. 102, pp. 396–406, 2017.

[22] W. Chen, H. Sun, X. Zhang, and D. Korošak, "Anomalous diffusion modeling by fractal and fractional derivatives," *Computers & Mathematics with Applications*, vol. 59, no. 5, pp. 1754–1758, 2010.

[23] W. Cai, W. Chen, and W. Xu, "Characterizing the creep of viscoelastic materials by fractal derivative models," *International Journal of Non-linear Mechanics*, vol. 87, no. 58–63, pp. 58–63, 2016.

[24] S. Qureshi, A. Atangana, and A. A. Shaikh, "Strange chaotic attractors under fractal-fractional operators using newly proposed numerical methods," *The European Physical Journal Plus*, vol. 134, no. 10, p. 523, 2019.

[25] S. Rashid, F. Jarad, and A. G. Ahmad, "A novel fractal-fractional order model for the understanding of an oscillatory and complex behavior of human liver with non-singular kernel," *Results in Physics*, vol. 35, p. 105292, 2022.

[26] J. Kongson, W. Sudsutad, C. Thaiprayoon, J. Alzabut, and C. Tearnbucha, "On analysis of a nonlinear fractional system for social media addiction involving Atangana-Baleanu-Caputo derivative," *Advances in Difference Equations*, vol. 2021, no. 1, p. 356, 2021.

[27] K. Diethelm, N. J. Ford, and A. D. Freed, "Detailed error analysis for a fractional adams method," *Numerical Algorithms*, vol. 36, no. 1, pp. 31–52, 2004.

[28] A. Atangana, "Mathematical model of survival of fractional calculus, critics and their impact: how singular is our world?" *Advances in Difference Equations*, vol. 2021, no. 1, p. 403, 2021.

[29] P. van den Driessche and J. Watmough, "Reproduction numbers and sub-threshold endemic equilibria for compartmental models of disease transmission," *Mathematical Biosciences*, vol. 180, no. 1-2, pp. 29–48, 2002.

[30] S. Ullah, M. Altaf Khan, and M. Farooq, "A fractional model for the dynamics of TB virus," *Chaos, Solitons & Fractals*, vol. 116, pp. 63–71, 2018.

[31] Y. Guo and T. Li, "Optimal control and stability analysis of an online game addiction model with two stages," *Mathematical Methods in the Applied Sciences*, vol. 43, pp. 4391–4408, 2020.

[32] H. F. Huo and Q. Wang, "Modelling the influence of awareness programs by media on the drinking dynamics," *Abstract and Applied Analysis*, vol. 2014, Article ID 938080, 2014.

[33] T. Li and Y. Guo, "Stability and optimal control in a mathematical model of online game addiction," *Filomat*, vol. 33, no. 17, pp. 5691–5711, 2019.

[34] A. Atangana and S. I. Araz, *Fractional Stochastic Differential Equations*, Springer, Singapore, 2021.

WILEY | Hindawi

Research Article

Hybrid Electro Search with Ant Colony Optimization Algorithm for Task Scheduling in a Sensor Cloud Environment for Agriculture Irrigation Control System

Murali Subramanian [iD],[1] **Manikandan Narayanan** [iD],[1] **B. Bhasker** [iD],[1] **S. Gnanavel** [iD],[2] **Md Habibur Rahman** [iD],[3] **and C. H. Pradeep Reddy** [iD][4]

[1]*School of Computer Science and Engineering, Vellore Institute of Technology, Vellore, Tamil Nadu, India*
[2]*Department of Computing Technologies, SRM Institute of Science and Technology, Chengalpattu, Tamil Nadu, India*
[3]*Department of Computer Science and Engineering, Faculty of Engineering and Technology, Islamic University, Kushtia 7003, Bangladesh*
[4]*School of Computer Science and Engineering, VIT-AP University, Amaravati, Andhra Pradesh, India*

Correspondence should be addressed to Md Habibur Rahman; habib@iu.ac.bd

Integrating cloud computing with wireless sensor networks creates a sensor cloud (WSN). Some real-time applications, such as agricultural irrigation control systems, use a sensor cloud. The sensor battery life in sensor clouds is constrained. The data center's computers consume a lot of energy to offer storage in the cloud. The emerging sensor cloud technology-enabled virtualization. Using a virtual environment has many advantages. However, different resource requirements and task execution cause substantial performance and parameter optimization issues in cloud computing. In this study, we proposed the hybrid electro search with ant colony optimization (HES-ACO) technique to enhance the behavior of task scheduling, for those considering parameters such as total execution time, cost of the execution, makespan time, the cloud data center energy consumption like throughput, response time, resource utilization task rejection ratio, and deadline constraint of the multicloud. Electro search and the ant colony optimization algorithm are combined in the proposed method. Compared to HESGA, HPSOGA, AC-PSO, and PSO-COGENT algorithms, the created HES-ACO algorithm was simulated at CloudSim and found to optimize all parameters.

1. Introduction

Food and agriculture are both important sources of income for many farmers worldwide. Irrigation is one of the most critical services supplied in agriculture. Most crops require irrigation in areas with low rainfall, as inadequate irrigation reduces crop quality and yield. Due to contemporary concerns such as water shortages, droughts, and resource scarcity, academics have tried to rationalize water usage in agriculture, one of the world's most water-intensive industries [1]. A large amount of water is required by the conventional irrigation method, resulting in water waste. The IIS is desperately needed to reduce water waste. In the wheat field, IoT sensors capture exact ground and environmental data. The collected data is sent to a cloud-based server, which analyzes and advises farmers on irrigation. This recommendation system has an embedded feedback mechanism to make it robust and flexible [2]. Sensor-cloud technology integrates WSNs with cloud computing to reduce storage, processing, and scalability issues. Sensor cloud technology has recently been deployed to several real-world applications, including agriculture irrigation [3]. Sensor-cloud technology integrates WSNs with cloud computing to reduce storage, processing, and scalability issues. Sensor cloud technology has recently been deployed to several real-world applications, including agriculture irrigation [4]. A

sensor cloud is a collection of WSNs that provide sensing as a service to various applications. Efficiently managing task requests from many applications is crucial [5]. Combining WSNs and cloud capabilities will offer good services provided by sensor cloud infrastructure. In a sensor network, huge volume of data is transported to the gateway, which is present in the cloud to offer such services [6].

Figure 1 clearly shows the overall architecture of the sensor cloud environment. Sensor networks act as a link between virtual and physical worlds. These SNs are made up of micro-electro-mechanical nodes that can detect their environment and communicate. A sensor cloud is a group of WSNs with several sensors. It is a heterogeneous environment and allows customers to purchase and use cloud services.

Because of this, large-scale networks benefit greatly from the cost-effectiveness and affordability of cloud computing. Similar to cloud computing, SCs allow for the dynamic deprovisioning of resources in response to demand, enhancing operational flexibility. Performance and dependability in the sensor cloud are determined by several factors: scheduling, which includes resource, job, workflow, task, and deadline scheduling, among others. Task scheduling maximizes resource usage and ensures that activities are completed in the most efficient manner possible, resulting in a satisfactory final result for customers. In cloud computing, task scheduling refers to the process of allocating a task to available virtual machines in order to perform it as quickly as possible [7].

This research concentrates on energy-efficient task scheduling, especially communication between the cloud and users in a sensor cloud environment for agriculture irrigation control systems. Here, user requests are treated as a task for accessing the required on-demand information from the cloud. Clouds provide users with virtual resources. Users use virtual resources to perform tasks. Cloud computing's elasticity supports multiple virtual apps at once. Multiobjective computers exchange resources. User requests determine resource allocation. An efficient scheduler module checks and issues resource status. A good scheduler is essential for optimal cloud computing real-time performance. The task scheduling algorithm maps virtual machines with the tasks in the cloud. It uses available resources, reducing request latency and response time while increasing resource utilization and system throughput.

The processing needs and features of tasks in cloud computing differ. Scheduling tasks for cloud computing is an unsolved NP-complete issue. Hybrid, heuristic, and metaheuristic approaches are preferred, which poor the performance of systems and service providers impacted by task scheduling. Task scheduling is challenging due to the task's nature, the variety of the cloud's resources, utility, and deadline restrictions. Among the best task scheduling methods are FCFS, PSO, MIN-MIN, ACO, GA, and others. The greatest remedy for cloud computing task scheduling problems is metaheuristic algorithms. Although it is not declared to be optimal, using heuristic techniques offers the best optimal solution. By combining both methods, the metaheuristic technique and the heuristic approach create a hybrid scheduling algorithm solution.

The survey provides Electro Search (ES) and ACO techniques for scheduling the Cloudlet in the virtual machine with balanced cloudlet distribution. This study offers a hybrid task scheduling method based on the electro search (ES) and ACO techniques. The job scheduling issue was typically solved using ES and ACO-based algorithms. In order to offer the cone to the global solution to the best solution in the search space, the authors apply the ES algorithm for the global search strategy. The VM is the most important asset in a cloud environment, and the ACO technique helps maximize VM use. The goal of this research is to lessen the deadline limitations, makespan, execution cost, overall execution time, energy consumption, and throughput. The legislative cloud customers are served smoothly by the sensor cloud services provider (SCSP), who also makes the greatest money. Typically, SCSP receives a variety of tasks as requests. Additionally, these jobs need to be organized based on the requirements and any limitations. The authors presented the HMTS algorithm after they examined the case.

2. Related Works

Task scheduling in the sensor cloud environment, particularly in cloud computing, is a significant difficulty because of the varied nature of cloud resources. Numerous real-time approaches have been put out to address the task scheduling issue in the context of cloud computing. The scheduling issue has been solved using a variety of task scheduling strategies, each of which has its own advantages and disadvantages as a result of the many QoS parameters. Scheduling strategies are generally divided into heuristic, metaheuristic, and algorithmic categories. Heuristic strategies rely on prediction to arrive at the best answer with minor complexity and the shortest time. Rather than heuristic procedures, metaheuristic strategies identify the most efficient solution results. Below are some of the most recent task scheduling approaches.

A study explored energy-efficient sensor cloud environment approaches. An energy-efficient algorithm detects a change in the environment. Most of the research looked at did not address QoS, scalability, or network longevity with energy efficiency. Real-time applications in agriculture, healthcare, and intelligent homes need maximizing QoS and energy. This study will help academics build better techniques that consider QoS measurements and energy [8].

Ojha et al. suggested a dynamic duty scheduling technique for on-field sensor networks to reduce energy usage. The sensor cloud framework helps field WSNs reduce processing demand. The authors demonstrated a suitable time interval selection technique for data uploading to the cloud in duty time intervals. The plan proposes improving energy efficiency while cutting expenses. The proposed method outperformed traditional energy efficiency, network longevity, cost-effectiveness, and utility. Real-time sensor cloud applications require testing. Consider QoS guarantee as a parameter [9].

Sivakumar and Al-Anbury proposed a CMSP for IoT-based sensor cloud systems. The approach divides a dense
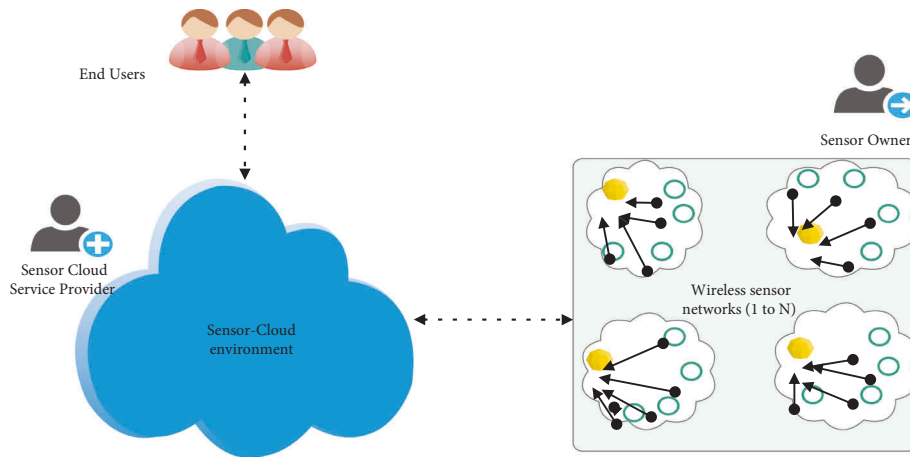
FIGURE 1: Sensor cloud architecture.

network into Voronoi structures. Each Voronoi division has its channel and data collector. They wanted to design a multichannel hybrid cluster protocol. It was made for static networks. ACMSP outperforms contemporary protocols such as MC-LMAC, MMSN, and TMCP in energy efficiency and throughput (Castalia tool). With IEEE 802.15.4, the proposed CMSP received intra- and intercluster data. The proposed CMSP must be tested in real time with real-time results for showing its effectiveness [10].

Chatterjee et al. optimized the selection algorithm for choosing suitable bridge nodes to reduce data transmission energy from sensor networks to sensor clouds. Research is focused on developing a multihop data transport system from PSNs to sensor clouds. One alternative was to save energy. Consider node heterogeneity, mobility, and other network factors to test real-time apps [11].

SC-iPaaS was proposed by Phan et al. SC-iPaaS has three layers: cloud, sensor, and edge. Between the layers, it uses push-pull communication. This study presents a Pareto optimal solution in the objective space. It uses evolutionary multiobjective optimization for its communication optimizer. The multiobjective analysis is critical in simulations. The results show that the proposed method obtains less bandwidth and energy consumption for more data yield. It is required to consider the real-time application and not QoS parameters [7].

Dinh et al. developed an effective sensor cloud interaction model to suit end-user QoS needs. We built a feedback control system to suit QoS requirements between physical WSN and sensor cloud. Optimize sensor energy utilization via feedback. This approach reduces latency compared to traditional protocols. A real-time application should be tested. Energy efficiency is a research issue—low signaling overhead [12].

A hybrid optimization model for effective VM task allocation was presented by Sreenivasulu and Paramasivam. The hybrid algorithm prioritizes workloads using cloud hierarchy and setting priorities using BAT/ BAR models and VM traits. MOML preemption lowered VM burden. The simulation findings suggest that the suggested hybrid model outperformed existing

algorithms such as BAT and ACO. The hybrid technique has proven beneficial in utilizing bandwidth and memory. The hybrid algorithm prioritizes workloads using cloud hierarchy and setting priorities using BAT/BAR models, and VM traits reduced VM burden. By using a hybrid strategy, you can get more. The author ignores energy usage and must demonstrate the suggested algorithm's efficiency with real-time workflows [13].

To set up cloud-based task scheduling and to address the complex work scheduling issue, the author developed a hybrid AC-PSO method. The hybrid strategy that is suggested combines ACO and PSO (PSO). Using the proposed methods, jobs are successfully distributed to cloud-based virtual computers. The metrics Makespan time, cost, and resource utilization are superior to the proposed method. The author disregards time complexity, throughput, and energy efficiency [14].

Dubey and Sharma created a hybrid CR-PSO technique to improve PSO restrictions and handle task scheduling. The author created a mathematical model of work scheduling and specified its purpose and fitness function. Using both CRO and PSO, a hybrid CR-PSO strategy is created. Experiments show that the suggested algorithm is faster, cheaper, and shorter. Cost-effective CR-PSO outputs increase cloud system performance. The author scheduled dependent tasks and checked the proposed approach's energy usage, load balancing, task rejection ratio, and turnaround time [15].

Task scheduling played the key role in cloud and sensor cloud systems, according to Proshikshya Mukherjee. The author looked into the various challenges and difficulties associated with task scheduling issues in the sensor cloud. The ability to efficiently manage and schedule duties is the most critical component of this job. As a result of this investigation, the researchers will obtain a lot of knowledge regarding task scheduling. Designing an efficient hybrid task scheduling mechanism in this work is required. In the sensor cloud, multicriteria decision-making is needed [16].

In order to solve the task scheduling problem in cloud computing, a MOPSO algorithm (multiobjective particle

swarm optimization) proposed by Jena. The proposed solution was suited for the cloud environment since it used system resources to reduce energy consumption and time to completion. The designed MOPSO outperformed both the BRS and the RSA, according to simulation findings. This effort necessitated more bandwidth, load balancing, and cost, among other things. A more robust algorithm is required [17].

Swagatika et al. conducted a complete examination of conventional scheduling algorithms for efficient VM allocation in a cloud context. A modified Markov chain model is utilized to anticipate resource utilization. An upgraded PSO algorithm is employed for efficient resource allocation optimally in the cloud, with dynamic load balancing based on the VM allocation mechanism and required to focus on a more robust algorithm. Work needed to consider the many characteristics such as makespan time, energy consumption, and cost [18].

Nayak et al. proposed a novel approach for deadline-based work scheduling. Every lease has a current (CT) and gap time (GT). Previous methods did not include CT and GT as scheduling criteria. The proposed scheduling method is based on the lease acceptance rate. The proposed mechanism eliminates the necessity for a decision-maker such as AHP to resolve lease issues. In MATLAB R2015a, 10 different workloads are simulated and assessed. The proposed technique determined the average task rejection and acceptance ratios. The new mechanism outperforms the current backfilling process. Consider aspects such as VM switching costs, energy consumption, and makespan time for further work [19].

The author proposed using a hybrid cuckoo and particle swarm optimization technique to schedule jobs with multiple objectives. This task scheduling approach can achieve a close-to-optimal solution in a heterogeneous cloud environment because to the qualities of the recommended CPSO technique, which include being immediately convergent and simple to apply. When compared to existing algorithms such as ACO Min-Min, PBACO, and FCFS, the suggested CPSO approach obtains the lowest rate of deadline violations. Energy usage and other QoS service elements need to be taken into account [20].

Huang et al. developed a PSO algorithm with time-varying inertia weights for cloud work scheduling. This paper proposes a PSO-based scheduler with five update methods (i.e., simulated annealing, linear, chaotic, sigmod decreasing, and logarithm decreasing). Logarithm PSO trumps alternative cloud work scheduling methods, experiments show. The suggested PSO-based scheduler outperforms the average GSA, ABC, and DA algorithms. Various criteria must be considered, such as load balance and energy usage. In addition, the proposed technique will have to be used in a variety of contexts and application workflows [21].

The proposed electro search algorithm adopts a three-phase scheme using the Bohr model and Rydberg formulae. The ES algorithm's new features enable it to find optimal global points without initializing tuning parameters. It was found that the optimal results outperformed selected algorithms such as GA and SA in terms of computation time

and success rate. The proposed algorithm outperformed the others. This method required testing for task scheduling and considering other performance parameters in cloud [22].

Bansal and Malik introduced a PSO-based multifaceted scheduling framework (MFOSF). This work presented a resource cost timeline model (RCTM) to define task resource needs. An updated PBPSO-based model was proposed to maximize performance scheduling and user cost. Third, better PBPSO was proposed to prevent PSO from going local. P_{best} and G_{best} changed the solution's quality based on performance and budget. Enhanced PBPSO is superior to similar approaches in cost, violation rate, and resource utilization, confirming its effectiveness. The proposed algorithm must be tested using specified QoS and energy usage statistics [23].

According to Khan and Santhosh, task scheduling can reduce time of waiting and increase service quality in cloud. The support vector machine loads first categorize it. PSGWO is used in the hybrid technique to find the best virtual machines and resource allocation. Traditional ant colony and PSGWO are compared to the proposed scheduling paradigm. In every parameter, the proposed hybrid optimization-based work scheduling outperforms previous approaches. This work cannot explore better QoS with VM allocation [24].

Kumar and Sharma proposed a resource allocation model employing PSO-COGENT scheduling to maximize execution cost, makespan time, throughput, task rejection ratio, and energy consumption based on fitness function while taking deadline considerations into account. The proposed PSO-COGENT method outperformed the already employed PSO, honeybee, and min-min strategies in terms of execution cost, execution time, and energy consumption. Consideration of various QoS factors, SLA, and testing for real-time applications such as agricultural is required for this task [25].

For instance, to enhance task scheduling behavior, a hybrid electro search with a genetic algorithm (HESGA) was proposed by Velliangiri et al. The advantages of genetic and electro search algorithms were integrated. Globally, electro search outperforms genetic algorithm. The proposed HESGA algorithm is compared to existing approaches. HESGA approach obtains better results than HEPSOGA, GA, ES, and ACO. This work required an enhanced version that took energy consumption, QoS metrics, and real-time applications such as agriculture [26].

Gokuldhev and Singaravel proposed the LPMSA algorithm for cloud job scheduling. Moth search and floral pollination algorithms were combined (FPA). The proposed LPMSA picks the best cloud job scheduling solution. The suggested LPMSA is evaluated on machines with low and high heterogeneity. The suggested LPMSA saves time and energy over existing methods. The Wilcoxon test compares makespan minima and energy usage. This work's limitations are the necessity to test with real-time applications and add more parameters to the algorithm [27]. The local pollination-based gray wolf optimizer (LPGWO) method was used by Gokuldhev et al. to efficiently schedule jobs. GWO and FPA are both used in the hybrid algorithm. In the presence of GWO, data are distributed via local pollination to the

subsequent potential solution packet. These methods are used to solve early tasks. Work scheduling in low and high machine heterogeneity was enhanced.

Finally, comparing simulation results revealed the slowest convergence of makespan and energy consumption. This work required testing with real-time applications and adding more parameters to the method are needed [28]. Compare the various scheduling algorithms in this work. The HEFT algorithm ranks tasks and assigns them to processors. Give the heterogeneous processor tasks to reduce makespan time. The proposed algorithm outperforms load balancing and task makespan time with HEFT and CPOP. However, the algorithm can be improved by considering various deadlines, QoS parameters, and application tests [29]. This research proposed a SACO method with slave ants for cloud computing task scheduling. To avoid long routes with pheromones erroneously accumulated by leading ants, we use slave ants to diversify and reinforce—no preprocessing overhead for slave ants and beats existing ACO-based cloud work scheduling algorithms. SACO solves the NP-hard issue efficiently while maximizing cloud server utilization. Heterogeneous clusters cannot be considered because computing instances decide costs [30]. An ICMPACO approach is proposed in this work for solving complicated large-scale optimization issues. The algorithms ACO and IACO perform better than ICMPACO when dealing with gate assignment and travelling salesman issues. The gate assignment problem and typical TSP cases are both successfully solved by ICMPACO. A total of 132 flights can be efficiently routed to 20 gates (83.5%). ICMPACO outperforms ACO and IACO in terms of optimization and stability. The ICMPACO algorithm requires more research because it takes longer to solve difficult optimization issues [31]. Q-ACOA is suggested for work scheduling and resource allocation in cloud computing based on current problems. For the first time, critical performance for task scheduling is established. Utilize Q-ACOA to efficiently execute processes, move data, and delight consumers. The work scheduling and resource allocation in cloud computing are optimized by Q-ACOA. Despite these successes, there are still problems with research. For some reason, there is no correlation between the tasks. To aid in resource allocation and scheduling in cloud computing, the research's limitations should concentrate on task correlation [32]. This study presents a FACO algorithm for cloud computing virtual machine load balancing. Ragmani et al. proposed a FACO cloud virtual machine scheduling algorithm. Due to scalability, ant colony optimization was used. CloudSim optimizes ACO settings. FACO uses evaporation to avoid nonoptimal early convergence. The proposed approach can cut response time by 80%, processing time by 90%, and total cost by 9%. We want to define pheromones beyond FACO. FACO has not been tested in a multicloud scenario [33].

When we think of implementing a new framework, we may have few merits and demerits. For example, smart bluetooth is one of the emerging wireless technologies used for data transfer between short distances. It is also cheaper than other technologies having advantage of being available on almost every smart phone [34]. The practice of current traditional centralized security measures may lead us with limitations because of single point of failure, traceability, verifiability, as well as scalability [35]. When we chose multiclass model, development should be done with the consideration of the relative status of the factors taken [36].

Abualigah and Diabat offer a hybrid antlion optimization method with elite-based differential evolution to solve multi-objective task scheduling challenges in cloud computing. The MALO solution must maximize resource efficiency while minimizing makespan time [37]. Two experimental series on artificial and real trace data sets were run with CloudSim. MALO outperformed other well-known optimization methods.

This paper suggests a more efficient task scheduling method and an approach to optimal power minimization to help with dynamic resource allocation. Using a prediction mechanism and a dynamic resource table update approach can increase the effectiveness of resource allocation in terms of job completion and reaction time [38]. This architecture is successful in lowering total power consumption because it decreases data center power consumption. The proposed approach can be used to update the resource table. In order to achieve an effective resource deployment, improved job scheduling and a mechanism that uses less power are implemented. The simulation produces results that are 8% more accurate when compared to other approaches. To solve those problems, a hybrid machine learning (RATS-HM) technique is created. Finally, by simulating the suggested RATSHM technique with a new simulation setup and comparing the outcomes with those of other existing techniques, its utility is shown [39]. With regard to resource usage, energy consumption, response time, and other factors, the proposed method performs better than the existing one.

The task scheduling issue for tasks in the sensor cloud computing architecture has been addressed in the literature using a variety of metaheuristic- and heuristic-based algorithms, including PSO, GA, ES, ACO, and CRO. The majority of these algorithms are not effective enough for scheduling jobs in a multicloud setting, according to a review of pertinent studies. The algorithm used in related works lacks both global and local optimum solutions. The parameters necessary to improve task scheduling performance are not taken into account by many algorithms. Based on these conclusions, we developed the hybrid electro search-ant colony optimization technique (HES-ACO) to enhance task scheduling behavior by optimizing parameters such as makespan time, execution cost, total execution time, energy consumption, throughput, response time, resource utilization, and deadline constraints of the sensor cloud. Table 1 describes about the literature review of metaheuristic hybrid task scheduling algorithms with limitations

3. System Model and Problem Statement Formation of Problem Statement

Cloud computing has seized control of the computing market in the recent decade, offering users a wide range of services. The popularity of cloud computing is causing a significant increase in cloud users. As the number of users grows, the system encounters several challenges. Mapping

TABLE 1: iterature review of metaheuristic hybrid task scheduling algorithms with limitations.

S. no.	Author and year	Methodology	Parameters	Limitations	Tool
1	Sreenivasulu and Paramasivam (2021) [13]	Hybrid optimization algorithm (BAT and BAR), hierarchy process model, and MOML preemption policy	Turnaround time, response time, memory utilization, bandwidth utilization, and resource utilization	(i) The author does not consider energy consumption and is required to prove the efficiency of the proposed algorithm with real-time workflows	CloudSim
2	Dubey and Sharma 2021) [14]	Hybrid AC-PSO algorithm and task scheduling	Makespan rate, cost, and resource utilization rate	(i) The author does not define the fitness function for energy (ii) The work does not consider the parameters of energy consumption, throughput, and schedule length (iii) Need to improve the time complexity	CloudSim
3	Dubey and Sharma (2021) [15]	Hybrid CR-PSO algorithm	Makespan rate, cost, execution time, and energy consumption	(i) Author required plan scheduling for dependent tasks and needed to verify the effectiveness of proposed work on parameters such as energy consumption, load balancing, task rejection ratio, and turnaround time	CloudSim
4	Prem Jacob and Pradeep (2019) [20]	CPSO	Deadline, makespan time, and cost	(i) Required to consider various other QoS service parameters and energy consumption	CloudSim
5	Khan and Santhosh (2021) [24]	PSGWO	Makespan time and execution time Waiting time, energy efficiency, and resource utilization	(i) Required to apply this technique for various applications	NetBeans
6	Kumar and Sharma (2018) [25]	PSO-COGENT	Execution time, execution cost, makespan time, energy consumption, throughput, and task rejection ratio	(i) Required to consider various SLA and QoS parameters for verifying the algorithm's effectiveness (ii) need to test for various workflows in the cloud	CloudSim
7	Velliangiri et al. (2021) [26]	HESGA	Makespan time, cost, and response time	(i) Required to apply this approach with other applications such as agriculture and so on (ii) Need to consider various parameters such as energy consumption, load balancing, QoS, and so on	CloudSim
8	Gokuldhev and Singaravel (2020) [27]	LPMSA	Makespan time and energy consumption	(i) The proposed technique is required to test with real-time application and needs to consider various parameters and is still required to enhance the algorithm	CloudSim with Java
9	Gokuldhev and Singaravel (2020) [28]	LPGWO	Makespan time and energy consumption	(i) This work needs scheduling in low and high machine heterogeneity was enhanced and consider various QoS metrics is required	CloudSim with Java
10	Dubey et al. (2018) [29]	HEFT	Makespan time and load balancing	(i) The proposed method is required to consider various QoS parameters and need test its effectiveness	CloudSim

TABLE 1: Continued.

S. no.	Author and year	Methodology	Parameters	Limitations	Tool
11	Ragmani et al. (2020) [33]	FACO (ACO and fuzzy logic)	Total processing time, response time, cost, and load balancing index	The proposed approach needs to be evaluated within a real and multicloud computing architecture and required considering various parameters such as energy consumption	CloudSim
12	Bhasker and Murali (2022)	The proposed method (HES-ACO)	Total execution time, execution cost, makespan time, energy consumption, throughput, task rejection ratio, resource utilization, and deadline constraint	The proposed approach extends this work further to consider security issues while users access the cloud's information	CloudSim

desired tasks to virtual machines and determining the best schedule sequence is a complex problem in the cloud. The most delicate virtual machine in the cloud must be used to process the user's task request. Under deadline limitations, this efficient strategy can reduce energy consumption, costs, resource utilization, execution time, makespan, throughput, and response time parameters. This study attempts to provide an efficient solution for processing applications depending on user demand and priority (time, energy, cost, and deadline) while concurrently improving the QoS level.

Consider the k number of tasks and the p number of computational resources that can be used to handle the task requests in the cloud data center's virtual machines. Based on their demands, service providers choose the best resources for end customers. The following are the definitions for the task set, resource set, and virtual machine set:

$$T = \{T_1, T_2, T_3 \ldots \ldots T_K\}, \tag{1}$$

$$R = \{R_1, R_2, R_3, R_4 \ldots \ldots R_m\}, \tag{2}$$

$$V_m = \{V_{m1}, V_{m2}, V_{m3}, V_{m4} \ldots V_{mq}\}. \tag{3}$$

Every task T_a is defined as follows:

$$T_a = \{T_{id}, TL_i, D_i\}, \tag{4}$$

where the task identification number is denoted as T_{id}, MIPS length of the task is denoted as TL_i, and D_i is represented as deadline constraints associated with each task.

Similarly, each Vm_q is also characterized as follows:

$$Vm_q = \{Vm_{type}, Vm_{MIPS}, Vm_{speed}, Vm_{storage}, Vm_{id}\}, \tag{5}$$

where *MIPS* signifies the virtual machine computational power. The cloud type is denoted by Vm_{type} to which the Vm belongs and is expressed in integer ranges. Virtual machine identification number is represented as Vm_{id}. Vm_{speed} is the virtual machine's processing speed, while $Vm_{storage}$ is each virtual machine's storage capacity in the cloud data center [14].

When an application is scheduled at resources (R_m), it has the option of getting the resource right away or waiting until the current application at R_m is defined in the following equation:

$$FTE = \sum_{m=0}^{l} R_m + TEx_{T_k Vm_q}. \tag{6}$$

FTE of task T_i at resource R_m should be less than the deadline of the task request $(\delta(Di))$.

$$FTE \leq \delta(Di). \tag{7}$$

3.1. Objective Function.
The fundamental objective of the suggested approach is to enhance QoS metrics such energy consumption, makespan time, computation cost, execution time, resource utilization, throughput, task rejection ratio, and response time. Users of the cloud also need services that are as inexpensive as possible. As a result, we create a fitness function with the deadline taken into account as a QoS parameter, whose objective is to minimize time, execution cost, and energy usage. The following functions are described by the authors.

3.1.1. Execution Time.
A task's execution time is the length of time it takes the system to finish it.

$$TEx_{T_k Vm_q} = EEx_{T_k Vm_j} + TTime_{T_k Vm_j},$$

$$EEx_{T_k Vm_j} = \frac{TLen_{T_k}}{Vm_{MIPS}},$$

$$TTime_{T_k Vm_j} = \frac{TLen_{T_k}}{Bw_{Vm_j}}, \tag{8}$$

where $TEx_{T_k Vm_q}$ is the total time for processing the T_k task on the Vm_q virtual machines, and it is the total expected time $EEx_{T_k Vm_q}$ of the task T_k on the virtual machine Vm_q and the task transfer time $TTime_{T_k Vm_q}$.

3.1.2. Makespan Time.
When all tasks have been processed or the entire amount of time has passed between the start and conclusion of the tasks, this is referred to as the "makespan time" of a task schedule.

$$\text{Mspan}_{\text{time}} = \max\left\{\sum_{j=1}^{q} EEx_{T_k Vm_j}\right\}. \tag{9}$$

3.1.3. Execution Cost.

The second objevtive functions goal is to reduce the overall execution cost represented as $TExe_{cost}$. While considering the dealine constraints, the Task represented as Tk on a per-hour basis for virtual machines Vmj and cloud resources [25]. The execution cost is defined as follows:

$$TExe_{cost} = ExeC_{T_k Vm_j} * Cost_{Vm_j}, \tag{10}$$

where $ExeC_{T_k Vm_j}$ is the cost for executing the T_k task on the virtual machine Vm_j and $Cost_{Vm_j}$ is the resource cost of Vm_j in the cloud.

3.1.4. Energy Consumption (EC).

Both dynamic and static energy were consumed by each physical machine. We only evaluate active energy consumption in this study since we believe that static energy consumption has a minor impact and can be ignored. The proposed algorithm's third scheduling goal is to reduce carbon emissions by maximizing resource use. The number of Vm instances available determines the quantity of dynamic energy consumed. Equation below shows how much energy a virtual machine uses [15].

$$Vm_j = \begin{cases} \varphi_i \text{ if } Vm_i \text{ is in active state} \\ \omega_j \text{ if } Vm_j \text{ is in idle state} \end{cases}. \tag{11}$$

The following equation computes the energy consumption of all the VMs (active and idle):

$$Ec_{Vm_j} = FTT_j * \varphi + \left(Mspan_{time} - FTT_j\right) * \omega, \tag{12}$$

where $Ec_{\text{actualconsumption}}$ is actual energy consumption is computed by using the following equation:

$$Min\, Ec_{\text{actualconsumption}} = \left(Ec_{\max} - Ec_{\min}\right) * Resu_t + Ec_{\min}, \tag{13}$$

where Ec_{max} indicates resource usage R_m, while Ec_{min} denotes the ideal or minimum resource usage condition.

The total energy consumption of the data center is defined as follows:

$$Ec = \sum_{j=1}^{q} Ec_{Vm_j} + Min\, Ec_{\text{actualconsumption}}. \tag{14}$$

3.1.5. Throughput.

The throughput (ϑ) is evaluated by using the following equation:

$$\text{Throughput}(\vartheta) = \frac{\text{Total number of succesfully completed tasks}}{\text{total processing time}}. \tag{15}$$

3.1.6. Task Rejection Ratio (TR_i).

If the task is not completed within the deadline constraint, it is computed using the following equation:

$$\text{Task Rejection Ratio}(TR_i) = \frac{\text{Number of tasks rejected}}{\text{Total number of tasks}} * 100. \tag{16}$$

3.1.7. Deadline Constraint.

If the total time exceeds the deadline, it is defined as follows:

$$\delta(Di) = \frac{(\text{number of tasks violating the deadline constraint} * 100)}{\text{total number of tasks}}. \tag{17}$$

3.1.8. Fitness Function ft (R_m).

All cloudlets should be handled prior to the deadline in order to meet our objective of reducing the amount of energy required by the specified operation or cloudlet (makespan, cost, time, throughput, and task rejection percentage). The fitness function of the problem of work scheduling with various objectives is defined by the following equation:

$$\text{ft}(Rm) = \alpha * Mspan_{time} + \beta * TExe_{cost} + \gamma * Ec. \tag{18}$$

Subject to

$$\sum_{j=1}^{q} \partial_{ij} = 1, \forall i \in T_i \forall j \in Vm_j. \tag{19}$$

Equation (17) shows that each application has only one resource assigned to it.

$$ft_{i,j} = ft_{i-1,j} \forall i \in T_i \forall j \in Vm_j. \tag{20}$$

Some assumptions and constraints are needed to consider for the tasks submitted in the cloud. α, β, and γ are the weight metrics of makespan $Mspan_{time}$, cost $TExe_{cost}$, and Energy consumption Ec, respectively [15].

4. Hybrid ES-ACO Task Scheduling Algorithm

The dynamic nature of task scheduling makes it difficult to identify the best resource. By taking into account a number of variables, we examine the issue of energy consumption and makespan, which must be reduced, and system performance, which must be optimized, because it directly affects the revenue and scalability of sensor cloud resource suppliers. This section covers the hybrid ES-ACO strategies for finding the ideal task scheduling solution in the sensor cloud environment as well as the sensor cloud model for the task scheduling algorithm. The recommended approach produced a hybrid ES-ACO task scheduling framework by fusing the advantages of ESO and ACO. The suggested hybrid ES-ACO architecture is depicted in Figure 2. The suggested architecture includes several WSNs, and it makes obvious how work scheduling was carried out in the cloud environment.
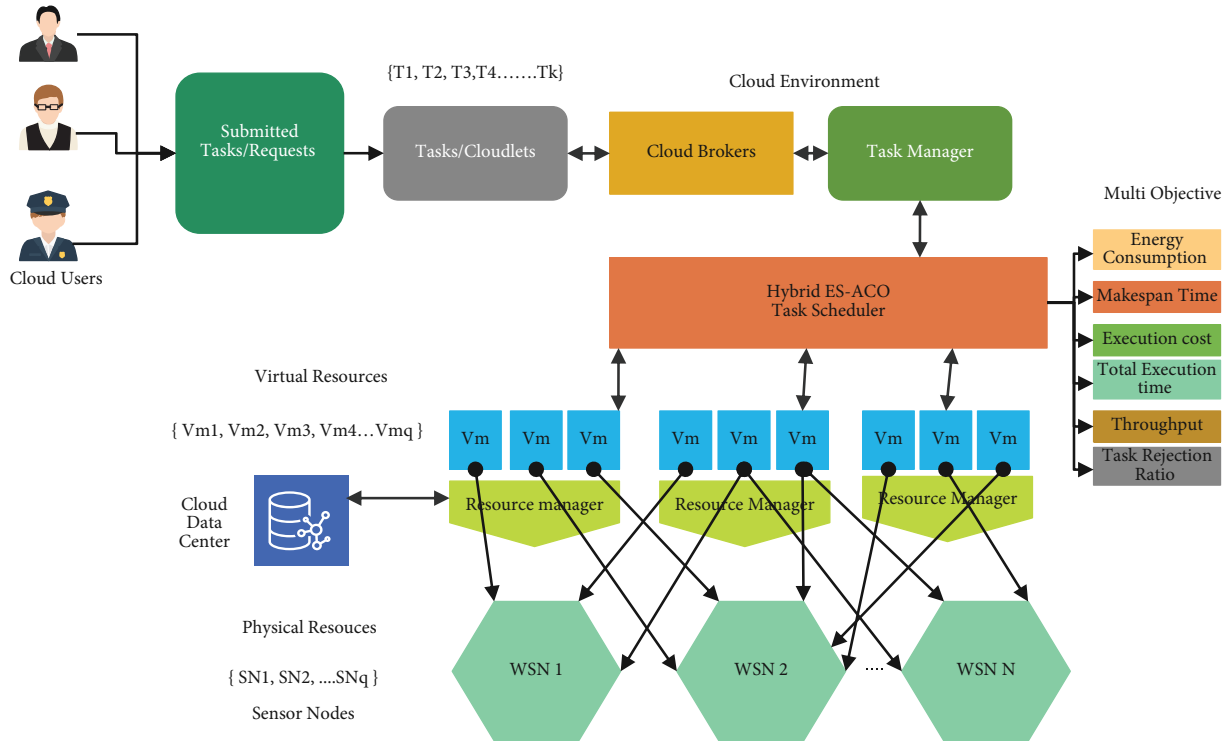
FIGURE 2: Proposed infrastructure model for task scheduling in sensor cloud environment.

4.1. Traditional Electro Search Optimization Algorithm (ESO). The electro search algorithm's domain of potential solutions is comparable to the molecular space in which various atoms are arranged. The electrons of every atom are arranged around its nucleus. To reach the highest energy level of molecular states, the orbits of the electrons that surround the nucleus of each atom gradually alter. It is equivalent to the maximum of the objective function [22].

4.1.1. Overview of the Standard Electro Search Procedure. The electro search algorithm can be divided into the following three phases:

(1) Atom spreading
(2) Orbital transition
(3) Nucleus relocation

4.1.2. Atom Spreading Phase. The possible solutions are distributed at random in this step. Each potential candidate is an atom. They have a nucleus, which the electrons orbit around. The electrons are limited to precise orbits around the nucleus, and when they move between them, a certain amount of energy is either absorbed or released.

4.1.3. Orbital Transition Phase. The electrons around each nucleus expand their orbits during this phase in an effort to reach orbits with greater energies. The idea of quantized energy levels in a hydrogen atom served as inspiration for this orbital transition.

4.1.4. Nucleus Relocation Phase. The energy of a photon that is emitted during this phase, which is determined by the energy level difference between the two atoms, is used to determine the position of the new nucleus.

4.1.5. Traditional Ant Colony Optimization (ACO). Traditional ACO is a metaheuristic technique created by Italian researchers based on the foraging behavior of ant colonies [14]. When ants seek for food away from their nests and colonies, they leave a trail of pheromones in their wake. The likelihood of discovering the quickest route from the food source to the ant colonies was influenced by the density of pheromones. Once the food source is located, each ant travels in that direction using the quickest route and highest pheromone concentration. The shortest path is discovered using the ACO techniques in the subsequent steps.

Step 1: Set the number of ant colonies and iterations

Step 2: Set the beginning point at random

Step 3: Each node chooses a direction based on pheromone concentrations

Step 4: Then add the traverse path to the list

Step 5: Update the pheromones after each iteration

Step 6: Reiterate till the halting criteria are not reached

4.2. Hybrid ES-ACO Algorithm. Both evolutionary computational techniques and metaheuristic approaches are based on nucleus instincts and quickly produce an ideal

solution. ACO and ES are two terms that are used interchangeably.

The HES-PSO work scheduling method combines electro search with ant colony optimization. The hybrid ES-ACO strategy reduces makespan time, minimizes energy consumption, reduces computing cost, increases resource utilization, reduces execution time, reduces task rejection ratio, reduces throughput, and improves reaction time. Both approaches were used to quickly find an optimal solution with reduced time complexity.

To develop a metaheuristic method, the electro search (ES) algorithm with ant colony optimization (ACO) is employed. The three stages of the optimization of the electro-search method are spreading atom phase, orbital transition phase, and nucleus relocation phase.

This modification of the conventional electro search (ESO) is a first by incorporating the ACO to raise the standard of the ideal answer [26]. The recommended approach is broken down into the following four steps:

(1) Initialization
(2) Spreading of atoms
(3) Transition of orbital
(4) Relocation of nucleus

Tasks ($T1$, $T2$, $T3$, $T4$,..., Tk) and resources ($Vm1$, $Vm2$, $Vm3$, $Vm4$,..., Vmq) are dispersed throughout the cloud datacenter in the first phase. The second phase designates the atoms as the tasks, that is, the cloud permits the release of the nucleus agent, which stores the locations and details of the virtual machines.

The state diagrams of atom spreading, orbital alteration, and nucleus relocation are shown in Figures 3–5. Similar to atoms, these agents are dispersed throughout the search space. This stage involves randomly dispersing the competitor configurations throughout the research area. Each user interacts with an iota, which is made up of an orbiting core and electrons. According to Velliangiri et al. [26], the electrons are confined to particular rings that encircle the core and can only move between them while emitting or maintaining particular levels of liveliness. The atoms scour the search space in quest of the best answer. The current and previous resource information will be stored in the third space, and each agent will follow atom around the resource pool, or virtual machine, to choose the best one. Following the best virtual machines, the atoms choose the optimal solution in the last step using the data stored in the agent. The jobs are consequently delegated to virtual machines.

This study introduces the ES-ACO algorithm, a multi-objective task scheduling system that combines the benefits of both traditional electro search and the ant colony optimization method. Schedule the work to a virtual machine in an inefficient manner, which reduces makespan time, minimizes energy consumption, decreases computation cost, increases resource use, decreases execution time, decreases task rejection ratio, increases throughput, and improves reaction time. When comparing HES-ACO methods to ES methods, PSO methods, GA methods, ACO methods, HESGA methods, and AC-PSO methods, the HES-ACO
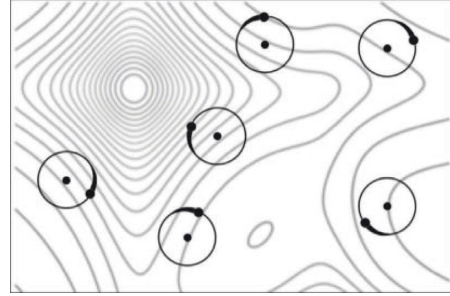
FIGURE 3: State diagram of atom spreading.
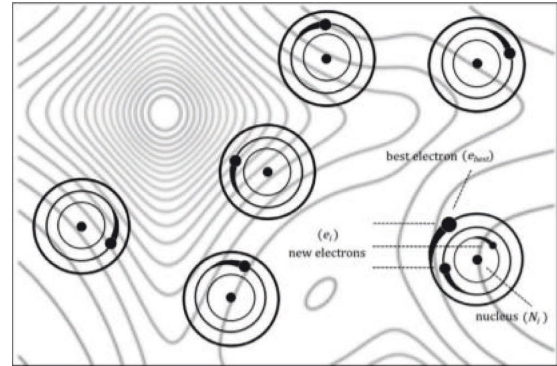
FIGURE 4: State diagram of orbital transition.
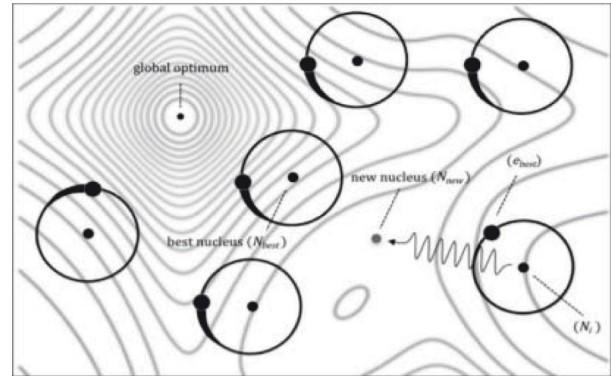
FIGURE 5: State diagram of nucleus relocation.

methods record a significantly higher space utilization. Algorithm 1 describes about hybrid ES-ACO task scheduling approach.

Figure 6 shows the flow diagram of proposed hybrid ES-ACO technique for task scheduling in sensor cloud environment.

4.2.1. Selection of Parameters

(1) Number of Particles (h). The number of particles in the underlying population, such as the needed calculation

Input 1: Set of subtasks, that is, $T_1, T_2, T_3, T_4, \ldots, T_k$. 2. Set of virtual machines, that is, $Vm_1, Vm_2, Vm_3, Vm_4, \ldots, Vm_q$
Output: Mapping of the tasks to set the Vms (optimal schedule)
Step 1: Initialize the set of ant colonies
Step 2: Set the parameters of ACO
Step 3: Initialize the set of subtasks, that is, $T_1, T_2, T_3, T_4, \ldots, T_k$
Step 4: Initialize the set of virtual machines, that is, $Vm_1, Vm_2, Vm_3, Vm_4, \ldots, Vm_q$
Step 5: Compute pheromone value $\rho_{i,j}(0) = (c/TEx_{T_k Vm_q})$
Step 6: Submit the Vm list, which was created successfully in the data center, and set of tasks to the cloud broker
Step 7: For 1 to Q do( )
Step 8:   Generate nucleus $Q[i]$
Step 9:   Initialize nucleus agent randomly
Step 10: End for
Step 12: $Rm = 0$
Step 13: Define the fitness function ft (Rm)
Step 14: $\mathrm{ft}(Rm) = \alpha * Mspan_{time} + \beta * TExe_{cost} + \gamma * Ec$
Step 15: Compute G_{best} and P_{best}
Step 16: While (Max iterations X) // $\forall i \in T_i$ & $\forall j \in Vm_j$
Step 17:   Update the pheromone, that is, monitor the status of resources using the following equation
Step 18: $\partial_{i,j}(t+1) = (1-\theta) * \partial_{i,j}(t) + \sum_{b=1}^{\sigma} \partial_{i,j}^{\sigma}(t)$
Step 19: $\partial_{i,j}^{\sigma}(t) = \begin{cases} (\varepsilon/L_n)\sigma \text{th passes on the each nucleus} \\ 0, \text{else the growth of aunt } 0 \end{cases}$
Step 20: $i = 0$
Step 21:   Compute the fitness value for each nucleus of $Q[i]$
Step 22: $G_{best} = $ best nucleus of $Q[i]$
Step 23: $i{++}$
Step 24:   for $a = 1$ to Q
Step 25: $P_{best}[a] = Q[i]$
Step 26:   End for
Step 27: End while
Step 28: Return the global best solution of atom

ALGORITHM 1: Hybrid ES-ACO task scheduling algorithm.

emphasis, work assessment, accomplishment rate, and so on, typically raises the thoroughness of the chase space inspection in an arbitrary hunt approach. Meanwhile, as we will see in the following section, increasing the number of molecules decreases the number of calculation cycles needed to fulfill the goal, hence boosting the achievement rate. Regardless of how significant the aforementioned criterion may be, the quantity of capacity assessments is viewed as the fundamental execution regulation for applications. Fewer molecules in a population result in a lower success rate and more cycles. A huge population, on the other hand, increases the achievement rate and requires an excessive number of capacity evaluations.

(2) The span of Orbital (a). Electrons in each core might be able to move to larger rings. The orbital distance is the size of the greatest possible circle. Because of the electrons that orbit each nucleus, it is now feasible to shift the emphasis to any location. The migration removes (and consequently the orbital range of every core) change during the course of the cycles as the particle travels closer to the ideal place. As the orbital sweep is dynamically compressed, the transition region for electrons shrinks. This decrease permits the computation to merge toward the target by constraining

electron movement in the vicinity of the hypothetical global ideal point.

(3) Number of Electrons (e). Electro Search's electrons around each core represent the randomness of scientific exploration into the cosmos. An increase in the merging rate is seen when arbitrary electrons in each focus are far off from one another. This method avoids hastily joining imperfect focal points together. Even when the underlying molecules are less than ideal, this method makes space exploration more efficient. It improves the inquiry space investigation, especially when the underlying molecules are far from ideal. Furthermore, the iterative procedure's modest compression of orbital sweep bounds the territory is taken into account orbital movement, preventing additional arbitrary electrons from being placed far from the core

(4) Convergence Criteria. Population mixing owing to emphasis is taken into account using stopping criteria in transformative calculations. When the total number of people living in the applicant setups reaches a "stale" number, the analysis is done. Different end criteria were utilized in the development writing, such as reaching the maximum number of cycles, arriving at a desirable
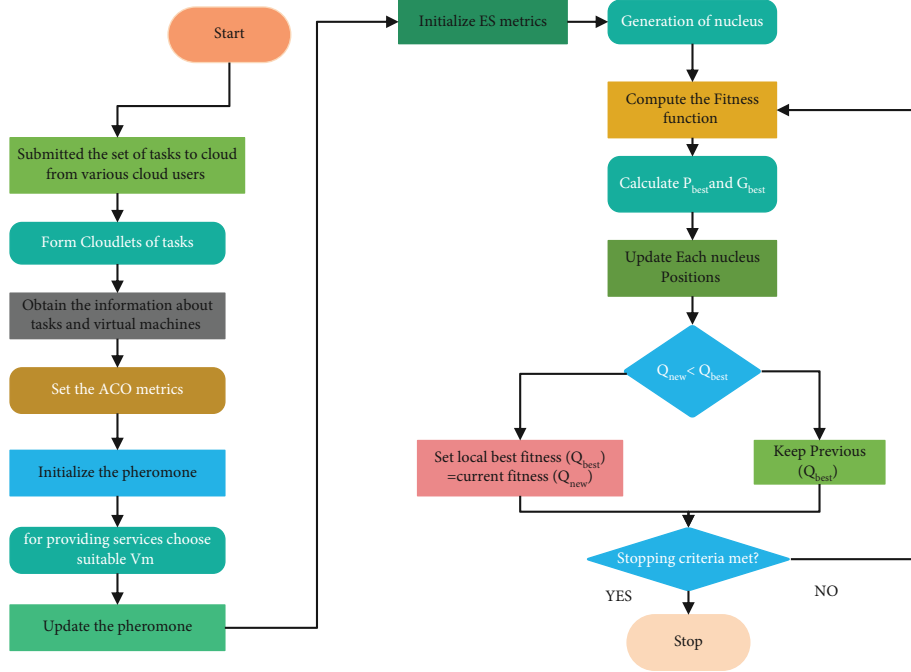
Figure 6: The flow chart of the proposed hybrid ES-ACO.
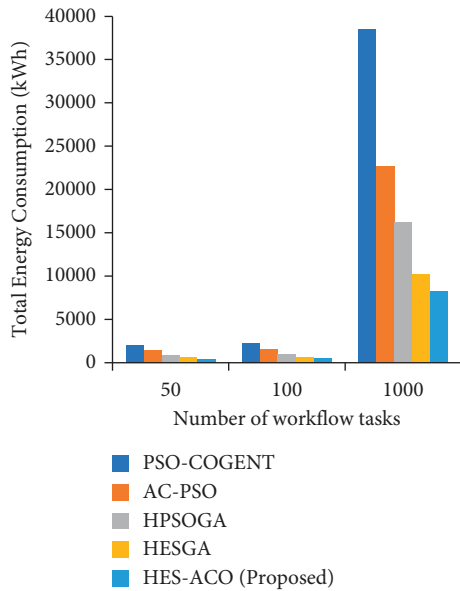
Figure 7: Energy consumption.
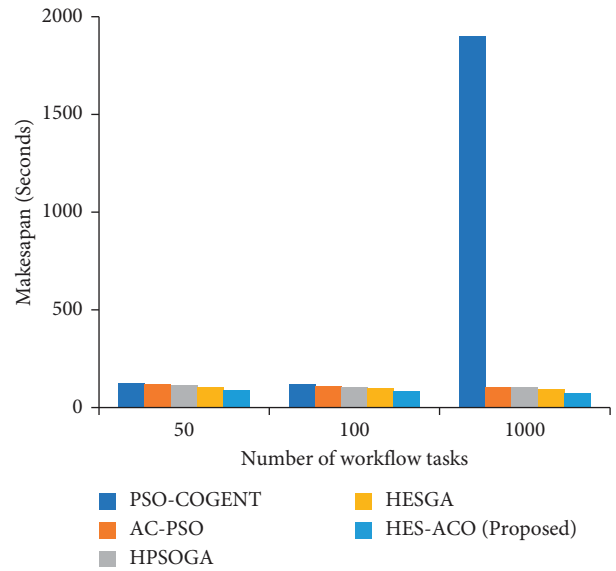
Figure 8: Makespan time.

arrangement, and so on. For the purpose of the electro search calculation, the highest number of cycles served as the ending rule [26].

5. Experimental Result and Discussion

The developed hybrid electro search with ant colony optimization (HES-ACO) task scheduling algorithm was compared to the HESGA, HPSOGA, AC-PSO, PSO-COGENT, and the proposed algorithm in a comparative analysis (HES-ACO). Energy consumption, execution cost, total execution time, throughput, makespan time, task rejection ratio, response time, and resource usage are all used to evaluate the proposed model HES-ACO performance.

5.1. Simulation and Results Analysis. Task scheduling experiments are described here so that their results can be analyzed. To ensure that the suggested scheduling paradigm works well in a cloud setting, we use the CloudSim simulator to replicate the environment. When it comes to simulating the infrastructure as a service (IaaS) cloud, the CloudSim simulator is a useful framework. In order to carry out the
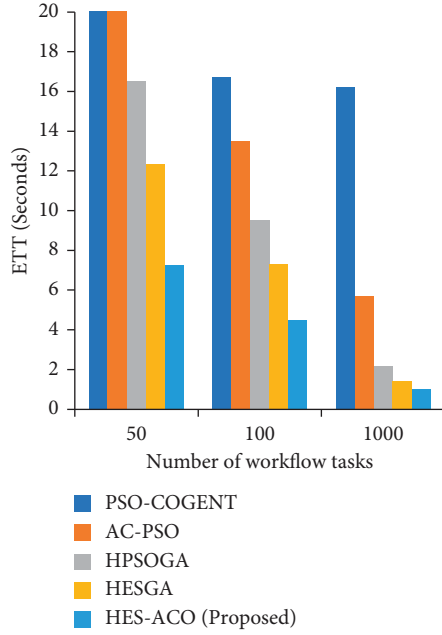
Figure 9: Execution time.

Figure 10: Throughput.

scientific workflow sustainably, new algorithms are implemented (including task scheduling, VM deployment, energy model, etc.). The efficacy of the HES-ACO algorithm is measured in an empirical fashion.

5.1.1. Simulation Parameters

(i) Two distinct hosts are used, the HP ProLiant ML110 G5 and the HP ProLiant ML110 G4 [37], which use 135 W/s and 117 W/s of power, respectively.

(ii) 2.3 W Energy consumption rate is consider to transfer 1 GB data.

(iii) Four VMs with different CPU (in MIPS) and RAM (in MB) capacities are installed. On an average VM start-up time is 96.9 s. Around 2,500 MIPS with 870 MB RAM, 52,000 MIPS with 1740 MB, 1,000 MIPS with 1740 MB RAM, and 500 MIPS with 613 MB RAM run the scientific procedure. Based on the workflow requirements, the VMs are deployed/undeployed dynamically.

(iv) Amazon Web Services offers 20 MBPS as average VM bandwidth.

5.2. Performance Metric and Simulation Parameters

Energy consumption: Total energy consumed by the servers to execute scientific workflows is computed using equation (13).

Makespan or total execution time: It is the total time to execute the workflow from entry tasks to the exit task. Equation (11) is used to calculate the makespan.

Execution time (ETT): Average execution time per task is calculated by equations (8)–(10).
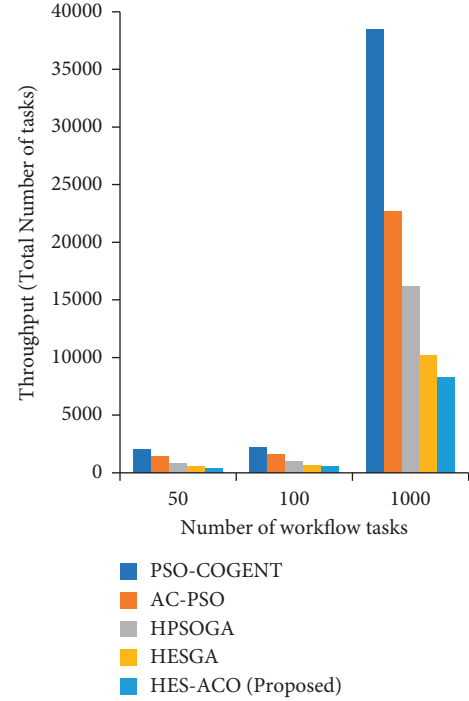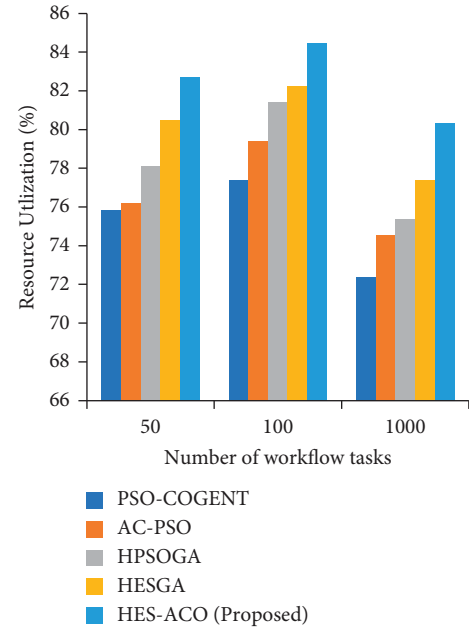
Figure 11: Resource utilization.

Throughput: It is evaluated by division of number tasks successfully executed and total number of tasks. It is calculated by using equation (17).

Execution cost: It is calculated by using equation (12).

pAverage RU: It is the ratio of allocated computing resources (such as CPU in MIPS) to execute the scientific workflow tasks and total computing resources of the server.
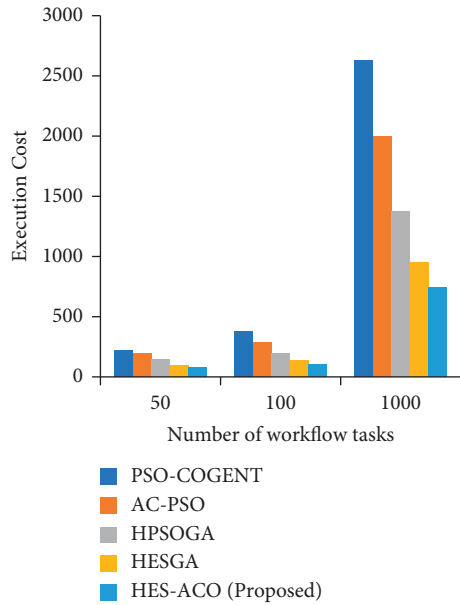
Figure 12: Execution cost for tasks.

Figure 7 clearly shows that proposed mechanism HES-ACO method outperformed existing methods such as AC-PSO, HPSOGA, and HESGA for energy consumption versus number of tasks workflow.

Figure 8 clearly show that proposed mechanism HES-ACO method outperformed existing methods such as AC-PSO, HPSOGA, and HESGA for makespan time versus number of tasks workflow.

Figure 9 clearly shows that proposed mechanism HES-ACO method outperformed existing methods such as AC-PSO, HPSOGA, and HESGA for execution time versus number of tasks workflow.

Figure 10 clearly shows that proposed mechanism HES-ACO method outperformed existing methods such as AC-PSO, HPSOGA, and HESGA for throughput versus number of tasks workflow.

Figure 11 clearly shows that proposed mechanism HES-ACO method outperformed existing methods such as AC-PSO, HPSOGA, and HESGA for resource utilization versus number of tasks workflow.

Figure 12 clearly shows that proposed mechanism HES-ACO method outperformed than existing methods such as AC-PSO, HPSOGA, and HESGA for execution cost versus number of tasks workflow.

6. Conclusion

There are not many task scheduling techniques for sensor clouds; hence, in this work, we mainly focus on user and cloud interaction. This study took into account a number of factors at once, including execution time, execution cost, throughput, energy use, makespan time, resource utilization, and deadline constraint parameters. In this essay, we have spoken about how customers' high processing needs are causing a daily increase in the number of cloud servers. Nevertheless, these servers use a lot of electricity. Both

sensor and cloud settings have significant issues with energy consumption. As a result, energy-efficient job scheduling is crucial for reducing energy use and improving the other variables. A hybrid electro search with ant colony optimization (HES-ACO) strategy is suggested in this research. Tasks are inefficiently scheduled using the proposed HES-ACO approach at virtual machine resources (V_m). It utilizes a fitness function to optimize the parameters (execution time, execution cost, throughput, reaction time, and energy consumption) while taking the task deadline into account as a quality-of-service parameter. The proposed method efficiently increases resource usage while minimizing energy consumption, cost, make-span time, execution time, throughput, and task rejection ratio when compared to HESGA, HPSOGA, AC-PSO, and PSO-COGENT algorithms. The created algorithm can be applied in the future to various SLA, QoS, and security criteria that are also taken into consideration for further research.

Data Availability

The data used to support the findings of this study are available from the corresponding author upon request.

Conflicts of Interest

The authors declare that they have no conflicts of interest.

References

[1] L. Hamami and B. Nassereddine, "Application of wireless sensor networks in the field of irrigation: a review," *Computers and Electronics in Agriculture*, vol. 179, p. 105782, 2020.

[2] A. Bhoi, R. P. Nayak, S. K. Bhoi et al., "IoT-IIRS: internet of Things based intelligent-irrigation recommendation system using machine learning approach for efficient water usage," *PeerJ Computer Science*, vol. 7, pp. 5788–e615, 2021.

[3] M. Zhang and S. Xiong, "Sensor-cloud based precision sprinkler irrigation management system," in *CWSN 2019*, C. S. Guo, Ed., Springer Nature Singapore Pte Ltd, 2019.

[4] T. Ojha, S. Misra, and N. S. Raghuwanshi, "Sensing-cloud: leveraging the benefits for agricultural applications," *Computers and Electronics in Agriculture*, vol. 135, pp. 96–107, 2017.

[5] R. Dalvi and S. K. Madria, "Energy-efficient scheduling of fine-granularity tasks in a sensor cloud," *Lecture Notes in Computer Science*, vol. 9050, pp. 498–513, 2015.

[6] M. T. Rahman, T. F. Shuva, and R. T. Khan, "Efficient sensor-cloud communication using data classification and compression," *International Journal of Information Technology and Computer Science*, vol. 9, no. 6, pp. 9–17, 2017.

[7] D. H. Phan, J. Suzuki, S. Omura, and K. Oba, "Toward sensor-cloud integration as a service: optimizing three-tier communication in cloud-integrated sensor networks," *Proceedings of the th International Conference on Body Area Networks*, vol. 1, pp. 355–362, 2013.

[8] K. Das, S. Das, R. K. Darji, and A. Mishra, *Review Article Survey of Energy-Efficient Techniques for the Cloud-Integrated Sensor Network*, Springer, America, 2018.

[9] T. Ojha, S. Bera, S. Misra, and N. S. Raghuwanshi, "Dynamic duty scheduling for green sensor-cloud applications," in *Proceedings of the International Conference on Cloud*

Computing Technology and Science, pp. 841–846, CloudCom, 2015-February.

[10] S. Sivakumar and A. Al-anbuky, "Dense clustered multi-channel wireless sensor cloud," *Journal of Sensor and Actuator Networks*, vol. 4, no. 3, pp. 208–225, 2015.

[11] S. Chatterjee, S. Sarkar, and S. Misra, *Energy-Efficient Data Transmission in Sensor-Cloud*, pp. 1–6, IEEE, China, 2015.

[12] T. Dinh and Y. Kim, "An efficient sensor-cloud interactive model for on-demand latency requirement guarantee," *IEEE International Conference on Communications*, vol. 6, pp. 1–6, 2017.

[13] G. Sreenivasulu and I. Paramasivam, "Hybrid optimization algorithm for task scheduling and virtual machine allocation in cloud computing," *Evolutionary Intelligence*, vol. 14, no. 2, pp. 1015–1022, 2021.

[14] K. Dubey and S. C. Sharma, "A hybrid multi-faceted task scheduling algorithm for the cloud computing environment," *International Journal of Systems Assurance Engineering and Management*, vol. 32, p. 56845, 2021.

[15] K. Dubey and S. C. Sharma, "A novel multi-objective CR-PSO task scheduling algorithm with deadline constraint in cloud computing," *Sustainable Computing: Informatics and Systems*, vol. 32, p. 100605, 2021.

[16] T. S. Proshikshya Mukherjee, *Issues Of Some Task Scheduling Strategies On Sensor Cloud Environment (Smart Inte)*, Springer Nature, Singapore, 2020.

[17] R. K. Jena, "Multi-objective task scheduling in cloud environment using nested PSO framework," *Procedia Computer Science*, vol. 57, pp. 1219–1227, 2015.

[18] S. Swagatika, A. K. Rath, and P. K. Pattnaik, "Markov chain model and PSO technique for dynamic heuristic resource scheduling for system-level optimization of cloud resources," *ARPN Journal of Engineering and Applied Sciences*, vol. 13, no. 3, pp. 1042–1052, 2018.

[19] S. C. Nayak, S. Parida, C. Tripathy, and P. K. Pattnaik, "An enhanced deadline constraint-based task scheduling mechanism for cloud environment," *Journal of King Saud University - Computer and Information Sciences*, vol. 832, 2018.

[20] T. Prem Jacob and K. Pradeep, "A multi-objective optimal task scheduling in cloud environment using cuckoo particle swarm optimization," *Wireless Personal Communications*, vol. 109, no. 1, pp. 315–331, 2019.

[21] X. Huang, C. Li, H. Chen, and D. An, "Task scheduling in cloud computing using particle swarm optimization with time-varying inertia weight strategies," *Cluster Computing*, vol. 23, no. 2, pp. 1137–1147, 2020.

[22] A. Tabari and A. Ahmad, "A new optimization method: electro-Search algorithm," *Computers & Chemical Engineering*, vol. 103, pp. 1–11, 2017.

[23] M. Bansal and S. K. Malik, "A multi-faceted optimization scheduling framework based on the particle swarm optimization algorithm in cloud computing," *Sustainable Computing: Informatics and Systems*, vol. 28, p. 100429, 2020.

[24] M. S. A. Khan and R. Santhosh, "Task scheduling in cloud computing using hybrid optimization algorithm," *Soft Computing*, vol. 5, p. 457, 2021.

[25] M. Kumar and S. C. Sharma, "PSO-COGENT: cost and energy efficient scheduling in cloud environment with deadline constraint," *Sustainable Computing: Informatics and Systems*, vol. 19, no. January, pp. 147–164, 2018.

[26] S. Velliangiri, P. Karthikeyan, V. M. Arul Xavier, and D. Baswaraj, "Hybrid electro search with genetic algorithm for task scheduling in cloud computing," *Ain Shams Engineering Journal*, vol. 12, no. 1, pp. 631–639, 2021.

[27] M. Gokuldhev and G. Singaravel, "Local pollination-based moth search algorithm for task-scheduling heterogeneous cloud environment," *The Computer Journal*, vol. 65, no. 2, pp. 382–395, 2020.

[28] M. Gokuldhev, G. Singaravel, and N. R. Ram Mohan, "Multi-objective local pollination-based Gray Wolf optimizer for task scheduling heterogeneous cloud environment," *Journal of Circuits, Systems, and Computers*, vol. 29, no. 07, pp. 2050100–2050124, 2020.

[29] K. Dubey, M. Kumar, and S. C. Sharma, "Modified HEFT algorithm for task scheduling in cloud environment," *Procedia Computer Science*, vol. 125, pp. 725–732, 2018.

[30] Y. J. Moon, H. C. Yu, J. M. Gil, and J. B. Lim, "A slave ants-based ant colony optimization algorithm for task scheduling in cloud computing environments," *Human-Centric Computing and Information Sciences*, vol. 7, no. 1, p. 28, 2017.

[31] W. Deng, J. Xu, and H. Zhao, "An improved ant colony optimization algorithm based on hybrid strategies for scheduling problem," *IEEE Access*, vol. 7, pp. 20281–20292, 2019.

[32] Y. Su, Z. Bai, and D. Xie, "The optimizing resource allocation and task scheduling based on cloud computing and Ant Colony Optimization Algorithm," *Journal of Ambient Intelligence and Humanized Computing*, vol. 12, p. 0123456789, 2021.

[33] A. Ragmani, A. Elomri, N. Abghour, K. Moussaid, and M. Rida, "FACO: a hybrid fuzzy ant colony optimization algorithm for virtual machine scheduling in high-performance cloud computing," *Journal of Ambient Intelligence and Humanized Computing*, vol. 11, no. 10, pp. 3975–3987, 2020.

[34] P. K. Reddy Maddikunta, S. Hakak, M. Alazab et al., "Unmanned aerial vehicles in smart agriculture: applications, requirements, and challenges," *IEEE Sensors Journal*, vol. 21, no. 16, pp. 17608–17619, 2021.

[35] R. Kumar, P. Kumar, R. Tripathi, G. P. Gupta, T. R. Gadekallu, and G. Srivastava, "Sp2f: a secured privacy-preserving framework for smart agricultural unmanned aerial vehicles," *Computer Networks*, vol. 187, p. 107819, 2021.

[36] N. Deepa, M. Z. Khan, B. Prabadevi, D. R. Vincent Pm, P. K. R. Maddikunta, and T. R. Gadekallu, "Multiclass model for agriculture development using multivariate statistical method," *IEEE Access*, vol. 8, pp. 183749–183758, 2020.

[37] L. Abualigah and A. Diabat, "A novel hybrid antlion optimization algorithm for multi-objective task scheduling problems in cloud computing environments," *Cluster Computing*, vol. 24, no. 1, pp. 205–223, 2021.

[38] J. Praveenchandar and A. Tamilarasi, "Retracted article: dynamic resource allocation with optimized task scheduling and improved power management in cloud computing," *Journal of Ambient Intelligence and Humanized Computing*, vol. 12, no. 3, pp. 4147–4159, 2021.

[39] P. K. Bal, S. K. Mohapatra, T. K. Das, K. Srinivasan, and Y. C. Hu, "A joint resource allocation, security with efficient task scheduling in cloud computing using hybrid machine learning techniques," *Sensors*, vol. 22, no. 3, p. 1242, 2022.

WILEY | Hindawi

Research Article

Keyword Extraction for Medium-Sized Documents Using Corpus-Based Contextual Semantic Smoothing

Osama A. Khan [ID],[1] **Shaukat Wasi** [ID],[1] **Muhammad Shoaib Siddiqui** [ID],[2] **and Asim Karim** [ID][3]

[1]*Department of Computer Science, Mohammad Ali Jinnah University (MAJU), Karachi 75400, Pakistan*
[2]*Faculty of Computer and Information Systems, Islamic University of Madinah, Madinah 42351, Saudi Arabia*
[3]*Department of Computer Science, Lahore University of Management Sciences (LUMS), Lahore 54792, Pakistan*

Correspondence should be addressed to Osama A. Khan; osamaahmedkhan@hotmail.com

Keyword extraction refers to the process of selecting most significant, relevant, and descriptive terms as keywords, which are present inside a single document. Keyword extraction has major applications in the information retrieval domain, such as analysis, summarization, indexing, and search, of documents. In this paper, we present a novel supervised technique for extraction of keywords from medium-sized documents, namely Corpus-based Contextual Semantic Smoothing (CCSS). CCSS extends the concept of Contextual Semantic Smoothing (CSS), which considers term usage patterns in similar texts to improve term relevance information. We introduce four more features beyond CSS as our novel contributions in this work. We systematically compare the performance of CCSS with other techniques, when implemented over INSPEC dataset, where CCSS outperforms all state-of-the-art keyphrase extraction techniques presented in the literature.

1. Introduction

Keyword extraction can be defined as the process of selecting most significant, relevant, and descriptive terms as keywords, which are present inside a single document, where "terms" refer to distinct n-grams of any size. Keywords represent distinguished and specialized concepts and are bound to convey the informational content load of a document. Keyword extraction has major applications in the information retrieval domain, such as summarization [1, 2], indexing [3], search [4], tagging [5, 6], contextual advertising [7, 8], and personalized recommendation [9].

Documents can generally be classified into long-, medium-, and short-sized documents, where webpages, news articles, and research papers represent long-sized documents, research papers' abstracts, emails, and question-and-answer conversations characterize medium-sized documents, while microposts and Short Message Service (SMS) denote short-sized documents. Each type of document possesses unique characteristics and challenges that need to

be dealt with before any keyword extraction technique can be successfully applied on it. Long-sized documents comprise large vocabulary, medium-sized documents include lack of context, while short-sized documents contain challenges related to low signal-to-noise ratio, extensive preprocessing, and multivaried text composition [10].

Replacing author-assigned keywords in research papers' abstracts, topic identification of emails, and topic recommendation for question-and-answer conversations are a few significant applications of keyword extraction from medium-sized documents in the real world.

A research paper abstract can provide a user the summary of the respective research article, in absence of his/her access to the latter. Hence, keywords extracted from research abstracts would represent the ones extracted from respective research articles. Also, research papers contain keywords that are manually tagged by respective authors. Manually tagged keywords contain bias that helps respective research papers to appear in top results, when searched by users utilizing those index terms. This can be observed by looking

at examples of ACM (https://www.acm.org/) and IEEE (https://www.ieee.org/), both of which are leading research organizations in the domains of Computer Science and Engineering, respectively, and hence possess a majority of authors in these domains, when considered together. For ACM, authors need to provide Computing Classification System (CCS) (https://dl.acm.org/ccs) Concepts that are defined by ACM, but also keywords that are defined by authors. For IEEE, authors need to provide their own defined keywords as index terms. Upon automatic selection, keywords or index terms should exclude associated bias in the search process upto a certain level, e.g., in terms of $F-$measure (see Section 4.2).

Keyword extraction has been performed in the literature on all types of documents (long-sized [11], medium-sized [12], and short-sized [13]), while utilizing various techniques. Keyword extraction techniques developed so far have been either supervised [14] or unsupervised [15]. Unsupervised techniques can be used on multiple document collections without the need for costly and time-consuming prior labeling. On the other hand, supervised techniques although require periodic training from human-labeled document collections, they still can be more accurate [16, 17].

In this paper, we present a novel supervised technique for extraction of keywords from medium-sized documents, namely Corpus-based Contextual Semantic Smoothing (CCSS). CCSS extends the concept of Contextual Semantic Smoothing (CSS) [10], which considers term usage patterns in similar texts to improve term relevance information for short-sized documents. In fact, CSS performs smoothing of the TFIDF matrix using a semantic feature, namely Phi coefficient, while keeping the corpus context into consideration. We introduce four more features beyond CSS as our novel contributions in this work in order to handle further challenges associated with medium-sized documents.

2. Related Work

PageRank is a graph-based unsupervised language-independent ranking algorithm, presented by Page et al. [18], which uses link information to iteratively assign global importance scores to webpages. PageRank is based upon the principle: "A vertex is important if there are other important vertices pointing to it," which can be regarded as voting or recommendation among vertices. In PageRank for keyword extraction, the ranking score of a candidate keyword is computed by summing up the ranking scores of all unigrams within the keyword [19–21]. Then, candidate keywords are ranked in descending order of ranking scores, and the top N candidates are selected as keywords.

Various methods have been proposed in the literature to infer latent topics of words and documents. These methods are known as latent topic models that derive latent topics from a large-scale document collection according to word occurrence information. Latent Dirichlet allocation (LDA), developed by Blei et al. [22] is a generative statistical model that allows sets of observations to be explained by

unobserved groups that explain why some parts of the data are similar. It is representative of the latent topic models, embeds supervised learning, has more feasibility for inference, and can reduce the risk of overfitting.

Topical PageRank (TPR), proposed by Liu et al. [23], is based upon PageRank [18], which measures the importance of a word with respect to different topics. Given the topic distribution of a document, ranking scores of words are calculated with respect to those topics, and top ranked words for each topic are extracted as its keywords, thus resulting in a good coverage of the document's major topics. TPR combines the advantages of both LDA and TFIDF/PageRank, by utilizing both external topic information (like LDA) and internal document structure (like TFIDF/PageRank).

Liu et al. [24] devised an unsupervised technique for keyword extraction, which first finds exemplar terms in a document by leveraging, clustering, and semantic relatedness, which guarantees the document to be semantically covered by these exemplar terms (centroids of clusters). Then, keywords are extracted from the document using these exemplar terms. The technique incorporates term cooccurrence information and considers Noun Phrases only for keyword candidates.

Tsatsaronis et al. [25] designed SemanticRank, which is again based upon PageRank [18], but ranks both keywords and sentences in a document based on their respective relevance to the document. The technique constructs a semantic graph using terms as nodes, and their implicit links while utilizing Omiotis similarity measure, WordNet, and Wikipedia as knowledge-bases and statistical information.

3. Corpus-Based Contextual Semantic Smoothing for Medium-Sized Documents

Given a collection of medium-sized documents $D = \{d_1, d_2, \ldots, d_N\}$ and domain-specific information (stopword and standardization lists), a keyword extraction technique outputs the top K keywords from a document d_i. We divide our methodology into two phases, namely (*i*) keyword extraction (unigrams) and (*ii*) keyphrase extraction (*n*-grams, where $n > 1$). First, all experiments were conducted to optimize the process of keyword extraction, and then the parameters were revisited to optimize the process of keyphrase extraction.

Corpus-based contextual semantic smoothing (CCSS, see Figure 1) extends the concept of Contextual Semantic Smoothing (CSS) [10], which considers term usage patterns in similar texts to improve term relevance information. In fact, CSS performs smoothing of the TFIDF matrix using a semantic feature, namely Phi coefficient, while keeping the corpus context into consideration.

3.1. Parts of Speech Tagging. In the literature, different combinations of Parts of Speech (POS) have been employed in order to filter unlikely keywords from a document, as presented in Table 1.
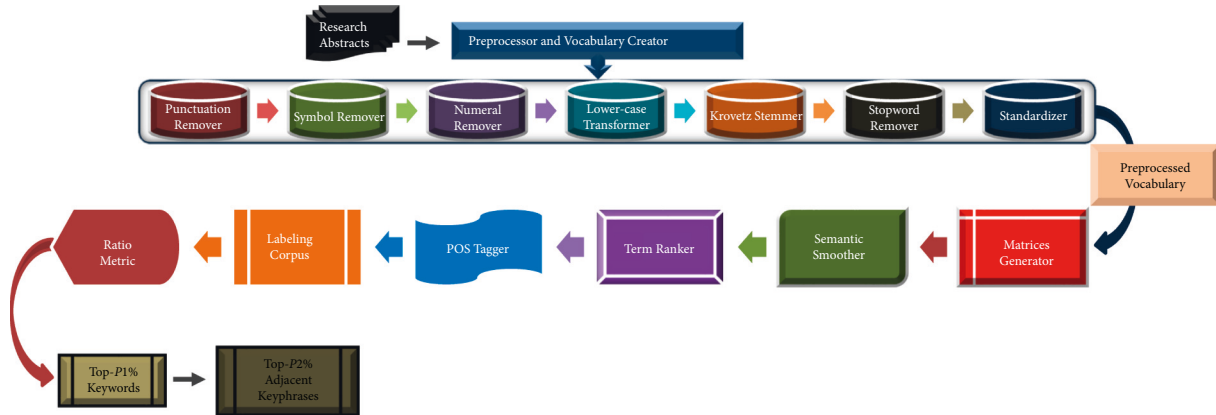
FIGURE 1: Corpus-based contextual semantic smoothing.

TABLE 1: Different combinations of POS in the literature.

S#	Reference	POS
1	[26–30]	Nouns only
2	[9, 31]	Nouns and verbs only
3	[6, 20–23, 32, 33]	Nouns and adjectives only
4	[15, 34–37]	Nouns, verbs, and adjectives only
5	[16]	Nouns, verbs, adjectives, and adverbs only
6	[38]	Verbs and adverbs only

As the first feature, we experimented with various combinations of POS (including some mentioned in Table 1), and selected the combination that considered all POS except Modal Verbs, as candidate keywords in a document. Modal Verbs are auxiliary verbs, such as "can" or "will," which are used to express modality. This combination of POS has not been used in the literature before, as evident from Table 1. Experiments related to this feature are presented in Section 5.1.

3.2. Labeling Corpus. As the second feature, we utilized a corpus consisting only of labels. We state our hypothesis as "A term should be considered as candidate keyword in a document, if it has been assigned as a label atleast once in the labeling corpus." We acquired INSPEC (https://www.theiet.org/publishing/inspec/) and ACM (https://doc.novay.nl/dsweb/Get/Document-115737/ACM-URLs.txt) collections to combine all of their labels into a single corpus. Both INSPEC and ACM collections consist of abstracts in English from scientific journal papers. Further details about the corpora are provided in Section 4.1. We experimented with various frequencies (f) of terms assigned as labels in the labeling corpus, and finally found our hypothesis to be true. In the literature, corpora have been utilized as a feature [1, 28, 39–44], however both labeling corpus in general, and this combination of corpora in particular, have not been used earlier. Experiments related to this feature are presented in Section 5.2.

3.3. Ratio Metric. As the third feature, we introduced a novel metric for each term's (t_j) eligibility for being a candidate keyword.

$$\frac{f_d}{f_l} \le x, \qquad (1)$$

where f_d represents frequency of t_j in the source document (d) under consideration, f_l represents frequency of t_j in the labeling corpus (l) under consideration, and x represents a threshold value under which the ratio of f_d and f_l should remain in order for t_j to be considered as a candidate keyword. The motivation behind developing this metric was to filter those terms as candidate keywords whose $f_d \gg f_l$. Experiments related to this feature are presented in Section 5.3.

3.4. Keyphrase Extraction. Once we had identified the significant keywords in the first phase, we moved on towards forming significant keyphrases in the second phase, through four different combinations of the two phases.

First, we considered the simplest way where all adjacently located keywords in d were utilized to form keyphrases.

Second, for all adjacently located keywords in each d, we selected the Top-P% (P is an integer between 0 and 100) keyphrases from them as significant keyphrases in order to take into consideration the varying sizes of documents.

Third, similar to selecting Top-P% keyphrases in each d as significant keyphrases, we revisited and improved the keyword extraction process by selecting Top-P1% ($P1$ is an integer between 0 and 100) keywords in each d as its significant keywords, and then selecting all adjacently located keywords in each d as significant keyphrases.

Fourth, we first selected Top-P1% (same value as resulted from the third combination of the two phases) keywords in each d as its significant keywords, and then selected Top-P2% ($P2$ is an integer between 0 and 100) keyphrases in each d as significant keyphrases. In the literature, keywords have been selected using the Top-P% metric; however, the process of Top-P2% keyphrases' selection after Top-P1% keywords have been selected has not been proposed earlier. Experiments related to the combinations of the two phases are presented in Section 5.4.

TABLE 2: Different combinations of POS.

S#		POS	Precision	Recall	F – measure
1		NO and AD only	0.3267	0.8641	0.4741
2		**NO, AD, and F only**	**0.3270**	**0.8836**	**0.4774**
3		NO, AD, and I only	0.3156	0.9176	0.4697
4	Top-N, $N = All$	NO, AD, I, and F only	0.3161	0.9370	0.4727
5		NO, AD, and V only	0.2891	0.9048	0.4382
6		NO, AD, I, V, NU, G, and AG only	0.2781	0.9631	0.4315
7		All POS except MV	0.3303	0.8195	0.4708

Bold values represent the best results achieved in terms of F-measure.

4. Data Analysis and Experimental Setup

4.1. Data Analysis. INSPEC dataset contains abstracts in English of journal papers from the disciplines of Computers and Control, and Information Technology, from 1998 to 2002, and is a collection of 2, 000 documents. The keywords assigned by a professional indexer may or may not be present in the abstracts. However, the indexers had access to the full-length documents when assigning the keywords. The abstracts in this dataset contain two sections; Title and Abstract, while in this work our focus is on the Abstract section only. All experiments presented in Section 5 have been conducted over this dataset.

ACM dataset contains abstracts in English of journal, conference, and workshop papers published by ACM in four domains of Computer Science, Distributed Systems, Information Search and Retrieval, Learning, and Social and Behavioral Sciences, and it consists of a total of 10, 935 documents. This dataset has only been used to create a labeling corpus (see Section 3.2).

4.2. Experimental Setup. The following evaluation metrics will be employed in the experiments:

(i) Precision is the fraction of relevant instances among the retrieved instances.

$$\text{Precision} = \frac{tp}{tp + fp}, \quad (2)$$

where tp and fp denote true positives and false positives, respectively.

(ii) Recall is the fraction of relevant instances that were retrieved.

$$\text{Recall} = \frac{tp}{tp + fn}, \quad (3)$$

where fn denotes false negatives.

(iii) F – measure is the harmonic mean of Precision and Recall.

$$F - \text{measure} = \frac{2 * \text{Precision} * \text{Recall}}{\text{Precision} + \text{Recall}}. \quad (4)$$

5. Experimental Results and Discussion

We follow experiments in the same sequence as mentioned in Section 3.

5.1. POS Tagging. As discussed in Section 3.1, Table 2 presents different combinations of POS experimented for the task of keyword extraction.

Here, NO = Nouns, AD = Adjectives, F = Foreign Words, I = Irrelevant Terms, V = Verbs, NU = Numbers, G = Genitive Markers, AG = Agents, and MV = Modal Verbs.

Foreign Words include non-English words, and Irrelevant Terms are represented by a union of all prepositions, conjunctions, determiners, possessive pronouns, particles, adverbs, and interjections [45], while Genitive Markers show ownership, measurement, association, or source, e.g., "boy's" and "of the boy."

Although the combination of POS selected for our methodology ranks fourth among the different ones experimented, we, for obvious reasons, avoided those combinations that included either foreign words or irrelevant terms.

5.2. Labeling Corpus. As discussed in Section 3.2, Table 3 displays various frequencies of terms assigned as labels in the labeling corpus, which were experimented for the task of keyword extraction.

5.3. Ratio Metric. As discussed in Section 3.3, we experimented with different threshold values for x for the task of keyword extraction, and found $x = 5$ to be the optimal value in terms of F-measure, as mentioned in Table 4.

All results related to different stages for the process of keyword extraction are summarized in Table 5, as discussed in Sections 3.1–3.3.

Here, $F1$, $F2$, and $F3$ represent the POS Tagging, Labeling Corpus, and Ratio Metric features, respectively.

5.4. Keyphrase Extraction. As discussed in Section 3, the optimal values yielded for the first three features for the process of keyword extraction were then revisited to yield the optimal values for the process of keyphrase extraction. Although the same optimal values were yielded for the first two features, the Ratio Metric feature produced an optimal value at $x = 8$, as mentioned in Table 6, and also reflected in Tables 4 and 5.

This is the simplest combination of keyword extraction and keyphrase extraction processes where all adjacently located keywords in d were utilized to form keyphrases.

As discussed in Section 3.4, for our second combination of keyword extraction and keyphrase extraction processes, we experimented with different values for P, and found $P = 55$ to be the optimal value in terms of F-measure, as mentioned in Table 7.

TABLE 3: Various frequencies of terms as labels in Labeling Corpus.

S#		Frequency of Term as Label	Precision	Recall	F − measure
1		$\mathbf{f \geq 1}$	**0.4106**	**0.8194**	**0.5471**
2		$1 \leq f \leq 15$	0.3277	0.3237	0.3257
3	Top-N, N = All	$1 \leq f \leq 28$	0.3504	0.4363	0.3886
4		$1 \leq f \leq 80$	0.3821	0.6466	0.4803
5		$1 \leq f \leq 294$	0.4030	0.7796	0.5313

Bold values represent the best results achieved in terms of F-measure.

TABLE 4: Different threshold values for x.

S#		x	Precision	Recall	F − measure
1		**5**	**0.6115**	**0.7195**	**0.6611**
2	Top-N, N = All	6	0.5901	0.7497	0.6604
3		7	0.5716	0.7704	0.6563
4		8	0.5589	0.7833	0.6523

Bold values represent the best results achieved in terms of F-measure.

TABLE 5: Different stages for the process of keyword extraction.

S#		Stage	Precision	Recall	F − measure	Change in F − measure
1		CSS	0.2790	0.9073	0.4268	—
2	Top-N, N = All	CSS + $F1$	0.3303	0.8195	0.4708	↑4%
3		CSS + $F1$ + $F2$	0.4106	0.8194	0.5471	↑8%
4		**CSS + F1 + F2 + F3**	**0.5589**	**0.7833**	**0.6523**	**↑11%**

Bold values represent the best results achieved in terms of F-measure.

TABLE 6: Different threshold values for x.

S#		x	Precision	Recall	F − measure
1		4	0.2174	0.4441	0.2919
2		5	0.2269	0.5156	0.3152
3	Top-N, N = All	6	0.2274	0.5491	0.3217
4		7	0.2274	0.5775	0.3263
5		8	0.2276	0.5953	0.3293
6		9	0.2249	0.6064	0.3282

TABLE 7: Different values for P.

S#	$P1$	Precision	Recall	F − measure
1	40	0.4316	0.4730	0.4513
2	50	0.4031	0.5597	0.4687
3	**55**	**0.3927**	**0.5820**	**0.4690**
4	60	0.3764	0.6028	0.4635
5	70	0.3418	0.6366	0.4447

Bold values represent the best results achieved in terms of F-measure.

TABLE 8: Different values for $P1$.

S#	$P1$	Precision	Recall	F − measure
1	40	0.4048	0.4469	0.4248
2	50	0.3965	0.5556	0.4628
3	59	0.3818	0.6075	0.4689
4	60	0.3791	0.6138	0.4687
5	70	0.3502	0.6592	0.4574

TABLE 9: Different values for $P2$.

S#	$P2$	Precision	Recall	F − measure
1	40	0.4294	0.4746	0.4509
2	50	0.4075	0.5700	0.4752
3	55	0.3984	0.5954	0.4774
4	60	0.3837	0.6207	0.4742
5	70	0.3516	0.6616	0.4592

As discussed in Section 3.4, for our third combination of keyword extraction and keyphrase extraction processes, we experimented with different values for $P1$, and found $P1 = 59$ to be the optimal value in terms of F-measure, as mentioned in Table 8.

As discussed in Section 3.4, for our fourth combination of keyword extraction and keyphrase extraction processes, we experimented with different values for $P2$, and found $P2 = 55$ to be the optimal value in terms of F-measure, as mentioned in Table 9.

All results related to different combinations of keyword extraction and keyphrase extraction processes are summarized in Table 10, as discussed in Section 3.4.

TABLE 10: Different combinations of keyword extraction and keyphrase extraction processes.

S#	Combination of processes	Precision	Recall	F – measure	Change in F – measure
1	Keyword extraction + adjacent keywords in d to form keyphrases	0.2276	0.5953	0.3293	—
2	Keyword extraction + adjacent keywords in d to form top-P% keyphrases	0.3927	0.5820	0.4690	↑13%
3	Keyword extraction (top-$P1$% unigrams) + adjacent keywords in d to form keyphrases	0.3818	0.6075	0.4689	—
4	**Keyword extraction (top- P1% unigrams) + adjacent keywords in d to form top-P2% keyphrases**	**0.3984**	**0.5954**	**0.4774**	**↑1%**

Bold values represent the best results achieved in terms of F-measure.

TABLE 11: Systematic comparison of CCSS with other techniques over INSPEC dataset.

S#	Technique	Precision	Recall	F – measure
1	PageRank [18] evaluated by Liu et al. [23]	0.3300	0.1710	0.2250
2	Term frequency inverse document frequency (TFIDF) evaluated by Liu et al. [23]	0.3330	0.1730	0.2270
3	LDA [22] evaluated by Liu et al. [23]	0.3320	0.1720	0.2270
4	TPR [23]	0.3540	0.1830	0.2420
5	Liu et al. [24]	0.3270	0.6530	0.4360
6	SemanticRank [25]	0.4210	0.5320	0.4700
7	CCSS	0.3984	0.5954	0.4774

5.5. CCSS Vs. State-of-the-Art Techniques. We systematically compared the performance of CCSS with other techniques, when implemented over INSPEC dataset, as presented in the literature, and such analysis is presented in Table 11. It is clear that CCSS has outperformed all state-of-the-art keyphrase extraction techniques presented in the literature.

6. Conclusion and Future Work

In this paper, we have presented a novel supervised technique for extraction of keywords from medium-sized documents, namely Corpus-based Contextual Semantic Smoothing (CCSS). CCSS extended the concept of Contextual Semantic Smoothing (CSS), which considered term usage patterns in similar texts to improve term relevance information. We introduced four more features beyond CSS as our novel contributions in this work. We systematically compared the performance of CCSS with other techniques, when implemented over INSPEC dataset, where CCSS clearly outperformed all state-of-the-art keyphrase extraction techniques presented in the literature.

Our future work includes utilizing CCSS in the applications of indexing and search, summarization, and multilingual summarization, of medium-sized documents. We are also currently working on compiling the literature review for all keyword extraction-based applications beyond and including the abovementioned ones.

Data Availability

Previously reported INSPEC and ACM datasets were used to support this study and are available at https://www.theiet.org/publishing/inspec/and https://www.innovalor.nl/, respectively. The datasets used in this study are available from the corresponding author upon reasonable request.

Conflicts of Interest

The authors declare that there are no conflicts of interest regarding the publication of this paper.

Acknowledgments

References

[1] V. Qazvinian, D. R. Radev, and A. Özgür, "Citation summarization through keyphrase extraction," in *Proceedings of the 23rd International Conference on Computational Linguistics (Beijing, China) (COLING '10)*, pp. 895–903, Association for Computational Linguistics, Stroudsburg, PA, USA, August 2010.

[2] H. Zha, "Generic summarization and keyphrase extraction using mutual reinforcement principle and sentence clustering," in *Proceedings of the 25th Annual International ACM SIGIR Conference on Research and Development in Information Retrieval (Tampere, Finland) (SIGIR '02)*, pp. 113–120, ACM, New York, NY, USA, August 2002.

[3] A. Hliaoutakis, K. Zervanou, G. Euripides, E. G. M. Petrakis, and E. E. Milios, "Automatic document indexing in large medical collections," in *Proceedings of the International Workshop on Healthcare Information and Knowledge Management (Arlington, VA, USA) (HIKM '06)*, pp. 1–8, ACM, New York, NY, USA, November 2006.

[4] Z. Bar-Yossef and M. Gurevich, "Estimating the impressionrank of web pages," in *Proceedings of the 18th International Conference on World Wide Web (Madrid, Spain)*,

WWW '09). ACM, pp. 41–50, New York, NY, USA, April 2009.

[5] O. Medelyan, E. Frank, and I. H. Witten, "Human-competitive tagging using automatic keyphrase extraction," in *Proceedings of the 2009 Conference on Empirical Methods in Natural Language Processing: Volume 3 – Volume 3 (Singapore) (EMNLP '09)*, pp. 1318–1327, Association for Computational Linguistics, Stroudsburg, PA, USA, August 2009.

[6] W. Wu, B. Zhang, and M. Ostendorf, "Automatic generation of personalized annotation tags for twitter users," in *Proceedings of Human Language Technologies: The 2010 Annual Conference of the North American Chapter of the Association for Computational Linguistics (Los Angeles, CA, USA) (HLT '10)*, pp. 689–692, Association for Computational Linguistics, Stroudsburg, PA, USA, June 2010.

[7] K. S. Dave and V. Varma, "Pattern based keyword extraction for contextual advertising," in *Proceedings of the 19th ACM International Conference on Information and Knowledge Management (Toronto, ON, Canada) (CIKM '10)*, pp. 1885–1888, ACM, New York, NY, USA, October 2010.

[8] W.-T. Yih, J. Goodman, and V. R. Carvalho, "Finding advertising keywords on web pages," in *Proceedings of the 15th International Conference on World Wide Web (Edinburgh, Scotland) (WWW '06)*, pp. 213–222, ACM, New York, NY, USA, May 2006.

[9] C. Wartena, R. Brussee, and W. Slakhorst, "Keyword extraction using word co-occurrence," in *Proceedings of the 2010 Workshops on Database and Expert Systems Applications (DEXA '10) (Bilbao, Spain)*, pp. 54–58, IEEE Computer Society, Washington, DC VA, USA, August 2010.

[10] O. A. Khan and A. Karim, "MIKE: an interactive microblogging keyword extractor using contextual semantic smoothing," in *Proceedings of the 24th International Conference on Computational Linguistics (Mumbai, India) COLING '12*, pp. 289–296, Association for Computational Linguistics, Stroudsburg, PA, USA, December 2012.

[11] X. Wu, F. Xie, G. Wu, and W. Ding, "Personalized news filtering and summarization on the web," in *Proceedings of the 2011 IEEE 23rd International Conference on Tools with Artificial Intelligence (ICTAI '11)*, pp. 414–421, Boca Raton, FL, USA, November 2011.

[12] S. A. Hossain, A. S. M. M. Rahman, T. T. Tran, and A. E. Saddik, "Location aware question answering based product searching in mobile handheld devices," in *Proceedings of the 2010 IEEE/ACM 14th International Symposium on Distributed Simulation and Real Time Applications (DS-RT '10)*, pp. 189–195, Fairfax, VA, USA, October 2010.

[13] K. Zoltán and S. Johann, "Semantic analysis of microposts for efficient people to people interactions," in *Proceedings of the 2011 RoEduNet International Conference 10th Edition: Networking in Education and Research*, pp. 1–4, Iasi, Romania, June 2011.

[14] E. Frank, G. W. Paynter, I. H. Witten, C. Gutwin, and C. G. Nevill-Manning, "Domain-specific keyphrase extraction," in *Proceedings of the 16th International Joint Conference on Artificial Intelligence, (IJCAI '99)*, pp. 668–673, San Francisco, CA, USA, July 1999.

[15] F. Liu, D. Pennell, F. Liu, and Y. Liu, "Unsupervised approaches for automatic keyword extraction using meeting transcripts," in *Proceedings of the Human Language Technologies: The 2009 Annual Conference of the North American Chapter of the Association for Computational Linguistics (HLT-NAACL '09) (Boulder, CO)*, pp. 620–628, Association for Computational Linguistics, Stroudsburg, PA, USA, 2009.

[16] F. Liu, F. Liu, and Y. Liu, "A supervised framework for keyword extraction from meeting transcripts," *IEEE Transactions on Audio Speech and Language Processing*, vol. 19, no. 3, pp. 538–548, March 2011.

[17] A. Hulth, "Improved automatic keyword extraction given more linguistic knowledge," in *Proceedings of the 2003 Conference on Empirical Methods in Natural Language Processing (EMNLP '03) (Sapporo, Japan)*, pp. 216–223, Association for Computational Linguistics, Stroudsburg, PA, USA, July 2003.

[18] L. Page, S. Brin, R. Motwani, and T. Winograd, "*The PageRank Citation Ranking: Bringing Order to the Web*", Stanford InfoLab, Stanford, CA, USA, 1999.

[19] R. Mihalcea and P. Tarau, "Textrank: bringing order into texts," in *Proceedings of the 2004 Conference on Empirical Methods in Natural Language Processing (EMNLP '04)*, pp. 404–411, (Barcelona, Spain), Association for Computational Linguistics, Stroudsburg, PA, USA, July 2004.

[20] X. Wan and J. Xiao, "Collabrank: towards a collaborative approach to single-document keyphrase extraction," in *Proceedings of the 22nd International Conference on Computational Linguistics (COLING '08)*, (Manchester UK), pp. 969–976, Association for Computational Linguistics, Stroudsburg, PA, USA, August 2008.

[21] X. Wan and J. Xiao, "Single document keyphrase extraction using neighborhood knowledge," in *Proceedings of the 23rd National Conference on Artificial Intelligence: Volume 2 (AAAI '08)*, pp. 855–860, Chicago, IL, USA, July 2008.

[22] D. M. Blei, A. Y. Ng, and M. I. Jordan, "Latent dirichlet allocation," *Journal of Machine Learning Research*, vol. 3, pp. 993–1022, January 2003.

[23] Z. Liu, W. Huang, Y. Zheng, and M. Sun, "Automatic keyphrase extraction via topic decomposition," in *Proceedings of the 2010 Conference on Empirical Methods in Natural Language Processing (EMNLP '10) (Cambridge, MA, USA)*, pp. 366–376, Association for Computational Linguistics, Stroudsburg, PA, USA, October 2010.

[24] Z. Liu, P. Li, Y. Zheng, and M. Sun, "Clustering to find exemplar terms for keyphrase extraction," in *Proceedings of the 2009 Conference on Empirical Methods in Natural Language Processing: Volume 1 – Volume 1 (EMNLP '09) (Singapore)*, pp. 257–266, Association for Computational Linguistics, Stroudsburg, PA, USA, August 2009.

[25] G. Tsatsaronis, I. Varlamis, and K. Nørvåg, "SemanticRank: ranking keywords and sentences using semantic graphs," in *Proceedings of the 23rd International Conference on Computational Linguistics*, pp. 1074–1082, Association for Computational Linguistics, Stroudsburg, PA, USA, August 2010.

[26] L. Zhang, J. Wu, Y. Zhuang, Y. Zhang, and C. Yang, "Review-oriented metadata enrichment: a case study," in *Proceedings of the 9th ACM/IEEE-CS Joint Conference on Digital Libraries (JCDL '09)*, pp. 173–182, ACM, New York, NY, USA, June 2009.

[27] M. Wenchao, L. Lianchen, and D. Ting, "A modified approach to keyword extraction based on word-similarity," in *Proceedings of the 2009 IEEE International Conference on Intelligent Computing and Intelligent Systems (ICICISYS '09)*, pp. 388–392, Shanghai, China, November 2009.

[28] A. Panunzi, M. Fabbri, and M. Moneglia, "Keyword extraction in open-domain multilingual textual resources," in *Proceedings of the First International Conference on Automated Production of Cross Media Content for Multi-Channel Distribution AXMEDIS'05*, p. 4, Florence, Italy, November 2005.

[29] T. Takehara, S. Miki, N. Nitta, and N. Babaguchi, "Extracting Context Information from Microblog Based on Analysis of Online Reviews," in *Proceedings of the 2012 IEEE International Conference on Multimedia and Expo (ICME '12) Workshops*, pp. 248–253, Melbourne, VIC, Australia, July 2012.

[30] J. Tang, Z. Liu, M. Sun, and J. Liu, "Portraying user life status from microblogging posts," *Tsinghua Science and Technology*, vol. 18, no. 2, pp. 182–195, April 2013.

[31] J. Liu and J. Wang, "Keyword extraction using language network," in *Proceedings of the 2007 International Conference on Natural Language Processing and Knowledge Engineering (NLPKE '07)*, pp. 129–134, Beijing, China, August 2007.

[32] Y. Ouyang, W. Li, and R. Zhang, "273. Task 5. Keyphrase extraction based on core word identification and word expansion," in *Proceedings of the 5th International Workshop on Semantic Evaluation (SemEval '10). Association for Computational Linguistics*, pp. 142–145, Stroudsburg, PA, USA, July 2010.

[33] J. Hauffa, T. Lichtenberg, and G. Groh, "Towards an NLP-based topic characterization of social relations," in *Proceedings of the 2012 International Conference on Social Informatics (ICSI '12)*,, pp. 289–294, Alexandria, VA, USA, December 2012.

[34] G. Berend and R. Farkas, "SZTERGAK: feature engineering for keyphrase extraction," in *Proceedings of the 5th International Workshop on Semantic Evaluation (SemEval '10)*, pp. 186–189, Association for Computational Linguistics, Stroudsburg, PA, USA, July 2010.

[35] Y. J. Lui, R. Brent, and A. Calinescu, "Extracting Significant Phrases from Text," in *Proceedings of the 21st International Conference on Advanced Information Networking and Applications Workshops (AINAW'07)*, pp. 361–366, Niagara Falls, ON, Canada, May 2007.

[36] G. Fang, C. Yuan, X. Wang, J. Li, and Z. Song, "From keywords to social tags: tagging for dialogues," in *Proceedings of the 2011 7th International Conference on Natural Language Processing and Knowledge Engineering (NLPKE '11)*, pp. 106–113, Tokushima Japan, November 2011.

[37] C. Chitra and A. Julian, "Searching video blogs with integration of context and content analysis," in *Proceedings of the 2010 International Conference on Innovative Computing Technologies (ICICT) '10)*, pp. 1–5, Karur, India, February 2010.

[38] G. B. Colombo, M. J. Chorley, V. Tanasescu, S. M. Allen, C. B. Jones, and R. M. Whitaker, "Will you like this place? A tag-based place representation approach," in *Proceedings of the 2013 IEEE International Conference on Pervasive Computing and Communications Workshops (PERCOM Workshops)*, pp. 224–229, San Diego, CA, USA, March 2013.

[39] A. Hulth, "Enhancing linguistically oriented automatic keyword extraction," in *Proceedings of the Human Language Technologies: The 2004 Annual Conference of the North American Chapter of the Association for Computational Linguistics: Short Papers (HLT-NAACL-Short '04)*, pp. 17–20, Association for Computational Linguistics, Stroudsburg, PA, USA, May 2004.

[40] L.-F. Chien, "PAT-tree-based keyword extraction for Chinese information retrieval," in *Proceedings of the 20th Annual International ACM SIGIR Conference on Research and Development in Information Retrieval (SIGIR '97)*, pp. 50–58, ACM, New York, NY, USA, July 1997.

[41] E. Pianta and S. Tonelli, "KX: a flexible system for keyphrase extraction," in *Proceedings of the 5th International Workshop on Semantic Evaluation (SemEval '10)*, pp. 170–173, Association for Computational Linguistics, Stroudsburg, PA, USA, July 2010.

[42] P. Treeratpituk, P Teregowda, J. Huang, and C. Lee Giles, "SEERLAB: a system for extracting key phrases from scholarly documents," in *Proceedings of the 5th International Workshop on Semantic Evaluation (SemEval '10)*, pp. 182–185, Association for Computational Linguistics, Stroudsburg, PA, USA, July 2010.

[43] S. Muresan, E. Tzoukermann, and J. L. Klavans, "Combining linguistic and machine learning techniques for email summarization," in *Proceedings of the 2001 Workshop on Computational Natural Language Learning - Volume 7 (ConLL '01)*, p. 8, Stroudsburg, PA, USA, July 2001.

[44] M. Paukkeri, A. P. García-Plaza, S. Pessala, and T. Honkela, "Learning taxonomic relations from a set of text documents," in *Proceedings of the International Multiconference on Computer Science and Information Technology (IMCSIT '10)*, pp. 105–112, Wisla, Poland, October 2010.

[45] K. M. Carley, "AutoMap User's Guide," *Center for Computational Analysis of Social and Organizational Systems (CASOS), Institute for Software Research International (ISRI), School of Computer Science, Carnegie Mellon University*, June 2013.

WILEY | Hindawi

Research Article

On Curvilinear Regression Analysis via Newly Proposed Entropies for Some Benzene Models

Guangwu Liu,[1] Muhammad Kamran Siddiqui,[2] Shazia Manzoor ⓘ,[2] Muhammad Naeem ⓘ,[3] and Douhadji Abalo ⓘ[4]

[1]*Green & Smart River-Sea-Going Ship, Cruise and Yacht Research Center, Wuhan University of Technology, Wuhan, China*
[2]*Department of Mathematics, COMSATS University Islamabad, Lahore Campus, Lahore, Pakistan*
[3]*Department of Computer Science, TIMES Institute, Multan, Pakistan*
[4]*Department of Mathematics, University of Lome, P.O. Box 1515, Lome, Togo*

Correspondence should be addressed to Douhadji Abalo; douhadjiabalo@gmail.com

To avoid exorbitant and extensive laboratory experiments, QSPR analysis, based on topological descriptors, is a very constructive statistical approach for analyzing the numerous physical and chemical properties of compounds. Therefore, we presented some new entropy measures which are based on the sum of the neighborhood degree of the vertices. Firstly, we made the partition of the edges of benzene derivatives which are based on the degree sum of neighboring vertices and then computed the neighborhood version of entropies. Secondly, we made use of the software SPSS for developing a correlation between newly introduced entropies and the physicochemical properties of benzene derivatives. Our obtained results demonstrated that the critical temperature ($\mathscr{CT}$), critical pressure ($\mathscr{CP}$), and critical volume ($\mathscr{CV}$) can be predicted through fifth geometric arithmetic entropy, second SK entropy, and fifth ND entropy, respectively. Other remaining physical characteristics include Gibb's energy ($q\mathscr{E}$), $\log(P)$, molar refractivity ($\mathscr{MR}$), and Henry's law ($\mathscr{HL}$) that can be predicted by using sixth ND entropy.

1. Introduction

In chemistry, models are classified into two types. The first type of modeling is based on the quantum-chemical method and theoretically identical models derived from statistical mechanics. The second type consists of chemical thinking, which compares related systems. According to the core principle of chemistry, all the features of matter correlate with its molecular structure, and thus, molecules with similar structures have similar properties. This has resulted in several empirical approaches such as SAR, SPC, QSPR, and QSAR [1, 2].

The identical factor of all these methods is the correlation between physicochemical properties and molecular descriptors. There are numerous descriptors to utilize [3], but one family of descriptors has been demonstrated exceptionally basic and valuable in foreseeing multiple molecular properties. These are known as topological indices ($\mathscr{TIS}$).

Topological indices ($\mathscr{TIS}$) are numerical parameters that are correlated with a graph and help identify its topology. There are three types of $\mathscr{TIS}$: degree-based $\mathscr{TIS}$, spectrum-based $\mathscr{TIS}$, and distance-based $\mathscr{TIS}$ [4, 5]. Degree-based $\mathscr{TIS}$, which are defined in terms of the degrees of the vertices of a graph, are one of the most studied $\mathscr{TIS}$ used in mathematical chemistry [6]. Imran et al. [7] discuss the topological properties of symmetric chemical structures. Zou et al. [8] computed topological indices for polyphenylene. Recently, some neighborhood versions of $\mathscr{TIS}$ have also been introduced [9, 10]. Zhang et al. [11–13] discuss the topological indices of generalized bridge molecular graphs, carbon nanotubes, and the product of chemical graphs.

The idea of entropy first appeared in thermodynamics in the nineteenth century, when it was closely linked to the heat flow and a key component of the second law of thermodynamics. Subsequently, statistical mechanics used the

notion to illuminate thermodynamics physically. Leading physicists such as Boltzmann and Gibbs [14, 15], who employed entropy as a measure of the disorder of the massive dynamical system underlying molecule collections, were responsible for this. Fisher employed similar notions in the establishment of the foundations of theoretical statistics in 1920 [16]. In the 1950s, Kullback and Leibler [17] developed this concept further. Zhang et al. [18–20] provided the physical analysis of heat for the formation and entropy of ceria oxide.

Claude Shannon, a mathematician and electrical engineer who worked at Bell Labs in New Jersey in the midtwentieth century, identified the link between entropy and information content [21]. The concept formed a key element of the emerging field of information theory at that time. Afterward, in the 1950s, Jaynes explained the explicit association between Shannon's entropy and that of statistical mechanics in a series of excellent works [22, 23]. Since then, information theory has found applications in a variety of fields, including networking analysis, mathematical statistics, complexity theory, and financial mathematics.

We made a bibliometric analysis grounded on the Scopus database https://www.scopus.com. This analysis is based upon 986 research articles with entropy and graph entropy [24–26] as key factors. The percentage of publications in different subjects is shown in Figure 1.

We made a bibliometric analysis of the research conducted in different countries on the concept of entropy in Figure 2.

In recent times, another approach which is a bit different in the literature, namely, using the concept of Shannon's entropy in terms of topological indices was introduced by Manzoor et al. in [27]. Continuing their work, they also introduced eccentricity-based graph entropies [28, 29] and bond additive graph entropies [30]. In this paper, the present authors formulated some new graph entropies, namely, neighborhood versions of graph entropies. The graph entropy is represented in the following formula:

$$\mathfrak{E}_{\mathbb{I}}(\mathfrak{B}) = - \sum_{\mathfrak{u}'\mathfrak{v}' \in \mathfrak{E}(\mathfrak{B})} \frac{\mathbb{I}(\mathfrak{u}'\mathfrak{v}')}{\sum_{\mathsf{uv} \in \mathfrak{E}(\mathfrak{B})} \mathbb{I}(\mathsf{uv})} \log_2\left[\frac{\mathbb{I}(\mathfrak{u}'\mathfrak{v}')}{\sum_{\mathsf{uv} \in \mathfrak{E}(\mathfrak{B})} \mathbb{I}(\mathsf{uv})}\right], \tag{1}$$

where $\mathscr{V}(\mathfrak{B})$ is the vertex set, $\mathfrak{E}(\mathfrak{B})$ is the edge set, and $\mathbb{I}(\mathsf{uv})$ is the edge weight of the edge (uv).

(i) Neighborhood version of forgotten entropy
If $\mathbb{I}(\mathsf{uv}) = \mathfrak{A}(\mathfrak{u})^2 + \mathfrak{A}(\mathfrak{v})^2$, then

$$\sum_{\mathsf{uv} \in \mathfrak{E}(\mathfrak{B})} \mathbb{I}(\mathsf{uv}) = \sum_{\mathsf{uv} \in \mathfrak{E}(\mathfrak{B})} \left[\mathfrak{A}(\mathfrak{u})^2 + \mathfrak{A}(\mathfrak{v})^2\right] = \mathbb{F}_N^*. \tag{2}$$

So, equation (1) is called the neighborhood version of forgotten entropy.
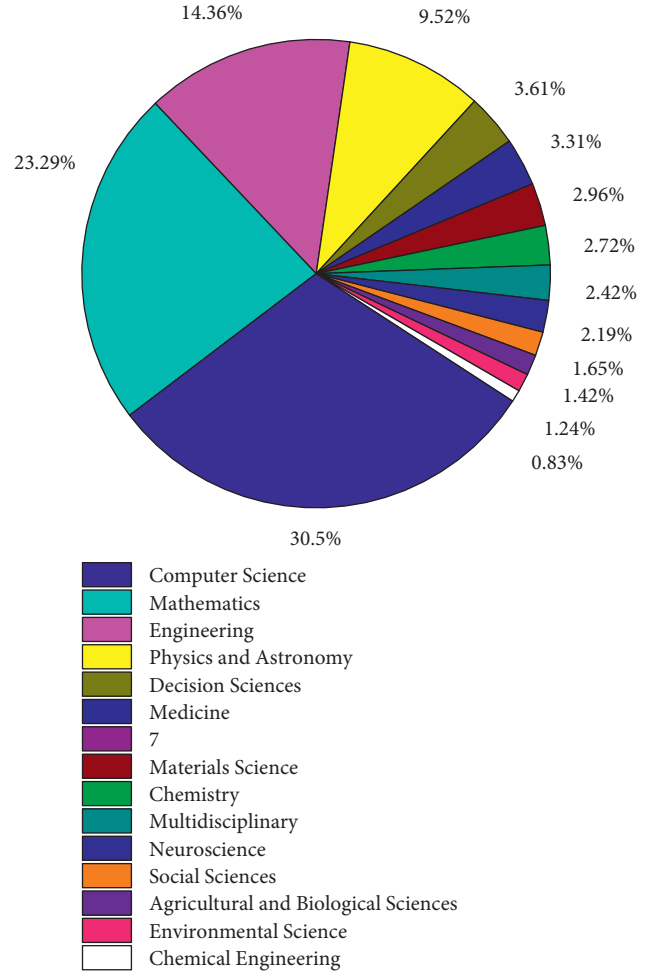
FIGURE 1: Bibliometric analysis of the publications of entropy in various disciplines.

$$\mathfrak{E}_{\mathbb{F}_N^*}(\mathfrak{B}) = \log_2\left(\mathbb{H}_N^*\right) - \frac{1}{\mathbb{H}_N^*} \sum_{i=1}^{\mathfrak{q}} \sum_{\mathsf{uv} \in \mathfrak{E}_i(\mathfrak{B})}$$
$$\cdot \left[\mathfrak{A}(\mathfrak{u})^2 + \mathfrak{A}(\mathfrak{v})^2\right] \log_2\left[\mathfrak{A}(\mathfrak{u})^2 + \mathfrak{A}(\mathfrak{v})^2\right]. \tag{3}$$

(ii) Neighborhood version of second Zagreb entropy
If $\mathbb{I}(\mathsf{uv}) = \mathfrak{A}(\mathfrak{u}) \times \mathfrak{A}(\mathfrak{v})$, then

$$\sum_{\mathsf{uv} \in \mathfrak{E}(\mathfrak{B})} \mathbb{I}(\mathsf{uv}) = \sum_{\mathsf{uv} \in \mathfrak{E}(\mathfrak{B})} \left[\mathfrak{A}(\mathfrak{u}) \times \mathfrak{A}(\mathfrak{v})\right] = \mathbb{M}_2^*. \tag{4}$$

So, equation (2) is called the neighborhood version of second Zagreb entropy.

$$\mathfrak{E}_{\mathbb{M}_2^*}(\mathfrak{B}) = \log_2\left(\mathbb{M}_2^*\right) - \frac{1}{\mathbb{M}_2^*} \sum_{i=1}^{\mathfrak{q}} \sum_{\mathsf{uv} \in \mathfrak{E}_i(\mathfrak{B})} \tag{5}$$
$$\cdot \left[\mathfrak{A}(\mathfrak{u}) \times \mathfrak{A}(\mathfrak{v})\right] \log_2\left[\mathfrak{A}(\mathfrak{u}) \times \mathfrak{A}(\mathfrak{v})\right].$$
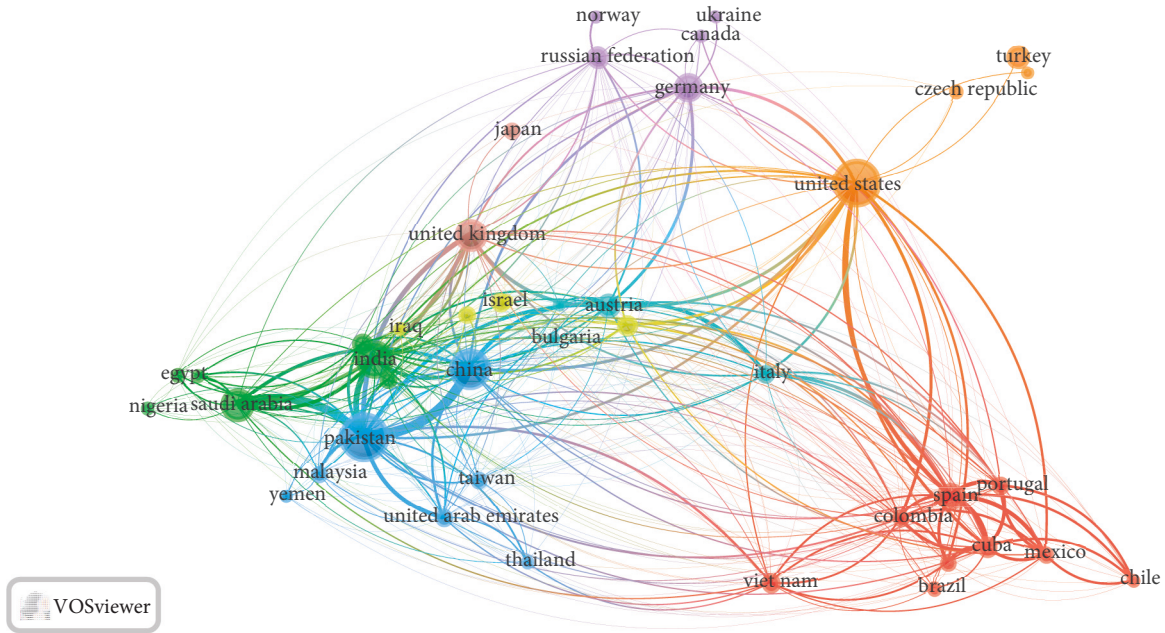
FIGURE 2: Bibliometric analysis of countrywide research based on the topic of entropy. The size of the circles denotes the frequency of articles, and distinct colors are used to signify distinct clusters.

(iii) Neighborhood version of hyper-Zagreb entropy

If $\mathbb{I}(\mathsf{uv}) = [\mathfrak{A}(\mathfrak{u}) + \mathfrak{A}(\mathfrak{v})]^2$, then

$$\sum_{\mathsf{uv}\in\mathfrak{E}(\mathfrak{B})} \mathbb{I}(\mathsf{uv}) = \sum_{\mathsf{uv}\in\mathfrak{E}(\mathfrak{B})} [\mathfrak{A}(\mathfrak{u}) + \mathfrak{A}(\mathfrak{v})]^2 = \mathbb{HM}_N. \quad (6)$$

So, equation (3) is called the neighborhood version of hyper-Zagreb entropy.

$$\mathfrak{E}_{\mathbb{HM}_N}(\mathfrak{B}) = \log_2\left(\mathbb{HM}_N\right) - \frac{1}{\left(\mathbb{HM}_N\right)} \sum_{i=1}^{\mathfrak{q}} \sum_{\mathsf{uv}\in\mathfrak{E}_i(\mathfrak{B})}$$

$$\cdot\, [\mathfrak{A}(\mathfrak{u}) + \mathfrak{A}(\mathfrak{v})]^2 \log_2 [\mathfrak{A}(\mathfrak{u}) + \mathfrak{A}(\mathfrak{v})]^2. \quad (7)$$

(iv) First ND entropy

If $\mathbb{I}(\mathsf{uv}) = \sqrt{\mathfrak{A}(\mathfrak{u}) \times \mathfrak{A}(\mathfrak{v})}$, then

$$\sum_{\mathsf{uv}\in\mathfrak{E}(\mathfrak{B})} \mathbb{I}(\mathsf{uv}) = \sum_{\mathsf{uv}\in\mathfrak{E}(\mathfrak{B})} [\sqrt{\mathfrak{A}(\mathfrak{u}) \times \mathfrak{A}(\mathfrak{v})}] = \mathbb{ND}_1. \quad (8)$$

So, equation (4) is called the first ND entropy.

$$\mathfrak{E}_{\mathbb{ND}_1}(\mathfrak{B}) = \log_2\left(\mathbb{ND}_1\right) - \frac{1}{\left(\mathbb{ND}_1\right)} \sum_{i=1}^{\mathfrak{q}} \sum_{\mathsf{uv}\in\mathfrak{E}_i(\mathfrak{B})}$$

$$\cdot\, [\sqrt{\mathfrak{A}(\mathfrak{u}) \times \mathfrak{A}(\mathfrak{v})}] og_2 [\sqrt{\mathfrak{A}(\mathfrak{u}) \times \mathfrak{A}(\mathfrak{v})}] 1. \quad (9)$$

(v) Second ND entropy

If $\mathbb{I}(\mathsf{uv}) = 1/\sqrt{\mathfrak{A}(\mathfrak{u}) + \mathfrak{A}(\mathfrak{v})}$, then

$$\sum_{\mathsf{uv}\in\mathfrak{E}(\mathfrak{B})} \mathbb{I}(\mathsf{uv}) = \sum_{\mathsf{uv}\in\mathfrak{E}(\mathfrak{B})} \left[\frac{1}{\sqrt{\mathfrak{A}(\mathfrak{u}) + \mathfrak{A}(\mathfrak{v})}}\right] = \mathbb{ND}_2. \quad (10)$$

So, equation (5) is called the second ND entropy.

$$\mathfrak{E}_{\mathbb{ND}_2}(\mathfrak{B}) = \log_2\left(\mathbb{ND}_2\right) - \frac{1}{\left(\mathbb{ND}_2\right)} \sum_{i=1}^{\mathfrak{q}} \sum_{\mathsf{uv}\in\mathfrak{E}_i(\mathfrak{B})}$$

$$\cdot \left[\frac{1}{\sqrt{\mathfrak{A}(\mathfrak{u}) + \mathfrak{A}(\mathfrak{v})}}\right] \log_2 \left[\frac{1}{\sqrt{\mathfrak{A}(\mathfrak{u}) + \mathfrak{A}(\mathfrak{v})}}\right]. \quad (11)$$

(vi) Third ND entropy.

If $\mathbb{I}(\mathsf{uv}) = [\mathfrak{A}(\mathfrak{u}) \times \mathfrak{A}(\mathfrak{v})][\mathfrak{A}(\mathfrak{u}) + \mathfrak{A}(\mathfrak{v})]$, then

$$\sum_{\mathsf{uv}\in\mathfrak{E}(\mathfrak{B})} \mathbb{I}(\mathsf{uv}) = \sum_{\mathsf{uv}\in\mathfrak{E}(\mathfrak{B})} [\mathfrak{A}(\mathfrak{u}) \times \mathfrak{A}(\mathfrak{v})]$$

$$\cdot [\mathfrak{A}(\mathfrak{u}) + \mathfrak{A}(\mathfrak{v})] = \mathbb{ND}_3. \quad (12)$$

So, equation (6) is called the third ND entropy.

$$\mathfrak{E}_{\mathbb{ND}_3}(\mathfrak{B}) = \log_2\left(\mathbb{ND}_3\right) - \frac{1}{\left(\mathbb{ND}_3\right)} \sum_{i=1}^{\mathfrak{q}} \sum_{\mathsf{uv}\in\mathfrak{E}_i(\mathfrak{B})}$$

$$\cdot [\mathfrak{A}(\mathfrak{u}) \times \mathfrak{A}(\mathfrak{v})][\mathfrak{A}(\mathfrak{u}) + \mathfrak{A}(\mathfrak{v})]\log_2$$

$$\cdot [\mathfrak{A}(\mathfrak{u}) \times \mathfrak{A}(\mathfrak{v})][\mathfrak{A}(\mathfrak{u}) + \mathfrak{A}(\mathfrak{v})]. \quad (13)$$

(vii) Fourth ND entropy.

If $\mathbb{I}(\mathsf{uv}) = 1/\sqrt{\mathfrak{A}(\mathfrak{u}) \times \mathfrak{A}(\mathfrak{v})}$, then

$$\sum_{\mathsf{uv}\in\mathfrak{E}(\mathfrak{B})} \mathbb{I}(\mathsf{uv}) = \sum_{\mathsf{uv}\in\mathfrak{E}(\mathfrak{B})} \left[\frac{1}{\sqrt{\mathfrak{A}(\mathfrak{u}) \times \mathfrak{A}(\mathfrak{v})}}\right] = \mathbb{ND}_4. \quad (14)$$

So, equation (7) is called the fourth ND entropy.

$$\mathfrak{E}_{\mathbb{ND}_4}(\mathfrak{B}) = \log_2\left(\mathbb{ND}_4\right) - \frac{1}{\left(\mathbb{ND}_4\right)}\sum_{i=1}^{q}\sum_{\mathsf{uv}\in\mathfrak{E}_i(\mathfrak{B})}$$

$$\cdot\left[\frac{1}{\sqrt{\mathfrak{A}(\mathfrak{u})\times\mathfrak{A}(\mathfrak{v})}}\right]\log_2\left[\frac{1}{\sqrt{\mathfrak{A}(\mathfrak{u})\times\mathfrak{A}(\mathfrak{v})}}\right].$$

$$(15)$$

(viii) Fifth ND entropy.

If $\mathbb{I}(\mathsf{uv}) = \mathfrak{A}(\mathfrak{u})/\mathfrak{A}(\mathfrak{v}) + \mathfrak{A}(\mathfrak{v})/\mathfrak{A}(\mathfrak{u})$, then

$$\sum_{\mathsf{uv}\in\mathfrak{E}(\mathfrak{B})}\mathbb{I}(\mathsf{uv}) = \sum_{\mathsf{uv}\in\mathfrak{E}(\mathfrak{B})}\left[\frac{\mathfrak{A}(\mathfrak{u})}{\mathfrak{A}(\mathfrak{v})} + \frac{\mathfrak{A}(\mathfrak{v})}{\mathfrak{A}(\mathfrak{u})}\right] = \mathbb{ND}_5. \quad (16)$$

So, equation (8) is called the fifth ND entropy.

$$\mathfrak{E}_{\mathbb{ND}_5}(\mathfrak{B}) = \log_2\left(\mathbb{ND}_5\right) - \frac{1}{\left(\mathbb{ND}_5\right)}\sum_{i=1}^{q}\sum_{\mathsf{uv}\in\mathfrak{E}_i(\mathfrak{B})}$$

$$\cdot\left[\frac{\mathfrak{A}(\mathfrak{u})}{\mathfrak{A}(\mathfrak{v})} + \frac{\mathfrak{A}(\mathfrak{v})}{\mathfrak{A}(\mathfrak{u})}\right]\log_2\left[\frac{\mathfrak{A}(\mathfrak{u})}{\mathfrak{A}(\mathfrak{v})} + \frac{\mathfrak{A}(\mathfrak{v})}{\mathfrak{A}(\mathfrak{u})}\right].$$

$$(17)$$

(ix) Sixth ND entropy

If $\mathbb{I}(\mathsf{uv}) = \mathfrak{d}(\mathfrak{r})\mathfrak{A}(\mathfrak{u}) + \mathfrak{d}(\mathfrak{s})\mathfrak{A}(\mathfrak{v})$, then

$$\sum_{\mathsf{uv}\in\mathfrak{E}(\mathfrak{B})}\mathbb{I}(\mathsf{uv}) = \sum_{\mathsf{uv}\in\mathfrak{E}(\mathfrak{B})}\left[\mathfrak{d}(\mathfrak{r})\mathfrak{A}(\mathfrak{u}) + \mathfrak{d}(\mathfrak{s})\mathfrak{A}(\mathfrak{v})\right] = \mathbb{ND}_6. \quad (18)$$

So, equation (9) is called the sixth ND entropy.

$$\mathfrak{E}_{\mathbb{ND}_6}(\mathfrak{B}) = \log_2\left(\mathbb{ND}_6\right) - \frac{1}{\left(\mathbb{ND}_6\right)}\sum_{i=1}^{q}\sum_{\mathsf{uv}\in\mathfrak{E}_i(\mathfrak{B})}$$

$$\cdot\left[\mathfrak{d}(\mathfrak{r})\mathfrak{A}(\mathfrak{u}) + \mathfrak{d}(\mathfrak{s})\mathfrak{A}(\mathfrak{v})\right]\log_2 \quad (19)$$

$$\cdot\left[\mathfrak{d}(\mathfrak{r})\mathfrak{A}(\mathfrak{u}) + \mathfrak{d}(\mathfrak{s})\mathfrak{A}(\mathfrak{v})\right].$$

(x) Neighborhood version of SK entropy

If $\mathbb{I}(\mathsf{uv}) = \mathfrak{A}(\mathfrak{u}) + \mathfrak{A}(\mathfrak{v})/2$, then

$$\sum_{\mathsf{uv}\in\mathfrak{E}(\mathfrak{B})}\mathbb{I}(\mathsf{uv}) = \sum_{\mathsf{uv}\in\mathfrak{E}(\mathfrak{B})}\left[\frac{\mathfrak{A}(\mathfrak{u}) + \mathfrak{A}(\mathfrak{v})}{2}\right] = \mathbb{SK}_N. \quad (20)$$

So, equation (10) is called the neighborhood version of SK entropy.

$$\mathfrak{E}_{\mathbb{SK}_N}(\mathfrak{B}) = \log_2\left(\mathbb{SK}_N\right) - \frac{1}{\left(\mathbb{SK}_N\right)}\sum_{i=1}^{q}\sum_{\mathsf{uv}\in\mathfrak{E}_i(\mathfrak{B})}$$

$$\cdot\left[\frac{\mathfrak{A}(\mathfrak{u}) + \mathfrak{A}(\mathfrak{v})}{2}\right]\log_2\left[\frac{\mathfrak{A}(\mathfrak{u}) + \mathfrak{A}(\mathfrak{v})}{2}\right].$$

$$(21)$$

(xi) Neighborhood version of first SK entropy.

If $\mathbb{I}(\mathsf{uv}) = \mathfrak{A}(\mathfrak{u}) \times \mathfrak{A}(\mathfrak{v})/2$, then

$$\sum_{\mathsf{uv}\in\mathfrak{E}(\mathfrak{B})}\mathbb{I}(\mathsf{uv}) = \sum_{\mathsf{uv}\in\mathfrak{E}(\mathfrak{B})}\left[\frac{\mathfrak{A}(\mathfrak{u}) \times \mathfrak{A}(\mathfrak{v})}{2}\right] = \mathbb{SK}_{1N}. \quad (22)$$

So, equation (11) is called the neighborhood version of SK entropy.

$$\mathfrak{E}_{\mathbb{SK}_{1N}}(\mathfrak{B}) = \log_2\left(\mathbb{SK}_{1N}\right) - \frac{1}{\left(\mathbb{SK}_{1N}\right)}\sum_{i=1}^{q}\sum_{\mathsf{uv}\in\mathfrak{E}_i(\mathfrak{B})}$$

$$\cdot\left[\frac{\mathfrak{A}(\mathfrak{u}) \times \mathfrak{A}(\mathfrak{v})}{2}\right]\log_2\left[\frac{\mathfrak{A}(\mathfrak{u}) \times \mathfrak{A}(\mathfrak{v})}{2}\right].$$

$$(23)$$

(xii) Neighborhood version of second SK entropy.

If $\mathbb{I}(\mathsf{uv}) = [\mathfrak{A}(\mathfrak{u}) + \mathfrak{A}(\mathfrak{v})/2]^2$, then

$$\sum_{\mathsf{uv}\in\mathfrak{E}(\mathfrak{B})}\mathbb{I}(\mathsf{uv}) = \sum_{\mathsf{uv}\in\mathfrak{E}(\mathfrak{B})}\left[\frac{\mathfrak{A}(\mathfrak{u}) + \mathfrak{A}(\mathfrak{v})}{2}\right]^2 = \mathbb{SK}_{1N}. \quad (24)$$

So, equation (12) is called the neighborhood version of SK entropy.

$$\mathfrak{E}_{\mathbb{SK}_{2N}}(\mathfrak{B}) = \log_2\left(\mathbb{SK}_{2N}\right) - \frac{1}{\left(\mathbb{SK}_{2N}\right)}\sum_{i=1}^{q}\sum_{\mathsf{uv}\in\mathfrak{E}_i(\mathfrak{B})}$$

$$\cdot\left[\frac{\mathfrak{A}(\mathfrak{u}) + \mathfrak{A}(\mathfrak{v})}{2}\right]^2\log_2\left[\frac{\mathfrak{A}(\mathfrak{u}) + \mathfrak{A}(\mathfrak{v})}{2}\right]^2.$$

$$(25)$$

(xiii) Neighborhood version of modified Randić entropy.

If $\mathbb{I}(\mathsf{uv}) = 1/\max\{\mathfrak{A}(\mathfrak{u}), \mathfrak{A}(\mathfrak{v})\}$, then

$$\sum_{\mathsf{uv}\in\mathfrak{E}(\mathfrak{B})}\mathbb{I}(\mathsf{uv}) = \sum_{\mathsf{uv}\in\mathfrak{E}(\mathfrak{B})}\left[\frac{1}{\max\{\mathfrak{A}(\mathfrak{u}), \mathfrak{A}(\mathfrak{v})\}}\right] = {}^m\mathbb{R}_N. \quad (26)$$

So, equation (13) is called the neighborhood version of modified Randić entropy.

$$\mathfrak{E}_{m\mathbb{R}_N}(\mathfrak{B}) = \log_2\left({}^m\mathbb{R}_N\right) - \frac{1}{\left({}^m\mathbb{R}_N\right)}\sum_{i=1}^{q}\sum_{\mathsf{uv}\in\mathfrak{E}_i(\mathfrak{B})}$$

$$\cdot\left[\frac{1}{\max\{\mathfrak{A}(\mathfrak{u}), \mathfrak{A}(\mathfrak{v})\}}\right]\log_2\left[\frac{1}{\max\{\mathfrak{A}(\mathfrak{u}), \mathfrak{A}(\mathfrak{v})\}}\right].$$

$$(27)$$

(xiv) Neighborhood version of redefined first Zagreb entropy.

If $\mathbb{I}(\mathsf{uv}) = \mathfrak{A}(\mathfrak{u}) + \mathfrak{A}(\mathfrak{v})/\mathfrak{A}(\mathfrak{u}) \times \mathfrak{A}(\mathfrak{v})$, then

$$\sum_{\mathsf{uv}\in\mathfrak{E}(\mathfrak{B})}\mathbb{I}(\mathsf{uv}) = \sum_{\mathsf{uv}\in\mathfrak{E}(\mathfrak{B})}\left[\frac{\mathfrak{A}(\mathfrak{u}) + \mathfrak{A}(\mathfrak{v})}{\mathfrak{A}(\mathfrak{u}) \times \mathfrak{A}(\mathfrak{v})}\right] = \mathbb{R}ez_{1N}. \quad (28)$$

So, equation (14) is called the neighborhood version of redefined first Zagreb entropy.

$$\mathfrak{E}_{\mathbb{R}ez_{1N}}(\mathfrak{B}) = \log_2\left(\mathbb{R}ez_{1N}\right) - \frac{1}{\left(\mathbb{R}ez_{1N}\right)} \sum_{i=1}^{q} \sum_{uv \in \mathfrak{E}_i(\mathfrak{B})}$$

$$\cdot \left[\frac{\mathfrak{A}(\mathfrak{u}) + \mathfrak{A}(\mathfrak{v})}{\mathfrak{A}(\mathfrak{u}) \times \mathfrak{A}(\mathfrak{v})}\right] \log_2\left[\frac{\mathfrak{A}(\mathfrak{u}) + \mathfrak{A}(\mathfrak{v})}{\mathfrak{A}(\mathfrak{u}) \times \mathfrak{A}(\mathfrak{v})}\right]. \tag{29}$$

(xv) Neighborhood version of redefined second Zagreb entropy.

If $\mathbb{I}(uv) = \mathfrak{A}(\mathfrak{u}) \times \mathfrak{A}(\mathfrak{v})/\mathfrak{A}(\mathfrak{u}) + \mathfrak{A}(\mathfrak{v})$, then

$$\sum_{uv \in \mathfrak{E}(\mathfrak{B})} \mathbb{I}(uv) = \sum_{uv \in \mathfrak{E}(\mathfrak{B})}\left[\frac{\mathfrak{A}(\mathfrak{u}) \times \mathfrak{A}(\mathfrak{v})}{\mathfrak{A}(\mathfrak{u}) + \mathfrak{A}(\mathfrak{v})}\right] = \mathbb{R}ez_{2N}. \tag{30}$$

So, equation (15) is called the neighborhood version of redefined second Zagreb entropy.

$$\mathfrak{E}_{\mathbb{R}ez_{2N}}(\mathfrak{B}) = \log_2\left(\mathbb{R}ez_{2N}\right) - \frac{1}{\left(\mathbb{R}ez_{2N}\right)} \sum_{i=1}^{q} \sum_{uv \in \mathfrak{E}_i(\mathfrak{B})}$$

$$\cdot \left[\frac{\mathfrak{A}(\mathfrak{u}) \times \mathfrak{A}(\mathfrak{v})}{\mathfrak{A}(\mathfrak{u}) + \mathfrak{A}(\mathfrak{v})}\right] \log_2\left[\frac{\mathfrak{A}(\mathfrak{u}) \times \mathfrak{A}(\mathfrak{v})}{\mathfrak{A}(\mathfrak{u}) + \mathfrak{A}(\mathfrak{v})}\right]. \tag{31}$$

(xvi) Neighborhood version of atom bond connectivity entropy.

If $\mathbb{I}(uv) = \sqrt{\mathfrak{A}(\mathfrak{u}) + \mathfrak{A}(\mathfrak{v}) - 2/\mathfrak{A}(\mathfrak{u}) \times \mathfrak{A}(\mathfrak{v})}$, then

$$\sum_{uv \in \mathfrak{E}(\mathfrak{B})} \mathbb{I}(uv) = \sum_{uv \in \mathfrak{E}(\mathfrak{B})}\left[\sqrt{\frac{\mathfrak{A}(\mathfrak{u}) + \mathfrak{A}(\mathfrak{v}) - 2}{\mathfrak{A}(\mathfrak{u}) \times \mathfrak{A}(\mathfrak{v})}}\right] = ABC_N. \tag{32}$$

So, equation (16) is called the neighborhood version of atom bond connectivity entropy [31].

$$\mathfrak{E}_{ABC_N}(\mathfrak{B}) = \log_2\left(ABC_N\right) - \frac{1}{\left(ABC_N\right)} \sum_{i=1}^{q} \sum_{uv \in \mathfrak{E}_i(\mathfrak{B})}$$

$$\cdot \left[\sqrt{\frac{\mathfrak{A}(\mathfrak{u}) + \mathfrak{A}(\mathfrak{v}) - 2}{\mathfrak{A}(\mathfrak{u}) \times \mathfrak{A}(\mathfrak{v})}}\right] \log_2 \tag{33}$$

$$\cdot \left[\sqrt{\frac{\mathfrak{A}(\mathfrak{u}) + \mathfrak{A}(\mathfrak{v}) - 2}{\mathfrak{A}(\mathfrak{u}) \times \mathfrak{A}(\mathfrak{v})}}\right].$$

(xvii) Neighborhood version of geometric arithmetic entropy.

If $\mathbb{I}(uv) = 2 \times \sqrt{\mathfrak{A}(\mathfrak{u}) \times \mathfrak{A}(\mathfrak{v})}/\mathfrak{A}(\mathfrak{u}) + \mathfrak{A}(\mathfrak{v})$, then

$$\sum_{uv \in \mathfrak{E}(\mathfrak{B})} \mathbb{I}(uv) = \sum_{uv \in \mathfrak{E}(\mathfrak{B})}\left[\frac{2 \times \sqrt{\mathfrak{A}(\mathfrak{u}) \times \mathfrak{A}(\mathfrak{v})}}{\mathfrak{A}(\mathfrak{u}) + \mathfrak{A}(\mathfrak{v})}\right] = GA_N. \tag{34}$$

So, equation (17) is called the neighborhood version of geometric arithmetic entropy [31].

$$\mathfrak{E}_{GA_N}(\mathfrak{B}) = \log_2\left(GA_N\right) - \frac{1}{\left(GA_N\right)} \sum_{i=1}^{q} \sum_{uv \in \mathfrak{E}_i(\mathfrak{B})}$$

$$\cdot \left[\frac{2 \times \sqrt{\mathfrak{A}(\mathfrak{u}) \times \mathfrak{A}(\mathfrak{v})}}{\mathfrak{A}(\mathfrak{u}) + \mathfrak{A}(\mathfrak{v})}\right] \log_2 \tag{35}$$

$$\cdot \left[\frac{2 \times \sqrt{\mathfrak{A}(\mathfrak{u}) \times \mathfrak{A}(\mathfrak{v})}}{\mathfrak{A}(\mathfrak{u}) + \mathfrak{A}(\mathfrak{v})}\right].$$

2. Curvilinear Regression Analysis of Proposed Entropies

In this section, we analyze the entropies given above with the following physical characteristics of the benzene derivatives [32, 33]: critical pressure ($\mathscr{CP}$), critical temperature ($\mathscr{CT}$), critical volume ($\mathscr{CV}$), Gibb's energy ($\mathsf{q}\mathscr{E}$), $\log(P)$, molar refractivity ($\mathscr{MR}$), and Henry's law ($\mathscr{HL}$). The experimental values of physical characteristics of benzene derivatives have been referred to from [34] and presented in Table 1. We have presented the values of the proposed indices for the benzene derivatives in Tables 2 and 3. Figures 3 and 4 illustrate the structure of benzene derivatives.

We analyze the topological indices vis a vis the physical characteristics using the following regression models:

$$\mathfrak{P} = \tilde{a} + \tilde{b}\mathsf{X}, \tag{36}$$

where $\mathfrak{P}$ is the physical property, $\mathfrak{X}$ is the entropy, and $\tilde{a}$ and $\tilde{b}$ represent the coefficient and constant, respectively. For the seven physicochemical properties, we found the correlation between the properties and the seventeen entropies proposed by us. We now present the analysis of the linear model based on the R^2 value. Based on the recommendations of the International Academy of Mathematical Chemistry (IAMC), we have only considered regression models with $R^2 \geq 0.8$.

2.1. Linear Regression Models. Using equation (36), we obtained the linear regression models (LRM) for the seven physicochemical properties via each of the proposed indices, and the results are presented in Tables 4–9.

Table 4 shows the relation between entropy and critical temperature. In Table 4, we can easily see that all the entropies show the highest positive correlation with critical temperature. The most significant regression models are shown as follows:

$$\mathscr{CT} = -159.668 + 185.780\mathfrak{E}_{GA_N}$$

$$\mathscr{CT} = -168.156 + 191.581\mathfrak{E}_{\mathbb{ND}_6}$$

$$\mathscr{CT} = -111.034 + 177.475\mathfrak{E}_{\mathbb{ND}_4}$$

$$\mathscr{CT} = -161.636 + 187.887\mathfrak{E}_{\mathbb{R}ez_{1N}} \tag{37}$$

$$\mathscr{CT} = -148.444 + 182.909\mathfrak{E}_{ABC_N}$$

$$\mathscr{CT} = -165.387 + 664\mathfrak{E}_{\mathbb{R}ez_{2N}}.$$

Figure 5 shows that all the points fall near the fitted line. From all entropies, the fifth geometric arithmetic entropy

TABLE 1: The physical characteristics of benzene derivatives.

Chemical structures	CP	HL	GE	CT	$\log(P)$	CV	MR
Benzene ($\mathfrak{S}_1$)	47.69	0.66	121.68	323.79	2.03	263.5	25.28
Naphthalene ($\mathfrak{S}_2$)	38.97	1.67	252.38	484.95	3.03	409.5	42.45
Phenanthrene ($\mathfrak{S}_3$)	32.43	2.68	383.08	586.11	4.03	555.5	59.62
Anthracene ($\mathfrak{S}_4$)	32.43	2.68	383.08	586.11	4.03	555.5	59.62
Chrysene ($\mathfrak{S}_5$)	27.41	3.69	513.78	650.8	5.03	701.5	76.79
Benz[a]anthrene ($\mathfrak{S}_6$)	27.41	3.69	513.78	650.8	5.03	701.5	76.79
Triphenylene ($\mathfrak{S}_7$)	27.41	3.69	513.78	650.8	5.03	701.5	76.79
Tetracene ($\mathfrak{S}_8$)	27.41	3.69	513.78	650.8	5.9	701.5	76.79
Benzo[a]pyrene ($\mathfrak{S}_9$)	26.08	4.48	621.88	689.17	5.34	765.5	85.53
Benzo[e]pyrene ($\mathfrak{S}_{10}$)	26.08	4.48	621.88	689.17	5.34	765.5	85.53
Perylene ($\mathfrak{S}_{11}$)	26.08	4.48	621.88	689.17	5.34	765.5	85.53
Benzo[ghi]perylene ($\mathfrak{S}_{12}$)	24.85	5.27	729.98	728.06	5.66	829.5	94.28
Dibenzo[a, c]anthracene ($\mathfrak{S}_{13}$)	23.47	4.7	644.48	714.53	6.02	847.5	93.96
Dibenzo[a, h]anthracene ($\mathfrak{S}_{14}$)	23.47	4.7	644.48	714.53	6.02	847.5	93.96
Dibenzo[a, j]anthracene ($\mathfrak{S}_{15}$)	23.47	4.7	644.48	714.53	6.02	847.5	93.96
Picene ($\mathfrak{S}_{16}$)	23.47	4.7	644.48	714.53	6.02	847.5	93.96
Coronene ($\mathfrak{S}_{17}$)	23.7	6.06	838.08	767.68	5.98	893.5	103.02
Pyrene ($\mathfrak{S}_{18}$)	30.73	3.47	491.18	625.65	5.08	619.5	68.36

TABLE 2: Numerical values of neighborhood version of entropies.

Compound	$\mathfrak{E}_{F_N^*}$	$\mathfrak{E}_{M_2^*}$	$\mathfrak{E}_{HM_N}$	$\mathfrak{E}_{ND_1}$	$\mathfrak{E}_{ND_2}$	$\mathfrak{E}_{ND_3}$	$\mathfrak{E}_{ND_4}$	$\mathfrak{E}_{ND_5}$	$\mathfrak{E}_{ND_6}$
$\mathfrak{S}_1$	2.5850	2.5850	2.5850	2.5849	2.5849	2.5849	2.5849	2.5849	2.5849
$\mathfrak{S}_2$	3.3565	3.3599	3.3583	3.4344	3.4532	3.2416	3.4359	3.4591	3.3767
$\mathfrak{S}_3$	3.8466	3.8645	3.8647	3.9651	3.9911	3.7126	3.9032	3.9991	3.8986
$\mathfrak{S}_4$	3.9062	3.9048	3.9056	3.9739	3.9928	3.8095	3.9710	3.9997	3.8981
$\mathfrak{S}_5$	4.2601	4.2575	4.2591	4.3568	3.3413	4.1134	3.7453	4.3912	4.2926
$\mathfrak{S}_6$	4.2712	4.2832	4.2720	4.3628	4.3842	4.1699	4.3599	4.3918	4.3107
$\mathfrak{S}_7$	4.2158	4.2103	4.2135	4.3429	4.3794	4.0333	4.3426	4.3908	4.3401
$\mathfrak{S}_8$	4.3140	4.3120	4.3131	4.3694	4.3856	4.2373	4.3642	4.3921	4.3302
$\mathfrak{S}_9$	4.4504	4.4433	4.4485	4.3480	4.5756	4.2959	4.5477	4.5843	4.4903
$\mathfrak{S}_{10}$	4.4259	4.3587	4.3633	4.5403	4.2838	4.4725	4.5395	4.5839	4.4729
$\mathfrak{S}_{11}$	4.4286	4.4206	4.4249	4.5410	4.5738	4.2550	4.5408	4.5840	4.4736
$\mathfrak{S}_{12}$	4.6133	4.6055	4.6097	4.7157	4.7451	5.2290	4.7159	4.7542	4.6580
$\mathfrak{S}_{13}$	4.5561	4.5506	4.5538	4.6600	4.6984	4.3997	4.6580	4.6935	4.5958
$\mathfrak{S}_{14}$	4.5925	4.5901	4.5915	4.6704	4.6922	4.4770	4.6671	4.6998	4.6181
$\mathfrak{S}_{15}$	4.5925	4.5901	4.5915	4.6704	4.6922	4.4770	4.6671	4.6998	4.6181
$\mathfrak{S}_{16}$	4.5753	4.5711	4.5736	4.6659	4.6912	4.4366	4.6640	4.6991	4.6118
$\mathfrak{S}_{17}$	4.7805	4.7735	4.7771	4.8729	4.8988	4.6252	4.8752	4.9064	4.8235
$\mathfrak{S}_{18}$	4.1111	4.1079	4.1096	4.2131	4.2396	4.1095	4.2160	4.2476	4.1527

TABLE 3: Numerical values of neighborhood version of entropies.

Compound	$\mathfrak{E}_{SK_N}$	$\mathfrak{E}_{SK_{1N}}$	$\mathfrak{E}_{SK_{2N}}$	$\mathfrak{E}_{mR_N}$	$\mathfrak{E}_{Rez_{1N}}$	$\mathfrak{E}_{Rez_{2N}}$	$\mathfrak{E}_{ABC_N}$	$\mathfrak{E}_{GA_N}$
$\mathfrak{S}_1$	2.5849	2.5849	2.5849	2.5849	2.5849	2.5849	2.5849	2.5849
$\mathfrak{S}_2$	3.4338	3.3599	3.3624	3.4244	3.4367	3.4350	3.4561	3.4594
$\mathfrak{S}_3$	3.2830	3.6126	3.8647	3.9533	3.9096	3.9479	3.9950	3.9999
$\mathfrak{S}_4$	3.9265	3.9048	3.9056	3.8641	3.9603	3.9738	3.9959	3.9990
$\mathfrak{S}_5$	4.3567	4.2575	4.1429	4.3448	4.3569	4.3491	3.3869	4.3922
$\mathfrak{S}_6$	4.3628	4.2832	4.2841	4.3182	4.3603	4.3627	4.3875	4.3923
$\mathfrak{S}_7$	4.3431	4.2103	4.2985	4.3334	4.3436	4.3426	3.3847	4.3922
$\mathfrak{S}_8$	4.3695	4.3120	4.3131	4.3609	4.3642	4.3691	3.3884	4.3923
$\mathfrak{S}_9$	4.5488	4.4462	4.4485	4.5563	4.5480	4.5482	4.5791	4.5849
$\mathfrak{S}_{10}$	4.5409	4.4183	4.4224	4.5360	4.5397	4.5395	4.7898	4.5849
$\mathfrak{S}_{11}$	4.5417	4.4206	4.4249	4.2940	4.5213	4.5401	4.5777	4.5849
$\mathfrak{S}_{12}$	4.7165	4.6353	4.6097	4.7149	4.7158	4.7148	4.7483	4.7548
$\mathfrak{S}_{13}$	4.6603	4.5506	4.7847	4.6495	4.6588	4.6208	4.6940	4.7004
$\mathfrak{S}_{14}$	4.6535	4.5901	4.5915	4.6583	4.6675	4.6702	4.6702	4.6955
$\mathfrak{S}_{15}$	4.6535	4.5901	4.5915	4.6583	4.6675	4.6702	4.6702	4.6955
$\mathfrak{S}_{16}$	4.6660	4.5711	4.5736	4.6537	4.6647	4.6656	4.6949	4.7004
$\mathfrak{S}_{17}$	4.8736	4.7735	4.7771	4.8707	4.8750	4.8819	4.9012	4.9069
$\mathfrak{S}_{18}$	4.2132	4.1079	4.1096	4.2111	4.2162	4.2129	4.2426	4.2479
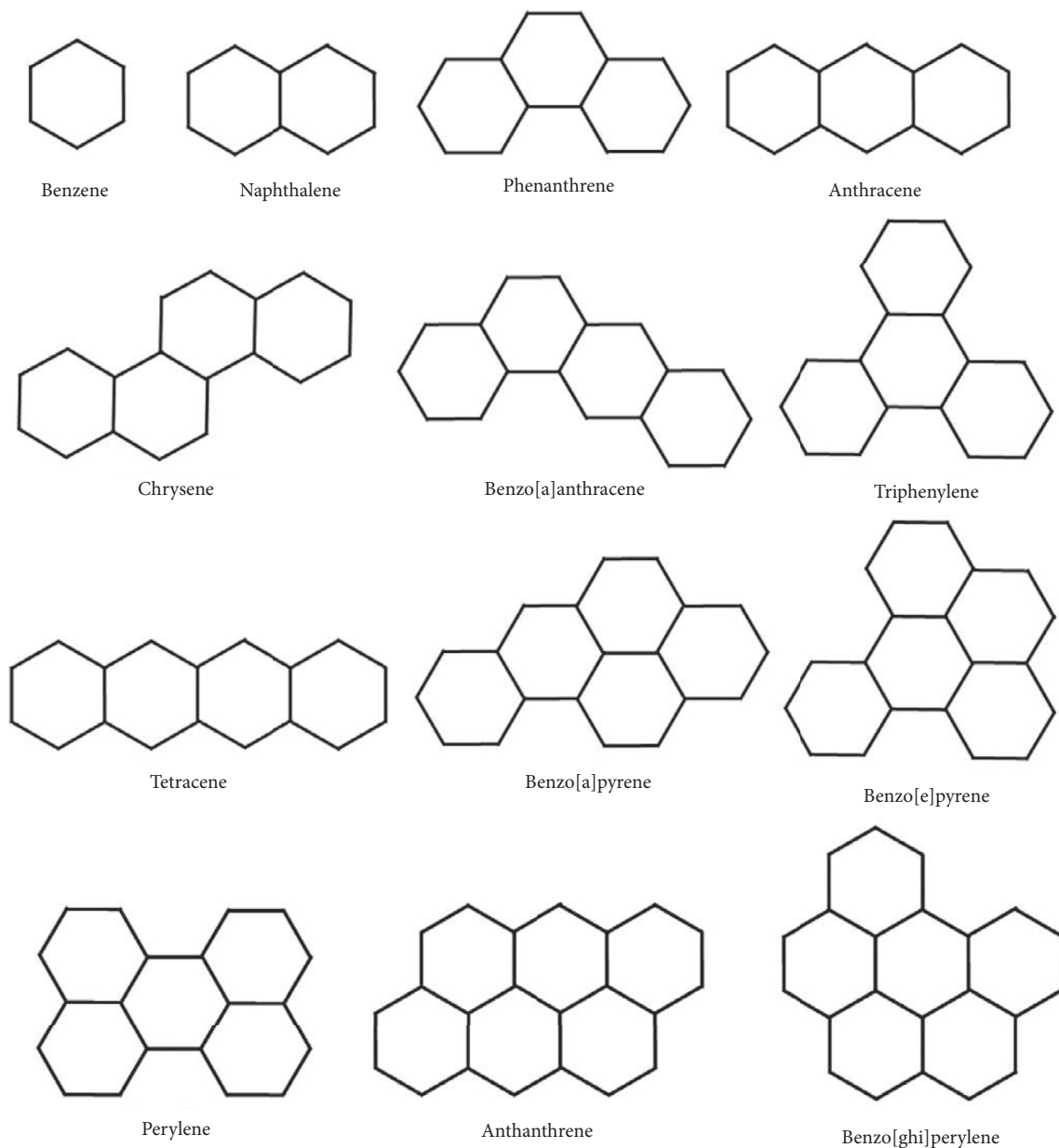
FIGURE 3: An illustration of benzene derivatives for the first type.

shows the best relation with critical temperature ($\mathscr{CT}$). So, the critical temperature can be predicted by using the fifth geometric arithmetic entropy.

Table 5 shows the relation between entropy and critical pressure ($\mathscr{CP}$), and all the entropies show the highest positive correlation with critical pressure. The most significant regression models are shown as follows:

$$\begin{aligned}
\mathscr{CP} &= 77.137 - 11.477\mathfrak{C}_{\mathbb{SK}_{2N}} \\
\mathscr{CP} &= 96.285 - 11.005\mathfrak{C}_{\mathbb{ND}_4} \\
\mathscr{CP} &= 77.014 - 11.192\mathfrak{C}_{\mathbb{ND}_5} \\
\mathscr{CP} &= 77.547 - 11.545\mathfrak{C}_{\mathbb{ND}_6} \\
\mathscr{CP} &= 76.958 - 11.329\mathfrak{C}_{\mathfrak{m}\mathbb{R}_N} \\
\mathscr{CP} &= 77.121 - 11.314\mathfrak{C}_{\mathbb{R}ez_{1N}}.
\end{aligned} \tag{38}$$

Dibenzo(a,c)anthracene

Dibenzo(a,h)anthracene

Dibenzo(a,j)anthracene

Picene

Coronene

Dibenzo(a,h)pyrene

Dibenzo(a,i)pyrene

Dibenzo(a,l)pyrene

Pyrene
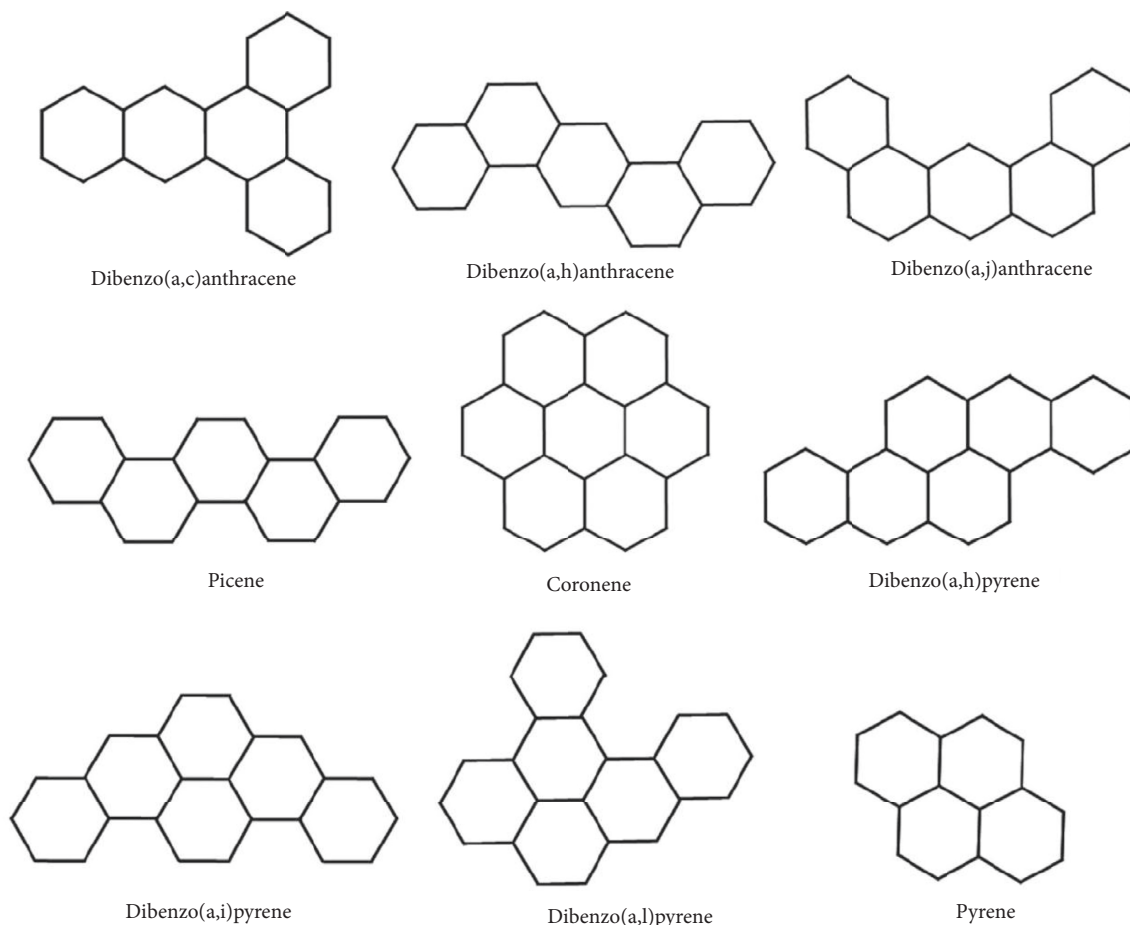
Figure 4: An illustration of benzene derivatives for the second type.

Table 4: The significant LRM: critical temperature of benzene derivatives on indices.

Entropies	$\mathfrak{R}$	$\mathfrak{R}$-square	Adj ($\mathfrak{R}^2$)	$\mathfrak{s}$
Modified neighborhood version of forgotten entropy	0.998	0.996	0.996	6.66225
Neighborhood version of second Zagreb entropy	0.998	0.996	0.996	6.87851
First ND entropy	0.998	0.997	0.996	6.59836
Second ND entropy	0.999	0.997	0.997	5.94872
Third ND entropy	0.999	0.997	0.996	6.18795
Fourth ND entropy	0.999	0.998	0.996	6.41912
Fifth ND entropy	0.999	0.998	0.997	6.12268
Sixth ND entropy	0.999	0.998	0.996	6.43054
SK entropy	0.961	0.923	0.918	29.78877
First SK entropy	0.997	0.993	0.992	9.06386
Second SK entropy	0.997	0.994	0.993	8.62473
Neighborhood version of modified Randic entropy	0.997	0.995	0.993	8.55077
Neighborhood version of redefined first Zagreb entropy	0.999	0.998	0.997	5.48691
Fourth atom bond connectivity entropy	0.999	0.998	0.997	5.71456
Neighborhood version of hyper-Zagreb entropy	0.998	0.995	0.995	7.23697
Neighborhood version of redefined second Zagreb entropy	0.999	0.998	0.997	5.4923
Fifth geometric arithmetic entropy	**0.999**	**.998**	**0.997**	**5.45456**

From all the entropies, the second *SK* entropy shows the best relation with critical pressure ($\mathscr{CP}$), and all the points fall near the fitted line shown in Figure 6. So, the critical pressure ($\mathscr{CP}$) can be predicted by using the second *SK* entropy.

Table 6 shows the relation between entropy and critical volume. From Table 6, we can easily see that all the entropies

Table 5: The significant LRM: critical pressure (CP) of benzene derivatives on indices.

Entropies	$\mathfrak{R}$	$\mathfrak{R}$-square	Adj $(\mathfrak{R}^2)$	$\mathfrak{s}$
Neighborhood version of second Zagreb entropy	0.993	0.985	0.983	0.81336
First ND entropy	0.993	0.986	0.983	0.8299
Second ND entropy	0.993	0.986	0.981	0.85676
Third ND entropy	0.994	0.988	0.983	0.812
Fourth ND entropy	0.994	0.988	0.982	0.8429
Fifth ND entropy	0.994	0.989	0.98	0.8797
Sixth ND entropy	0.995	0.989	0.979	0.90475
SK entropy	0.958	0.917	0.912	1.87022
First SK entropy	0.991	0.982	0.98	0.88984
Second SK entropy	**0.995**	**0.989**	**0.987**	**0.72501**
Neighborhood version of modified Randic entropy	0.995	0.989	0.986	0.72720
Neighborhood version of redefined first Zagreb entropy	0.995	0.989	0.985	0.77312
Fourth atom bond connectivity entropy	0.995	0.990	0.984	0.7966
Neighborhood version of hyper-Zagreb entropy	0.992	0.985	0.984	0.79918
Neighborhood version of redefined second Zagreb entropy	0.992	0.985	0.983	0.825
Fifth geometric arithmetic entropy	0.994	0.988	0.986	0.75756

Table 6: The significant LRM: critical volume of benzene derivatives on indices.

Entropies	$\mathfrak{R}$	$\mathfrak{R}$-square	Adj $(\mathfrak{R}^2)$	$\mathfrak{s}$
Modified neighborhood version of forgotten entropy	0.981	0.963	0.961	33.08152
Neighborhood version of second Zagreb entropy	0.982	0.964	0.959	33.90248
First ND entropy	0.982	0.965	0.957	34.7795
Second ND entropy	0.982	0.965	0.954	36.03779
Third ND entropy	0.982	0.965	0.95	37.50893
Fourth ND entropy	0.982	0.965	0.946	39.09405
Fifth ND entropy	**0.991**	**0.983**	**0.967**	**30.46046**
Sixth ND entropy	0.987	0.974	0.956	35.1254
SK entropy	0.961	0.923	0.918	47.88923
First SK entropy	0.982	0.965	0.961	33.26689
Second SK entropy	0.984	0.968	0.961	33.15523
Neighborhood version of modified Randic entropy	0.984	0.968	0.958	34.26668
Neighborhood version of redefined first Zagreb entropy	0.985	0.971	0.959	34.09436
Fourth atom bond connectivity entropy	0.986	0.971	0.956	35.26197
Neighborhood version of hyper-Zagreb entropy	0.981	0.962	0.959	33.85292
Neighborhood version of redefined second Zagreb entropy	0.982	0.964	0.959	33.95369
Fifth geometric arithmetic entropy	0.982	0.964	0.956	35.14404

Table 7: The significant LRM: Gibb's energy (GE) of benzene derivatives on indices.

Entropies	$\mathfrak{R}$	$\mathfrak{R}$-square	Adj $(\mathfrak{R}^2)$	$\mathfrak{s}$
Modified neighborhood version of forgotten entropy	0.957	0.917	0.911	51.08458
Neighborhood version of second Zagreb entropy	0.960	0.922	0.912	50.92216
First ND entropy	0.962	0.925	0.908	51.96242
Second ND entropy	0.963	0.927	0.904	53.0685
Third ND entropy	0.967	0.935	0.909	51.91691
Fourth ND entropy	0.967	0.936	0.901	54.00602
Fifth ND entropy	0.973	0.946	0.908	52.04307
Sixth ND entropy	**0.978**	**0.956**	**0.917**	**49.48688**
SK entropy	0.943	0.889	0.882	58.99765
First SK entropy	0.959	0.92	0.91	51.58078
Second SK entropy	0.960	0.921	0.904	53.17509
Neighborhood version of modified Randic entropy	0.960	0.922	0.898	54.93049
Neighborhood version of redefined first Zagreb entropy	0.960	0.922	0.889	57.16546
Fourth atom bond connectivity entropy	0.960	0.922	0.879	59.6619
Neighborhood version of hyper-Zagreb entropy	0.955	0.913	0.907	52.24284
Neighborhood version of redefined second Zagreb entropy	0.956	0.913	0.902	53.85496
Fifth geometric arithmetic entropy	0.959	0.92	0.903	53.56609

TABLE 8: The significant LRM: $\log(P)$ of benzene derivatives on indices.

Entropies	$\mathfrak{R}$	$\mathfrak{R}$-square	Adj ($\mathfrak{R}^2$)	$\mathfrak{s}$
Modified neighborhood version of forgotten entropy	0.969	0.94	0.936	0.28258
Neighborhood version of second Zagreb entropy	0.970	0.94	0.932	0.29159
First ND entropy	0.970	0.94	0.928	0.30098
Second ND entropy	0.971	0.943	0.926	0.30508
Third ND entropy	0.971	0.943	0.92	0.31671
Fourth ND entropy	0.972	0.944	0.914	0.32831
Fifth ND entropy	0.981	0.963	0.936	0.28207
Sixth ND entropy	**0.985**	**0.971**	**0.945**	**0.26278**
SK entropy	0.951	0.905	0.899	0.35614
First SK entropy	0.971	0.943	0.935	0.28406
Second SK entropy	0.972	0.945	0.933	0.28894
Neighborhood version of modified Randic entropy	0.972	0.945	0.928	0.29977
Neighborhood version of redefined first Zagreb entropy	0.977	0.955	0.936	0.28365
Fourth atom bond connectivity entropy	0.977	0.955	0.93	0.29626
Neighborhood version of hyper-Zagreb entropy	0.969	0.94	0.936	0.2827
Neighborhood version of redefined second Zagreb entropy	0.975	0.951	0.944	0.2637
Fifth geometric arithmetic entropy	0.975	0.951	0.94	0.27288

TABLE 9: The significant LRM: molar refractivity (MR) of benzene derivatives on indices.

Entropies	$\mathfrak{R}$	$\mathfrak{R}$-square	Adj ($\mathfrak{R}^2$)	$\mathfrak{s}$
Modified neighborhood version of forgotten entropy	0.981	0.962	0.96	4.02512
Neighborhood version of second Zagreb entropy	0.982	0.964	0.959	4.09119
First ND entropy	0.982	0.964	0.957	4.1829
Second ND entropy	0.982	0.964	0.954	4.34063
Third ND entropy	0.982	0.965	0.95	4.49344
Fourth ND entropy	0.982	0.965	0.946	4.67932
Fifth ND entropy	0.987	0.975	0.957	4.18104
Sixth ND entropy	**0.992**	**0.983**	**0.969**	**3.56484**
SK entropy	0.961	0.924	0.92	5.70614
First SK entropy	0.982	0.965	0.96	4.03334
Second SK entropy	0.983	0.966	0.958	4.10153
Neighborhood version of modified Randic entropy	0.983	0.966	0.955	4.25288
Neighborhood version of redefined first Zagreb entropy	0.984	0.968	0.954	4.31552
Fourth atom bond connectivity entropy	0.984	0.968	0.951	4.47577
Neighborhood version of hyper-Zagreb entropy	0.980	0.96	0.958	4.14024
Neighborhood version of redefined second Zagreb entropy	0.980	0.961	0.956	4.21432
Fifth geometric arithmetic entropy	0.981	0.962	0.953	4.34898

FIGURE 5: Graphical representation of LRM between critical temperature and the fifth geometric arithmetic entropy.
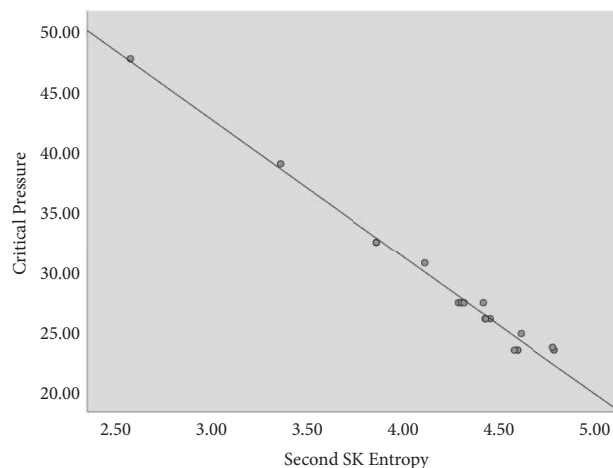
FIGURE 6: Graphical representation of LRM between critical pressure (CP) and the second SK entropy.

show the highest positive correlation with critical volume. The most significant regression models are shown as follows:

$$\mathscr{CV} = -569.955 + 293.079\mathfrak{E}_{\mathbb{ND}_5}$$

$$\mathscr{CV} = -589.308 + 303.572\mathfrak{E}_{\mathbb{ND}_6}$$

$$\mathscr{CV} = -576.671 + 297.184\mathfrak{E}_{\mathbb{R}ez_{1N}}$$

$$\mathscr{CV} = -551.360 + 288.287\mathfrak{E}_{ABC_N} \qquad (39)$$

$$\mathscr{CV} = -577.343 + 65.676\mathfrak{E}_{\mathbb{SK}_{2N}}$$

$$\mathscr{CV} = -573.522 + 297.843\mathfrak{E}_{\mathbf{m}\mathbb{R}_N}.$$

From all the entropies, the fifth ND entropy shows the best relation with critical volume ($\mathscr{CV}$), and all the points fall near the fitted line as can be seen in Figure 7. So, the critical temperature can be predicted by using the fifth ND entropy.

Table 7 shows the relation between entropy and Gibb's energy ($\mathsf{q}\mathscr{E}$) of benzene derivatives. From Table 7, we can easily see that all the entropies show the highest positive correlation with Gibb's energy ($\mathsf{q}\mathscr{E}$).

$$\mathsf{q}\mathscr{E} = -751.66 + 303.591\mathfrak{E}_{\mathbb{ND}_6}$$

$$\mathsf{q}\mathscr{E} = -732.155 + 293.063\mathfrak{E}_{\mathbb{ND}_5}$$

$$\mathsf{q}\mathscr{E} = -674.923 + 284.469\mathfrak{E}_{\mathbb{ND}_4}$$

$$\mathsf{q}\mathscr{E} = -639.259 + 283.942\mathfrak{E}_{\mathbb{ND}_3} \qquad (40)$$

$$\mathsf{q}\mathscr{E} = -725.293 + 293.202\mathfrak{E}_{\mathbb{SK}_{2N}}$$

$$\mathsf{q}\mathscr{E} = -739.593 + 297.729\mathfrak{E}_{\mathbb{ND}_1}.$$

Of all the entropies, the fifth ND entropy shows the best relation with Gibb's energy ($\mathsf{q}\mathscr{E}$), and all the points fall near the fitted line as seen in Figure 8. So, Gibb's energy can be predicted by using the sixth ND entropy.

Table 8 shows the relation between entropy and $\log(P)$. From Table 8, we can easily see that all the entropies show the highest positive correlation with critical volume. The most significant regression models are shown as follows:

$$\log(P) = -3.443 + 1.998\mathfrak{E}_{\mathbb{ND}_6}$$

$$\log(P) = -3.304 + 1.927\mathfrak{E}_{\mathbb{ND}_5}$$

$$\log(P) = -3.159 + 1.890\mathfrak{E}_{\mathbb{ND}_4}$$

$$\log(P) = -3.357 + 1.956\mathfrak{E}_{\mathbb{R}ez_{1N}} \qquad (41)$$

$$\log(P) = -3.300 + 1.925\mathfrak{E}_{GA_N}$$

$$\log(P) = -3.371 + 1.958\mathfrak{E}_{\mathbb{R}ez_{2N}}.$$

From all the entropies, the sixth ND entropy shows the best relation with $\log(P)$, and all the points fall near the fitted line as can be seen in Figure 9. So, the $\log(P)$ can be predicted by using the sixth ND entropy.

Table 9 shows the relation between entropy and molar refractivity ($\mathscr{MR}$) of benzene derivatives. From Table 9, we can easily see that all the entropies show the highest positive correlation with molar refractivity ($\mathscr{MR}$).

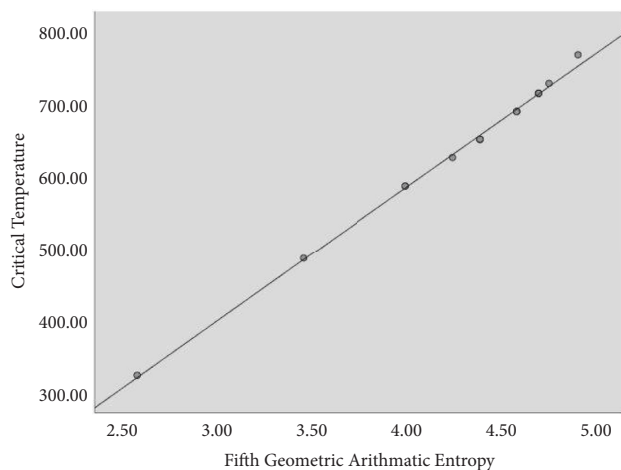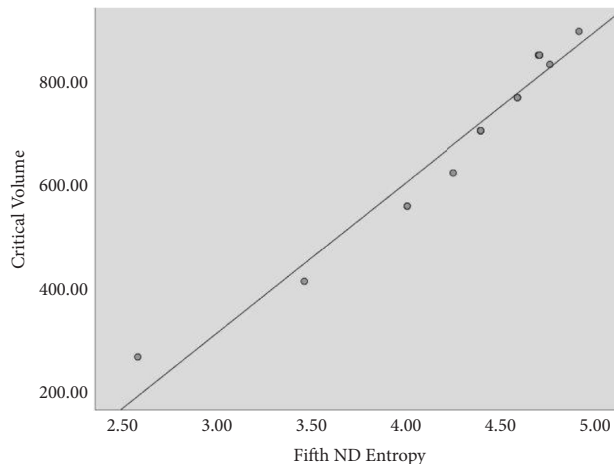Figure 7: Graphical representation of LRM between critical volume and the fifth ND entropy.
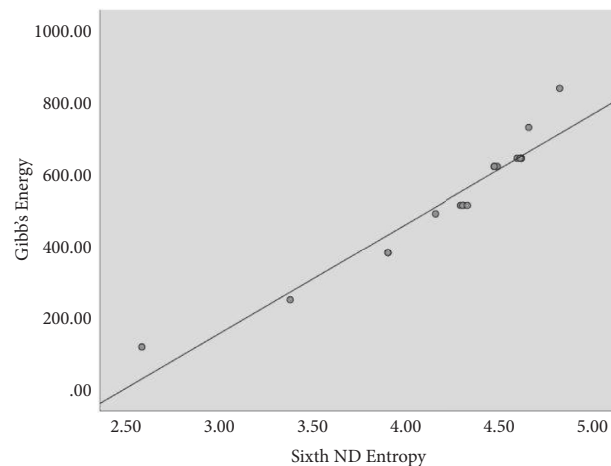
Figure 8: Graphical representation of LRM between Gibb's energy (GE) and the sixth ND entropy.
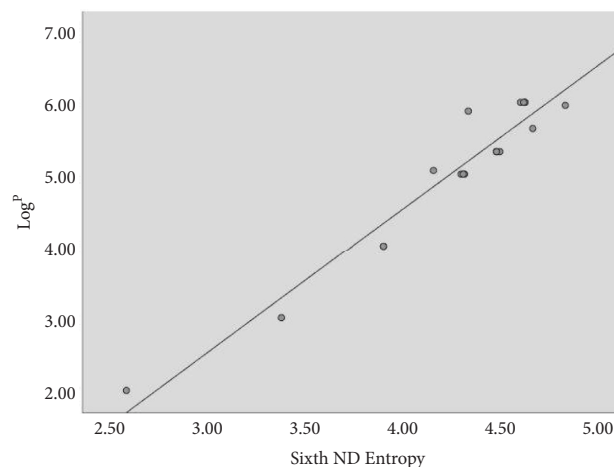
Figure 9: Graphical representation of LRM between $\log(P)$ and the sixth ND entropy.
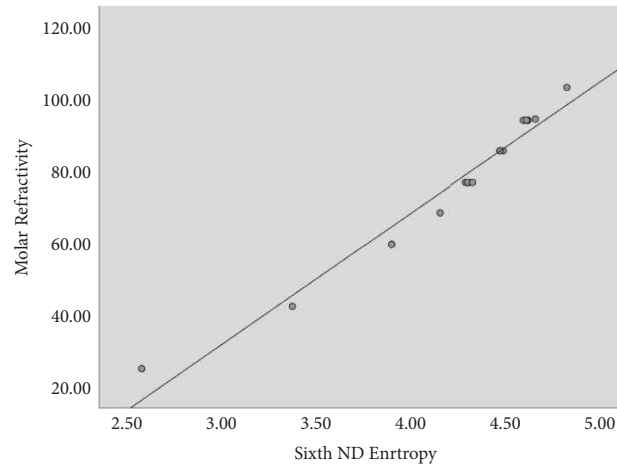
FIGURE 10: Graphical representation of LRM between molar refractivity and the sixth ND entropy.

TABLE 10: The significant LRM: Henry's law of benzene derivatives on indices.

Entropies	$\mathfrak{R}$	$\mathfrak{R}$-square	Adj ($\mathfrak{R}^2$)	$\mathfrak{s}$
Modified neighborhood version of forgotten entropy	0.962	0.926	0.921	0.36535
Neighborhood version of second Zagreb entropy	0.965	0.931	0.922	0.36445
First ND entropy	0.966	0.933	0.919	0.37174
Second ND entropy	0.967	0.935	0.915	0.38046
Third ND entropy	0.970	0.942	0.918	0.37439
Fourth ND entropy	0.971	0.942	0.911	0.38944
Fifth ND entropy	0.976	0.952	0.919	0.37152
Sixth ND entropy	**0.981**	**0.962**	**0.929**	0.3485
SK entropy	0.947	0.897	0.89	0.43156
First SK entropy	0.964	0.93	0.92	0.36835
Second SK entropy	0.964	0.93	0.915	0.38044
Neighborhood version of modified Randic entropy	0.965	0.93	0.909	0.39337
Neighborhood version of redefined first Zagreb entropy	0.965	0.93	0.901	0.40943
Fourth atom bond connectivity entropy	0.965	0.931	0.893	0.42717
Neighborhood version of hyper-Zagreb entropy	0.960	0.922	0.918	0.37422
Neighborhood version of redefined second Zagreb entropy	0.961	0.923	0.912	0.38616
Fifth geometric arithmetic entropy	0.963	0.928	0.913	0.38561

$$\mathscr{MR} = -77.645 + 36.463\mathfrak{C}_{\mathbb{ND}_6}$$
$$\mathscr{MR} = -75.316 + 35.202\mathfrak{C}_{\mathbb{ND}_5}$$
$$\mathscr{MR} = -76.136 + 35.698\mathfrak{C}_{\mathbb{R}ez_{1N}}$$
$$\mathscr{MR} = -73.151 + 34.642\mathfrak{C}_{ABC_N} \qquad (42)$$
$$\mathscr{MR} = -75.860 + 36.134\mathfrak{C}_{\mathbb{SK}_{2N}}$$
$$\mathscr{MR} = -75.730 + 35.771\mathfrak{C}_{\mathfrak{m}\mathbb{R}_N}.$$

Of all the entropies, the sixth ND entropy shows the best relation with molar refractivity ($\mathscr{MR}$), and all the points fall near the fitted line as seen in Figure 10. So, the molar refractivity can be predicted by using the sixth ND entropy.

Table 10 shows the relation between entropy and Henry's law. From Table 10, we can easily see that all the entropies show the highest positive correlation with Henry's law. The most significant regression models are shown as follows:
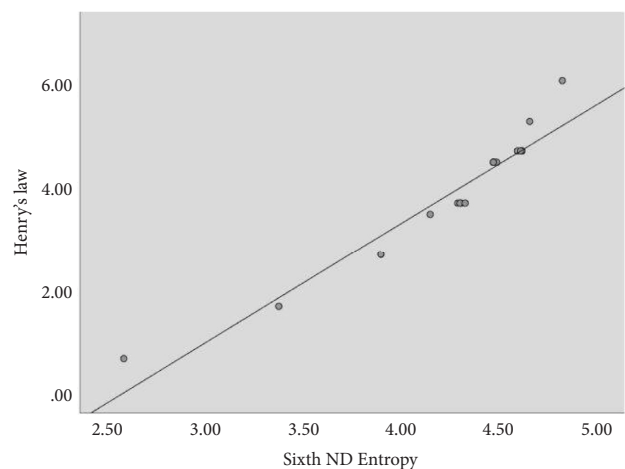
FIGURE 11: Graphical representation of LRM between Henry's law and the sixth ND entropy.

$$\mathscr{HL} = -5.991 + 2.318\mathfrak{E}_{\mathrm{ND}_6}$$

$$\mathscr{HL} = -5.842 + 2.237\mathfrak{E}_{\mathrm{ND}_5}$$

$$\mathscr{HL} = -5.395 + 2.169\mathfrak{E}_{\mathrm{ND}_4}$$

$$\mathscr{HL} = -5.102 + 2.160\mathfrak{E}_{\mathrm{ND}_3} \qquad (43)$$

$$\mathscr{HL} = -5.793 + 2.239\mathfrak{E}_{\mathrm{ND}_2}$$

$$\mathscr{HL} = -5.902 + 2.074\mathfrak{E}_{\mathrm{ND}_1}.$$

From all the entropies, the sixth ND entropy shows the best relation with Henry's law ($\mathscr{HL}$), and all the points fall near the fitted line as can be seen in Figure 11. So, Henry's law ($\mathscr{HL}$) can be predicted by using the sixth ND entropy.

3. Concluding Remarks

Quantitative structure-property relationships (QSPRs) mathematically link physical or chemical properties with the structure of a molecule. Entropies are defined on molecular structures for a better understanding of the physical features [35] and chemical reactivity. In this paper, we developed the QSPR between ND entropy and the physical characteristics of benzene derivatives. Based on the linear regression model, we analyzed that critical temperature ($\mathscr{CT}$), critical pressure ($\mathscr{CP}$), and critical volume ($\mathscr{CV}$) can be predicted through the fifth geometric arithmetic entropy, second SK entropy, and fifth ND entropy, respectively. Other remaining physical characteristics such as Gibb's energy ($\mathsf{q}\mathscr{E}$), $\log(P)$, molar refractivity ($\mathscr{MR}$), and Henry's law ($\mathscr{HL}$) can be predicted by using the sixth ND entropy.

Data Availability

The data used to support the findings of this study are cited at relevant places within the text as references.

Conflicts of Interest

The authors declare that they have no conflicts of interest.

Authors' Contributions

This work was equally contributed by all writers.

References

[1] R. Dagani, "Toxicologists seek structure-activity links," *Chemical & Engineering News Archive*, vol. 59, no. 10, pp. 26–29, 1981.

[2] M. Randic, "Quantitative structure-property relationship. Boiling points of planar benzenoids," *New Journal of Chemistry*, vol. 20, no. 10, pp. 1001–1009, 1996.

[3] H. Van De Waterbeemd and S. Rose, "Quantitative approaches to structure–activity relationships," in *The Practice of Medicinal Chemistry*, pp. 491–513, Academic Press, Cambridge, MA, USA, 2008.

[4] S. Mondal, N. De, and A. Pal, "On some new neighbourhood degree based indices," 2019, https://arxiv.org/abs/1906.11215.

[5] S. Mondal, N. De, and A. Pal, "On neighborhood Zagreb index of product graphs," *Journal of Molecular Structure*, vol. 1223, Article ID 129210, 2021.

[6] D. H. Rouvray, *Chemical Graph Theory: Introduction and Fundamentals*, D. Bonchev, Ed., vol. 2, pp. 191–200, Abacus Press, Hachette UK, 1991.

[7] M. Imran, M. K. Siddiqui, M. Naeem, and M. A. Iqbal, "On topological properties of symmetric chemical structures," *Symmetry*, vol. 10, no. 5, pp. 173–221, 2018.

[8] X. Zuo, M. Numan, S. I. Butt, M. K. Siddiqui, R. Ullah, and U. Ali, "Computing topological indices for molecules structure of Polyphenylene via M-polynomials," *Polycyclic Aromatic Compounds*, vol. 42, no. 4, pp. 1103–1112, 2022.

[9] V. Ravi and K. Desikan, "Neighbourhood degree-based topological indices of graphene structure," *Biointerface Research in Applied Chemistry*, vol. 11, no. 5, Article ID 13681, 2021.

[10] M. C. Shanmukha, N. S. Basavarajappa, A. Usha, and K. C. Shilpa, "Novel neighbourhood redefined first and second Zagreb indices on carborundum structures," *Journal of Applied Mathematics and Computing*, vol. 66, no. 1-2, pp. 263–276, 2021.

[11] X. Zhang, X. Wu, S. Akhter, M. K. Jamil, J. B. Liu, and M. R. Farahani, "Edge-version atom-bond connectivity and geometric arithmetic indices of generalized bridge molecular graphs," *Symmetry*, vol. 10, no. 12, pp. 751–786, 2018.

[12] X. Zhang, H. M. Awais, M. Javaid, and M. K. Siddiqui, "Multiplicative Zagreb indices of molecular graphs," *Journal of Chemistry*, vol. 2019, Article ID 5294198, 19 pages, 2019.

[13] X. Zhang, A. Rauf, M. Ishtiaq, M. K. Siddiqui, and M. H. Muhammad, "On degree based topological properties of two Carbon Nanotubes," *Polycyclic Aromatic Compounds*, vol. 42, no. 3, pp. 866–884, 2020.

[14] L. Boltzmann, *Lectures on gas theory*, pp. 501–512, Courier Corporation, Chelmsford, 2012.

[15] J. Gibbs, *Elementary Principles in Statistical Mechanics*, pp. 544–454, Dover Publications, New York, NY, USA, 1960.

[16] R. A. Fisher, "On the mathematical foundations of theoretical statistics," *Philosophical Transactions of the Royal Society of London - A*, vol. 222, pp. 309–368, 1922.

[17] S. Kullback and R. A. Leibler, "On information and sufficiency," *The Annals of Mathematical Statistics*, vol. 22, no. 1, pp. 79–86, 1951.

[18] X. Zhang, H. Jiang, J. B. Liu, and Z. Shao, "The cartesian product and join graphs on edge-version atom-bond connectivity and geometric arithmetic indices," *Molecules*, vol. 23, no. 7, pp. 1731–1817, 2018.

[19] X. Zhang, M. Naeem, A. Q. Baig, and M. A. Zahid, "Study of hardness of superhard crystals by topological indices," *Journal of Chemistry*, vol. 2021, Article ID 9604106, 10 pages, 2021.

[20] X. Zhang, M. K. Siddiqui, S. Javed, L. Sherin, F. Kausar, and M. H. Muhammad, "Physical analysis of heat for formation and entropy of Ceria Oxide using topological indices," *Combinatorial Chemistry & High Throughput Screening*, vol. 25, no. 3, pp. 441–450, 2022.

[21] C. E. Shannon, "A mathematical theory of communication," *Bell System Technical Journal*, vol. 27, no. 3, pp. 379–423, 1948.

[22] E. T. Jaynes, "Information theory and statistical mechanics. II," *Physical Review*, vol. 108, no. 2, pp. 171–190, 1957.

[23] E. T. Jaynes, "Information theory and statistical mechanics," *Physical Review*, vol. 106, no. 4, pp. 620–630, 1957.

[24] M. Dehmer and A. Mowshowitz, "A history of graph entropy measures," *Information Sciences*, vol. 181, no. 1, pp. 57–78, 2011.

[25] A. Mowshowitz, "Entropy and the complexity of graphs: I. An index of the relative complexity of a graph," *Bulletin of Mathematical Biophysics*, vol. 30, no. 1, pp. 175–204, 1968.

[26] N. Rashevsky, "Life, information theory, and topology," *Bulletin of Mathematical Biophysics*, vol. 17, no. 3, pp. 229–235, 1955.

[27] S. Manzoor, M. K. Siddiqui, and S. Ahmad, "On entropy measures of molecular graphs using topological indices," *Arabian Journal of Chemistry*, vol. 13, no. 8, pp. 6285–6298, 2020.

[28] R. Huang, M. K. Siddiqui, S. Manzoor, S. Ahmad, and M. Cancan, "On eccentricity-based entropy measures for dendrimers," *Heliyon*, vol. 7, no. 8, Article ID e07762, 2021.

[29] M. A. Rashid, S. Ahmad, M. K. Siddiqui, S. Manzoor, and M. Dhlamini, "An analysis of eccentricity-based invariants for biochemical hypernetworks," *Complexity*, vol. 2021, Article ID 1974642, 14 pages, 2021.

[30] S. Manzoor, M. K. Siddiqui, and S. Ahmad, "Computation of entropy measures for phthalocyanines and porphyrins dendrimers," *International Journal of Quantum Chemistry*, vol. 122, no. 5, pp. 1–15, 2022.

[31] X. L. Wang, M. K. Siddiqui, S. A. K. Kirmani, S. Manzoor, S. Ahmad, and M. Dhlamini, "On topological analysis of entropy measures for silicon carbides networks," *Complexity*, vol. 2021, Article ID 4178503, 26 pages, 2021.

[32] I. Gutman and S. J. Cyvin, *Introduction to the theory of benzenoid hydrocarbons*, pp. 542–152, Springer Science & Business Media, Berlin/Heidelberg, Germany, 2012.

[33] J. R. Dias, "Handbook of polycyclic hydrocarbons," *Part A: Benzenoid Hydrocarbons*, pp. 921–934, CRC Press, Boca Raton, Florida, 1987.

[34] R. Kanabur and V. Shigehalli, "Qspr analysis of degree-based topological indices with physical properties of benzenoid hydrocarbons," *General Letters in Mathematics*, vol. 2, no. 3, pp. 150–169, 2017.

[35] M. M. Adeva-Andany, M. Gonzalez-Lucan, C. Donapetry-Garcia, C. Fernández-Fernandez, and E. Ameneiros-Rodríguez, "Glycogen metabolism in humans," *BBA clinical*, vol. 5, pp. 85–100, 2016.

WILEY | Hindawi

Research Article

A Combined Deep CNN: LSTM with a Random Forest Approach for Breast Cancer Diagnosis

Almas Begum ⓘ,¹ V. Dhilip Kumar ⓘ,¹ Junaid Asghar ⓘ,² D. Hemalatha ⓘ,¹ and G. Arulkumaran ⓘ³

¹*Computer Science and Engineering, Vel Tech Rangarajan Dr.Sagunthala R&D Institute of Science and Technology, Avadi, Chennai, India*
²*Faculty of Pharmacy, Gomal University, Dera Ismail Khan 29050, Khyber Pakhtunkhwa, Pakistan*
³*Department of Electrical and Computer Engineering, Bule Hora University, Bule Hora, Ethiopia*

Correspondence should be addressed to G. Arulkumaran; erarulkumaran@gmail.com

The most predominant kind of disease that is normal among ladies is breast cancer. It is one of the significant reasons among ladies, regardless of huge endeavors to stay away from it through screening developers. An automatic detection system for disease helps doctors to identify and provide accurate results, thereby minimizing the death rate. Computer-aided diagnosis (CAD) has minimum intervention of humans and produces more accurate results than humans. It will be a difficult and long task that depends on the expertise of pathologists. Deep learning methods proved to give better outcomes when correlated with ML and extricate the best highlights of the images. The main objective of this paper is to propose a deep learning technique in combination with a convolution neural network (CNN) and long short-term memory (LSTM) with a random forest algorithm to diagnose breast cancer. Here, CNN is used for feature extraction, and LSTM is used for extracted feature detection. The experimental results show that the proposed system accomplishes 100% of accuracy, a sensitivity of 99%, recall of 99%, and an F1-score of 98% compared to other traditional models. As the system achieved correct results, it can help doctors to investigate breast cancer easily.

1. Introduction

Breast cancer is probably the deadliest infection influencing ladies around the world. This infection is the main source for cancer growth passing. Women may develop tumors due to the breast cells' unusual development. These huge tumor cells divide into cancer and noncancer cells depending on the region, size, and location. The term "benign" refers to the original tumor area of the noncancerous tumor, while the term "malignant" refers to the secondary tumor area of the cancerous tumor. The lives of women are not at risk from benign tumor since they are curable, and their growth can be slowed down by taking the right treatments. A malignant tumor can only be treated if the patient receives the necessary medical care, such as surgery or radiation. The disease assessment includes classes such as tumor class or not, intermittent occasion or no-repetitive occasion, and harmless

or threatening. Numerous past investigations are directed through the machine learning methods such as K-nearest neighbor, decision tree, support vector machine, and so on, which give the better presentation. However presently, an advanced approach is utilized to characterize breast cancer called deep learning to defeat machine learning. It is a procedure that is often utilized in data science, with top methods used in deep learning as convolution neural networks (CNN), recurrent neural networks (RNN), classic neural networks (multilayer perceptrons), long short term-memory networks (LSTMs), and others. Lately, deep learning has drawn in wide consideration inside the field. The calculation of clinical requirements is still deeply dependent upon, particularly related with deep learning. The utilization of significant learning demand applications has been extensively applied and has ended up in a strong methodology to face composite issues. To classify breast

cancer, some of the studies used a pretrained network or created fresh deep neural networks [1].

Worldwide, among women breast cancer is a frequent disease according to the World Health Organization. One in every three women who are impacted will die. The current analysis strategies for the disease incorporate mammography, MRI, and pathology examinations. A physical pathologist should compute what the anatomical pathology research center has created while conveying results. Due to a breast cancer patient's conclusion, a doctor's computations are out of date. As a result, it encourages the employment of computer-assisted procedures. MRI has been recognized as a better imaging technique for detecting any kind of tumor [1].

Deep learning is a computer science approach that is used. It has received a lot of interest in the field of categorization in recent years. In clinical necessities, the order calculation actually has a ton of clout, particularly assuming that it is joined with deep learning. These applications have been widely used and have shown an effective way of dealing with complicated challenges. Recent deep learning-based research has focused on the idea of medical imaging on automated CAD systems. The greatest method for classifying and recognizing medical images is deep learning. Three processes in consecutive are necessary for a deep learning-based CAD system: preprocessing and parameter, setup, and deep feature extraction and diagnosis. From the same original breast picture, deep learning techniques can be used to immediately build massive low-high levels deep hierarchical feature maps. This demonstrates that deep learning is the most effective and reliable medical imaging method when using breast image data from the same source. Deep learning is the most effective and reliable medical imaging technique.

1.1. Motivation.

Breast tumors can be successfully considered over their initial identification. Hence, the accessibility about appropriate masking strategies persists in significant recognition of an underlying indication of the disease. Different imaging techniques are used for utilization for masking and recognizing the sickness, and the notable procedures are ultrasonography, sonography, and thermography. Among these commonly used strategies for early identification of bosom disease is ultrasonography. The techniques that are prominently utilized are that ultrasonography is not successful for robust cancer.

A convolution neural network (CNN) comprises various convolution layers which can separate elements that address the different settings of images without highlight designing. Thus, CNN has turned into the most broadly involved strategy for picture translation errands in numerous areas such as the discovery and analysis of breast cancer [2]. After the accomplishment of CNNs in object location assignment [3], a few investigations have taken advantage of the benefits of deep CNNs to conquer the downsides of traditional mass identification models [4–13].

Deep learning is a classification of machine learning. According to the data selected, deep learning utilizes unsupervised learning to study the data either as unstructured or unlabeled [14]. Considering the above-said problems, little multitude can be circumvented by emission from radioactivity and thermometry which might be more compelling than the ultrasound method in diagnosing more modest but dangerous commonalities.

In this paper, we intend to bring in the concepts of deep learning techniques to diagnose breast cancer by combining CNN and LSTM, where CNN is used for feature extraction and LSTM is used for extracted feature detection.

1.2. Related Work.

Breast cancer has been adequately studied since its initial recognition. So, accessing appropriate masking strategies is significant as distinguishing every underlying indication of the disease. Different imaging methods are utilized over masking to recognize this illness; the most famous methodologies are mammography, ultrasound, and the thermograph. One of the biggest strategies for early detection of breast cancer growth is mammography. Illustrative monograph techniques are available, that are commonly used as mammography, and are not convincing over some types of breast cancer. Thinking about these complexities, little groups can be skirted by emissions from radiography, and the monograph may be more suitable than the ultrasound system in diagnosing more unassuming harmful masses [15].

These days, important evolution in computer science has occurred, for example, artificial intelligence, machine learning, and CNN are the fastest growing fields in the medical care industry [16]. These technologies are found in the examination field that manages and works on mechanical frameworks to determine complex errands by lessening the need for human insight. An investigation was performed by [17] to assess the determination of bosom disease with mammograms utilizing CNN. They show that exhibition appraisal in determination is completed on two datasets of mammographic mass, for example, DDSM-400 and CBIS-DDSM, with variations in the exactness of the comparing division guides of ground truth. In a paper [18], authors have used deep CNN to detect breast cancer automatically from various classes of images with five layers on mammograms and ultrasound.

In the earlier examination, authors [19] utilized CNNs to research mechanized identification of breast malignant growth using IDC-type. A few researchers utilized ML-based programmed location procedures to distinguish something similar, and it is intended to acquire the right results to reduce the blunders found in the finding technique. A few past investigations have proposed involving AI too such as CNN for picture recognition and medical services observing [20]. However, as for clinical side arrangement, which is about 60% for all group recognition, 75% for as it was categorized, and 100% calculative, the precision rate is excessively lacking [21]. In the paper [22], the authors have proposed a novel approach combining class structure-based deep convolution neural networks for providing reliable and accurate multi classification of breast cancer.

1.2.1. CNN Using ML.

The authors [23], proposed a framework that utilizes different convolution neural organization (CNO) models to consequently identify bosom

malignant growth, contrasting the outcomes and those from AI (ML) calculations. All structures were directed by an enormous dataset of around 275,000, 50×50-pixel RGB picture patches. The authors used machine learning classifiers such as logistic regression, logistic regression, and support vector machines.

The implementation is conducted using the sci-kit-learn machine learning framework in Python with pandas, NumPy, Matplotlib functions, and Seaborn frameworks. Four CNN models have been used to predict invasive cancer such as CNN models 1, 2, 3, and 4. To boost the quantity of highlights, convolution layers are significantly increased by three times here [6]. In CNN Model 3, the disease is more profound than Models 1 and 2, with a five-layer CNN used to distinguish the disease [24].

1.2.2. Multilayer Perceptron.

Multilayer perceptron includes generally utilized to be a strategy fit for managing complex issues. The author [25] has performed research to utilize multilayer perceptron to identify and validate by using x-fold cross-validation. A fabricated model using a dataset from Medical Center University uses multilayer perceptron, Weka 3.8, and 5-fold cross approval assessments. This model can be used to assist clinical social affairs with choosing the sorts of redundant and nonintermittent bosom harmful development [26].

Followed by Mujarad's examination that identified cancer malignant growth utilizing multifacet perceptron with a prescient exactness upsides of 65.21%. Amidst of various methodologies, multilayer perceptrons are broadly used methods for detecting cancer. They are also widely used for predicting complex types of issues in cancer with higher rates in accuracy [27]. Similar work has been carried out by authors [28] that combines CNN–LSTM to detect COVID-19 using X-rays that automatically identify the diseases before they spread. Recent research focuses on how to use deep learning-based network models to build an automated system with LSTM that accepts a patient's health records to determine the probability of being infected by breast cancer [29].

1.2.3. Random Forest Classifier.

In paper, [30] presents the exploration foundation of machine learning structure, and connected with the generally involved random forest calculation, advances the exploration destinations and content, proposes a work on versatile adaptive random forest algorithm (ARF), and based on the ARF method, construction is carried out. In another paper [31], the authors used an active contour that implies one of divisions.

Methods are used to separate the pixels of interest from the representation for examination and handling the same. In another paper [9], authors have proved random forest classifiers with decision trees that give better results during the segmentation process. Thus, in [12], authors have showed that the random forest technique has given better performance compared to other machine learning techniques. Similarly, in [32], authors have created a random
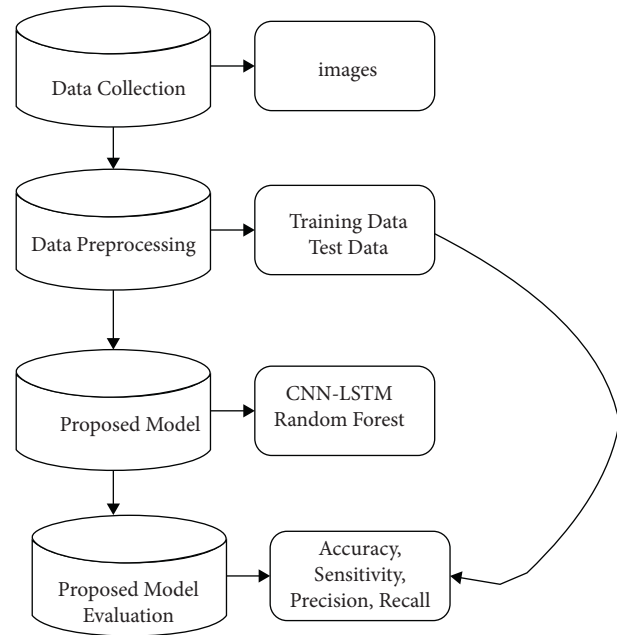
FIGURE 1: Proposed model for breast cancer.
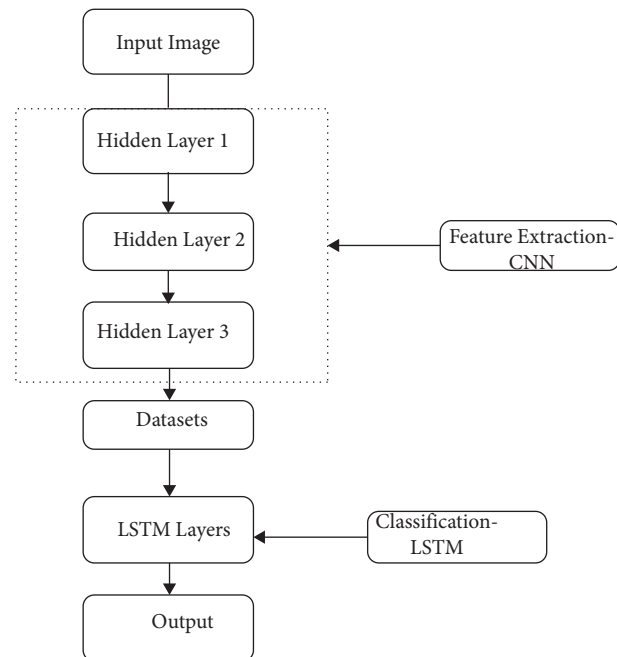
FIGURE 2: Feature extraction and classification.

forest classifier with LSTM to encode amino acids called as LEMP that gives better performance.

In a recent work, the authors [33] suggested a method that uses the modified contrast enhancement technique to improve the edges of source mammography images. To improve performance, the transferable texture convolutional neural network (TTCNN) was then proposed. In this study, the authors used an energy layer, and methods of classification are merged to extract the texture features from the layer of convolution. In another work, authors [34] proposed
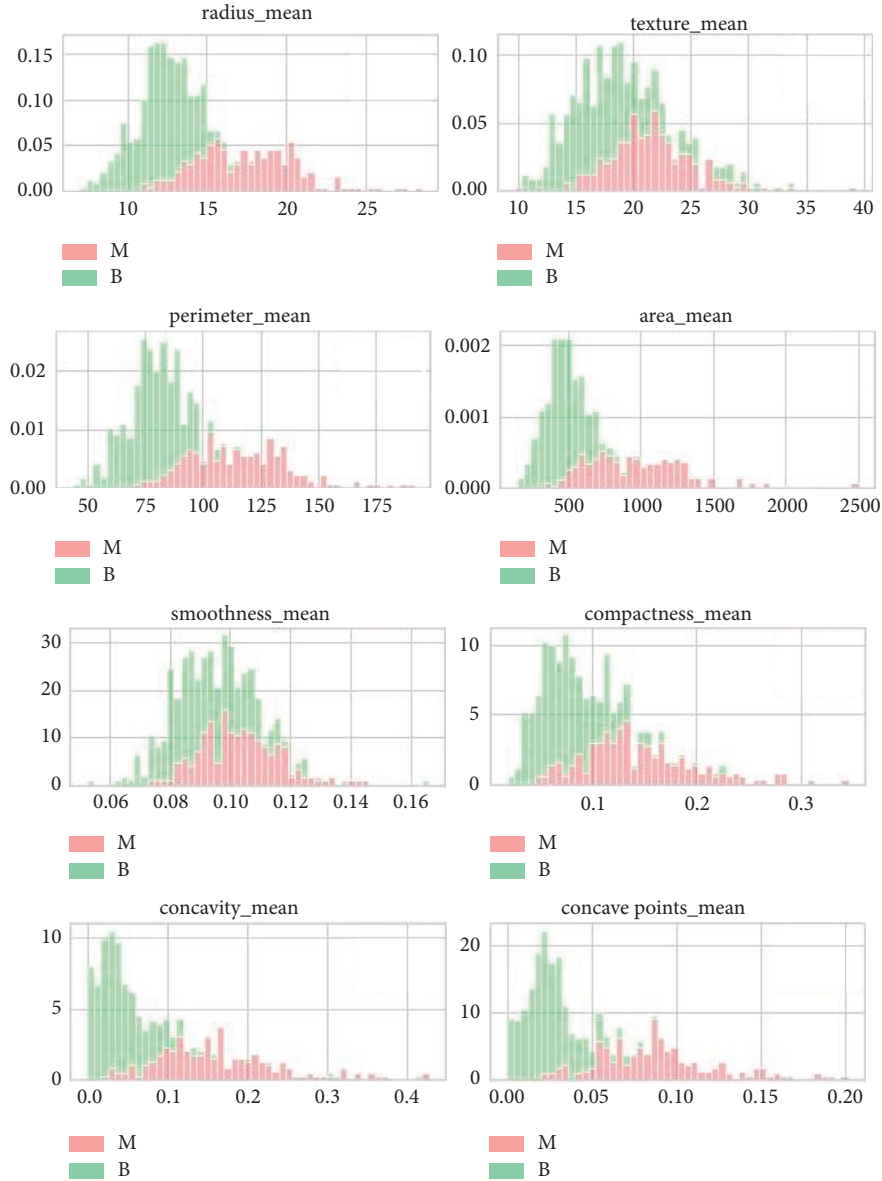
FIGURE 3: Prediction values shown by the graph.

a quantization-assisted U-Net approach for segmentation of breast lesions in two steps such as (1) U-Net and (2) quantization. U-Net-based segmentation assists quantization to identify the isolated regions of specific lesions with sonography images.

2. Proposed Methodology to Analyze Novel Deep-CNN LSTM

In this article, the breast cancer data are forecasted using a random forest classifier. The data from the UCI Repository's Wisconsin Breast *Cancer* Database (WBCD) have been used in this work. Malignant and benign types of cancer are the two major categories of information. The above dataset is used by most of the researchers for detecting cancer in the breast. The Wisconsin Breast *Cancer* Database data are

analyzed using the random forest algorithm, and it may be diagnosed based on 32 attributes.

2.1. Data Processing. All of the characteristics in the data have been scaled. On the data, we planned to use deep learning classification algorithms. As a result, we designed the scale to work with the approaches. Since the current dataset is arbitrary and there is no information mark yet, the principal phase of prehandling is to upgrade it by arranging and naming information and depicting the many kinds of cycles that interaction crude information to set it up for later cycles.

2.2. Methodology. The dataset was used as an input to the random forest classifier, which was used to classify breast
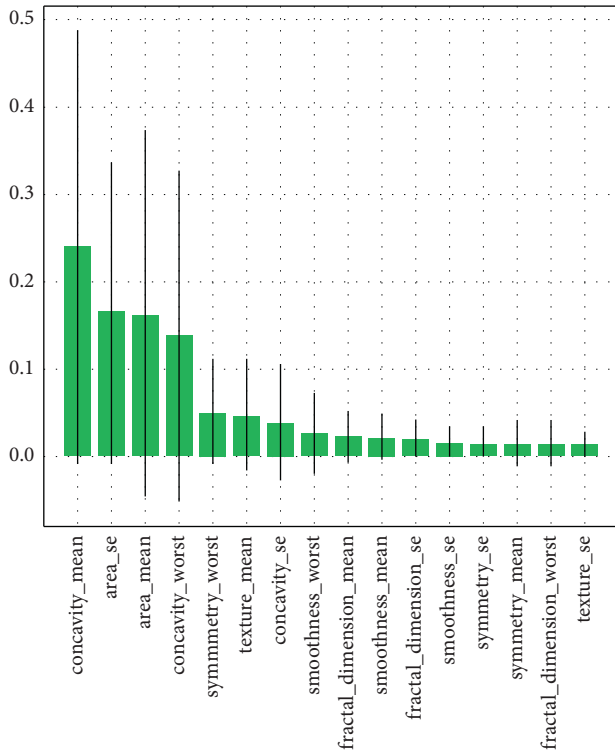
Figure 4: Feature ranking.

cancer. We trained the deep forest algorithm in the suggested architecture after feeding it the input. For convolution layers, we employed Leaky RELU nonlinearity as shown in the following equation:

$$f(a) = \begin{cases} a, \text{if } a > 0, \\ ya, \text{otherwise.} \end{cases} \quad (1)$$

The above Figure 1 illustrates breast cancer detection with different phases. During the collection phase, various image datasets are collected. In the preprocessing phase, resizing of images is performed to classify the data into training and test data. In each epoch, by using a 5 fold cross-validation confusion matrix, accuracy sensitivity and F1 scores are determined. To solve the grading problem from the dataset of the images, a network-based LSTM model is utilized along with CNN. The following Figure 2 shows that feature extraction is performed with CNN and classification with LSTM.

2.3. Combined Network: CNN and LSTM.
A CNN is a form of multilayer perceptron, unlike with a deep learning architecture, a simple neural network cannot learn complicated features. In a variety of applications, CNNs have been shown to be extremely effective. The objective principle of CNN is that it can extract local features from high-layer inputs and pass them down to lower layers for more complicated features. Convolutional, pooling, and fully connected (FC) layers make up a CNN. LSTM is an improved RNN (recurrent neural network) that consists of memory blocks rather than traditional RNN to solve

vanishing and gradient problems. The key difference between LSTM and RNNs is that it adds a cell state to save long-term states; also, an LSTM network can recall and connect information from the past with data from the present. The network has various convolutional layers, pooling layers, one fully connected layer, one LSTM layer, and finally one output layer with a softmax function.

3. Results and Discussion

To prepare and test the model, the random forest grouping procedure is utilized. The credits of inward focusing on the mean, region mean, span mean, border mean, and concavity mean have been utilized to depict the expectation. Assuming the consequence of the expectation to be 1, the UI will show that the 'Individual is in danger of being determined to have cancer disease later on.' 'Individual is not at risk of being determined to have bosom malignant growth in what's to come' is introduced on the UI in the event that the forecast accomplished is 0.

The following Figure 3 shows the prediction values that stacks the data based on the features selected, where the features are separated into two groups according to malignant and benign types of cancer. From the selected features, mean values for radius, texture, perimeter, area, smoothness, compactness, concavity, and concave values are determined.

3.1. Data Structure.
The datasets employed produced two groups of non-recurrence events and recurrence events as a result of the data structure. For the medical image tasks, models from the pretrained images are fine-tuned using a random forest classifier, which is called as "Transfer Learning."

Because of the great computational expense, convergence difficulty, and restricted amount of good quality labelled samples, gaining from clinical imaging information without any preparation is by and large not the most attainable method.

3.2. Quantitative Analysis by the Graph.
To visualize the performance of a classifier, curves of receiver operating characteristics (ROC) are used. It employs a diagrammatic design to show the proposed neural network's diagnostic capabilities in distinguishing between malignant and benign breast cancer samples.

We were able to pick the best feasible optimum forest model for BC classification using the random forest classifier method. The ROC bends likewise show how a huge neural organization based model works. The greater the classifier's performance, the higher the values. The following graph depicts some of the features that have been selected according to their importance, and ranking is obtained as shown in Figure 4.

3.3. Exploratory Data Analysis (EDA).
Information perception is an incredibly important piece of expertise in AI. It
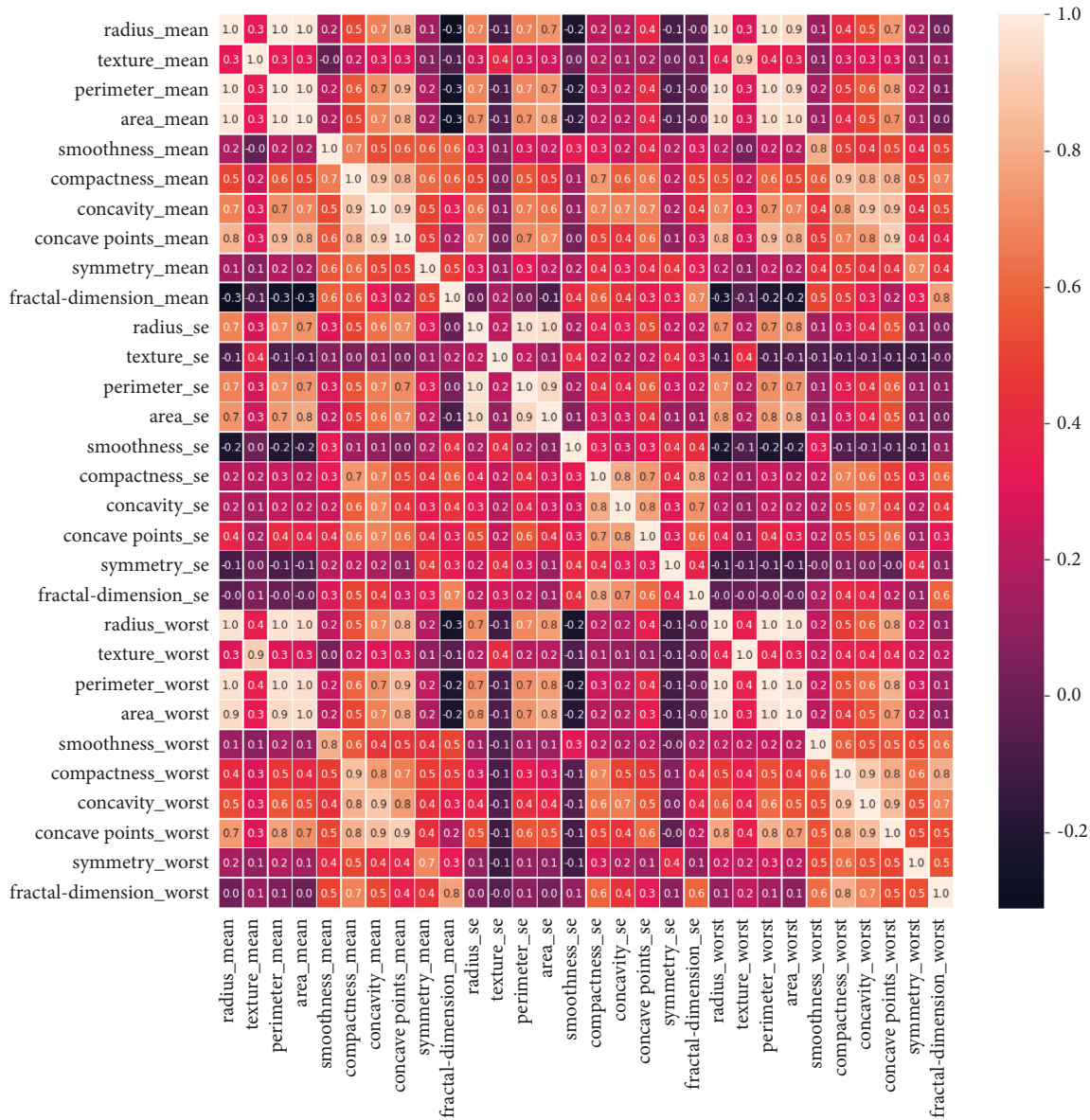
FIGURE 5: Correlation heat map for the breast cancer data set.
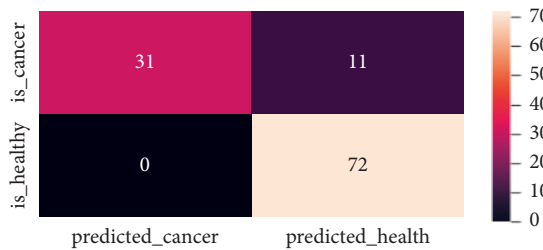
FIGURE 6: Confusion Matrices (without cross validation).
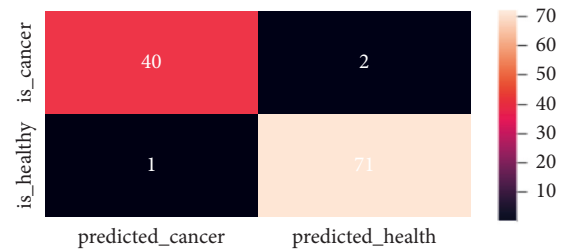
FIGURE 7: Confusion matrices (with cross validation by using the random forest classifier).

is liable for giving a subjective comprehension of the given information. Exploratory data analysis (EDA) is utilized to track down examples and connections in information. The perceptions we use in this venture are heat maps and a couple plot of the relative multitude of boundaries being

thought off. Simple data analysis and visualization were used to gain a better grasp of the data set and determine which features would be relevant to a deep learning model. Heat maps are exceptionally helpful to utilize while

TABLE 1: Classification report.

Model	Accuracy (%)	Sensitivity (%)	Precision (%)	Recall (%)	F1—score (%)
CNN model 1	95.5	91.2	59	80	68
CNN model 2	96.1	91.6	72	91	81
Multilayer perceptron	96.23	93.7	97.1	97.5	97.5
Proposed model	100	99.3	97	99	98

understanding complex informational collections. A heat map is a 2D portrayal of information in which values can be addressed by various shading plans. Heat maps are primarily used to observe solid connections between different boundaries as they are an extraordinary sign of relationship [35].

This map highlights which features add new information to the problem and which features are comparable to others in the collection. The correlation heat map matrix is shown with colored dimensions for mapping data to be visually represented in a scatterplot as shown in Figure 5.

In our work, CNN-LSTM and multilayer perceptron models were compared and executed with a proposed model based on random forest classifier tests which were determined with measures up to 5-fold cross validation.

3.4. Qualitative Analysis by Confusion Matrices.

We input the data to an excellent model of the data to receive output in probabilities after it has been cleaned and preprocessed. It is, after all, a deep learning classification performance metric. A confusion matrix, otherwise called an error matrix, is a unique table development that licenses the portrayal of the introduction of estimation, regularly a managed learning one, in the issue of measurable grouping. The confusion matrix without cross validation is shown in Figure 6 and with cross validation is shown in Figure 7.

The system has successfully played out 20 evaluations by using 5-fold cross endorsement of the chest threatening development data and using unpredictable boondocks estimation. Table 1 summarizes the classification report, and the graphical representation in Figure 8 shows that the proposed model has better performance than other conventional models.

3.5. Limitations.

Due to the considerable heterogeneity among images of the cancer subtype, standard machine learning algorithms for multiclass classification perform poorly. Thus, to enhance computer-aided diagnosis, complex approaches such as deep CNN with LSTM are employed. The algorithm is used with the random forest classifier to generalize big data sets using data properties with amazing results. These findings are mostly due to the design, which takes into consideration the tasks implied in the field of computer vision that use the two-convolution method. The proposed model mentioned above has certain weaknesses in addition to the excellent accuracy it has attained. Sufficiently labelled data and an uneven number of classes are two of the most common problems encountered while using deep learning models. The absence of labelled data causes the models to provide biased findings, which is
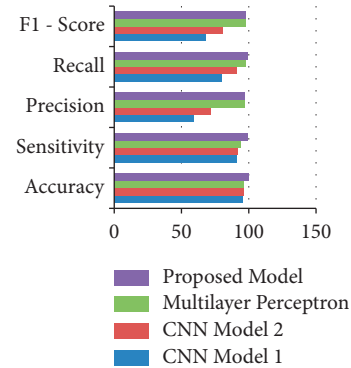
FIGURE 8: Graphical representation of the proposed model.

referred to as the "over-fitting problem." Also, data augmentation approaches are required to handle issues and generate efficient categorization.

4. Conclusion

It is a difficult challenge to automate breast cancer screening in order to improve patient care. In this study, we have suggested a deep CNN–LSTM with a random forest approach that automates predicting systems for the identification of breast cancer. Convolutional, max-pooling, and fully connected layers were used in the pretraining phase, and a classification layer was used to separate the benign samples from the malignant samples after the pretraining phase. We have fostered an assessment model to decide malignant growth repetitive and no-intermittent utilizing multifacet perceptron. The accuracy is obtained after execution of 5-fold cross-validation tests, and performance measures are calculated. It tends to expand the dataset as here we have considered estimation of mass-circularity in the dataset, and from factual examination, we observed that this quantitative estimation prompts straightforwardness in our decision obtaining 100% accuracy, and other performance metrics are also attained at high levels when compared with other models. In the future, the proposed model can be compared with other datasets available with a greater number of images [36, 37].

Data Availability

No data were used to support the findings of this study.

Conflicts of Interest

The authors declare that they have no conflicts of interest.

References

[1] H. Mohsen, E. S. A. El-Dahshan, E. S. M. El-Horbaty, and A. B. M. Salem, "Classification using deep learning neural networks for brain tumors," *Future Computing and Informatics Journal*, vol. 3, no. 1, pp. 68–71, 2018.

[2] G. Hamed, M. A. E. R. Marey, S. E. S. Amin, and M. F. Tolba, "Deep learning in breast cancer detection and classification," in *The International Conference on Artificial Intelligence and Computer Vision*, pp. 322–333, Springer, Cham, 2020.

[3] Y. LeCun, B. Boser, J. Denker et al., "Handwritten digit recognition with a back-propagation network," *Advances in Neural Information Processing Systems*, vol. 2, 1989.

[4] A. S. Becker, M. Marcon, S. Ghafoor, M. C. Wurnig, T. Frauenfelder, and A. Boss, "Deep learning in mammography: diagnostic accuracy of a multipurpose image analysis software in the detection of breast cancer," *Investigative Radiology*, vol. 52, no. 7, pp. 434–440, 2017.

[5] T. Kooi, G. Litjens, B. Van Ginneken et al., "Large scale deep learning for computer aided detection of mammographic lesions," *Medical Image Analysis*, vol. 35, pp. 303–312, 2017.

[6] N. Dhungel, G. Carneiro, and A. P. Bradley, "Automated mass detection in mammograms using cascaded deep learning and random forests," in *Proceedings of the 2015 International Conference on Digital Image Computing: Techniques and Applications*, pp. 1–8, IEEE, Adelaide, SA, Australia, November 2015.

[7] N. Dhungel, G. Carneiro, and A. P. Bradley, "A deep learning approach for the analysis of masses in mammograms with minimal user intervention," *Medical Image Analysis*, vol. 37, pp. 114–128, 2017.

[8] A. Akselrod-Ballin, L. Karlinsky, S. Alpert, S. Hasoul, R. Ben-Ari, and E. Barkan, "A region based convolutional network for tumor detection and classification in breast mammography," in *Deep Learning and Data Labeling for Medical Applications*, pp. 197–205, Springer, Cham, 2016.

[9] J. Ali, R. Khan, N. Ahmad, and I. Maqsood, "Random forests and decision trees," *International Journal of Computer Science Issues*, vol. 9, no. 5, p. 272, 2012.

[10] A. Akselrod-Ballin, L. Karlinsky, A. Hazan et al., "Deep learning for automatic detection of abnormal findings in breast mammography," in *Deep Learning in Medical Image Analysis and Multimodal Learning for Clinical Decision Support*, pp. 321–329, Springer, Cham, 2017.

[11] D. Ribli, A. Horváth, Z. Unger, P. Pollner, and I. Csabai, "Detecting and classifying lesions in mammograms with deep learning," *Scientific Reports*, vol. 8, no. 1, pp. 4165–4167, 2018.

[12] D. Bazazeh and R. Shubair, "Comparative study of machine learning algorithms for breast cancer detection and diagnosis," in *Proceedings of the 2016 5th International Conference on Electronic Devices, Systems and Applications*, pp. 1–4, IEEE, Ras Al Khaimah, United Arab Emirates, December 2016.

[13] Y. Choukroun, R. Bakalo, R. Ben-Ari, A. Akselrod-Ballin, E. Barkan, and P. Kisilev, "Mammogram classification and abnormality detection from nonlocal labels using deep multiple instance neural network," in *Proceedings of the VCBM*, pp. 11–19, Germany, January 2017.

[14] K. S. Priyanka, "A review paper on breast cancer detection using deep learning IOP conference series: materials science and engineering," *IOP Conference Series: Materials Science and Engineering*, vol. 1022, no. 1, Article ID 012071, 2021.

[15] G. Muhammad, M. S. Hossain, and N. Kumar, "EEG-based pathology detection for home health monitoring," *IEEE Journal on Selected Areas in Communications*, vol. 39, no. 2, pp. 603–610, 2021.

[16] M. Masud, A. E. Eldin Rashed, and M. S. Hossain, "Convolutional neural network-based models for diagnosis of breast cancer," *Neural Computing & Applications*, vol. 34, no. 14, pp. 11383–11394, 2020.

[17] L. Tsochatzidis, P. Koutla, L. Costaridou, and I. Pratikakis, "Integrating segmentation information into CNN for breast cancer diagnosis of mammographic masses," *Computer Methods and Programs in Biomedicine*, vol. 200, Article ID 105913, 2021.

[18] D. Muduli, R. Dash, and B. Majhi, "Automated diagnosis of breast cancer using multi-modal datasets: a deep convolution neural network based approach," *Biomedical Signal Processing and Control*, vol. 71, Article ID 102825, 2022.

[19] N. Wahab and A. Khan, "Multifaceted fused-CNN based scoring of breast cancer whole-slide histopathology images," *Applied Soft Computing*, vol. 97, Article ID 106808, 2020.

[20] M. S. Hossain, G. Muhammad, and N. Guizani, "Explainable AI and mass surveillance system-based healthcare framework to combat COVID-I9 like pandemics," *IEEE Network*, vol. 34, no. 4, pp. 126–132, 2020.

[21] P. Kumar, S. Srivastava, R. K. Mishra, and Y. P. Sai, "End-to-end improved convolutional neural network model for breast cancer detection using mammographic data," *The Journal of Defense Modeling and Simulation*, 2020.

[22] Z. Han, B. Wei, Y. Zheng, Y. Yin, K. Li, and S. Li, "Breast cancer multi-classification from histopathological images with structured deep learning model," *Scientific Reports*, vol. 7, no. 1, pp. 4172–4210, 2017.

[23] S. A. Alanazi, M. M. Kamruzzaman, M. N. Islam Sarker et al., "Boosting breast cancer detection using convolutional neural network," *Journal of Healthcare Engineering*, vol. 2021, pp. 1–11, Article ID 5528622, 2021.

[24] Y. Zhang, S. Chan, V. Y. Park et al., *Automatic Detection and Segmentation of Breast Cancer on MRI Using Mask R-CNN Trained on Non–fat-sat Images and Tested on Fat-Sat Images*, Academic Radiology, USA, 2020.

[25] S. A. Mojarad, S. S. Dlay, W. L. Woo, and G. V. Sherbet, "Breast cancer prediction and cross validation using multi-layer perceptron neural networks," in *Proceedings of the 2010 7th International Symposium on Communication Systems, Networks & Digital Signal Processing*, pp. 760–764, IEEE, Newcastle Upon Tyne, UK, July 2010.

[26] S. Nurmaini, R. F. Malik, D. Z. Abidin, A. Zarkasi, and Y. N. Kunang, "Breast cancer classification using deep learning," in *Proceedings of the International Conference on Electrical Engineering and Computer Science*, pp. 237–242, IEEE, Pangkal Pinang, Indonesi, October 2018.

[27] F. F. Ting and K. S. Sim, "Self-regulated multilayer perceptron neural network for breast cancer classification," in *Proceedings of the 2017 International Conference on Robotics, Automation and Sciences*, pp. 1–5, IEEE, Melaka, Malaysia, November 2017.

[28] M. Z. Islam, M. M. Islam, and A.nullah Asraf, "A combined deep CNN-LSTM network for the detection of novel coronavirus (COVID-19) using X-ray images," *Informatics in Medicine Unlocked*, vol. 20, Article ID 100412, 2020.

[29] S. Dutta, J. K. Mandal, T. H. Kim, and S. K. Bandyopadhyay, "Breast cancer prediction using stacked GRU-LSTM-BRNN," *Applied Computer Systems*, vol. 25, no. 2, pp. 163–171, 2020.

[30] Q. Ren, H. Cheng, and H. Han, "Research on machine learning framework based on random forest algorithm," in

Proceedings of the AIP conference proceedings, vol. 1820, AIP Publishing LLC, Melville, United States, March 2017.

[31] M. Malathi, P. Sinthia, F. Farzana, and G. Aloy Anuja Mary, "Breast cancer detection using active contour and classification by deep belief network," *Materials Today Proceedings*, vol. 45, pp. 2721–2724, 2021.

[32] Z. Chen, N. He, Y. U. Huang, W. T. Qin, X. Liu, and L. Li, "Integration of A Deep learning classifier with A random forest approach for predicting malonylation sites," *Genomics, Proteomics & Bioinformatics*, vol. 16, no. 6, pp. 451–459, 2018.

[33] S. Maqsood, R. Damasevicius, and R. Maskeliunas, "TTCNN: a breast cancer detection and classification towards computer-aided diagnosis using digital mammography in early stages," *Applied Sciences*, vol. 12, no. 7, p. 3273, 2022.

[34] T. Meraj, W. Alosaimi, B. Alouffi et al., "A quantization assisted U-Net study with ICA and deep features fusion for breast cancer identification using ultrasonic data," *PeerJ Computer Science*, vol. 7, Article ID e805, 2021.

[35] P. R. Anisha, C. K. K. Reddy, K. Apoorva, and C. M. Mangipudi, "Early diagnosis of breast cancer prediction using random forest classifier IOP conference series: materials science and engineering," *IOP Publishing*, vol. 1116, no. 1, Article ID 012187, April 2021.

[36] G. Murtaza, L. Shuib, A. W. Abdul Wahab et al., "Deep learning-based breast cancer classification through medical imaging modalities: state of the art and research challenges," *Artificial Intelligence Review*, vol. 53, no. 3, pp. 1655–1720, 2020.

[37] M. Nawaz, A. A. Sewissy, and T. Hassan, "Multi-class breast cancer classification using deep learning convolutional neural network," *International Journal of Advanced Computer Science and Applications*, vol. 9, no. 6, pp. 316–332, 2018.

WILEY | Hindawi

Research Article

Friend Recommender System for Social Networks Based on Stacking Technique and Evolutionary Algorithm

Aida Ghorbani,[1] Amir Daneshvar [ID],[2] Ladan Riazi,[2] and Reza Radfar[3]

[1]*Department of Information Technology Management, Science and Research Branch, Islamic Azad University, Tehran, Iran*
[2]*Department of Information Technology Management, Electronic Branch, Islamic Azad University, Tehran, Iran*
[3]*Department of Technology Management, Science and Research Branch, Islamic Azad University, Tehran, Iran*

Correspondence should be addressed to Amir Daneshvar; a_daneshvar@iauec.ac.ir

In recent years, social networks have made significant progress and the number of people who use them to communicate is increasing day by day. The vast amount of information available on social networks has led to the importance of using friend recommender systems to discover knowledge about future communications. It is challenging to choose the best machine learning approach to address the recommender system issue since there are several strategies with various benefits and drawbacks. In light of this, a solution based on the stacking approach was put out in this study to provide a buddy recommendation system in social networks. Additionally, a decrease in system performance was caused by the large amount of information that was accessible and the inefficiency of some functions. To solve this problem, a particle swarm optimization (PSO) algorithm to select the most efficient features was used in our proposed method. To learn the model in the objective function of the particle swarm algorithm, a hybrid system based on stacking is proposed. In this method, two random forests and Extreme Gradient Boosting (XGBoost) had been used as the base classifiers. The results obtained from these base classifiers were used in the logistic regression algorithm, which has been applied sequentially. The suggested approach was able to effectively address this issue by combining the advantages of the applied strategies. The results of implementation and evaluation of the proposed system show the appropriate efficiency of this method compared with other studied techniques.

1. Introduction

In recent years, by the development of social networks, individuals and organizations can easily interact with each other. People can get their favorite connections in different fields and share their knowledge as well. Most of the connections that individuals are making on social networks exist only in the virtual world and are not often accessible there. A social network is a graph in which each node stands for a person, group, or organization, and each link between nodes depicts the relationships among them. Understanding and describing the processes that create social interactions is one of the fundamental problems in social network analysis. In this regard, the problem of link prediction in social networks states that two nodes in a network will be connected in the near future or not[1].

One of the most important issues in social networks, which leads to its superiority over other networks, is the friend recommender system in it. In recent years, many methods were proposed to suggest a friend recommender system that had been used machine learning techniques and artificial intelligence [2, 3]. The performance of its methods is not, however, clearly categorized in the area of machine learning. This is mostly because there are so many methods and suggested adjustments in the literature. As a result, choosing a proper machine learning algorithm is difficult and confusing that fits the needs of the issue when developing a recommender system. Thus, considering that each machine learning method has its advantages and limitations, an approach based on stacking technique is presented that can combine the advantages of machine learning methods and improve the results.

Before moving on to the next phase of this study, a review of earlier techniques is provided. The different parts of the research's suggested system are then discussed. The outcomes of the system's implementation are then examined using a number of tests, and conclusions are provided at the end.

2. Related Work

The problem of link prediction, which first raised by Getoor and Diehl, is presented as a problem of predicting the presence of a link between two entities. The prediction is based on the properties of other objects and other observed links [4]. This is widely used in a wide range of real and important areas, especially those involving the detection of complex events from highly structured data [5]. A thorough summary of link prediction in various networks was given in a research by Daud et al. The report gave thorough descriptions of link prediction algorithms, cutting-edge technology, programs, problems, and future research objectives. Besides, several directions for future research in the field of link prediction in social networks were expressed [6].

In a research by Chen et al. [7], the encoder-LSTM-decoder (E-LSTM-D) system is proposed as a new deep learning model based on stacked long short-term memory (LSTM) in the encoder-decoder architecture. The various experiments performed in this paper show that the E-LSTM-D model in different datasets performs significantly better than the existing dynamic link prediction methods. Behera et al. used potential future linkages using a variety of machine learning algorithms, including K-NN, MLP, bagging, SVM, and decision trees, based on attributes retrieved from the topological structure. The performance of the proposed system of this research was evaluated in terms of various criteria [8].

In a research by Chonghuan [9], to solve the problem of sparsity of recommender systems, a new recommendation method for social network using matrix factorization technique proposed. In this method, users clustered and various complex factors considered as well. The simulation results showed that the proposed socialized recommendation method based on matrix factorization (SRM-MF) system performed better than the methods available on the tested dataset. For instance, the precision of the real dataset and the Book-Crossing dataset are 0.088 and 0.095, respectively, assuming the Hamming distance is 20. While 0.073 and 0.086, respectively, represent the greatest accuracy for other procedures used in similar circumstances, Pecli et al.'s experiments were performed on three datasets (Microsoft Academic Network, Amazon, and Flickr) that included more than twenty different features, including topological features and domain-specific features. The program combines three feature selection strategies, six different classification algorithms (support vector machines (SVM), k-nearest neighbors (K-NN), simple Bayesian, Classification and Regression Tree (CART), random forest, and multilayer perceptron) and three evaluation criteria (precision, F-measure, and area under the curve). Their research's findings revealed an intriguing relationship between the majority of the chosen characteristics and the dataset. The findings demonstrated that using feature selection techniques to condense the feature set

produces better classification models than classifiers built using the whole set of features [10]. In the paper by Manshad et al., a new time series link prediction (TSLP) method based on irregular cellular learning automaton (ICLA) and evolutionary computation (EC) proposed. ICLA-EC had been used to analyze network evolution through neighborhood dynamicity. Based on experiments performed on different datasets, ICLA-EC-TSLP achieved significant results (0.7212–0.8650) in AUC criterion compared with other methods [11].

In Cai et al.'s research, a new link prediction model based on line graph neural networks is proposed that achieves good performance for the link prediction problem. Studies on 14 datasets revealed that the suggested approach of this study consistently outperformed all fundamental techniques in terms of area under the curve (AUC) by identifying more relevant features [12]. In the research of Parveen et al., the friends' recommendation system performed using different types of machine learning algorithms, such as Random Forest Classifier, XGBoost, Light GBM, and Cat Boost. The performance of the mentioned methods compared in F1-score criteria, accuracy, recall, and confusion matrix. The results of this study showed that Random Forest and Light GBM are less accurate than the XGBoost and CatBoost algorithms. The accuracy of the XGBoost and CatBoost algorithms was the same and equal to 95% [13].

Kumar et al. proposed a friend recommendation system that uses a random forest to advise a buddy. The data collection used in this study has 94,000 nodes. The achieved accuracy for this suggested model is 89%. It is stated that the accuracy obtained in relation to the available hardware and data volume is quite reasonable [14]. In the research of Murali et al., a recommendation system presented in which each user is offered the best research articles in this field. This recommendation method is based on the individual queries and similarities found from other users based on their queries. This recommendation system uses a collaborative filtering approach and helps to avoid user time-consuming [15].

In the research done by ZhengWei et al. [16], a solution based on XGBoost is proposed for classifying and recommending journals to researchers. The doc2vec is used to get better results. The accuracy of this method was measured at 84.24 percent after testing on Common SCI English publications in the computing industry to verify the findings. A unique Graph Neural Network for Reciprocal Recommendation (GraphRR) was suggested for exploiting multiplex user interactions in the research written by Chang et al. [17]. To display each user's preference, attraction, and likeness, three ego graphs are created for each user depending on the directions of interaction. Then, multiplexity-aware GNN modules are applied to measure participation. Extensive tests were conducted on large-scale real-world online gaming datasets from NetEase Games, which demonstrated the system's good performance.

As it is clear from the reviewed researches, recommender systems used in different fields and have of special importance. Studies shown that using machine learning techniques in this field is high and could be developed due to the nature of artificial intelligence methods. In Table 1, a summary of the reviewed related works is given.

Research	Field	Method	Dataset
[7]	Link prediction	Encoder-LSTM-decoder (E-LSTM-D) system	CONTACT, ENRON, RADOSLAW, FB-FORUM, LKML
[8]	Link prediction	K-NN, MLP, bagging, SVM, and decision tree	Collected dataset
[9]	Recommendation system in social network	SRM-MF	Actual dataset, Book-Crossing
[10]	Link prediction applications	Selected feature method with SVM, K-NN, simple Bayesian, CART, random forest, and multilayer perceptron	Microsoft Academic Network, Amazon, and Flickr
[11]	Link prediction	ICLA-EC-TSLP	Hep-th, Hep-ph, Astro-ph, Email-Enron, CollegeMsg
[12]	Link prediction	Line graph neural networks	14 various datasets
[13]	Friend recommendation system	Random Forest Classifier, XGBoost, Light GBM, and Cat Boost	Facebook dataset
[14]	Friend recommendation system	Random forest	Facebook recruiting
[15]	Research recommendation system	Collaborative filtering	Collected dataset
ZhengWei et al. [16]	Classification and recommendation of academic journals	XGBoost with doc2vec	Common SCI English journals
Chang et al. [17]	Reciprocal recommendation	GraphRR	Real-world large-scale online games from NetEase Games

3. Proposed System

This paper aims to propose a new way as an effective approach based on the use of particle swarm optimization and ensemble methods for friend recommendation in social network. Details of the proposed system are shown in Figure 1.

The proposed system of this research uses particle swarm optimization algorithm to select effective features. Each particle in this method represents a set of characteristics that iteratively progress toward the best answer. In this algorithm, a particle that chooses the optimal attributes for the issue is ultimately chosen. The method used to learn the objective function of the particle swarm optimization algorithm involves a stacked model of several machine learning algorithms.

There are several ways to learn the model, and usually each of them has power in a particular area, and to use one of them, the necessary studies must be done to understand how they work. There is no algorithm that is always the best, and each approach performs differently depending on the data and the situation. This is a key concept in these algorithms and models. In these situations, combining the output of many classifiers is preferable than selecting a specific approach or technique. Since each of them may have different strengths and weaknesses, it is expected that their participation would have a good compensatory effect.

One of the best and most effective combining methods is the use of stacking technique in which multiple models are combined. This method is used to increase the accuracy of models and improve results and reliability in a wide range of business and research programs. Stacking is a learning-based method, which combines multiple classification models or regression models. There are two stages to the categorization process based on this model. The output of the first level of classifiers serves as the input for the classifiers at the second level in the stacking approach. In other words, it can be said that classifier prediction at one level is considered as a feature for the next level classifier.

In this regard, in the proposed method of this research, XGBoost methods and two forms of random forest are implemented for the first level. The results of the first-level algorithms are used in logistic regression, which is implemented in the second level of the proposed system. Finally, the obtained results are used as the fitness result in the objective function of the particle swarm optimization algorithm.

3.1. Data Preparation. The link prediction collection has been used. This collection could be find at Noesis, nd. This collection of information has collected 22 networks from different sources and fields. This dataset includes a wide range of different features and information. A summary of the information in these datasets is given in Table 2. Name of the network, number of nodes, number of edges, average degree, average clustering coefficient, and average length of shortest route, dimension, heterogeneity, and assortativity are all listed in the table from left to right [21]. BUP dataset and a few additional datasets were used to test the proposed system. The BUP dataset represents the network information of political blogs. This dataset includes 105 nodes, 441 links, and 8.4 degrees (Table 2).
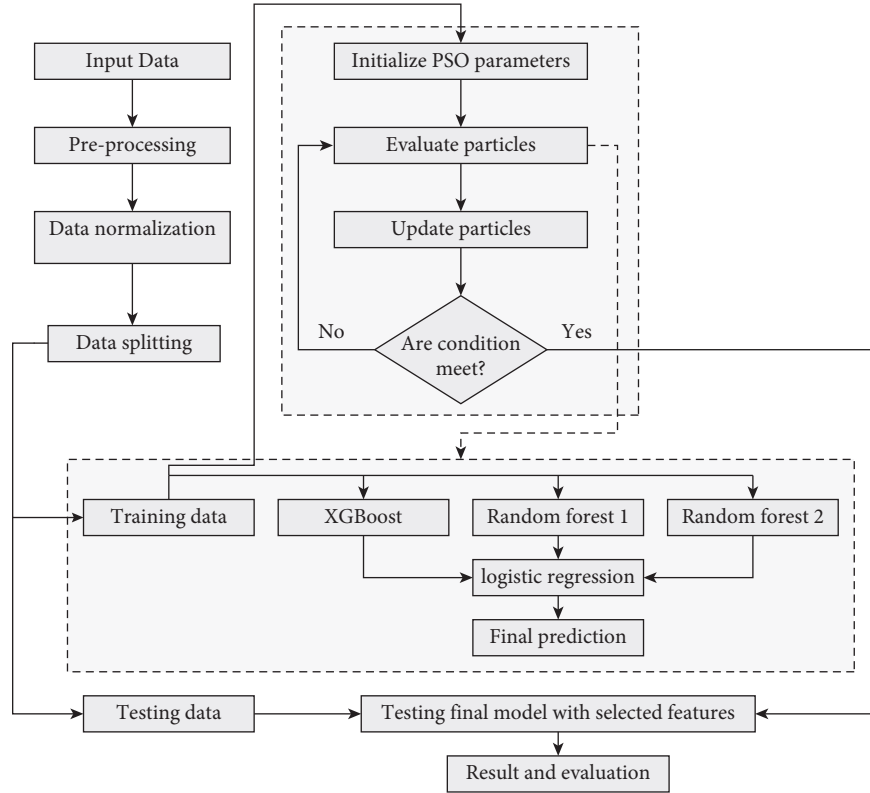
Figure 1: Proposed system.

Table 2: Topological properties of networks [21].

Name	$|V|$	$|E|$	k	C	ASPL	D	H	r
UPG	4941	6594	2.67	0.08	18.99	46	1.4504	0.0035
HPD	8756	32331	7.38	0.11	4.19	14	4.5133	−0.051
ERD	6927	11850	3.42	0.12	3.78	4	12.6708	−0.1156
YST	2284	6646	5.82	0.13	4.29	11	2.8479	−0.0991
EML	1133	5451	9.62	0.22	3.61	8	1.9421	0.0782
ADV	5155	39285	15.24	0.25	3.22	9	5.4060	−0.0951
KHN	3772	12718	6.74	0.25	3.63	12	9.422	−0.1205
PGP	10680	24316	4.55	0.27	7.49	24	4.1465	0.2382
CEG	297	2148	14.46	0.29	2.46	5	1.8008	−0.1632
LDG	8324	41532	9.98	0.31	4.37	16	6.188	−0.0997
SMG	1024	4916	9.6	0.31	2.98	6	3.9475	−0.1925
ZWL	6651	54182	16.29	0.32	3.85	10	2.5851	0.0006
INF	410	2765	13.49	0.46	3.63	9	1.3876	0.2258
BUP	105	441	8.4	0.49	3.08	7	1.4207	−0.1279
HTC	7610	15751	4.14	0.49	5.68	19	2.0986	0.2939
CGS	6158	11898	3.86	0.49	3.62	14	3.9467	0.2426
GRQ	5241	14484	5.53	0.53	5.05	17	3.0523	0.6593
EMT	2426	16630	13.71	0.54	3.15	10	3.1011	0.0474
FBK	4024	87887	43.68	0.59	3.98	13	2.432	0.0707
UAL	332	2126	12.81	0.63	2.74	6	3.4639	−0.2079
CDM	16264	47594	5.85	0.64	5.82	18	2.2087	0.1846
NSC	1461	2742	3.75	0.69	2.59	17	1.8486	0.4616

3.1.1. Normalization. Normalization is an operation on raw data that rescale the data or transform the data so that each attribute has a uniform contribution. Doing this will solve the problem of dominant features and outliers. Based on statistical criteria, there are many techniques for normalizing data within a certain range. The Z-score normalizing approach is used in this case for normalization. In this method, the criteria of mean and standard deviation are used to rescale the data so that the resulting features have a zero mean and a unit variance.

Each instance, $x_{i,n}$, of the data is transformed into $x'_{i,n}$ as follows:

$$X'_{i,n} = \frac{X_{i,n} - \mu_i}{\sigma_i}, \qquad (1)$$

where μ and σ denote the mean and standard deviation of ith feature, respectively [22].

3.1.2. Feature Engineering. Nod2vec and NetworkX packages are used for feature engineering in this research. One of the introduced solutions for selecting features from a graph is known as Node2Vec. Node2vec is a flexible neighborhood sampling strategy that allows us to gently interpolate between BFS (Breadth First Search) and DFS (Depth First Search). This method is implemented by developing a biased flexible random walking method that can explore neighbors in both BFS and DFS methods [20].

A random walk is defined by two parameters p and q. We assume that the current random walking position is node v. The position of the previous step is node t. In order to determine the next position, the probabilities of π_{vx} transfer at the edges (v, x) leading to v must be evaluated. We set the probability of anomalous transfer to $\pi_{vx} = \alpha_{pq}$ (t, x)·w_{vx}. In particular, α_{pq} is defined as follows:

$$\alpha_{pq} = \begin{cases} \dfrac{1}{p}, & d_{tx} = 0, \\ 1, & d_{tx} = 1, \\ \dfrac{1}{q}, & d_{tx} = 2, \end{cases} \qquad (2)$$

where d_{tx} defines the shortest distance between node t and node x, and the value of d_{tx} must be 0, 1, or 2. The p parameter controls the possibility of revisiting a node during a random walk. When the p value is high, the visited nodes are rarely sampled. This strategy promotes moderate exploration and eliminates redundant sampling across two hops. Alternatively, if p is small, the walk is directed backward by one step (Figure 2), keeping it "local" and near to the initial node u.

The q parameter allows the search to distinguish between "local" and "global" nodes. As shown in Figure 2, if $q > 1$, a random walk is more likely to be sampled from nodes around the node. BFS samples the nodes in a small location. Conversely, if $q < 1$, the random walk is farther away from v, which can receive more general information about the features. Therefore, the distance between the sampling node and the given source node does not increase strictly [21].

Recently, huge amounts of network data in various fields such as web pages, social networks, and power grids are being generated and collected. NetworkX package was created in April 2005 to analyze these massive and complex networks in Python [22]. This Python package is intended for building, modifying, and researching the composition
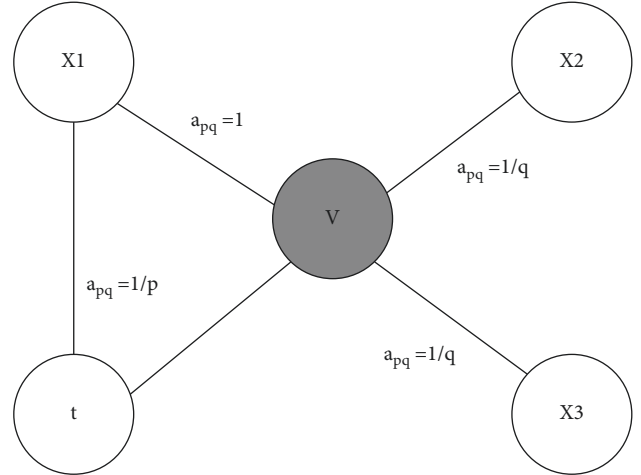
Figure 2: Node selection in Node2Vec algorithm. The current position in a random walk is at node v, and the previous step is at node (*t*). In this example, x1, x2, and x3 are neighbors. The values of a_{pq} are calculated based on the distance between v and t. [21].

and operation of complicated networks. A variety of networks or diagrams are shown using its data structures. In contrast to many other technologies, NetworkX is extremely versatile and built to handle data at a scale appropriate for contemporary issues. In this package, nodes can represent any object in Python, and edges can contain arbitrary data. In Figure 3, a graph plot of BUP data that created by NetworkX is shown. This figure shows the nodes and how they (edges) are connected.

3.1.3. Data Splitting. To implement and evaluate the efficiency of the proposed system, the data studied in this research are divided into two segments: training data and test data. In this classification, 70% of the total data examined is used for system training. To evaluate the system, the remaining 30% is considered as test data.

3.2. Classification Model. In these methods, classifiers had been combined to produce better predictions compared with single-level models. To do this, the stacking technique is used to implement several consecutive classifiers. As mentioned in the proposed system, several XGBoost is execution technique to increase the accuracy and performance of the Gradient Boosting Machine (GBM) and especially to increase the classification accuracy of regression trees proposed in [23], and two random forest algorithms have been ran in the first level, and finally, logistic regression model is one of the statistical tools used for data analysis, in which the relationship between a dependent variable and independent variables defined based on a series of observational values [24] and in the second level combined with them sequentially. The results of the first-level classifiers combined as the input of the second level and the final prediction in the second level are based on the results obtained from the first level.
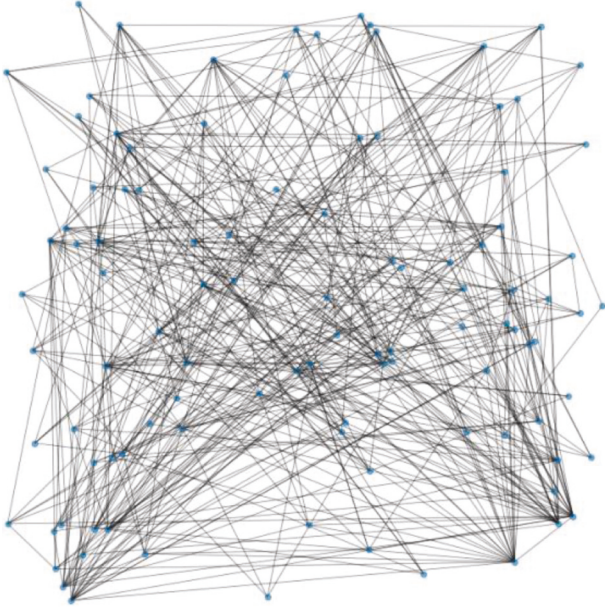
Figure 3: A graph plot of BUP data that created by NetworkX.

Because of the regular and parallel processing, XGBoost outperforms GBM. This approach integrates all predictors simultaneously for enhanced training [25]. The XGBoost algorithm is a system that successively generates decision trees. This algorithm can perform calculations relatively faster than all computing environments. XGBoost is widely used in modeling and classification for its performance.

Many decision trees grow in the classification of random forest algorithms, which is a batch algorithm. A decision tree algorithm can easily perform classification operations on events. The random forest algorithm uses several decision trees. In fact, a set of decision trees together produce a forest, and this forest can make better decisions (than a tree). In general, the decision tree is prone to overtraining and has little generalizability. The volatility of the decision tree's findings in the presence of noise in the input data is another drawback. A slight shift in learning patterns during the construction of a decision tree may result in significant changes to the tree's structure. Random forest, which operates by averaging the outcomes of all decision trees, is used to tackle these issues. The most important feature of stochastic forests is their high performance to measure the importance of variables, thus determining the role of each variable in predicting the response [26].

3.3. Feature Selection.

In solving many problems, machine learning methods have difficulty in dealing with a large number of input features. One of the most crucial strategies in data preparation and feature selection is crucial for the efficient and accurate use of machine learning technologies. One of the important steps in the machine learning process is feature selection. This process identifies relevant features and removes irrelevant and additional data [27]. This process speeds up data mining algorithms, improves prediction accuracy, and increases comprehensibility. Irrelevant features are those that do not provide any useful information, and additional features do not provide more information than currently selected features.

In the proposed method of this research, particle swarm optimization algorithm is used to select the features. In this section, more relevant features are selected so that the performance of the friend recommender system is improved. The particle swarm optimization algorithm is a social search algorithm based on the social behavior and regular collective movements of birds and fish [28]. Despite the limited ability of each particle to find the best pattern, their collective behavior has a great ability to find the best path (in other words the best answer to optimization problems) as the position of each particle changes based on the particle's experience in previous movements and neighboring particle experiences. In fact, each particle is aware of its superiority or lack of superiority over neighboring particles as well as the whole group.

Two perspectives were considered to model the order in the collective movement of these particles. One dimension is the social interactions between group members, and the other dimension is the individual superiority that each group member may have. In the first dimension, all members of the group are obliged to always change their position by following the best person in the group. In the second dimension, it is necessary for each member to keep in their memory the best situation they have personally experienced and to have a tendency toward the best perceived situation of their past. Each of these members may become the leader of the group so that the other members have the duty to follow them.

After generating the initial population (particles) and considering an initial velocity for each particle, the fitness of each particle is calculated based on its position. Each particle in the search space represents one solution for the problem and changes its speed based on the best answer obtained in the particle group (best person in the group) and the best place that it has ever been. This velocity is added to the position of the particle, and a new position of the particle is obtained. In subsequent iterations, the best particle in terms of fitness helps the other particles and corrects their motion, and after successive iterations, the problem will converge towards the optimal answer.

The position vector for the ith particle with dimension d is $X_i = [x_{i,1}, x_{i,2}, \ldots, x_{i,d}]$. The velocity vector is defined as $V_i = [v_{i,1}, v_{i,2}, \ldots, v_{i,d}]$.

During motion, the best position that each particle can reach during the execution of the algorithm is called pbest = $[p_{b,1}, p_{b,2}, \ldots, p_{b,d}]$, and the best position that all particles have gained during the execution of the algorithm is called gbest = $[g_{b,1}, g_{b,2}, \ldots, g_{b,d}]$. The position and velocity vectors of each particle are defined as follows:

TABLE 3: Some of important parameters considered for different methods.

Method	Parameters
XGBoost	Number of boosting stages = 100 loss function = "log_loss" Learning rate = 0.1 Maximum depth of the individual regression estimators = 3
RandomForest_1	The number of trees in the forest = 20 measures the quality of a split = "gini" The number of features to consider when looking for the best split = "sqrt (n_features)"
RandomForest_2	The number of trees in the forest = 30 measures the quality of a split = "gini" The number of features to consider when looking for the best split = "sqrt (num of features)"
Logistic regression	Solver = "lbfgs" penalty term = "L2" Tolerance for stopping criteria = 1e-4

TABLE 4: Result for class 1 in BUP dataset.

	Precision	Recall	F-measure	Accuracy
XGBoost	0.59	0.57	0.58	0.59
RandomForest_1 (n_estimators = 20)	0.67	0.63	0.65	0.66
RandomForest_2 (n_estimators = 30)	0.66	0.64	0.65	0.65
Logistic regression	0.58	0.59	0.59	0.58
Proposed method	0.68	**0.70**	**0.69**	0.69

$$v_{i,d}(t+1) = w_t \cdot v_{i,d}(t) + c_1$$
$$\cdot \text{rand}_1\left(p\text{best}_{i,d}(t) - x_{i,d}(t)\right) + c_2, \quad (3)$$
$$x_{i,d}(t+1) = x_{i,d}(t) + v_{i,d}(t+1).$$

c_1 is learning coefficient related to personal experiences of each particle and c_2 is learning coefficient related to group experiences. The rand_1 is random number between [0 1]. The w_t is a control parameter that controls the effect of the current particle velocity on the next velocity and creates a balance between the algorithm's ability to search locally and globally.

4. Results

In this section, the results of the implementation of proposed system reviewed. To do this, the performance of the friend recommender system has been examined in 5 different modes. In these 5 modes, the XGBoost, first Random Forest, second Random Forest, Logistic Regression, and the proposed system were used as learning models. First, some of important parameters considered for different methods are stated in Table 3.

The results of this implementation are given in Table 4. The values obtained for precision, recall, F-measure, and accuracy criteria for the mentioned methods for class one are given in this table. Based on the results of this table, the values of the criteria if the proposed system is used are 0.68, 0.70, 0.69, and 0.69, respectively. These findings demonstrate that if the suggested stacking strategy is used, the best results are achieved for every analyzed criterion. Better outcomes than individual base models are attained in the proposed system because basic

learning models are stacked and their unique capabilities are used. The confusion matrix obtained from the stacking for the train and test data is given in Figure 4. Each column of the confusion matrix represents a sample of the predicted value, and each row contains actual sample. To classify two classes, each member sample will be either positive or negative. Therefore, for each data sample, four states may occur that are represented by the confusion matrix.

The sample is a member of a positive class and is recognized as a member of the same class (true positive). The sample is a member of the positive class and is recognized as a member of the negative class (false negative). The sample is a member of a negative class and is recognized as a member of the same class (true negative). Finally, the sample is a member of the negative class and is recognized as a positive class member (false positive).

Since the elements on the main diameter show the correct samples (true positive and true negative), as shown in Figure 4 for the training dataset, their sum is equal to the total number of samples. The values of the elements on the subdiameter show the incorrect samples (false negative and false positive), which are zero for the training dataset. Therefore, the confusion matrix for training data showed the highest possible performance.

The confusion matrix findings for the test data show that there are not many false positive instances or false negative cases, which is acceptable. This demonstrates how well the suggested stacking approach works in both classes.

4.1. Results for Other Datasets.
In this section, the proposed method on other datasets was also examined. These datasets are INF, CEG, and UAL, respectively. The results
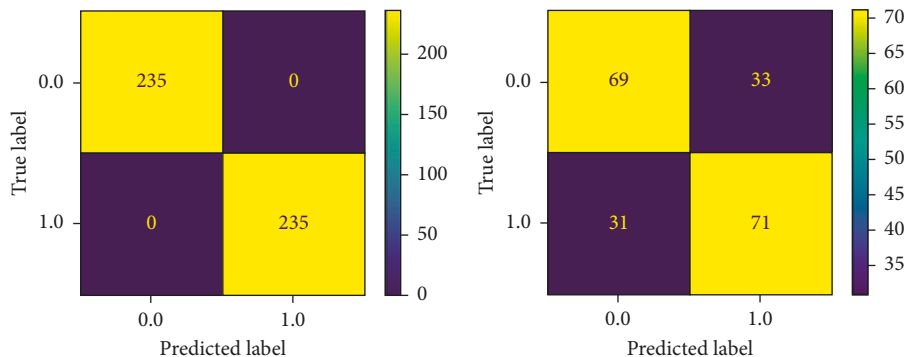
FIGURE 4: Confusion matrix for proposed method for BULP dataset. Left figure is for training, and right figure is for testing dataset.

TABLE 5: Result for class 1 in INF dataset.

	Precision	Recall	F-measure	Accuracy
XGBoost	0.66	0.63	0.69	0.67
RandomForest_1 (n_estimators = 20)	0.71	0.67	0.69	0.70
RandomForest_2 (n_estimators = 30)	0.71	0.67	0.69	0.70
Logistic regression	0.53	0.53	0.53	0.53
Proposed method	0.73	0.68	0.70	0.71

TABLE 6: Result for class 1 in CEG dataset.

	Precision	Recall	F-measure	Accuracy
XGBoost	0.57	0.54	0.55	0.57
RandomForest_1 (n_estimators = 20)	0.65	0.61	0.63	0.64
RandomForest_2 (n_estimators = 30)	0.66	0.62	0.64	0.65
Logistic regression	0.53	0.54	0.54	0.53
Proposed method	0.63	0.66	0.64	0.64

of applying different methods to INF dataset are listed in Table 5.

The results of applying different methods to CEG dataset are listed in Table 6.

The results of applying different methods to UAL dataset are listed in Table 7.

As can be observed, the suggested method performs rather well on the investigated datasets. The findings from the INF and UAL datasets demonstrated that the suggested system of this study outperformed the alternative algorithms in every analyzed criterion. In these two experiments, Random Forest_2 had the best performance after the proposed system. In testing the methods on CEG dataset, Random Forest_2 performed better in the precision and accuracy criteria, and the proposed system performed better in the recall and F-measure criteria. However, due to the fact that in the case of this study, overlooked cases (false negatives) are more costly than false alarms (false positive), and recall is more important than other criteria. Therefore, like the other two datasets, the proposed system of this research performs better on this dataset.

4.2. Research Limitations. Because a portion of the methodology utilized in this work is based on stacking several machine learning techniques, training the system takes a disproportionately long amount of time. The training procedure for huge graphs might take a long time if hardware resources were limited. For future work, according to the stated point, one can focus on reducing system training time. Applying intelligent sampling methods and using a subset of data for the training process can be considered.

TABLE 7: Result for class 1 in UAL dataset.

	Precision	Recall	F-measure	Accuracy
XGBoost	0.65	0.64	0.64	0.64
RandomForest_1 (n_estimators = 20)	0.68	0.68	0.68	0.68
RandomForest_2 (n_estimators = 30)	0.68	0.68	0.68	0.68
Logistic regression	0.63	0.59	0.61	0.62
Proposed method	0.75	0.75	0.75	0.75

5. Conclusion

In this research, a friend recommender system based on a combination of XGBoost, random forest, and logistics regression techniques is proposed. The results of this approach's implementation of XGBoost methods and two types of random forests were integrated using the stacking method and the logistics regression algorithm. The particle swarm optimization algorithm in this method chooses the most efficient characteristics to achieve the highest efficiency. For better investigation, in addition to the proposed stacking system, XGBoost-based system, linear regression, and random forest were implemented The results of this comparison showed that the proposed stacking system can achieve higher precision, recall, F-measure, and accuracy than other implemented approaches. This system has been able to make good diagnoses in both existing classes and achieve good results.

6. Introducing the Tool

Python programming language is used to implement the proposed solution. Python is a powerful programming language that is easy for people to learn. High-level data structures in this programming language are very efficient, and object-oriented programming is made possible. Python Interpreter and the extensive standard library are freely available on all major platforms on the Python website [29]. For the Python programming language, there are several libraries on machine learning and data mining issues. These features have led to the widespread use of this language in the field of artificial intelligence.

Appendix

Some of the codes used in this article are shown in this appendix.

```
Load Data
with open ("Dataset\\files\\INF_full.net") as f:
    fb_links = f.read ().splitlines ()
counter = 0
for tmp in fb_links:
    counter += 1
    if (tmp == " * edges"):
        break;
fb_links = fb_links[counter:]
Process Graph Data
node_list_1 = []
node_list_2 = []
for i in tqdm (fb_links):
    node_list_1.append (i.split (" ")[0])
    node_list_2.append (i.split (" ")[1])
fb_df = pd.DataFrame ({"node_1": node_list_1, "node
_2": node_list_2})
G = nx.from_pandas_edgelist (fb_df, "node_1", "node_
2", create_using = nx.Graph ())
node_list = node_list_1 + node_list_2
node_list = list (dict.fromkeys (node_list))
adj_G = nx.to_numpy_matrix (G, nodelist = node_list)
all_unconnected_pairs = []
offset = 0
for i in tqdm (range (adj_G.shape[0])):
    for j in range (offset, adj_G.shape[1]):
        if i != j:
            #print (str (i), str (j))
            if nx.shortest_path_length (G, str (i+1), str (j+1))
                if adj_G[i,j] == 0:
                    all_unconnected_pairs.append ([node_list
[i],node_list[j]])
```

```
        offset = offset + 1
node_1_unlinked = [i[0] for i in all_unconnected_pairs]
node_2_unlinked = [i[1] for i in all_unconnected_pairs]
data = pd.DataFrame ({"node_1":node_1_unlinked,
"node_2": node_2_unlinked}) data["link"] = 0
initial_node_count = len (G.nodes)
fb_df_temp = fb_df.copy ()
omissible_links_index = []
for i in tqdm (fb_df.index.values):
    G_temp = nx.from_pandas_edgelist (fb_df_temp.-
drop (index = i), "node_1", "node_2", crea-
te_using = nx.Graph ())
    if (nx.number_connected_components (G_temp)
== 1) and (len (G_temp.nodes) == initial_node
_count):
omissible_links_index.append (i)
fb_df_temp = fb_df_temp.drop (index = i)
Balancing Data
ytrain = np.reshape (ytrain.values, (-1, 1))
total_train = np.append (xtrain, ytrain, axis = 1)
total_train_class0 = total_train[total_train[:,-1] == 0]
total_train_class1 = total_train[total_train[:,-1] == 1]
total_train_class0_sampled = total_train_class0[0:
total_train_class1.shape[0],:]
totalTrainBalanced = np.append      (total_train_class0
_sampled, total_train_class1, axis = 0)
xtrain = totalTrainBalanced[:,  0:  totalTrainBalanced.
shape[1]-1]
ytrain = totalTrainBalanced[:, -1]
ytest = np.reshape (ytest.values, (-1, 1))
total_test = np.append (xtest, ytest, axis = 1)
total_test_class0 = total_test[total_test[:,-1] == 0]
total_test_class1 = total_test[total_test[:,-1] == 1]
total_test_class0_sampled = total_test_class0[0:total_-
test_class1.shape[0],:]
totalTestBalanced = np.append (total_test_class0_samp
led, total_test_class1, axis = 0)
xtest = totalTestBalanced[:,  0:  totalTestBalanced.shape
[1]-1]
ytest = totalTestBalanced[:, -1]
Modeling and Evaluation
def confusion_matrix_scorer (clf, X, y):
    y_pred = clf.predict (X)
    cm = confusion_matrix (y, y_pred)
    return {"accuracy": accuracy_score (y, y_pred),
        "precision": precision_score (y, y_pred),
        "recall": recall_score (y, y_pred),
        "f1": f1_score (y, y_pred),}
def numpy2dataframe (nparray):
```

```
panda_df = pd.DataFrame (data = nparray,
        index = [“Row_” + str (i + 1)
        for i in range (nparray.shape[0])],
        columns = [“Column_” + str (i + 1)
        for i in range (nparray.shape[1])])
    return panda_df
def showReuslt (clf, xtrain, xtest, ytrain, ytest):
    print (“------------Train Result---------------”)
    y_pred = predictions = clf.predict (xtrain)
    plot_confusion_matrix (clf, xtrain, ytrain)
    print (classification_report (ytrain, y_pred))
    print (“------------Test Result---------------”)
    y_pred = predictions = clf.predict (xtest)
    plot_confusion_matrix (clf, xtest, ytest)
    print (classification_report (ytest, y_pred))
maxScore = 0
final_xTrain = []
final_xTest = []
def objective_function_topass (model, X_train, y_train,
X_valid, y_valid):
    global maxScore
    global final_xTrain
    global final_xTest
    model.fit (X_train, y_train)
    P = accuracy_score (y_valid, model.predict (X_valid))
# accuracy_score, precision_score, f1_score, recall_score
    if (P > maxScore):
        maxScore = P
        final_xTrain = X_train
        final_xTest = X_valid
    return P
estimators = [ (“xg”, GradientBoostingClassifier (n_esti
mators = 100,   learning_rate = 1.0,   max_depth = 1,
random_state = 0)),
    (“rf_1”, RandomForestClassifier (n_estimators = 20,
random_state = 10)),
    (“rf_2”, RandomForestClassifier (n_estimators = 30,
random_state = 100))]
clf = StackingClassifier (
    estimators = estimators,   final_estimator = Logistic
RegressionCV ()
)
algo_object = ParticleSwarmOptimization (objective_-
function_topass,   n_iteration = 10,   population_
size = 10, minimize = False)
best_feature_list = algo_object.fit   (clf,   xtrain_df,
pd.DataFrame (ytrain), xtest_df, pd.DataFrame (ytest),
verbose = True)
#plot your results algo_object.plot_history ()
```

Data Availability

The data are tabulated in the article and included in the appendix.

Conflicts of Interest

The authors declare that they have no conflicts of interest.

References

[1] C. P. Muniz, R. Goldschmidt, and R. Choren, “Combining contextual, temporal and topological information for unsupervised link prediction in social networks,” *Knowledge-Based Systems*, vol. 156, pp. 129–137, 2018.

[2] I. Portugal, P. Alencar, and D. Cowan, “The use of machine learning algorithms in recommender systems: a systematic review,” *Expert Systems with Applications*, vol. 97, pp. 205–227, 2018.

[3] A. P. Chobar, M. A. Adibi, and A. Kazemi, “Multi-objective Hub-Spoke Network Design of Perishable Tourism Products Using Combination Machine Learning and Meta-Heuristic Algorithms,” *Environment, Development and Sustainability*, pp. 1–28, 2022.

[4] L. Getoor and C. P. Diehl, “Link mining,” *Acm Sigkdd Explorations Newsletter*, vol. 7, no. 2, pp. 3–12, 2005.

[5] T. E. Senator, “Link mining applications,” *ACM SIGKDD Explorations Newsletter*, vol. 7, no. 2, pp. 76–83, 2005.

[6] N. N. Daud, S. H. Ab Hamid, M. Saadoon, F. Sahran, and N. B. Anuar, “Applications of link prediction in social networks: a review,” *Journal of Network and Computer Applications*, vol. 166, Article ID 102716, 2020.

[7] J. Chen, J. Zhang, X. Xu et al., “E-lstm-d: a deep learning framework for dynamic network link prediction,” *IEEE Transactions on Systems, Man, and Cybernetics: Systems*, vol. 51, no. 6, pp. 3699–3712, 2021.

[8] R. K. BeheraBehera, K. S. Sahoo, D. Naik, S. K. Rath, and B. Sahoo, “Structural Mining for Link Prediction Using Various Machine Learning Algorithms,” *International Journal of Social Ecology and Sustainable Development*, vol. 12, no. 3, pp. 66–78, 2021.

[9] C. Xu, “A novel recommendation method based on social network using matrix factorization technique,” *Information Processing & Management*, vol. 54, no. 3, pp. 463–474, 2018.

[10] A. Pecli, M. C. Cavalcanti, and R. Goldschmidt, “Automatic feature selection for supervised learning in link prediction applications: a comparative study,” *Knowledge and Information Systems*, vol. 56, no. 1, pp. 85–121, 2018.

[11] M. Khaksar, M. R. Meybodi, A. Salajegheh, and A. Salajegheh, “A new irregular cellular learning automata-based evolutionary computation for time series link prediction in social networks,” *Applied Intelligence*, vol. 51, no. 1, pp. 71–84, 2021.

[12] L. Cai, J. Li, J. Wang, and S. Ji, “Line Graph Neural Networks for Link Prediction,” *IEEE Transactions on Pattern Analysis and Machine Intelligence*, vol. 44, no. 9, 2021.

[13] R. Parveen and N. S. Varma, “Friend’s recommendation on social media using different algorithms of machine learning,” *Global Transitions Proceedings*, vol. 2, no. 2, pp. 273–281, 2021.

[14] K. N. Kumar and K. Vineela, “Friend Recommendation Using Graph Mining on Social Media,” vol. 4, no. 5, 2020.

[15] M. V. Murali, T. G. Vishnu, and N. Victor, “A collaborative filtering based recommender system for suggesting new trends in any domain of research,” in *Proceedings of the 2019*

5th International Conference on Advanced Computing & Communication Systems (ICACCS), pp. 550–553, IEEE, Coimbatore, India, March 2019.

[16] H. ZhengWei, M. JinTao, Y. YanNi, H. Jin, and T. Ye, "Recommendation method for academic journal submission based on doc2vec and XGBoost," *Scientometrics*, vol. 127, pp. 2381–2394, 2020.

[17] Y. Chang, L. Shu, E. Du et al., "GraphRR: a multiplex graph based reciprocal friend recommender system with applications on online gaming service," *Knowledge-Based Systems*, vol. 251, Article ID 109187, 2020.

[18] M. Gómez-Víctor, "Supervised Data Mining in Networks: Link Prediction and Aplications," Doctoral Thesis, University of granda, Spain, 2018.

[19] D. Singh and B. Singh, "Investigating the impact of data normalization on classification performance," *Applied Soft Computing*, vol. 97, Article ID 105524, 2020.

[20] A. Grover and A. J. Leskovec, "node2vec: scalable feature learning for networks," in *Proceedings of the 22nd ACM SIGKDD International Conference on Knowledge Discovery and Data Mining*, pp. 855–864, San Francisco, CA, USA, August 2016.

[21] J. Peng, J. Guan, and X. Shang, "Predicting Parkinson's disease genes based on node2vec and autoencoder," *Frontiers in Genetics*, vol. 10, p. 226, 2019.

[22] A. Hagberg and D. Conway, "NetworkX: Network Analysis with Python," 2020.

[23] T. Chen and C. Guestrin, "XGBoost: a scalable tree boosting system,"vol. 13, pp. 785–794, in *Proceedings of the 22nd acm sigkdd international conference on knowledge discovery and data mining*, vol. 13, pp. 785–794, ACM, San Francisco CA USA, August 2016.

[24] M. Saadi and R. Abolfazl, "Analysis and estimation of deforestation using satellite imagery and GIS," *GIS Application in Environment*, 2000.

[25] J. Fan, X. Wang, L. Wu et al., "Comparison of Support Vector Machine and Extreme Gradient Boosting for predicting daily global solar radiation using temperature and precipitation in humid subtropical climates: a case study in China," *Energy Conversion and Management*, vol. 164, pp. 102–111, 2018.

[26] L. Braiman, "Random forests," *Machine Learning*, vol. 45, pp. 5–32, 2001.

[27] V. Kumar and S. Minz, "Feature selection: a literature review," *The Smart Computing Review*, vol. 4, no. 3, pp. 211–229, 2014.

[28] R. Eberhart and J. Kennedy, "A New Optimizer Using Particle Swarm Theory, Sixth International Symposium on Micro Machine and Human Science," in *Proceedings of the 1995 MHS'95. Proceedings of the Sixth International Symposium on Micro Machine and Human Science*, October 1995.

[29] G. V. Rossum, *Python Tutorial*, Vol. 3, 12th Media Services, Suwanee GA USA, 2018.

WILEY | Hindawi

Research Article

Experimental and Computational Approaches for the Classification and Correlation of Temperament (*Mizaj*) and Uterine Dystemperament (*Su'-I-Mizaj Al-Rahim*) in Abnormal Vaginal Discharge (*Sayalan Al-Rahim*) Based on Clinical Analysis Using Support Vector Machine

Arshiya Sultana [iD],[1] **Wajeeha Begum** [iD],[1] **Rushda Saeedi** [iD],[1] **Khaleequr Rahman** [iD],[2] **Md Belal Bin Heyat** [iD],[3,4,5] **Faijan Akhtar** [iD],[6] **Ngo Tung Son** [iD],[7] **and Hadaate Ullah** [iD][8]

[1]*Department of Amraze Niswan Wa Ilmul Qabalat, National Institute of Unani Medicine, Ministry of Ayush, Bengaluru, Karnataka, India*
[2]*Department of Ilmul Saidla, National Institute of Unani Medicine, Ministry of Ayush, Bengaluru, Karnataka, India*
[3]*IoT Research Center, College of Computer Science and Software Engineering, Shenzhen University, Shenzhen, Guangdong 518060, China*
[4]*International Institute of Information Technology, Centre for VLSI and Embedded System Technologies, Hyderabad, Telangana 500032, India*
[5]*Department of Science and Engineering, Novel Global Community Educational Foundation, Hebersham, NSW 2770, Australia*
[6]*School of Computer Science and Engineering, University of Electronic Science and Technology of China, Chengdu, Sichuan, China*
[7]*ICT Department, FPT University, Hanoi, Vietnam*
[8]*Department of EEE, Southern University, Chittagong, Bangladesh*

Correspondence should be addressed to Arshiya Sultana; drarshiya@yahoo.com, Md Belal Bin Heyat; belalheyat@gmail.com, and Hadaate Ullah; hadaate@southern.edu.bd

The temperament (*Mizaj*) of the body is an essential constituent for health conservancy and diagnosis of several diseases. Hence, general body temperament and uterine dystemperament (*Su'-i-Mizaj*) with abnormal vaginal discharge (*Salayan al-Rahim*) need evaluation. In addition, we also applied a computational intelligence technique for enhancing scientific validity to classify the warm-cold and wet-dry temperaments. This trial included a total of 66 participants with a vaginal discharge of reproductive age. Data included demographic characteristics of the participants, symptoms associated with vaginal discharge, women's general temperament, and symptoms of uterine dystemperament. Correlation between general body temperament and age, abnormal vaginal discharge, and its associated symptoms was also performed. Additionally, we used the Support Vector Machine-Radial Basis Function (SVM-RBF) model to classify the warm-cold and wet-dry temperaments. Warm general temperament was highly prevalent (77.27%), followed by moderate (19.69%) on the warm-cold temperament scale. In wet-dry temperament, moderate general body temperament (50%) was more prevalent. In warm-cold and wet-dry scores, 78.78% and 74.24% had warm and wet uterine dystemperament, respectively. The age and symptoms were correlated with general temperament. A strong positive correlation was found between warm general temperament and warm dystemperament of the uterus ($r = 0.40$, $p < 0.009$). In addition, our SVM-RBF CV-5 classification model achieved the highest accuracy (99.2%). Our results showed that vaginal discharge is more common in warm general temperament and warm-wet dystemperament of the uterus. The same has been proven by computational intelligence. Nevertheless, vaginal discharge can also happen in normal and other temperaments.

1. Introduction

As per the Unani concept, the body of a human is made up of four elements (*Arkan*) that influence each other and produce unique qualities, known as *Mizaj* (temperament). These elements and temperaments produced by them are responsible for the growth, nutrition, and metabolism of the organism [1]. The temperament concept is a basic modality of the Unani system of medicine, CAM, widely practised in the subcontinent of India and some other parts of the world. Temperament is one of the fundamental components in defining human health and disease. Hence, the *Mizaj* assessment is used as a tool to determine the physiopathology of disease, diagnosis, prevention of disease, and management in Unani medicine [1, 2]. An individual's temperament directly affects his state of health, and its disruption leads to an imbalance, called dystemperament (*Su'-i-Mizaj*), causing one or more type/s of illnesses [3]. An individual's temperament is maintained and preserved by humour (*Akhlat*) [2]. There are four types of temperaments, namely, warm, cold, wet, and dry, in Unani medicine [4], and they are related to four humours, namely, sanguine, phlegmatic, choleric, and melancholic [1, 2]. Each organ also has its specific temperament in addition to general body temperament [3, 5]. The most common cause of disease of an individual organ is dystemperament, which is represented by various symptoms of that individual organ. Numerous gynaecologic disorders are conceptually associated with the dystemperament of the uterus, including dysmenorrhoea, menstrual disorders, abnormal uterine bleeding (AUB), abnormal vaginal discharge, and infertility [4].

Vaginal discharge (VD) is the commonest complaint [6] and the common reason for which women seek medical attention [7] in their reproductive age group. It can be a normal physiologic variance or a pathological manifestation [6]. AVD is the second most common problem after menstrual disorder or AUB, and 1 in 10 women represents vaginal discharge in a year [8]. In the healthcare setting, approximately 11% to 38.4% of Indian women seek care for vaginal discharge [9]. A study disclosed that about 21% of Indian women are estimated to have any one type of reproductive tract infection/sexually transmitted infection at any given point in time [10]. Abnormal vaginal discharge (AVD) occurs frequently among women with candidiasis, trichomoniasis, bacterial vaginosis, gonorrhoea, and chlamydia [6].

Unani classical manuscripts elucidate the concept of vaginal discharge [11]. Avicenna [12] (980–1037 AD) opined that leucorrhoea (*Sayalan al-Mani*) is an excessive flow of normal discharge from the uterus and vaginal discharge (*Sayalan al-Rahim*) is an infected discharge pouring out from the uterus. Furthermore, he states that normal vaginal discharge is also noted at the time of sexual arousal; however, if the discharge is seen without sexual arousal, then the cause of the discharge is the weakness of the uterine digestive faculty (*Du'fe Quwwat-i-Hadima al-Rahim*). The various aetiological factors of abnormal vaginal discharge are the

dominance of humour (*Ghalaba-i-Akhlat*) causes, an imbalance in the four senses of humour leading to abnormal vaginal discharge, reproductive tract infection/metritis (*Waram al-Rahim*), vaginitis (*Waram al-Mahbil*), syphilis (*Aatshak*), gonorrhoea, and so on [11]. The pathological vaginal discharge may be white, yellow, red, or black [13].

Organ temperament is associated with the humour predominant in that organ, and any qualitative or quantitative change in humour leads to disease. Unani philosophers surmised that the human body is regulated by three major faculties/powers (*Quwa*). Natural faculty (*Quwa Tabiiyya*) is a specific faculty for metabolism, growth, and reproduction [14]. Disturbance of the power of the uterus may cause vaginal discharge. Uterine dystemperament (*Su'-i-Mizaj al-Rahim*) leads to weakness of nutritive faculty (*Du'fe Quwwat Ghadhiya*) that weakens digestive faculty (*Quwwat Hadima*) and uterine retentive faculty (*Quwwat-i-Masika al-Rahim*) [13].

Various studies have shown the relationship between some gynaecological diseases and temperament such as dysmenorrhoea [15], infertility, mixed urinary incontinence [16], and menopausal transition [17]. The principle of disease management in Unani medicine is to correct the changed temperament, as general temperament (*Mizaj Shakhsi*) or uterine dystemperament is considered an important cause of disease. Thus, the patient's general and/or organ temperament needs to be assessed before initiating the treatment. Furthermore, other traditional medicine studies also indicated that clinical practice with syndrome differentiation perhaps leads to the innovation and improvement of biomedical diagnoses [18]. To date, none of the studies has determined the association between the general temperament and dystemperament of the uterus in AVD, its associated symptoms, and gynaecological infections.

Additionally, computational intelligence plays a significant role in the medical field, such as localization, treatment, detection, and recommendation. Presently, some intelligence techniques such as deep learning machine learning and the Internet of Things (IoT) [19] with processing techniques such as text, image, signal, video, and audio processing are used in medical areas. Previously, physiological signals are used to detect sleep disorders [20–22]. The authors applied intelligence techniques for the analysis of experimental data related to oxidative stress and mRNA [23–25]. Ali et al. [26] designed an automatic system for the detection of Parkinson's disease based on the ensemble learning technique. Ukwuoma et al. [27] used different deep learning to classify and detect medical diseases. Lai's group used medical machine learning and deep learning techniques to automatically detect bruxism sleep disorder [28–31] and cardiac diseases [32]. However, we used the computational intelligence technique to classify the temperament in AVD data in this study.

Thus, the objective of this study was to determine and correlate the general body and dystemperament of the uterus in AVD and its associated symptoms. In addition, we also

applied computational intelligence for enhancing scientific validity to classify the warm-cold and wet-dry general temperament.

The main contributions of this study are as follows:

(i) This study will provide the scientific basis for the traditional concept of the role of temperament in health and disease.

(ii) This study will help clinicians to diagnose gynaecological disorders and to treat them accurately and easily by quantifying the temperament of organs and the patient's general temperament.

(iii) This study will provide support to the clinician to select proper diet and Unani drugs as per temperament based on the general body or uterine temperament as the treatment modality is a heteropathy regimen as in Unani medicine, the basic principle of treatment is treatment contrasts with the nature and temperament of the disease or heteropathic regimen (*Ilaj-bil-Zid*).

(iv) This study will design a heatmap based on a clinical experiment and classify warm and wet general body temperament and uterine dystemperament in AVD using the Support Vector Machine-Radial Basis Function (SVM-RBF) model.

(v) This study may facilitate clinicians in their day-to-day diagnosis and treatment.

The proposed paper is organized in the standard format: Introduction, Materials and Methods, Result, Discussion, and Conclusion (Figure 1).

2. Materials and Methods

2.1. Study Design. A single-centre, retrospective study included a total of 66 participants with the AVD of reproductive age who fulfilled the inclusion criteria. The data were collected from March 2018 to November 2018. This study was conducted in the Department of Ilmul Qabalat wa Amraze Niswan (OBG), National Institute of Unani Medicine, Bengaluru, India.

2.2. Institutional Review Board and Ethical Consideration. The scientific and ethical committee approved the intramural research protocol with reference IEC No. NIUM/IEC/2019–20/IMR/02. This study was completed based on the Helsinki Declaration and the GCP guidelines, Ministry of Ayush, GOI. The study is registered with the Central Trial Registry of India with reference No. CTRI/2021/01/030553 (dated: 15/01/2021).

2.3. Informed Consent Statement. Written informed consent was obtained from each participant included in the study.

2.4. Participant's Description. Sixty-six were included of the 97 participants who were initially screened, and 31 were excluded because of various reasons (fibroid and ovarian cysts ($n = 10$), severe PID ($n = 11$), cervical cancer ($n = 1$),

lactation ($n = 3$), positive urine pregnancy test ($n = 2$), and intrauterine contraceptive device ($n = 4$)). Thus, 66 participants were included.

2.4.1. Eligibility Criteria. The inclusion criteria included married women aged 18–50 years who had a history of AVD or/and associated with symptoms such as dyspareunia, dysuria, burning micturition, vulvar itching, and vaginal malodour. The exclusion criteria were participants with any undiagnosed vaginal or uterine bleeding, ulceration, genital malignancies, pregnancy, and lactating women. Participants with any clinical manifestation of venereal disease were also excluded.

2.4.2. Procedure. Sociodemographics included information such as name, age, address, contact number, education, occupation, socioeconomic status as per the Kuppuswamy scale, and habitat. The detailed menstrual history of the age of onset of menarche, menstrual cycle pattern, last menstrual period (LMP), and associated symptoms was noted. Detailed obstetrical and contraceptive history was recorded. VAS score for the symptoms associated with AVD was also noted. Furthermore, severity grading of symptoms as none (0), mild (1–3), moderate (4–6), and severe (7–10) was also noted. Per speculum and vaginum examination findings recorded were noted and analysed. Furthermore, a validated questionnaire for general temperament and clinical features to assess the uterine dystemperament described in the Unani literature was retrieved. Specific investigation such as human immunodeficiency virus (HIV), hepatitis B surface antigen (HbsAg), Venereal Disease Research Laboratory (VDRL), Pap smear, vaginal wet mount, and pelvic ultrasonography was carried out to diagnose the cause of the vaginal discharge.

2.5. Assessment Tool

2.5.1. Validated Temperament Questionnaire. A well-validated questionnaire included 10 questions to assess the general temperament of the body based on the clinical features of the ten determinants mentioned by Avicenna. Cronbach's α coefficient was 0.71 for this questionnaire [33], and the reliability was 0.82 through the test-retest technique with Spearman-Brown correlation coefficient ($P < 0.05$) [34].

2.5.2. Dystemperament of the Uterus. The clinical features were scored on a rating scale of 2 through 1. The total score of each patient was added up, and the inferences for the dystemperament of the uterus were taken based on an equal-interval scale developed from the total score of the questionnaire. The reliability was 0.87 for split-half reliability for the questionnaire [17].

2.5.3. Sample Size. The sample size was calculated as 60 based on the scores of the scales. After including 10% dropout in total, the sample size was calculated as 66 shown in (1) [16]:
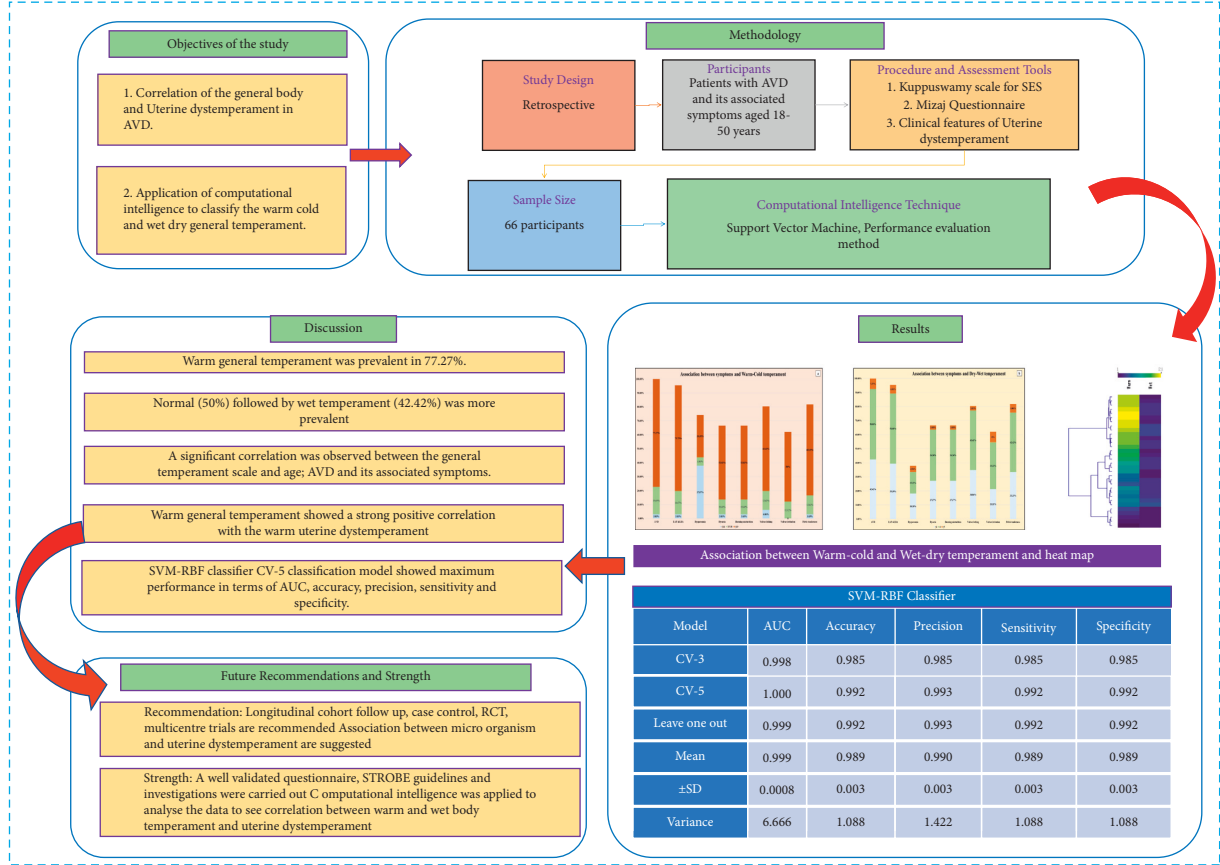
FIGURE 1: Schematic representation of the whole study.

$$\text{Sample size} = \left[\frac{\partial}{\mu 1 - \mu 2}\right]^2 = \left[\frac{6.0}{10 - 7.2}\right]^2 x15 = 60. \quad (1)$$

2.5.4. Statistical Methods.

The data analysis was performed by the statistical software SPSS 28 version. The mean ± SD and number (%) were imputed for continuous and categorical data measurements, respectively. The coefficient correlation was calculated to observe the association between age, abnormal vaginal discharge, associated symptoms, and temperament.

2.6. Computational Intelligence Technique

2.6.1. Support Vector Machine.

One of the supervised machine learning techniques is the Support Vector Machine (SVM). It is utilized in the classification and regression methods of data analysis. For data prediction, an SVM creates a hyperplane in infinite-dimensional space. The hyperplane with the greatest distance to the nearest training point of the class achieves the maximum accuracy. SVM was initially established in 1963 by prominent scientists Alexey and Vladimir. After 29 years, Vapnik's team created SVM for nonlinear data using a kernel method to boost the hyperplanes' maximum margin [35]. We used SVM-Radial Basis Function (SVM-RBF) kernel classifier in the present classification [36].

2.6.2. Performance Evaluation Method.

General temperament and dystemperament of the uterus, warm-cold, and dry-wet temperament scores were analysed in terms of accuracy, sensitivity, precision, specificity, and Area Under the Curve (AUC). We used SVM-RBF with leave-one-out cross-validation (CV) 3- and 5-fold models. The warm and wet general body temperament and dystemperament of the uterus in AVD were analysed in terms of accuracy, sensitivity, precision, specificity, and area under the curve (AUC) [37–39], as shown in equations (2)–(5).

$$\text{Accuracy} = \left(\frac{(TP + TN)}{(TP + TN + FP + FN)}\right), \quad (2)$$

$$\text{Sensitivity} = \left(\frac{TP}{(FN + TP)}\right), \quad (3)$$

$$\text{Specificity} = \left(\frac{TN}{(FP + TN)}\right), \quad (4)$$

$$\text{precision} = \left(\frac{TP}{(TP + FP)}\right), \quad (5)$$

where TP is a true positive, FP is a false positive, TN is a true negative, and FN is a false negative.

3. Results

3.1. Demographic Variables. Participants with AVD were in the age group of 19 to 40 years, and the mean age was 29.61 ± 5.65 years. Out of 66 participants, 21.21% ($n = 24/66$) and 78.78% ($n = 52/66$) were Hindus and Muslims, respectively. The mean weight of the participants was 61.65 ± 14.02 kg. The mean height of the participants was 155.60 ± 5.14 cm. The mean BMI was 25.59 ± 5.54 kg/m². Two (3.03%) and 64 (96.96%) participants were from rural and urban areas, respectively (see Figure 2).

3.2. Socioeconomic Status. The highest number of participants was from the upper-middle class ($n = 29/66$, 43.93%), followed by the lower middle class ($n = 25/66$, 37.87%). Further details are summarized in Figure 3.

3.3. Menstrual and Obstetrics History. The menarche's mean age was 13.22 ± 0.87 years. The duration of the menstrual cycle was 27.91 ± 1.17 days, and the duration of flow was 3.90 ± 1.40 days. The past menstrual cycle was regular in 57 (86.36%) participants. Normal vaginal delivery (NVD) was noted in 51 (77.27%) participants. Further obstetrics details are summarized in Figure 4.

3.4. Clinical Examination Findings. Maximum participants had moderate ($n = 43/66$, 65.15%) and foul-smelling abnormal vaginal discharge ($n = 50/66$, 75.75%), and 57 (86.36%) participants had abnormal cervical findings (Figure 5).

3.5. Specific Investigations. Pap smear, vaginal wet mount, and pelvic ultrasonography were specific investigations carried out to diagnose the causes of vaginal discharge. Maximum participants had inflammatory Pap smear ($n = 44/66$, 66.66%) followed by bacterial vaginosis ($n = 13/66$, 19.69%). Amsel's criteria showed that the Whiff test and blue cells were positive in 17 (25.75%) participants. KOH test was positive in one (1.15%) patient. The normal saline test for trichomonas was negative in all participants. The vaginal pH was 4.56 ± 0.46, and normal HIV, HbsAg, and VDRL were negative in all participants. Maximum participants (54.54%) had pus cells between 21 and 30/HPF. Maximum participants had pathological findings in ultrasonography ($n = 35/66$, 53.03%) (Figure 6).

3.6. Prevalence of Infections (Alone and/or Mixed Infections). Maximum participants had mixed infections ($n = 48/66$, 72.72%) (Table 1 and Figure 7).

3.7. Age, General Body Temperament, and Dystemperament of the Uterus. Participants with AVD had a high prevalence of warm ($n = 51/66$, 77.27%) in warm-cold and normal ($n = 33/$ 66, 50%) in wet-dry general body temperament. Likewise, participants had a high prevalence of warm ($n = 52/66$, 78.78%) in warm-cold and wet ($n = 49/66$, 74.24%) in wet-dry uterine dystemperament. Warm ($n = 48/66$, 72.22%) in warm-cold and normal ($n = 30/66$, 45.45%) in wet-dry general temperament were more common between the age of 21–40 years (Table 2).

3.8. Distribution of Participants. Participants with abnormal vaginal discharge had a high prevalence of warm ($n = 51/66$, 77.27%) in warm-cold and normal ($n = 33/66$, 50%) in wet-dry general body temperament (Table 3). High prevalence of warm temperament in warm-cold and normal in wet-dry general body temperament was noted in participants with lower abdominal pain (75.75%, 50%), dyspareunia (30.30%, 15.15%), dysuria (53.03%, 36.36%), burning micturition (53.03%, 36.36%), vulval itching (60.60%, 42.42%), vulvar irritation (50%, 33.33%), and pelvic tenderness (65.65%, 42.42%) signs and symptoms (Table 3 and Figure 8). Table 4 summarizes the data according to the severity of symptoms and general body temperament.

3.9. Correlation between General Temperament and Age, Abnormal Vaginal Discharge, and Its Associated Symptoms

3.9.1. Warm-Cold Temperament. Between age 20–30 years and normal temperament, a very strong positive coefficient correlation ($r = 0.94$) was noted, followed by a moderate positive coefficient correlation ($r = 0.31$) between age 20–40 years and normal temperament, and a weak negative coefficient correlation ($r = -0.22$) between warm temperament and age 20–40 years was observed in the warm-cold temperament scale (Table 5).

3.9.2. Wet-Dry Temperament. A weak negative coefficient correlation ($r = -0.22$) between wet temperament age and 20–30 years was observed in the wet-dry temperament scale (Table 5).

3.9.3. AVD and Its Associated Symptoms. The correlations between AVD and its associated symptoms are summarized in Table 5. A strong negative correlation between vulvar irritation and normal general body temperament was noted in the warm-cold temperament scale ($r = -0.53$).

3.9.4. Correlation of General Temperament and Dystemperament of the Uterus. The warm general temperament had a strong positive correlation with warm dystemperament of the uterus ($r = 0.403$, $P < 0.009$).

3.10. Computational Result. Our SVM-Radial Basis Function (SVM-RBF) CV-5 classification model achieved maximum performance in terms of AUC (100%), accuracy (99.2%), precision (99.3%), sensitivity (99.2%), and specificity (99.2%). In addition, our SVM-RBF CV-3 classification
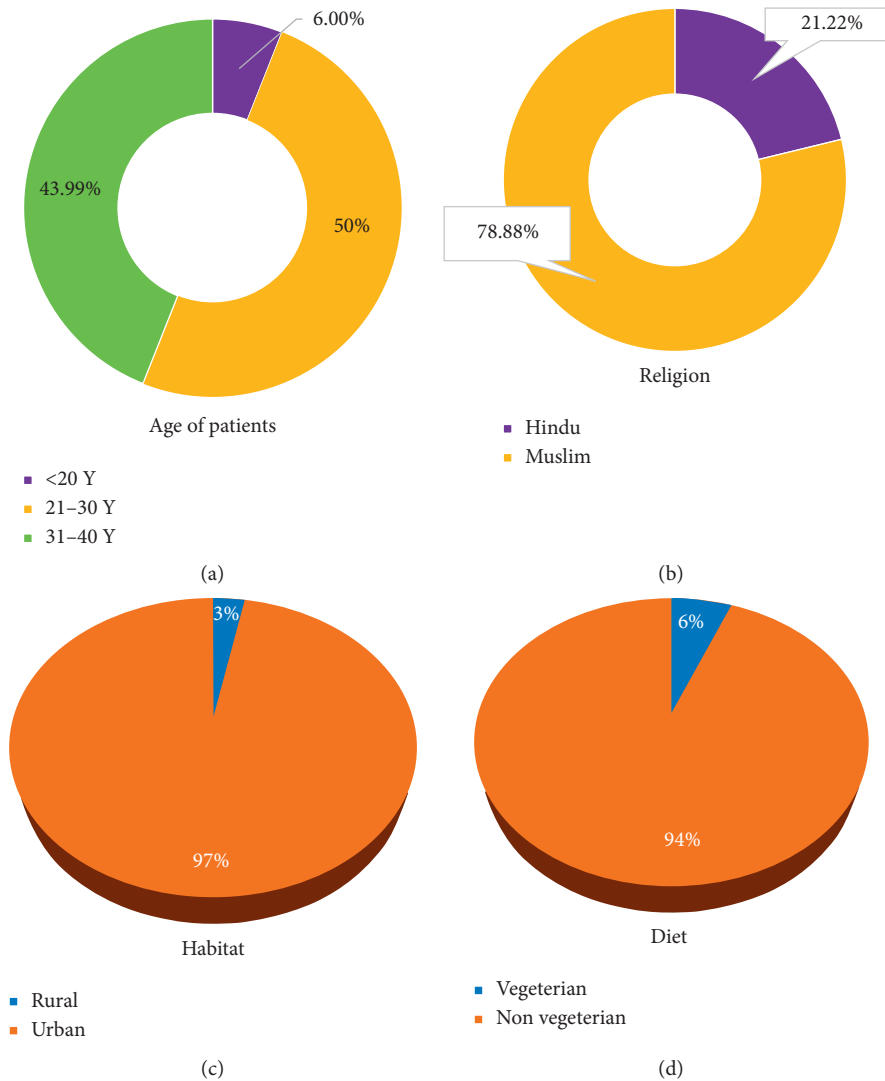
FIGURE 2: Demographic variables of patients with abnormal vaginal discharge. (a) Age of patients. (b) Religion. (c) Habitat. (d) Diet.

model has minimum performance in terms of AUC (99.8%), accuracy (98.5%), precision (98.5%), sensitivity (98.5%), and specificity (98.5%). However, our SVM-RBF CV-5 model is more suitable for the classification of warm and wet general body temperament and uterine dystemperament (Table 6). However, we also designed the heatmap for the relationship between general body temperament and uterine dystemperament in abnormal vaginal discharge mentioned in Figure 9.

4. Discussion

4.1. Major Findings. We explored the correlation between the general temperament and dystemperament of the uterus with age, AVD, and its associated symptoms. The data shows that warm general temperament was prevalent in 77.27% of participants with AVD. Normal (50%) followed by wet temperament (42.42%) was more prevalent in participants with AVD. A significant correlation was observed between the general temperament scale and age, AVD, and its

associated symptoms. Moreover, it was observed that the warm general temperament showed a strong positive correlation with the warm dystemperament of the uterus. In addition, SVM-RBF classifier CV-5 classification model showed maximum performance in terms of AUC (100%), accuracy (99.2%), precision (99.3%), sensitivity (99.2%), and specificity (99.2%).

4.2. Sociodemographic Characteristics, Gynaecological, and Obstetrical History. In this study, the majority of participants were urban ($n = 64/66$, 96.96%). Similarly, Mulu et al. [40] also reported that the majority of participants were urban. Educational levels showed that 75.75% of participants had higher and above education levels. The middle socioeconomic class was the highest prevalence of AVD, 81.81%, followed by the upper lower class (18.18%). This shows that AVD is more common in middle and low socioeconomic status people. Previous research has observed associations between socioeconomic status, disease prevalence, and mortality [41, 42]. A previous study found that low
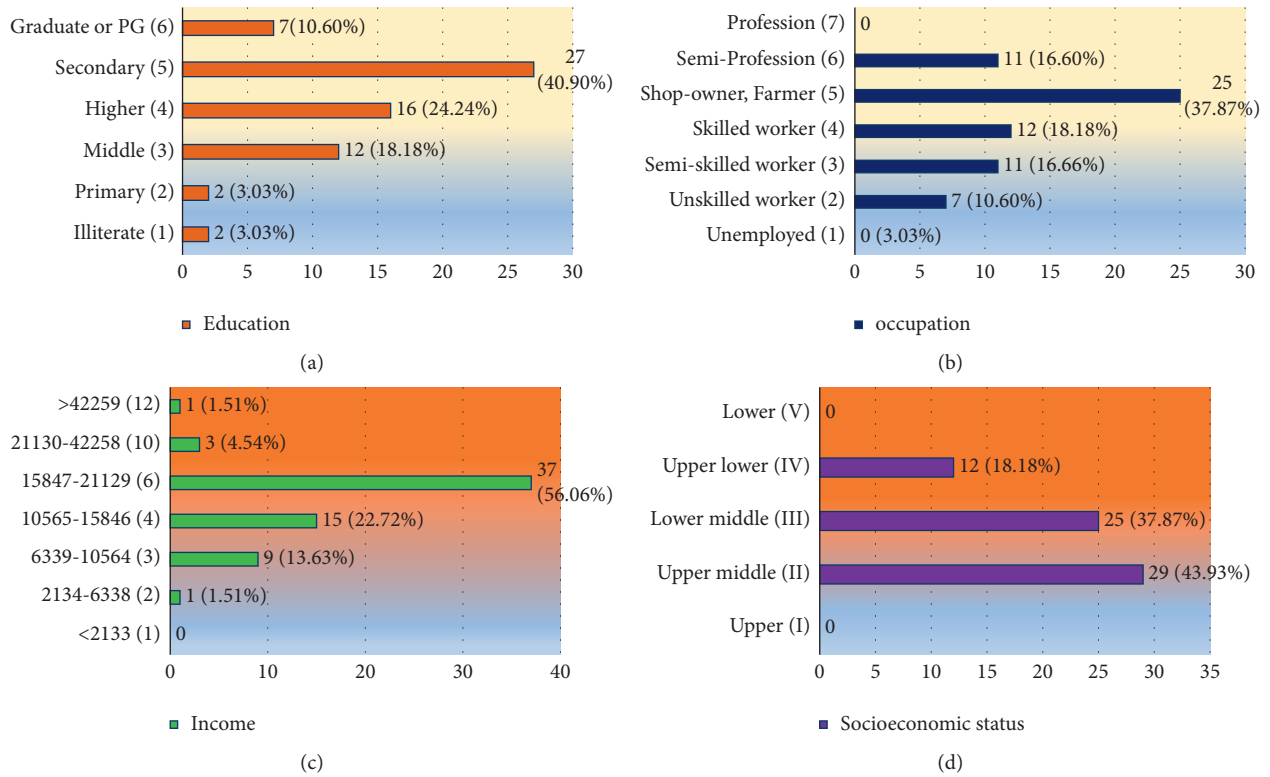
FIGURE 3: Socioeconomic status of patients with abnormal vaginal discharge. (a) Education. (b) Occupation. (c) Income. (d) Socioeconomic status.
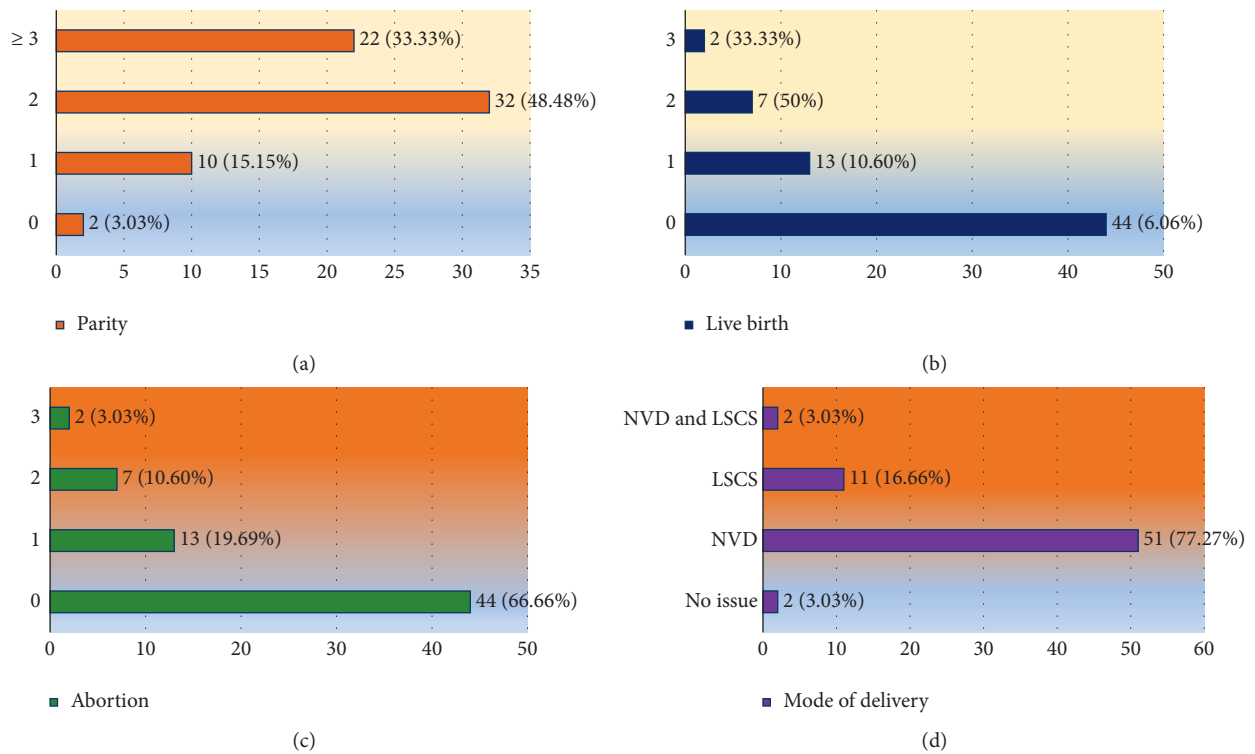
FIGURE 4: Obstetrics history of participants with abnormal vaginal discharge. (a) Parity. (b) Live birth. (c) Abortion. (d) Mode of delivery.
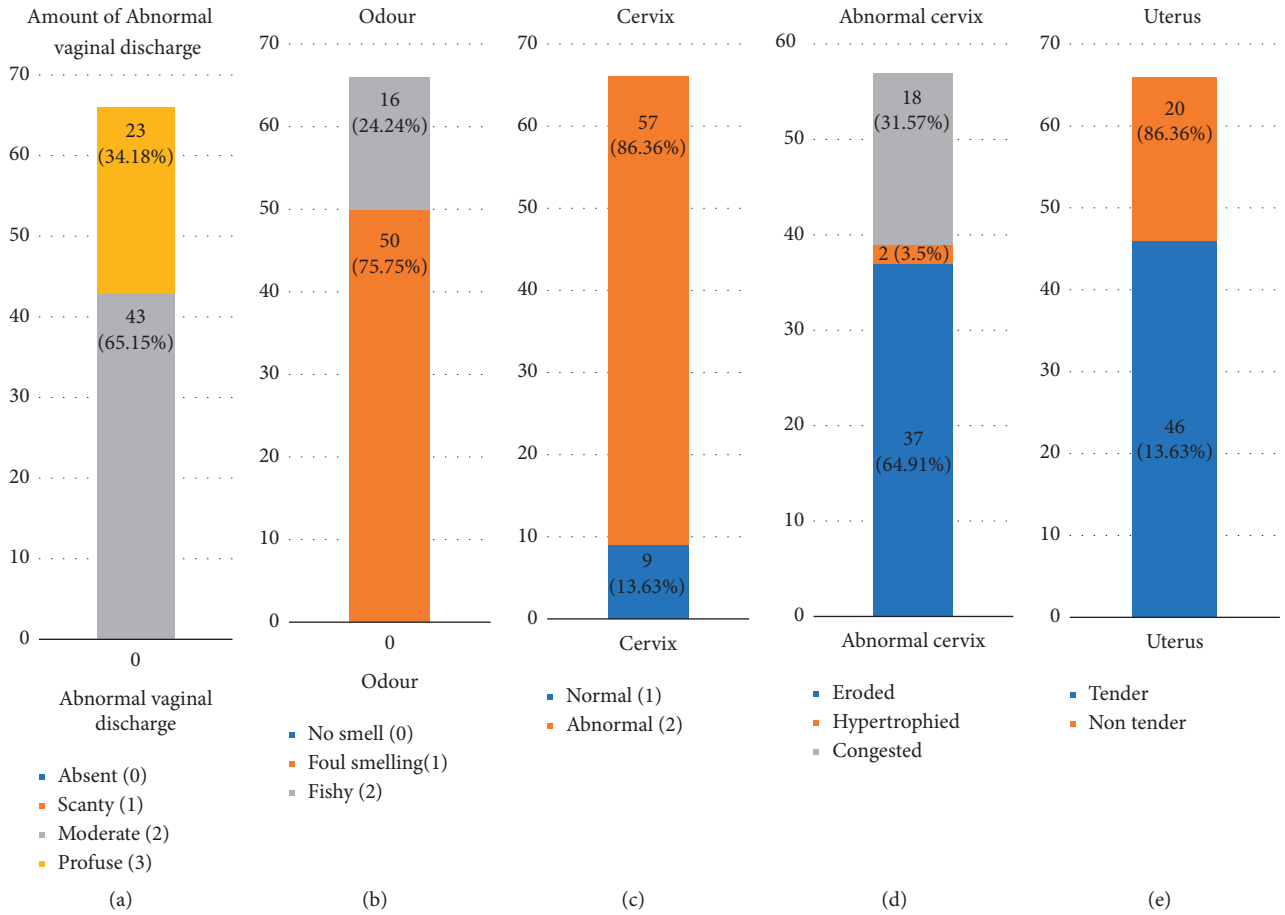
FIGURE 5: Clinical examination findings of participants with abnormal vaginal discharge. (a) Abnormal vaginal discharge. (b) Odour. (c) Cervix. (d) Abnormal cervix. (e) Uterus.
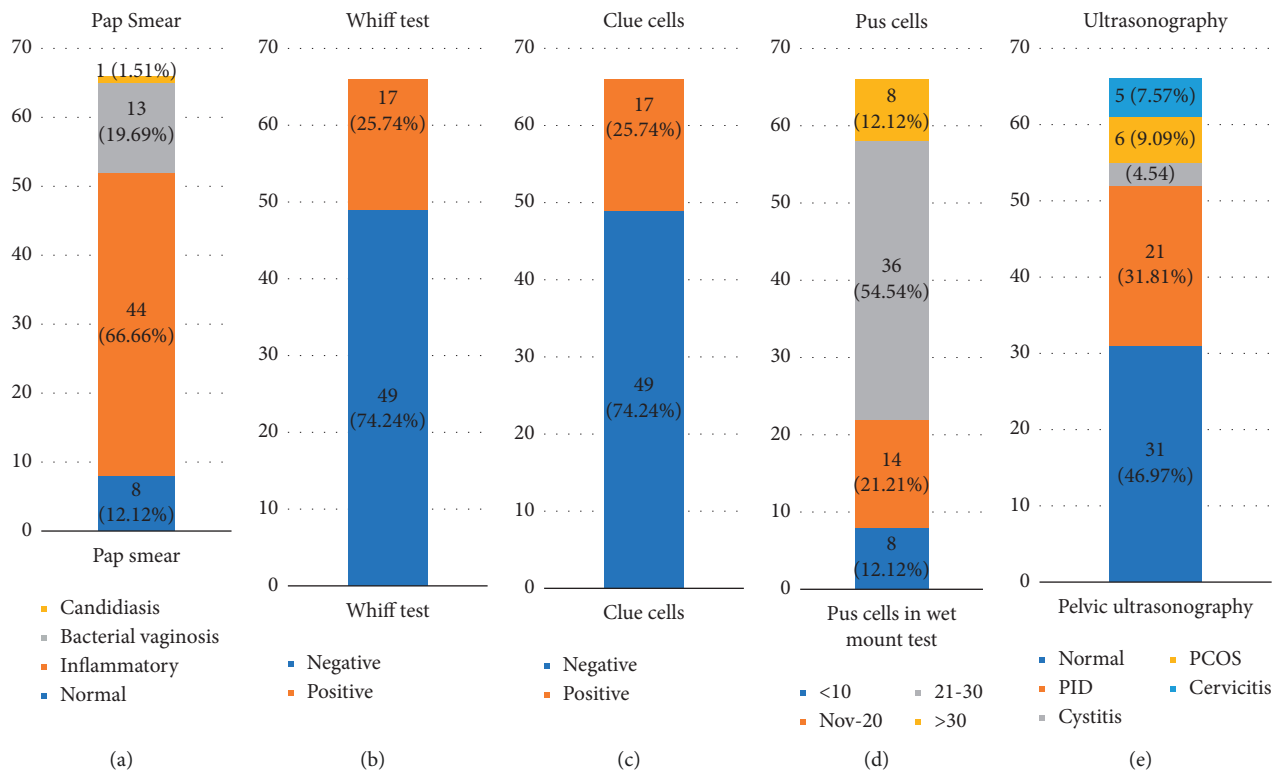
FIGURE 6: Specific investigations of participants with abnormal vaginal discharge. (a) Pap smear. (b) Whiff test. (c) Clue cells. (d) Pus cells. (e) Ultrasonography.

TABLE 1: Prevalence of infections alone and/or mixed infections.

Infections	No. of participants ($n = 66$)	%
Bacterial vaginosis	1	1.51
Cervicitis	5	7.57
Cervical ectopy	7	10.60
Total	**13**	**27.27**
Mixed infections		
PID + cervicitis	4	6.06
PID + CE	2	3.03
PID + BV	7	10.60
BV + CE	6	9.09
CE + cervicitis	21	31.81
Cervicitis + CE + PID	9	13.63
PID + BV + CE	3	4.54
Total	**53**	**80.80**

BV: bacterial vaginosis; CE: cervical ectopy; PID: pelvic inflammatory disease.
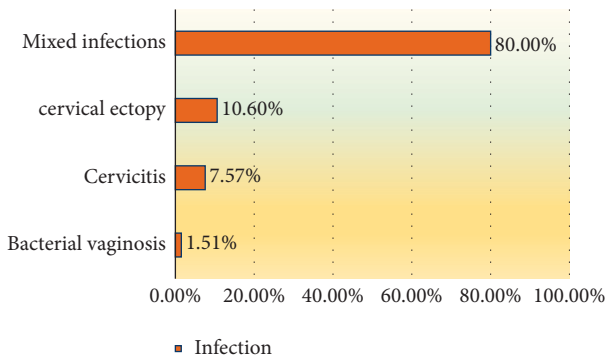
FIGURE 7: Prevalence of infection in participants with abnormal vaginal discharge.

TABLE 2: Age, general temperament (*Mizaj*), and dystemperament of the uterus (*Su'-i-Mizaj al-Rahim*) in abnormal vaginal discharge.

Age and general temperament								
Warm-cold temperament								
Age (y)	≤14 (cold)		15–18 (normal)		≥19 (warm)		Total ($n = 66$)	
	No	%	No	%	No	%	No	%
≤20	0	0	1	1.15	3	4.54	4	6.06
21–30	0	0	6	9.09	27	40.90	33	50
31–40	2	3.03	6	9.09	21	31.81	29	43.93
Total	2	3.03	13	19.69	51	77.27	66	100
Wet-dry temperament								
	≤3 (wet)		4 (normal)		≥5 (dry)		Total	
≤20	1	1.51	3	4.54	0	0	4	6.06
21–30	14	21.21	14	21.21	5	7.57	33	50
31–40	13	19.69	16	24.24	0	0	29	43.93
Total	28	42.42	33	50	5	7.57	66	100
Age and dystemperament of the uterus								
Age	≥6 (warm)		<6 (cold)		≥4 (wet)		<4 (dry)	
	No	%	No	%	No	%	No	%
≤20	3	4.54	1	1.51	3	4.54	1	1.51
21–30	23	34.84	10	15.14	24	36.36	9	13.63
31–40	26	39.39	3	4.54	22	33.33	7	10.60
Total	52	78.78	14	21.21	49	74.24	17	25.75

socioeconomic status, malnutrition, and unhygienic conditions may be accountable for AVD [43]. This study is similar to previous studies where abnormal vaginal discharge was common in low socioeconomic groups [44, 45]. The majority of participants were Muslim (78.78%). Similarly, a study conducted in Bangladesh also showed that the prevalence of AVD is more common in Muslims [45]. The age of menarche was 13.22 ± 0.87 years, and 81.81% had two or more two children, comparable to the previous study. Besides, 93.33% of the participants had experienced childbirth [46].

4.3. General Temperament. We found that 57.5% and 42.42% had warm and wet temperaments, respectively. Unani philosophers inferred that not only does warm-wet temperament cause AVD but also occasionally dry, warm, or normal or warm-dry temperament may also cause AVD. Furthermore, AVD may occur because of an abnormality in the quantity and quality of matter in the dystemperament. Cold, dry, warm or warm-dry, and dystemperament (simple or compound) cause derangement of expulsive faculty [12–14]. A previous study also reported that AVD was predominant in warm humour (*Khilt Harr*) participants [47].

4.4. General Temperament and Age. The mean age was 29.61 ± 5.65 years, similar to the previous studies [48]. Khan [13] observed that AVD was more prevalent in reproductive age due to the predominance of warm dystemperament of the uterus (*Su'-i-Mizaj al-Rahim Harr*) or warm humour in the body at reproductive age. However, he also surmised that dominance of all humour causes AVD. This study observed that AVD was more prevalent in warm-normal/wet temperament participants. In addition, a few participants also had cold-dry temperaments. Bhat and Begum found that AVD is more prevalent in women aged 25–35 years [47], and similarly, another study observed that the active reproductive age group is more predisposed to AVD [49]. We found the highest prevalence of AVD in the age group of 21–30 years ($n = 33/66$, 50%), followed by 31–40 years ($n = 29/66$, 43.93%). Our study reported the highest prevalence of warm (72.71%) and normal/wet general temperament (45.45%) above 21 years of age. Furthermore, a very strong positive coefficient (0.94) between age 21–30 years and normal temperament was noted. This shows that as age increases, the warmth decreases, and at a young age, the temperament is warm. Unani physicians describe that the human life period is divisible into four age groups. Each age group may have its specific temperament; namely, temperament in growing age (*Sinn -i-Namu*-21–30 years) is warm-wet temperament as in this period of growth, both innate humour (*Rutubat-i-Ghariziyya*) and innate heat (*Hararat-i-Ghariziyya*) are dominant. Adulthood (*Sin-i-Shabab*) ranges from thirty to forty (30–40 years) years and possesses a normal temperament [47, 50]. In this period, the quantity of innate humour *is* equal to the quantity required for the preservation of innate heat, neither excessive nor deficient, and maintains the continuance of normal

TABLE 3: Abnormal vaginal discharge, its associated symptoms, and general temperament.

VAS score for symptoms	No. of participants ($n = 66$)	General body temperament					
		Warm-cold			Wet-dry		
		≤14 (cold)	15–18 (normal)	≥19 (warm)	≤3 (wet)	4 (normal)	≥5 (dry)
AVD	6.30 ± 0.65						
Absent	0	0	0	0	0	0	0
Present	66 (100)	2 (3.03)	13 (19.69)	51 (77.27)	28 (42.42)	33 (50)	5 (7.57)
LAP and LBA	4.92 ± 1.50						
Absent	3 (4.54)	0	2 (3.03)	1 (1.51)	2 (3.03)	0	1 (1.51)
Present	63 (95.45)	2 (3.03)	11 (16.67)	50 (75.75)	26 (39.39)	33 (50)	4 (6.06)
Dyspareunia	1.65 ± 2.31 41 (62.12)						
Absent	41 (62.12)	1 (1.51)	9 (13.63)	31 (46.97)	16 (24.24)	23 (34.84)	2 (3.03)
Present	25 (37.87)	1 (1.51)	4 (6.06)	20 (30.30)	12 (18.18)	10 (15.15)	3 (4.54)
Dysuria	1.77 ± 2.41						
Absent	40 (60.60)	0	6 (9.09)	16 (24.24)	10 (15.15)	8 (12.12)	4 (6.06)
Present	26 (39.39)	2 (3.03)	7 (10.60)	35 (53.03)	18 (27.27)	24 (36.36)	2 (3.03)
Burning micturition	3.24 ± 2.46						
Absent	22 (33.33)	0	6 (9.09)	16 (24.24)	10 (15.15)	8 (12.12)	4 (6.06)
Present	44 (66.67)	2 (3.03)	7 (10.60)	35 (53.03)	18 (27.27)	24 (36.36)	2 (3.03)
Vulvar itching	4.27 ± 2.31						
Absent	13 (19.69)	0	4 (6.06)	9 (13.63)	5 (7.57)	5 (7.57)	3 (4.54)
Present	53 (80.30)	4 (6.06)	9 (13.63)	40 (60.60)	23 (34.84)	28 (42.42)	2 (3.03)
Vulvar irritation	3.09 ± 2.62						
Absent	25 (37.87)	2 (3.03)	5 (7.57)	18 (27.27)	14 (21.21)	9 (13.63)	2 (3.03)
Present	41 (62.12)	0	8 (12.12)	33 (50)	14 (21.21)	22 (33.33)	5 (7.57)
McPS (pelvic tenderness)	2.27 ± 1.39						
Absent	12 (18.18)	0	4 (6.06)	8 (12.12)	6 (9.09)	5 (7.57)	1 (1.51)
Present	54 (81.81)	2 (3.03)	9 (13.63)	43 (65.15)	22 (33.33)	28 (42.42)	4 (6.06)

Data presented: no. (%) or mean ± SD; AVD: abnormal vaginal discharge; LAP: lower abdominal pain; LBA: low backache; McPS: modified McCormack pain scale for abdominopelvic tenderness; VAS: Visual Analogue Scale.
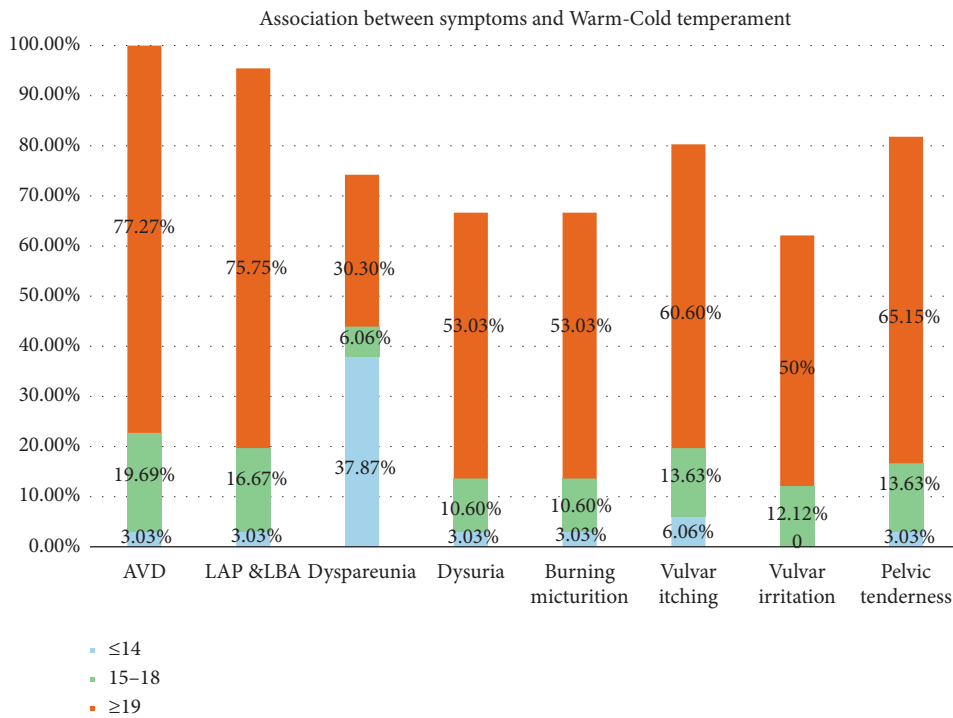
(a)

FIGURE 8: Continued.
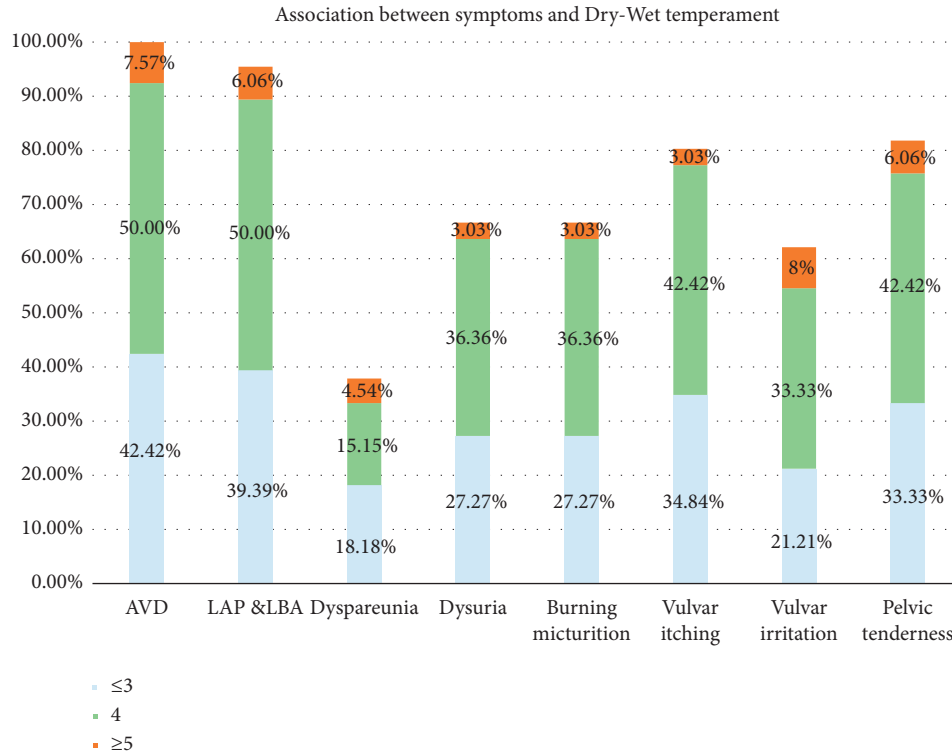
Figure 8: Association between symptoms with temperament. (a) Warm-cold and (b) dry-wet temperament.

metabolism. In this period, neither any growth nor any dissolution or degeneration occurs in the organs. Thus, the temperament of this period is normal. Usually, sanguine and bilious diseases are most common in this period. We also observed that AVD participants had warm (40.90%) and wet (21.21%) general body temperaments between the age of 21–30 years. A previous study also reported that AVD was predominant in warm temperament participants [47].

4.5. General Temperament, Abnormal Vaginal Discharge, and Associated Symptoms. In our study, AVD was associated with other gynaecological complaints such that 95.95% had lower abdominal pain (LAP) and backache (LBA), 37.87% had dyspareunia, 39.39% had dysuria, 66.67% had burning micturition, 80.30% had vulvar itching, and 62.12% had vulvar irritation. A previous study reported that all participants who had abnormal vaginal discharge also had associated symptoms [47]. Another study also reported that vaginal discharge was associated with pruritus, pain in the lower abdomen (84.1%), backache (72.96%), and burning micturition (66.7%). The majority of participants reported foul smell (75.75%) [44] discharge in our study, and a similar previous study also reported foul smell discharge in 60.4% of women. One more study also reported vaginal discharge associated with other clinical features [48]. Unani philosophers opined that AVD is associated with other gynaecological complaints such as pruritus, vulvae, low backache, increased frequency of urine, heaviness in the lower abdomen, lethargy, generalized weakness, giddiness,

dysmenorrhoea, constipation, burning sensation in extremities, cramps in lower limbs, and irritable mood. Furthermore, they also stated that sometimes it is also noted during pregnancy, which is copious and associated with severe itching [12, 13].

The commonest symptoms associated with AVD were LBA and abdominal pain in the present study. Various studies demonstrated the positive association between temperament and pain profiles in many diseases. Knaster et al. [51] showed that, in participants with chronic pain, temperament evaluation could improve the professionals' understanding of pain and behavioural experience. The traditional medicine texts review proposes that temperament correction can affect psychological and physical symptoms [15].

4.6. Dystemperament of the Uterus. Warm-wet uterine dystemperament prevalence was the highest (78.78%–74.74%) in AVD participants. Dystemperament of the uterus holds significant importance in uterine diseases; hence diagnosis and treatment depend upon the determination of individual and organ temperament [4]. A study found dry dystemperament of the uterus in all menopausal transition participants [17]. We found a significant correlation between general temperament and warm uterine dystemperament in AVD. As per the literature, warm dystemperament diseases are more common in reproductive age. In addition, the dystemperament of the uterus could also diffuse to the entire body and cause the body's dystemperament [52]. In our study, AVD

TABLE 4: Severity of symptoms and general temperament.

Severity grading of symptoms	Warm and cold			Wet and dry			Total ($n=66$)
	≤14	15–18	≥19	≤3	4	≥5	
AVD							
None	0 (0)	0 (0)	0 (0)	0 (0)	0 (0)	0 (0)	0 (0)
Mild	0 (0)	0 (0)	0 (0)	0 (0)	0 (0)	0 (0)	0 (0)
Moderate	2 (3.03)	9 (13.63)	36 (54.54)	20 (30.30)	24 (36.36)	3 (4.54)	47 (66.66)
Severe	0	4 (6.06)	15 (22.72)	8 (12.12)	9 (13.63)	2 (3.03)	19 (33.33)
LBA and LAP							
None	0	2 (3.03)	1 (1.15)	2 (3.03)	0	1 (1.51)	3 (4.54)
Mild	0	1 (1.51)	2 (3.03)	2 (3.03)	1 (1.51)	0	3 (4.54)
Moderate	2 (3.03)	10 (15.15)	43 (65.15)	23 (34.84)	29 (43.93)	3 (4.54)	55 (83.33)
Severe	0	0	5 (7.57)	1 (1.51)	3 (4.54)	1 (1.51)	5 (7.57)
Dyspareunia							
None	1 (1.51)	9 (13.63)	31 (46.96)	16 (24.24)	23 (34.84)	2 (3.03)	41 (62.12)
Mild	0	0	8 (12.12)	4 (6.06)	4 (6.04)	0	8 (12.12)
Moderate	0	4 (6.06)	11 (16.66)	8 (12.12)	6 (9.09)	2 (3.03)	16 (24.24)
Severe	1 (1.51)	0	1 (1.51)	0	0	1 (1.15)	1 (1.51)
Dysuria							
None	1 (1.51)	8 (12.12)	31 (46.96)	16 (24.24)	20 (30.30)	4 (6.06)	40 (60.60)
Mild	1 (1.51)	0	7 (10.60)	1 (1.51)	7 (10.60)	0	8 (12.12)
Moderate	0	5 (7.57)	13 (19.69)	11 (16.66)	6 (9.09)	1 (1.51)	18 (27.27)
Severe	0	0	0	0	0	0	0 (0)
Burning micturition							
None	0	6 (9.09)	16 (24.24)	10 (15.15)	8 (12.12)	4 (6.06))	22 (33.33)
Mild	0	1 (1.51)	4 (6.06)	0	4 (6.06)	1 (1.51)	5 (7.57)
Moderate	2 (3.03)	5 (7.57)	31 (46.96)	18 (27.27)	19 (28.78)	1 (1.51)	38 (57.57)
Severe	0	1 (1.51)	0	0	1 (1.51)	0	1 (1.51)
Vulvar itching							
None	0	4 (6.06)	9 (13.63)	5 (7.57)	5 (7.57)	3 (4.54)	13 (19.69)
Mild	0	1 (1.51)	2 (3.03)	0	3 (4.54)	0	3 (4.54)
Moderate	2 (3.03)	8 (12.12)	38 (57.57)	22 (33.33)	24 (36.36)	2 (3.03)	48 (72.72)
Severe	2 (3.03)	0	0	1 (1.51)	1 (1.51)	0	2 (3.03)
Vulvar irritation							
None	2 (3.03)	5 (7.57)	18 (27.27)	14 (21.21)	9 (13.63)	2 (3.03)	25 (37.87)
Mild	0	1 (1.51)	4 (6.06)	2 (3.03)	3 (4.54)	0	5 (7.57)
Moderate	0	7 (10.60)	27 (40.90)	12 (18.18)	19 (28.78)	3 (4.54)	34 (51.51)
Severe	0	0	2 (3.03)	0	0	2 (3.03)	2 (3.03)

Data presented: no. (%); AVD: abnormal vaginal discharge; LAP: lower abdominal pain; LBA: low backache; McPS: modified McCormack pain scale for abdominopelvic tenderness; VAS: Visual Analogue Scale.

was prominent in warm and wet dystemperament of the uterus, and it was also observed in other temperaments. Similarly, Avicenna, a great Unani scholar, surmised that any type of uterine dystemperament may lead to abnormal vaginal discharge [12]. The study found an association between general and uterine temperament with some diseases of women. Another study showed that the majority of participants (73.7% in the case group and 26.3% in the control group) had a cold temperament with vaginitis [53].

It may be said that the dystemperament of the uterus of a person probably leads to genital tract infections, thereby causing AVD and its associated symptoms, which can be ameliorated by using appropriate therapeutic measures and amending temperament imbalance.

4.7. Future Recommendations, Limitations, and Strength. A longitudinal cohort follow-up study is recommended to evaluate the temperament relationship between genital tract infection, aetiology, and abnormal vaginal discharge. It is also recommended to study the association between different microorganisms and the dystemperament of the uterus. If agreed with strong studies, the dystemperament of the uterus can be used as a measure for the prognostic criteria for female genital tract infection [54]. Furthermore, a case-control cohort and a randomized clinical trial are suggested to enhance the precision of the study. Furthermore, multicentre trials to see the variation in the population as per location and country for generalisability.

Regardless of such limitations, to date, to the best of our knowledge, this is the first study where we experienced significant associations between general and uterine temperament with age and associated clinical features of abnormal vaginal discharge. A well-validated temperament questionnaire for general temperament was used. Furthermore, the adaptation of STROBE guidelines was also a strength of the study. Amsel's criteria, ultrasonography, Pap smear, HIV, HbsAg, VDRL, and wet-mount vaginal smear

TABLE 5: Correlation between age, abnormal vaginal discharge, associated symptoms, and temperament.

	General temperament								
	Warm-cold						Wet-dry		
	Normal temperament (15–18)			Warm temperament (≥19)			Wet temperament (≤3)		
Variables	r value	95%CI lower	95%CI upper	r value	95%CI lower	95%CI upper	r value	95%CI lower	95%CI upper
Age									
20–30 (y)	0.94****	0.57	0.99	−0.12	−0.47	0.25	−0.22*	−0.68	0.36
31–40 (y)	−0.19	−0.86	0.73	0.005	−0.42	0.43	−0.05	−0.51	0.58
20–40 (y)	0.31**	−0.35	0.71	−0.22*	−0.46	0.03	0.03	−0.35	0.4
Clinical features: abnormal vaginal discharge and its associated symptoms									
AVD (n = 66)	0.28*	−0.31	0.72	−0.21*	−0.46	0.06	−0.05	−0.4	0.3
LAP and LBA (n = 63)	0.22*	−0.43	0.72	0.08	−0.19	0.35	−0.17	−0.5	0.24
Dyspareunia (n = 25)	0	0	0	0.04	−0.4	0.48	−0.15	−0.66	0.46
Dysuria (n = 26)	−0.25*	−0.92	0.8	0.13	−0.32	0.5	−0.30**	−0.74	0.3
BM (n = 44)	−0.07	−0.78	0.7	0.01	−0.32	0.34	−0.17	−0.58	0.30
Vulvar itching (n = 53)	−0.31**	−0.81	0.4	−0.08	−0.38	0.08	−0.10	−0.49	0.32
Vulvar irritation (n = 41)	−0.53 ***	−0.90	0.2	0.09	−0.25	0.42	00.13	−0.62	0.42
McPS (pelvic tenderness) (n = 54)	0.08	−0.61	0.7	−0.05	−0.35	0.24	−0.04	−0.45	0.3

Data presented: no. (%); mean ± SD; AVD: abnormal vaginal discharge; LAP: lower abdominal pain; LBA: low backache; McPS: modified McCormack pain scale for abdominopelvic tenderness; VAS: Visual Analogue Scale; BM: burning micturition; r value:**** ±0.70 or higher: very strong positive or negative relationship;**** ±0.40 to ±0.69: strong positive or negative relationship;** ±0.30 to ±0.39: moderate positive or negative relationship;* ± 0.20 to ± 0.29: weak positive or negative relationship; ±0.01 to ±0.19: no relationship.

TABLE 6: Performance of the warm and wet general body temperament and dystemperament of the uterus in AVD using Support Vector Machine- Radial Basis Function (SVM-RBF) classifier.

Model	AUC	Accuracy	Precision	Sensitivity	Specificity
CV-3	0.998	0.985	0.985	0.985	0.985
CV-5	**1.000**	**0.992**	**0.993**	**0.992**	**0.992**
Leave-one-out	0.999	0.992	0.993	0.992	0.992
Mean	0.999	0.989	0.990	0.989	0.989
±SD	0.0008	0.003	0.003	0.003	0.003
Variance	6.666	1.088	1.422	1.088	1.088

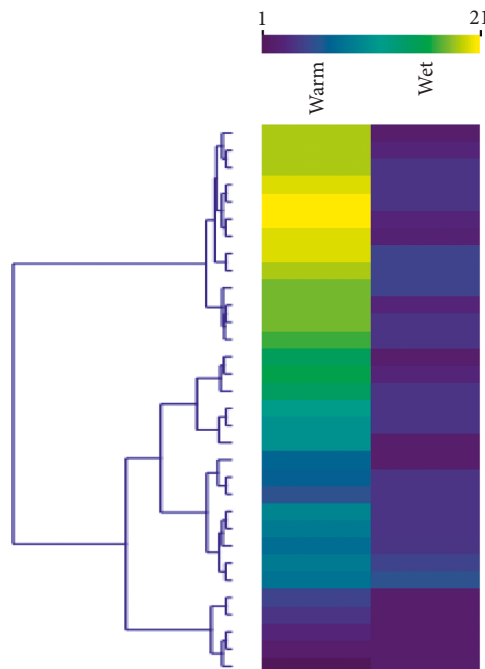Bold means higher performance as compared to the others.

FIGURE 9: Heatmap for the relationship between general body temperament (wet and warm) and uterine dystemperament (wet and warm) in abnormal vaginal discharge.

were also performed to find the aetiological cause of the abnormal vaginal discharge. In addition, to enhance scientific validation, computational intelligence was applied to analyse the data to see the accuracy, precision, specificity, and sensitivity of the correlation between warm and wet body temperament and uterine dystemperament.

5. Conclusion

In the present study, 21–30 years was the most prevalent age group for AVD. Warm temperament in warm-cold general body temperament and normal or wet temperament were more predominant in wet-dry general body temperament in this disease. Warm-wet dystemperament of the uterus was more prevalent in AVD. Additionally, the warm general temperament was strongly associated with uterine warm temperament, while our SVM-RBF computational model is better for classifying the warm and wet conditions. This study may recommend innovative treatment methods and prevention in the field of female genital tract infections. However, it needs to be further evaluated.

Data Availability

The data used to support the findings of this study are available from the first authors upon request.

Conflicts of Interest

The authors declare that they have no conflicts of interest.

Authors' Contributions

Arshiya Sultana designed and planned the study, analysed the data, drafted, critically reviewed, and proofread the paper, and interpreted the data; Wajeeha Begum supervised the trial and proofread the paper; Rushda Saeedi was involved in carrying out the clinical trial and collating and interpreting the data; Khaleequr Rahman contributed to drafting, critically reviewing, and proofreading the paper; Md Belal Bin Heyat, Faijan Akhtar, Ngo Tung Son, and Hadaate Ullah designed the computational intelligence methodology, results, interpretation, and references. Arshiya Sultana, Md Belal Bin Heyat, and Faijan Akhtar contributed equally to this work.

Acknowledgments

References

[1] H. R. S. Roshandel, F. Ghadimi, and R. S. Roshandel, "Developing and standardization of a structured questionnaire to determine the temperament (Mizaj) of individuals," *Indian J. Tradit. Knowl.*vol. 15, pp. 341–346, 2016.

[2] M. S. R. Chamanzari Hamid, S. S. Ahmad, H. Khadije, H. Seyyed Musa, Z. Nazila, and S. R. Mazlum, "Evaluation of temperament–based diet education on quality of life in patients with gerd," *Evid. Based Care.*vol. 3, pp. 29–38, 2014.

[3] F. Rajabzadeh, S. Mohammad, B. Fazljou, L. Khodaie, and L. Sahebi, "The association between temperament and gynecological disease from Persian medicine," *Point of View*, vol. 6, pp. 69–73, 2018.

[4] A. Saeidi, M. Tansaz, M. Saberi et al., "Evaluation of uterine warm and cold distemperament (Su-e Mizaj) in Persian medicine: a qualitative study," *Crescent J. Med. Biol. Sci.*vol. 7, pp. 177–185, 2020.

[5] H. Salmannezhad, M. Mojahedi, A. Ebadi et al., "An assessment of the correlation between happiness and Mizaj (temperament) of university students in Persian medicine," *Iranian Red Crescent Medical Journal*, 2017, In Press.

[6] Z. M. Chirenje, N. Dhibi, H. H. Handsfield et al., "The etiology of vaginal discharge syndrome in Zimbabwe: results from the Zimbabwe STI etiology study," *The Sexually Transmitted Diseases*, vol. 45, no. 6, pp. 422–428, 2018.

[7] R. E. Moreira Mascarenhas, M. Sacramento Cunha MacHado, B. F. Borges Da Costa E Silva et al., "Prevalence and risk factors for bacterial vaginosis and other vulvovaginitis in a population of sexually active adolescents from Salvador, Bahia, Brazil," *Infectious Diseases in Obstetrics and Gynecology*, vol. 2012, pp. 1–6, Article ID 378640, 2012.

[8] R. Saeedi, J. T. Deoband, A. Sultana, and M. U. Z. N. Farzana, *A Conceptual Literary Exploration of Sayalan Al-Rahim (Abnormal Vaginal Discharge) in Unani Medicine*, A Conceptual Literary Exploration of Sayalan Al-Rahim (Abnormal Vaginal Discharge) in Unani Medicine, 2020.

[9] C. Zemouri, T. E. Wi, J. Kiarie et al., "The performance of the vaginal discharge syndromic management in treating vaginal and cervical infection: a systematic review and meta-analysis," *PLoS One*, vol. 11, no. 10, 21 pages, Article ID e0163365, 2016.

[10] V. Durai, S. Varadharajan, A. R. Muthuthandavan, V. Durai, S. Varadharajan, and R. Anitha, "Reproductive tract infections in rural India – a population-based study," *Journal of Family Medicine and Primary Care*, vol. 8, no. 11, pp. 3578–3583, 2019.

[11] M. Qarshi and J. Al-Hikmat, IdaraeKitabus Shifa, New Delhi, India, vol. 1, pp. 1121–1123, 2011.

[12] I. Sina and A. Q. Fit Tib, Idara Kitabus Shifa, New Delhi, India, pp. 1030–1069, 2010.

[13] A. Khan, Iksir-i-A'zam, Idarae Kitab us Shifa, New Delhi, vol. 2, pp. 806–808, 2011.

[14] A. H. Tabri and F. Firdaws Al-HikmatFi'l-Tibb, Idarae Kitabus Shifa, New Delhi, India, 2010, p.25-7.

[15] F. Kaviani, Z. Tavakol, and H. Salehiniya, "The relationship between warm and cold temperament and dysmenorrhea," *Clinical Epidemiology and Global Health*, vol. 8, no. 3, pp. 858–861, 2020.

[16] A. Sultana, A. G. F. Najeeya, K. Rahman, and M. U. Z. N. Farzana, "Determination of Mizaj (Temperament) in women with mixed urinary incontinence," *A preliminary study*, vol. 5, pp. 352–358, 2020.

[17] L. Fatima and A. Sultana, "Efficacy of Tribulus terrestris L. (fruits) in menopausal transition symptoms: a randomized placebo controlled study," *Advances in Integrative Medicine*, vol. 4, no. 2, pp. 56–65, 2017.

[18] W. X. Lin, X. Du, L. L. Yang et al., "Differences in the composition of vaginal microbiota between women exhibiting spleen-deficiency syndrome and women with damp-heat syndrome, two of the most common syndromes of vaginitis in traditional Chinese medicine," *Evidence-based Complementary and Alternative Medicine*, vol. 2019, pp. 1–11, Article ID 5456379, 2019.

[19] C. Chola, B. H. Md Belal, and A. Faijan, "IoT based intelligent computer-aided diagnosis and decision making system for health care," in *Proceedings of the 2021 International Conference on Information Technology (ICIT)*, pp. 184–189, IEEE, Amman, Jordan, July 2021.

[20] M. B. Bin Heyat, F. Akhtar, M. Ansari et al., "Progress in detection of insomnia sleep disorder: a comprehensive review," *Current Drug Targets*, vol. 22, no. 6, pp. 672–684, 2021.

[21] M. B. Bin Heyat, *Insomnia: Medical Sleep Disorder & Diagnosis*, Anchor Academic Publishing, Hamburg, Germany, 2016.

[22] M. B. Bin Heyat, A. Faijan, B. H. Mohd Ammar, and A. Shajan, *Short time frequency analysis of theta activity for the diagnosis of bruxism on EEG sleep record*, K.D. Gupta and A. Hassanien, Eds., pp. 63–83, Springer, 2020.

[23] F. Akhtar, P. K. Patel, M. B. B. Heyat et al., "Smartphone addiction among students and its harmful effects on mental health, oxidative stress, and neurodegeneration towards future modulation of anti-addiction therapies: a comprehensive survey based on slr, research questions, and network visualization techniques," *CNS & Neurological Disorders - Drug Targets*, vol. 21, 2022.

[24] M. S. Iqbal, R. Abbasi, M. B. Bin Heyat et al., "Recognition of mRNA N4 acetylcytidine (ac4C) by using non-deep vs. Deep learning," *Applied Sciences*, vol. 12, no. 3, pp. 1344–1416, 2022.

[25] A. K. Nawabi, S. Jinfang, R. Abbasi et al., "Segmentation of drug-treated cell image and mitochondrial-oxidative stress using deep convolutional neural network," *Oxidative Medicine and Cellular Longevity*, vol. 2022, pp. 1–14, Article ID 5641727, 2022.

[26] L. Ali, Z. He, W. Cao, H. T. Rauf, Y. Imrana, and M. B. Bin Heyat, "MMDD-ensemble: a multimodal data–driven ensemble approach for Parkinson's disease detection," *Frontiers in Neuroscience*, vol. 15, pp. 754058–754111, 2021.

[27] C. C. Ukwuoma, B. H. Md Belal, and M. Mahmoud, "Image inpainting and classification agent training based on reinforcement learning and generative models with attention mechanism," in *Proceedings of the 2021 International Conference on Microelectronics (ICM)*, pp. 96–101, IEEE, New Cairo City, Egypt, January 2021.

[28] M. B. B. Heyat, D. Lai, F. I. Khan, and Y. Zhang, "Sleep bruxism detection using decision tree method by the combination of C4-P4 and C4-A1 channels of scalp EEG," *IEEE Access*, vol. 7, pp. 102542–102553, 2019.

[29] D. Lai, M. B. B. Heyat, F. I. Khan, and Y. Zhang, "Prognosis of sleep bruxism using power spectral density approach applied on EEG signal of both EMG1-EMG2 and ECG1-ECG2 channels," *IEEE Access*, vol. 7, pp. 82553–82562, 2019.

[30] M. B. Bin Heyat, D. Lai, F. Akhtar et al., *Bruxism detection using single-channel C4-A1 on human sleep S2 stage recording*, D. Gupta, S. Bhattacharyya, and A. Khanna, Eds., pp. 347–367, John Wiley & Sons, 1st ed edition, 2020.

[31] M. B. Bin Heyat, F. Akhtar, A. Khan et al., "A novel hybrid machine learning classification for the detection of bruxism patients using physiological signals," *Applied Sciences*, vol. 10, no. 21, p. 7410, 2020.

[32] D. Lai, Y. Zhang, X. Zhang, Y. Su, and M. B. Bin Heyat, "An automated strategy for early risk identification of sudden cardiac death by using machine learning approach on measurable arrhythmic risk markers," *IEEE Access*, vol. 7, pp. 94701–94716, 2019.

[33] M. Mojahedi, M. Naseri, R. Majdzadeh et al., "Reliability and validity assessment of Mizaj questionnaire: a novel self-report scale in Iranian traditional medicine," *Iranian Red Crescent Medical Journal*, vol. 16, no. 3, Article ID e15924, 2014.

[34] M. Dehnavi, Z. Jafarnejad, F. Mojahedi, M. Shakeri, and M. T. Sardar, "Investigation of warm and cold temperament with symptoms of premenstrual syndrome, Iranian Journal of Obstetrics, Gynecology and Infertility, Iran," *Journal of Obstetrics & Gynaecology of India*, vol. 18, pp. 17–24, 2016.

[35] B. E. Boser, V. N. Vapnik, and I. M. Guyon, *Training Algorithm Margin for Optimal Classifiers*, pp. 144–152, Perception, New York, 1992.

[36] Q. Liu, C. Chen, Y. Zhang, and Z. Hu, "Feature selection for support vector machines with RBF kernel," *Artificial Intelligence Review*, vol. 36, no. 2, pp. 99–115, 2011.

[37] O. AlShorman, M. Masadeh, M. B. B. Heyat et al., "Frontal lobe real-time EEG analysis using machine learning techniques for mental stress detection," *Journal of Integrative Neuroscience*, vol. 21, no. 1, p. 020, 2022.

[38] M. B. Bin Heyat, F. Akhtar, S. J. Abbas et al., "Wearable flexible electronics based cardiac electrode for researcher mental stress detection system using machine learning models on single lead electrocardiogram signal," *Biosensors*, vol. 12, no. 6, p. 427, 2022.

[39] H. Ullah, M. B. Bin Heyat, H. AlSalman et al., "An effective and lightweight deep electrocardiography arrhythmia recognition model using novel special and native structural regularization techniques on cardiac signal," *Journal of Healthcare Engineering*, vol. 2022, pp. 1–18, Article ID 3408501, 2022.

[40] W. Mulu, M. Yimer, Y. Zenebe, and B. Abera, "Common causes of vaginal infections and antibiotic susceptibility of aerobic bacterial isolates in women of reproductive age attending at Felegehiwot referral Hospital, Ethiopia: a cross sectional study," *BMC Women's Health*, vol. 15, pp. 42–49, 2015.

[41] A. Langhammer, S. Krokstad, P. Romundstad, J. Heggland, and J. Holmen, "The HUNT study: participation is associated with survival and depends on socioeconomic status, diseases and symptoms," *BMC Medical Research Methodology*, vol. 12, p. 143, 2012.

[42] M. Laaksonen, K. Talala, T. Martelin et al., "Health behaviours as explanations for educational level differences in cardiovascular and all-cause mortality: a follow-up of 60 000 men and women over 23 years," *The European Journal of Public Health*, vol. 18, no. 1, pp. 38–43, 2008.

[43] S. Yasmin, N. A. Zaman, and F. Zafreen, "Socio-demographic characteristics of women having vaginal discharge attending a military hospital," *Journal of Armed Forces Medical College, Bangladesh*, vol. 14, no. 2, pp. 183–185, 2020.

[44] V. Chaudhary, V. Prakesh, K. Agarwal, V. Agrawal, A. Singh, and S. Pandey, "Clinico-microbiological profile of women with vaginal discharge in a tertiary care hospital of northern India," *International Journal of Medical Science and Public Health*, vol. 1, no. 2, p. 75, 2012.

[45] A. Mukherjee and S. Yasmin, "A cyto-epidemiological study on married women in reproductive age group (15-49 years) regarding reproductive tract infection in a rural community of West Bengal," *Indian Journal of Public Health*, vol. 56, no. 3, pp. 204–209, 2012.

[46] Y. Kwak, Y. Kim, and K. A. Baek, "Prevalence of irregular menstruation according to socioeconomic status: a population-based nationwide cross-sectional study," *PLoS One*, vol. 14, no. 3, 12 pages, Article ID e0214071, 2019.

[47] T. A. Bhat, "Efficacy of Tamarindus Indicus, Melia Azadirach and Santalum Album in Syndromic Management of Abnormal Vaginal Discharge," *A Single-Blind Randomised Controlled Trial*, pp. 1–8, 2017.

[48] T. Modak, P. Arora, C. Agnes et al., "Diagnosis of bacterial vaginosis in cases of abnormal vaginal discharge: comparison of clinical and microbiological criteria," *J. Infect. Dev. Ctries.*vol. 5, no. 5, pp. 353–360, 2010.

[49] T. K. Roberts-Wilson, J. B. Spencer, and C. R. Fantz, "Using an algorithmic approach to secondary amenorrhea: avoiding diagnostic error," *Clinica Chimica Acta*, vol. 423, pp. 56–61, 2013.

[50] M. H. Shah, *The General Principles of Avicenna's Canon of Medicine*, Interservices Preso, Karachi, 1998.

[51] P. Knaster, A. M. Estlander, H. Karlsson, J. Kaprio, and E. Kalso, "Temperament traits and chronic pain: the association of harm avoidance and pain-related anxiety," *PLoS One*, vol. 7, no. 10, Article ID e45672, 2012.

[52] M. Tansaz, F. Sohrabvand, S. Adhami et al., "Evaluation of uterine temperament in Iranian infertile women using a quantitative instrument for uterine temperament detection," *International Journal of Preventive Medicine*, vol. 11, p. 39, 2020.

[53] S. Adhami, T. Mojgan, M. Amal Saki, and J. Mozhgan, "The relationship between uterine temperament and vaginitis from Iranian traditional medicine point of view," *Indo Am. J. Pharm. Sci*, vol. 4, pp. 3589–3595, 2017.

[54] R. Saeedi, A. Sultana, K. Rahman, M. Belal Bin Heyat, M. A. Kamal, and M Ishawu, "Efficacy of Acacia nilotica linn. Pod's sitz bath plus vaginal pessary in syndromic management of abnormal vaginal discharge: a randomized controlled trial," *Evidence-based Complementary and Alternative Medicine*, vol. 2022, pp. 1–11, Article ID 5769555, 2022.

WILEY | Hindawi

Research Article

Performance Analysis of an Optimized ANN Model to Predict the Stability of Smart Grid

Ayushi Chahal [ID],[1] **Preeti Gulia** [ID],[1] **Nasib Singh Gill** [ID],[1] **and Jyotir Moy Chatterjee** [ID][2]

[1]*Department of Computer Science & Applications, Maharshi Dayanand University, Rohtak, Haryana, India*
[2]*Department of Information Technology, Lord Buddha Education Foundation, Kathmandu, Nepal*

Correspondence should be addressed to Jyotir Moy Chatterjee; jyotir.moy@lbef.edu.np

The stability of the power grid is concernment due to the high demand and supply to smart cities, homes, factories, and so on. Different machine learning (ML) and deep learning (DL) models can be used to tackle the problem of stability prediction for the energy grid. This study elaborates on the necessity of IoT technology to make energy grid networks smart. Different prediction models, namely, logistic regression, naïve Bayes, decision tree, support vector machine, random forest, XGBoost, k-nearest neighbor, and optimized artificial neural network (ANN), have been applied on openly available smart energy grid datasets to predict their stability. The present article uses metrics such as accuracy, precision, recall, $f1$-score, and ROC curve to compare different predictive models. Data augmentation and feature scaling have been applied to the dataset to get better results. The augmented dataset provides better results as compared with the normal dataset. This study concludes that the deep learning predictive model ANN optimized with Adam optimizer provides better results than other predictive models. The ANN model provides 97.27% accuracy, 96.79% precision, 95.67% recall, and 96.22% $F1$ score.

1. Introduction

An electric grid is said to be smart if it tends to replace traditional appliances with smart ones. A smart grid helps in the smart distribution of electric energy, provides smart meter infrastructure, etc. The smart grid also motivates the use of renewable energy resources rather than nonrenewable ones [1]. Smart grids can be used to enhance the smooth functioning of every domain like electricity generation either from renewable or nonrenewable energy resources, distribution of energy according to the demand and supply for different smart sectors like smart homes, smart offices, smart factories, electric vehicles, and so on as shown in Figure 1.

Nowadays, renewable energy resources dominate the market for electricity generation [2]. Smart grid faces multiple problems like power grid resilience, cyber security in a smart power grid system, smart energy management or distribution, etc. [3]. With the growing demand for renewable energy resources, grid topology used for electricity distribution has become more and more decentralized.

Consumer of the electricity can also behave like its producer. So unlike traditional grids, power generation and consumption can occur from any terminal point [4]; such terminals are called Prosumers. Generation and distribution of power are not limited to a central node anymore.

With this decentralized approach, it becomes very difficult to manage and keep track of the generation and consumption of energy. This creates chaos to maintain information on the demand and supply of electric power among the producers and consumers. This, in turn, makes it difficult to maintain the stability of the grid system. To remove this overhead, a decentralize smart grid control (DSGC) is proposed [5]. This control system keeps track of the power demand and supply frequency on every producer-consumer node of the grid. Different decentralized topologies can be used in smart energy grids for power consumption and production as shown in Figure 2.

DSGC increases the stability of the smart grid. DSGC model considers some parameters like price elasticity, balancing power flow, and reaction time of nodes. These
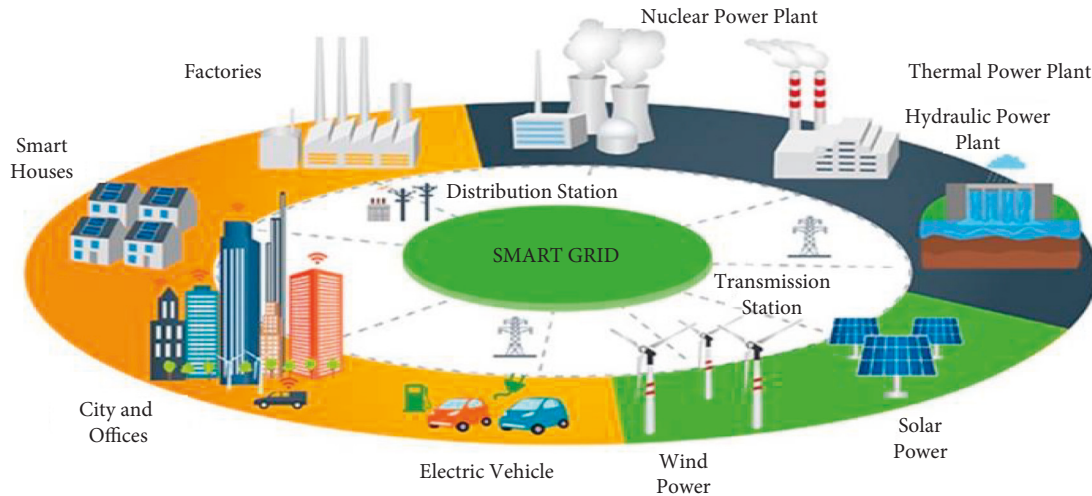
FIGURE 1: Smart grid. Source: Smart grid evolution, 2018. Eolas Magazine. URL: https://www.eolasmagazine.ie/smart-grid-evolution/ (accessed 2.18.22).

(a)	(b)	(c)
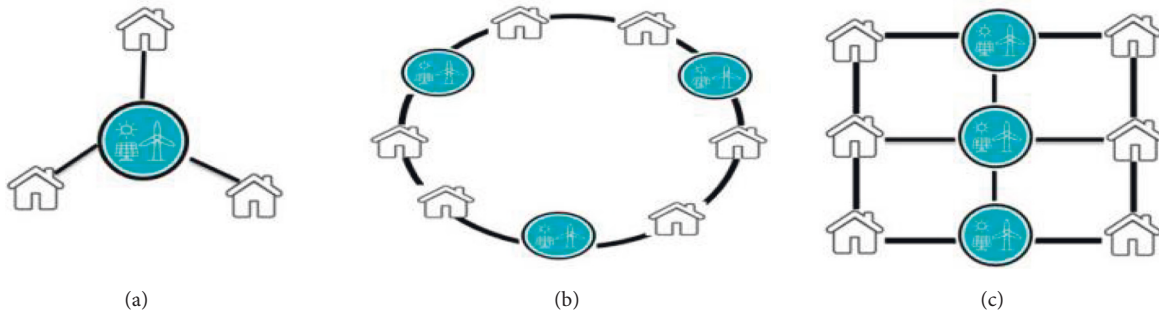
FIGURE 2: Decentralized smart grid topologies: (a) star with a central node as producer; (b) ring topology with decentralized 3 producer and 6 consumer nodes; (c) lattice topology with 3 producer and 6 consumer nodes.

parameters help to check the stability of the energy grid network. Balancing power flow deals with the units produced or consumed by producer or consumer, respectively. The reaction time of nodes deals with the change in the response according to the rise or fall in the price of power units. The most careful part of the decentralized smart energy grid is the information flow of electricity distribution. This information flow helps in deciding the stability of the decentralized smart grid. For predicting stability, different ML and DL models play an indispensable role [6].

The main objectives of this study are

(i) This study provides a detailed overview of the integration of IoT with a smart energy grid with the help of three-layered architecture

(ii) This article discusses the behavior of a smart grid dataset

(iii) This study helps to understand the effect of data augmentation on prediction accuracy

(iv) "ANN" model is proposed for the stability prediction of a decentralized grid system

(v) This study outlines the comparative analysis of traditional machine learning algorithms with optimized ANN

The article is organized as follows: integration of IoT and the electric grid is very well explained in Section 2 with a layered architecture. The related literature review is given in Section 3. Section 4 describes a stepwise approach used in methodology for analysis purposes. It also provides a detailed overview of different prediction models used in this study. Section 5 discusses the experimental results and presents them in graphical form. Also, it provides a comparative analysis of all the models.

2. Layered Architecture for IoT and Smart Grid Integration

The Internet of Things (IoT) has provided innovative solutions to real-life problems [7]. IoT has upgraded different technologies like computational, sensing, communicational, etc. IoT can be integrated with grid systems which further helps to resolve problems of smart grids like balancing demand and supply of energy grid. [8].

IoT-integrated smart grid system is divided into three layers [9]. Figure 3 presents a layered structure of the IoT-integrated smart grid system. In bottom-up fashion,

(i) *First layer* is the data collection layer. Different IoT devices like sensors and actuators are used over a
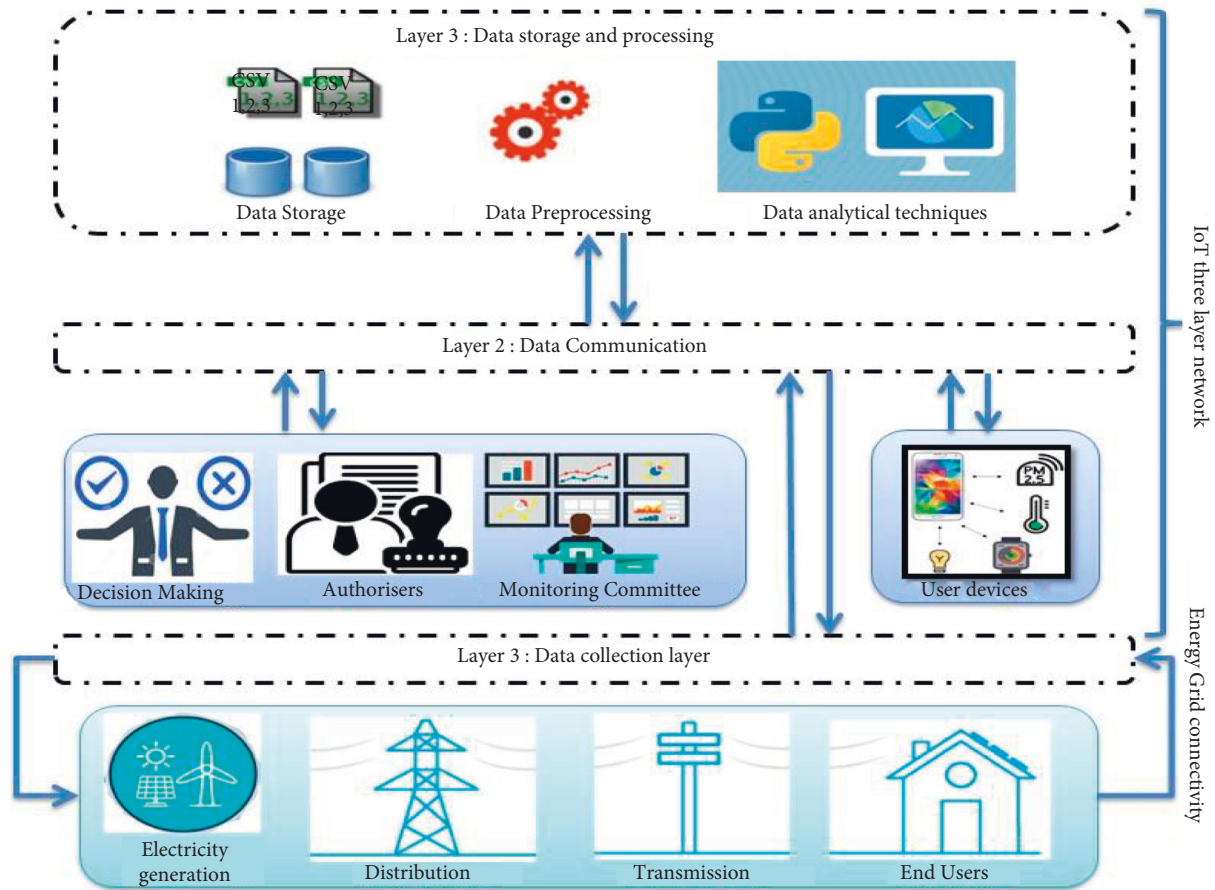
FIGURE 3: IoT-integrated smart energy grid three-layered network. This concept is partially adapted from Babar et al. [10].

wireless sensor network to collect data from smart homes, distribution centers, smart factories, or smart renewable energy generation systems. This data are fed into layer 2.

(ii) *Second layer* is the data communication layer. In this layer, data are communicated to decision-makers, different monitoring centers, and authorities to determine priorities and parameters. User devices are also attached on the second layer only.

(iii) *Third layer* is the data storage and processing. In this layer, data are processed and analyzed using intelligent techniques like artificial intelligence, machine learning, big data analytics, cloud computing, fog computing, edge computing, etc. These techniques process the data according to the guidelines and results required by the authorities and decision-makers presented in layer 2. This processed data are presented to the user in graphical, tabular, or textual form.

IoT can enhance the functioning of the smart grid by improving sensing and measurement [11]. It helps in automatic monitoring and remote control. IoT can help in forecasting the usage of renewable resources. The distribution of electricity is a very important part of the energy grid, which is automated by IoT. The smart meter is one of the most popular applications of IoT in the smart energy grid [12, 13].

3. Related Work

In the smart grid, work like assigning renewable energy resources, delivering short-term energy forecasting, and sensing the motion of the occupants are to be analyzed to enhance its efficiency. Yao et al. use machine learning models for the same and have given Machine Learning Energy-Efficient Framework (MLEEF) [14]. The authors used solar energy for this study. Occupant's profiles and energy profiles are studied in depth before applying machine learning frameworks to the dataset. Findings of the analysis are measured as accuracy for checking energy consumption and load forecasting. A hybrid machine learning model is proposed by Sharmila et al. for smart energy management by optimizing energy distribution from the energy sources to the recipient. In this model, SVM is used for regression and classification problems with the Big data five V's paradigm [15].

Energy Management Model (EMM) is presented by Ahmed et al. which uses ML models to manage energy flow for smart grid [16]. Both optimization techniques and machine learning models are used to manage the energy distribution. This study concluded that machine learning-based energy management models outperform the results of optimization-based EMM. Hourly data are collected from national renewable energy resources in the US for this study. Collected data statistics are used for its simulation. This

average dataset of 10 years is then distributed in three seasons: winter, summer, and spring. Season-wise energy management models are used for analysis to check which model performs better.

Arzamasov et al. focused on the DSGC system [17]. They focus on the frequency of the alternate current (AC) to check the stability of the system. It is discussed that frequency increases at the time of excess electricity generation and decreases at the time of reduced amount of electricity production. The authors focus to identify the instability of four node star network DSGC system after accessing the mathematical model discussed in the study of Schäfer et al.

Chen et al. used a deep residue learning model called Short-Term Long Forecast (SLTF) to forecast electric load over the network for a day ahead [18]. Authors have used ANN as a base. End-to-end complete new neural network is proposed in the study. Multiple neural networks ensemble in a single model. This ensemble is done in two phases. The first phase is to take snapshots of the training model. Authors have used Adam for optimization to enhance the learning rate. In the second phase, authors initialize different models independently. All models are trained by hyper-parameter tuning and then the average output of all the models is used for forecasting. A similar forecasting model using STLF is proposed by Y. Wang et al. in their study [47]. Ensemble Markov model is proposed to forecast the industrial electric load. In this model, authors have combined novel time series data mining techniques and then ensembled different prediction frameworks of the Hidden Markov Model (HMM). Min-Max normalization is used to normalize the data and this data are fed to the bagging algorithm for resampling. After sampling, hyper-parameters are set and HMM is applied to every sample. All results are ensemble based on log-likelihood. Different parameters like average absolute percentage error (MAPE), root mean square error (RMSE), and average absolute error (MAE) help to measure the efficiency of the model. Wang et al. use SVM and XGBoost machine learning models for forecasting industrial load [20]. Bayesian optimization algorithm is used to optimize the hyper-parameters of the XGBoost model. Different state-of-the-art methods are used to predict model accuracy.

An SVM model is proposed by Gupta et al. to predict blackout in smart grid [21]. This model is trained on the historic dataset and evaluated probabilistically. Ge et al. used a hybrid algorithm to forecast industrial power load [22]. At first, the k-means algorithm classifies the data in different clusters. After that, the reinforcement learning model is used with the SVM model. To optimize the reinforcement model, the author has used swarm optimization. This optimized hybrid algorithm has increased the accuracy of the model to predict the load over a real-time dataset.

Wei et al. have used Deep Belief Network (DBN) over the smart grid network to detect attacks for false data injection. Initially, researchers have used unsupervised machine learning algorithms to feed the Boltzmann machine with initial weights that will be used in DBN. Back-propagation technique of DBN helps to reduce errors in the top to bottom fashion and hence refine the model. This proposed approach of the researchers provides good results as compared with the false data injection attacks detected through the SVM model [23].

Amarasinghe et al. used deep neural network models to forecast energy load balancing. Convolutional neural network (CNN) forecasts the load. Also, the results of CNN are compared with other predictive models like LSTM sequence-to-sequence, shallow ANN, restricted Boltzmann model, and SVM over the same kind of dataset. Root mean square error (RMSE) helps in the comparative analysis of different prediction models [24]. Muzumdar et al. presented the reasonableness of using ML predictive models to forecast the balance and imbalance of energy flow in the energy grid [25]. Authors have used historic communication and supplied data from the data source. After that, data preprocessing steps are applied. Refined data is split into training and testing datasets on which different machine learning models like multi-layer perceptron (MLP), bagging, AdaBoost, decision tree, random forest, naïve Bayes model, KNN, SVM, and gradient boosting. Accuracy, RMSE (for both 10 cross fold and random split), and MAE (for both random split and 10 cross fold) are tried to find the correct predictive model among all the ML models applied to the dataset. Z. Guan et al. use a nonparametric Bayesian clustering model in a smart grid system in order to preserve the privacy of the big data one gets from the smart grid. For this proposed model, the Infinite Gaussian mixture model (IGMM) is used in the implementation process. The Laplace mechanism is used to release data so that the privacy of data can be maintained [48].

Wang et al. proposed a data reduction technique for wireless sensor networks (WANs) to predict forthcoming data. This technique is divided into two phases: the first one is the data reduction phase (DRP). DRP helps in reducing the amount of data to be transmitted over WAN. The second phase is the data prediction phase (DPP), in which nontransmitted data are predicted at the base station itself. Data predictions are done on the basis of the Kalman filter [27].

Alsamhi et al. used the ANN model to predict signal strength emitted from drones. These signals are used to communicate with the IoT devices in a smart city environment. This signal strength is used to find the next location in the path of a flying drone [28]. Nyangaresi and Alsamhi presented a study for secure signal transfer in a smart grid. In smart metering, data are being transferred from consumers to power management centers. This study has proposed a traffic signaling protocol developed for preserving the privacy of the data. This protocol is found to be effective against Man-in Middle attacks, desynchronization attacks, and impersonating attacks [29].

4. Methodology

4.1. Dataset Used and Its Preprocessing. This study has used a data set from the UCI repository [30]. This dataset has the readings of a renewable smart energy grid that is supposed to satisfy the needs of three consumers. This dataset contains 10,000 records originally. But this dataset is augmented for better results and the augmented version of the dataset contains 60,000 observations. This dataset contains 14

features, out of which 12 are independent primary features and 2 are dependent secondary features. Table 1 describes all the features of the dataset used for the study.

4.2. Stepwise Methodology Used.

Figure 4 presents the stepwise approach used to predict the stability of the smart grid. A detailed explanation of the approach used in the research is as follows:

(i) Firstly, a raw dataset is taken, and then it is augmented. Initially, the dataset has 6000 observations. Since the grid is considered to be symmetric and we are assuming three consumers in this study, this dataset is augmented by 3! $(3 * 2 * 1 = 6$ times). Data augmentation helps to get better accuracy in results.

(ii) Next is the data preprocessing step. No feature engineering overhead is required because data are acquired from simulation exercises so there are no NaN or duplicate values.

(iii) After that, some machine learning models like logistic regression, k-nearest neighbor (KNN), decision tree, support vector machine (SVM), random forest, naïve Bayes, and XGBoost are applied to the dataset to predict future values. Hyper-parameter tuning of these models is performed in order to get the best results. All the specifications of these ML models are explained in a subsection in Section 4.

(iv) After hyper-parameter tuning, the performance of all the predictive models is measured based on the evaluation matrices used (explained in Section 5.1).

(v) Deep learning model is applied to the scaled dataset. For applying ANN with the "Relu" activation function, the dataset is needed to be scaled. So, by importing the "StandardScalar" function of preprocessing package, the features of the dataset are scaled properly.

(vi) After feature scaling, the proposed ANN model for smart grid is applied. Specification of the proposed ANN model is explained in detail in Section 4.2.8.

In this study, ML and DL models are deployed to predict the stability of the decentralized energy grid. Also, an artificial neural network (ANN), a deep neural network model, is used for the same. In the following subsection, these models are explained in detail.

4.2.1. Logistic Regression.

Logistic regression works somewhat similar to linear regression. Logistic regression predicts the outcome on the basis of the individual characteristics of each feature [31]. The logistic regression model is very easy to regularize. It calibrates output based on predicted possibilities [32]. Suppose Y is a predicted output feature that depends on the predictor variable X and X can be given as $\{x1, x2, x3, \ldots, x_n\}$. y is regarded as the output variable given as follows:

$$y = a_0 + a_1 x_1 + a_2 x_2 + \ldots + a_n x_n + e,$$

$$y = \begin{cases} 1, if\ a0 + a1x1 > 0, \\ 0, if\ a0 + a1x1 \leq 0, \end{cases} \quad (1)$$

where $a_0, a_1, a_2, \ldots, a_n$ are the regression coefficients. It uses logarithmic or logistic function for cost evaluation.

4.2.2. KNN.

K-nearest neighbor (KNN) is a supervised machine learning model [33]. This supervised learning technique works on the principle of similarity among the neighbors. Classification of the data points is done on the basis of the distance between them. It is also called a lazy learner algorithm. KNN algorithm is used in many energy grid scenarios like to forecast low-voltage demand, and to measure current and its state [34, 35].

4.2.3. Naïve Bayes.

Naïve Bayes network is also a prediction model that works on conditional probability [36]. For understanding purpose, let Z be a class label that will be classified on the basis of the conditional probability of independent features X and Y. Naïve Bayes [37] model will learn using the Bayes rule to calculate a conditional probability for class Z using instances $Y_0, Y_1, Y_2, \ldots, Y_n$ of attribute Y. Posterior probability is used to predict the class. When attribute Y is independent of attribute X, then the posterior probability of Z can be calculated, when the following condition is hold [38]:

$$P(Y \mid X, Z) = P\left(\frac{Y}{Z}\right), \forall X, Y, Z, \text{ whenever } P(C) > 0. \quad (2)$$

4.2.4. Decision Tree.

Decision tree is used to predict the categorical dataset. Nodes of the decision tree are applied with decision rules which help in categorizing the dataset in particular classes [39]. It helps to analyze the instance of a feature and predict the target value. Any kind of null value in data does not create any hurdle for the decision tree model. Data normalization or scaling is not necessary but any small change in data can make this model unstable [40].

4.2.5. SVM.

It is a supervised machine learning model in which the type of kernel used plays an important part. Statistical learning is considered the base of this predictive model. Support vector machine (SVM) is used in classification as well as regression problems. Kernel used in SVM takes the input data and plots it to high-dimensional actual feature space. SVM model then creates a hyper-plane in feature space which is used to categorize the data points into different classes and to find out patterns for classification and regression problems. The cost function used in SVM to calculate prediction cost is given in equation (4).

$$C = \sum_{i=1}^{l} Lo + W(l, h), \quad (3)$$

where Lo = loss function and $W(l, h)$ = capacity of learning model.

TABLE 1: Performance parameters for prediction models.

S No.	Feature	Type	Significance
1	tau1, tau2, tau3, tau4	Primary, independent, and predictive	Represents reaction time of producer and three consumers (range: from 0.5 to 10)
2	p1, p2, p3, p4	Primary, independent, and predictive	Represents power produced (positive value) and consumed (negative value) by producers and consumers, respectively
3	g1, g2, g3, g4	Primary, independent, and predictive	Price elasticity coefficient of producer and consumer (range: from 0.05 to 1.00)
4	Stab	Secondary and dependent	Numerical real value (if positive, then linearly unstable, if negative, linearly stable)
5	Stabf	Secondary and dependent	Categorical feature, binary value labeled as stable/unstable
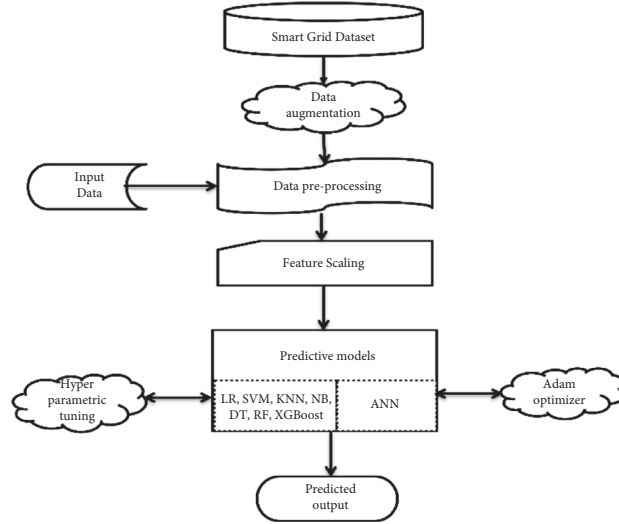
FIGURE 4: Flow chart of the methodology.

4.2.6. Random Forest.

Random forest is made up of many decision trees. Random forest is one of the ensemble learning techniques which uses trees as a base to learn and predict [41]. Prediction is made by taking an average of the aggregate given by each tree individually. Random forest can also adapt sacristy very well [42]. Random forest supervised learning model cannot work efficiently on high-dimensional datasets. M number of multiple decision trees are combined to form a forest with a finite value.

$$m_{M,n}(x; \theta_1, \ldots, \theta_m, D_n) = \frac{1}{M} \sum_{j=1}^{M} m_n(x; \theta_j, D_n), \quad (4)$$

where query decision query x is denoted as $m_n(x; \theta_j, D_n)$ and $\theta_1, \ldots, \theta_m$ are random variables which are independent of each other and independent of D_n.

4.2.7. XGBoost.

Exclusive gradient boosting technique has become very popular since it came into existence [43]. It is a tree boosting technique that is scalable in nature. It provides an easy way to prevent over-fitting problems [44]. It can be very helpful while using a sparse and low sample size dataset. When a dataset $D = \{(x_i, y_i)\}$ is given with n number of records and m number of features, then prediction of y_i represented as $\hat{y}_i$ can be given with the mathematical principle of XGBoost as follows:

$$\hat{y_i} = \Phi(x_i) = \sum_{k=1}^{k} f_k(x_i), \quad (5)$$

where k is the adaptive functions used to predict the output and f_k is the regression tree decisive space [45].

4.2.8. Proposed ANN.

Deep learning (DL) is a subset of machine learning. DL models like ANN (artificial neural network) [46], CNN (convolutional neural network) [47], RNN (recurrent neural network), and RBM (restricted Boltzmann machine) are one of the supervised deep learning techniques. Also, deep learning models like AE (AutoEncoders), RM, CNN, RNN, and RBM can be used as unsupervised model also [45]. For this study, we have used an optimized ANN as shown in Figure 5. ANN model has a single input layer, three hidden layers, and a single output layer. The input layer contains 12 nodes, the first and second hidden layers have 24 nodes, the third hidden layer has 24 nodes, and the output layer has a single node.

For the activation function, we choose rectified linear activation function which is popularly known as ReLU. ReLU function generally chooses the maximum value from the linear combination of inputs from the previous nodes for the output [48]. ReLU is chosen because this function gives output as either all zeros or ones. And with respect to our
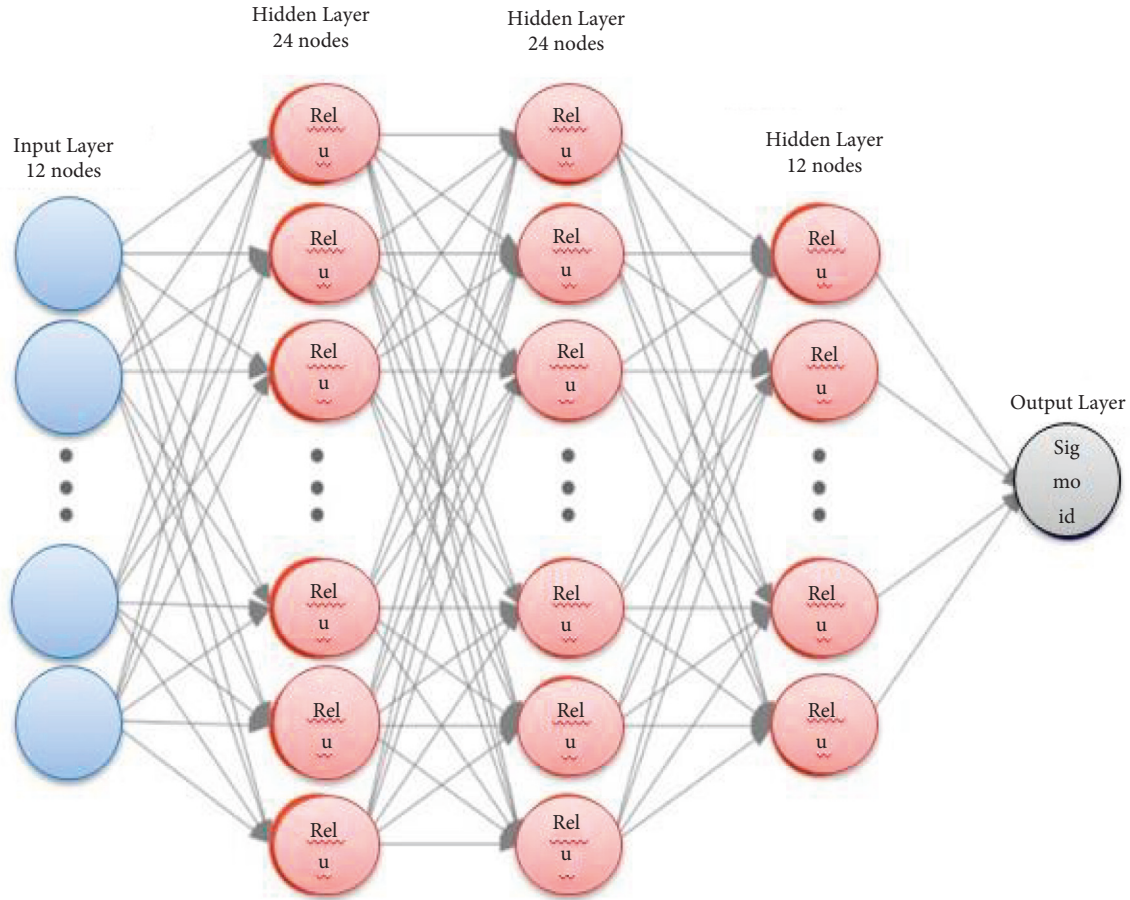
Figure 5: ANN model used for predictive analysis.

dataset, either the grid is stable represented as "1" or the grid is unstable represented as "0" and it has all numerical functions within a given range. "Sigmoid" function is used as an activation function for the output layer because the dataset has only two prediction classes, this implies the dataset will be classified logistically.

$$\text{ReLU}(x) = \begin{cases} 0, if\ x < 0 \\ 1, if\ x \ge 0 \end{cases}, \text{Sigmoid}(x) = \frac{1}{1 + e^{-z}}. \quad (6)$$

To enhance the functioning of ANN, an optimization technique named adaptive optimization algorithm also referred to as "Adam" is used to predict stability of the grid. Adam optimizer function helps to optimize the weights of ANN network. Adam optimizer helps to optimize the learning rate of ANN model [49].

Table 2 presents values of hyper-parameters of different machine learning and deep learning models used for this study.

5. Experimental Result and Discussion

In this section, details of the dataset used for this study are elaborated. All kinds of necessary evaluation matrices used for the analysis of the model are also elaborated in this section. Finally, performance comparison results are presented for all predictive models used.

5.1. Evaluation of Metrics. Repeated random test-train split validation method is used for consistency of machine learning models used for predictions. Repeated random test-train split is basically a hybrid technique of the Hold-out validation approach and K-Fold cross-validation method. Hold-out validation approach is basically known as train and test split.

In this method, the dataset is randomly split into training and testing datasets which may lead to under-fitting or over-fitting. K-Fold cross-validation is a technique in which the data set is divided into K folds and for all the splits, predictive models are applied. And for every split, accuracy is calculated. This helps to avoid over-fitting.

In the repeated random test-train split approach, one split the dataset in testing and training datasets, and then the splitting and evaluating processes are repeated for model prediction multiple times (as one does in K-cross-validation method). For repeated random test-train split, ShuffleSplit and cross_val_score libraries of sklearn are used in python. The number of splits used is 10 and the test dataset is 30% of the total dataset. Accuracy for each fold in repeated random test-train split approach is shown in Table 3. For every model, the highest accuracy achieved is highlighted.

In this analysis experiment, binary classification accuracy, precision, recall, F1-score, and ROC curve are considered for evaluation. This study has focused on the

TABLE 2: Hyper-parameters for predictive models.

Predictive models	Logistic regression	KNN	Naïve Bayes	Decision tree	SVM	Random forest	XGBoost	Optimized ANN
Hyper-parameters used	✓ Penalty = l2 ✓ Multi_class = auto ✓ $c = 1.0$ ✓ max_iter = 100 ✓ tol = $1e − 4$	✓ n_neighbour = 3 ✓ Weight = uniform ✓ algo = auto ✓ leafsize = 30 ✓ $p = 2$ ✓ Metric = minkowski	✓ n_class priors = none ✓ var_smoothening = $1e − 09$	✓ Splitter = best ✓ Criterion = entropy ✓ Max_depth = 90 ✓ Min_samples_split = 10	✓ Random_state = 1 ✓ Probability = true	✓ n_estimator = 100 ✓ criterion = gini ✓ min_sample_split = 10 ✓ max_feature = auto	✓ object = binary_logisticz ✓ n_estimator = 10 ✓ max_depth = 15	✓ Three hidden layers ✓ ReLU + Sigmoid activation function ✓ Adam optimizer

TABLE 3: Accuracy for every fold using repeated random test-train split.

S.No.	Model	Accuracy Fold1	Accuracy Fold2	Accuracy Fold3	Accuracy Fold4	Accuracy Fold5	Accuracy Fold6	Accuracy Fold7	Accuracy Fold8	Accuracy Fold9	Accuracy Fold10
1	Logistic regression	0.81405	0.81527	0.8145	**0.81838***	0.8146	0.81561	0.8131	0.81116	0.81361	0.81272
2	KNN	0.813889	**0.82283***	0.81522	0.82078	0.81656	0.81267	0.81639	0.81561	0.81628	0.81789
3	Naïve Bayes	0.832556	0.8315	0.82444	0.83039	0.83056	**0.83256***	0.83239	0.82828	0.83311	0.83156
4	Decision tree	0.83305	0.83156	0.83183	0.837	**0.83328***	0.83244	0.83178	0.8315	0.8345	0.83139
5	SVM	0.927667	0.92706	0.92622	**0.92944***	0.92806	0.92628	0.92789	0.92767	0.92844	0.92911
6	Random forest	0.907056	0.90939	0.90572	0.90983	**0.90928***	0.909	0.90772	0.91183	0.90817	0.91056
7	XGBoost	0.92983	0.92894	0.92806	0.9275	**0.93406***	0.93206	0.92817	0.93133	0.93078	0.92794
8	Optimized ANN	0.9571	0.9705	0.9724	0.9771	0.9802	0.981	0.9781	**0.9836***	0.9821	0.98

Bold face represents the highest accuracy achieved for every model among different folds.

accuracy of the model. Accuracy measures the correct values that are predicted as compared with the false value predicted and any prediction model is considered to be the best if it predicts maximum correct values. The more the accuracy is given by the model, the more it is considered to be suitable for prediction.

Accuracy (A) is calculated as a ratio of rightfully predicted and classified testing samples to the total testing sample size.

$$A = \frac{(\text{Correct predictions})}{(\text{total samples})}. \tag{7}$$

Precision (P) is also known as false alarm rate. It is calculated as the ratio of the number of correctly classified stable test samples to the total number of samples predicted as stable samples.

$$P = \frac{(\text{True Positives})}{(\text{True Positives} + \text{False Positives})}. \tag{8}$$

Recall (R) referred to as sensitivity or true positive rate, is the ratio of correctly classified stable test samples to total testing samples.

$$R = \frac{(\text{True Positives})}{(\text{True Positives} + \text{False Negative})}. \tag{9}$$

F1-score (F) is a weighted average of precision and recall. ROC curve is basically a graph that helps in the visualization of binary classifier performance on all possible thresholds. ROC curve is plotted between true positive rate against false positive rate. In this analysis, all machine learning models are compared and visualized with the help of the ROC curve as shown in Figure 6.

As shown in Figure 6, SVM is providing the highest true positive rate with the lowest false positive value. Next, close to SVM is XGBoost classifier. So, among all machine learning models, SVM gave the best performance and KNN and logistic regression model gave the least performance.

5.2. Performance Comparison Analysis. Seven machine learning models and deep learning models are for the prediction of the stability of distributed smart energy grid.

Different parameters used for predictive analysis like accuracy, precision, recall, and F1-score are already described in Section 4.2. Performance of different machine learning models is compared and shown in Table 4. In this table, all parameters are taken as an average of repeated random test-train splits.

Table 4 shows the performance parameters of every model used for the study. Logistic regression model gave the least performance with an accuracy of 81.2%, precision as 75.8%, recall as 69.7%, and F1-score as 72.6%. Now, as compared with the logistic regression model, KNN model gave a better performance. KNN prediction model gave an accuracy of 81.61%. Precision score for KNN is 76.3% and recall is 70.7%. F1-score which is a harmonic mean of both precision and recall came out to be 73.4%.

After KNN next, Naïve Bayes is next in line. In terms of accuracy score, naïve Bayes and decision tree gave almost similar performance as accuracy for naïve Bayes model is 83.04%. But, true positive rate and correct prediction rate for decision tree are much better than that of naïve Bayes. Because precision for naïve Bayes came out to be 82.9% and recall is 66.2% for the same, F1-score for naïve Bayes is 73.6%. Decision tree performs better than logistic regression, KNN model, and naïve Bayes. Accuracy for decision tree came out to be 83.28%. Precision is 86.5%, recall is 84.5%, and F1-score is 85.5% for the same. According to the parameter results, random forest is next in line for better performance. Accuracy for random forest is 90.88%, precision value is 90.6%, recall is 82.4%, and F1-score is 86.3% for random forest. SVM and XGBoost perform best among all machine learning models. Accuracy value for SVM and XGBoost came out to be 92.77% and 92.88%, respectively, Precision is 92.1% and 91.2%, respectively, recall is 87.1% and 88.5%, respectively, F1-score is 89.5% and 89.8%, respectively.

Proposed deep learning model for smart grid, that is, optimized ANN model outperforms all other predictive models with accuracy as 97.27%, precision is 96.79%, recall is 95.67%, and F1-score came out to be 96.22%. Following bar charts are used to visualize the comparative analysis of different predictive models on the basis of accuracy (Figure 7), precision (Figure 8), recall (Figure 9), and F1-score

TABLE 4: Performance parameters for prediction models.

S. no.	Model	Accuracy	Precision	Recall	F1 score
1	Logistic regression	81.2	75.8	69.7	72.6
2	KNN	81.61	76.3	70.7	73.4
3	Naïve Bayes	83.04	82.9	66.2	73.6
4	SVM	92.77	92.1	87.1	89.5
5	Decision tree	83.28	86.5	84.5	85.5
6	Random forest	90.88	90.6	82.4	86.3
7	XGBoost	92.98	91.2	88.5	89.8
8	Proposed ANN	**97.27**	**96.79**	**95.67**	**96.22**

Bold face represents the best model among all other models.
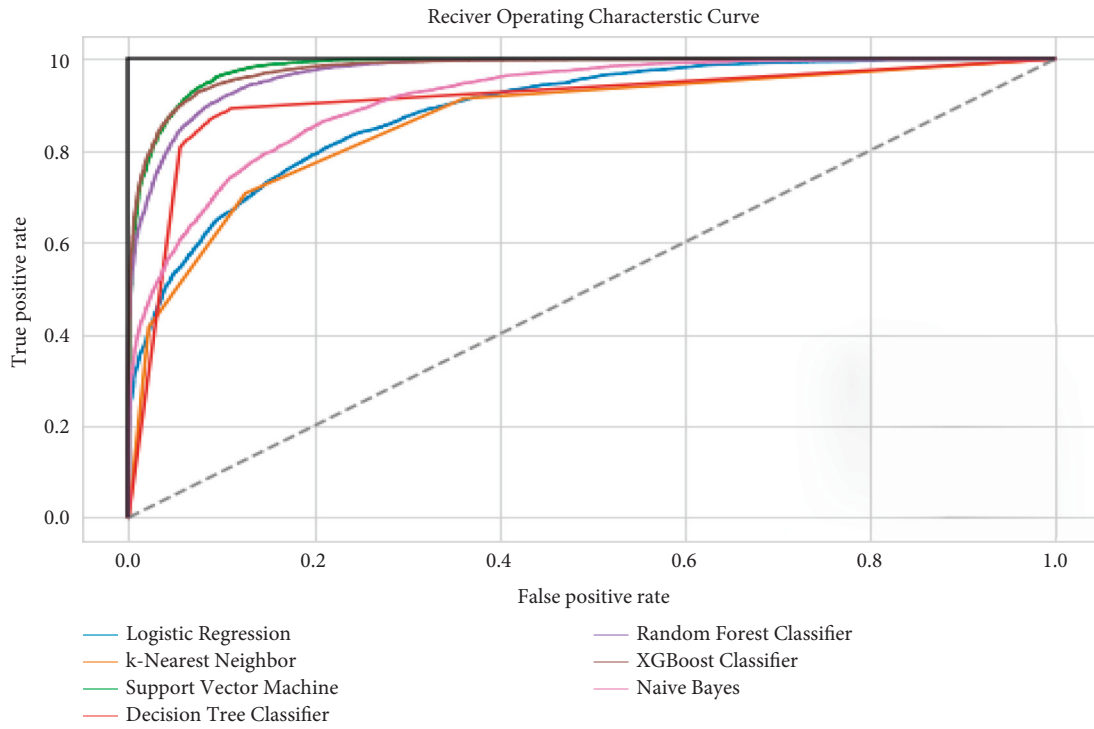
FIGURE 6: ROC curve of all machine learning models.
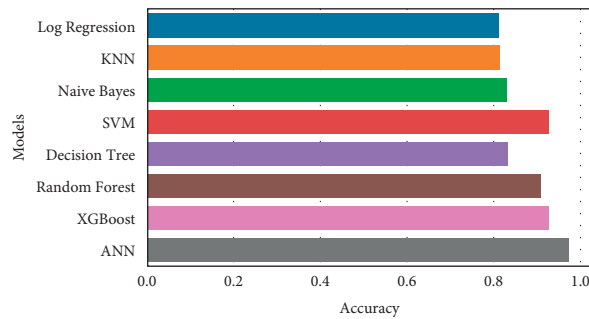
FIGURE 7: Comparative analysis of accuracy using different prediction models.

(Figure 10). On the basis of these charts and Table 4, this study concludes that ANN is the best model for stability prediction in smart grid.

Also, an augmented dataset helps to achieve better accuracy than that of the normal dataset. Dataset used in the study of Arzamasov et al. [17] used normal dataset which
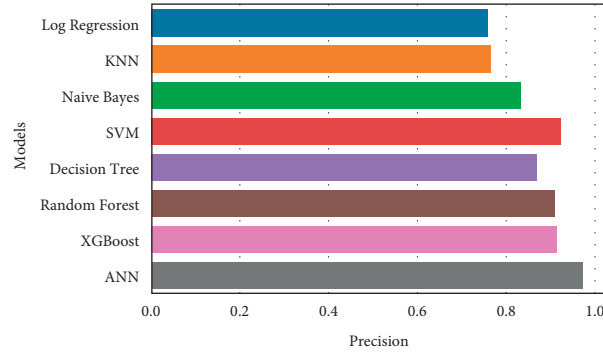
FIGURE 8: Comparative analysis of precision using different prediction models.
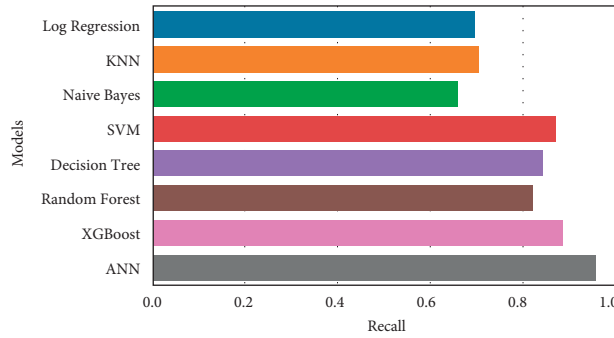
FIGURE 9: Comparative analysis of recall using different prediction models.
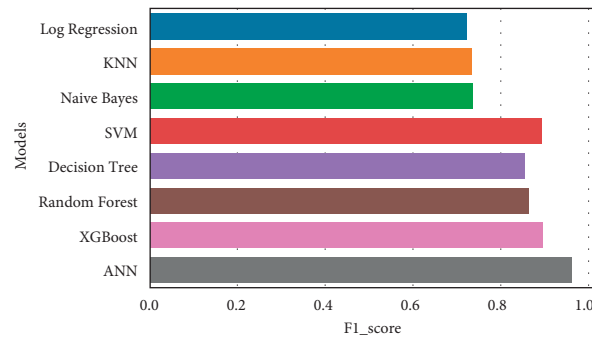
FIGURE 10: Comparative analysis of F1-score using different prediction models.

TABLE 5: Comparison of the proposed model with the existing approach.

S. No.	Model	Accuracy (%)
1	Decision tree (Arzamasov et al. [17])	80
2	Proposed optimized ANN	97.27

gave an accuracy of around 80% for decision tree while augmented dataset with proposed model gave an accuracy of 97.27%. Table 5 shows the comparison of the proposed optimized ANN model with the model in this field with respect to accuracy.

6. Conclusion

Industry 4.0 has shown its impact by means of Industrial Internet viz. through IoT enabling technologies, taking smart decisions, automating industries deploying machine learning, deep learning, data analytics, etc. Power grid is one of the domains where all these technologies are used to make it smart. In smart grid, producers and consumers are connected through communication lines or the Internet. IoT can help to convert conventional energy networks to smart energy grids. This article presents a three-layered integrated smart grid IoT network. This integration can play a very major role to predict the stability of smart power grid in near future using data collected from these communication lines or the Internet.

Different predictive models like logistic regression, naïve Bayes, KNN, decision tree, SVM, random forest, XGBoost, and optimized ANN are used to analyze openly available smart grid datasets. These predictive models are then compared based on accuracy, precision, recall, and $F1$-score. Also, ROC curve is used for the comparison of all the predictive models. Dataset is available on UCI machine learning repository and this dataset is firstly augmented and then scaled to find better results. As a result, we found that the decision tree predictive model on normal dataset gave an accuracy of 80% and the augmented dataset gave an accuracy of 83.28% for the same model.

Among all the predictive models, ANN optimized with Adam optimizer with ReLU and Sigmoid activation function gave an accuracy of 97.27% that wins the race. All comparative matrices are presented using bar charts. These bar charts help to conclude that optimized ANN which is a deep learning model outperformed the remaining machine learning predictive models. Further, other deep learning models will be proposed which may give much better results for prediction. A real-time dataset may be used in near future, to apply the same predictive models and analyze their efficiency for it.

Data Availability

Data will be available on request from the submitting author.

Conflicts of Interest

The authors declare that they have no conflicts of interest.

References

[1] F. A. Almalki, S. H. Alsamhi, R. Sahal et al., "Green IoT for eco-friendly and sustainable smart cities: future directions and opportunities," *Mobile Networks and Applications*, vol. 19, p. 3, 2021.

[2] V. V. S. Lanka, M. Roy, S. Suman, and S. Prajapati, "Renewable energy and demand forecasting in an integrated smart grid," in *2021 Innovations in Energy Management and Renewable Resources(Iemre 2021)*, A. K. Bar, M. Pal, S. Ghosh et al., Eds., IEEE, New York, 2021.

[3] M. Jayachandran, C. R. Reddy, S. Padmanaban, and A. H. Milyani, "Operational planning steps in smart electric power delivery system," *Scientific Reports*, vol. 11, no. 1, p. 17250, 2021.

[4] M. A. Mahmoud, A. Y. C. Tang, A. Maseleno, F.-C. Lim, H. Kasim, and C. Yong, "Towards the development of a smart energy grid," in *Emerging Trends in Intelligent Computing and Informatics: Data Science, Intelligent Information Systems and Smart Computing*, F. Saeed, F. Mohammed, and N. Gazem, Eds., Springer International Publishing Ag, Cham, pp. 673–682, 2020.

[5] B. Schäfer, M. Matthiae, M. Timme, and D. Witthaut, "Decentral smart grid control," *New Journal of Physics*, vol. 17, no. 1, p. 015002, 2015.

[6] S. Azad, F. Sabrina, and S. Wasimi, "Transformation of smart grid using machine learning," in *2019 29th Australasian Universities Power Engineering Conference (Aupec)*IEEE, New York, 2019.

[7] G. Kaur, P. Tomar, and P. Singh, "Design of cloud-based green IoT architecture for smart cities," in *Internet of Things and Big Data Analytics toward Next-Generation Intelligence, Studies in Big Data*, N. Dey, A. E. Hassanien, C. Bhatt, A. S. Ashour, and S. C. Satapathy, Eds., Springer International Publishing, Cham, pp. 315–333, 2018.

[8] N. M. Kumar, A. A. Chand, M. Malvoni et al., "Distributed energy resources and the application of ai, iot, and blockchain in smart grids," *Energies*, vol. 13, no. 21, p. 5739, 2020.

[9] S. M. A. A. Abir, A. Anwar, J. Choi, and A. S. M. Kayes, "IoT-Enabled smart energy grid: applications and challenges," *IEEE Access*, vol. 9, pp. 50961–50981, 2021.

[10] M. Baba, M. U. Tariq, and M. A. Jan, "Secure and resilient demand side management engine using machine learning for IoT-enabled smart grid," *Sustainable Cities and Society*, vol. 62, 2020.

[11] P. Tomar, G. Kaur, and P. Singh, "A prototype of IoT-based real time smart street parking system for smart cities," in *Internet of Things and Big Data Analytics toward Next-Generation Intelligence, Studies in Big Data*, N. Dey, A. E. Hassanien, C. Bhatt, A. S. Ashour, and S. C. Satapathy, Eds., Springer International Publishing, Cham, pp. 243–263, 2018.

[12] M. Elsisi, K. Mahmoud, M. Lehtonen, and M. M. F. Darwish, "Reliable industry 4.0 based on machine learning and IoT for analyzing, monitoring, and securing smart meters," *Sensors*, vol. 21, no. 2, p. 487, 2021.

[13] M. Babar, M. U. Tariq, and M. A. Jan, "Secure and resilient demand side management engine using machine learning for IoT-enabled smart grid," *Sustainable Cities and Society*, vol. 62, p. 102370, 2020.

[14] R. Yao, J. Li, B. Zuo, and J. Hu, "Machine learning-based energy efficient technologies for smart grid," *International Transactions on Electrical Energy Systems*, vol. 31, no. 9, p. e12744, 2021.

[15] P. Sharmila, J. Baskaran, C. Nayanatara, and R. Maheswari, "A hybrid technique of machine learning and data analytics for optimized distribution of renewable energy resources targeting smart energy management," in *2nd International Conference on Recent Trends in Advanced Computing Icrtac-Disrup - TivInnovation, 2019*, P. Nithyanandam, R. Parvathi, R. J. Kannan, and A. N. Khan, Eds., Elsevier Science Bv, Amsterdam, pp. 278–284, 2019.

[16] W. Ahmed, H. Ansari, B. Khan et al., "Machine learning based energy management model for smart grid and renewable energy districts," *IEEE Access*, vol. 8, pp. 185059–185078, 2020.

[17] V. Arzamasov, K. Böhm, and P. Jochem, "Towards concise models of grid stability," in *Proceedings of the 2018 IEEE International Conference on Communications, Control, and Computing Technologies for Smart Grids (SmartGridComm)*, pp. 1–6, IEEE, Aalborg, Denmark, 29-31 October 2018.

[18] K. Chen, K. Chen, Q. Wang, Z. He, J. Hu, and J. He, "Short-term load forecasting with deep residual networks," *IEEE Transactions on Smart Grid*, vol. 10, no. 4, pp. 3943–3952, 2019.

[19] Y. Wang, Y. Kong, X. Tang et al., "Short-term industrial load forecasting based on ensemble hidden Markov model," *IEEE Access*, vol. 8, pp. 160858–160870, 2020.

[20] Y. Wang, S. Sun, X. Chen et al., "Short-term load forecasting of industrial customers based on SVMD and XGBoost," *International Journal of Electrical Power & Energy Systems*, vol. 129, p. 106830, 2021.

[21] S. Gupta, R. Kambli, S. Wagh, and F. Kazi, "Support-vector-machine-based proactive cascade prediction in smart grid using probabilistic framework," *IEEE Transactions on Industrial Electronics*, vol. 62, no. 4, pp. 2478–2486, 2015.

[22] Q. Ge, C. Guo, H. Jiang et al., "Industrial power load forecasting method based on reinforcement learning and PSO-lssvm," *IEEE Transactions on Cybernetics*, vol. 52, no. 2, pp. 1112–1124, 2022.

[23] L. Wei, D. Gao, and C. Luo, "False data injection attacks detection with deep Belief networks in smart grid," in *Proceedings of the 2018 Chinese Automation Congress, CAC*, pp. 2621–2625, Xi'an, China, 30 November 2018 - 02 December 2018.

[24] K. Amarasinghe, D. L. Marino, and M. Manic, "Deep neural networks for energy load forecasting," in *Proceedings of the 2017 IEEE 26th International Symposium on Industrial Electronics (ISIE)*, pp. 1483–1488, IEEE, Edinburgh, UK, 19-21 June 2017.

[25] A. Muzumdar, C. N. Modi, G. M. Madhu, and C. Vyjayanthi, "Analyzing the feasibility of different machine learning techniques for energy imbalance classification in smart grid," in *Proceedings of the 2019 10th International Conference on Computing, Communication and Networking Technologies (Icccnt)*, 06-08 July 2019.

[26] Z. Guan, Z. Lv, X. Sun et al., "A differentially private big data nonparametric bayesian clustering algorithm in smart grid," *IEEE Transactions on Network Science and Engineering*, vol. 7, no. 4, pp. 2631–2641, 2020.

[27] H. Wang, Z. Yemeni, W. M. Ismael, A. Hawbani, and S. H. Alsamhi, "A reliable and energy efficient dual prediction data reduction approach for WSNs based on Kalman filter," *IET Communications*, vol. 15, no. 18, pp. 2285–2299, 2021.

[28] S. H. Alsamhi, F. Almalki, O. Ma, M. S. Ansari, and B. Lee, "Predictive estimation of optimal signal strength from drones over IoT frameworks in smart cities," *IEEE Transactions on Mobile Computing*, vol. 1, p. 1, 2021.

[29] V. O. Nyangaresi and S. H. Alsamhi, "Towards secure traffic signaling in smart grids," in *Proceedings of the 2021 3rd Global Power, Energy and Communication Conference (GPECOM)*, pp. 196–201, IEEE, Antalya, Turkey, 05-08 October 2021.

[30] *UCI Machine Learning Repository: Electrical Grid Stability Simulated Data Data Set*, Available at: https://archive.ics.uci.edu/ml/datasets/Electrical+Grid+Stability+Simulated+Data+# accessed, 2018.

[31] S. Sperandei, "Understanding logistic regression analysis," *Biochemia Medica*, vol. 24, no. 1, pp. 12–18, 2014.

[32] R. H. Myers, *Classical and Modern Regression with Applications*, Duxbury press, vol. 2, p. 488, Belmont, CA, 1990.

[33] S. Zhang, X. Li, M. Zong, X. Zhu, and D. Cheng, "Learning k for kNN Classification," *ACM Trans. Intell. Syst. Technol.*vol. 8, no. 3, pp. 1–43, 2017.

[34] Y. Weng, R. Negi, C. Faloutsos, and M. D. Ilić, "Robust data-driven state estimation for smart grid," *IEEE Transactions on Smart Grid*, vol. 8, no. 4, pp. 1956–1967, 2017.

[35] O. Valgaev, F. Kupzog, and H. Schmeck, "Low-voltage power demand forecasting using K-nearest neighbors approach," in *Proceedings of the 2016 IEEE Innovative Smart Grid Technologies - Asia (ISGT-Asia)*, pp. 1019–1024, IEEE, Melbourne, VIC, Australia, 28 November 2016 - 01 December 2016.

[36] D. Vidaurre, C. Bielza, and P. Larrañaga, "Forward stagewise naïve Bayes," *Progress in Artificial Intelligence*, vol. 1, pp. 57–69, 2012.

[37] N. F. Lepora, M. Evans, C. W. Fox, M. E. Diamond, K. Gurney, and T. J. Prescott, "Naive Bayes texture classification applied to whisker data from a moving robot," in *Proceedings of the 2010 International Joint Conference on Neural Networks (IJCNN)*, pp. 1–8, IEEE, Barcelona, Spain, 18-23 July 2010.

[38] I. H. Wijesinghe and S. D Viswakula, "Machine learning for pre-auction sample selection," in *Proceedings of the 2018 National Information Technology Conference (NITC)*, pp. 1–8, IEEE, Colombo, Sri Lanka, 02-04 October 2018.

[39] C. T. Yildiz and E. Alpaydin, "Omnivariate decision trees," *IEEE Transactions on Neural Networks*, vol. 12, no. 6, pp. 1539–1546, 2001.

[40] P. H. Swain and H. Hauska, "The decision tree classifier: design and potential," *IEEE Transactions on Geoscience Electronics*, vol. 15, no. 3, pp. 142–147, 1977.

[41] E. Scornet, "Random forests and kernel methods," *IEEE Transactions on Information Theory*, vol. 62, no. 3, pp. 1485–1500, 2016.

[42] E. Scornet, G. Biau, and J.-P. Vert, "Consistency of random forests," *Annals of Statistics*, vol. 43, no. 4, pp. 1716–1741, 2015.

[43] T. Chen and C. Guestrin, "XGBoost: a scalable tree boosting system," in *Proceedings of the 22nd ACM SIGKDD International Conference on Knowledge Discovery and Data Mining, KDD '16*, pp. 785–794, Association for Computing Machinery, New York, NY, USA, 2016.

[44] M. Ding, L. Zhao, H. Pei, and M. Song, "An XGBoost based evaluation methodology of product color emotion design," *Journal of Advanced Mechanical Design, Systems, and Manufacturing 15*, vol. 15, p. 6, 2021 JAMDSM0075–JAMDSM0075.

[45] A. Chahal and P. Gulia, "Deep learning: a predictive IoT data analytics method," *International Journal of Engineering Trends and Technology*, vol. 68, no. 7, pp. 25–33, 2022.

[46] A. Sagu, N. S. Gill, and P. Gulia, "Artificial neural network for the internet of Things security," *International Journal of Engineering Trends and Technology*, vol. 68, no. 11, pp. 129–136, 2018.

[47] G. Altan, "DeepOCT: an explainable deep learning architecture to analyze macular edema on OCT images," *Engineering Science and Technology, an International Journal*, vol. 34, p. 101091, 2022.

[48] G. Katz, C. Barrett, D. L. Dill, K. Julian, and M. J. Kochenderfer, "Reluplex: an efficient SMT solver for verifying deep neural networks," in *Computer Aided Verification, Lecture Notes in Computer Science*, R. Majumdar and V. Kunčak, Eds., Springer International Publishing, Cham, pp. 97–117, 2017.

[49] Z. Zhang, "Improved Adam optimizer for deep neural networks," in *Proceedings of the 2018 IEEE/ACM 26th International Symposium on Quality of Service*, Banff, AB, Canada, 04-06 June 2018.

WILEY | Hindawi

Research Article

Future of Business Culture: An Artificial Intelligence-Driven Digital Framework for Organization Decision-Making Process

Navaneetha Krishnan Rajagopal,[1] Naila Iqbal Qureshi,[2] S. Durga,[3] Edwin Hernan Ramirez Asis [iD],[4] Rosario Mercedes Huerta Soto [iD],[5] Shashi Kant Gupta,[6] and S. Deepak [iD][7]

[1]*Business Studies, University of Technology and Applied Sciences, Salalah, Oman*
[2]*Department of Business and Administration, College of Business Administration, Princess Nourah Bint Abdulrahman University, Riyadh, Saudi Arabia*
[3]*KL Business School, Koneru Lakshmaiah Education Foundation, KL University, Vaddeswaram, Andhra Pradesh, India*
[4]*Universidad Señor de Sipan, Chiclayo, Peru*
[5]*Universidad Nacional Santiago Antunez de Mayolo, Huaraz, Peru*
[6]*CSE, Integral University, Lucknow, Uttar Pradesh, India*
[7]*Department of Accounting and Finance School of Business and Economics, Ambo University, Woliso Campus, P.O. Box 217, Ambo, Ethiopia*

Correspondence should be addressed to S. Deepak; deepak.sankaran@ambou.edu.et

Technological efforts are currently being used across a broad array of industries. Through the combination of consumer choice and matching principle, the goal of this paper is to investigate the prospective implications of artificial intelligence systems on businesses' outcomes. From an entrepreneurship standpoint, the research revealed that artificial intelligence systems can help with better decision-making. What impact does the introduction of AI-based decision-making technologies have on organizational policymaking? The quirks of human and AI-based policymaking are identified in this research based on five important contextual factors: precision of the choice search area, contribution to the innovation of the policymaking process and result, volume of the replacement collection, policymaking pace, and generalizability. We create a novel paradigm comparative analysis of conventional and automation judgment along these criteria, demonstrating how both judgment modalities can be used to improve organizational judgment efficiency. Furthermore, the research shows that, by involving internal stakeholders, they can manage the correlation among AI technologies and improve decision for businessmen. Furthermore, the research shows that customer preferences and industry norms can moderate the link between AI systems and superior entrepreneurial judgment. The goal of this work is to conduct a thorough literature analysis examining the confluence of AI and marketing philosophy, as well as construct a theoretical model that incorporates concerns based on established studies in the areas. This research shows that, in a setting with artificial intelligence systems, customer expectation, industry standards, and participative management, entrepreneurial strategic decisions are enhanced. This research provides entrepreneurs with technology means for enhancing decision-making, illustrating the limitless possibilities given by AI systems. A conceptual approach is also formed, which discusses the four factors of profit maximization: relationship of AI tools and IT with corporate objectives; AI, organizational learning, and decision-making methodology; and AI, service development, and value. This study proposes a way to exploit this innovative innovation without destroying society. We show real-world examples of each of these frameworks, indicate circumstances in which they are likely to improve decision-making performance in organizations, and provide actionable implications into their constraints. These observations have a wide variety of implications for establishing new management methods and practices from both academic and conceptual viewpoints.

1. Introduction

Organizational behavior and behavioral economics have long debated how to construct managerial decision that would be, where certain, but when, like, and how to originate and incorporate choices regarding classes of individuals. Herbert Simon defines the method of choosing the variant that is expected to occur in perhaps the most preferable option from a set of available options. This technique includes identifying and documenting the possibilities, assessing their significance, and assessing the appropriateness and insufficiency of each set of results. Businesses can be conceived of as "judgment systems" that must be organized to meet organizational goals. Identifying the right judgment framework for your company, for instance, deferring choices to specialists or combining the judgments of a bunch of participants, has a big impact on how well it runs. While the challenges of developing judgment frameworks that influence actual participants are very well, a primary motivating factor underlying AI's explosive development has been the prospect of speedy, specific, reproducible, and minimal decisions with accuracy surpassing human understanding. While AI's rising usage bears witness to its multiple verifiable positives, its usage in executive decision necessitates a complete understanding of its abilities and weaknesses. Executives that employ AI to make judgments are eventually responsible for their choices. Current revelations and evidence suggesting from the research showed, however, that using AI-based judgment may introduce and worsen a plethora of major and often concealed biases and barriers to evidence brought, responsibility, and openness, jeopardizing faith in AI-based decisions. Despite the attractiveness of intelligent decision-making, institutional culture development is a topic of discussion.

Certain businesses have embraced a "statistics" perspective to operational decision-making. Analytics can assist you in making smarter judgments, but you will need the right technology to do so. Many individuals assume that the processor is a human being. According to the term "information," data are vetted by—and summarized for—humans to comprehend. Firms should, nevertheless, adopt artificial intelligence (AI) into their activities and, in some situations, eliminate individuals from the mix in order to fully comprehend the value of data. Processes based on data must make room for AI-driven frameworks. Firms in the electronic era need to know long waits and, as a result, a better awareness of a dynamic market than in past eras. Depending upon the perspective, numerous companies have implemented advancing technology to attain high effectiveness and a strategic edge [1]. Between all these advancements, AI has taken center stage [2], garnering the attention of both research and industrial applications. The potential of a machine to adapt from its lessons, respond to different inputs, and conduct human-like behaviors is described as AI [3]. AI may now be one intellectual force with the fullest chance for upheaval, as per [3]. Likewise, AI is a critical multipurpose technology in the area of [4]. In the latest period, the vast volume of data generated in various formats has been quicker now than ever. It advocated for the use of new technologies in order to accelerate technological developments such as computing processing capacities and the development of new AI techniques [5]. Businesses can utilize AI to process in the form of these breakthroughs [6, 7].

AI is less susceptible to selection dissonance than people. Even if the results are counterintuitive to our multiple viewpoints, AI can be taught to locate population sections that better describe variation at delicate levels. Thousands, if not millions, of categories are no problem for AI. And AI is perfectly capable of dealing with nonlinear relationships of any kind, including exponentially dynamic equations, geometrical sequences, and binomial probabilities.

The approach shown in Figure 1 provides an excellent use of the evidence and draws more reliable and unbiased inferences. It can assist in finding the optimum ad creativity, commodity quantities, and investment portfolios to make. While individuals are no longer affiliated, it is important to note that AI-driven activities are not just about mechanization. Sure, it might save money, but that is just a bonus. The value of AI stems from its ability to make better decisions than humans. As a result, effectiveness is significantly improved, and new possibilities are introduced.

Humans are not outdated only because they are removed from processes that only entail the analysis of structure data. Many business choices are based on factors other than organized data. Long-term goals, business strategies, organizational ideals, and competitive dynamics are all instances of knowledge that exists only in our thoughts and is transmitted through heritage and other quasichannels. This information is unavailable to AI but crucial to business decisions. For instance, AI could identify the optimal inventories realistically in order to optimize revenues. In a competitive setting, however, a corporation may choose to keep higher inventory levels to deliver a better customer experience at the expense of earnings. In other circumstances, AI may calculate that increasing marketing spending will provide the best return on investment among the options accessible to the organization. However, in order to maintain quality standards, a corporation may choose to limit growth. Individuals have more knowledge in terms of tactics, ethics, and economic conditions; hence they may deviate from AI's objective reasonableness. In such cases, AI can be used to generate possibilities from whom individuals can select the best one depending on the supplementary information available. The order in which such operations are carried out is case-specific. Sometimes AI is the first to relieve human workload. Human judgment can also be used as an input to AI processing in some situations. There may be iteration between AI and human processing in various circumstances (see Figure 2). The point is that people are interacting with the possibilities created by AI's data processing rather than the data itself. Our approach to reconciling our decisions with objective rationality is through values, strategy, and culture. This is best accomplished in an
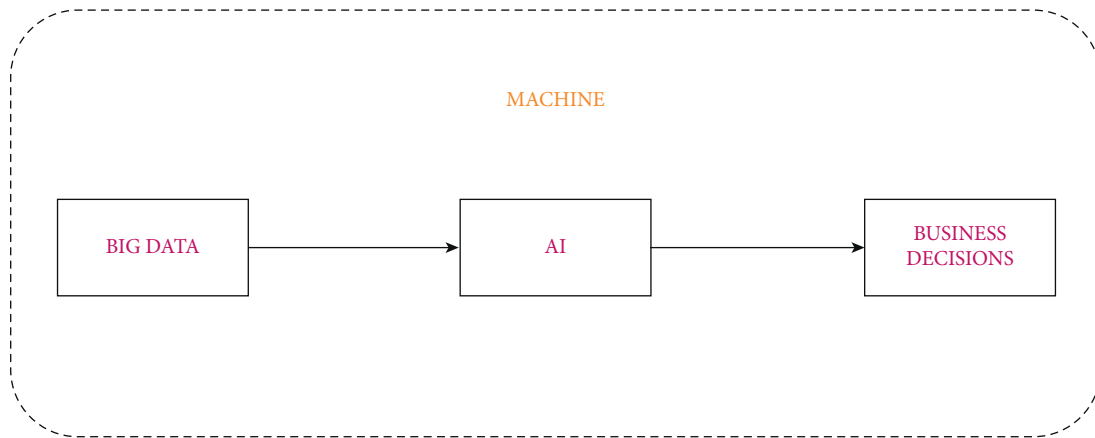
FIGURE 1: AI-driven workflow.
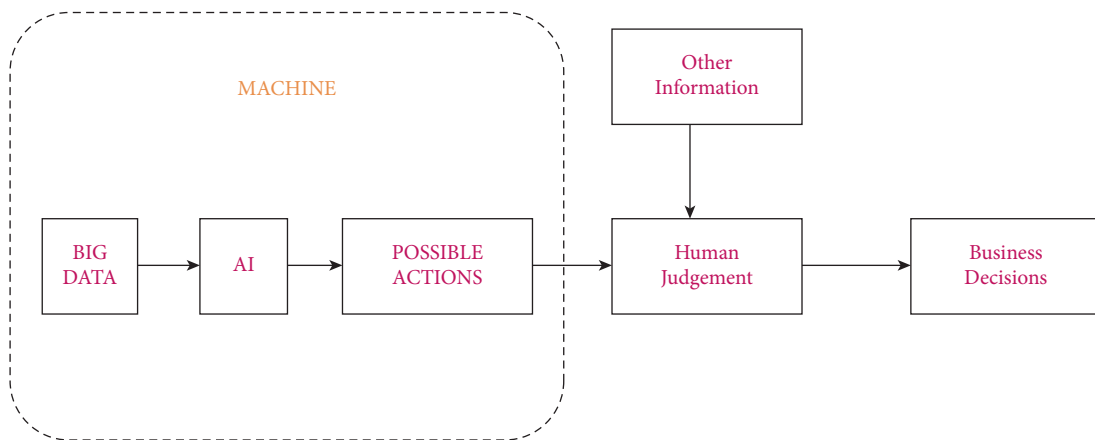
FIGURE 2: AI and human judgment-based DM model.

open and knowledgeable manner. We can make better decisions by combining AI and humans, rather than relying solely on one.

Firms are born and formed as a result of the serious consequence up and define their strategy. Strategy implementation is a continual and sophisticated process since companies invest in diverse systems, and decisions can have explicitly or implicitly consequences on participants [8]. Choices made in the presence of risk are distinguished from those made in the face of uncertainty, according to conventional causal inference. In the first group, all conceivable outcomes, including their chances of occurring, are known and statistically or empirically available. Several factors, however, influence the level and kind of uncertainty in strategic organizational choices that fall into the latter group [9]. To handle complexity, such decisions must be made in an adaptive way, which organizations enable by introducing hierarchies and departments to specify roles. While this enhances operational decision speed and efficiency, it has been discovered that having a variety of perspectives, experiences, and knowledge improves the quality of strategic judgments [9].

1.1. Research Gap and Challenges. Recently, the study of AI has become a growing field. AI and organizations, AI and judgment, and AI within KIFs, yet let alone AI with structuring organization and judgment within KIFs, have received little interest from scholars. Many academics studied the topic of ES, an AI methodology, in the 1980s and 1990s, but it appears that the current tendency is to research the AI technologies world in general. Because of this, when studying the literature on AI, we noticed a surge in the publication of studies discussing ES and AI in the 1980s and 1990s, but this surge subsided until this past decade. Due to the Second Machine Age's restricted computing power and storage, as well as a dearth of data, AI faced a winter throughout the 1990s and the first decade of 2000. To the state of the art, the survey has thus far mostly concentrated on the use of AI in certain sectors or functional departments. According to Martnez-López and Casillas (2013), who performed an outline of AI-based implementation within business markets, and Syam and Sharma (2018), who looked at the effect of AI and machine learning on profits, some researchers have performed a thorough search about the use of AI inside a singular purpose of the venture. Design and research approaches have recently encouraged the

establishment of innovative management practices as well as program management, civic engagement, marketing, and use of social media, among other things.

According to this perspective, the term "change initiatives" refers to a concept that covers cutting-edge problems and procedures for innovative processes [10]. The term "intellectual capital" relates to the governance of expertise, the administration of process innovations within organizations, and the innovation-centered processes that draw on outside ideas to promote effective innovation. Therefore, open innovation advises businesses to go beyond their comfort zones while developing their strategic innovations by collaborating and forming collaborations with various institutions, individuals, and specialists. The boundaries of open innovation, according to some writers, need to be studied and debated in terms of risk, processes and practices, administration, communication, economics, or techniques, even if open innovation has been thoroughly researched in academic study.

McCarthy originally used the phrase artificial intelligence in 1956, defining it as "the science and engineering of creating intelligent machines." Since then, there have been moments of false optimism and cycles of success. AI researchers were confident in their projections of their success in the near future from the start, based on intriguing findings. Instead, the development of AI took longer than anticipated and was dependent on shifting research priorities throughout time, including eras where new approaches were introduced and old ones were improved. However, in the past ten years, the enormous amount of data being produced at a faster rate than ever before necessitated the creation of new technologies, which sped up the advancement of science and technology, including an increase in computational processing. Performing tasks that are simple for a human to complete but difficult to formalize in terms of numerical constraints was (and remains) a major difficulty for AI in its early stages [11]. The challenge of formulating guidelines to explain this kind of activity suggested that AI systems needed the capacity to spot trends in information and develop their own knowledge. Machine learning is the capability that allows computer-based programs to intuitively recognize trends in information and to behave without being explicitly programmed. As a result, AI research has progressed not only in the direction of process rules that humans previously specified for replicating people's behavior to make judgments but also in the path of emulating human experience.

Today, fresh data are produced quickly, providing possible input for developing strategies. This easy access to a lot of data comes with its own set of complications. Large amounts of data must be transformed into workable options as part of the strategy-building process in order for decisions to be made. Strategic decision-making, however, continues to be a cognitively taxing process that necessitates the accurate identification of and selection from among viable possibilities. Human decision-makers frequently choose from limited possibilities based on their existing knowledge base in the interest of time rather than optimizing. On the other side, AI offers a methodical capacity for data processing and interpretation and learns to accomplish certain objectives by permitting suitable adaptability [12]. In fact, the use of AI is more and more ingrained in our daily lives, and its applications in the corporate world are growing in importance. Human attention is a finite resource in and of itself, and AI has already started taking over jobs that formerly required administrative involvement. According to McKinsey (2017), useable AI is "the next frontier," and its emergence has been dubbed one of the most significant evolvements ever since industrialization. Today, AI is starting to become an essential part of company expansion, driving a significant increase in mechanization. Some judgments in the promotional interaction with stakeholders are already automated by AI. The paper makes the claim that AI can be used as an efficacious response to external uncertainties of big datasets and unclear climatic circumstances and was an appropriate reaction to the situational factors of insufficient management consciousness, based on the preliminary research results of [12]. It would be worthwhile to look into the use restrictions, such as corporate culture and digital readiness. The idea that all businesses are created equally surfaced during the interviews. Further investigation is required to determine the conditions under which businesses will truly profit from utilizing AI and more specifically if the expense and effort required to implement change would be worthwhile.

The pace of innovation and intelligent systems has had a significant impact on the B2B ecosystem over the past ten years. The adoption of methods and software that make use of artificial intelligence (AI) to improve operational efficiencies and effectiveness by autonomous algorithms or networks has been one of the most massive modifications. Integrated environments, where research methodology is essential for effective approaches and where AI plays a significant role, decide the next business problems (Saura and Ribeiro-Soriano) [13]. Since data-driven decision-making processes are becoming more prevalent in the corporate world, it is crucial for business success to develop and use customer relationship management systems (CRMs) correctly. However, despite its potential and advantages for businesses, AI is difficult to deploy technically. There is a void in the literature surrounding the identification of the uses that specifically AI-based CRMs can offer to the B2B digital marketing ecosystem, despite the fact that the use of CRM in B2B marketing has been investigated and debated in the past, as was previously mentioned.

In light of the aforementioned, our study intends to provide knowledge relating to the role of AI in developing marketing strategies and to offer managerial and academic insights by exploring whether and how AI might influence the development of marketing strategies [4, 14]. The authors answer this question using a contingency theory approach, doing an exploratory investigation to confirm the current situation, and looking for any potential insights into potential future applications. The following is the structure of this paper. The methods used to carry out the literature review based on the gaps identified are described in Section 2. The results of the article analysis are then provided in

Section 3. The final portion discusses the findings and future research directions.

2. Research Survey and Methodologies

As stated in the media, the state of the art is not necessarily ready for every application. The hype curve, which Gartner publishes on a regular basis, has proved very useful in defining the readiness of various technologies. The hype curve indicates when a technology is ready and when it reaches a high level of production. The graph in Figure 3 depicts the hype curve for new technologies based on a 2019 assessment. Many of the terms associated with artificial intelligence are still a few years away from becoming commonplace.

In terms of developing financial returns, Borges et al. [15] undertook academic analysis to evaluate the association between AI and policy. In view of this, the objective of this report was to narrow the gap by undertaking a thorough systematic review concentrating on the interplay of AI and market tactics, incorporating modern practice with frameworks, showcasing anticipated results, complexities, and possibilities, and kicking off a conversation about future studies. By picking publications from peer-reviewed journals and conference proceedings, they developed a system for introducing research gaps.

Caner and Bhatti [16] analyzed peer-reviewed scientific journal manuscripts to construct a conceptual framework for predicting AI organizational strategy. Only research articles between 2015 and 2019 were considered. They found that AI capabilities and constraints, economic arrangements and AI, organizational units and AI, personnel, sectors, and AI, and AI laws and morals are the crucial parts of the AI business model.

A literature evaluation by Trunk et al. [17] examined the correlation between AI as well as decision-making in quickly transforming company scenarios. The writer completed a textual evaluation of peer-reviewed newspapers to provide an introduction to the preexisting scientific studies which investigated the possibility of linking AI to difficult factors. Results are provided inside a conceptual viewpoint, which demonstrates exactly how people are able to make use of AI within powerful scenarios in addition to consequences and hurdles to look at.

Models are referred to as AI when compared with traditional quantitative theories, which is described as corporeal and precise software applications which could deal with intricacy. There are different research and opinions on whether AI may be just like the man mind in decision-making; however, the methods taken into account differ in terms of focus, expertise, and then purpose. Models are components of manufacturing operations to help human beings for ages; therefore, including know-how straight into company is not a brand new occurrence. Devices, nonetheless, are much more of something completely handled by people as well as much less unique compared to groups in genuine cultural connection scenarios. AI proposes that devices respond and also respond to people, a change within the human-machine connection. Possibilities as well as

chances are not agreed upon or perhaps analyzed extensively, necessitating additional studies.

Figure 4 depicts an equivalent curve, presuming that observation is more closely linked to planned rationality, whereas understanding and reacting necessitate the inclusion of other experienced and recording systems. There is no comprehensive definition of an AI application. Different aspects of intelligence are thought to exist in humans, and according to Nilsson's description and the rational behavior continuum (see Figure 4), AI applications span from simple to complicated [18]. Table 1 shows the literature carried out on various dimensions of AI application in an organizational context.

3. AI-Driven Framework Methodologies and Analysis

By improving consumers' perception and engagement with digital strategy-based applications, AI solutions can help businesses gain a competitive advantage. Entrepreneurial orientation through the development of new products will supply innovative features focused on the social cognitive capabilities of the AI age. The end result is often that combat and mental preparation should focus on securing the introduction of AI to produce ground-breaking goods and providers. Incorporating next-generation AI technologies having a well-defined electronic Internet business strategy that features company objectives, efficiency, and legislation can give businesses competitive by nature benefits. The preexisting research has determined a good base, and the literature comment could today be utilized to create a theoretical style. It assisted the audience with a definite indication of the problem by utilizing a suitable experimental method to evaluate the information in thirteen posts together with the aim of isolating the suggestions to become incorporated within the categorization of all of the publications (Figure 5).

As previously stated, tactical policymaking falls under the heading of uncertain conclusions. Apiece substitute is given a probability and utility level in order to make the optimal decision, and the option with the uppermost biased value is picked. Coherence, conditionalization, and completion are characteristics of probability levels. The influence of frequency is referred to as coherence. Expertise grows as a result of a huge recurrence of analogous claims in analogous situations, which molds the assessment in a given direction. The amount of people included is referred to as convergence. The control body is expected to rise as this number grows. We try comparing the characteristics of AI along five key decision-making circumstances before attempting to address the administrative models by which mortal and AI-based decision-making can be merged: precision of the search area, understandability of the policymaking processes and outcomes, size of the alternate solution collection, policymaking tempo, and replicability. The features of human and AI-based policymaking under these settings are summarized in Table 2.

Our comparability of standard, as well as AI-based strategic preparation, indicates a framework that

Gartner Hype Cycle for
Emerging technologies, 2019
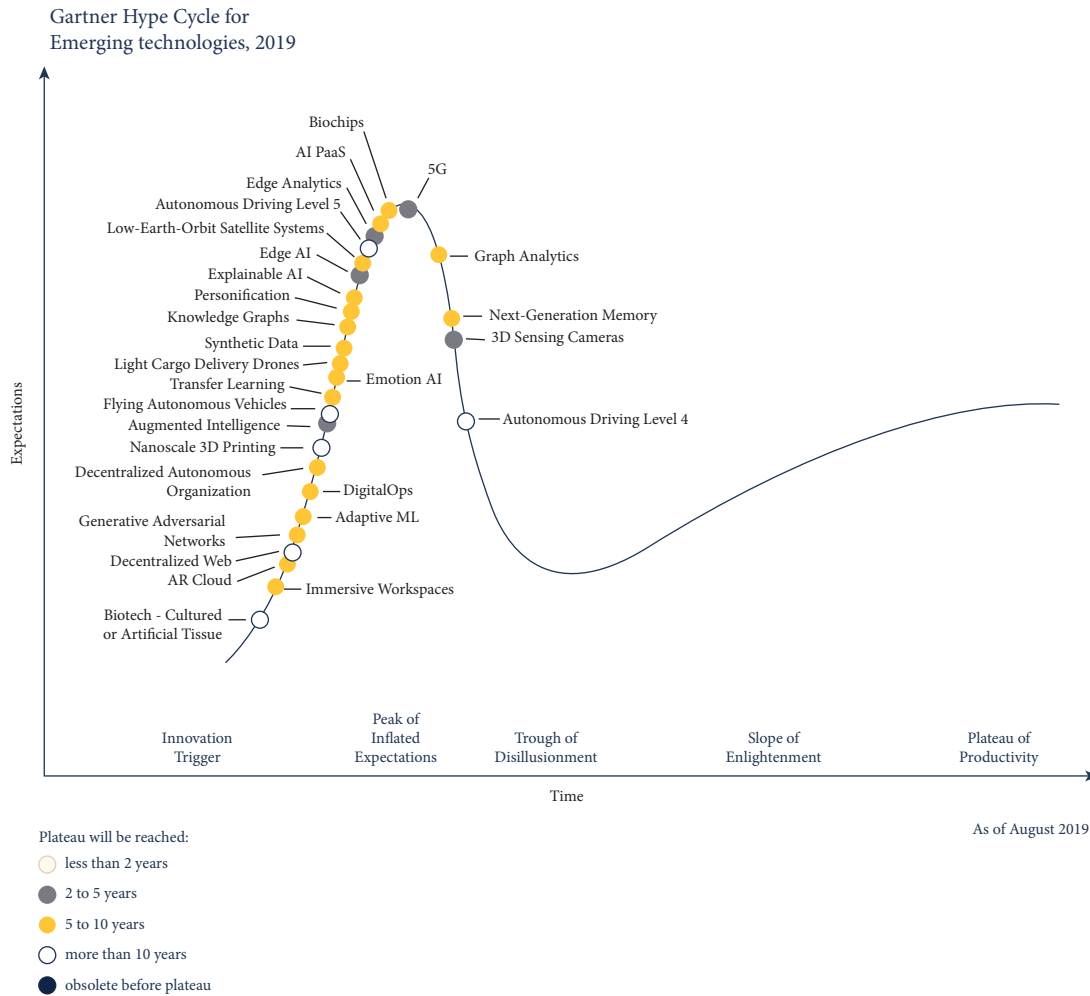
FIGURE 3: Gartner hype chart.

demonstrates the way in which the modalities could be mixed to improve the usefulness of strategic preparation. Within our strategy, the 3 important organizations are complete human AI delegation, crossbreed human AI as well as AI human sequential choice producing, and also aggregated human AI choice-generating (see Figure 6).

3.1. AI Structures. Complete abdication frameworks, which are equivalent to organizational contexts where leaders transmit choice authority to personnel professionals, use AI-based techniques to make choices without human assistance. But on the other hand, intellect retains influence over the conclusion. When the dimensionality on the realization is now much less valuable compared to the generalization reliability, the substitute approach established is great, the decision-making speed is crucial and brought on by organic verdicts, and the total envoy is very beneficial. There are severe drawbacks to deferring decision-making to AI. Scientific studies show that printer mastering algorithms are able to master from Internet textual materials and then replicate concealed man prejudices from gender and race, to come up with insights as well as generate choices (see Figure 7).

Resolving these challenges will involve the collaboration of lawmakers, academics, corporate executives, and computational decision-making system designers. A starting place for this kind of try will be the realization that supervisors are able to designate power to AI, however, not accountability. Enterprise supervisors have to find out how growing authorized buildings such as *RB_IN* the European General Data Protection Regulation (GDPR) is able to change algorithmic quality, fairness, openness, and accountability as well as attend a hands-on method of guaranteeing the moral page layout of computational choice producing realizing the benefits of total envoy to AI-based stakeholders while reducing the chances. Types of these pursuits incorporate switching to fresh new details constructivist coaching strategies as well as leading to the development of completely new methods for reasonable, transparent, and responsible algorithms.

People as well as AI-based solutions can make options to come down with diverse selection methods consecutively, using the end result of just one policy developer moving in the ingestion of other people. The company planners are able to take advantage of the strengths of equally AI as well as man strategic preparation of crossbreed methods, though
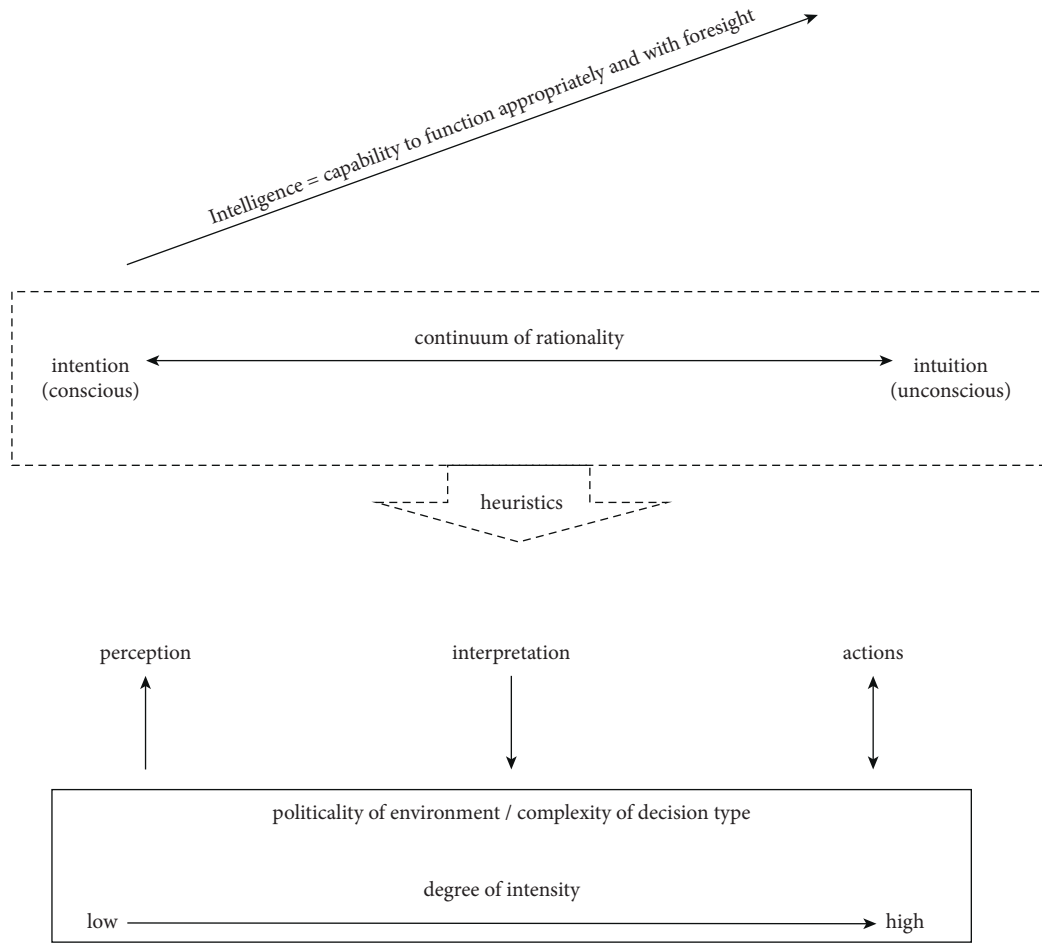
Figure 4: Continuum of rational behavior.

Table 1: Categorization of publications based on organizational environment and the implementation of AI component.

Feature of AI domain	References cited
Decision-making process	Akthar et.al., 2019, and Duan et al. [3]
Stakeholder relationship	Carbone et al. [8], Trunk et al. [17], and Sujata et al. [7]
Machine-to-machine communication	Balog et al. [2] and Lich et al. [4]
AI and machine learning in organization	Yin et al. [14] and Goralski and Tan, 2020

they might additionally earn more intense every other's flaws. The analytic options as inputs to man choice producing and man choices as inputs to computational strategic preparation are 2 stylized crossbreed components that are analyzed.

Information gathering technique for human decision-making: strategic options. This particular building moves within 2 phases. Within the initial action, the original group of options is put through AI-based policymaking. AI provides a filtering system, getting rid of identical or maybe unsuitable choices, as well as delivering in the 2nd stage a subset of practical alternatives which a man policy developer picks because of one of them.

Strategic planning uses human decisions as input. In this structure, people policymakers first target a specific number of possibilities from a higher proportion and additionally send out the mailing list to AI algorithms for selection and

estimation of the smartest choice. The framework pertains nicely to instances in which man choice creators work with a top self-belief within a tiny group of ideal options, but analyzing that little established efficiently demands the computation of big details sets or maybe the thing to consider of crucial stakeholders more than an extended time period. The places where people are unsure regarding the perfect option are coming from a few of choices; this particular framework is able to take advantage of the predictive opportunity of algorithms effectively.

Equally, individuals and AI policymakers are given portions or choices of choices in between the distant relative abilities in this particular product. AI-based judgments and the person are next incorporated utilizing an aggregation method like democratic greater part or maybe typical right into a communal judgment. In this regard, the AI-based policy developer could be viewed together with the reasoning crew's choice that influences
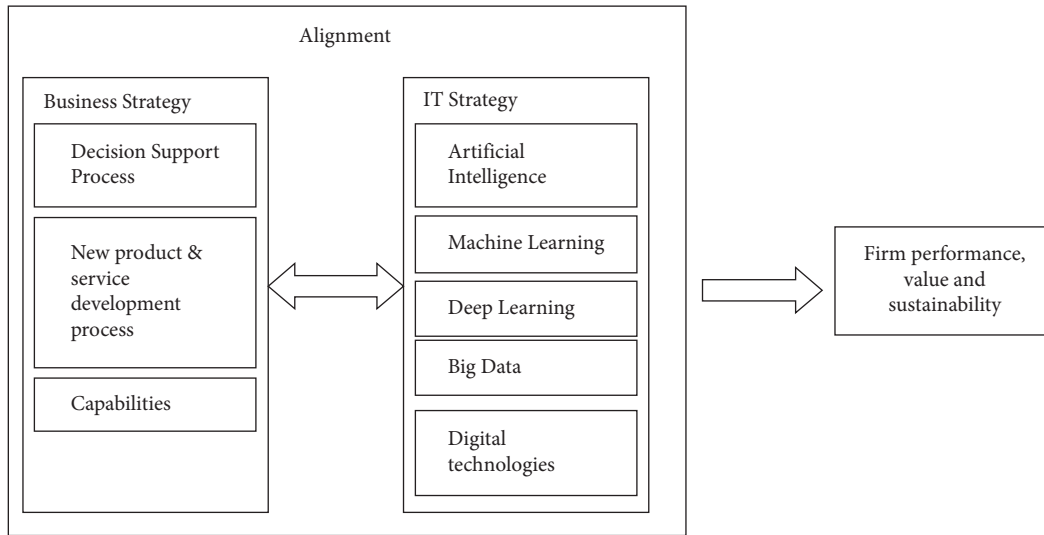
FIGURE 5: Conceptual framework.

TABLE 2: Personnel versus AI-policymaking process.

Conditions	AI	Human
Specificity	A well-defined selection feature selection with precise optimization algorithms is required.	It allows for a broad and vague decision-making environment.
Interpretability	The intricacy of the representations might make interpreting the choice and consequences challenging.	Decisions can be explained and interpreted; however, they are susceptible to retrospective interpretation.
Size	Massive variant combinations can be handled.	Insufficient ability to analyze a wide variety of choices consistently.
Speed	Speedy in comparison. There is a minimal balance among precision.	Slow in comparison. There is a massive trade among exactness.
Replicability	Because of the regular computational approach, the decision-making process and outputs are highly repeatable.	Interpersonal and transcharacteristics such as variances in knowledge, attentiveness, background, and the judgment producer's psychological response make replication susceptible.
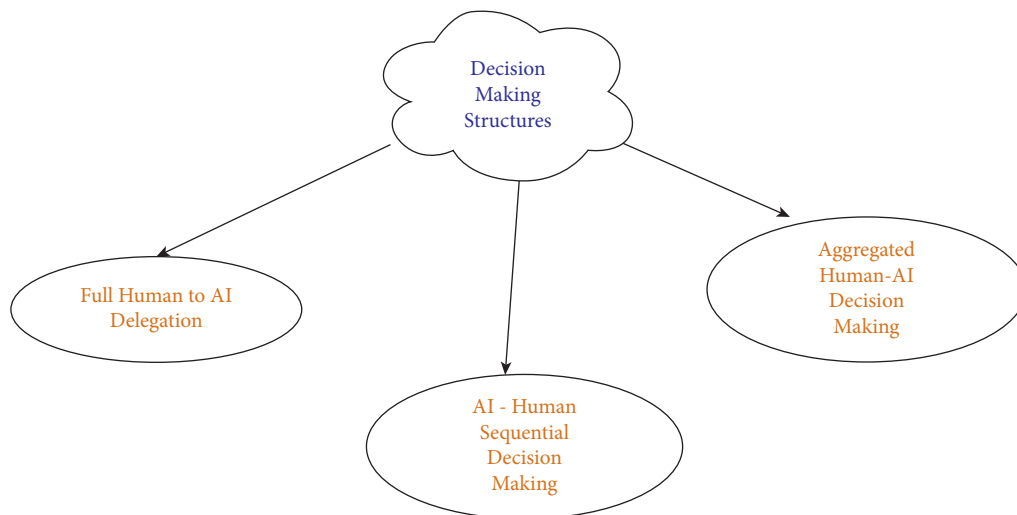
FIGURE 6: Structures related to AI.

the end result of a situation. Because of the pros and cons of individuals in addition to AI-based policymakers, individuals and AI-based policymakers are able to concentrate on different or even disagreeing facets of the options.

3.2. Key Challenges in Using AI-Frameworks in Organization Decision-Making Process. Although "it is not like every strategic decision requires the use of science," AI knowledge has been shown to be essential in understanding when,
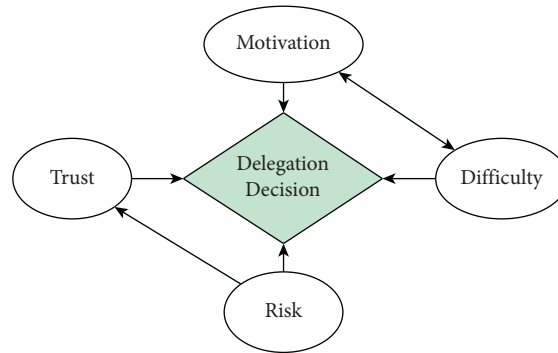
Figure 7: Data delegation process.

where, and why to include AI into operating models. AI literacy, according to researchers, is a deep awareness of the technology and its capabilities and limitations, which is often lacking. Scholars have stated that involving personnel who would be exaggerated by AI incorporation, rather than just top administration, is critical to increasing AI literacy because acceptability varies at different levels. Stakeholders have been shown to need to feel a sense of ownership, and they can define their position by acquainting themselves with the skill and energetically contributing to the integration. As a result, according to the literature, education and training are critical tasks. Capabilities, in particular, have been stated towards becoming extremely relevant as AI enters managerial decision, with an emphasis on employee training in collaboration, inventiveness, and excellent reasoning. AI should be introduced progressively as expertise and comprehension of the technology increase. Personnel get used to using it for jobs that used to be done by computers. Clarity, which is described as "documentation insight into the nature and exchange of information, and also the circumstances with which it is interpreted" to reach a consensus, is also necessary for successful adoption and use. The publications in this genre recommend assembling a varied introductory team composed of new and seasoned business managers, as well as individuals who have obtained adequate guidance. Governance, according to scholars, is responsible for establishing an appropriate introductory team and giving guidance throughout the approach.

By presenting the material of the techniques for dealing, the paradigm examines the recent academic debate on activities and, on the other hand, has been proven to be dependent on the AI application in question, as seen in Figure 8. Furthermore, while utility calculations are claimed to be human-dependent, researchers argue that AI can predict how each option alternative will affect the company or its partners. This could have an impact on the weighing of options, for which AI can also perform pure mathematical calculations. The final choice, on the other hand, must be made solely by the human decision group.

Organizational architecture and resource distribution have an impact on application selection. However, research reveals that this effect is reciprocal, meaning that AI applications have an impact on the definition of organizational structures. Like a nutshell, utilizing AI to aid in this essential

organizational process implies a shift in rational decision roles. According to the study, they become managers.

AI deployment considerations at agencies are based on the operational aim that the innovation is advancing. As illustrated in Tables 3 and 4, the administration may achieve better successful outcomes by using a three-part structure in which AI risks vary depending on the requirement for human decision.

The sophistication of the task grows, and so does the need for effective prevention technologies; according to the report's findings, "confiscating the possibilities and trying to mitigate the dangers connected with trying to adopt automated tools includes paying great consideration to the contest among innovation and endeavor." This continuous spectrum approach can assist government in determining which tasks can be automated rapidly and which ones demand more preparation and collaboration with professional and corporate Allies.

4. Results and Discussions

The Gartner AI survey showed that 17% of firms use AI-based tools for managing HR activities, and this percentage will increase to 30% by 2023. 60% of firms that employ AI use it for the decision-making process (see Figure 9.)

Based on the above structures involved in the effective decision-making process in firms, it is evident that AI performs better when compared to decisions upheld by professionals. Figures 10 and 11 and Table 5 depict the effectiveness of AI tools in the decision-making process.

5. Implications for Further Research and Practice

5.1. Implications. To effectively use and utilize the potential of AI to manage knowledge, it is crucial to understand how AI enables various categories of knowledge. The authors of this paper want to advance knowledge and open up new avenues for investigation into the application of AI to strategy development. The outcomes show that AI may support, replace, or supplement human decision-making when developing marketing strategies. It particularly serves to emphasize the possibility of a beneficial partnership between management and machines. The study has offered

INPUT   PROCESS   OUTPUT
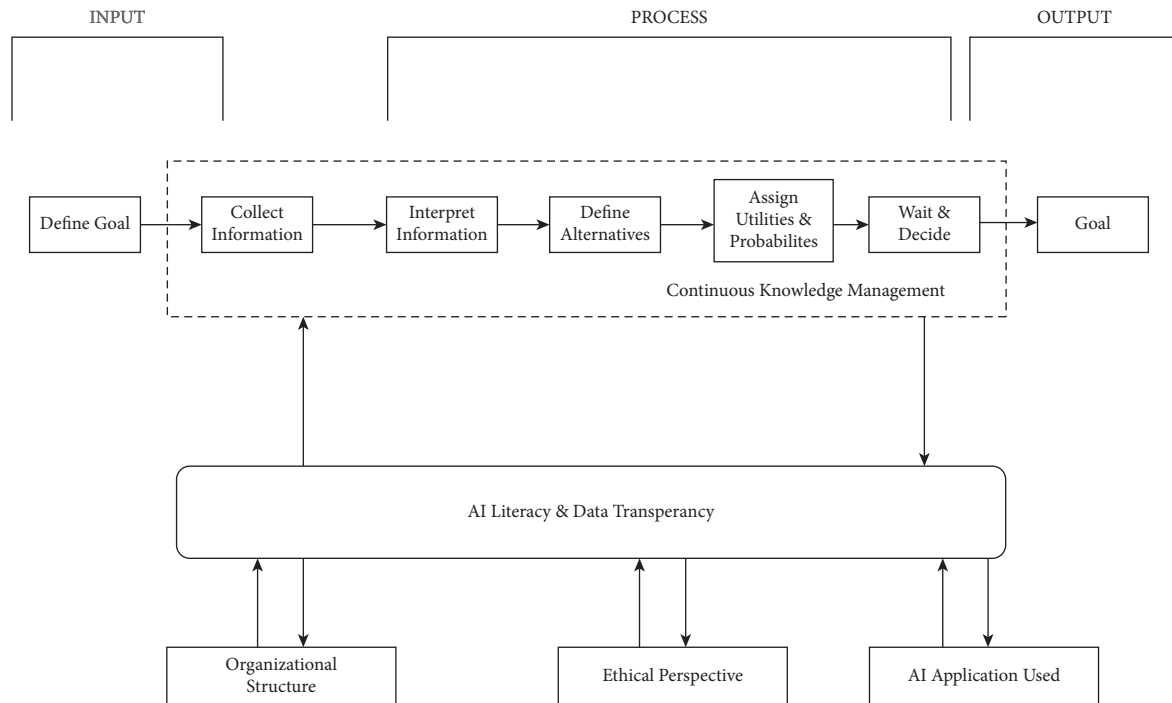

FIGURE 8: Conceptual model for AI.

empirical proof that AI can be used as a tool for developing marketing strategies. What the paper advises to refer to as a creative-possibility perspective is one topic that emerged from the interviews. The authors are hoping that this creative-possibility perspective opens up a new line of inquiry into how managers may collaborate with AI during the process of formulating strategies. Additionally, the expert interviews underline the chance in terms of business school curricula. They noted how many businesses are still ill-prepared for the changes AI would bring about. The establishment of a connection between academia and industry is the primary aspect that will aid in fostering change. For instance, this started in Italy with the establishment of eight competence centers and a number of projects financed by the Italian government. The evidence of how AI may be a tool for developing marketing strategies may be used as input for upcoming business school partnerships and projects.

Furthermore, the current study suggests that this point of view could guide the inclusion of a pragmatic analysis maturity stage dubbed Creative Analytics to the GAAM viewpoint. This suggests the potential for Prescriptive Analytics ("how can we make it happen") to develop into AI ("what innovation can we envisage") used for creative strategy design. It takes both science and art to formulate a campaign. In the world we live in today, data is widely accessible and can be used to influence advertising. Instead, the authors argue that, by providing ways in which AI can supplement human attention for alternative creation, human cognition is "freed up" to provide the art. This is because current AI is suitable for automating some tasks requiring managerial attention. Instead of asking "what is

the appropriate response" tactically, managers need to strategically concentrate on "what are the proper questions." This exploratory work suggests that this is feasible by allowing AI to assist in both the rational view it offers and the creative identification and analysis of the current issue.

The findings of the current investigation have relevant conceptual ramifications. First, additional researches could use research methods outlined in the original investigation as a foundation for fresh proposals for intellectual capital and the excavation of perspectives from significant social networks, taking into account the dearth of prior research that would investigate the innovation process using machine learning strategies. Second, using predictive modeling that aims for statistical significance, the themes found in the current study can be operationalized and investigated as variables. To put it another way, the open innovation and Twitter-based insights learned in this study can be used as factors in further empirical studies. Since our goal was to find characteristics that may be employed in the formulation of future hypotheses in empirical research rather than testing them, the present investigation, despite its explorative, can serve as a forerunner of future statistical inquiries on open innovation.

The findings of this investigation are really useful. As a result, managers of businesses or organizations—both public and private—can effectively use our findings as a guide for developing new organizational or communication norms that would support the growth of open innovation in their own organizations. The many emotions that were discovered in this study also provide us a better grasp of how employees or outside experts feel about open innovation and related issues. Additionally, our findings shed light on how

TABLE 3: Analysis of task by level and decision degree.

Level/degree	Low	Medium	High
Micro	Filling of data	Foster care	Response to emergency
Meso	Operational capabilities	Recruitment process	Decisive planning
Macro	Constitutional responsibilities	Creation of policy	Problem recital and management

TABLE 4: Provision for AI paradigms for tasks by degree of decision.

Low	Medium	High
Automation	Predictive analytics	Relationship inventory
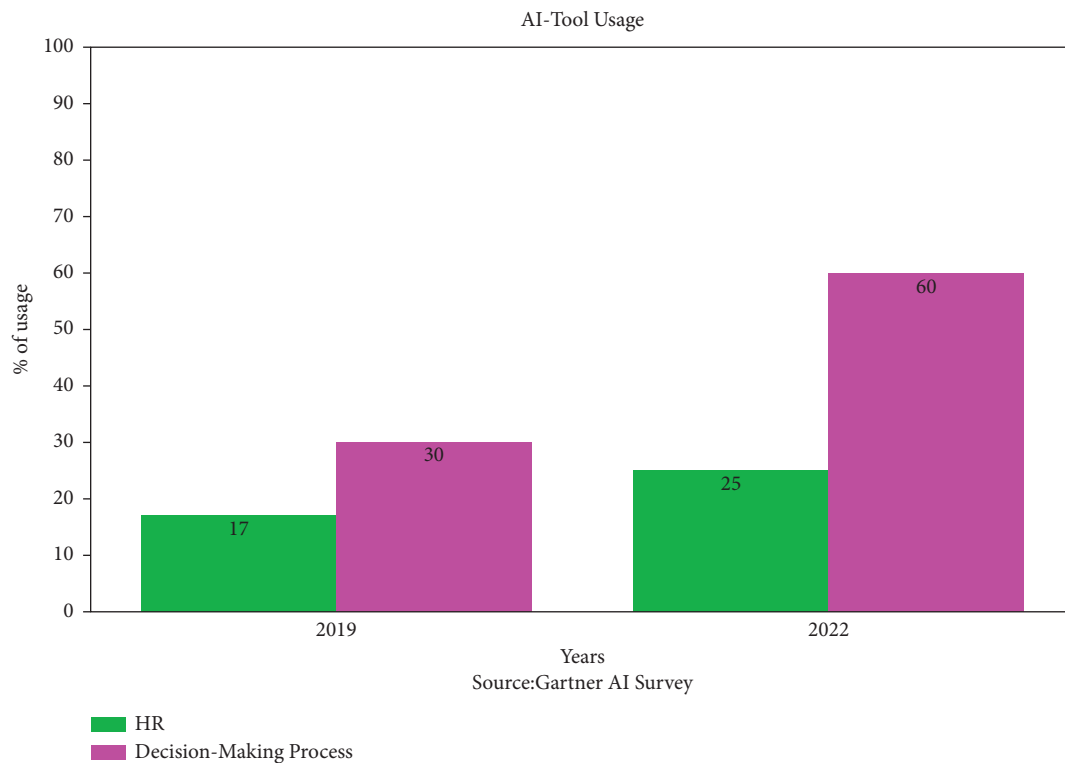
FIGURE 9: Gartner AI survey of AI tools usage.

businesses should structure and promote their cultures, communities, project development and management, support for entrepreneurial endeavors, organization and promotion of ideas, team structure and organization, the use of technology in organizations, and the significance of business models and management for open innovation. In particular, the practitioners can comprehend the idea of open innovation from numerous analysis viewpoints and not just those linked to restrictions, dangers, and characteristics based on our results and the 8 highlighted subjects. More specifically, businesses can use these findings to enhance creative concepts, facilitate knowledge sharing among the company's stakeholders, foster employee innovation, and hence support the development of internal open innovation initiatives or both. Finally, by providing fresh approaches to foster creativity and produce value through open innovation, CEOs and executives of organizations might advise enhancements to their business models and conventional procedures. By

answering the research questions put forth in each of the subjects chosen as pertinent for open innovation strategies, businesses can also apply open innovation.

5.2. Limitations and Future Research Perspectives. The current study contains a number of drawbacks. First, because we utilized a nonprobability sampling design, the results cannot be applied to other settings or samples on the same topic. However, they can be used to explain the UGC components that make up the sample. The second restriction of the present study is the number of tweets we utilized to train our model because all machine learning models are concerned with the accuracy of the findings (i.e., the more trained the machine learning model is, the better the results are). Another drawback of the current study is that we only focused on the information that was taken from one social network (Twitter). Therefore, it would be required to

Effectiveness of AI Tools in Firm Decision-Making Process (2018)
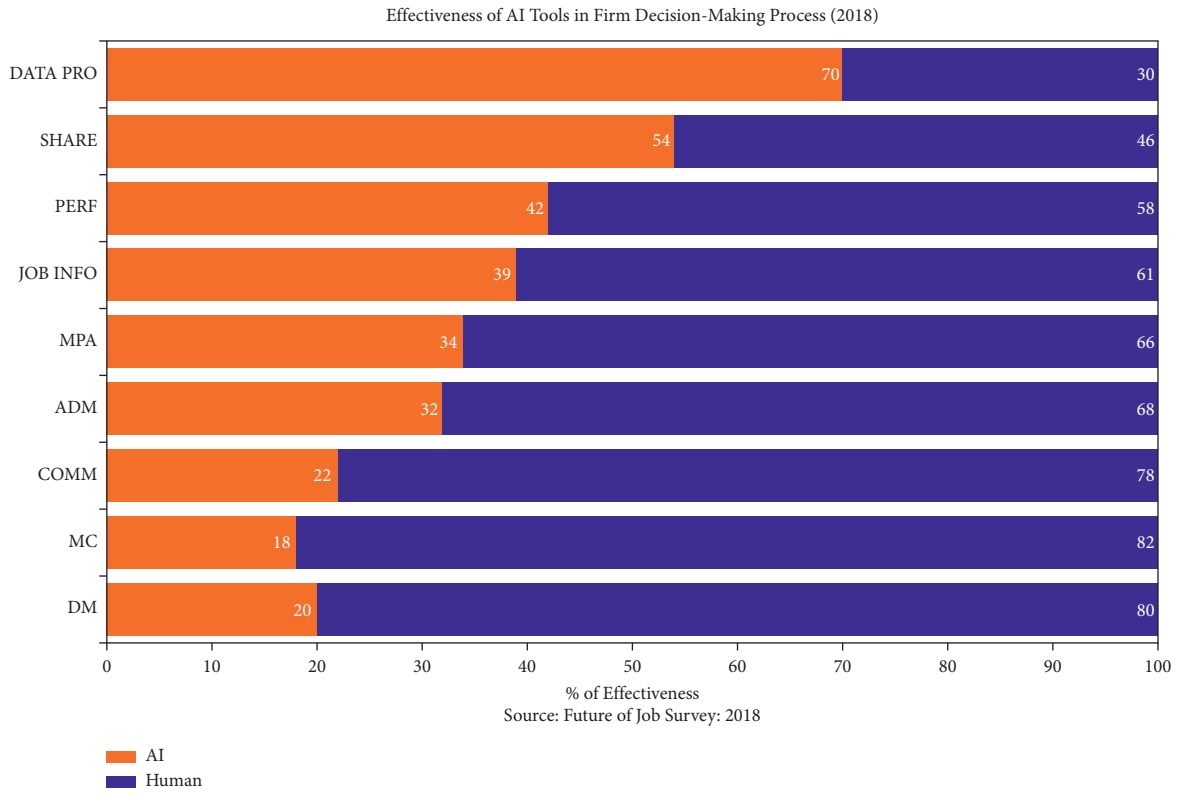
FIGURE 10: Effectiveness of AI tools in firm decision-making process (2018).

Effectiveness of AI Tools in Firm Decision-Making Process (2022)
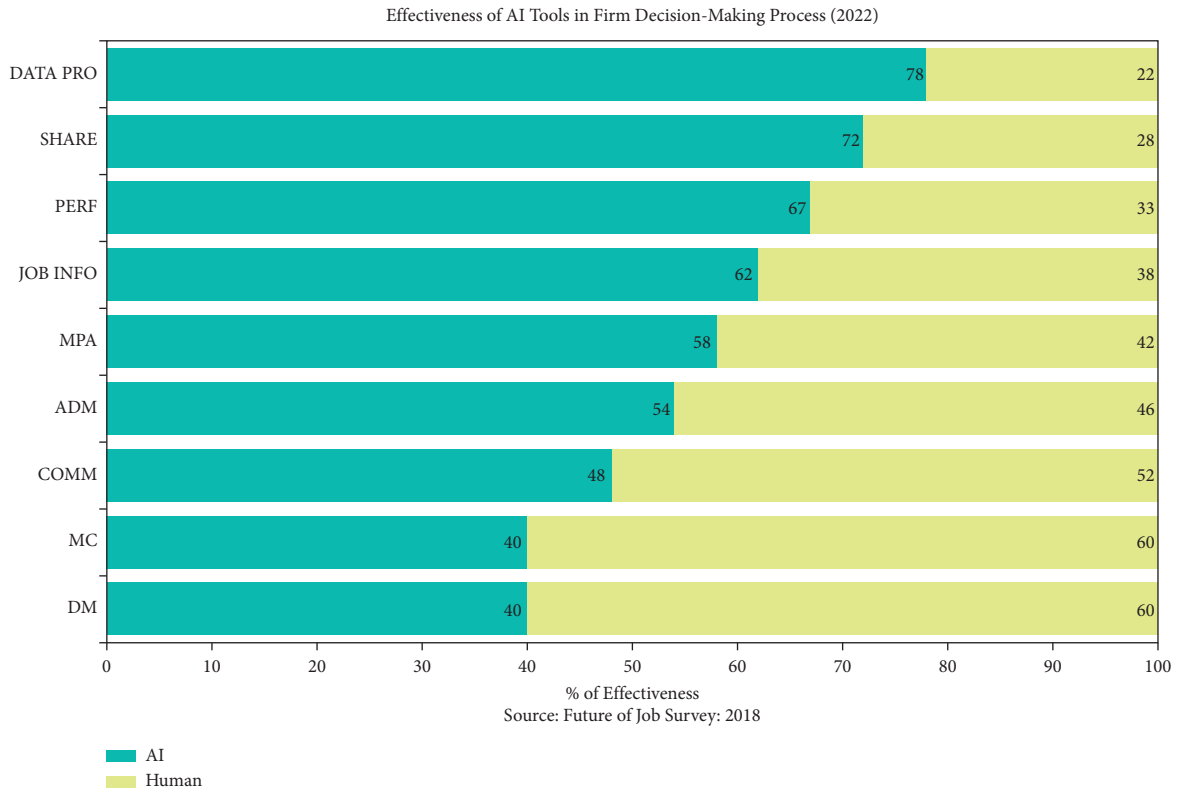
FIGURE 11: Effectiveness of AI tools in firm decision-making process (2022).

TABLE 5: Effectiveness of AI tools in firm decision-making process.

Factors	Human proportionate hours		AI proportionate hours	
	2018	2022	2018	2022
Reasoning and decision-making	80	60	20	40
Managing and coordinating	82	60	18	40
Communication	78	52	22	48
Administration	68	46	32	54
Mental and physical activities	66	42	34	58
Identifying job-related information	61	38	39	62
Complex activities performance	58	33	42	67
Job-related data sharing	46	28	54	72
Data processing	30	22	70	78

confirm our findings using information from other significant social network platforms in future research. Thirdly, this study was an exploratory examination that produced high-quality findings. It is therefore necessary to conduct more quantitative research to quantitatively test the variables found in the current study.

Although it has several limitations, this exploratory effort seeks to scratch the surface of whether and how AI may be used in the development of marketing strategies. First, the study has solely examined the purposeful process of strategy design. Only some strategies, or those that are proactively developed by patterns of strategic decisions, are purposeful, according to Mintzberg (1978). By virtue of initially unconscious patterns of strategic decision-making, further strategies emerge. Furthermore, Hart (1992) suggested that organizational actor autonomy and management intentionality (the extent to which marketing strategy is intentionally generated) be used to establish a practically applicable strategy formulation process (the degree of involvement of organizational actors in the strategy creation process).

The research is limited by the number of studies included in the sample, the databases used to conduct the systematic review of the literature, and the researchers' in-depth analysis of the chosen studies. Additionally, it can be argued that the MAC process's visual outcome interpretation is a restriction. Last but not least, since the technology corresponding to the growth of AI-based CRMs in B2B digital marketing is constantly changing, future studies should keep going in the directions of research that have been suggested so far to continue building strong foundations for the use of AI-based CRMs in B2B digital marketing.

Although the literature study demonstrates how AI is used in relation to business goals and strategies, the findings show that the academy has not given much attention to this confluence and that there are still many unanswered concerns and difficulties. The new generation of AI (or cognitive technologies), which incorporate cognition-related technologies and largely rely on or do away with humans for labor-intensive tasks, was only discussed in specific application-related contexts without any emphasis on the tool-related aspects of AI or for introducing conceptually managerial implications. Based on the findings of the literature assessment, difficulties and potential areas for further research were identified.

Thus, in terms of the sources of value creation with the application of AI and its connection with business strategy, knowledge gaps and research propositions were developed.

6. Conclusion

Managers and organization experts have long been concerned about how to design organizational decision-making frameworks. Algorithmic choice creators are starting to be more and more essential organizational players together with the fast development of AI. The furnished paradigm sets the groundwork for understanding how you can incorporate computational and human choice producing to take full advantage of the advantages of every tactic and talk to greater conclusions. This may improve businesses, though it should be completed with extreme caution. The study discovered that the conventional perspective of devices as tools is contradictory to AI. To make usage of the technologies efficiently, man decision-makers should shift their functions to be interpreters and translators on the results, in the place of merely managing the device inside the delivery associated with a fixed procedure. This means an increased shift and responsibility inabilities. As a result, exactly how people view AI is going to be substantially affected by the way they see themselves, while the context, as well as goal, is going to be seriously affected by AI. Based on present scientific studies, nonetheless, the presumption that computer systems, as well as people, are the same is neither realistic nor honest.

Our paper starts up brand new studies' concerns: Just how can we determine exactly how effectively an AI constitutes a choice? Just how does algorithmic reasoning influence managing accountability? Just how does our framework influence organizational results? Exactly how crucial would be the decision-making context within figuring out the suitability of alternate tactics? What will function as the effect on accountability and trust for a realm in which AI is starting to be more and more vital only in decision-making? By dealing with these along with other issues, supervisors, as well as organizational scholars as well, are going to be much better ready for an unsure long term.

In corporate environments, AI technologies have taken center stage. This enthusiasm is in part because of the potential, which has been shown in reports from top consultancies, technological companies, and white papers. In turn, the business competitive environment is tied to high

expectations. Research on the strategic application of AI to gain competitive advantages is thus becoming more and more in demand. This research also provides a theoretical foundation that identifies these areas for future research and aids in comprehending how company strategy and the deployment of AI technologies interact. This interaction was described in the framework in terms of the sources used to create financial returns. The suggested framework can serve as a guide for management and organizational practices with regard to managerial implications, necessitating new models for managerial decision-making and transforming organizational culture. Additionally, by showing how AI and business strategy are related, executives will be better able to implement these new technologies while being more aware of the opportunities, difficulties, and potential advantages that AI may present for their companies. This work has several limitations even though it makes contributions, such as the state of the field today and potential directions for future research on the subject at hand. Without mentioning other business strategy dimensions like operational strategy and financial strategy, the research was conducted using terminology linked to business strategy or IT strategy. Future research might broaden the search criteria and take these viewpoints into account. Furthermore, the dimensions shown in the conceptual model may serve as a catalyst for further study going in a certain direction. Future field studies that can investigate these claims should ideally be vital to the issues and hypotheses raised by this study.

Data Availability

No data were used to support this study.

Conflicts of Interest

The authors declare that they have no conflicts of interest.

References

[1] P. Akhtar, J. G. Frynas, K. Mellahi, and S. Ullah, "Big data-savvy teams' skills, big data-driven actions and business performance," *British Journal of Management*, vol. 30, no. 2, pp. 252–271, 2019.

[2] K. Balog, "The concept and competitiveness of agile organization in the fourth industrial revolution's drift," *Strategic Management*, vol. 25, no. 3, pp. 14–27, 2020.

[3] Y. Duan, J. S. Edwards, and Y. K. Dwivedi, "Artificial intelligence for decision making in the era of Big Data–evolution, challenges and research agenda," *International Journal of Information Management*, vol. 48, pp. 63–71, 2019.

[4] U. Lichtenthaler, "Building blocks of successful digital transformation: complementing technology and market issues," *International Journal of Innovation and Technology Management*, vol. 17, no. 01, p. 2050004, 2020.

[5] K. Božič and V. Dimovski, "Business intelligence and analytics use, innovation ambidexterity, and firm performance: a dynamic capabilities perspective," *The Journal of Strategic Information Systems*, vol. 28, no. 4, p. 101578, 2019.

[6] X. Chen and K. Siau, "Business analytics/business intelligence and IT infrastructure: impact on organizational agility," *Journal of Organizational and End User Computing*, vol. 32, no. 4, pp. 138–161, 2020.

[7] J. Sujata, D. Aniket, and M. Mahasingh, "Artificial intelligence tools for enhancing customer experience," *International Journal of Recent Technology and Engineering*, vol. 2, pp. 700–706, 2019.

[8] E. Carbone, K. Georgalos, and G. Infante, "Individual vs. group decision-making: an experiment on dynamic choice under risk and ambiguity," *Theory and Decision*, vol. 87, no. 1, pp. 87–122, 2019.

[9] D. M. Rousseau, "Making evidence-based organizational decisions in an uncertain world," *Organizational Dynamics*, vol. 49, no. 1, p. 100756, 2020.

[10] J. R. Saura, D. Palacios-Marqués, and D. Ribeiro-Soriano, "Exploring the boundaries of open innovation: evidence from social media mining," *Technovation*, vol. 4, p. 102447, 2022 ISSN 0166-4972.

[11] A. F. Borges, F. J. Laurindo, M. M. Spínola, R. F. Gonçalves, and C. A. Mattos, "The strategic use of artificial intelligence in the digital era: systematic literature review and future research directions," *International Journal of Information Management*, vol. 57, p. 102225, 2021 ISSN 0268-4012.

[12] T. Eriksson, A. Bigi, and M. Bonera, "Think with me, or think for me? On the future role of artificial intelligence in marketing strategy formulation," *The TQM Journal*, vol. 32, no. 4, pp. 795–814, 2020.

[13] J. R. Saura, D. Ribeiro-Soriano, and D. Palacios-Marqués, "Setting B2B digital marketing in artificial intelligence-based CRMs: a review and directions for future research," *Industrial Marketing Management*, vol. 98, no. October 2021, pp. 161–178, 2021a.

[14] J. Yin, S. Wei, X. Chen, and J. Wei, "Does it pay to align a firm's competitive strategy with its industry IT strategic role," *Information Management*, vol. 57, no. 8, p. 103391, 2020.

[15] A. F. Borges, F. J. Laurindo, M. M. Spínola, R. F. Gonçalves, and C. A. Mattos, "The strategic use of artificial intelligence in the digital era: systematic literature review and future research directions," *International Journal of Information Management*, vol. 57, p. 102225. in press, 2020.

[16] S. Caner and F. Bhatti, "A conceptual framework on defining businesses strategy for artificial intelligence," *Contemporary Management Research*, vol. 16, no. 3, pp. 175–206, 2020.

[17] A. Trunk, H. Birkel, and E. Hartmann, "On the current state of combining human and artificial intelligence for strategic organizational decision making," *Bus. Res*, vol. 13, pp. 875–919. in press, 2020.

[18] N. J. Nilsson, *The Quest for Artificial Intelligence: A History of Ideas and Achievements*, Cambridge University Press, Cambridge, 2010.

WILEY | Hindawi

Research Article

A Comprehensive Skills Analysis of Novice Software Developers Working in the Professional Software Development Industry

Imdad Ahmad Mian [ID],[1] **Ijaz-ul-Haq** [ID],[2] **Aamir Anwar** [ID],[3] **Roobaea Alroobaea** [ID],[4] **Syed Sajid Ullah** [ID],[5] **Fahad Almansour,**[6] **and Fazlullah Umar** [ID][7]

[1]*Department of Science, SZABIST University Islamabad, Islamabad, Pakistan*
[2]*Faculty of Education, Psychology and Social Work, University of Lleida, Lleida, Spain*
[3]*School of Computing and Engineering, University of West London, London, UK*
[4]*Department of Computer Science, College of Computers and Information Technology, Taif University, P.O. Box 11099, Taif 21944, Saudi Arabia*
[5]*Department of Information and Communication Technology, University of Agder (UiA), Grimstad N-4898, Norway*
[6]*Department of Computer Science, College of Sciences and Arts in Rass, Qassim University, Buraydah 51452, Saudi Arabia*
[7]*Department of Information Technology, Khana-e-Noor University, Pol-e-Mahmood Khan, Shashdarak 1001, Kabul, Afghanistan*

Correspondence should be addressed to Syed Sajid Ullah; sajidullah718@yahoo.com and Fazlullah Umar; fazlullahumir@gmail.com

Measuring and evaluating a learner's learning ability is always the focus of every person whose aim is to develop strategies and plans for their learners to improve the learning process. For example, classroom assessments, self-assessment using computer systems such as Intelligent Tutoring Systems (ITS), and other approaches are available. Assessment of metacognition is one of these techniques. Having the ability to evaluate and monitor one's learning is known as metacognition. An individual can then propose adjustments to their learning process based on this assessment. By monitoring, improving, and planning their activities, learners who can manage their cognitive skills are better able to manage their knowledge about a particular subject. It is common knowledge that students' meta-cognitive and self-assessment skills and abilities have been extensively studied, but no research has been carried out on the mistakes that novice developers make because they do not use their self-assessment abilities enough. This study aims to assess the metacognitive skills and abilities of novice software developers working in the industry and to describe the consequences of awareness of metacognition on their performance. In the proposed study, we experimented with novice software developers and collected data using Devskiller and a self-assessment log to analyze their use of self-regulation skills. The proposed study showed that when developers are asked to reflect upon their work, they become more informed about their habitual mistakes, and using a self-assessment log helps them highlight their repetitive mistakes and experiences which allows them to improve their performance on future tasks.

1. Introduction

The development of software is a logically complex task. The main four components of software development and its value ability are (i) the process applied, (ii) the tool used in the development, (iii) stakeholders, and (iv) timeline and budget [1]. Producing quality software is the key component to the success of any software product. The implementation of the best development process, quality characteristics, and sophisticated technology have immense effects on the quality of the software [2].

Software quality can be affected by two main components: (a) software process quality and (b) software product quality. Product quality is dependent on process quality [2]. The process quality has received more attention from the research community [3]. Whereas the implementation phase

of the development process has received less attention, particularly from a behavioral perspective [4, 5]. The implementation phase consists of coding, testing, installing, and supporting the system [6]. As mature tools are available for coding, testing, installing, and supporting (troubleshooting) the system, along with these tools, the programmer's ability and skills have additional importance and effect on the software quality.

The programmer's ability and skills can be commonly viewed as the experience he/she has, different certifications, products developed (portfolio), and communication skills of the individual person [7]. These are the common methods that are generally applied to check the talent and capability of a programmer and have positive measures [4]. However, these factors do not show the individual thinking ability or self-judgment of the programmer during development. To achieve this goal, it is important to measure individual metacognitive skills such as self-exploration, self-assessment, understanding from example (example-based learning) [8], and most importantly learning from their mistakes. These measures can have diverse effects on individual performance and therefore require an in-depth analysis to highlight their importance and influence on young software programmers.

Since metacognitive skills are used subconsciously, many people are either unaware of this phenomenon or unable to manage them properly. Research shows that people who use their self-assessment skills are more progressive than those who do not use their self-assessment skills. Normally, people ignore these types of learning skills in many learning environments. A programming job is a very mentally challenging job, where a programmer's intellectual abilities, knowledge, and cognitive and metacognitive skills are used aggressively. Different types of studies have been carried out to assess the metacognition skills of different learners in different academic domains. However, minimal work has focused on the industry and no such work has been proposed for young professionals working in the software industry.

Our research objective is to analyze the self-assessment skills of novice developers, which affect their development work and to evaluate their performance on awareness of using self-assessment. The research will focus on

(1) Analysis of metacognitive abilities and their usage by novice software developers.

(2) Correlation of different types of novice developer groups and their performance on the basis of their improvement/diminishment.

To resolve these issues, the following research question is to be addressed:

(i) What role can self-assessment play in the lives of novice software developers in minimizing repetitive mistakes?

To answer this main question, we will ask further (sub) research questions as follows:

(i) What are self-assessment skills?

(ii) How self-assessments skills help people perform better?

(iii) How can self-assessment skills help novice software developers in the field of programming?

(iv) What is the effect of self-assessment on novice developers' work?

(v) What is the difference between developers who use self-assessment and those who do not?

(vi) What kinds of mistakes a novice developer makes without analyzing their work?

2. Related Work

As like metadata can be defined as data about data, similarly metacognition can be defined as cognition about cognition [2]. Metacognitive learning involves specific knowledge of knowing that what are the different aspects of individual actions and what are the relations between these aspects that affect the learning of that individual [9]. Research on metacognition found that by applying different methods and awareness of metacognition, the learner's learning ability can improve significantly. Özsoy and Ataman [10] argue that metacognition practices are very important for successful learning strategies for teacher training, students' learning, and content development [11]. Özsoy and Ataman [10] conducted a study on students with mathematical disabilities and revealed the importance of metacognition in adulthood. He concluded that some students overestimated and some underestimated their mathematics results. The study on metacognition presents two different terms of mistake, which affect the learning process, made by the learner during learning: (1) Underuse: which means not asking for help when the subjects need help and (ii) Overuse: the learner asks for help repeatedly while not using his own mind to think about some problem [12].

2.1. The Social Cognitive Theory (SCT). In the paper [13], the authors relate the different factors of person metacognition as personal factors, behaviour, and environmental influence. The author [13] relates these factors and concludes that there is a relation between these components which affect the metacognition of students. These factors described in Figure 1 describe the social cognitive theory (SCT). The SCT describe that:

(i) The interaction between the person and their behaviour is influenced by their thoughts and actions [14].

(ii) The interaction between the person and environment involves beliefs and cognitive competencies developed and modified by social influences.

The interaction between the environment and their behaviours involves the person's behaviour determining their environment, which in turn affects their behaviour [15].

This SCT has got reputation because it explains individual acts specifically point (i) above. More precisely, the
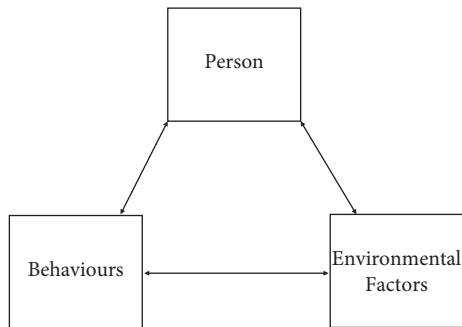
FIGURE 1: Social cognitive theory (SCT).

SCT argue that the person's cognition like self-assessment can guide the behaviour without the actual skills an individual has [4]. For example, the authors have defined a social cognitive conceptual framework using SCT, to simplify theory integration in the field of presenteeism research [16].

Metacognitive knowledge has been described as the knowledge and a deeper understanding of the cognitive process and product [6]. For example, a programmer knows that they must test the function that has a specific task but does not need to test a simply declared variable. Metacognitive knowledge has three important components. Declarative metacognitive knowledge was found to be "what is known in a propositional manner" [17] or the assertion about the world and the knowledge of the influencing factors of human thinking. Procedural metacognitive knowledge can be described as the awareness of processes of thinking [17] or the knowledge of the methods for achieving goals and the knowledge of how skills work and how they are to be applied. Conditional or strategic metacognitive knowledge is "the awareness of the conditions that influence learning such as why strategies are effective, when they should be applied, and when they are appropriate" [17].

2.2. Metacognitive Monitoring.
Metacognitive monitoring means the ability to successfully judge one's own cognitive process [7]. According to the author in [9], "metacognitive monitoring is the conscious monitoring, control, and active regulation of the self-cognitive activities in the whole process of cognitive activity." The author argues that metacognitive monitoring is self-monitoring for which the individual must have to require some knowledge and experience of metacognition. The real taste of metacognition can be felt in metacognitive monitoring. Metacognitive monitoring affects the regulation of study, which in turn affects overall learning [18].

2.3. Metacognitive Control.
Metacognitive control can be defined as the ability to regulate cognitive activity. Metacognitive control is used to control the memory process and to use strategy to improve comprehension. By using a learning strategy, the learner gains knowledge in the area of concentration. The learner will learn to ask themselves whether they are looking for directly stated, implied, or need to connect information from their own backgrounds with

the material [17]. Recently, the author in [19] found that due to cognitive control training, the key neural region has been improved in terms of active and proactive activities. To understand the conceptual mapping of different learning strategies, we have represented these different learning strategies in Figure 2.

2.4. Self-Assessment.
Self-assessment is defined by the author in [20] as "Self-assessment is a process of formative assessment during which students reflect on and evaluate the quality of their work and their learning, judge the degree to which they reflect explicitly stated goals or criteria, identify strengths and weaknesses in their work, and revise accordingly" (2007, p.160). Investigating the present abilities of oneself is the basic step to learning. Self-assessment builds a way to check out the progress of oneself, after that, one can understand the further improvement in the learning process. It can motivate the learner about his/her responsibility and work. It makes the learner possible to focus on improvement by awarding him/her about their cognition abilities.

Self-assessment abilities commonly can repair what students do not see as superior to anything educators can, in light of the fact that instructors for the most part cannot analyze as absolutely the student comprehension problem [21]. Mostly, learners do not assess themselves until they are guided or made aware to do so [22]. Hence, it is important to assess those individuals so that they can use their self-assessment abilities to solve a problem in any situation.

The authors in [23] argue that "the way in which self-assessment is implemented is critical to its acceptance by students". Different techniques have been used to assess the self-assessment of different types of learners. For example, the authors in [21] use ACE in ITS to assess the student self-exploration on rum time, Behlau et al. [24] used questionnaires to find the impact of voice problems on individual life, Binali et al. [4] use PSE to assess the student of programming, Boud [23] in their study used State University data to measure self-assessment ads Questionnaire Tutors and to assess the self-assessment of learners, also the Self-Assessment Manikin [3, 25] used ELM-PE to measure the self-assessment of a student in the ITS system [8], professional judgment and expertise oriented framework have been developed by the authors in [26] by postulating on the aspirant/developing coach's capacity for and development of metacognition within the reflective process, and a lot more.

2.5. Aspects of Self-Assessment.
To promote the metacognition aspects of novice developers working in the software industry, we focused on the three well-known aspects of self-assessment skills [10].

2.5.1. Planning.
Learners plan better and learn when their attention focuses on learning objectives [27]. A clear discussion of the learning goals starts the metacognitive process by prioritizing the significance of thinking about the learning process over the content. The authors [28] in their study stated that goal setting and strategic planning
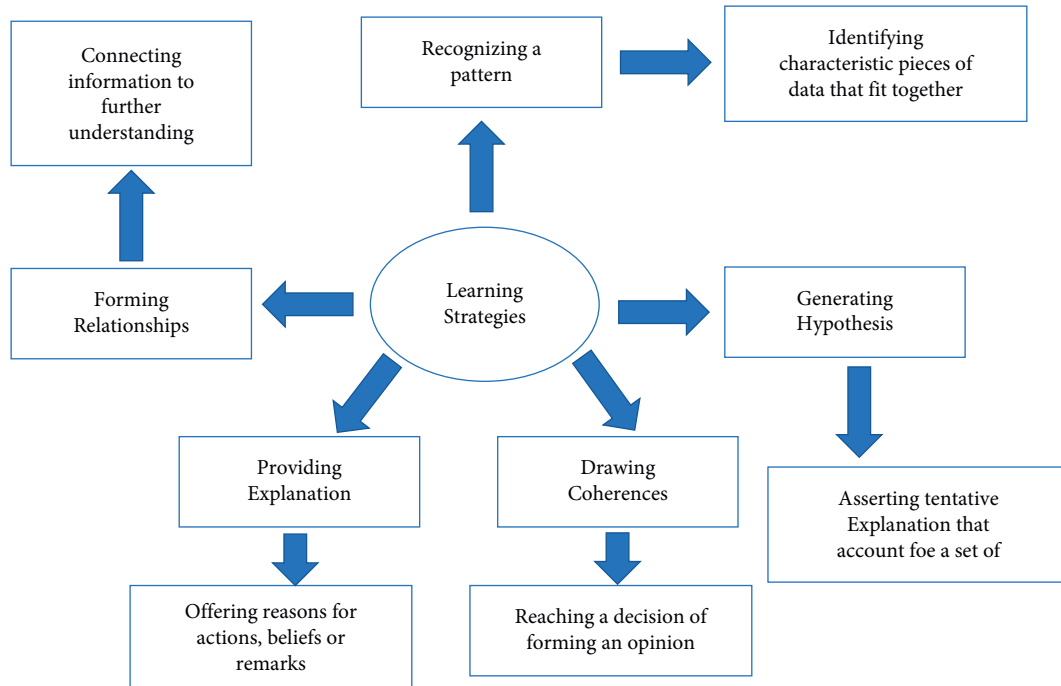
FIGURE 2: Learning strategies.

positively anticipate objective fulfilment in Massive Open Online Course [28]. It is important for every learner to review what is already known about the topic or task on which he/she is working [29]. Also, it is important for the learner to assess the time it will take to complete this task and also to have a clear idea of the resources needed for the successful completion of that task to help him/her think about the process of learning.

While solving a problem, we can divide the type of learner into different categories:

(i) Learner with initial planning:

(ii) Learner with continuous planning or partial planning.

(iii) Learner with no planning

2.5.2. Monitoring. Every learner benefits from monitoring their understanding during learning activities [2]. Grainger et al. [30] also originated that impaired metacognitive monitoring in developmental disorders in children has important educational implications. The importance of the learning process can be reminded by monitoring learning behaviors throughout the learning process. This can be done by chunking, connecting, elaborating, and organizing the materials in such a way that the learner can recognize patterns and associations [31]. In the monitoring process during the work/problem solving, it is easy to figure out the errors and correct them in the thinking process.

2.5.3. Evaluating. By evaluating self-assessment skills, the learner becomes more aware of the self-assessment process and its direct impact on learning [32]. By evaluating

students, the authors describe and allocate value or merit to the quality of their knowledge outcomes [33]. Different types of evaluation methods such as a checklist, rating scales, and questionnaires can help the learners evaluate their thinking during problem-solving. The study conducted by Sierra and Frodden [34] concluded that those learners who evaluate their learning process can decide whether they want to continue or need to change the learning process.

Students with self-evaluation judgment ability have high-performance feedback from those who do not evaluate their learning process [35].

2.6. Implicit Thinking. Implicit thinking refers to unconscious effects such as knowledge, perception, or memory that impact a person's behaviour even while the individual is unaware of those influences [36]. There are times when we act on something and then consider how we might handle it in a different setting or approach. That is implicit cognition at work; the mind will then proceed based on ethical and comparable scenarios when engaging with a certain notion. Implicit cognition and its automatic cognitive process allow a person to make a decision on the occasion. It is frequently characterized as an automatic process in which actions are easily performed without conscious awareness.

3. Analysis of Self-Assessment Skills

This study followed a qualitative approach where we used observation-based research to observe five novice developers at coding tasks. These developers were also required to fill in self-assessment logs daily for five days.

The design of the research is as follows:

(i) Define the target participants and select the sampling process.

(ii) Task preparation

(iii) Tools used

(iv) Prepare experiment environment

(v) Procedure

(vi) Develop and design self-assessment log

(vii) Data collection

3.1. Defining the Target Participants and Select the Sampling Process. The populations of our research were novice software developers working in the professional software development industry. The criterion was set to choose those professional developers whose work experience is less than two years. As it was not feasible to analyze the whole population, we selected a convenience sample of five novice developers for experiment and assessment. All these developers were working on Android game development using C# as a development language at a local software firm.

3.2. Task Preparation. We assigned a set of tasks to each developer for five days. The experiment included five tasks, one task for each developer daily, divided into three categories:

(i) Simple task (ST)

(ii) Intermediate task (IT)

(iii) Complex task (CT)

3.3. Tools Used. We selected the Devskiller for observation assessment. Devskiller is a tool that records the time and actions performed by the programmer while performing their coding tasks. Devskiller has been used in other studies for the same purpose [37]. It provides a 14-day trial which was enough for us as our experiment was only five days. On each day, we assigned a specific task in the Devskiller user dashboard and sent invitations to each developer through e-mail. We used Devskiller to investigate different attributes of the developers. These attributes will be discussed in the following section.

3.4. Preparation of Experiment Environment. The five developers were provided seating on separate tables in the same room. As the surrounding environment is also an important factor in self-assessment, the environment was set to be more comfortable and conducive. They were briefed about the purpose of the experiment, the 5-day activities, the plan, and the ultimate goal of the research.

3.5. Procedure. The five tasks that the developers had to complete were divided into three categories. For the first and second days of the experiment, every developer was given a simple task (ST) to complete. The reason to assign simple tasks on days 1 and 2 was to help the programmer revise the

basics of coding. On the third and fourth days, some intermediate-level complex task was assigned. On the last day of the experiment, a complex task was assigned to the developers. Table 1 shows the specific task against each day. Aside from the practical task, the developers also filled out the self-assessment log at the end of the daily task.

3.6. Develop and Design Self-Assessment Log. To complement our findings from the data collected through Devskiller, we used a self-assessment log that the developers had to fill out at the end of the daily task. Figure 3 provides an overview of the questionnaire. The log helped us to make our observations reliable. Both, Devskiller log data and data collected through self-assessment log were used to answer our research questions, which are given below:

(i) What role can self-assessment play in the lives of novice software developers in minimizing repetitive mistakes?

(ii) How can self-assessment skills help novice software developers in the field of programming?

(iii) What is the effect of self-assessment on novice developers' work?

(iv) What is the difference between developers who use self-assessment and those who do not?

(v) What kinds of mistakes a novice developer makes without analyzing their work?

3.7. Data Collection. To analyze a developer in terms of self-assessment, data could be obtained in two ways: direct source or indirect source. Directly sourced data comes from the developers' first-hand, which means that the data are collected through the log file of Devskiller and a self-assessment log from developers. Indirect sources are the managerial staff of the software house, where data can be collected through interviews with the team managers and team leads. We used the direct source to collect the data. All the data were collected through the log file of Devskiller and the self-assessment log in Figure 3.

The process of self-assessment includes three main steps, i.e., planning, monitoring, and evaluation. We have considered these three parameters for the self-assessment of developers (see section 3.2.8). In the planning phase, the two other parameters, time taken to make a plan and construct used for planning, were assessed. In the monitoring phase, the number of repetitive mistakes and the type of repetitive mistakes were analyzed and measured, and in the evaluation phase, the technique used by the developer to evaluate his/ her solution was analyzed. At the end of the task, the developers were asked to fill in the self-assessment log. The experiment continued for five days.

4. Experiment Evaluation

4.1. Calculating the Attribute of Individual Developers. As discussed, we selected the planning, monitoring, and evaluation phases of self-assessment. A total of seven attributes

TABLE 1: Developers' daily tasks.

Day	Task
1	Write a function that returns the largest element in a list.
2	Write a function that computes the list of the first 100 Fibonacci numbers.
3	Handle the switch statement for the buttons in the first scene for a game.
4	Show the complete panel in the game when an object reaches a specific point.
5	Lock and unlock the levels of the game on the basis of previous level conditions.

Developer Survey Questionnaire	
S.No	Questions
1	What was your task?
Answer	
2	How did you planned your task?
Answer	
3	Did you used internet for help? If yes, what did you used it for?
Answer	
4	While coding, did you make mistakes? If yes, did you solved them?
Answer	
5	Did you completed your task?
Answer	
6	If you completed your task? How did you evaluated you rsolution?
Answer	

FIGURE 3: Self-assessment log.

for these phases were used to assess the self-assessment skills of individual developers. The data about these attributes were collected from the log file of Devskiller and the self-assessment log filled in by the developers on a daily basis. The different attributes that were selected for each phase are shown in Figure 4.

The data about the planning phase were collected from two attributes.

(i) The time taken by the developer to plan for the task

(ii) The construct used by the developer for planning. This included any pen and paper planning and workflow designs.

The number of repetitive mistakes done by the developer was gathered from the Devskiller log. The log data stores information about all the actions performed by the developer including typos and edits.

The evaluation phase was analyzed by the strategy used by the developer to evaluate his solution. We categorized these strategies into three types.

(i) Run code directly; the developer did not spend time in evaluating his code before trying to run it.

(ii) Dry run: the developer did a dry run of their code to ensure it would work as required.

(iii) Used test cases: the developer generated test cases to test his solution for completeness.

4.2. Assessing Developers Based on Attributes. The self-assessment log was designed to collect information regarding the knowledge and ability of self-assessment of developers in terms of planning, monitoring, and evaluation. Table 2 shows an overview of the data collected from the self-assessment log.
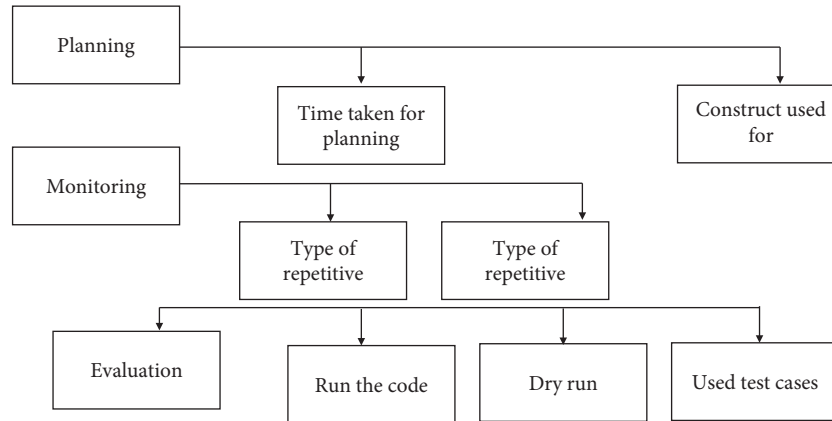
FIGURE 4: Selected attributes for self-assessment phases.

TABLE 2: Developer planning, monitoring, and evaluation data from the assessment log.

| Developer | Days | Planning | | Evaluation | |
		Planned or not	Construct used for planning	Evaluate solution or not	The method used for evaluation
	1	No	Search Internet	Not	Run
	2	No	Search Internet	Not	Run
1	3	No	Search Internet	Not	Run
	4	Yes	Implicit thinking	Yes	Dry run
	5	Yes	Implicit thinking	Yes	Dry run

TABLE 3: Developer planning, monitoring, and evaluation data from the Devskiller log.

Developer	Day	Planning Time taken for planning	Monitoring Number of repetitive mistakes	Evaluation Task completed?
	1	0	15	No
	2	0	14	No
1	3	0	13	No
	4	1 minute	12	Yes
	5	2 minutes	8	Yes

TABLE 4: Developer planning, monitoring, and evaluation data.

| Developer | Days | Planning | | | Monitoring | Evaluation | | |
		Plan made for the task	Time taken for planning	Construct used for planning	Number of repetitive mistakes	Solution evaluated before running	The method used for evaluation	Task completed
	1	No	0	Search Internet	15	No	Run	No
	2	No	0	Search Internet	14	No	Run	No
	3	No	0	Search Internet	13	No	Run	No
1	4	Yes	1 minute	Implicit thinking	12	Yes	Dry run	Yes
	5	Yes	2 minutes	Implicit thinking	8	Yes	Dry run	Yes

Along with the data collected from the self-assessment log, we also collected data from the Devskiller log file. Table 3 shows an overview of the data collected from the Devskiller log file.

Collectively, the data gathered from the assessment log and Devskiller log file is presented in Table 4.

Table 4 shows the use of self-assessment skills of developer 1 for five days from three perspectives. The first subcolumn of the planning phase tells us that if the developer made any plan to solve the task assigned. If the developer made any plan, the value will be YES, and if they did not make any plan the value will be NO. The next column shows the time taken by the developer for planning. If no plan was made, then the value will be 0. The next column of the planning phase tells us about the strategy used by the developer for making their plan. The specific value was

TABLE 5: All developers planning, monitoring, and evaluation data.

| Dev | Days | Planning | | | Monitoring | Evaluation | |
		Plan made for the task	Time taken for planning	Construct used for planning	Number of repetitive mistakes	Solution evaluated before running	The method used for evaluation
	1	0	0	Search Internet	10	No	Run
	2	1	2 minutes	Implicit thinking	5	Yes	Dry run
2	3	1	3 minutes	Mind mapping	3	Yes	Dry run
	4	1	5 minutes	Mind mapping	3	Yes	Used test cases
	5	1	1 minute	Mind mapping	2	Yes	Used test cases
	1	No	0	Search Internet	15	Not	Run
	2	No	0	Search Internet	14	Not	Run
3	3	Yes	2 minutes	Implicit thinking	8	Yes	Dry run
	4	Yes	3 minutes	Implicit thinking	5	Yes	Dry run
	5	Yes	2 minutes	Mind mapping	2	Yes	Used test cases
	1	No	0	Search Internet	15	Not	Run
	2	Yes	1 minute	Implicit thinking	8	Not	Run
4	3	Yes	2 minutes	Implicit thinking	7	Yes	Dry run
	4	Yes	3 minutes	Thinking	3	Yes	Dry run
	5	Yes	2 minutes	Mind mapping	2	Yes	Used test cases
	1	Yes	2 minutes	Implicit thinking	5	Not	Dry run
	2	Yes	2 minutes	Implicit thinking	4	Not	Dry run
5	3	Yes	3 minutes	Implicit thinking	2	Yes	Dry run
	4	Yes	2 minutes	Mind mapping	2	Yes	Used test cases
	5	Yes	4 minutes	Mind mapping	1	Yes	Used test cases

populated using the strategy used by the developer. The next column monitoring has one subcolumn "Number of repetitive mistakes." This column shows the number of repetitive mistakes made by the developer. The value of this parameter was retrieved from the Devskiller log file. For the evaluation phase, we checked whether the developer evaluated their code before trying to run it. If they did, the next column specifies the method used by the developer to evaluate his solution. The last column task completed or not shows the status of the task given to the developer on the corresponding day. All the collected data from five developers are presented in Table 5.

4.3. Effect of Self-Assessment on Task Completion.
From Table 5 and the self-assessment log, we generated Table 6 to show the effect of self-assessment on the task completion of the developers. For self-assessment, it is important that the individual uses his self-assessment abilities uniformly in all the important phases of assessment such as planning, monitoring, and evaluation. The table shows the values of self-assessment and status of task of Developer 1 for five days.

Table 6 shows a positive correlation between the use of self-assessment skills and task completion. The data for the rest of the developers are presented in Table 7.

From the data in Table 7, it is evident that there is always a positive correlation between the use of self-assessment and task completion status. However, there was an exception in the case of developer 3 where on the first day, he did not use any self-assessment ability but still completed the task. On further investigation, it was revealed that the developer had actually used an Internet source and copy-pasted the code that he had found online to complete his task. This does not

TABLE 6: Effect of self-assessment on task completion.

Days	Self-assessment	Task status
1	No	Not completed
2	No	Not completed
3	No	Not completed
4	Yes	Completed
5	Yes	Completed

TABLE 7: Effect of self-assessment on task completion.

Developer	Day	SA	Task status
	1	No	Not completed
	2	Yes	Completed
2	3	Yes	Completed
	4	Yes	Completed
	5	Yes	Completed
	1	No	Completed
	2	No	Not completed
3	3	Yes	Not completed
	4	Yes	Completed
	5	Yes	Completed
	1	No	Not completed
	2	No	Not completed
4	3	Yes	Completed
	4	Yes	Completed
	5	Yes	Completed
	1	Yes	Completed
	2	Yes	Completed
5	3	Yes	Completed
	4	Yes	Completed
	5	Yes	Completed

stand true for all situations in the professional industry since there are many situations for which readily available code is
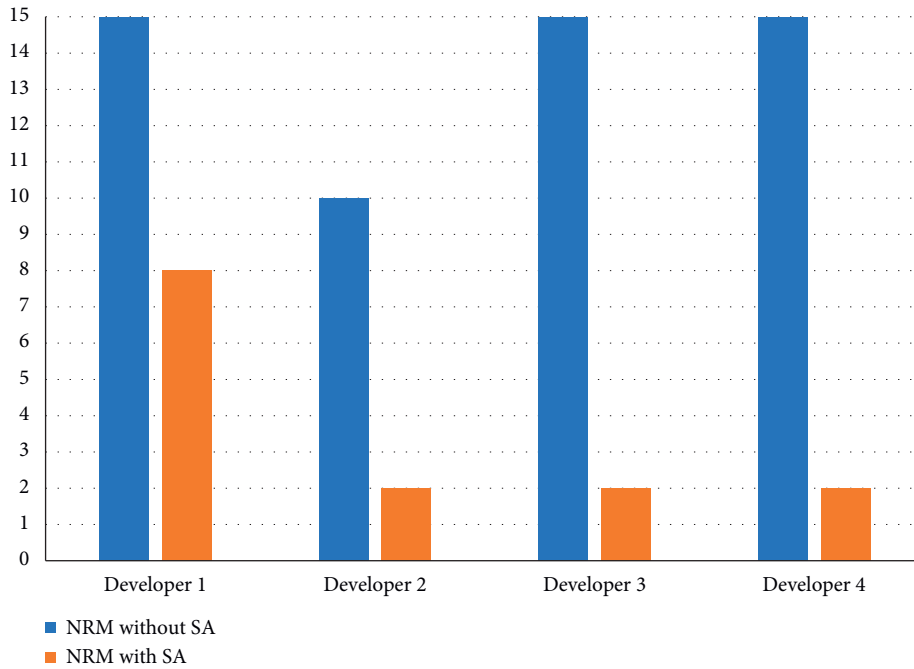
Figure 5: Comparison of NRM with SA status.
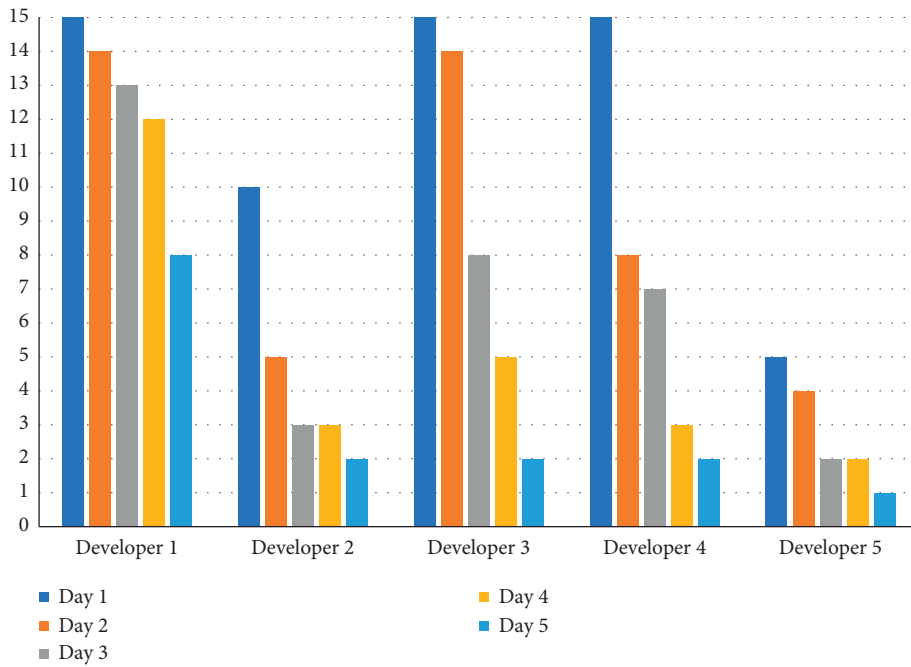
Figure 6: Number of repetitive mistakes of five developers.

not available and the developer needs to use their experience and skills to solve such problems.

4.4. Effect of Self-Assessment on Repetitive Mistakes. The overall effect of self-assessment on repetitive mistakes is reported in Figure5.

Figure 6 shows the effects of self-assessment on repetitive mistakes. From the results, it can be analyzed that the use of self-assessment skills is negatively correlated to the number of repetitive mistakes. Taking the case of developer 2, on the first day, he did not assess himself and made 10 repetitive mistakes. Since he was more informed on the second day, he was careful to assess himself and be vigilant about what was expected of him. As a result, the number of mistakes he made during the coding exercise decreased to 5. Developer 1's performance showed the least effect of using self-assessment skills on task performance. His number of mistakes

did not see a very big change; however, this number continued to decrease with every passing day, which was a positive sign. This result showed that while still not assessing himself thoroughly, there was still some improvement in his performance due to the awareness of self-assessment. This could also have been affected by the notion of the experiment and therefore would require further investigation which was not the scope of this study.

4.5. Types of Repetitive Mistakes. From the programming perspective, we analyzed only three types of mistakes which were frequent to occur. These were

  (i) Syntax errors

 (ii) Semantic errors

(iii) Logical errors

The complete data about these mistakes made by developers are shown in Table 8.

For the purpose of analysis, we compared the data on the number of repetitive mistakes (NRMs) for each developer from day 1 and day 5. This was done to investigate whether the experiment had any effect on the use of self-assessment skills by developers and whether this affected the frequency of repetitive mistakes. Table 9 shows the number of mistakes repeated by developers on both day 1 and day 5, respectively.

Figure 5 visualizes the data of Table 9 with categories: NRM (number of repetitive mistakes) without using SA (self-assessment) and NRM with SA.

5. Results and Findings

From the above-performed experiments, we tried to find answers to the following questions.

5.1. What Role Can Self-Assessment Play in the Lives of Novice Software Developers in Minimizing Repetitive Mistakes? The analysis of the results from the experiment conducted revealed a negative correlation between the use of self-assessment abilities and the number of repetitive mistakes. The results showed a clear diminishment in the number of mistakes made by the developers as the experiment progressed. One of the major factors influencing this trend was the awareness of the intent of the experiment which implicitly led the developers into engaging self-assessment activities. The results provide a clear insight that developers who used self-assessment made fewer repetitive mistakes compared to those who did not assess their work. It is also clear from the results that the awareness of self-assessment has a greater impact on the developer's aptitude.

5.2. What Kinds of Mistakes a Novice Developer Makes without Analyzing Their Work? There are three types of mistakes that every developer makes repetitively in everyday work. These mistakes along with their repetition times are presented in Table 9 and visualized in Figure 5. Syntactic mistakes have more frequency compared to other types of mistakes. Syntax mistakes are mostly related to the

TABLE 8: Number of repetitive mistakes of 5 developers.

Developer	Day	Syntax	Semantic	Logical
1	1	8	4	3
	2	7	5	2
	3	8	3	2
	4	9	2	1
	5	3	3	2
2	1	6	2	2
	2	3	1	1
	3	3	0	0
	4	2	0	1
	5	2	0	0
3	1	8	4	3
	2	9	3	2
	3	5	2	1
	4	4	1	0
	5	2	0	0
4	1	7	5	3
	2	4	2	2
	3	4	2	1
	4	3	0	0
	5	2	0	0
5	1	3	1	1
	2	3	1	0
	3	2	0	0
	4	2	0	0
	5	1	0	0

TABLE 9: Developers' NRMs on days 1 and 5.

Developer	NRMs without SA for day 1			NRMs with SA for day 5		
	Syntax	Semantic	Logical	Syntax	Semantic	Logical
1	8	4	3	3	3	2
2	6	2	2	2	0	0
3	8	4	3	2	0	0
4	7	5	3	2	0	0

knowledge of a certain language. Since all the developers involved in this experiment were fresh graduates, they were expected to have an acceptable level of knowledge of the language syntax. Most of the syntax errors that were seen were due to negligence and the fact that the developer did not monitor their own coding practice. The developers showed haste to finish the task and in doing so made plenty of syntax errors. Another important aspect that was discovered here was the dependence on the Integrated Development Environment (IDE) tool. Most of the developers were unsure about their mistakes because of their experience with IDEs. Since all current IDEs provide the IntelliSense feature which highlights syntax errors, most young developers depend upon such tools to keep track of syntax errors. This affects their performance as this allows them to be careless which is why they do not monitor their own coding while performing tasks.

5.3. What Is the Difference between Developers Who Use Self-Assessment and Those Who Did Not? The experiment was

conducted for five days, and during these five days, we saw a clear pattern emerge in terms of the developers who used their self-assessment skills and those who did not. The self-assessment log provided us with first-hand data about the understanding of self-assessment by each developer. It was noted that the developers who were not sure about their metacognitive abilities provided short answers and were reluctant to share more details about the procedures they followed. In contrast, the developers who were more confident about the use of self-assessment were also able to describe their processes more clearly. The performance evaluation also increased with the experiment since the developers started producing fewer errors in their code because they were continuously monitoring and evaluating their work.

6. Conclusion

The purpose of this research was to evaluate novice professional software developers in terms of planning, monitoring, and evaluation to assess their self-assessment skills to improve their work by minimizing repetitive mistakes they make every day. A thorough literature review, a planned experiment and an assessment log were used to identify the factors affecting the performance of developers and reasons for repetitive mistakes and verify the effectiveness of self-assessment on repetitive mistakes through an experiment.

There is a need for self-assessment awareness in the professional software development industry to enhance the self-assessment skills and work of novice software developers. By applying different methods to analyze the self-assessment skills of novice developers like collecting the log data from Devskiller, use of self-assessment log and static observation of developers during a planned experiment. We identified important factors of self-assessment that can influence the work of young developers. From the Devskiller log, self-assessment log data and results can be extracted that self-assessment has a positive correlation with the performance of novice software developers.

This research also addresses the type of mistakes that novice software developer makes repetitively during coding. From the Devskiller log file and static observation of the experiment, it is concluded that most of the developers make syntactic mistakes repetitively because they do not monitor themselves while coding. One of the main reasons for this was found to be their dependence on the latest IDEs which provide them with the facilities of syntax highlighting syntax errors [38–40].

Data Availability

The data used in this research can be obtained from the corresponding author.

Conflicts of Interest

The authors declare that they have no conflicts of interest.

Acknowledgments

References

[1] D. Emiliano de Souza, C. Favoretto, and M. M. Carvalho, "Knowledge management, absorptive and dynamic capacities and Project success: a review and framework," *Engineering Management Journal*, vol. 28, pp. 1–20, 2021.

[2] I. U. Haq, A. Anwar, I. Basharat, and K. Sultan, "Intelligent tutoring supported collaborative learning (itscl): a hybrid framework," *Learning*, vol. 11, no. 8, 2020.

[3] S. Aamir and Q. Rifat, "A study of metacognitive knowledge and metacognitive regulation among biology teachers at secondary level," *Journal of Science Education*, vol. 2, no. 2, 2021.

[4] T. Binali, C. C. Tsai, and H. Y. Chang, "University students' profiles of online learning and their relation to online metacognitive regulation and internet-specific epistemic justification," *Computers & Education*, vol. 175, Article ID 104315, 2021.

[5] A. Little, J. Tarbox, and K. Alzaabi, "Using acceptance and commitment training to enhance the effectiveness of behavioral skills training," *Journal of Contextual Behavioral Science*, vol. 16, pp. 9–16, 2020.

[6] M. Z. Khan, R. Naseem, A. Anwar et al., "A novel approach to automate complex software modularization using a fact extraction system," *Journal of Mathematics*, vol. 2022, 2022.

[7] S. Surakka, "What subjects and skills are important for software developers?" *Communications of the ACM*, vol. 50, no. 1, pp. 73–78, 2007.

[8] P. Brusilovsky, E. Schwarz, and G. Weber, "ELM-ART: an intelligent tutoring system on World Wide Web," in *Intelligent Tutoring Systems*Springer, Heidelberg, Germany, 1996.

[9] J. H. Flavell, "Metacognition and cognitive monitoring: a new area of cognitive-developmental inquiry," *American Psychologist*, vol. 34, no. 10, pp. 906–911, 1979.

[10] G. Özsoy and A. Ataman, "The effect of metacognitive strategy training on mathematical problem-solving achievement," *International Electronic Journal of Environmental Education*, vol. 1, no. 2, pp. 67–82, 2017.

[11] E. Railean, "Metacognition in higher education," in *Metacognition and Successful Learning Strategies in Higher Education*, pp. 1–21, IGI Global, Pennsylvania, PA, USA, 2017.

[12] I. Roll, V. Aleven, and Mcl, "Improving students' help-seeking skills using metacognitive feedback in an intelligent tutoring system," *Learning and Instruction*, vol. 21, no. 2, pp. 267–280, 2011.

[13] A. Bandura, *Self-Efficacy, Socialfoundations for Thought and Action: A SocialCognitive Theory*, Prentice-Hall, New Jersey, NJ, USA, 1986.

[14] J. E. Maddux, "Self-efficacy," *Interpersonal and Intrapersonal Expectancies*, pp. 55�60, Routledge, England, UK, 2016.

[15] R. Yılmaz and HafizeKeser, "The impact of interactive environment and metacognitive support on academic achievement and transactional distance in online learning," *Journal of Educational Computing Research*, vol. 55, no. 1, pp. 95–122, 2017.

[16] C. Cooper and L. Lu, "Presenteeism as a global phenomenon: unraveling the psychosocial mechanisms from the perspective of social cognitive theory," *Cross Cultural & Strategic Management*, vol. 23, no. 2, pp. 216–231, 2016.

[17] E. P. Ross and B. D. Roe, "The case for basic skills programs in higher education," Phi Delta Kappa, Eighth and Union, Box 789, Article ID 47402, Indiana, IN, USA, 1986.

[18] M. Baars and VD, "Effects of problem solving after worked example study on secondary school children's monitoring

accuracy," *Educational Psychology*, vol. 37, no. 7, pp. 810–834, 2017.

[19] K. D. Vohs and R. F. Baumeister, *Handbook of Self-Regulation: Research, Theory, and Applications*, Guilford Publications, New York, NY, USA, 2016.

[20] H. Andrade and Y. Du, "Student responses to criteria-referenced self-assessment," *Assessment & Evaluation in Higher Education*, vol. 32, no. 2, pp. 159–181, 2007.

[21] C. Conati and V. Kurt, "Toward computer-based support of meta-cognitive skills: a computational framework to coach self-explanation," *International Journal of Artificial Intelligence in Education*, vol. 11, pp. 389–415, 2000.

[22] J. B. Biggs, *Teaching for Quality Learning at university: What the Student Does*, McGraw-Hill Education, Chennai, Tamilnadu, 2011.

[23] D. Boud, *Enhancing Learning through Self-Assessment*, Routledge, England, UK, 2013.

[24] M. Behlau, G. Madazio, F. Moreti et al., "Efficiency and cutoff values of self-assessment instruments on the impact of a voice problem," *Journal of Voice:Official Journal of the Voice Foundation*, vol. 30, no. 4, pp. 506–e18, 2016.

[25] G. McBeath and S. Webb, "Cities, subjectivity and cyberspace," *Imagining Cities: Scripts, Signs, Memory*, pp. 249–260, Routledge, London, UK, 1997.

[26] L. Collins, H. J. Carson, and D. Collins, "Metacognition and professional judgment and decision making in coaching: importance, application and evaluation," *International Sport Coaching Journal*, vol. 3, no. 3, pp. 355–361, 2016.

[27] I. U. Haq, A. Anwar, I. U. Rehman et al., "Dynamic group formation with intelligent tutor collaborative learning: a novel approach for next generation collaboration," *IEEE Access*, vol. 9, Article ID 143406, 2021.

[28] R. F. Kizilcec and Pérez, "Self-regulated learning strategies predict learner behavior and goal attainment in Massive Open Online Courses," *Computers & Education*, vol. 104, pp. 18–33, 2017.

[29] J. Ehrlinger, A. L. Mitchum, and C. S. Dweck, "Understanding overconfidence: theories of intelligence, preferential attention, and distorted self-assessment," *Journal of Experimental Social Psychology*, vol. 63, pp. 94–100, 2016.

[30] C. Grainger, D. M. Williams, and S. E. Lind, "Metacognitive monitoring and control processes in children with autism spectrum disorder: diminished judgement of confidence accuracy," *Consciousness and Cognition*, vol. 42, pp. 65–74, 2016.

[31] A. Macb, A. Gumley, M. Schwannauer, A. Carcione, R. Fisher, and Mcl, "Metacognition, symptoms and premorbid functioning in a First Episode Psychosis sample," *Comprehensive Psychiatry*, vol. 55, no. 2, pp. 268–273, 2014.

[32] L. M. Blaschke, "Heutagogy and lifelong learning: a review of heutagogical practice and self-determined learning," *International Review of Research in Open and Distance Learning*, vol. 13, no. 1, pp. 56–71, 2012.

[33] E. Panadero, G. T. L. Brown, and J.-W. Strijbos, "The future of student self-assessment: a review of known unknowns and potential directions," *Educational Psychology Review*, vol. 28, no. 4, pp. 803–830, 2016.

[34] A. M. Sierra and C. Frodden, "Promoting student autonomy through self-assessment and learning strategies," *HOW Journal*, vol. 10, no. 1, pp. 133–166, 2017.

[35] S. Stolp and K. M. Zabrucky, "Contributions of metacognitive and self-regulated learning theories to investigations of calibration of comprehension," *International Electronic Journal of Environmental Education*, vol. 2, no. 1, pp. 7–31, 2017.

[36] S. Braun, S. Stegmann, A. S. Hernandez Bark, N. M. Junker, and R. van Dick, "Think manager-think male, think follower-think female: g," *Journal of Applied Social Psychology*, vol. 47, no. 7, pp. 377–388, 2017.

[37] 2015, https://devskiller.com/37-best-articles-from-2015-on-recruiting-programmers-and-tech-talents/.

[38] J. E. Jacobs and G. P. Scott, "Children's metacognition about reading: issues in definition, measurement, and instruction," *Educational Psychologist*, vol. 22, no. 3-4, pp. 255–278, 1987.

[39] D. Mukherjee and T. Singh, "Effects of metacognitive awareness, self-efficacy and goal orientations on programming performance of software professionals," *Recent Advances in Psychology: An International Journal*, vol. 3, p. 116, 2016.

[40] A. Desoete, "Mathematics and metacognition in adolescents and adults with learning disabilities," *International Electronic Journal of Environmental Education*, vol. 2, no. 1, pp. 82–100, 2017.

WILEY | Hindawi

Research Article

COCO: Coherent Consensus Schema For Dynamic Spectrum Allocation For 5G

C. Rajesh Babu [iD],[1] Kadiyala Ramana,[2] R. Jeya [iD],[3] and Asadi Srinivasulu [iD][4]

[1]*Department of Network and Communications, SRM Institute of Science and Technology, Chennai, India*
[2]*Department of Information Technology, Chaitanya Bharathi Institute of Technology, Hyderabad, India*
[3]*Department of Computing Technologies, SRM Institute of Science and Technology, Chennai, India*
[4]*Data Science Research Lab, BlueCrest University, Monrovia, Liberia*

Correspondence should be addressed to Asadi Srinivasulu; head.research@bluecrestcollege.com

Numerous wireless technologies have been integrated to provide 5th generation (5G) communication networks capable of delivering mission-critical applications and services. Despite considerable developments in a variety of supporting technologies, next-generation cellular deployments may still face severe bandwidth constraints as a result of inefficient radio spectrum use. To this end, a variety of appropriate frameworks have recently emerged that all aid mobile network operators (MNOs) in making effective use of the abundant frequency bands that other incumbents reserve for their own use. The proposed COCO model for Dynamic Spectrum Allocation (DSA) has 2 functionalities such as 1. Coherent PU-SU packet acceptance algorithm for Secondary User (SU) in DSA. 2. Consensus Algorithm for PU-SU Channel Reservation in DSA. To enable a 5G service with one-millisecond latency, interconnection ports between operators are expected to be required at every base station, which would have a significant influence on the topological structure of the core network. Additionally, just one radio network infrastructure would need to be created, which all operators would then be able to use. We allow change of PU SU characteristics to satisfy the needs of new services. These modifications are accomplished via the use of Coherent and Consensus Algorithms that regulate PU and SU through negotiation and allocation procedures. Our primary objective was to decrease interference, handoff latency, and the chance of blocking. In this paper, we describe our idea for employing COCO Model to address the issues of spectrum mobility, sharing, and handoff for Cognitive Radio Networks in 5G.

1. Introduction

In order to meet the technical requirements for 5G, the sub 1 ms latency rate must be achieved. Content must be supplied from a location near to the user's device if a delay time of less than 1 millisecond is required. In order to provide a service with such low latency, content must be placed extremely near to the client, potentially at the base of every cell, including the numerous tiny cells that are expected to be important in achieving densification needs [1].To enable a 5G service with one millisecond latency, interconnection ports between operators are expected to be required at every base station, which would have a significant influence on the topological structure of the

core network [2]. Additionally, just one radio network infrastructure would need to be created, which all operators would then be able to use.

Figure 1 illustrates the "overlay distribution" strategy by radio regulating bodies, which allows wide access to the majority of the frequency band, even if the frequency band is authorized for a certain application. Uncoordinated use of spectrum in both the time and frequency domains can be achieved by using the overlay information exchange. Techniques are used to disperse the generated signal across a wide range of frequencies so that existing licensed radio equipment does not detect an unacceptable level of power [3]. Examples of these approaches include frequency hopping, Multiplexing, and Ultra-Wide Band. This kind of
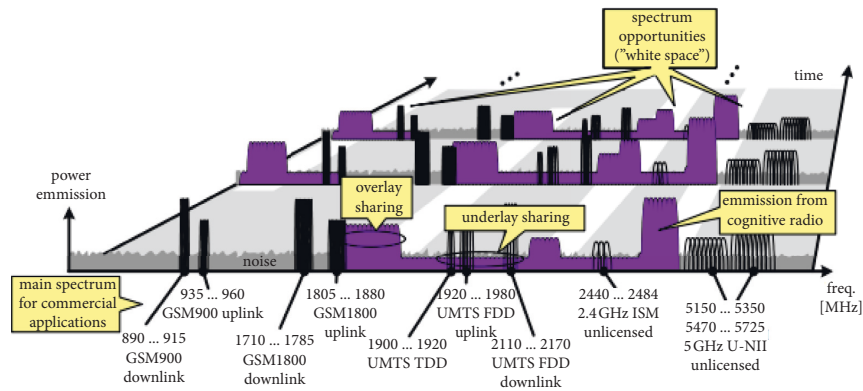
Figure 1: Cognitive radio and spectrum management in 5G.

interference is minimized by placing rigorous limits on the transmission power in the underlying dynamic spectrum.

1.1. Motivation for the Work. The Primary and Secondary users' activation and addition are dynamic with the fluctuating modalities of their interest and their requirements. The resource availability changes according to the usability, and the spectrum wastage occurs due to unused spectrum utilization. A dynamic spectrum sensing and sharing framework based on user needs is the need of the hour topic in Cognitive Radio [4]. There are disruptions possible while providing effective and efficient services meeting the QoS aspects. There is a precondition required to understand the users' requirements with a satisfactory resource provisioning mechanism along with validation with artificial intelligence in place, which remain a community hole to be filled through research.

2. Related Work

Liu et al. (2020) [5] presented a blockchain-based safe FL architecture for creating smart contracts and preventing hostile or untrustworthy parties from participating in FL. To fight against poisoning assaults, the central aggregator identified harmful and untrustworthy individuals by automatically executing smart contracts. Furthermore, membership inference attacks are prevented using local differential privacy approaches. The proposed approach, according to numerical findings, may effectively prevent poisoning and membership inference attacks, thereby boosting the security of FL in 5G networks. According to Rubayet Shafi et al. (2020) [6], Resilience, performance, and complexity were major technological hurdles to overcome while using AI in 5G and beyond 5G. Beyond-5G and sixth generation (6G) networks with AI-enabled cell networks were presented as a possible roadmap for future research to identify top challenges such as training issues, lack of bounding performance, and uncertainty in generalization, as well as a possible roadmap to realize the vision. In order to safeguard the user's identity and location, Hui Li et al. (2019) [7] implemented UGG, IPP, and LPP algorithms in the SBMs upload of a blockchain-based VANET. Two factors were used to assess the availability of k-anonymity unity: connection and average distance. Extensive simulations have

shown the effectiveness of a blockchain-based VANET. The simulation took into account a number of elements, such as system time, average distance, connection quality, and privacy breaches. In terms of processing time, the suggested design outperforms the current designs, according to the simulation results. They also demonstrate that their proposed architecture provides a higher degree of privacy for their users' identities and locations. Huijuan Jiang et al. (2019) [8] proposed a distributed user association strategy based on multi-agent reinforcement learning to offer load balancing for cognitive radio networks with several independent APs. APs used reinforcement learning to find the optimum user association rules in the technique they proposed. It is portrayed as a dynamic match game between the APs and SUs. Every iteration, the APs picked which SUs they wanted to be associated with, and the SUs then choose which AP they wanted to be affiliated with based on all the APs' offers. Comparing the suggested multi-agent reinforcement learning technique to the classic max-SINR method, simulation results demonstrate that system performance is greatly improved while excellent resilience is maintained by the latter. According to Semba Yawada et al., (2019) [9] the spectrum mobility in cognitive radio networks has many key aspects. Despite the difficulty of upkeep and upgrading, the novel methods to mobility and connection management attempt to decrease latency and information loss during spectrum handoff. The reasons for spectrum handoff and the methods that lead to it were examined. Protocols have been developed to show how the handoff process works. The different spectrum handoff methods were compared. The suggested technique outperformed the pure reactive handoff method in simulations. There are still many unanswered questions about software-defined networks in 5G and 6G networks that have yet to be addressed by Long et al. (2019) [10]. (SDN). SDN technologies are utilized to introduce 5G and 6G mobile network system designs. It was thus necessary to draw attention to the main issues and common SDN-5G/6G application scenarios. There are also comparisons and descriptions of three kinds of software-defined 5G/6G mobility management frameworks. We took a look at how wireless cellular networks handle interference right now. An overview of interference control techniques was provided in SDN-5G/6G. For software-defined 5G and 6G networks, the mm-Wave spectrum, the absence of

standard channel models, huge MIMO, low latency and Quality of Experience (QoE), energy efficiency, and scalability are all investigated. According to Daniel Minoli et al. (2019) [11] in IEEE Spectrum, IoT applications in Smart City environments face a number of challenges, including the requirement for small cells and millimeter-wave transmission issues, building penetration issues, the requirement for Distributed Antenna Systems, and the near-term introduction of pre-5G IoT technologies such as NB-IoT and LTE-M, which could serve as proxies for commercial deployment and acceptance of 5G. An improved target channel selection method was developed by Atif Shakeel et al., (2019) [12] in order to facilitate spectrum handoffs among the SUs in a CRAHN. It was recommended that SUs be organized during channel access according to the shortest job first idea using an improved frame structure that facilitates in cooperation among them in an ad hoc setting. By enabling SUs affected by inaccurate channel state predictions to compete for channel access within a single transmission cycle, the proposed system improves throughput over previous prediction-based spectrum handoff techniques. Since there are less collisions in the proposed method, it outperformed conventional spectrum handoff techniques in terms of throughput and data delivery time. Priority was given to Base Stations, PUs, and SUs in addressing the issue of spectrum resource distribution, according to Wang Bin Song et al. In the research, a multi-layer network model and a multi-agent system model were introduced. The RF Plan's BS structure and the number of Base Stations were both reduced thanks to the use of MAS for resource distribution. Designing a stratified multi-layer Multi Agent System that works in a dispersed environment and provides higher network performance while using less power is the research gap highlighted. A network environment for algorithm simulation is set up by Xiaomo Yu et al (2022) [13], after which they analyse the overall performance of the improved genetic algorithm and investigate the influence of genetic algorithm-related parameters and network environment-related parameters on the overall performance of the algorithm. The findings demonstrate the effectiveness of the enhanced genetic algorithm. It is possible to enhance network efficiency by approximately 2% while simultaneously reducing the frequency of spectrum switching by approximately 69%.

The summary of related work is shown in Table 1.

2.1. Research Gap. The basic purpose of cognitive radio is to detect interference on the channel that will be shared, as well as to protect the mobile user (PU) from interference. Due to the passive nature of cognitive radio, there is currently no practical means for identifying its impact on a given channel. According to popular belief, recognising PU signals is the same as finding spectrum possibilities, which is not the case [14].

3. Dynamic Spectrum Management Framework

As shown in figure 2, the DSMF incorporates the important components of a Licensed Spectrum Access domain. The Spectrum Manager is composed of 2 sub system blocks namely, Request Manager, which does the management of prioritizing

based on DSA domain spectrum application rules, and Radio Spectrum Resource component, computes accessible resources for allocating the PU, on the basis of spectrum application rules and details saved in a Repository [15]. Regarding the PU block, a multi-PU channel is applied where a licensed system has User Equipment or UE associated to PU's Base Station (BS) provides optimal power which is received. Primary users, the DSA Repository, the DSA Spectrum Manager, and a number of Secondary Users are all implemented in the DSMF. Spectrum sharing policies may be implemented in both macro and small-cell scenarios using the framework's techniques for centralized and distributed allocation of resources. There are two separate modules in the Spectrum Manager, one for managing priority based on DSA spectrum use rules, and one for calculating available resources for Primary Users based on spectrum consumption rules and data stored in the Repository. It is now possible to have each UE (User Equipment) in the licensed network associate with the Base Station (BS) that offers the strongest received power for the PU frame, which is currently the case. The Secondary User's behavior is recorded in the DSA Repository as an array of "pixels." Each SU relates to a specific DSA channel since there is only one array for each DSA channel. It is necessary for DSA licensees to comply to an Interference-to-Noise Ratio (INR) of -6dB inside the SU's zone of protection. By sharing resources that might otherwise go unused, DSA aims to increase the framework's utility [16]. It is possible that greedy operators may pursue their own interests at the expense of other Research on node misbehavior was conducted utilizing the cognitive radio analogy. An analysis of a fictional cognitive radio system revealed that hostile or selfish nodes may engage in acts to disrupt or enhance their own value in the community of cognitive radio nodes. For enforcing shared access agreements both before and after the fact, the authors provide a variety of options. It is hoped that the preventative measures and punitive measures would inhibit tampering with the devices' software and hardware layers, while the latter is designed to identify and punish disobedient users. Instead, we advocate for the creation of a grading system to keep tabs on the DSA's behavior.

4. Network Model

The model analyzes a single channel Cognitive Radio Network. As in practice, with the consensus policy with mobile network operators, the arrival of PU in a channel is arbitrary and has the right to access the channel. SU packets come in two forms: SU1 packets and SU2 packets, and they're both utilized by the system. Priority is given to SU1 packets over SU2 packets. When it comes to taking up a single channel, the PU packets of the system take precedence. Additionally, this research makes the assumption that the spectrum sensing for the SUs is optimal. This suggests that the system model does not take into account the interactions between distinct SUs.

There is, in fact, to limit the contention of SU flooding over the channel, a Secondary User buffer prepared for packets from Secondary User2. If the channel is already full at the time of an incoming Secondary User2 packet, the newly arriving Messages from Secondary User2 will be held

TABLE 1: Related work Summary.

Reference	Proposed Technique	Allocation/ Sharing/ Sensing	Centralized/ Distributed	Simulation/Frequency Band	Efficiency	Parameters Improved
[5]	Blockchain-based safe FL framework has been presented by the authors in order to build smart contracts and prohibit malevolent or unreliable FL players.	Sharing	Centralized	MATLAB	Improved	PU Arrival Service time Number of Hand-offs
[6]	AI-enabled cellular networks for Beyond-5G and 6th generation (6G) networks are on the horizon.	Sharing	Centralized	Google Tensorflow on MNIST dataset and CIFAR-10 dataset, respectively.	Improved	Data Accuracy
[7]	SBMs are uploaded to the blockchain-based VANET in a revolutionary decentralized architecture employing blockchain technology that integrates UGG, IPP, and LPP algorithms with the method of dynamic threshold encryption and k-anonymity unity.	Sharing and Allocation	Centralized	-	-	AI-enabled fault identification Self-Recovery Mechanism
[8]	User association rules are learned via a reinforcement learning process by access points on their own in order to pick secondary user protocols for handoff and mobility management.	Sharing/ Privacy Protection	Distributed	MATLAB	Improved	system time, average distance, connectivity,
[9]	Protocols for Handoff and Mobility Management	Sharing and Allocation	Distributed	Simulated OFDM based CR	Improved	System Throughput SU Transmission Rate
[10]	Examined new 5G and 6G software defined networks (SDN) technology, which encompasses system design, resource management, mobility management, and interference control. SDN is a cutting-edge technology.	Sharing	Distributed	MATLAB	Improved	Bandwidth Collision Probability Delay
[11]	The millimeter wave spectrum must be addressed in order to accommodate high data rates in 5G cellular technology.	Sharing	Distributed	MAC Protocol from IEEE 802.11a	Improved	Collision with SU Extended Data Delivery Throughput
[12]	The spectrum handoff between SUs in a CRAHN is improved using an upgraded frame structure that promotes coordination among SUs based on an imperfect channel state prediction.	Sharing and Allocation	Distributed	Deployed a Hierarchical Multi Agent System Model for 5G	Improved	Channel Resource Allocation
[13]	A new paradigm for 5G cellular communication networks has been proposed, which balances resource distribution between main users, secondary users, and base stations.	sharing	Distributed	MATLAB	Improved	Switching probability

in the Secondary User2 buffer until they are ready to be sent out. To configure the buffers for Primary User and Secondary User1 packets, there are no alternatives Because Primary User packets have the greatest priority, if a Primary User packet arrives while a Secondary User packet is being sent, the transmission of the Secondary User packet will be immediately halted. For the sake of efficiency, the

transmission of a freshly received Secondary User1 packet may only be temporarily halted by another Secondary User1. In both Secondary User1 and Secondary User2 packets, the interrupted packet's heightened need for transmission continuation causes both to become impatient. If a Secondary User packet is stopped during transmission, it will not be saved in the system and will not be able to be sent
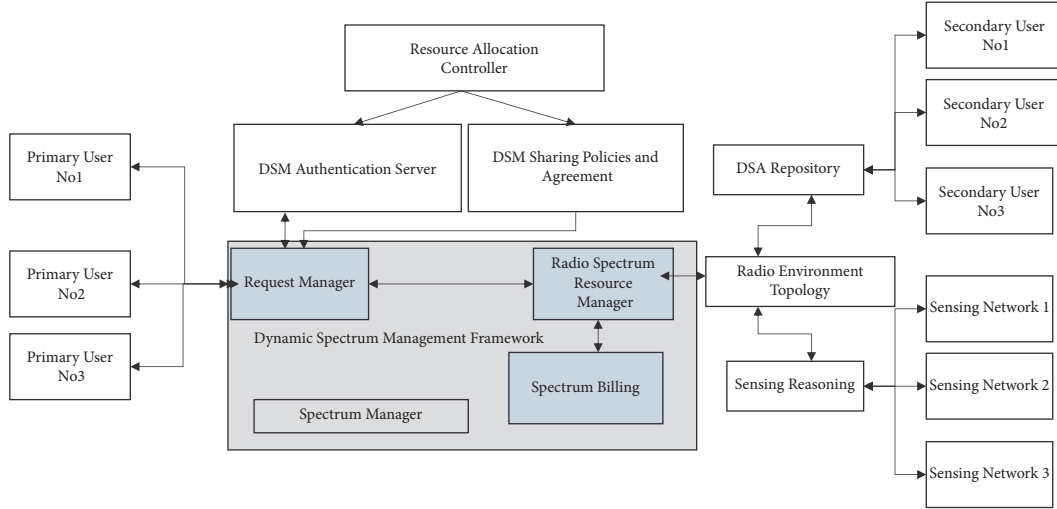
Figure 2: Dynamic Spectrum Management Framework.

again. It is possible for Secondary User packets to exit the system and broadcast on another open channel if they are interrupted. In light of the digital nature of current networks, the discrete-time Markov chain model shown below may be constructed by using the spectrum allocation approach described above. R = 1, 2,... is a convenient way to represent the division of time into equal-sized slots on an axis. Estimated arrival rates of Primary User, Secondary User 1, and Secondary User 2 packet transmission rates are predicted to follow geometric distributions at intervals determined by their respective rates of service μ_1, μ_{21}, and μ_{22}. If PU arrives back in channel, it is the responsibility of the algorithm to release the channel from SU to PU.

A system with a large number of Secondary User2 packets, a large number of Secondary User1 packets, and an even larger number of Primary User packets may be described by the following equation: A three-dimensional process comprised of the number $S(2)$ of Secondary User packets, the number $S(1)$ of Secondary User1 packets, and the number Pn of Primary User packets may be used to abstract the changes in the number of distinct packet types in the system. A discrete-time three-dimensional Markov chain is thus formed by $S(2)$, $S(1)$, and Pn. The state-space of $S(2)$, $S(1)$, and Pn may be expressed using the model assumption mentioned before.

$$\theta = \{(K, 0, 1) \cup (K, 0, 0) \cup (K, 1, 0): 0 \le K \le \infty\}. \quad (1)$$

5. EVALUATION OF MODEL

Assume that P is the probability matrix of state transitions in the Markov chain $S(2)$, $S(1)$, and Pn. The system model implies that the buffer capacity of Secondary User2 packets is limitless in order to accommodate additional Secondary User2 packets in the system. A consequence of this is that P is unlimited in its size by the number of packets experiencing state change for Secondary User2. Here's an example of how you can represent P and it is shown in (1).

$$P = \begin{pmatrix} a & b & & & \\ d & a & b & & \\ & d & a & b & \\ & & \ddots & \ddots & \end{pmatrix}. \quad (2)$$

Secondary User1 packet transmissions are unaffected by Secondary User2 packets in the analyzed cognitive radio network with categorized Secondary Users and impatient packets. The primary and secondary user1 packet transmission operations may be seen as a single-server pure losing priority queueing architecture.

The transmissions of the Secondary User2 packets, on the other hand, are impacted not only by the transmissions of the Primary User packets, but also by the transmissions of the Secondary User1 packets. As a consequence, the performance of Secondary User2 packets will be the exclusive emphasis of this section. The γ rate of interruptions, throughput, and average latency of Secondary User2 packets are among the key performance measures that we create algorithms for. The number of Secondary User2 packets that are interrupted and leave the system per slot is what is meant by the interruption rate for Secondary User2 packets. The rate at which Secondary User2 packets are being interrupted may be described as in (3):

$$\gamma = \sum_{a=0}^{\infty} \pi_{a,0,0} \mu_{22} \left(1 - \lambda_{21}\lambda_{22}\right). \quad (3)$$

The throughput ϕ of total number of the Secondary User2 packets successfully sent per slot is defined as Secondary User2 packets. A Secondary User2 packet may be successfully broadcast if and only if it is not interrupted during transmission. Equation (4) may be used to describe the throughput of packets transmitted by Secondary User2:

$$\phi = \lambda_{22} - \gamma. \quad (4)$$

The average delay β in arrival of a Secondary User2 packets and their exit from system is defined as the Secondary User2 packets. Little's calculation for the mean delay of Secondary User2 traffic is expressed in (5)

$$\beta = \frac{E[SU2]}{\lambda_{22}}, \tag{5}$$

where the system's mean SU2 traffic in steady-state is denoted in (6)

$$E[SU2] = \sum_{a=0}^{\infty} \pi_{a,0,0} + \pi_{a,0,1} + \pi_{a,1,0}. \tag{6}$$

The Secondary User2 packet cannot ascertain the total traffic in the CRN prior to making a decision. If a Secondary User2 successfully sent a packet, it may receive the reward indicated by R, but if it decides to join the system, it incurs the penalty indicated by C per slot. If a single Secondary User2 packet elects to join the system, the Secondary User2 packet's individual net benefit function $We(\lambda_{22})$ may be expressed in (7)

$$We(\lambda_{22}) = \left(1 - \frac{\gamma}{\lambda_{22}}\right)R - \beta C. \tag{7}$$

6. Coherent Pu-Su Packet Acceptance Algorithm for DSA

In contrast to standard cognitive radios, adaptive transceivers transmit data using "dynamic" resources, which are always changing. In order to make use of this special quality of cognitive radio systems, the proposed adaptive algorithm distributes bandwidth for individual traffic regarding the knowledge of congestion queues' Quality of Service standards and the related data of the currently available spectrum. As an added bonus, the suggested method, which is applicable to multimedia applications that generate both genuine and quasi traffic, dynamically adapts the distribution probabilities between actual and potential real-time traffic based on the fluctuation of accessible spectrums.

To minimize the latency of SU packets, they are allocated a limited buffer with a capacity of N (N > 0). On the other hand, no buffer is supplied for the PUs, ensuring that the PUs' latency requirements are satisfied to the maximum degree feasible [16].

(1) In an adaptive admission control strategy, the central controller counts the number of packets in the system on a regular basis. A fresh SU packet will be accepted or rejected by the system's central controller based on its likelihood with acceptance probability as $\beta = 1/(\lambda + 1)$ or reject it with probability β to the packet count of the system multiplied by the Coherent Factor. The system access probability is inversely proportional to the system packet count.

(2) When an SU packet is permitted into the system, it is queued in the buffer if the channel is currently in use by another packet. If the buffer is full, this SU packet will be terminated.

(3) To prevent conflict, the newly coming PU packet will be stopped if the channel is already in use by another packet of the same type [17]. If a packet of the same type is already in use by another PU, the newly arriving PU packet will interrupt this SU packet's transmission and take over the channel.

A packet from an SU that was in transit is returned to the SUs' buffer and placed at the front of the queue if the transmission was interrupted. If the buffers of the SUs become full, the system will force the last SU packet queued to exit. Since there is only one gap in the buffer when a fresh admission of an SU packet happens concurrently with an interruption of an SU packet, the newly admitted SU packet will be rejected by the system. Since the interrupted packet has a greater priority than the newly accepted one, it takes precedence. The greater the number of packets in a system, the greater the likelihood that it will be accessed. When the system is overloaded with packets, it's less probable that one of the freshly arrived SU packets will be accepted. Coherent PU-SU Packet Acceptance Procedure is represented inj figure 3.

7. Algorithm Analysis

7.1. Spectrum Analyzer Setup. Each cellular band was measured throughout the day where table 1 detail the spectrum analyzer and antenna specifications, respectively. The spectrum analyzer's frequency range is set at 100KHz to 3GHz. The spectrum occupancy measurement is recorded and plotted using the Rohde & Schwarz FSH Remote and MATLAB software. Spectrum occupancy was determined using a spectrum analyzer operating at frequencies ranging from 100 kHz to 3GHz.

7.2. Parameters and Values. Typical Wi-Fi network parameters, such as RTS = 44 bytes, CTS = 38 bytes, payload = 250 bytes, SIFS and DIFS = respectively 15, 34 microseconds and a slot size of 1 ms are used in the numerical results. We also employ a transmission rate of 10 Mbps while operating in the 2.4 GHz frequency range. The packet transmission rate is determined as $\mu 1$, $\mu 2 = 0.5$.

Additionally, the Malleable or Coherent Factor β data set is set to = {0.0 through 0.1 to, 1.0} with $\beta = 0$ being the standard access to system method without using admission control. This demonstrates the Coherent Factor's effect on the system's performance and the suggested adaptive admission control scheme's efficiency.

Simultaneously, we adjust the arrival rates of the PU and SU packets to $\lambda 1 = 0.2$ and 0.3 and $\lambda 2 = 0.4$ and 0.6 and investigate the impacts of the arrivals of the Primary User and Secondary User packets on measuring performance in a novel approach. For the sake of illustration, we assume that the SU's buffer capacity is set at $N = 10$. We derive that increasing the Secondary User buffer capacity increases the throughput and mean delay of the Secondary User packets.

From Figure 4, we infer that as the Factor of Coherent Function grows, SU packets' throughput decreases in the same way with the $\lambda 1$, the arrival rate of the packets from PU
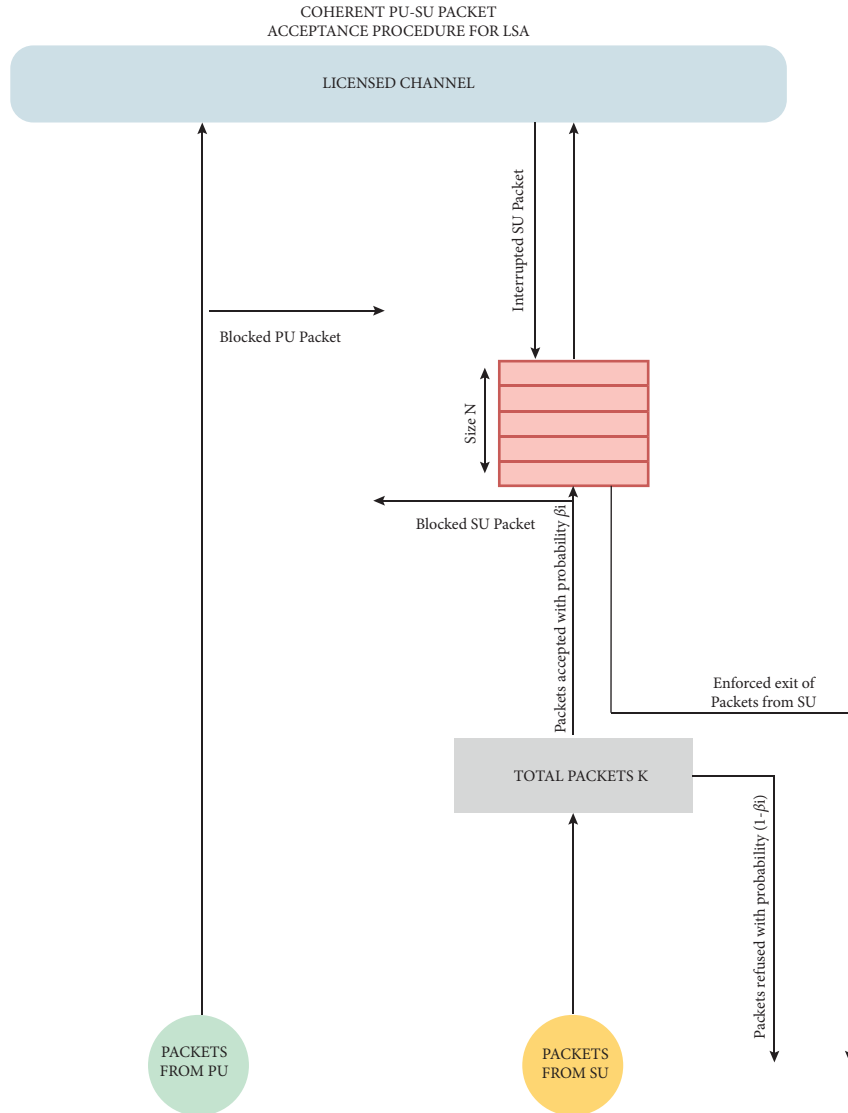
FIGURE 3: Coherent PU-SU Packet Acceptance Procedure.

and $\lambda 2$ of the SU packets. The reason for this is that when the Coherent Factor β increases, the likelihood of a fresh incoming Secondary User packet being acknowledged for the system decreases, resulting in a throughput decrease of the Secondary User packets.

7.3. Performance Optimization Assumptions. Certain assumptions are made that will be used in further optimizations.

(1) In this scenario, it is assumed that an arriving SU packet does not know the current number of packets in the system and is unsure whether the system would allow it. This is a distinct assumption. A SU packet will either enter the system permanently or not at all, depending on its state when received.
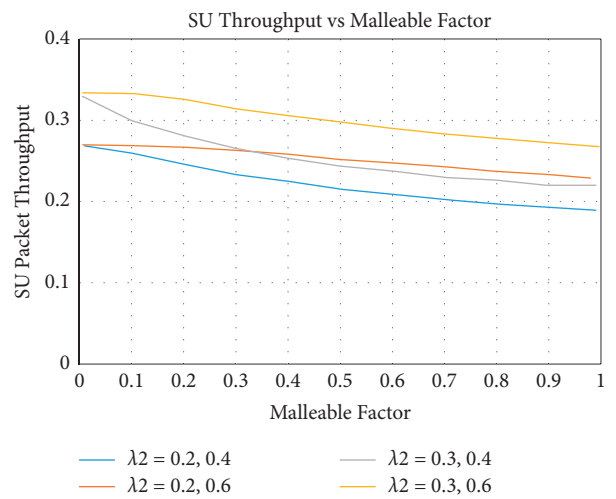
FIGURE 4: SU throughput versus Malleable factor.

TABLE 2: SU packet arrival scenarios for analysis.

Scenario 1	Scenario 2	Scenario 3
$\beta(0^+)$	$\beta(T)$	$\beta(0^+) > 0$ and $\beta(0^+) < 0$
Even if no additional SU packets enter the system, the SU packet that attempts to join will get no advantage. Thus, the trial strategy with probability $\eta_e = 0$ is the ideal approach, and there is no alternative optimal strategy [18].	Even if all prospective incoming SU packets attempt to enter the system, they will all get non-negative advantages in this situation. Thus, the trial strategy with probability $\eta_e = 1$ is the ideal approach, and there is no alternative optimal strategy.	If all SU packets enter the system with probability q=1, the Secondary User traffic packet that attempts to join will get a negative net benefit. As a result, q=1 is not the best option. On the other hand, if all SU packets enter the process with probability q=0, the packet from SU that attempts to combine will get a net positive benefit. Thus, q=0 is also not an ideal option. As a result, the best trial probability is $\eta e = e$, where e is determined by solving the equation $\beta(\Gamma) = 0$

(2) Assume R is the reward for successfully transmitting an SU packet. Because the admission of SU packets into the system is not assured, the introduction of a new SU packet is known as a trial. Each trial is charged of fee T. (T R). That is, whenever a SU packet is received in the system, regardless of whether it is effectively delivered, it incurs a cost T for attempting to enter the system.

(3) Γ represents the expected pace of arrival of the SU packages

We would get the following equation for the likelihood of sending an SU packet successfully:

$$\omega(\lambda^2) = \frac{S}{\lambda_2}. \tag{8}$$

S denotes the throughput of Secondary User traffic, and λ_2 denotes the arrival rate of Secondary user traffic. The individualized net positive $\beta(\lambda_2)$ for an SU packet seeking to enter the service is calculated as in eqaution (9):

$$\beta(\lambda_2) = \omega(\lambda_2)(R-T) - (1 - \omega(\lambda^2))T = \omega(\lambda^2)R - T. \tag{9}$$

The unique net gain of an SU packet decreases asymptotically as the rate of SU packet arrival rises. We analyze three scenarios to determine the ideal trial technique for a single SU packet as given in the Table 2:

The term "Collective Net Gain" refers to the following in equation (10):

$$\beta c(\lambda_2) = (\lambda^2)\omega(\lambda^2)R - T. \tag{10}$$

Additionally, we investigate the consistent characteristic of BS(2) in ith numerical findings. We demonstrate through the following figure 5, how the Collective Net Gain varies with the arrival rate 2 of SU packets for various Coherent Factors.

8. Inference From Numberical Results

From Table 3, as PU packets' arrival rate of λ^1 or SU1 packets' arrival rate of λ^{21} rises, both the optimum indivual and collective access rate of effectiveness drop. Since when the arrival rate of Primary User packets or Secondary User1 packets rises, the probability of successfully transmitting
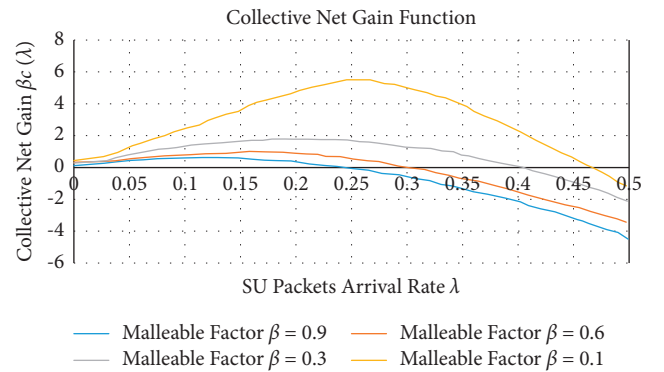
FIGURE 5: Collective net gain variation.

Secondary User2 packets always decreases. As a consequence, a greater number of Secondary User2 packets will decline in reaching the system. Additionally, when incentive R grows, both the individually optimum and collectively ideal access rates increase. The explanation for this trend is self-evident: if the incentive is bigger, the additional Secondary User2 packets will prefer to contact the system since their interests are higher. The numerical findings for establishing the appropriate additional price are shown in the table. However if the rate of arrival of Primary User or Secondary User1 packets improves, decline in the ideal extra price f is observed. Secondary User2 packets are more likely to drop out of the system if Primary User or Secondary User1 packet rates rise.

8.1. Discussions. We concentrated on the limits imposed by channel dynamics and the varying attitudes of PU and SU during times when research must be enforced. We proposed a new algorithm called Coherent PU-SU Packet Acceptance Algorithm For DSA that deals with Channel Reservation using white space terminology, Spectrum Selection and Allocation to the CR-SU by taking into account the functional outputs of the PU-SU dynamics, which involves the contention of SUs for a defined frequency and the constraints imposed by the PUs on the same frequency. The proposed algorithm offers additional services for 5G CORE such as User behaviour based spectrum resource allocation and Policy based dynamic spectrum management framework.

Table 3: Numerical results of individual and Collective Net Gain of cognitive radio users.

Reward R	PU Arrival Rate λ^1	SU Arrival Rate λ^{21}	Individual Gain λ^g		Collective Net Gain $\beta(\Gamma)$		λ^*	β^*	Additional Price A^P
			MIN	MAX	MIN	MAX			
8	0.09	0.14	0.13	0.14	0.6	0.59	0.07	0.3	1.3
8	0.09	0.19	0.09	0.10	0.4	0.34	0.05	0.2	0.8
11	0.09	0.19	0.12	0.13	0.5	0.45	0.07	0.3	1.4
11	0.14	0.19	0.09	0.10	0.4	0.34	0.05	0.2	1.12

9. Conclusion and Future Work

As a result of the discussion above, we can affirm that the Dynamic Spectrum Management framework used to control spectrum in Cognitive Radio networks is capable of providing very efficient solutions to a variety of cognitive radio difficulties. The use of DSMF in cognitive radio networks is intriguing and represents an unexplored research topic. The Dynamic Spectrum Allocation Framework for the 5G environment did not consider the applications which operate on 5G radio environmental dynamics. To address the Application Specific QoS parameters in a 5G scenario, we need to focus on collaborating our proposed Dynamic Spectrum Management framework with the 5G CORE [19]. A fundamental promise of 5G is to offer stakeholders with significantly faster speeds. 5G networks are projected to operate at higher frequencies, including 3-6GHz, which intersects with satellite C-band, and 26-30GHz, which intersects with satellite Ka-band. To allow CR-enabled spectrum management at these frequencies, CORE functionality must be separated from wireless networks [20,21]. Our proposed algorithm in conjunction with 5G CORE is intended to give the ideal solutions for such a high-capacity 5G network situation. As a future direction customized Access Modification Function (AMF) with our proposed algorithm in 5G-CORE is suggested for better performance.

Data Availability

The data used to support the findings of this study are available from the corresponding author upon request (head.research@bluecrestcollege.com).

Conflicts of Interest

"The authors declare that they have no conflicts of interest to report regarding the present study."

Authors' Contributions

C.Rajesh Babu: Conceptualization, Data curation, Formal Analysis, Methodology, Software, Writing - original draft; Kadiyala Ramana: Supervision, Writing – review & editing, Project administration, Visualization; R.Jeya: Visualization, Investigation, Formal Analysis, Software; Asadi Srinivasulu: Data Curation, Investigation, Resources, Software, Writing - original draft, Methodology

References

[1] Y. Zhang and Z. Fang, "Dynamic double threshold spectrum sensing algorithm based on block chain," in *Proceedings of the IEEE 3rd International Conference on Electronic Information Technology and Computer Engineering*, pp. 1090–1095, Xiamen, China, October 2019.

[2] A. Agarwal and R. Gangopadhyay, "Predictive spectrum occupancy probability-based spatio-temporal dynamic channel allocation map for future cognitive wireless networks," *Transactions on Emerging Telecommunications Technologies*, vol. 29, no. 8, Article ID e3442, 2018.

[3] V. Frascolla, M. M. Butt, N. Marchetti et al., "Dynamic licensed shared access - a new architecture and spectrum allocation techniques," in *Proceedings of the IEEE Vehicular Technology Conference*, pp. 1–5, Montreal, Canada, September 2016.

[4] A. A. Cheema and S. Salous, "Spectrum occupancy measurements and analysis in 2.4 GHZ WLAN," *Electronics*, vol. 8, no. 9, p. 1011, 2019.

[5] Y. Liu, J. Peng, J. Kang, A. M. Iliyasu, D. Niyato, and A. A. A. El-Latif, "A secure federated learning framework for 5G networks," *IEEE Wireless Communications*, vol. 27, no. 4, pp. 24–31, 2020.

[6] R. Shafin, L. Liu, V. Chandrasekhar, H. Chen, J. Reed, and J. C. Zhang, "Artificial intelligence-enabled cellular networks: a critical path to beyond-5G and 6G," *IEEE Wireless Communications*, vol. 27, no. 2, pp. 212–217, 2020.

[7] H. Li, L. Pei, D. Liao, G. Sun, and D. Xu, "Blockchain meets VANET: an architecture for identity and location privacy protection in VANET," *Peer-to-Peer Networking and Applications*, vol. 12, no. 5, pp. 1178–1193, 2019.

[8] H. Jiang, T. Wang, and S. Wang, "Multi-agent reinforcement learning for dynamic spectrum access," in *Proceedings of the IEEE International Conference on Communications*, pp. 1–6, Shanghai, China, May 2019.

[9] P. S. Yawada and M. T. Dong, "Intelligent process of spectrum handoff/mobility in cognitive radio networks," *Journal of Electrical and Computer Engineering*, vol. 2019, Article ID 7692630, 12 pages, 2019.

[10] Q. Long, Y. Chen, H. Zhang, and X. Lei, "Software defined 5G and 6G networks: a survey," *Mobile Networks and Applications*, 2019.

[11] D. Minoli and B. Occhiogrosso, "Practical aspects for the integration of 5G networks and IoT applications in smart cities environments," *Wireless Communications and Mobile Computing*, vol. 2019, Article ID 5710834, 30 pages, 2019.

[12] A. Shakeel, R. Hussain, A. Iqbal, I. L. Khan, Q. U. Hasan, and S. A. Malik, "Spectrum handoff based on imperfect channel state prediction probabilities with collision reduction in

cognitive radio ad hoc networks," *Sensors*, vol. 19, no. 21, p. 4741, 2019.

[13] X. Yu, Y. Cai, W. Li, X. Zhou, and L. Tang, "Research on dynamic spectrum allocation algorithm based on cyclic neural network," *Wireless Communications and Mobile Computing*, vol. 2022, Article ID 7928300, 14 pages, 2022.

[14] F. Beltrán, S. K. Ray, and J. Gutiérrez, "Dynamic Spectrum management in 5G: lessons from technological breakthroughs in unlicensed bands use," *Social-Informatics and Telecommunications Engineering, LNICST*, vol. 245, pp. 250–259, 2018.

[15] M. B. H. Weiss, K. Werbach, D. C. Sicker, and C. E. C. Bastidas, "On the application of blockchains to spectrum management," *IEEE Transactions on Cognitive Communications and Networking*, vol. 5, no. 2, pp. 193–205, 2019.

[16] P. Ren, Y. Wang, and Q. Du, "CAD-MAC: a channel-aggregation diversity based MAC protocol for spectrum and energy efficient cognitive Ad Hoc networks," *IEEE Journal on Selected Areas in Communications*, vol. 32, no. 2, pp. 237–250, 2014.

[17] C. R. Babu and B. Amutha, "A novel energy-efficient data aggregation protocol for cognitive radio based wireless multimedia networks," *Peer-to-Peer Networking and Applications*, vol. 14, pp. 2452–2461, 2020.

[18] C. Rajesh Babu and B. Amutha, "Blockchain and extreme learning machine based spectrum management in cognitive radio networks," *Transactions on Emerging Telecommunications Technologies*, pp. 1–13, 2020.

[19] Y. Xu, J. Yu, and R. M. Buehrer, "The application of deep reinforcement learning to distributed spectrum access in dynamic heterogeneous environments with partial observations," *IEEE Transactions on Wireless Communications*, vol. 19, no. 7, pp. 4494–4506, 2020.

[20] E. Z. Tragos, S. Zeadally, A. G. Fragkiadakis, and V. A. Siris, "Spectrum assignment in cognitive radio networks: a comprehensive survey," *IEEE Communications Surveys & Tutorials*, vol. 15, no. 3, pp. 1108–1135, 2013.

[21] C. Jothikumar, V. Kadiyala Ramana, D. Chakravarthy, S. Singh, S. Singh, and I. H. Ra, "An efficient routing approach to maximize the lifetime of IoT-based wireless sensor networks in 5G and beyond," *Mobile Information Systems*, vol. 2021, Article ID 9160516, 11 pages, 2021.

WILEY | Hindawi

Research Article

A Deep Neural Network-Based Approach for Sentiment Analysis of Movie Reviews

Kifayat Ullah (ID),[1] **Anwar Rashad** (ID),[1] **Muzammil Khan** (ID),[1] **Yazeed Ghadi** (ID),[2] **Hanan Aljuaid** (ID),[3] **and Zubair Nawaz** (ID)[4]

[1]*Department of Computer and Software Technology, University of Swat, Swat, Pakistan*
[2]*Department of Software Engineering/Computer Science, Al Ain University, Al Ain, UAE*
[3]*Computer Sciences Department, College of Computer and Information Sciences,*
Princess Nourah bint Abdulrahman University (PNU), P.O. Box 84428, Riyadh 11671, Saudi Arabia
[4]*Department of Data Science, University of the Punjab, Lahore, Pakistan*

Correspondence should be addressed to Kifayat Ullah; kifayat@uswat.edu.pk

The number of comments/reviews for movies is enormous and cannot be processed manually. Therefore, machine learning techniques are used to efficiently process the user's opinion. This research work proposes a deep neural network with seven layers for movie reviews' sentiment analysis. The model consists of an input layer called the embedding layer, which represents the dataset as a sequence of numbers called vectors, and two consecutive layers of 1D-CNN (one-dimensional convolutional neural network) for extracting features. A global max-pooling layer is used to reduce dimensions. A dense layer for classification and a dropout layer are also used to reduce overfitting and improve generalization error in the neural network. A fully connected layer is the last layer to predict between two classes. Two movie review datasets are used and widely accepted by the research community. The first dataset contains 25,000 samples, half positive and half negative, whereas the second dataset contains 50,000 specimens of movie reviews. Our neural network model performs sentiment classification among positive and negative movie reviews called binary classification. The model achieves 92% accuracy on both datasets, which is more efficient than traditional machine learning models.

1. Introduction

The most pleasant passage of time in the modern world is watching movies. People like to give their opinion on movies [1]. Movie reviews are comments or views of persons who have watched the movie. The collection of all these reviews assists the users in knowing whether the movie is worth watching [2].

Sentiment analysis is a field of study in which we examine people's sentiments, opinions, attitudes, and emotions based on some entities like services, products, organizations, topics, events, and their attributes [1]. The objective of sentiment analysis is to find whether these pieces of text convey negative, positive, or neutral opinions.

There are some dissimilarities between sentiment analysis and opinion mining. The first significant difference is that opinion must always have an owner (holder/owner of the comment) and target (about which holder is commenting), whereas sentiment does not have to. Spontaneously, opinion mining is used to find out people's viewpoints (e.g., disagree, agree) on someone or something [3]. Sentiment analysis is used to mine someone's feelings or attitude. If we respond, "I share your sentiment or feeling," this is called sentiment, while if someone's expression can be answered by "I disagree/agree," it is an opinion. It is not required to differentiate between sentiment and opinion in most cases explicitly. This paper considers the words sentiment analysis and opinion mining interchangeably.

To solve the problem of sentiment analysis, three methods are used: lexicon-based, machine learning, and hybrid-based methods [4].

Lexicon-based techniques use either dictionary-based techniques or corpus-based techniques. Dictionary-based methods use dictionary terms, like SentiWordNet and WordNet, and corpus-based approaches use statistical analysis [4].

Machine learning is automatically used to learn from labeled or unlabeled data automatically, called supervised learning or unsupervised learning. At the same time, a hybrid is a combination of both. Machine learning is further divided into traditional machine learning and deep learning.

Machine learning techniques are also known as traditional machine learning techniques, where some of the most popular techniques are SVM (Support Vector Machine), Decision Tree, NB (Naïve Bayes), and RF (Random Forest).

Deep learning mimics the working of the human brain to process data and creates patterns. These patterns are used for the decision-making process. The deep learning approach can learn automatically and get improved from experience without any explicit programming.

This research work proposes a seven-layer deep neural network model for larger datasets. First, the data is converted into word vectors. According to [5], Word2Vec is one of the most powerful techniques that Keras offers in an embedding layer. We use two layers of the convolutional layer. The first 1D convolutional layer is used to extract features from the input data to produce a feature map. The second convolution layer summarizes the features selected by the first convolutional layer. The global max-pooling layer reduces the resolution features of the output and prevents overfitting of the data (Dang, Moreno-García, & De la Prieta, 2020).

The dropout layer is used to solve the problem of generalization and overfitting. This layer randomly drops units from the network, while these units are dropped temporarily, along with all the outgoing and incoming connections [6].

The dense layer uses the loss function on the trained dataset to classify the input features into positive or negative.

The remainder of the paper is organized as follows: Section 1.1 introduces the related research work about movie reviews and machine learning and sentiment analysis, Section 2 describes the proposed seven-layer deep neural network model, Section 3 describes the experiments and results of our proposed model, Section 4 presents discussions, and Section 5 is the conclusion of the research work.

1.1. Related Works. Reference [7] proposed a deep neural network model for sentiment analysis applied to comments of YouTube videos, written in Brazilian Portuguese. The model has six layers. This model achieves an accuracy of 60% to 84% [7].

Reference [6] showed that overfitting is a severe problem in deep neural networks. A deep neural network with large parameters is a powerful but slow machine. The problem of overfitting is handled using the dropout technique. This paper shows that dropout improves the neural network's performance in supervised learning.

There are certain challenges in processing natural languages. In recent years, it has been observed that a neural network is a favorable solution to the challenges of natural language processing [8]. Moreover, according to [9, 10], the deep learning approach with two hidden layers is more accurate than the approach with a single hidden layer.

Reference [11] categorized the sentiment analysis into three levels. The first level is the document level, which is used to categorize the whole document as negative or positive. The second is sentence level, which classifies the sentence. The third is the aspect or feature level that classifies the document or sentence based on some aspect.

Reference [12] proposed an unsupervised-based method in which WordNet dictionary is used to determine opinion words and their antonyms and synonyms. This method is applied to movie reviews classifying each document as negative, positive, or neutral. This model uses POS tagger on the collected reviews, which tags all words of the document. Reference [12] prepared a seed list that holds some opinion words and their polarity. WordNet is used to find its synonyms if the extracted word is not in the seed list. The results have concluded that the proposed model achieves 63% accuracy on document classification using movie reviews.

In [13], the proposed SLCABG model combines the advantages of deep learning and sentiment lexicon. To enhance the sentiment features within the review, a sentiment lexicon is used at the first stage of the model, and then a convolutional neural network and GRU (Gated Recurrent Unit) are used. These layers extract sentiment features and then use the attention mechanism to weigh.

References [14, 15] presented the key challenges faced in sentiment analysis. Reference [16] presented the two most essential comparisons of sentiment analysis. First, it discussed the comparisons between sentiment review structure and analysis challenges. This challenge reveals another factor that challenges faced in sentiment analysis are domain-dependent. Reference [16] shows that the negation challenge is very popular in all types of reviews when there is a minor difference in explicit or implicit meaning. It is also concluded that the nature and review structure present a suitable challenge. Second, it examines the significance of sentiment analysis challenges to improve accuracy. Another hot area of research is the theoretical type of sentiment analysis. These two comparisons are collected from 47 research studies [16].

The WHO (World Health Organization) declared an illness on 11th March 2020 because of COVID-19 (Coronavirus Disease of 2019). As a result, a significant amount of pressure has mounted on each country to assess the cases of COVID-19 and efficiently utilize the available resources, as there was fear, panic, and anxiety as the number of cases increased [17]. More than 24 million people had positive tests worldwide as of 27th August 2020 [17].

Reference [17] extracted facts from tweets related to WHO and COVID-19 and believes that World Health Organization is ineffectual in guiding the public. The authors therein described that two types of tweets were analyzed. First, they gathered tweets from 01-01-2019 to 23-03-2020,

which were around 23,000. These tweets were analyzed and concluded that most of the tweets conveyed negative or neutral sentiments.

The second dataset collected from December 2019 to May 2020, which contained about 226,668 tweets, was analyzed and it was concluded that most of the tweets conveyed positive or neutral sentiments [17]. The authors claimed that the people had posted mostly positive tweets. This claim was then validated using a deep neural network classifier having 81% accuracy.

Reference [18] focused on the multilingual text data of social media to discover the concentration of extremism in sentiment. The authors therein used four classifications, neutral, moderate, low extreme, and high extreme. Reference [18] extracted Urdu data from a different source, which was then authenticated by Urdu domain professionals, and it achieved 88% accuracy. Naïve Bayes and SVM were applied for classification purposes and achieved 82% accuracy.

According to [19], data encoding has a vital role in convolutional neural network training. One of the most popular and simplest encoding methods is one-hot encoding. But when the dataset becomes large, data does not spread the full-label set. Therefore, in one-hot encoding, the relationship between words is independent. However, when the larger dataset is used, the dimension of the word vector will be very large.

Reference [19] had two contributions. First, the authors therein showed that random projections are an effective tool for calculating embedding having lower dimensions. Second, they proposed a normalized eigenrepresentation of the class, which encodes targets with minimal information loss and improves the accuracy of random projections with the same convergence rates.

Reference [20] used an artificial neural network trained on a movie review database with two large lists of negative and positive words. This model achieved 91% accuracy on training and 86.67% accuracy on validation.

The study performed by [6] showed that overfitting is a severe problem in deep neural networks. The deep neural network having an enormous parameter is a powerful but slow machine. This research work addresses the issue of overfitting, which means too much learning will be performed poorly on new data but, on the other hand, there is good performance on the training dataset. These problems are handled using the dropout technique. This paper demonstrates that the neural network performs better by using a dropout on supervised learning. The dropout value may be between 20% and 50%; small value has minimal effect and too large value results in underlearning by the network.

CNN is the most famous technique in computer vision; however, recent studies show that convolutional neural networks perform well on natural language processing. Reference [21] presented Facebook fast-text word embedding to represent words for sentiment analysis instead of word embeddings and trained a convolutional neural network.

Reference [22] proposed a deep neural network model and conducted experiments using a different number of CNN layers and different numbers and sizes of filters. Reference [22] also performed sentiment analysis of Hindi movie reviews, 50% of the dataset was used for training, and the other 50% of the dataset was used for testing the model. The model proposed by [22] achieved 95% accuracy and performed superior to traditional machine learning techniques.

The model proposed by [22] comprises four layers, embedding layer, convolutional layer, global max-pooling layer, and dense layer.

The first layer, that is, the embedding layer, represents a sequence of words as vectors, where the dimension must be less than vocabulary size. Reference [22] used Word2Vec to capture semantic properties. The trained model maps a word to its corresponding vector representation. Softmax probability is used to calculate high-dimensional vectors for every word.

Every hidden neuron accepts a one-word vector. This means that there must be a hidden neuron in the model for every word vector.

Reference [22] used the convolutional layer having "m" kernels/filters to a frame of size "h" over every sentence. These "m" kernels operate in parallel generating several features.

The features map produced by the convolutional layer is given to the global max-pooling layer, which samples these features and generates the local optimum. This layer aggregates information/data and reduces representation.

In [22], the experimental results claimed that the CNN which has two convolutional layers and kernel sizes of 4 and 3 performs better and achieves 95.4% accuracy. In contrast, CNN with three convolutional layers achieves 93.44% accuracy. When the quantity of the convolution layers and kernel size increase, the training time also increases.

Reference [8] reviewed the latest studies and showed that deep learning solves the problems of sentiment analysis and natural language processing. RNN, DNN, and CNN are applied using TF-IDF and word embeddings to many datasets. Word embedding performs well against TF-IDF. The convolution neural network outperforms other models, which present a good balance between CPU runtime and accuracy.

Reference [23] showed that deep learning is better for sentiment analysis. That paper explains the sigmoid function and how weights are learned in neural networks, and a particular convolution layer and pooling operations are used.

2. Methods

Alexandre Cunha proposed a six-layer neural network model for sentiment analysis to mine features and classified the comments [7]. However, he recommended that further work is needed to make this model efficient for analyzing large datasets (Figure 1).

In this research work, to check the performance of [7], we implemented the same neural network model in Python and applied it to larger movie review datasets. Unfortunately, the model does not give satisfactory results. So we
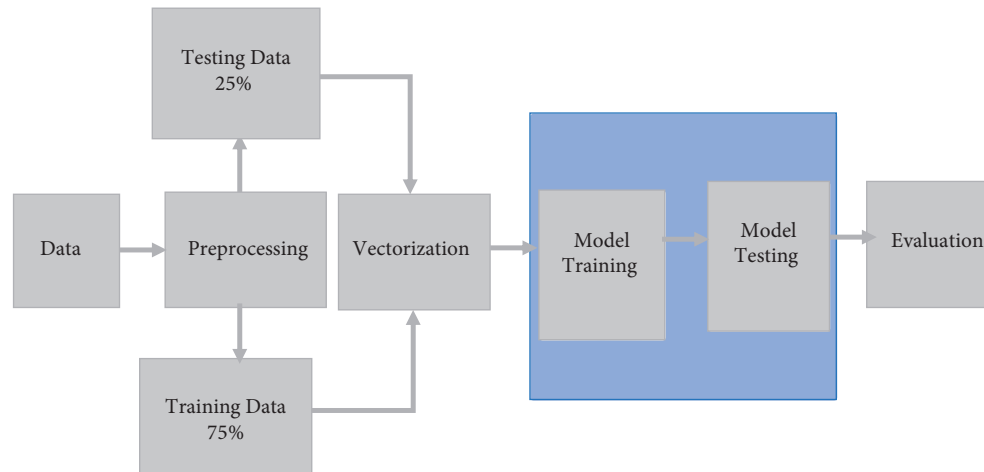
FIGURE 1: Methodology workflow.

have proposed a seven-layer deep neural network model for larger datasets. Furthermore, in this research work, one more hidden layer (one-dimensional global max-pooling layer) was added with default parameters and some parameters were changed in the proposed model of Alexandre Cunha, which increased the model's accuracy.

Our proposed model has seven layers. The first layer is the embedded layer, followed by two consecutive convolutional layers, a global max-pooling layer, a fully connected layer, a dropout layer, and a dense layer.

2.1. Embedding Layer.

The embedding layer is the first layer of the model and is provided with labeled data. The embedding layer requires that the dataset must be cleaned. The datasets are prepared so that one-hot encoding is generated for each word. Size of the vector space must be specified as it is part of the model. We used 256-dimensions.

The word embedding vectors are initialized in the first step with small random vectors. One option is one-hot encoding to map words into word vectors, but there is no relationship between words in one-hot encoding, as each word is independent [19]. Furthermore, the dimensions of the word vector will be very large if the number of words is large. Therefore, the researchers proposed encoding the words into vectors to solve the problem of one-hot encoding [24].

In this study, word embedding is used to convert words into vectors. The vocabulary size is restricted to the top 78,000 most common words for dataset-I and 1,08,000 for dataset-II. 256 dimensions are used and cut off the review after 1200 words, which we select from the experimental results of Table 1. The weights of embedding layers are taken randomly from the dictionary created from the datasets, and then these vectors are adjusted through backpropagation [25].

2.2. Convolution Layer.

In the convolution layer, the name "convolution" comes from or means to extract features from the input data, also called filters. In a one-dimensional convolutional layer (1D-CNN), features are extracted from the input data to produce a feature map using a filter or kernel.

The convolutional layer is a feed-forward deep neural network primarily applicable in computer vision, natural language processing, and recommending systems [8]. The objective of a convolutional layer is to extract the most significant features from the input [26].

We used a convolutional layer to effectively extract important features using fewer neurons compared to the dense layer [7]. However, more layers of the convolutional layer will extract more features from the input vectors. Therefore, we have used a two convolutional layers. These convolutional layers have 128 and 64 filters size, respectively.

We have used a 1D convolutional layer. Therefore, it summarizes along with one dimension. Its advantage is that it automatically detects important features without any human supervision.

The second convolutional layer summarizes the features selected by the first convolutional layer because filter size is reduced in this layer.

2.3. Global Max-Pooling Layer.

The global max-pooling layer reduces the resolution features in the output and prevents data overfitting [8]. Furthermore, according to [23], pooling layer is used to decrease dimensionality by releasing the number of factors and hence shortening the execution time.

We use the global max-pooling 1D layer. In this layer, the dimensionality of features is decreased without losing key information. The features generated by the convolutional layer are summarized in this layer and thee features of the global region are presented into a feature map. The next layer will perform operations on the summarized features. Now, if there are any variations in the position of input features, the model can identify them. Pooling operations are divided into max-pooling and average pooling. In max-pooling operation, maximum elements are selected from the feature map of the region, which is converted by the filter. In contrast, global max-pooling gives a single value by reducing each channel in the feature map.

TABLE 1: Effect of the input statement using fixed-length dataset I.

Length of sentence	Accuracy (%)	Precision (%)	Recall (%)	F1-Score (%)
10	73.19	73.46	73.56	72.83
2375	87.95	88.05	88.65	87.77
1200	88.89	88.22	87.83	87.35

2.4. Dropout Layer. Multiple nonlinear hidden layers in deep neural networks make the model more expressive which can learn the complicated relationship between input and output [6].

Generalization and overfitting are two significant problems in the neural network. The model's ability to perform well on new data is called generalization. In contrast, when you train the model on large data and the model works well on that data but performs poorly on the test dataset, this problem is called overfitting.

Dropout is a technique that effectively addresses these problems and combines many different architectures of neural networks efficiently [6]. Dropout means dropping visible or hidden units from the network, which are temporarily removed from the network and all its outgoing and incoming connections.

Reference [6] proposed that a typical dropout value for hidden units will be in the range of 0.5 to 0.8 because a shallow value has a very slight effect on the model and a very high value results in underlearning by the neural network.

The dropout layer is used with a dropout rate of 0.3, which we obtained from the experimental results in Table 2. When the dropout layer is used in the neural network, its neurons become less sensitive to specific weights, which will result in a neural network that is less likely to overfit the training data and can be better generalized.

2.5. Fully Connected Layer. Dense layer (densely connected layer) means fully connected layer. A fully connected layer performs primary classification. We have used two dense layers, one hidden layer, and another is the last layer. The hidden dense layer will return an array of 50 probability scores. It takes a feature vector as input and gives an output of a 50-dimensional vector. At the same time, the last dense layer is used to classify features of the input into various classes.

The seven-layer sequential neural network model is shown in Figure 2.

3. Experiments

This section evaluates the neural network model for sentiment analysis.

3.1. Data Collections. There are several sources for movie review datasets like GitHub, Kaggle.com, UCI (machine learning repository), and IMDb. We extracted movie review datasets from IMDb. The critics frequently use movie rating websites like IMDb to post remarks and rate movies, which assist users in deciding whether to watch the movie or not. In this study, we have used two datasets on IMDb, an online

TABLE 2: Effect of dropout value.

Dropout	Accuracy (%)	Precision (%)	Recall (%)	F1-Score (%)
0.3	90.23	90.88	89.91	89.78
0.4	89.81	90.33	89.99	89.52
0.6	89.35	89.45	89.96	89.18
0.8	88.89	88.22	87.83	87.35

```
Model: "sequential"
_____
Layer (type)              Output Shape          Param #
=================================================
embedding (Embedding)     (None, 1500, 256)     19968000

conv1d (Conv1D)           (None, 1494, 128)     229504

conv1d_1 (Conv1D)         (None, 1490, 64)      41024

global_max_pooling1d (Global  (None, 64)        0

dense (Dense)             (None, 50)            3250

dropout (Dropout)         (None, 50)            0

dense_1 (Dense)           (None, 1)             51
=================================================
Total params: 20, 241, 829
Trainable params: 20, 241, 829
Non-trainable params: 0
_____
None
```

FIGURE 2: Seven-layer neural network model.

database of information about movies. These datasets are available and broadly accepted by researchers [8]. The first dataset (dataset I) is available on Kaggle.com [27], which contains IMDb movie reviews from the audience, with 25,000 samples having half positive and half negative [28]. The second dataset (dataset II) is also available on Kaggle.com [29], and it is a binary classification dataset containing 50,000 reviews of movies.

3.2. Preprocessing. To improve the quality of sentiment analysis and reduce errors and inconsistencies in sentiment analysis, we need to clean the data [1]. We observed from the datasets that they contain HTML tags and punctuations. Therefore, we removed the HTML tags and special characters from these datasets. After removing punctuations, which result in single characters that make no sense, we removed all the strings having single characters. We replaced them with a space that creates multiple spaces in our dataset. Then we removed multiple spaces from our text, and, finally, we converted the text to lowercase. After cleaning, each dataset is divided into two pairs, training and testing; 75% of the dataset is used to train the proposed model and the remaining 25% for testing. In dataset I, from 25,000 samples, 18,750 sequences or samples are used for training, while the

remaining 6,250 sequences or samples are used for testing. Meanwhile, in dataset II, 37,500 sequences or samples are used for training and 12,500 sequences or samples are used for testing from 50,000 samples.

3.3. Performance Metrics.

3.3. Performance Metrics. The evaluation metric of the model used in this research work is accuracy. The parameters of the accuracy are defined as follows:

TP: The total number of reviews is is categorized as positive, and the reviews are positive.

FP: The total number of reviews is categorized as negative, and the reviews are positive.

TN: The total number of reviews is categorized as negative, and the reviews are negative.

FN: The total number of statements/reviews is categorized as positive, and the reviews are negative.

Accuracy is calculated by taking the ratio between the predicted reviews and the total number of reviews.

$$\text{Accuracy} = \frac{(TP + TN)}{(TP + TN + FP + FN)}. \tag{1}$$

Precision is calculated by taking the ratio between the reviews predicted correctly as positive and the total number of predictable positive reviews.

$$\text{Precision} = \frac{TP}{(TP + FP)}. \tag{2}$$

Recall is calculated by taking the ratio between the reviews that are predicted correctly as positive reviews to all of the reviews in that class.

$$\text{Recall} = \frac{TP}{(TP + FN)}. \tag{3}$$

*F*1-Score is calculated by taking the weighted average between recall and precision.

$$F1 - \text{Score} = \frac{(2 * \text{Precision} * \text{recall})}{(\text{Precision} + \text{recall})}. \tag{4}$$

3.4. Experiment Results. These experiments are performed using datasets I and II. We took the largest review, average review, and smallest review length to conduct experiments. The parameters of the proposed model are shown in Table 3. We record the experimental results in Tables 1, 4, and 5. We discovered from the experimental results that using the longest review and average review length as a fixed length of the input gives better results compared to the smallest review length. Furthermore, the average length review is more effective in terms of processing speed and accuracy, which affects the performance of the proposed neural network model. The experiments in Table 5 are performed on the six-layer model proposed by [7]. It is shown in Table 5 that the accuracy of the six-layer model is less than that of our proposed model.

TABLE 3: Parameters of the model.

Parameters	Values
The length of the input sentence	1200
The dimension of the word vector	256
The thesaurus size	78000, 108000
The size of the convolution kernel	7×5
The number of hidden neurons in the convolution layer	128
Dropout	0.3

TABLE 4: Effect of the input statement using fixed-length dataset II.

Sentence length	Accuracy (%)	Precision (%)	Recall (%)	F1-Score (%)
6	73.28	74.74	71.40	72.28
2375	90.85	91.03	90.93	90.47
1200	91.04	91.13	91.09	90.66

TABLE 5: Effect of the input statement using fixed-length six-layer model.

Length of sentence	Accuracy (%)	Precision (%)	F1-Score (%)
10	68.41	66.51	89.35
2375	50.28	50.05	99.78
1200	52.39	53.97	99

The generalization performance of the neural network model is improved by using a dropout layer. Different dropout values are used in the experiment. It has been observed from the experiments that when the dropout value is set to 0.3, the model's performance is optimum. The results of the experiments are shown in Table 2. The experimental result of Table 2 is on the seven-layer model and the experimental results of Table 6 are on the six-layer model [7], whose accuracy is not more than 52.39%.

It has also been observed from the experiments that the model's performance is affected by the number of iterations. When we increase the number of iterations, the performance of the model also improves. It is presented in Tables 7 and 8 and also shown in Figures 3 and 4. The experiments in Table 9 are performed on the six-layer model, with accuracy not more than 55%.

The testing accuracy, recall, precision, and *F*1-Score are shown in Tables 10 and 11.

From Tables 10 and 11, it is noted that the model achieved a final accuracy of 91.18% on dataset I and 91.98% accuracy on dataset II. Meanwhile, from Table 12, it is noted that the six-layer model achieved a final accuracy of 53.70%, which is less than that of our proposed model.

4. Discussions

We proposed a seven-layer deep neural network model for sentiment analysis to classify movie reviews in this research work. Before the word vector is input into the model, the data is preprocessed to improve the quality of sentiment analysis. We remove HTML tags, punctuation marks, and spaces in preprocessing as they do not contain any

TABLE 6: Effect of dropout value.

Dropout	Accuracy (%)	Precision (%)	F1-Score (%)
0.3	52.39	53.97	99
0.4	52.10	53.67	100
0.6	52.25	53.18	100
0.8	51.74	52.08	100

TABLE 7: Effect of the iterations on the model's dataset I.

Epoch	Accuracy (%)	Precision (%)	Recall (%)	F1-Score (%)
1	89.99	90.58	90.01	89.52
2	97.13	97.29	97.01	97.02
3	99.63	99.63	99.64	99.62
4	99.89	99.92	99.88	99.89

TABLE 8: Effect of the iterations on the model's dataset II.

Epoch	Accuracy (%)	Precision (%)	Recall (%)	F1-Score (%)
1	91.04	91.13	91.09	90.66
2	96.84	97.00	96.75	96.74
3	99.18	99.16	99.20	99.14
4	99.42	99.44	99.38	99.38

FIGURE 3: Accuracy on dataset I.

FIGURE 4: Accuracy on dataset II.

TABLE 9: Effect of the number of iterations.

Epoch	Precision (%)	Accuracy (%)	F1-Score (%)
1	54.09	52.48	100
2	54.59	53.14	100
3	54.58	53.65	100
4	54.93	53.87	100

TABLE 10: Test results of the model's dataset I.

Epoch	Accuracy (%)	Recall (%)	F1-Score (%)	Precision (%)
Testing	92.18	92.53	91.94	91.79

TABLE 11: Test results of the model using dataset II.

Epoch	Accuracy (%)	Precision (%)	Recall (%)	F1-Score (%)
Testing	91.98	94.14	89.93	91.72

TABLE 12: Test results using dataset I.

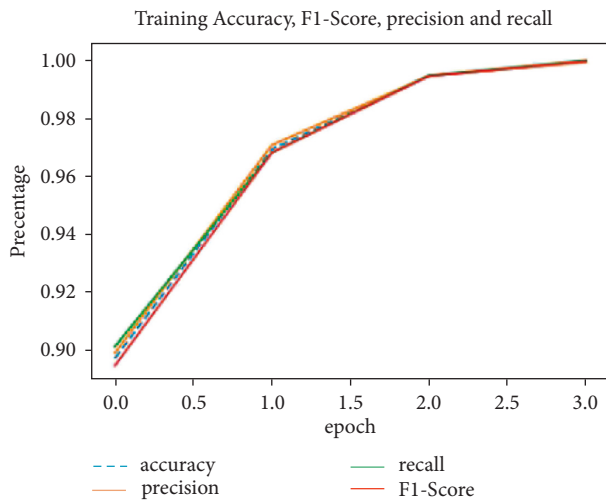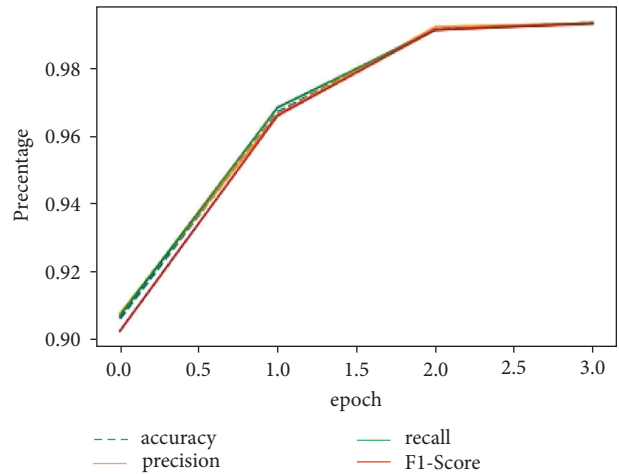| Epoch	Accuracy (%)	F1-Score (%)	Precision (%)
Testing	53.70	100	52.14

information. For feature selection, we have different options, but the most effective method is word embedding. So we used word embedding (embedding layer), which is used to convert text into vectors so that words with similar meanings get a closer vector.

In addition, we found that the length of the input review affects the model's performance. Therefore, we select small, average, and maximum review lengths, where the average review length gives better results on the model. After the embedding layer, two consecutive convolution layers are used to extract the essential features from the data. We use the convolution layer because it extracts features from fewer neurons compared to the traditional dense layer. The second convolutional layer summarizes the features selected by the first convolutional layer. Then we use the global max-pooling layer to decrease dimensionality without losing key

features and prevent the model from overfitting data. A fully connected layer takes the features vector generated by the global max-pooling layer as input and provides an array of probability as output. A dropout layer is used to randomly drop hidden layer neurons to reduce overfitting and improve generalization error. The value of the dropout layer is set to 0.3 because when the value of dropout is set to 0.3, the model's performance is optimum. Finally, a dense layer is used to classify sentiment features as positive or negative.

5. Conclusion

The model proposed by [7] is a deep neural network consisting of six layers applied to two video comments on YouTube. The accuracy of this model is in the range of 60% to 84% [7]. It was suggested that this model would be applied to a larger dataset. We applied the same model to larger

datasets of movie reviews, but it gives 55% accuracy. We added one more layer called the global max-pooling layer in the same model as Alexandre Cunha and changed some parameters, improving the model's accuracy from 55% to 92%. The accuracy of the six-layer model proposed by [7] is less because the dataset used is large, and every review of the dataset is about 1500 words (cut-off review).

We have successfully implemented a deep neural network with seven layers on movie review data. Our model achieves accuracy of 91.18%, recall of 92.53%, $F1$-Score of 91.94%, and precision of 91.79% on dataset I, and, on dataset II, the model achieves accuracy of 91.98%, precision of 94.14%, recall of 89.93%, and $F1$-Score of 91.72%.

Data Availability

The code and data used to support the findings of this study have been deposited in the GitHub repository and are available at https://github.com/asifntu/sentimentanalysis. The readers can easily follow the steps to reproduce the study.

Conflicts of Interest

The authors have no conflicts of interest to report regarding this study.

Acknowledgments

References

[1] D. S. Sisodia, S. Bhandari, N. K. Reddy, and A. Pujahari, "A comparative performance study of machine learning algorithms for sentiment analysis of movie viewers using open reviews," in *Performance Management of Integrated Systems and its Applications in Software Engineering*, pp. 107–117, Springer, Salmon Tower Building, NY, USA, 2020.

[2] B. Lakshmi Devi, V. Varaswathi Bai, S. Ramasubbareddy, and K. Govinda, "Sentiment analysis on movie reviews," in *Emerging Research in Data Engineering Systems and Computer Communications*, pp. 321–328, Springer, Salmon Tower Building New York City, 2020.

[3] W. Zhang, M. Xu, and Q. Jiang, "Opinion Mining and Sentiment Analysis in Social media: Challenges and Applications," in *Proceedings of the 5th International Conference, HCIBGO 2018, Held as Part of HCI International 2018*, Las Vegas, NV, USA, July 15-20, 2018.

[4] B. Bhavitha, A. P. Rodrigues, and N. N. Chiplunkar, "Comparative Study of Machine Learning Techniques in Sentimental Analysis," in *Proceedings of the 2017 International Conference on Inventive Communication and Computational Technologies (ICICCT)*, Coimbatore, India, 10-11 March 2017.

[5] T. Mikolov, I. Sutskever, K. Chen, G. S. Corrado, and J. Dean, "Distributed representations of words and phrases and their compositionality," *Advances in Neural Information Processing Systems*, vol. 26, 2013.

[6] N. Srivastava, G. Hinton, A. Krizhevsky, I. Sutskever, and R. Salakhutdinov, "Dropout: a simple way to prevent neural networks from overfitting," *Journal of Machine Learning Research*, vol. 15, no. 1, pp. 1929–1958, 2014.

[7] A. A. L. Cunha, M. C. Costa, and M. A. C. Pacheco, "Sentiment analysis of youtube video comments using deep neural networks," *International Conference on Artificial Intelligence and Soft Computing*, China, 2019.

[8] N. C. Dang, M. N. Moreno-García, and F. De la Prieta, "Sentiment analysis based on deep learning: a comparative study," *Electronics*, vol. 9, no. 3, p. 483, 2020.

[9] A. Alharbi and O. Sohaib, "Technology readiness and cryptocurrency adoption: PLS-SEM and deep learning neural network analysis," *IEEE Access*, vol. 9, pp. 21388–21394, 2021.

[10] O. Sohaib, W. Hussain, M. Asif, M. Ahmad, and M. Mazzara, "A PLS-SEM neural network approach for understanding cryptocurrency adoption," *IEEE Access*, vol. 8, pp. 13138–13150, 2020.

[11] B. J. Liu, *Sentiment analysis and opinion mining*, vol. 5, no. 1, pp. 1–167, 2012.

[12] R. Sharma, S. Nigam, and R. J. Jain, "Opinion Mining of Movie Reviews at Document Level," 2014, https://arxiv.org/abs/1408.3829.

[13] L. Yang, Y. Li, J. Wang, and R. S. Sherratt, "Sentiment analysis for E-commerce product reviews in Chinese based on sentiment lexicon and deep learning," *IEEE Access*, vol. 8, pp. 23522–23530, 2020.

[14] R. Sujata, K. J. Parteek, and R. i. C. Science, "Challenges of Sentiment Analysis and Existing State of Art," 2014, https://www.researchgate.net/publication/308331478_Challenges_of_Sentiment_Analysis_and_Existing_State_of_Art.

[15] G. Vinodhini and R. J. I. J. Chandrasekaran, *Sentiment analysis and opinion mining: A Survey,* vol. 2, no. 6, pp. 282–292, 2012.

[16] D. M. E.-D. M. Hussein, "A survey on sentiment analysis challenges," *Journal of King Saud University - Engineering Sciences*, vol. 30, no. 4, pp. 330–338, 2018.

[17] K. Chakraborty, S. Bhatia, S. Bhattacharyya, J. Platos, R. Bag, and A. E. Hassanien, "Sentiment Analysis of COVID-19 tweets by Deep Learning Classifiers—A study to show how popularity is affecting accuracy in social media," *Applied Soft Computing*, vol. 97, Article ID 106754, 2020.

[18] M. Asif, A. Ishtiaq, H. Ahmad, H. Aljuaid, and J. Shah, "Sentiment analysis of extremism in social media from textual information," *Telematics and Informatics*, vol. 48, Article ID 101345, 2020.

[19] P. Rodríguez, M. A. Bautista, J. Gonzàlez, S. Escalera, and V. Computing, "Beyond one-hot encoding: lower dimensional target embedding," *Image and Vision Computing*, vol. 75, pp. 21–31, 2018.

[20] Z. Shaukat, A. A. Zulfiqar, C. Xiao, M. Azeem, and T. Mahmood, "Sentiment analysis on IMDB using lexicon and neural networks," *SN Applied Sciences*, vol. 2, no. 2, p. 148, 2020.

[21] I. Santos, N. Nedjah, and L. de Macedo Mourelle, "Sentiment analysis using convolutional neural network with fastText embeddings," in *Proceedings of the 2017 IEEE Latin American Conference on Computational Intelligence (LA-CCI)*, Arequipa, Peru, 08-10 November 2017.

[22] S. Rani and P. Kumar, "Deep learning based sentiment analysis using convolution neural network," *Arabian Journal for Science and Engineering*, vol. 44, no. 4, pp. 3305–3314, 2019.

[23] K. Chakraborty, S. Bhattacharyya, R. Bag, and A. A. Hassanien, "Sentiment analysis on a set of movie reviews using deep learning techniques," *Social Network Analytics:*

Computational Research Methods and Techniques, vol. 127, 2018.

[24] M. Giatsoglou, M. G. Vozalis, K. Diamantaras, A. Vakali, G. Sarigiannidis, and K. C. Chatzisavvas, "Sentiment analysis leveraging emotions and word embeddings," *Expert Systems with Applications*, vol. 69, pp. 214–224, 2017.

[25] F. Chollet, *Deep Learning with Python*, Simon & Schuster, Manhattan, New York City, 2017.

[26] Y. Chen, J. Wang, X. Chen, A. K. Sangaiah, K. Yang, and Z. Cao, "Image super-resolution algorithm based on dual-channel convolutional neural networks," *Applied Sciences*, vol. 9, no. 11, p. 2316, 2019.

[27] L. N, "Manhattan," 2019, https://www.kaggle.comhttps://www.kaggle.com/lakshmi25npathi/imdb-dataset-of-50k-movie-reviews.

[28] E. Ahmed, M. A. U. Sazzad, M. T. Islam, M. Azad, S. Islam, and M. H. Ali, "Challenges, Comparative Analysis and a Proposed Methodology to Predict Sentiment from Movie Reviews Using Machine Learning," in *Proceedings of the 2017 International Conference on Big Data Analytics and Computational Intelligence (ICBDAC)*, Chirala, Andhra Pradesh, India, 23-25 March 2017.

[29] L. Andrew, R. E. D. Maas, P. T. Pham, D. Huang, A. Y. Ng, and C. Potts, "Learning Word Vectors for Sentiment Analysis," 2011, https://www.kaggle.com/c/word2vec-nlp-tutorial/data.

WILEY | Hindawi

Research Article

Design and Implementation of Brain Tumor Segmentation and Detection Using a Novel Woelfel Filter and Morphological Segmentation

M Venu Gopalachari,[1] Morarjee Kolla,[2] Rupesh Kumar Mishra,[2] and Zarin Tasneem [iD][3]

[1]*Department of Information Technology, Chaitanya Bharathi Institute of Technology, Hyderabad, Telangana, India*
[2]*Department of Computer Science and Engineering, Chaitanya Bharathi Institute of Technology, Hyderabad, Telangana, India*
[3]*Department of Computer Science and Engineering, University of Science and Technology, Chattogram, Bangladesh*

Correspondence should be addressed to Zarin Tasneem; hodcse@ustc.ac.bd

Neuroimaging is critical in the diagnosis and treatment of brain cancers; however, the first detection of tumors is a challenge. Detection techniques like image segmentation are heavily reliant on the segmented image's resolution. Magnetic resonance imaging (MRI) tumor segmentation has emerged as a new study area in the medical imaging field. This spongy and delicate mass of tissue is the brain. Stable conditions allow for patterns to enter and interact with each other. To put it simply, a tumor is a mass of tissue that has grown unchecked by the natural mechanisms that keep it under control. When cells divide uncontrollably, they create a cancerous tumor. Brain tumors can be detected and segmented using a variety of methods. A new method for detecting brain tumors using MRI images is presented in this research. An innovative Woelfel filter is used for enhancement, and morphological segmentation approaches combined with anisotropic diffusion are used for segmentation. Segmentation of brain tumors can be accomplished using thresholding and morphological techniques, which are both effective. The tumor will be located and identified using morphological image processing. Image denoising refers to the process of removing artefacts such as noise and aliasing from digital images. Here MATLAB programming language is utilised as it incorporates all the toolboxes required for the application involved in the work.

1. Introduction

Medical imaging research has resulted in the development of diagnostic techniques such as computed tomography (CT), magnetic resonance imaging (MRI), and ultrasound. Each has its own set of pros and disadvantages. Medical imaging is the technique of creating images of the inside of the body in order to aid in the diagnosis of a medical condition. It not only aids in the treatment and identification of sickness but also allows for the discovery of inner structures that lay beneath the surface of the skin and bones, which is quite useful. It identifies abnormalities by comparing them to a database of normal anatomy and physiology. The segmentation of brain tumors is a crucial topic in the field of magnetic resonance imaging (MRI). Image segmentation is

the process of breaking down a complex image into smaller, more manageable segments for simpler analysis [1]. An MRI scan of the brain is one of the most regularly used diagnostic procedures for the detection of brain tumors. The magnetic resonance imaging (MRI) machine operates in the same way. During scanning by a radio transmitter, an antenna (coil) captures a radio wave generated by the patient's body. The radio transmitter then delivers a radio wave through the patient's body, shaking the protons in the process, which then generates a new radio wave. When the new radio wave is received, it is processed by a computer algorithm, which results in the creation of the magnetic resonance image (MRI). Tumors can be classified into two categories: primary tumors and secondary tumors [2]. Malignant tumors, on the other hand, are cancerous tumors that spread over a

prolonged period of time. They are rapidly expanding, but their borders are unclear. It is possible to develop primary and secondary malignancies [3–5]. It would be helpful to have an automated system for finding, locating, and classifying things [6]. It is possible to execute a range of medical imaging techniques in order to make an accurate diagnosis of tumors. Stroke lesions are investigated using magnetic resonance imaging (MRI) sequences depending on a range of factors, including the patient's age, location, and severity [7]. In the context of treatment, the adoption of a computerised system for determining the rate of sickness progression may be beneficial [8].

2. Related Works

Medical imaging techniques use direct observation of body tissues to provide a relatively accurate diagnosis of disease without surgery. There have been numerous advancements in nanoscale imaging techniques during the last few decades. It is possible to capture images of the internal organs and tissues of the body using medical imaging. To put it another way, the disease can be treated better and faster, resulting in less agony and less expense for the patient. Imaging can also be used to track the progression of a disease and determine whether or not a treatment is working. Medical image processing's primary goal is to extract relevant and accurate information from images with the least amount of error feasible. Because of the brain's intricacy, it is challenging to identify brain tumors using MRI imaging. A brain tumor is defined as an abnormal growth of brain tissue that impairs normal brain function. It is vital to obtain medically relevant information from magnetic resonance imaging (MRI) in order to diagnose and treat patients. When it comes to non-invasively diagnosing brain tumors, computer-aided detection (CAD) is favoured. When employing MRI to capture the pictures of the brain, noise and artefacts such as labelling and intensity changes are inevitable during the acquisition process [9]. There are also numerous other structures in the brain imaging, including cerebrospinal fluid, grey and white matter, and skull tissues, apart from the tumor.

The authors in [10] proposed a model in which the MRI brain images are first preprocessed using the median filter, and then the segmentation component of a particular image is completed. Region-based, threshold-based, cluster-based, and region-merging segmentation techniques were all discussed by the researchers in [11].

Another study can diagnose a brain tumor using a combination of handmade and deep learning characteristics [12–14]. Authors have presented malignant vs. benign and low-grade to high-grade glioma classification [15–18]. There are tumors in the human brain that are composed of a large number of abnormal cells or "tumors." The sooner the brain tumor is discovered, the better [19–22]. The segmentation of MR brain images to detect and extract tumor areas has been the subject of numerous studies. References [23–27] contain some of the related research on brain tissue segmentation using clustering and other approaches. It is difficult to segment images despite extensive research because of a variety of issues, such as diverse visual content and objects with non-uniform textures. While various algorithms and strategies exist, there is still a need for an effective, rapid method of segmenting medical images [28–30].

3. Methodology

The one-of-a-kind filter design would be selected almost universally since the complexity of the filter has little bearing on its implementation in a digital system. Both filters were the same size (order) and would process an image in around the same length of time.

The Woelfel method is used in this procedure (using two FIR filters). The employment of FIR filters, whether decimating or interpolating, allows for the omission of some calculations, resulting in significant computing savings. When IIR filters are employed, however, each output must be calculated individually, even if that output will be discarded (so, the feedback will be incorporated into the filter). They are suitable for multi-rate applications. We mean "decimation," which means lowering the sample rate, and "interpolation," which means increasing the sampling rate or both. FIR filters are used for decimating or interpolating, and they allow some calculations to be skipped, resulting in significant processing efficiency. When IIR filters are employed, however, each output must be calculated individually, even if that output will be discarded (so, the feedback will be incorporated).

An organised collection of structured data, or "data," is stored electronically in a computer system. In this way, it is possible to access and handle the data in a streamlined and efficient manner.

A brain MRI scan may be considered to evaluate the brain for tumors and other lesions, traumas, intracranial hemorrhages, and structural anomalies. The rgb2gray function removes the hue and saturation information from RGB images while keeping the luminance; this is referred to as the "color mapping" procedure.

The power spectral density (PSD), often known as the power spectrum, is a metric for evaluating a signal's power over its whole frequency range. By multiplying the Fourier terms by their complex conjugate and scaling by the number of samples, we can obtain an estimate of the PSD at frequency [31–33].

Roundoff noise causes a rise in the power spectral density (PSD) at the filter system object's output. Quantization mistakes in the filter are the causes of this noise. To calculate an average, L is the number of trials that were performed. The average of the L trials is used to calculate the PSD. The better the estimate is, the more trials you specify and the longer it takes to compute, but this comes at a cost. Ten trials are considered default when you do not specify L.

Filters are most typically used in image processing to suppress either the high frequencies in an image, resulting in a smoother image, or the low frequencies in an image, resulting in the augmentation or detection of edges in the image. Filters can be applied to an image in either the frequency domain or the spatial domain. Smoothing techniques are used in digital picture processing to remove noise. Image filtering is a critical step in the smoothing process.

Digital photos are enhanced and modified using filtering algorithms. Image filters are also used for blurring, noise reduction, sharpening, and edge identification. FIR filter design can be done using a variety of well-known and proven techniques. The implementation of FIR filters is straight-forward. It is possible to create distortion-free FIR filters by using linear phase design principles. Image processing applications do not benefit as much from the infinite impulse response (IIR) filter class as it does from others. Stability and ease of implementation are not inherent in this filter, as they are in the FIR filter. Because of this, this toolbox does not have IIR filtering capabilities. The picture quality improves and becomes clearer when using the Woelfel filter as compared to other filters, and an isotropic diffusion approach and these output images are utilised to do the morphological operation and discover brain tumors. Morphology refers to a broad range of image processing techniques that alters pictures based on the contours of the objects in the pictures. The output image of a morphological operation is always the same size as the input image because it is created by using a structural element. In a morphological process, the value of one pixel in a picture corresponds to the value of another pixel in its immediate neighborhood.

Only a limited amount of information was permitted to travel through the boundaries of the unique filtering image's PSD, which had no ringing.

There are advantages and cons to each strategy. We have compiled some of the most significant findings in the field of image denoising in this project. For this section, we begin by defining an image denoising problem and then discuss various image denoising approaches. MSE and SNR are used as the primary tools for noise removal in the project. To get an SNR of 20–30 dB, this filter would not degrade the image or lose crucial information. An issue noticed was that the SNR and blurriness appeared to be correlated. SNR, on the other hand, grew in proportion to the image's fuzziness. These methods are used to detect tumors.

Known also as Perona–Malik diffusion, anisotropic diffusion in the field of image processing and computer vision reduces noise in images while preserving critical characteristics such as edges and lines that aid in the interpretation of the image. If you think of anisotropic diffusion as an image generation method, it is similar to the diffusion process that produces a parameterized family of gradually blurrier images. When using the anisotropic diffusion filter, often known as ADF, it is possible to keep the image's borders while simultaneously adaptively reducing noise from the picture. Anisotropic diffusion filters frequently make use of the technique of spatial regularization. When building their models, anisotropic models take into account a number of other factors in addition to the modulus of the edge detector. Anisotropy was initially included into diffusion processes as a response to the need to manage one-dimensional features such as line-like forms.

An image processing approach that changes the pixels in the picture comes into play later in the process. There are two ways to identify pixels in a grayscale image: either utilising complex image processing techniques or a simpler set of

operations that do not require as much arithmetic. When we dilate an image, we are essentially expanding it. Adding pixels to an image's borders increases the number of pixels in an object's area. It is under the command of the structural element. After the dilation procedure is complete, the brain tumor is discovered.

3.1. Algorithm

Step 1. Import an image; in this case, MRI scan image is acquired from database.

Step 2. Take RGB image as input and convert it to grayscale before storing it in another variable to calculate the mean luminance (intensity of light).

Step 3. Display of PSD estimate via mesh grid image visualization.

The PSD of the signal is computed from discrete Fourier transform of image as

$$P((U,V)) = \frac{1}{N}|F(U,V)|^2, \tag{1}$$

where N is considered as the width of the frequency spectrum.

P (U, V) is the PSD of the image.

F (U, V) is the discrete Fourier transform of image $f(x, y)$ given by

$$F(U,V) = F\{f(x,y)\}. \tag{2}$$

We can estimate the visualization of base image using the mesh grid PSD.

Step 4. A grayscale PSD image estimates the PSD visualization of the base image.

Step 5. Random noise will be added to the PSD of the image's PSD.

Step 6. Noisy image as a result is obtained.

Step 7. Mesh grid PSD can be attained to estimate for the visualization of noisy image.

Step 8. Once again, we obtain the PSD of the noisy image.

Step 9. The PSD of the noisy image output is provided.

Step 10. The Woelfel filter output image is attained.

It provides the PSD of the output image, and the SNR of the output image is higher when compared to the existing method, which improves image quality.

Step 11. The highest quality image the detector receives is the output image of the Woelfel filter.

Step 12. The outcomes from filter are fed to the anisotropic diffusion to provide a thresholded image by highlighting the tumor.

Step 13. The morphological operation output image is subjected to dilation.

Let A and B be sets of image function, and the dilation of A by B is defined as

$$A \oplus B = \left\{ z | (\hat{B}) \cap A \neq \varnothing \right\}. \tag{3}$$

In dilatation, set B is frequently referred to as the structural element. This equation is based on finding B's reflection about its origin and shifting it by z; in the meantime, $\hat{B}$ and A overlap by at least one element.

Step 14. The tumor is detected in the brain after the dilation process is completed.

4. Experimental Results and Analysis

The brain BMP scan image was loaded from a medical database for the initial step of the inquiry and is depicted in Figure 1 as an example of what was done. The PSD estimate for the noiseless BMP scan was calculated and displayed using two different methods, as depicted in Figure 2. This is because the power spectral density (PSD) analysis of an image must be performed in two dimensions based on pixel value and position. A three-dimensional (3D) recording of the mesh grid portrayed the PSD estimation. The use of PSD analysis can be highly beneficial when attempting to determine the frequency content of photographs. Determining the frequency content of images is the first step in many different strategies for processing photos, such as compression, edge identification, and analysis.

Figure 3 depicts a 2D representation of the PSD estimation in greyscale, as depicted in Figure 4. These photographs were created with the help of the standard PSD code. It is possible to measure the power spectral density (PSD) or power spectrum of a signal by looking at how much power it has over a wide range of frequencies. It is possible to derive an estimate of the PSD at frequency by multiplying the Fourier components by their complex conjugate and scaling the result by the number of samples taken. Figure 5 illustrates how noise accumulates over time to produce a cluttered image.

This produces the mesh grid PSD estimate shown in Figure 6 as well as the corresponding grayscale PSD visualization in frequency domain shown in Figure 7. Both of these results are given in Figure 7. It was possible to acquire these results by without applying any filters during the preprocessing stage. Figure 8 shows the output picture obtained after applying an ideal low-pass filter to the imported input image. Figure 9 shows the PSD mesh grid plot visualization created in conjunction with the output image obtained after applying an ideal low-pass filter to the imported input image. It can be noticed that the image has been smoothed, and the effect is blurry in the eyesight since the

image's clear details have been obscured by the smoothing. An increase can also be noted in the PSD estimation visualization, which is also on the rise. For the ideal low-pass filter, as shown in Figure 10, the suitable frequency-domain transfer image, which has a ripple-like structure away from the estimate's center, is shown in Figure 11.

The work is further carried out by means of applying the novel Woelfel filter, and its output is displayed in Figure 11, and it indicates a smooth enhancement by highlighting the significant features in the original image even though it has been deteriorated by the additive noise. The corresponding mesh grid of the output image for its PSD values and a clear indication of the detail enhancement can be observed from the center of mesh grid (see Figure 12). Furthermore, its grayscale PSD estimate in frequency domain is achieved to see that the ripples have been reduced during the use of Woelfel filter (see Figure 13).

The obtained results for three stages such as no filter, low-pass filter, and after application of Woelfel filter are tabulated in Table 1 based on terms of the prominent attributes such as peak signal to noise ratio (PSNR), normalized absolute error (NAE), structural content (SC), and normalized cross-correlation (NCC). The graphical representation for these values is represented in Figure 14 for PSNR values and Figure 15 for normalized absolute error (NAE), structural content (SC), and normalized cross-correlation (NCC).

It is obvious from Figure 14 that the proposed filter during preprocessing stage can provide an optimal and best PSNR value when compared to no filter and ideal low-pass filter. From Figure 15, it can be noticed that normalized absolute error (NAE) and structural content (SC) values are less for proposed filter, whereas the normalized cross-correlation (NCC) value indicates the higher side which is the optimal solution during the preprocessing stage.

Using the PSNR, one may determine the quality of an image that has been distorted by noise and blur. The MSE is what determines the PSNR value. When comparing two images, the mean squared error (MSE) between the pixel intensities and the ratio of the greatest possible intensity to the computed value yields the PSNR (or peak signal to noise ratio).

This is the typical method for detecting blur in real-time images, and it may be applied to any image. This estimates the difference between the original image and the reconstructed image in terms of numerical values. An image's structural content is concerned with how its pixels are arranged in relation to each other. Correlation functions are another way of expressing how close two digital images are. In order to compare two collections of photographs, the NCC is a metric that is used. Images can initially be normalized in image processing applications where the brightness of the image can change owing to lighting and exposure situations. It is a tool for counting how many times a pattern or object appears in a photograph. The degree to which the original and rebuilt images are similar or distinct is one of the most commonly utilised parameters in image reconstruction.
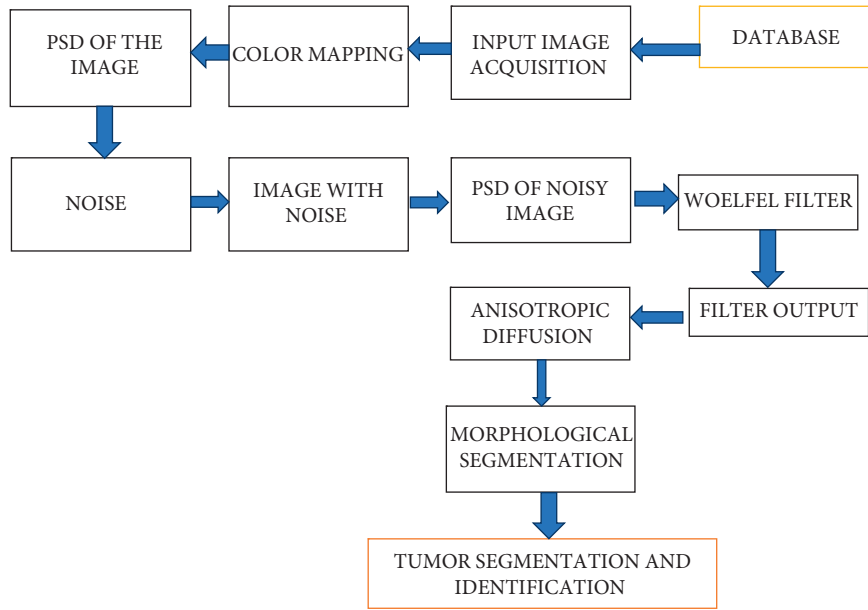
FIGURE 1: Block diagram for medical image denoising via Woelfel image noise filter.
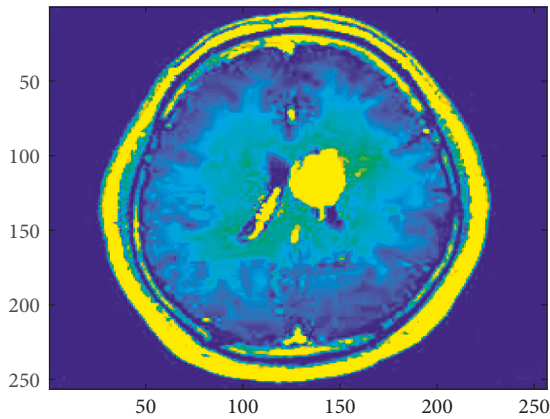
FIGURE 2: Brain BMP scan base image.
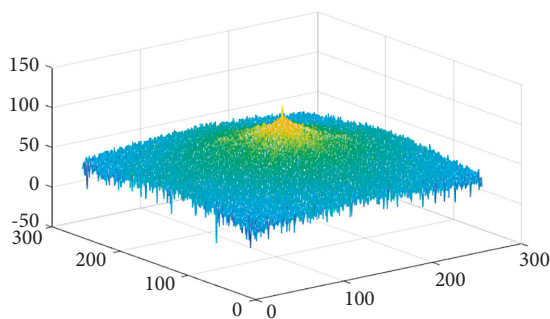
FIGURE 3: Grayscale PSD estimate.

FIGURE 4: Mesh grid PSD.
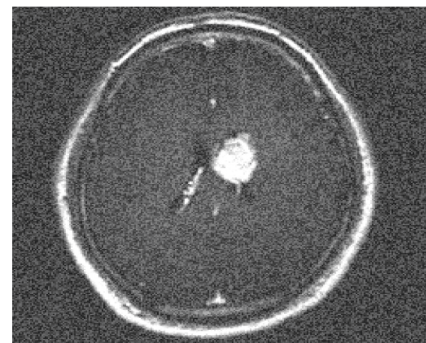
FIGURE 5: Noisy brain BMP scan image.

No filter, low-pass filter, and Woelfel filter findings are shown in Table 2 in terms of mean square error (MSE) and maximum difference (MD), respectively, for the three stages.

The difference between predicted and expected outcomes is calculated using the MSE. An image improvement technique that removes noise and blur is evaluated using this
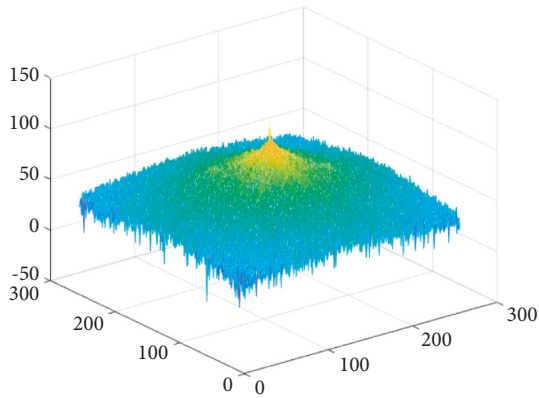
FIGURE 6: Mesh grid PSD estimate.
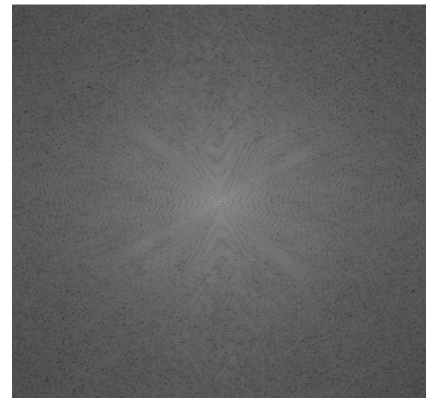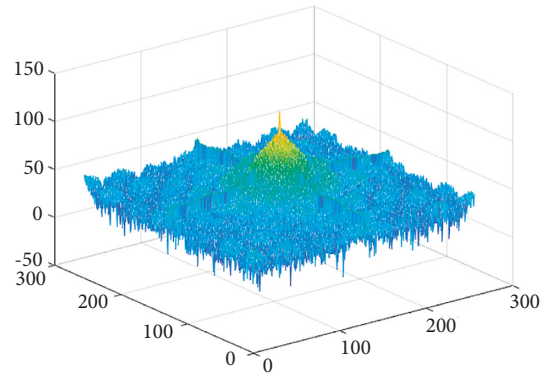

FIGURE 9: Mesh grid PSD estimate visualization.

FIGURE 7: Grayscale PSD visualization.
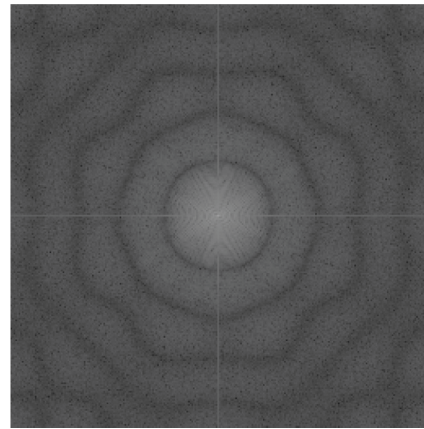
FIGURE 10: Grayscale PSD estimate.
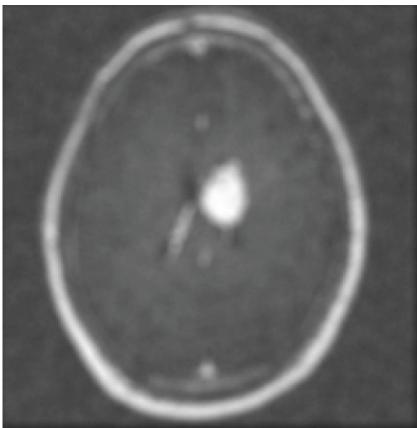
FIGURE 8: Ideal low-pass filter.
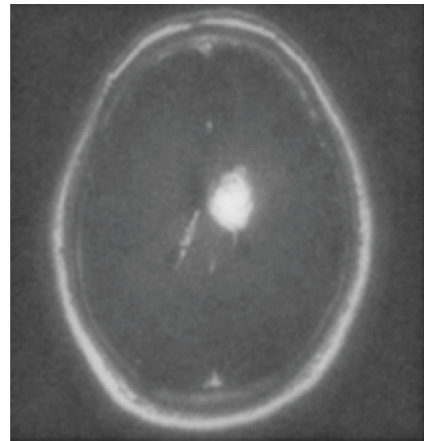
FIGURE 11: Novel Woelfel filter output.

metric, which is called the dispersion metric. It can be seen in Figure 16 that the proposed filter has a smaller mean square error (MSE), which implies that it is the best solution for preprocessing.

The dynamic range of a picture is determined by the MD, which is inversely proportional to contrast. To do this, a low-pass filter is used to suppress the image's higher frequency components, which correspond to the sharp edges in the
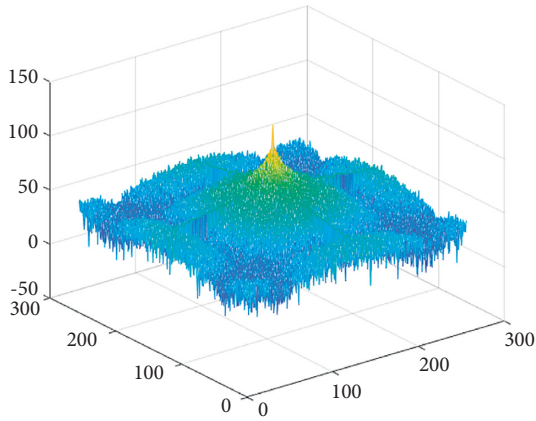
Figure 12: Mesh grid PSD estimate.
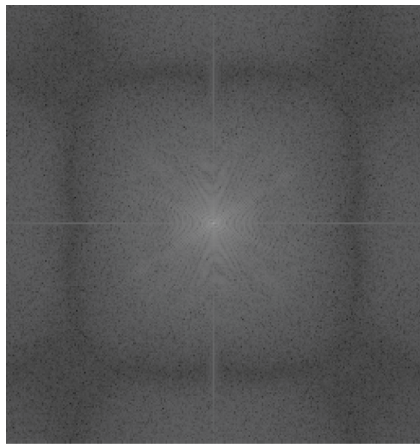
Figure 13: Grayscale PSD estimate.

Table 1: Parametric comparison for filters.

Parameters	Unfilter	LPF	Woelfel filter
PSNR	8.7833	21.8159	23.4202
Normalized absolute error (NAE)	0.3785	0.2545	0.1264
Structural content (SC)	1.086	1.074	0.9934
Normalized cross-correlation (NCC)	0.983	0.9918	0.9935
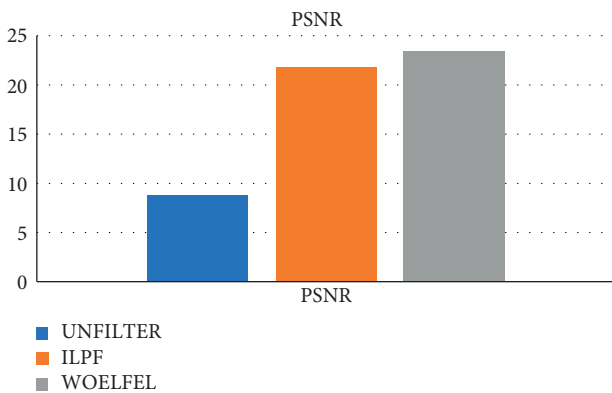
Figure 14: Comparison plot for PSNR values.
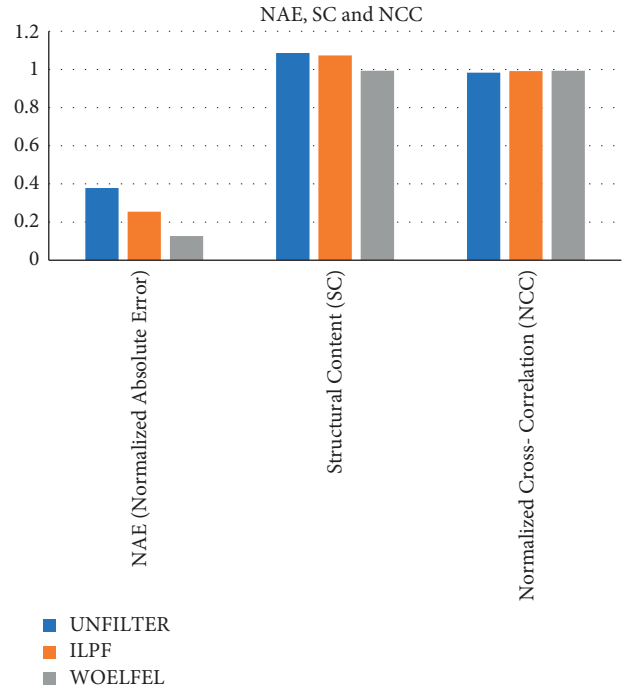
Figure 15: Comparison plot for NAE, SC, and NCC values.

Table 2: Parametric comparison of MSE and MD for filters.

Parameters	Unfilter	LPF	Woelfel filter
MSE	689.14	488.9	230.2
Maximum difference (MD)	673.32	453.54	132.76
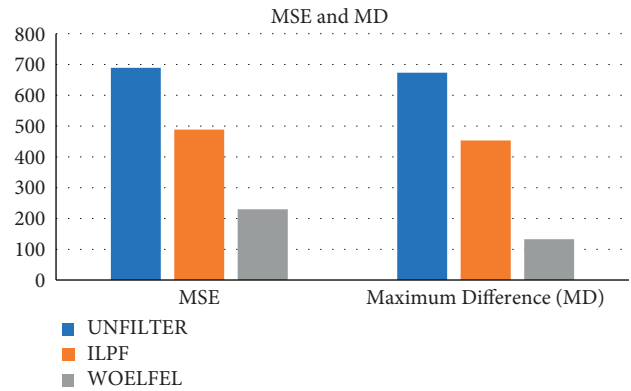
Figure 16: Comparison plot for MSE and MD values.

image. The image filtering technique that was carried out in this work has significant parameters that correspond well with the subjective sense of quality that a human observer can have on the images that were produced as a result of the procedure.

Images like the one shown in Figure 17 can be used to generate parameterized families of successively more and more blurred images using a diffusion process in order to achieve an exact detection of a brain tumor after superimposition on the original image as shown in Figure 18.
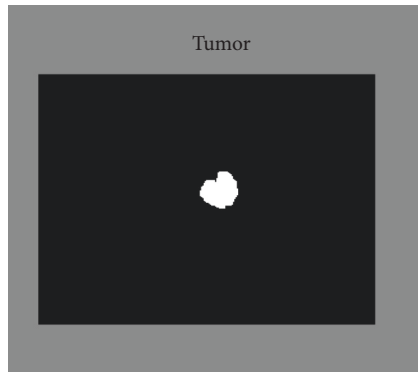
FIGURE 17: Brain tumor detection output.
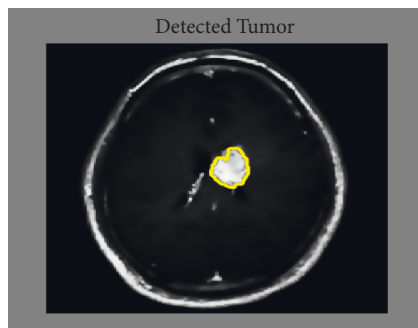
FIGURE 18: Exact brain tumor detection output after superimposition.

5. Conclusion

Radiation oncology researchers have developed a simple algorithm for tumor segmentation using MRI. Segmentation is carried out using morphological segmentation approaches mixed with anisotropic diffusion, and enhancement is accomplished using a new Woelfel filter. While keeping small details in the image, the new feature accurately detects the boundary. In order to perform morphological operations on tumors, a series of pretreatment steps must be completed beforehand. Before postprocessing, it is possible to see a clearer picture of the final image's PSD values and the degree to which the mesh grid has been enhanced in simulation results. A novel Woelfel filter reduces ripples to estimate grayscale PSD in the frequency domain. As a result, the new Woelfel filter has yielded better results in terms of important parameters such as peak signal to noise ratio (PSNR), normalized absolute error (NAE), structural content (SC), normalized cross-correlation (NCC), mean square error (MSE), and maximum difference (MD). As a further work, feature extraction procedures are required to work on all types of imagery by maintaining the integrity of the information, which can be a limitation of the work after repeated stage of filtering.

Data Availability

The processed data are available upon request from the corresponding author.

References

[1] K. Clark, B. Vendt, K. Smith et al., "The cancer imaging archive (TCIA): maintaining and operating a public information repository," *Journal of Digital Imaging*, vol. 26, no. 6, pp. 1045–1057, 2013.

[2] W.-C. Lin, E. C.-K. Tsao, and C.-T. Chen, "Constraint satisfaction neural networks for image segmentation," in *Artificial Neural Networks*, T. Kohonen, K. Mkisara, 0. Simula, and J. Kangas, Eds., vol. 25, no. 7, pp. 1087–1090, 1991.

[3] K. Khambhata, "Multiclass classification of brain tumor in MR images," *International Journal of Innovative Research in Computer and Communication Engineering*, vol. 4, no. 5, pp. 8982–8992, 2016.

[4] N. Singh and N. J. Ahuja, "Bug model based intelligent recommender system with exclusive curriculum sequencing for learner-centric tutoring," *International Journal of Web-Based Learning and Teaching Technologies*, vol. 14, no. 4, pp. 1–25, 2019.

[5] G. Kaur, "MRI brain tumor segmentation methods-a review," *International Journal of Current Engineering and Technology*, vol. 6, no. 3, pp. 760–764, 2016.

[6] V. Das, "Techniques for MRI brain tumor detection: a survey," *International Journal of Research in Computer Applications & Information Technology*, vol. 4, no. 3, pp. 53–56, 2016.

[7] G. Mohan and M. M. Subashini, "MRI based medical image analysis: survey on brain tumor grade classification," *Biomedical Signal Processing and Control*, vol. 39, pp. 139–161, 2018.

[8] A. Işın, C. Direkoğlu, and M. Şah, "Review of MRI-based brain tumor image segmentation using deep learning methods," *Procedia Computer Science*, vol. 102, pp. 317–324, 2016.

[9] L. Joo, S. C. Jung, H. Lee, S. Y. Park, M. Kim, and J. E. Park, "Stability of MRI radiomic features according to various imaging parameters in fast scanned T2-FLAIR for acute ischemic stroke patients," *Scientific Reports*, vol. 11, no. 1, Article ID 17143, 2021.

[10] H. Chen, Q. Zou, and Q. Wang, "Clinical manifestations of ultrasonic virtual reality in the diagnosis and treatment of cardiovascular diseases," *Journal of Healthcare Engineering*, vol. 2021, Article ID 1746945, 12 pages, 2021.

[11] E. S. A. El-Dahshan, H. M. Mohsen, K. Revett, and A. B. M. Salem, "Computer-aided diagnosis of human brain tumor through MRI: a survey and a new algorithm," *Expert Systems with Applications*, vol. 41, no. 11, pp. 5526–5545, 2014.

[12] B. Mishra, N. Singh, and R. Singh, "Master-slave group based model for co-ordinator selection, an improvement of bully algorithm," in *Proceedings of the 2014 International Conference on Parallel, Distributed and Grid Computing*, Solan, India, December 2014.

[13] E. Rashid, M. D. Ansari, V. K. Gunjan, and M. Ahmed, "Modern Approaches in Machine Learning and Cognitive Science," *A Walkthrough*, vol. 885, pp. 237–245, 2020.

[14] A. Aslam, E. Khan, and M. S. Beg, "Improved edge detection algorithm for brain tumor segmentation," *Procedia Computer Science*, vol. 58, pp. 430–437, 2015.

[15] S. Bauer, *Medical Image Analysis and Image-Based Modeling for Brain Tumor Studies*, Universita t Bern, Switzerland, 2013.

[16] E. Rashid, M. D. Ansari, V. K. Gunjan, and M. Khan, "Modern Approaches in Machine Learning and Cognitive Science," *A Walkthrough*, vol. 885, pp. 227–235, 2020.

[17] P. Natarajan and N. Krishnan, "Natasha sandeep kenkre, shraiya nancy, bhuvanesh pratap singh, "tumor detection using threshold operation in MRI brain images," in *Proceedings of the IEEE International Conference on Computational Intelligence and Computing Research*, Coimbatore, India, December 2014.

[18] D. D. Patil and S. G. Deore, "Medical image segmentation: a review," *International Journal of Computer Science and Mobile Computing*, vol. 2, no. 1, pp. 22–27, 2013.

[19] N. Singh and N. J. Ahuja, "Implementation and evaluation of intelligence incorporated tutoring system," *International Journal of Innovative Technology and Exploring Engineering*, vol. 8, no. 10C, pp. 4548–4558, 2019.

[20] T. Saba, A. Sameh Mohamed, M. El-Affendi, J. Amin, and M. Sharif, "Brain tumor detection using fusion of hand crafted and deep learning features," *Cognitive Systems Research*, vol. 59, pp. 221–230, 2020.

[21] A. Kashyap, V. K. Gunjan, A. Kumar, F. Shaik, and A. A. Rao, "Computational and clinical approach in lung cancer detection and analysis," *Procedia Computer Science*, vol. 89, pp. 528–533, 2016.

[22] V. Wasule, "Classification of brain MRI using SVM and KNN classifier," in *Proceedings of the Third International Conference on Sensing, Signal Processing and Security (ICSSS)*, pp. 218–223, Chennai, India, May 2017.

[23] F. Shaik, A. Kumar Sharma, S. Musthak Ahmed, V. Kumar Gunjan, and C. Naik, "An improved model for analysis of Diabetic Retinopathy related imagery," *Indian Journal of Science and Technology*, vol. 9, no. 44, p. 44, 2016.

[24] M. Al-Ayyoub, G. Husari, O. Darwish, and A. Alabed-alaziz, "Machine learning approach for brain tumor detection," in *Proceedings of the 3rd International Conference on Information and Communication Systems*, pp. 1–4, Irbid Jordan, April 2012.

[25] S. Javeed Hussain, T. Satya Savithri, and P. V. Sree Devi, "Segmentation of tissues in brain MRI images using dynamic neuro-fuzzy technique," *International Journal of Soft Computing and Engineering (IJSCE) ISSN*, vol. 1, p. 6, 2012.

[26] M. D. Ansari, V. K. Gunjan, and E. Rashid, *On Security and Data Integrity Framework for Cloud Computing Using Tamper-Proofing*, pp. 1419–1427, Springer, Berlin, Germany, 2021.

[27] K. S. Angel Viji and J. Jayakumari, "Performance evaluation of standard image segmentation methods and clustering algorithms for segmentation of MRI brain tumor images," *European Journal of Scientific Research ISSN*, vol. 79, no. 2, pp. 166–179, 2012.

[28] P. S. Prasad, B. Sunitha Devi, M. Janga Reddy, and V. K. Gunjan, "A survey of fingerprint recognition systems and their applications, Lecture Notes in Electrical Engineering," in *Proceedings of the International Conference on Communications and Cyber Physical Engineering*, pp. 513–520, Singapore, September 2018.

[29] S. Datta, Dr, and M. Chakraborty, "Brain tumor detection from pre-processed MR images using segmentation techniques," in *Proceedings of theIJCA Special Issue on "2nd National ConferenceComputing, Communication and Sensor Network" CCSN*, 2011.

[30] S. R. Kannan, "Segmentation of MRI using new unsupervised fuzzy C-mean algorithm," *ICGSTGVIP Journal*, vol. 5, 2005.

[31] N. Singh, A. Kumar, and N. J. Ahuja, "Implementation and evaluation of personalized intelligent tutoring system," *International Journal of Innovative Technology and Exploring Engineering*, vol. 8, pp. 46–55, 2019.

[32] N. Singh, N. J. Ahuja, and A. Kumar, "A novel architecture for learner-centric curriculum sequencing in adaptive intelligent tutoring system," *Journal of Cases on Information Technology*, vol. 20, no. 3, pp. 1–20, 2018.

[33] H. Sahu and N. Singh, "Software-defined storage, Advances in Systems Analysis, Software Engineering, and High Performance Computing," in *Proceedings of the Innovations in Software-Defined Networking and Network Functions Virtualization*, pp. 268–290, IGI Global, Hershey, PA, USA, 2018.

WILEY | Hindawi

Research Article

Two Complex Graph Operations and their Exact Formulations on Topological Properties

Shehla Hameed [ID],[1] Muhammad Kamran Jamil [ID],[1] Muhammad Waheed [ID],[1] Muhammad Azeem [ID],[1] and Senesie Swaray [ID][2]

[1]*Department of Mathematics, Riphah Institute of Computing and Applied Sciences, Riphah International University, Lahore, Pakistan*
[2]*Tree Crops Unit, Sierra Leone Agricultural Research Institute, Freetown, Sierra Leone*

Correspondence should be addressed to Senesie Swaray; senesieswaray74@gmail.com

Graph operations are utilized for developing complicated graph structures from basic graphs, and these basic graphs can help to understand the properties of complex networks. While on the other side, the topological descriptor is known as a numeric value that is associated with the graph of a network. It has enormous practical applications in chemistry and other fields of science. This particular work in this draft is the extended work and investigated the first, second, first multiplicative, first reformulated Zagreb indices, and the forgotten index of subdivision double corona and subdivision double neighborhood corona products.

1. Introduction

A topological index is a number associated with a graph of some network. With the help of this number, we can describe some properties of the network. Especially in organic chemistry, topological indices are used to predict some physical, chemical, or biological properties of organic compounds. Topological indices are key topics in the study of quantitative structural properties of a chemical network [1–5].

For a graph $\lambda = (V_\lambda, E_\lambda)$, the vertex and edge sets are denoted by V_λ and E_λ. The number of elements in V_λ and E_λ is called the order (n) and the size (m), respectively, of λ. A graph of order n and size m is denoted by $\lambda(n, m)$. The set of vertices adjacent to the vertex $v \in V_\lambda$ is called the neighborhood set of v and the number of elements in the neighborhood set the degree of v in λ is denoted by $d_\lambda(v)$ [6–10].

The study of the topological index started in 1947, and after that, hundreds of topological indices have been presented depending on the nature of applications for different

chemical compounds. In 1972, the researchers in [11] introduced the first and second Zagreb indices. For a graph λ, these topological indices are defined as

$$M_1(\lambda) = \sum_{v \in V_\lambda} d_\lambda(v)^2 = \sum_{uv \in E_\lambda} [d_\lambda(u) + d_\lambda(v)],$$

$$M_2(\lambda) = \sum_{uv \in E_\lambda} d_\lambda(u) d_\lambda(v). \tag{1}$$

The researchers of [12, 13], introduced multiplicative variants of ordinary Zagreb indices. These topological indices are used to study molecular chirality, complexity, heterosystems, and Ze-isomerism. The first and second multiplicative Zagreb indices are defined as

$$\prod_1(\lambda) = \prod_{v \in V_\lambda} d_\lambda(v)^2,$$

$$\prod_2(\lambda) = \prod_{uv \in E_\lambda} d_\lambda(u) d_\lambda(v). \tag{2}$$

In 2015, researchers in [14, 15] suggested a forgotten topological index that is comparable to the first Zagreb index in its applications. The forgotten topological index is also known as F-index, and it is defined as

$$F(\lambda) = \sum_{v \in V_\lambda} d_\lambda(v)^3 = \sum_{uv \in E_\lambda} \left[d_\lambda(u)^2 + d_\lambda(v)^2 \right]. \quad (3)$$

In 2004, Milicevic et al. [16] proposed reformulated Zagreb indices using edge-degrees rather than vertex-degrees. Mathematically, it is expressed as

$$EM_1(\lambda) = \sum_{e \in E_\lambda} d(e)^2 \text{where } d(e) = d(u) + d(v) - 2. \quad (4)$$

For $d(e) = d(u) + d(v)$, the above expression is known as the first hyper Zagreb index $HM_1(\lambda)$.

Complex network structures or large molecular structures can be constructed by applying some graph operations on simple graphs. Furthermore, these simple graphs can help to describe some properties of these structures. For example, the Cartesian product provides a significant model for connecting computers [17, 18].

For graphs $\lambda_1(n_1, m_1)$ and $\lambda_2(n_2, m_2)$, the corona product $\lambda_1 \circ \lambda_2$ is obtained by taking one copy of λ_1, n_1 copies of λ_2, and joining j^{th} vertex of λ_1 to every vertex J^{th} copy of λ_2 [19]. A special graph obtained by attaching a vertex in the each edge of λ is called the subdivision graph of λ and is symbolized by λ^s [20].

Let $\lambda(n, m)$, $\lambda_1(n_1, m_1)$, and $\lambda_2(n_2, m_2)$ be three graphs. The operation known as subdivision double corona product of λ, λ_1, and λ_2 and symbolized by $\lambda^s \circ (\lambda_1, \lambda_2)$, and is attained by making single copy of λ^s, n copies of λ_1, m copies of λ_2, and after that, by attaching the ith old vertex, $u(o)$, of λ^s to each vertex of the ith copy of λ_1 and j^{th} new vertex $u(N)$ of λ^s to each vertex of the jth copy of λ_2 [21]. An illustration of subdivision double corona product is shown in Figure 1.

For the above three graphs, the subdivision double neighborhood corona product, $\lambda^s \cdot (\lambda_1, \lambda_2)$, is the graph attained by making single copy of λ^s, n copies of λ_1, m copies of λ_2 and after that, by attaching the neighborhood vertices of the ith old vertex $u(o)$ of λ^s to every vertex of the ith duplicate of λ_1 and joining the neighborhood vertices of the jth new vertex $u(N)$ of λ^s to every vertex of the jth duplicate of λ_2 [21]. Figure 2 explains the notation of $(\lambda^s \cdot (\lambda_1, \lambda_2))$.

In [22], the authors investigated the first and second Zagreb indices of the Cartesian, composition, join, disjunction, and symmetric difference graph operations. The author in [23] computed the forgotten topological index of different corona products of graphs and the author in [24] gave the exact expressions of Zagreb indices of the generalized hierarchical product of graphs. For more discussion and results, we refer to [25, 26]. There are some new and recent topics related to this study is found, one can see [27–31].

The Laplacian spectrum of double neighborhood corona graphs are found in the literature of [21], and the main results are presented.

Theorem 1. *Let λ be a t-regular graph on n vertices, m edges, λ_1 and λ_2 be any two graphs on n_1 and n_2 vertices, respectively. Then, the Laplacian spectrum of $\lambda^s \circ (\lambda_1, \lambda_2)$ comprises*

  (i) $\eta^4 - (n_1 + n_2 + t + 4)\eta^4 + [(n_1 + 1)(n_2 + 3) + 2(t + 1) + n_2 t + \eta_j(\lambda)]\eta^2 - [t(n_2 + 1) + 2 (n_1 + \eta_j(\lambda) + 1)]\eta + \eta_j(\lambda) = 0$, for $1 \le j \le n$;

  (ii) $n_2 + 3 \pm \sqrt{(n_2 + 3)^2 - 8/2}$ repeated $m - n$ times each;

  (iii) $\eta_j(\lambda_1) + 1$ repeated n times, for $2 \le j \le n_1$;

  (iv) $\eta_j(\lambda_2) + 1$ repeated m times, for $2 \le j \le n_2$.

Theorem 2 (see [21]). *Let λ be a t-regular graph on n vertices, m edges, λ_1 and λ_2 be any two graphs on n_1 and n_2 vertices, respectively. Then, the Laplacian spectrum of $\lambda^s \cdot (\lambda_1, \lambda_2)$ comprises*

  (i) all the roots of the equation

$$
\begin{aligned}
&\eta - (n_1 + n_2 + t + 4) + \left[(n_2 + 4)(n_1 + t) + 1 - \left(2r - \eta_j(\lambda)\right)(n_1 + n_2)\right] \\
&- \sqrt{2t - \eta_j(\lambda)}\,\bigg]\eta^2 - \left[n_1 + n - 2 + t + 2 - \left(2t - \eta_j(\lambda)\right)n_1(n_1 + t + 1)\right. \\
&+ n_2(n_2 + 3)\bigg) + 2\left(\left(n_1 + t\right)(n_2 + 2) - \sqrt{2t\eta_j(\lambda)}\,\right)\bigg] + (n_1 + t)(n_2 + 2) - \\
&\sqrt{2t - \eta_j(\lambda)} + \left(2t - \eta_j(\lambda)\right)\left(n_1 n_2 - n_1 - n_2\right) = 0, \quad \text{for } 1 \ge j \ge n.
\end{aligned}
\tag{5}
$$

  (ii) $n_2 + 2$ repeated $m - n$ times;

  (iii) 1 repeated $m - n$ times;

  (iv) $\eta_i(\lambda_1) + 1$ repeated n times, for $2 \le i \le n_1$;

  (v) $\eta_i(\lambda_2) + 1$ repeated n times, for $2 \le i \le n_2$.

In this paper, we extend the work and investigated some degree-based topological indices of these graph operations.

2. Main Results

The current section contained the main results which include the formulation of some degree-based topological indices such as first and second Zagreb, first multiplicative Zagreb, first reformulated Zagreb, the forgotten indices of subdivision double corona product, and subdivision double neighborhood corona product of graphs.

Following is the famous relationship between arithmetic and geometric means.
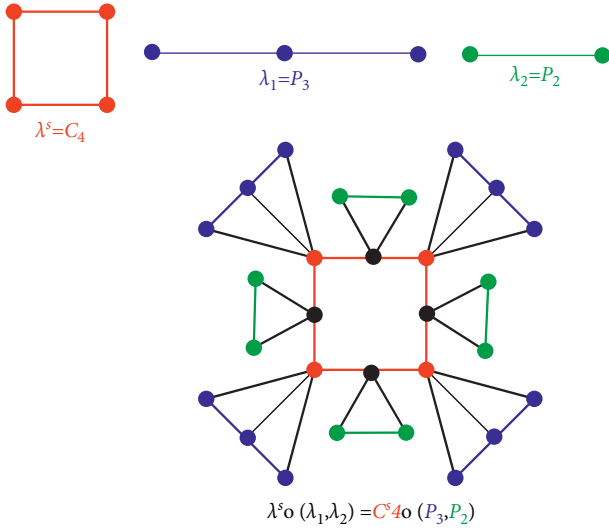
Figure 1: Subdivision double corona product $(C_4^s \circ (P_3, P_2))$.
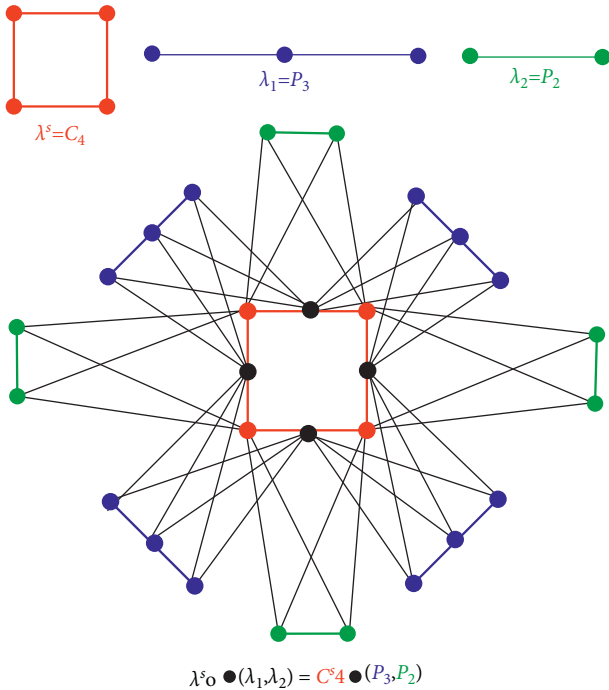
Figure 2: Subdivision double neighborhood corona product $(C_4^s \cdot (P_3, P_2))$.

Lemma 1 (AM-GM Inequality). *Let $a_1, a_2, \ldots, a_n$ be non-negative numbers. Then,*

$$\frac{a_1 + a_2 + \cdots + a_n}{2} \geq (a_1 a_2 \ldots a_n)^{1/n}, \quad (6)$$

and the equality holds if and only if $a_1 = a_2 = \ldots = a_n$ are equal.

Next to lemmas are the direct results from the definitions of the subdivision double corona product and subdivision neighborhood corona product of graphs.

Lemma 2. *Let λ, λ_1, and λ_2 are three graphs having order n, n_1, and n_2, respectively. Then, the degree behavior of the vertices in subdivision double corona product is given as*

$$d_{(\lambda^s \circ (\lambda_1, \lambda_2))}(v) = \begin{cases} d_\lambda(v) + n_1 & \text{if } v \in V_\lambda; \\ d_{\lambda_1}(v) + 1 & \text{if } v \in V_{\lambda_1}; \\ d_{\lambda_2}(v) + 1 & \text{if } v \in V_{\lambda_2}; \\ n_2 + 2 & \text{if } v \in V_{\lambda^s}. \end{cases} \quad (7)$$

Lemma 3. *Let λ, λ_1, and λ_2 are graphs having order n, n_1, and n_2, respectively, then the degrees of the vertices in subdivision double neighborhood corona product is*

$$d_{(\lambda^s \bullet (\lambda_1, \lambda_2))}(v) = \begin{cases} d_\lambda(v) + 2n_2 & \text{if } v \in V_\lambda; \\ d_{\lambda_1}(v) + 2 & \text{if } v \in V_{\lambda_1}; \\ d_{\lambda_2}(v) + 2 & \text{if } v \in V_{\lambda_2}; \\ 2(1 + n_1) & \text{if } v \in V_{\lambda^s}. \end{cases} \quad (8)$$

Following is our first main result, which gives the first Zagreb index of the subdivision double corona product in terms of the first Zagreb indices of basic graphs, their orders, and sizes.

Theorem 3. *Let $\lambda(n, m)$, $\lambda_1(n_1, m_1)$, and $\lambda_2(n_2, m_2)$ be the simple connected graphs. Then, the first Zagreb index of the subdivision double corona product, $(\lambda^s \circ (\lambda_1, \lambda_2))$, is given as*

$$\begin{aligned} M_1(\lambda^s \circ (\lambda_1, \lambda_2)) = {} & M_1(\lambda) + 4mn_1 + nn_1^2 \\ & + nM_1(\lambda_1) + 4m_1 n + nn_1 + mM_1(\lambda_2) \\ & + 4m_2 m + mn_2 + m(2 + n_2)^2. \end{aligned}$$

$$(9)$$

Proof. From the concept of topological descriptor named the first Zagreb index, we have got

$$M_1(\lambda^s \circ (\lambda_1, \lambda_2)) = \sum_{v \in V(\lambda^s \circ (\lambda_1, \lambda_2))} d_{\lambda^s \circ (\lambda_1, \lambda_2)}(v)^2. \quad (10)$$

Now, we apply Lemma 2,

$$M_1(\lambda^s \circ (\lambda_1, \lambda_2)) = \sum_{v \in V_\lambda} (d_\lambda(v) + n_1)^2$$

$$+ n \sum_{v \in V_{\lambda_1}} (d_{\lambda_1}(v) + 1)^2 + m \sum_{v \in V_{\lambda_2}} (d_{\lambda_2}(v) + 1)^2 + \sum_{v \in V_{\lambda^s}} (2 + n_2)^2$$

$$= \sum_{v \in V_\lambda} d_\lambda(v)^2 + 2n_1 \sum_{v \in V_\lambda} d_\lambda(v) + n_1^2 \sum_{v \in V_\lambda} 1 + n \left[\sum_{v \in V_{\lambda_1}} d_{\lambda_1}(v)^2 + 2 \sum_{v \in V_{\lambda_1}} d_{\lambda_1}(v) + \sum_{v \in V_{\lambda_1}} 1 \right]$$

$$+ m \left[\sum_{v \in V_{\lambda_2}} d_{\lambda_2}(v)^2 + 2 \sum_{v \in V_{\lambda_2}} d_{\lambda_2}(v) + \sum_{v \in V_{\lambda_2}} 1 \right] + (2 + n_2)^2 \sum_{v \in V_{\lambda^s}} 1$$

$$= M_1(\lambda) + 4mn_1 + nn_1^2 + nM_1(\lambda_1) + 4m_1 n + nn_1 + mM_1(\lambda_2) + 4m_2 m + mn_2 + m(2 + n_2)^2.$$

$$(11)$$

Hence, the required expression.

The next results put a bound on the first multiplicative Zagreb index for the subdivision double corona product. $\square$

Theorem 4. *Let $\lambda(n, m)$, $\lambda_1(n_1, m_1)$, and $\lambda_2(n_2, m_2)$ be the simple connected graphs. Then, the first multiplicative Zagreb index of the subdivision double corona product $(\lambda^s \circ (\lambda_1, \lambda_2))$ is given as*

$$\prod_1 (\lambda^s \circ (\lambda_1, \lambda_2)) \le \left[\frac{M_1(\lambda) + 4n_1 m + nn_1^2}{n} \right]^n \cdot \left[\frac{M_1(\lambda_1) + 4m_1 + n_1}{n_1} \right]^{nn_1}$$

$$(12)$$

$$\cdot \left[\frac{M_1(\lambda_2) + 4m_2 + n_2}{n_2} \right]^{mn_2} \cdot (2 + n_2)^{2m}.$$

Proof. From using the concept of the first multiplicative Zagreb index and Lemma 2, we have got

$$\prod_1 (\lambda^s \circ (\lambda_1, \lambda_2)) = \prod_{v \in V_{(\lambda^s \circ (\lambda_1, \lambda_2))}} d_{(\lambda^s \circ (\lambda_1, \lambda_2))}(v)^2$$

$$= \prod_{v \in V_\lambda} (d_\lambda(v) + n_1)^2 \times \left[\prod_{v \in V_{\lambda_1}} (d_{\lambda_1}(v) + 1)^2 \right]^n \times \left[\prod_{v \in V_{\lambda_2}} (d_{\lambda_2}(v) + 1)^2 \right]^m \times \prod_{v \in V_{\lambda^s}} (2 + n_2)^2$$

$$= \prod_{v \in V_\lambda} (d_\lambda(v)^2 + 2d_\lambda(v)(n_1) + n_1^2) \times \left[\prod_{v \in V_{\lambda_1}} (d_{\lambda_1}(v)^2 + 2d_{\lambda_1}(v) + 1) \right]^n$$

$$\times \left[\prod_{v \in V_{\lambda_2}} (d_{\lambda_2}(v)^2 + 2d_{\lambda_2}(v) + 1) \right]^m \times \prod_{v \in V_{\lambda^s}} (2 + n_2)^2$$

$$\le \left[\frac{\sum_{v \in V_\lambda} (d_\lambda(v)^2 + 2d_\lambda(v)n_1 + n_1^2)}{n} \right]^n \times \left[\frac{\sum_{v \in V_{\lambda_1}} (d_{\lambda_1}(v)^2 + 2d_{\lambda_1}(v) + 1)}{n_1} \right]^{nn_1}$$

$$\times \left[\frac{\sum_{v \in V_{\lambda_2}} (d_{\lambda_2}(v)^2 + 2d_{\lambda_2}(v) + 1)}{n_2} \right]^{mn_2} \times \left[\frac{\sum_{v \in V_{\lambda^s}} (2 + n_2)^2}{m} \right]^m$$

$$\le \left[\frac{\sum_{v \in V_\lambda} d_\lambda(v)^2 + 2n_1 \sum_{v \in V_\lambda} d_\lambda(v) + n_1^2 \sum_{v \in V_\lambda} 1}{n} \right]^n$$

$$\times \left[\frac{\sum_{v \in V_{\lambda_1}} d_{\lambda_1}(v)^2 + 2 \sum_{v \in V_{\lambda_1}} d_{\lambda_1}(v) + \sum_{v \in V_{\lambda_1}} 1}{n_1} \right]^{nn_1}$$

$$\times \left[\frac{\sum_{v\in V_{\lambda_2}} d_{\lambda_2}(v)^2 + 2\sum_{v\in V_{\lambda_2}} d_{\lambda_2}(v) + \sum_{v\in V_{\lambda_2}} 1}{n_2}\right]^{mn_2} \times \left[\frac{(2+n_2)^2 \sum_{v\in V_{\lambda^s}} 1}{m}\right]^{m}$$

$$= \left[\frac{M_1(\lambda) + 4n_1 m + nn_1^2}{n}\right]^{n} \times \left[\frac{M_1(\lambda_1) + 4m_1 + n_1}{n_1}\right]^{nn_1}$$

$$\times \left[\frac{M_1(\lambda_2) + 4m_2 + n_2}{n_2}\right]^{mn_2} \times (2+n_2)^{2m}.$$

(13)

The inequality is due to the Lemma 1. Equality in the last expression holds if and only if λ, λ_1, and λ_2 are regular graphs. □

Theorem 5. *Let* $\lambda(n, m)$, $\lambda_1(n_1, m_1)$, *and* $\lambda_2(n_2, m_2)$ *are three simple graphs and* $\lambda^s(nı, mı)$ *be the subdivided graph of* λ. *Then, the second Zagreb index of subdivision double corona product* $(\lambda^s\circ(\lambda_1, \lambda_2))$ *is given as*

$$M_2(\lambda^s\circ(\lambda_1, \lambda_2))$$
$$= nM_1(\lambda_1) + mM_1(\lambda_2) + nM_2(\lambda_1) + mM_2(\lambda_2) + 4m(m_1 + m_2)$$
$$+ (2n_1 + n_1 n_2)mı + mm_2 + n_1(3m + 2m_1 n + nn_1) + mn_2(2 + n_2 + 2m_2) +$$
$$\sum_{uv\in E_{\lambda^s}} (2d_\lambda(v) + n_2 d_\lambda(v)).$$

(14)

Proof. From using the concept of the second Zagreb index and Lemma 2, we have got

$$M_2(\lambda^s\circ(\lambda_1, \lambda_2)) = \sum_{uv\in E_{\lambda^s\circ(\lambda_1,\lambda_2)}} d_{\lambda^s\circ(\lambda_1,\lambda_2)}u \cdot d_{\lambda^s\circ(\lambda_1,\lambda_2)}v.$$

$$= \sum_{uv\in E_{\lambda^s}} (d_\lambda + n_1)(2 + n_2) + n \sum_{uv\in E_{\lambda_1}} (d_{\lambda_1}(u) + 1)(d_{\lambda_1}(v) + 1)$$

$$+ m \sum_{uv\in E_{\lambda_2}} (d_{\lambda_2}(u) + 1)(d_{\lambda_2}(v) + 1) + \sum_{\substack{u(o)\in V_{\lambda^s} \\ v\in V_{\lambda_1}}} (d_\lambda(u) + n_1)(d_{\lambda_1}(v) + 1)$$

$$+ \sum_{\substack{u(N)\in V_{\lambda^s} \\ v\in V_{\lambda_2}}} (2 + n_2)(d_{\lambda_2}(v) + 1)$$

$$= \sum_{uv\in E_{\lambda^s}} (2d_\lambda(u) + n_2 d_\lambda(u) + 2n_1 + n_1 n_2) + n \sum_{uv\in E_{\lambda_1}} (d_{\lambda_1}(u)d_{\lambda_1}(v) + d_{\lambda_1}(u))$$

$$+ d_{\lambda_1}(v) + 1) + m \sum_{uv\in E_{\lambda_2}} (d_{\lambda_2}(u)d_{\lambda_2}(v) + d_{\lambda_2}(u) + d_{\lambda_2}(v) + 1)$$

$$+ \sum_{\substack{u(o)\in V_{\lambda^s} \\ v\in V_{\lambda_1}}} (d_\lambda(u)d_{\lambda_1}(v) + d_\lambda(u) + n_1 d_{\lambda_1}(v) + n_1)$$

$$+ \sum_{\substack{u(N)\in V_{\lambda^s} \\ v\in V\lambda_2}} (2d_{\lambda_2}(v) + 2 + n_2 d_{\lambda_2}(v) + n_2)$$

$$= \sum_{uv \in E_{\lambda^s}} \left(2d_\lambda(u) + n_2 d_\lambda(u)\right) + \sum_{uv \in E_{\lambda^s}} \left(2n_1 + n_1 n_2\right) + n\left[\sum_{uv \in E_{\lambda_1}} d_{\lambda_1}(u) d_{\lambda_1}(v) + \sum_{uv \in E_{\lambda_1}} \left(d_{\lambda_1}(u) + d_{\lambda_1}(v)\right) + \sum_{uv \in E_{\lambda_1}} 1\right]$$

$$+ m\left[\sum_{uv \in E_{\lambda_2}} d_{\lambda_2}(u) d_{\lambda_2}(v) + \sum_{uv \in E_{\lambda_2}} \left(d_{\lambda_2}(u) + d_{\lambda_2}(v)\right) + \sum_{uv \in E_{\lambda_2}} 1\right] +$$

$$+ \sum_{\substack{u(o) \in V_{\lambda^s} \\ v \in V_{\lambda_1}}} d_\lambda(u) d_{\lambda_1}(v) + \sum_{\substack{u(o) \in V_{\lambda^s} \\ v \in V_{\lambda_1}}} \left(d_\lambda(u) + n_1 d_{\lambda_1}(v)\right)$$

$$+ n_1 \sum_{\substack{u(o) \in V_{\lambda^s} v \in V_{\lambda_1}}} 1 + \sum_{\substack{u(N) \in V_{\lambda^s} \\ v \in V_{\lambda_2}}} \left(2d_{\lambda_2}(v) + n_2 d_{\lambda_2}(v)\right) + \sum_{\substack{u(N) \in V_{\lambda^s} \\ v \in V_{\lambda_2}}} \left(2 + n_2\right)$$

$$\sum_{uv \in E_{\lambda^s}} \left(2d_\lambda(u) + n_2 d_\lambda(u)\right) + \left(2n_1 + n_1 n_2\right)\left|E_{\lambda^s}\right| + nM_2(\lambda_1) + nM_1(\lambda_1)$$

$$+ n\left|E_{\lambda_1}\right| + mM_2(\lambda_2) + mM_1(\lambda_2) + m\left|E_{\lambda_2}\right| + \sum_{u(o) \in V_{\lambda^s}} d_\lambda(u) \sum_{v \in V_{\lambda_1}} d_{\lambda_1}(v)$$

$$+ \sum_{u(o) \in V_{\lambda^s}} d_\lambda(u) \sum_{v \in V_{\lambda_1}} 1 + n_1 \sum_{u(o) \in V_{\lambda^s}} 1 \sum_{v \in V_{\lambda_1}} d_{\lambda_1}(v) + n_1 \sum_{u(o) \in V_{\lambda^s}} 1 \sum_{v \in V_{\lambda_1}} 1$$

$$+ 2 \sum_{u(N) \in V_{\lambda^s}} 1 \sum_{v \in V_{\lambda_2}} d_{\lambda_2}(v) + n_2 \sum_{u(N) \in V_{\lambda^s}} 1 \sum_{v \in V_{\lambda_2}} d_{\lambda_2}(v) + \left(2 + n_2\right) \sum_{u(N) \in V_{\lambda^s}} 1 \sum_{v \in V_{\lambda_2}} 1$$

$$= \sum_{uv \in E_{\lambda^s}} \left(2d_\lambda(u) + n_2 d_\lambda(u)\right) + \left(2n_1 + n_1 n_2\right)m\prime + nM_2(\lambda_1) + nM_1(\lambda_1) + nm_1$$

$$+ mM_2(\lambda_2) + mM_1(\lambda_2) + mm_2 + 4mm_1 + 2mn_1 + 2m_1 nn_1 + nn_1^2 + 4mm_2$$

$$+ 2mm_2 n_2 + mn_2 \left(2 + n_2\right).$$

$$(15)$$

After some simplification, we can get the required result.

The next result is about the first reformulated Zagreb index of the subdivision double corona product of graphs. □

Theorem 6. *Let $\lambda(n,m)$, $\lambda_1(n_1, m_1)$, and $\lambda_2(n_2, m_2)$ be the simple graphs and $\lambda^s(n\prime, m\prime)$ is the subdivision of the graph λ. Then, the first reformulated Zagreb index of the subdivision double corona product $(\lambda^s \circ (\lambda_1, \lambda_2))$ is given as*

$$EM_1\left(\lambda^s \circ (\lambda_1, \lambda_2)\right) = n_1 M_1(\lambda) + nM_1(\lambda_1) + mM_1(\lambda_2) + nHM_1(\lambda_1) + mHM_1(\lambda_2) +$$
$$\left(n_1 + n_2\right)^2 m\prime + 8mm_1 + nn_1\left(n_1 - 1\right)^2 + 2\left(n_1 - 1\right)\left(2mn_1 + 2nm_1\right) + \left(1 + n_2\right)^2 mn_2 +$$
$$4mm_2\left(1 + n_2\right) + \sum_{uv \in E_{\lambda^s}} \left(d_\lambda(u)^2 + 2\left(n_1 + n_2\right)d_\lambda(u)\right).$$

$$(16)$$

Proof. Using the Lemma 2 and the concept of the first reformulated Zagreb index, we have got

$$
EM_1\left(\lambda^s{\circ}(\lambda_1,\lambda_2)\right) = \sum_{uv\in E_{\lambda^s{\circ}(\lambda_1,\lambda_2)}} \left(d_{\lambda^s{\circ}(\lambda_1,\lambda_2)}(u) + d_{\lambda^s{\circ}(\lambda_1,\lambda_2)}(v) - 2\right)^2
$$

$$
= \sum_{uv\in E_{\lambda^s}} \left(d_\lambda(u) + n_1 + 2 + n_2 - 2\right)^2 + n \sum_{uv\in E_{\lambda_1}} \left(d_{\lambda_1}(u) + 1 + d_{\lambda_1}(v) + 1 - 2\right)^2
$$

$$
+ m \sum_{uv\in E_{\lambda_2}} \left(d_{\lambda_2}(u) + 1 + d_{\lambda_2}(v) + 1 - 2\right)^2 + \sum_{\substack{u(o)\in V_{\lambda^s}\\ v\in V_{\lambda_1}}} \left(d_\lambda(u) + n_1 + d_{\lambda_1}(v) + 1 - 2\right)^2
$$

$$
+ \sum_{\substack{u(N)\in V_{\lambda^s}\\ v\in V_{\lambda_2}}} \left(2 + n_2 + d_{\lambda_2}(v) + 1 - 2\right)^2 = \sum_{uv\in E_{\lambda^s}} \left[d_\lambda(u) + (n_1 + n_2)\right]^2 + n \sum_{uv\in E_{\lambda_1}} \left(d_{\lambda_1}(u) + d_{\lambda_1}(v)\right)^2
$$

$$
+ m \sum_{uv\in E_{\lambda_2}} \left(d_{\lambda_2}(u) + d_{\lambda_2}(v)\right)^2 + \sum_{\substack{u(o)\in V_{\lambda^s}\\ v\in V_{\lambda_1}}} \left[(d_\lambda(u) + d_{\lambda_1}(v)) + (n_1 - 1)\right]^2 + \sum_{\substack{u(N)\in V_{\lambda^s}\\ v\in V_{\lambda_2}}} \left[d_{\lambda_2}(v) + (1 + n_2)\right]^2
$$

$$
= \sum_{uv\in E_{\lambda^s}} \left[d_\lambda(u)^2 + (n_1 + n_2)^2 + 2d_\lambda(u)(n_1 + n_2)\right] + n \sum_{uv\in E_{\lambda_1}} \left(d_{\lambda_1}(u) + d_{\lambda_1}(v)\right)^2
$$

$$
+ m \sum_{uv\in E_{\lambda_2}} \left(d_{\lambda_2}(u) + d_{\lambda_2}(v)\right)^2 + \sum_{\substack{u(o)\in V_{\lambda^s}\\ v\in V_{\lambda_1}}} \left[(d_\lambda(u) + d_{\lambda_1}(v))^2 + (n_1 - 1)^2\right]
$$

$$
+ 2\left(d_\lambda(u) + d_{\lambda_1}(v)\right)(n_1 - 1)\right] + \sum_{\substack{u(N)\in V_{\lambda^s}\\ v\in V_{\lambda_2}}} \left[d_{\lambda_2}(v)^2 + (1 + n_2)^2 + 2d_{\lambda_2}(v)(1 + n_2)\right]
$$

$$
= \sum_{uv\in E_{\lambda^s}} d_\lambda(u)^2 + 2(n_1 + n_2) \sum_{uv\in E_{\lambda^s}} d_\lambda(u) + \sum_{uv\in E_{\lambda^s}} (n_1 + n_2)^2 + nHM_1(\lambda_1)
$$

$$
+ mHM_1(\lambda_2) + \sum_{\substack{u(o)\in V_{\lambda^s}\\ v\in V_{\lambda_1}}} \left(d_\lambda(u) + d_{\lambda_1}(v)\right)^2 + (n_1 - 1)^2 \sum_{\substack{u(o)\in V_{\lambda^s}\\ v\in V_{\lambda_1}}} 1 + 2(n_1 - 1)
$$

$$
\sum_{\substack{u(o)\in V_{\lambda^s}\\ v\in V_{\lambda_1}}} \left(d_\lambda(u) + d_{\lambda_1}(v)\right) + \sum_{\substack{u(N)\in V_{\lambda^s}\\ v\in V_{\lambda_2}}} d_{\lambda_2}(v)^2 + (1 + n_2)^2 \sum_{\substack{u(N)\in V_{\lambda^s}\\ v\in V_{\lambda_2}}} 1 + 2(1 + n_2)
$$

$$
\sum_{\substack{u(N)\in V_{\lambda^s}\\ v\in V_{\lambda_2}}} d_{\lambda_2}(v) = \sum_{uv\in E_{\lambda^s}} \left(d_\lambda(u)^2 + 2(n_1 + n_2)d_\lambda(u)\right) + (n_1 + n_2)^2 m\prime + nHM_1(\lambda_1)
$$

$$
+ mHM_1(\lambda_2) + \sum_{\substack{u(o)\in V_{\lambda^s}\\ v\in V_{\lambda_1}}} d_\lambda(u)^2 + \sum_{\substack{u(o)\in V_{\lambda^s}\\ v\in V_{\lambda_1}}} d_{\lambda_1}(v)^2 + 2 \sum_{\substack{u(o)\in V_{\lambda^s}\\ v\in V_{\lambda_1}}} d_\lambda(u)d_{\lambda_1}(v)
$$

$$
+ nn_1(n_1 - 1)^2 + 2(n_1 - 1) \sum_{\substack{u(o)\in V_{\lambda^s}\\ v\in V_{\lambda_1}}} \left(d_\lambda(u) + d_{\lambda_1}(v)\right) + \sum_{\substack{u(N)\in V_{\lambda^s}\\ v\in V_{\lambda_2}}} d_{\lambda_2}(v)^2
$$

$$
+ mn_2(1 + n_2)^2 + 2(1 + n_2) \sum_{u(N)\in V_{\lambda^s} v\in V_{\lambda_2}} d_{\lambda_2}(v)
$$

$$
= \sum_{uv\in E_{\lambda^s}} \left(d_\lambda(u)^2 + 2(n_1 + n_2)d_\lambda(u)\right) + (n_1 + n_2)^2 m\prime + nHM_1(\lambda_1) + mHM_1(\lambda_2)
$$

$$
+ \sum_{u(o)\in V_{\lambda^s}} d_\lambda(u)^2 \sum_{v\in V_{\lambda_1}} 1 + \sum_{u(o)\in V_{\lambda^s}} 1 \sum_{v\in V_{\lambda_1}} d_{\lambda_1}(v)^2 + 2 \sum_{u(o)\in E_{\lambda^s}} d_\lambda(u) \sum_{v\in V_{\lambda_1}} d_{\lambda_1}(v)
$$

$$+ nn_1 (n_1 - 1)^2 + 2(n_1 - 1)\left[\sum_{u(o)\in V_{\lambda^s}} d_\lambda(u) \sum_{v\in V_{\lambda_1}} 1 + \sum_{u(o)\in V_{\lambda^s}} 1 \sum_{v\in V_{\lambda_1}} d_{\lambda_1}(v)\right]$$

$$+ \sum_{u(N)\in V_{\lambda^s}} 1 \sum_{v\in V_{\lambda_2}} d_{\lambda_2}(v)^2 + mn_2(1 + n_2)^2 + 2(1 + n_2)\left[\sum_{u(N)\in V_{\lambda^s}} 1 \sum_{v\in V_{\lambda_2}} d_{\lambda_2}(v)\right]$$

$$= \sum_{uv\in E_{\lambda^s}} \left(d_\lambda(u)^2 + 2(n_1 + n_2)d_\lambda(u)\right) + (n_1 + n_2)^2 m\prime + nHM_1(\lambda_1) + mHM_1(\lambda_2)$$

$$+ n_1 M_1(\lambda) + nM_1(\lambda_1) + 2\cdot 2m\cdot 2m_1 + (n_1 - 1)^2 \cdot nn_1 + 2(n_1 - 1)(2mn_1 + 2m_1 n)$$

$$+ mM_1(\lambda_2) + (1 + n_2)^2 mn_2 + 2(1 + n_2).2m_2 m$$

$$= \sum_{uv\in E_{\lambda^s}} \left(d_\lambda(u)^2 + 2(n_1 + n_2)d_\lambda(u)\right) + (n_1 + n_2)^2 m\prime + nHM_1(\lambda_1)$$

$$+ mHM_1(\lambda_2) + n_1 M_1(\lambda) + nM_1(\lambda_1) + 8mm_1 + nn_1(n_1 - 1)^2$$

$$+ 4(n_1 - 1)(mn_1 + nm_1) + mM_1(\lambda_2) + mn_2(1 + n_2)^2 + 4mm_2(1 + n_2).$$

$$(17)$$

Hence, the proof is done.   □

Theorem 7. *For graphs $\lambda(n,m)$, $\lambda_1(n_1, m_1)$, and $\lambda_2(n_2, m_2)$, then, the first Zagreb index of the subdivision double neighborhood corona product $(\lambda^s \cdot (\lambda_1, \lambda_2))$ is given as*

$$M_1(\lambda^s \cdot (\lambda_1, \lambda_2)) = M_1(\lambda) + nM_1(\lambda_1) + mM_1(\lambda_2) + 8mn_2 + 4n_2^2 n + 8nm_1 + 4nn_1$$

$$+ 8mm_2 + 4mn_2 + m(2 + 2n_1)^2.$$

$$(18)$$

Proof. From the concept of the first Zagreb index we have

$$M_1(\lambda^s \cdot (\lambda_1, \lambda_2)) = \sum_{v\in V_{(\lambda^s \cdot (\lambda_1,\lambda_2))}} d_{(\lambda^s \cdot (\lambda_1,\lambda_2))}(v)^2.$$

$$(19)$$

Now, we apply Lemma 3,

$$= \sum_{v\in V_\lambda} (d_\lambda(v) + 2n_2)^2 + n\sum_{v\in V_{\lambda_1}} \left(d_{\lambda_1}(v) + 2\right)^2 + m\sum_{v\in V_{\lambda_2}} \left(d_{\lambda_2}(v) + 2\right)^2 + \sum_{v\in V_{\lambda^s}} (2 + 2n_1)^2$$

$$= \sum_{v\in V_\lambda} \left(d_\lambda(v)^2 + 2d_\lambda(v)(2n_2) + (2n_2)^2\right) + n\sum_{v\in V_{\lambda_1}} \left(d_{\lambda_1}(v)^2 + (2)2d_{\lambda_1}(v) + (2)^2\right)$$

$$+ m\sum_{v\in V_{\lambda_2}} \left(d_{\lambda_2}(v)^2 + 2d_{\lambda_2}(v)(2) + (2)^2\right) + \sum_{v\in V_{\lambda^s}} (2 + 2n_1)^2$$

$$= \sum_{v\in V_\lambda} d_\lambda(v)^2 + 4n_2\sum_{v\in V_\lambda} d_\lambda(v) + 4n_2^2\sum_{v\in V_\lambda} 1 + n\left[\sum_{v\in V_{\lambda_1}} d_{\lambda_1}(v)^2 + 4\sum_{v\in V_{\lambda_1}} d_{\lambda_1}(v) + 4\sum_{v\in V_{\lambda_1}} 1\right]$$

$$(20)$$

$$+ m\left[\sum_{v\in V_{\lambda_2}} d_{\lambda_2}(v)^2 + 4\sum_{v\in V_{\lambda_2}} d_{\lambda_2}(v) + 4\sum_{v\in V_{\lambda_2}} 1\right] + (2 + 2n_1)^2\sum_{v\in V_{\lambda^s}} 1$$

$$= M_1(\lambda) + 8mn_2 + 4n_2^2 n + nM_1(\lambda_1) + 8nm_1 + 4nn_1 + mM_1(\lambda_2) + 8mm_2$$

$$+ 4mn_2 + m(2 + 2n_1)^2.$$

Hence, the proof is done. □

Theorem 8. *Let* $\lambda(n,m)$, $\lambda^s(n\prime, m\prime)$, $\lambda_1(n_1, m_1)$, *and* $\lambda_2(n_2, m_2)$ *be the simple connected graphs. Then, the second*

Zagreb index of subdivision double neighborhood corona product ($\lambda^s \cdot (\lambda_1, \lambda_2)$) is given as

$$
\begin{aligned}
M_2\left(\lambda^s \cdot (\lambda_1, \lambda_2)\right) = {} & 2 \sum_{uv \in E_{\lambda^s}} \left(d_\lambda(u) + n_1 d_\lambda(u)\right) + 4n_2 m' + 4n_1 n_2 m' + n M_2(\lambda_1) \\
& + 2n M_1(\lambda_1) + 4nm_1 + m M_2(\lambda_2) + 2m M_1(\lambda_2) + 12mm_2 + 8mn_2 + 8nn_2 m_2 \\
& + 8nn_2^2 + 8mm_1 + 8mm_1 n_1 + 8mn_1 + 8mn_1^2.
\end{aligned}
\tag{21}
$$

Proof. From the concept of the second Zagreb index, we have

$$
M_2\left(\lambda^s \cdot (\lambda_1, \lambda_2)\right) = \sum_{uv \in E_{\lambda^s \cdot (\lambda_1, \lambda_2)}} d_{\lambda^s \cdot (\lambda_1, \lambda_2)} u \cdot d_{\lambda^s \cdot (\lambda_1, \lambda_2)} v. \tag{22}
$$

Now, we apply Lemma 3,

$$
= \sum_{uv \in E_{\lambda^s}} \left(d_\lambda(u) + 2n_2\right)\left(2 + 2n_1\right) + n \sum_{uv \in E_{\lambda_1}} \left(d_{\lambda_1}(u) + 2\right)\left(d_{\lambda_1}(v) + 2\right)
$$

$$
+ m \sum_{uv \in E_{\lambda_2}} \left(d_{\lambda_2}(u) + 2\right)\left(d_{\lambda_2}(v) + 2\right) + 2 \sum_{u(o) \in V_{\lambda^s}} \left(d_\lambda(u) + 2n_2\right)\left(d_{\lambda_2}(v) + 2\right)
$$

$$
+ 2 \sum_{\substack{u(N) \in V_{\lambda^s} \\ v \in V_{\lambda_1}}} \left(2 + 2n_1\right)\left(d_{\lambda_1}(v) + 2\right) = \sum_{uv \in E_{\lambda^s}}^{v \in V} \left(2d_\lambda(u) + 2n_1 d_\lambda(u) + 4n_2 + 4n_1 n_2\right)
$$

$$
+ n \sum_{uv \in E_{\lambda_1}} \left(d_{\lambda_1}(u) d_{\lambda_1}(v) + 2d_{\lambda_1}(u) + 2d_{\lambda_1}(v) + 4\right)
$$

$$
+ m \sum_{uv \in E_{\lambda_2}} \left(d_{\lambda_2}(u) d_{\lambda_2}(v) + 2d_{\lambda_2}(u) + 2d_{\lambda_2}(v) + 4\right) + 2 \sum_{\substack{u(o) \in V_{\lambda^s} \\ v \in V_{\lambda_2}}} \left[\left(d_\lambda(u) d_{\lambda_2}(v)\right) + 2d_\lambda(u) + 2n_2 d_{\lambda_2}(v) + 4n_2\right]
$$

$$
+ 2 \sum_{\substack{u(N) \in V_{\lambda^s} \\ v \in V_{\lambda_1}}} \left(2d_{\lambda_1}(v) + 4 + 2n_1 d_{\lambda_1}(v) + 4n_1\right)
$$

$$
= 2 \sum_{uv \in E_{\lambda^s}} \left(d_\lambda(u) + n_1 d_\lambda(u)\right) + 4n_2 \sum_{uv \in E_{\lambda^s}} 1 + 4n_1 n_2 \sum_{uv \in E_{\lambda^s}} 1 + n \left[\sum_{uv \in E_{\lambda_1}} d_{\lambda_1}(u) d_{\lambda_1}(v) + 2 \sum_{uv \in E_{\lambda_1}} \left(d_{\lambda_1}(u) + d_{\lambda_1}(v)\right) + 4 \sum_{uv \in E_{\lambda_1}} 1\right]
$$

$$
+ m \left[\sum_{uv \in E_{\lambda_2}} d_{\lambda_2}(u) d_{\lambda_2}(v) + 2 \sum_{uv \in E_{\lambda_2}} \left(d_{\lambda_2}(u) + d_{\lambda_2}(v)\right) + 4 \sum_{uv \in E_{\lambda_2}} 1\right]
$$

$$
+ 2 \left[\sum_{\substack{u(o) \in V_{\lambda^s} \\ v \in V_{\lambda_2}}} d_\lambda(u) d_{\lambda_2}(v) + \sum_{\substack{u(o) \in V_{\lambda^s} \\ v \in V_{\lambda_2}}} \left(2d_\lambda(u) + 2n_2 d_{\lambda_2}(v)\right) + 4n_2 \sum_{\substack{u(o) \in V_{\lambda^s} \\ v \in V_{\lambda_2}}} 1\right]
$$

$$
+ 2 \left[\sum_{u(N) \in V_{\lambda^s} v \in V_{\lambda_1}} \left(2d_{\lambda_1}(v) + 2n_1 d_{\lambda_1}(v)\right) + 4 \sum_{u(N) \in V_{\lambda^s} v \in V_{\lambda_1}} 1 + 4n_1 \sum_{u(N) \in V_{\lambda^s} v \in V_{\lambda_1}} 1\right]
$$

$$= 2 \sum_{uv \in E_{\lambda^s}} (d_\lambda(u) + n_1 d_\lambda(u)) + 4n_2 mI + 4n_1 n_2 mI + n[M_2(\lambda_1) + 2M_1(\lambda_1) + 4m_1]$$

$$+ m[M_2(\lambda_2) + 2M_1(\lambda_2) + 4m_2] + 2\left[\sum_{u(o) \in V_{\lambda^s}} d_\lambda(u) \sum_{v \in V_{\lambda_2}} d_{\lambda_2}(v) + 2 \sum_{u(o) \in V_{\lambda^s}} d_\lambda(u) \right.$$

$$\sum_{v \in V_{\lambda_2}} 1 + 2n_2 \sum_{u(o) \in V_{\lambda^s}} 1 \sum_{v \in V_{\lambda_2}} d_{\lambda_2}(v) + 4n_2 \sum_{u(o) \in V_{\lambda^s}} 1 \sum_{v \in V_{\lambda_2}} 1 \left. \right] + 2\left[2 \sum_{u(N) \in V_{\lambda^s}} 1 \sum_{v \in V_{\lambda_1}} d_{\lambda_1}(v) \right.$$

$$+ 2n_1 \sum_{u(N) \in V_{\lambda^s}} 1 \sum_{v \in V_{\lambda_1}} d_{\lambda_1}(v) + 4 \sum_{u(N) \in V_{\lambda^s}} 1 \sum_{v \in V_{\lambda_1}} 1 + 4n_1 \sum_{u(N) \in V_{\lambda^s}} 1 \sum_{v \in V_{\lambda_1}} 1 \left. \right]$$

$$= 2 \sum_{uv \in E_{\lambda^s}} (d_\lambda(u) + n_1 d_\lambda(u)) + 4n_2 mI + 4n_1 n_2 mI + n[M_2(\lambda_1) + 2M_1(\lambda_1) + 4m_1]$$

$$+ m[M_2(\lambda_2) + 2M_1(\lambda_2) + 4m_2] + 2[2m \cdot 2m_2 + 2 \cdot 2m \cdot n_2 + 2n_2 n \cdot 2m_2 + 4n_2 n \cdot n_2]$$

$$+ 2[2m \cdot 2m_1 + 2n_1 m \cdot 2m_1 + 4mn_1 + 4mn_1^2]$$

$$= 2 \sum_{uv \in E_{\lambda^s}} (d_\lambda(u) + n_1 d_\lambda(u)) + 4n_2 mI + 4n_1 n_2 mI + n[M_2(\lambda_1) + 2M_1(\lambda_1) + 4m_1]$$

$$+ m[M_2(\lambda_2) + 2M_1(\lambda_2) + 4m_2] + 2[4mm_2 + 4mn_2 + 4nn_2 m_2 + 4nn_2^2]$$

$$+ 2[4mm_1 + 4mm_1 n_1 + 4mn_1 + 4mn_1^2]$$

$$= 2 \sum_{uv \in E_{\lambda^s}} (d_\lambda(u) + n_1 d_\lambda(u)) + 4n_2 mI + 4n_1 n_2 mI + nM_2(\lambda_1) + 2nM_1(\lambda_1) + 4nm_1$$

$$+ mM_2(\lambda_2) + 2mM_1(\lambda_2) + 12mm_2 + 8mn_2 + 8nn_2 m_2 + 8nn_2^2 + 8mm_1$$

$$+ 8mm_1 n_1 + 8mn_1 + 8mn_1^2. \tag{23}$$

Hence, the proof is done.   □

Theorem 9. *Let $\lambda(n, m)$, $\lambda_1(n_1, m_1)$, and $\lambda_2(n_2, m_2)$ be the simple connected graphs. Then, the forgotten topological index of subdivision double neighborhood corona product $\lambda^s \cdot (\lambda_1, \lambda_2)$ is given as*

$$F(\lambda^s \cdot (\lambda_1, \lambda_2)) = F(\lambda) + 24mn_2^2 + 6n_2 M_1(\lambda) + 8nn_2^3 + nF(\lambda_1) + 24nm_1$$
$$+ 6nM_1(\lambda_1) + 8nn_1 + mF(\lambda_2) + 24mm_2 + 6mM_1(\lambda_2) + 8mn_2 + m(2 + 2n_1)^3. \tag{24}$$

Proof. From the concept of the forgotten index, we have

$$F(\lambda^s \cdot (\lambda_1, \lambda_2)) = \sum_{v \in V_{(\lambda^s \bullet (\lambda_1, \lambda_2))}} d_{(\lambda^s \cdot (\lambda_1, \lambda_2))}(v)^3. \tag{25}$$

Now, we apply Lemma 3,

$$= \sum_{v \in V_\lambda} (d_\lambda(v) + 2n_2)^3 + n \sum_{v \in V_{\lambda_1}} (d_{\lambda_1}(v) + 2)^3 + m \sum_{v \in V_{\lambda_2}} (d_{\lambda_2}(v) + 2)^3$$

$$+ \sum_{v \in V_{\lambda^s}} (2 + 2n_1)^3$$

$$
= \sum_{v \in V_\lambda} \left(d_\lambda(v)^3 + 3d_\lambda(v)(2n_2)^2 + 3d_\lambda(v)^2(2n_2) + (2n_2)^3 \right)
$$

$$
+ n \sum_{v \in V_{\lambda_1}} \left(d_{\lambda_1}(v)^3 + 3d_{\lambda_1}(v)(2)^2 + 3d_{\lambda_1}(v)^2 \cdot (2) + 2^3 \right)
$$

$$
+ m \sum_{v \in V_{\lambda_2}} \left(d_{\lambda_2}(v)^3 + 3d_{\lambda_2}(v)(2)^2 + 3d_{\lambda_2}(v)^2 \cdot 2 + 2^3 \right) + \sum_{v \in V_{\lambda^s}} (2 + 2n_1)^3
$$

$$
= \sum_{v \in V_\lambda} d_\lambda(v)^3 + 12n_2^2 \sum_{v \in V_\lambda} d_\lambda(v) + 6n_2 \sum_{v \in V_\lambda} d_\lambda(v)^2 + 8n_2^3 \sum_{v \in V_\lambda} 1 + n \sum_{v \in V_{\lambda_1}} d_{\lambda_1}(v)^3
$$

$$
+ 12n \sum_{v \in V_{\lambda_1}} d_{\lambda_1}(v) + 6n \sum_{v \in V_{\lambda_1}} d_{\lambda_1}(v)^2 + 8n \sum_{v \in V_{\lambda_1}} 1 + m \sum_{v \in V_{\lambda_2}} d_{\lambda_2}(v)^3 + 12m
$$

$$
\sum_{v \in V_{\lambda_2}} d_{\lambda_2}(v) + 6m \sum_{v \in V_{\lambda_2}} d_{\lambda_2}(v)^2 + 8m \sum_{v \in V_{\lambda_2}} 1 + (2 + 2n_1)^3 \sum_{v \in V_{\lambda^s}} 1
$$

$$
= F(\lambda) + 24mn_2^2 + 6n_2 M_1(\lambda) + 8nn_2^3 + nF(\lambda_1) + 24nm_1 + 6nM_1(\lambda_1)
$$

$$
+ 8nn_1 + mF(\lambda_2) + 24mm_2 + 6mM_1(\lambda_2) + 8mn_2 + m(2 + 2n_1)^3.
$$

$$(26)$$

Hence, the proof is done.   □

Theorem 10. *Let* $\lambda(n, m)$, $\lambda_1(n_1, m_1)$, *and* $\lambda_2(n_2, m_2)$ *be the simple connected graphs. Then, the first multiplicative Zagreb index of subdivision double neighborhood corona product* $(\lambda^s \cdot (\lambda_1, \lambda_2))$ *is given as*

$$
\prod_1 (\lambda^s \cdot (\lambda_1, \lambda_2)) \le \left[\frac{M_1(\lambda) + 8n_2 m + 4nn_2^2}{n} \right]^n \times \left[\frac{M_1(\lambda_1) + 8m_1 + 4n_1}{n_1} \right]^{nn_1}
$$

$$
\times \left[\frac{M_1(\lambda_2) + 8m_2 + 4n_2}{n_2} \right]^{mn_2} \times (2 + 2n_1)^{2m}.
$$

$$(27)$$

Proof. From the concept of the first multiplicative Zagreb index, we have

$$
\prod_1 (\lambda^s \cdot (\lambda_1, \lambda_2)) = \prod_{v \in V_{(\lambda^s \cdot (\lambda_1, \lambda_2))}} d_{(\lambda^s \cdot (\lambda_1, \lambda_2))}(v)^2.
$$

$$(28)$$

Now, we apply Lemma 3,

$$
= \prod_{v \in V_\lambda} (d_\lambda(v) + 2n_2)^2 \times \left[\prod_{v \in V_{\lambda_1}} (d_{\lambda_1}(v) + 2)^2 \right]^n \times \left[\prod_{v \in V_{\lambda_2}} (d_{\lambda_2}(v) + 2)^2 \right]^m \times \prod_{v \in V_{\lambda^s}} (2 + 2n_1)^2
$$

$$
= \prod_{v \in V_\lambda} (d_\lambda(v)^2 + 2d_\lambda(v)(2n_2) + (2n_2)^2) \times \left[\prod_{v \in V_{\lambda_1}} (d_{\lambda_1}(v)^2 + 2d_{\lambda_1}(v) \times 2 + 2^2) \right]^n
$$

$$
\times \left[\prod_{v \in V_{\lambda_2}} (d_{\lambda_2}(v)^2 + 2d_{\lambda_2}(v) \times 2 + 2^2) \right]^m \times \prod_{v \in V_{\lambda^s}} (2 + 2n_1)^2.
$$

$$(29)$$

By Lemma 1,

$$
\leq \left[\frac{\sum_{v \in V_\lambda}\left(d_\lambda(v)^2 + 4n_2 d_\lambda(v) + 4n_2^2\right)}{n}\right]^n \times \left[\frac{\sum_{v \in V\lambda_1}\left(d_{\lambda_1}(v)^2 + 4d_{\lambda_1}(v) + 4\right)}{n_1}\right]
$$

$$
{}^{nn_1} \times \left[\frac{\sum_{v \in V_{\lambda_2}}\left(d_{\lambda_2}(v)^2 + 4d_{\lambda_2}(v) + 4\right)}{n_2}\right]^{mn_2} \times \left[\frac{\sum_{v \in V_{\lambda^s}}(2 + 2n_1)^2}{m}\right]^m
$$

$$
\leq \left[\frac{\sum_{v \in V_\lambda} d_\lambda(v)^2 + 4n_2 \sum_{v \in V_\lambda} d_\lambda(v) + 4n_2^2 \sum_{v \in V_\lambda} 1}{n}\right]^n \times \left[\frac{\sum_{v \in V\lambda_1} d_{\lambda_1}(v)^2 + 4\sum_{v \in V_{\lambda_1}} d_{\lambda_1}(v) + 4\sum_{v \in V_{\lambda_1}} 1}{n_1}\right]^{nn_1}
$$

(30)

$$
\times \left[\frac{\sum_{v \in V_{\lambda_2}} d_{\lambda_2}(v)^2 + 4\sum_{v \in V_{\lambda_2}} d_{\lambda_2}(v) + 4\sum_{v \in V_{\lambda_2}} 1}{n_2}\right]^{mn_2} \times \left[\frac{(2 + 2n_1)^2 \sum_{v \in V_{\lambda^s}} 1}{m}\right]^m
$$

$$
= \left[\frac{M_1(\lambda) + 8n_2 m + 4nn_2^2}{n}\right]^n \times \left[\frac{M_1(\lambda_1) + 8m_1 + 4n_1}{n_1}\right]^{nn_1}
$$

$$
\times \left[\frac{M_1(\lambda_2) + 8m_2 + 4n_2}{n_2}\right]^{mn_2} \times (2 + 2n_1)^{2m}.
$$

Hence, equality holds in 13 iff λ, λ_1, and λ_2 are regular graphs.

Hence, the proof is done. □

Theorem 11. *Let $\lambda(n, m)$, $\lambda^s(n\prime, m\prime)$, $\lambda_1(n_1, m_1)$, and $\lambda_2(n_2, m_2)$ be the simple connected graphs. Then, the first reformulated Zagreb index of subdivision double neighborhood corona product $(\lambda^s \cdot (\lambda_1, \lambda_2))$ is given as*

$$
EM_1\left(\lambda^s \cdot (\lambda_1, \lambda_2)\right) = \sum_{uv \in E_{\lambda^s}}\left(d_\lambda(u)^2 + 4(n_1 + n_2)d_\lambda(u)\right) + 4(n_1 + n_2)^2 m\prime
$$

$$
+ nHM_1(\lambda_1) + 4nm_1 + 4nM_1(\lambda_1) + mHM_1(\lambda_2) + 4mm_2 + 4mM_1(\lambda_2)
$$

(31)

$$
+ 2n_2 M_1(\lambda) + 2nM_1(\lambda_2) + 6mm_2 + 8nn_2^3 + 16mn_2^2 + 16nn_2 m_2 + 2mM_1(\lambda_1)
$$

$$
+ 2mn_1(2 + 2n_1)^2 + 8mm_1(2 + 2n_1).
$$

Proof. From the concept of the first reformulated Zagreb, we have

$$
EM_1\left(\lambda^s \cdot (\lambda_1, \lambda_2)\right) = \sum_{uv \in E_{\lambda^s \cdot (\lambda_1, \lambda_2)}}\left(d_{\lambda^s \cdot (\lambda_1, \lambda_2)}(u) + d_{\lambda^s \cdot (\lambda_1, \lambda_2)}(v) - 2\right)^2.
$$

(32)

Now, we apply Lemma 3,

$$
= \sum_{uv \in E_{\lambda^s}}\left(d_\lambda(u) + 2n_2 + 2 + 2n_1 - 2\right)^2 + n \sum_{uv \in E_{\lambda_1}}\left(d_{\lambda_1}(u) + 2 + d_{\lambda_1}(v) + 2 - 2\right)^2
$$

$$
+ m \sum_{uv \in E_{\lambda_2}}\left(d_{\lambda_2}(u) + 2 + d_{\lambda_2}(v) + 2 - 2\right)^2 + 2 \sum_{u(o) \in V_{\lambda^s} v \in V_{\lambda_2}}\left(d_\lambda(u) + 2n_2 + d_{\lambda_2}(v) + 2 - 2\right)^2
$$

$$+ 2 \sum_{\substack{u(N)\in V_{\lambda s} \\ v\in V_{\lambda_1}}} \left(2 + 2n_1 + d_{\lambda_1}(v) + 2 - 2\right)^2 = \sum_{uv\in E_{\lambda s}} \left(d_\lambda(u) + 2(n_1 + n_2)\right)^2 + n \sum_{uv\in E_{\lambda_1}} \left(d_{\lambda_1}(u) + d_{\lambda_1}(v) + 2\right)^2$$

$$+ m \sum_{uv\in E_{\lambda_2}} \left(d_{\lambda_2}(u) + d_{\lambda_2}(v) + 2\right)^2 + 2 \sum_{\substack{u(o)\in V_{\lambda s}\, v\in V_{\lambda_2}}} \left(d_\lambda(u) + d_{\lambda_2}(v) + 2n_2\right)^2 + 2 \sum_{\substack{u(N)\in V_{\lambda s}\, v\in V_{\lambda_1}}} \left(d_{\lambda_1}(v) + 2 + 2n_1\right)^2$$

$$= \sum_{uv\in E_{\lambda s}} \left[d_\lambda(u)^2 + (2(n_1 + n_2))^2 + 2d_\lambda(u)(2(n_1 + n_2))\right] + n \sum_{uv\in E_{\lambda_1}} \left[\left(d_{\lambda_1}(u) + d_{\lambda_1}v\right)^2 + 4 + 4\left(d_{\lambda_1}(u) + d_{\lambda_1}(v)\right)\right]$$

$$+ m \sum_{uv\in E_{\lambda_2}} \left[\left(d_{\lambda_2}(u) + d_{\lambda_2}(v)\right)^2 + 4 + 4\left(d_{\lambda_2}(u) + d_{\lambda_2}(v)\right)\right] + 2 \sum_{\substack{u(o)\in V_{\lambda s} \\ v\in V_{\lambda_2}}} \left[\left(d_\lambda(u) + d_{\lambda_2}(v)\right)^2 + (2n_2)^2 + 2\left(d_\lambda(u) + d_{\lambda_2}(v)\right)2n_2\right]$$

$$+ 2 \sum_{u(N)\in V_{\lambda s}\, v\in V_{\lambda_1}} \left[d_{\lambda_1}(v)^2 + (2 + 2n_1)^2 + 2\left(d_{\lambda_1}(v)(2 + 2n_1)\right)\right]$$

$$= \sum_{uv\in E_{\lambda s}} d_\lambda(u)^2 + 4(n_1 + n_2)^2 \sum_{uv\in E_{\lambda s}} 1 + 4(n_1 + n_2) \sum_{uv\in E_{\lambda s}} d_\lambda(u)$$

$$+ n\left[\sum_{uv\in E_{\lambda_1}} \left(d_{\lambda_1}(u) + d_{\lambda_1}(v)\right)^2 + 4 \sum_{uv\in E_{\lambda_1}} 1 + 4 \sum_{uv\in E_{\lambda_1}} \left(d_{\lambda_1}(u) + d_{\lambda_1}(v)\right)\right]$$

$$+ m\left[\sum_{uv\in E_{\lambda_2}} \left(d_{\lambda_2}(u) + d_{\lambda_2}(v)\right)^2 + 4 \sum_{uv\in E_{\lambda_2}} 1 + 4 \sum_{uv\in E_{\lambda_2}} \left(d_{\lambda_2}(u) + d_{\lambda_2}(v)\right)\right]$$

$$+ 2\left[\sum_{\substack{u(o)\in V_{\lambda s} \\ v\in V_{\lambda_2}}} \left(d_\lambda(u) + d_{\lambda_2}(v)\right)^2 + 4n_2^2 \sum_{\substack{u(o)\in V_{\lambda s} \\ v\in V_{\lambda_2}}} 1 + 4n_2 \sum_{\substack{u(o)\in V_{\lambda s} \\ v\in V_{\lambda_2}}} \left(d_\lambda(u) + d_{\lambda_2}(v)\right)\right]$$

$$+ 2\left[\sum_{\substack{u(N)\in V_{\lambda s} \\ v\in V_{\lambda_1}}} d_{\lambda_1}(v)^2 + (2 + 2n_1)^2 \sum_{\substack{u(N)\in V_{\lambda s} \\ v\in V_{\lambda_1}}} 1 + 2(2 + 2n_1) \sum_{\substack{u(N)\in V_{\lambda s} \\ v\in V_{\lambda_1}}} d_{\lambda_1}(v)\right],$$

$$= \sum_{uv\in E_{\lambda s}} d_\lambda(u)^2 + 4(n_1 + n_2)^2 m\prime + 4(n_1 + n_2) \sum_{uv\in E_{\lambda s}} d_\lambda(u) + nHM_1(\lambda_1) + 4nm_1 + 4nM_1(\lambda_1)$$

$$+ mHM_1(\lambda_2) + 4mm_2 + 4mM_1(\lambda_2)$$

$$+ 2\left[\sum_{\substack{u(o)\in V_{\lambda s} \\ v\in V_{\lambda_2}}} \left(d_\lambda(u)^2 + d_{\lambda_2}(v)^2 + 2d_\lambda(u)d_{\lambda_2}(v)\right) + 4n_2^2 \sum_{\substack{u(o)\in V_{\lambda s} \\ v\in V_{\lambda_2}}} 1 + 4n_2\left(\sum_{\substack{u(o)\in V_{\lambda s} \\ v\in V_{\lambda_2}}} d_\lambda(u) + \sum_{\substack{u(o)\in V_{\lambda s} \\ v\in V_{\lambda_2}}} d_{\lambda_2}(v)\right)\right]$$

$$+ 2\left[\sum_{\substack{u(N)\in V_{\lambda s} \\ v\in V_{\lambda_1}}} d_{\lambda_1}(v)^2 + (2 + 2n_1)^2 \sum_{\substack{u(N)\in V_{\lambda s} \\ v\in V_{\lambda_1}}} 1 + 2(2 + 2n_1) \sum_{\substack{u(N)\in V_{\lambda s} \\ v\in V_{\lambda_1}}} d_{\lambda_1}(v)\right]$$

$$= \sum_{uv \in E_{\lambda^s}} d_\lambda(u)^2 + 4(n_1 + n_2)^2 m\prime + 4(n_1 + n_2) \sum_{uv \in E_{\lambda^s}} d_\lambda(u) + nHM_1(\lambda_1)$$

$$+ 2\left[\sum_{\substack{u(o) \in V_{\lambda^s} \\ v \in V_{\lambda_2}}} \left(d_\lambda(u)^2 + d_{\lambda_2}(v)^2 + 2d_\lambda(u)d_{\lambda_2}(v) \right) + 4n_2^2 \sum_{\substack{u(o) \in V_{\lambda^s} \\ v \in V_{\lambda_2}}} 1 + 4n_2 \left(\sum_{\substack{u(o) \in V_{\lambda^s} \\ v \in V_{\lambda_2}}} d_\lambda(u) + \sum_{\substack{u(o) \in V_{\lambda^s} \\ v \in V_{\lambda_2}}} d_{\lambda_2}(v) \right) \right]$$

$$+ 2\left[\sum_{u(N) \in V_{\lambda^s} v \in V_{\lambda_1}} d_{\lambda_1}(v)^2 + (2 + 2n_1)^2 \sum_{u(N) \in V_{\lambda^s} v \in V_{\lambda_1}} 1 + 2(2 + 2n_1) \sum_{u(N) \in V_{\lambda^s} v \in V_{\lambda_1}} d_{\lambda_1}(v) \right]$$

$$= \sum_{uv \in E_{\lambda^s}} d_\lambda(u)^2 + 4(n_1 + n_2)^2 m\prime + 4(n_1 + n_2) \sum_{uv \in E_{\lambda^s}} d_\lambda(u) + nHM_1(\lambda_1)$$

$$+ 4nm_1 + 4nM_1(\lambda_1) + mHM_1(\lambda_2) + 4mm_2 + 4mM_1(\lambda_2)$$

$$+ 2\left[\sum_{u(o) \in V_{\lambda^s}} d_\lambda(u)^2 \sum_{v \in V_{\lambda_2}} 1 + \sum_{u(o) \in V_{\lambda^s}} 1 \sum_{v \in V_{\lambda_2}} d_\lambda(v)^2 + 2 \sum_{u(o) \in V_{\lambda^s}} d_\lambda(u) \sum_{v \in V_{\lambda_2}} d_\lambda(v) + 4n_2^2 \sum_{u(o) \in V_{\lambda^s}} 1 \sum_{v \in V_{\lambda_2}} 1 \right.$$

$$\left. + 4n_2 \left(\sum_{u(o) \in V_{\lambda^s}} d_\lambda(u) \sum_{v \in V_{\lambda_2}} 1 + \sum_{u(o) \in V_{\lambda^s}} 1 \sum_{v \in V_{\lambda_2}} d_{\lambda_2}(v) \right) \right]$$

$$+ 2\left[\sum_{u(N) \in V_{\lambda^s}} 1 \sum_{v \in V_{\lambda_1}} d_{\lambda_1}(v)^2 + (2 + 2n_1)^2 \sum_{u(N) \in V_{\lambda^s}} 1 \sum_{v \in V_{\lambda_1}} 1 + 2(2 + 2n_1) \sum_{u(N) \in V_{\lambda^s}} 1 \sum_{v \in V_{\lambda_1}} d_{\lambda_1}(v) \right]$$

$$= \sum_{uv \in E_{\lambda^s}} d_\lambda(u)^2 + 4(n_1 + n_2)^2 m\prime + 4(n_1 + n_2) \sum_{uv \in E_{\lambda^s}} d_\lambda(u) + nHM_1(\lambda_1)$$

$$+ 4nm_1 + 4nM_1(\lambda_1) + mHM_1(\lambda_2) + 4mm_2 + 4mM_1(\lambda_2)$$

$$+ 2\left[n_2 M_1(\lambda) + nM_1(\lambda_2) + 2 \cdot 2m \cdot 2m_2 + 4nn_2 n_2^2 + 4n_2(2m \cdot n_2 + n \cdot 2m_2) \right]$$

$$+ 2\left[mM_1(\lambda_1) + (2 + 2n_1)^2 m \cdot n_1 + 2(2 + 2n_1)m \cdot 2m_1 \right]$$

$$= \sum_{uv \in E_{\lambda^s}} \left(d_\lambda(u)^2 + 4(n_1 + n_2)d_\lambda(u) \right) + 4(n_1 + n_2)^2 m\prime + nHM_1(\lambda_1) + 4nm_1$$

$$+ 4nM_1(\lambda_1) + mHM_1(\lambda_2) + 4mm_2 + 4mM_1(\lambda_2) + 2n_2 M_1(\lambda) + 2nM_1(\lambda_2)$$

$$+ 16mm_2 + 8nn_2^3 + 16mn_2^2 + 16nn_2 m_2 + 2mM_1(\lambda_1) + 2mn_1(2 + 2n_1)^2 + 8mm_1(2 + 2n_1). \tag{33}$$

Hence, the proof is done.   □

3. Conclusion

The first and second Zagreb indices, the first multiplicative Zagreb index, the first reformed Zagreb index, and the forgotten topological index were explored in this work, and their exact expressions were investigated. Other degree and distance-based topological indices of these complicated network operations could be calculated in the future work.

Data Availability

All the data supporting the results are included in the manuscript.

Conflicts of Interest

References

[1] C. Hansch and L. Leo, "Exploring QSAR fundamentals and applicability in chemistry and biology," Amer. Chem. Soc, Washington DC, USA, 1996.

[2] M. F. Nadeem, M. Imran, H. M. A. Siddiqui, M. Azeem, A. Khalil, and Y. Ali, "Yasir, "Topological aspects of metal-organic structure with the help of underlying networks" Arabian," *Journal of Chemistry*, vol. 14, no. 6, 2021.

[3] A. Shabbir, M. F. Nadeem, S. Mukhtar, and A. Raza, "On edge version of some degree-based topological indices of HAC5C7

[p,q] and VC5C7[p,q] nanotubes," *Polycyclic Aromatic Compounds*, vol. 42, no. 3, pp. 849–865, 2020.

[4] M. F. Nadeem, M. Azeem, and H. M. A. Siddiqui, "Comparative study of Zagreb indices for capped, semi-capped, and uncapped carbon nanotubes," *Polycyclic Aromatic Compounds*, vol. 1-18, pp. 1–18, 2021.

[5] M. F. Nadeem, M. Azeem, and I. Farman, "Comparative study of topological indices for capped and uncapped carbon nanotubes," *Polycyclic Aromatic Compounds*, vol. 1-18, pp. 1–18, 2021.

[6] M. F. Nadeem, S. Zafar, and Z. Zahid, "On topological properties of the line graphs of subdivision graphs of certain nanostructures," *Applied Mathematics and Computation*, vol. 273, pp. 125–130, 2016.

[7] A. Ahmad and S. C. López, "Distance-based topological polynomials associated with zero-divisor graphs," *Mathematical Problems in Engineering*, vol. 2021, Article ID 4959559, 8 pages, 2021.

[8] A. Ahmad, A. Ali, M. A. Asim, and M. F. Nadeem, "Polynomials of degree-based indices of metal-organic networks," *Combinatorial Chemistry & High Throughput Screening*, vol. 23, 2020.

[9] A. Ahmad, R. Hasni, K. Elahi, and M. A. Asim, "Polynomials of degree-based indices for swapped networks modeled by optical transpose interconnection system," *IEEE Access*, Institute of Electrical and Electronics Engineers, vol. 8, , Article ID 214293, 2020.

[10] N. A. Koam and A. Ahmad, "Polynomials of degree-based indices for three-dimensional mesh network," *Computers, Materials & Continua*, vol. 65, no. 2, pp. 1271–1282, 2020.

[11] I. Gutman and N. Tirnajsti, "Graph theory and molecular orbitals. III. Total pi-electron energy bydrocarbon," *Chemical Physics Letters*, vol. 17, pp. 535–538, 1972.

[12] R. Todeschini and V. Consonni, "New local vertex invariants and molecular descriptors based on functions of the vertex degrees," *MATCH Commun. Math. Comput. Chem.*vol. 64, pp. 359–372, 2010.

[13] M. Eliasi, A. Iranmanesh, and I. Gutman, "Multiplicative versions of first Zagreb index," *MATCH Commun. Math. Comput. Chem.*vol. 68, no. 1, pp. 217–230, 2012.

[14] B. Furtula and I. Gutman, "A forgotten topological index," *Journal of Mathematical Chemistry*, vol. 53, no. 4, pp. 1184–1190, 2015.

[15] B. Furtula, I. Gutman, Z. K. Vukicevic, G. Lekishvili, and G. Popivoda, "On an old degree-based topologicalindex," *Sci. Math.*vol. 148, pp. 19–31, 2015.

[16] A. Mili, evi, S. Ṇikolic and N. Tirnajsti, "On reformulated Zagreb indices č c c," *Molecular Diversity*, vol. 8, pp. 393–399, 2004.

[17] J. A. Bondy and U. S. R. Murty, *Graph Theory in Graduate Texts in Mathematics*, Vol. 29, Springer, , Berlin, Germany, 2008.

[18] F. Harary, *Graph Theory, Reading*, Addison-Wesley, Boston, Massachusetts, MA, USA, 1994.

[19] G. P. Singh, A. Borah, and S. Ray, "A review paper on corona product of graphs," *Advances and Applications in Mathematical Sciences*, vol. 19, no. 10, pp. 1047–1054, 2020.

[20] P. Sarkar, N. De, and A. Pal, "The forgotten topological index of double corona of graphs related to the different subdivision graphs," *Mathematical Advances in Pure and Applied Sciences*, vol. 2, no. 1, pp. 2636–8021, 2019.

[21] S. Barik and G. Sahoo, "On the Laplacian spectra of some variants of corona," *Linear Algebra Appl*, vol. 512, 2016.

[22] M. H. Khalifeh, H. Yousefi-Azari, and A. R. Ashrafi, "The first and second Zagreb indices of some graph operations," *Discrete Applied Mathematics*, vol. 157, no. 4, pp. 804–811, 2009.

[23] N. De, "Computing f-index of different corona products of graphs," *Bulletin of Mathematical Sciences and Applications*, vol. 19, pp. 24–30, 2017.

[24] M. Arezoomand and B. Taeri, "Zagreb indices of the generalized hierarchical product of graphs," *MATCH Commun. Math. Comput. Chem.*vol. 69, no. 1, pp. 131–140, 2013.

[25] A. R. Ashraf, A. R. Ashrafi, and H. Shabani, "The modified Wiener index of some graph operations," *ARS Mathematica Contemporanea*, vol. 11, no. 2, pp. 277–284, 2015.

[26] N. De, "The vertex Zagreb indices of some graph operations," *Carpathian Math. Publ.*vol. 8, no. 2, pp. 215–223, 2016.

[27] A. Ahmad, "On the degree based topological indices of benzene ring embedded in P-type-surface in 2D network," *Hacettepe Journal of Mathematics and Statistics*, vol. 4, no. 46, pp. 9–18, 2017.

[28] H. Alshehri, A. Ahmad, Y. Alqahtani, and M. Azeem, "Vertex metric-based dimension of generalized perimantanes diamondoid structure," *IEEE Access*, vol. 10, Article ID 43320, 2022.

[29] A. N. A. Koam, A. Ahmad, M. Azeem, and M. F. Nadeem, "Bounds on the partition dimension of one pentagonal carbon nanocone structure," *Arabian Journal of Chemistry*, vol. 15, no. 7, Article ID 103923, 2022.

[30] H. Raza, M. Waheed, M. K. Jamil, and M. Azeem, "Structures devised by the generalizations of two graph operations and their topological descriptors," *Main Group Metal Chemistry*, vol. 45, no. 1, pp. 44–56, 2022.

[31] A. N. A. H. Ahmad, A. Ahmad, and M. Azeem, "Computation of edge- and vertex-degree-based topological indices for tetrahedral sheets of clay minerals," *Main Group Metal Chemistry*, vol. 45, no. 1, pp. 26–34, 2022.

WILEY | Hindawi

Research Article

Blockchain-Based Contact Tracing and Information Sharing Model for COVID-19 Pandemic

Arwa Mashat and **Aliaa M. Alabdali**

Faculty of Computing & Information Technology, King Abdulaziz University, P.O. Box 344, Rabigh 21911, Saudi Arabia

Correspondence should be addressed to Aliaa M. Alabdali; amalabdali@kau.edu.sa

COVID-19 is the worst contagious disaster in the history of humankind, triggering a worldwide sickness pandemic. In lacking specialized treatments or immunizations, finding and eliminating the infection source is the best option to decrease disease transmission and lower sickness and degree of fatality among the general public. Generally, few significant barriers are present in the existing system of monitoring the contamination. One of the obstacles is regarding health-related data storage. The user's e-health data is kept in a traditional method that might have been compromised if shared with third parties. Secondly, the current disease tracking technologies fail to monitor diseases numerous ways. The tracing system is either personal or location-based. Apart from these, gathering individual consent and sharing their health data with unknown associations is a real-time problem. We propose a blockchain-based data system that maintains confidentiality with transparency. Users can acquire unlimited and nontampered vital routes as the suggested blockchain solution leverages to link the user/patient and approved solvers. Also, automatically executed smart contracts are constructed to desensitize the user ID and reallocation. The anonymous feature delivered by private blockchain with wireless technologies defends the customer's identity secrecy. We develop a matching approach using machine learning technology. Users may take safeguards in advance by employing our suggested analytical technique for predicting the risk due to infectious source presence.

1. Introduction

A new infirmity is known as COVID-19, and its variations are wreaking havoc throughout the globe. It was first originated in the Chinese Wuhan City in the province of Hubei. The virus's enormous proliferation has posed several obstacles, causing the foundations of human civilization to quiver. COVID-19 has infected about 11.5 million individuals and killed almost 529,090 people too far. South-East, in particular, has surpassed the United States as the country with the most known illnesses. Each country has its privacy policies to communicate information about sick patients [1–3]. Because various nations have their privacy policies for sharing the information of infected persons, sharing information across the world with reliable privacy protection is challenging. Users typically have slight control over the possible exploitation of personal data once uploaded to the

cloud [4, 5]. If a comprehensive data security solution is not in place, the cloud's private user data might be stolen for any number of malicious objectives [6]. The Globe Health Institution (WHO), a worldwide organization, engages with governments to share information and improve epidemic preventive strategy. However, some nations are losing faith in WHO, and the organization cannot get sufficient funding. Other authorities may withhold, incorrectly report, or prevent pandemic data from being reported. For worldwide pandemic prevention, this might result in a considerable security weakness. As a result, not a single system is present to share their personal details or data while protecting their confidentiality. Administration departments and governments may have availed to all people's health medical data, which is outside their area of authority and obligation. Some public healthcare offices, for example, may track down sick people's personal information and keep it in a conventional
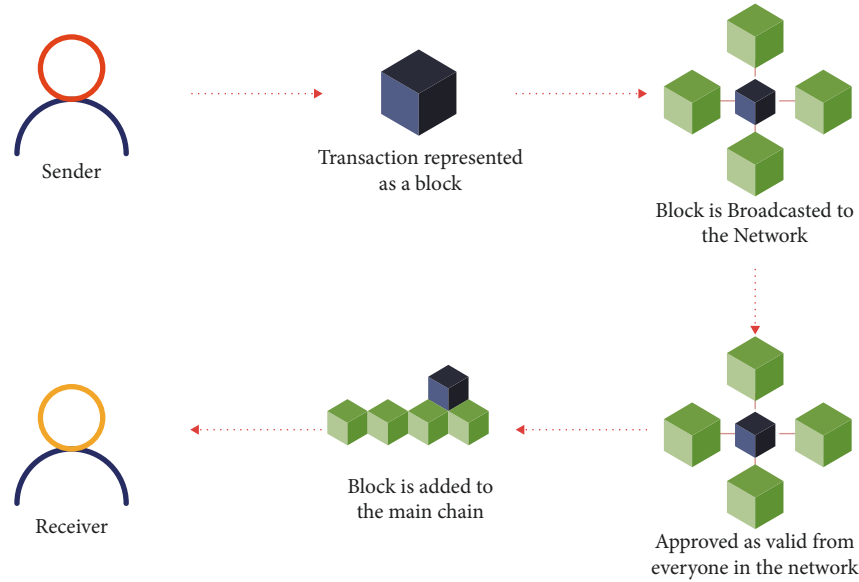
FIGURE 1: The basic structure of blockchain network.

isolation place, so this process actually helps to increase secondary contaminations and limits delicate liberty [7]. Several large tech companies will release the info of infected persons with health authorities, implying that users' data confidentiality and HR (human rights) will be infringed without their awareness [7, 8].

There are presently two types of contact tracking systems available: location-based and individual-based contact tracking. Without knowing about infection migration, position-based contact tracking always offers a conversational service and data contaminations in specified places. Individual-based tracing solutions are solely concerned with person-to-person Bluetooth interaction and do not track where users become infected. According to the WHO, the virus may persist on various surfaces. Therefore, it impacts people's daily activities [9]. On the other hand, the identification method cannot track and quantify the COVID-19 effect at a specific place [10].

Blockchain could equip a decentralized solution for sharing information and protecting confidentiality right out of the box. Each computer node may bundle user data into transactions and store it on the blockchain. Even if one node's data is tampered with, it will not affect its integrity since the tampered info will fail to pass validated by existing blocks. A smart contract is a blockchain-based application that can execute instructions distributed while maintaining output consistency. Current viral monitoring service solutions examine infection transmission variables that are too simplistic. Figure 1 shows the basic structure of blockchain network.

The key features of blockchain are as follows:

(1) Efficiency: a blockchain is simple to use and it can stalk large amounts of information. Moreover, it can bypass any complicated system.

(2) Transparency: because it shares resource information with all connected mobile devices, a blockchain

automatically opens all resource status and consumption data. This analysis looked at specific mobile devices' exclusive use of resources and infrastructure.

(3) Security: the security of a blockchain is superior to that of centralized data handling. Intruder invasions have the potential to do catastrophic damage to centralized data management. Giving misleading results is nearly tricky with a blockchain. It would need simultaneous control of all portable devices on which the data is disseminated, followed by a change to the data recorded in the machines.

1.1. Problem Definition.
Because the epidemic had such a negative impact on Saudi Arabia's economy, it is necessary to decrease the pandemic's ramifications and restore it to normalcy. The primary guideline for probable illness outbreak prevention is a set of limits and confinements. Many Android-based applications have been developed to remind people of these limits to stay healthy [11–13]. Everyone should follow the health professionals' safety recommendations; yet, these are insufficient in any public gathering. The main motivations are mentioned as follows:

(i) There is a growing demand for accurate and updated real-time COVID-19 tracking and prevention-based solutions. Daily updates, visiting locations monitoring, physical symptoms screening (to use a question-and-answer technique), report uploading, and other features are available in multitasking programs.

(ii) As a result, present Android-based applications lack data security and dependability, consume more bandwidth, and result in requests overlapping in public locations, making them unable to meet the
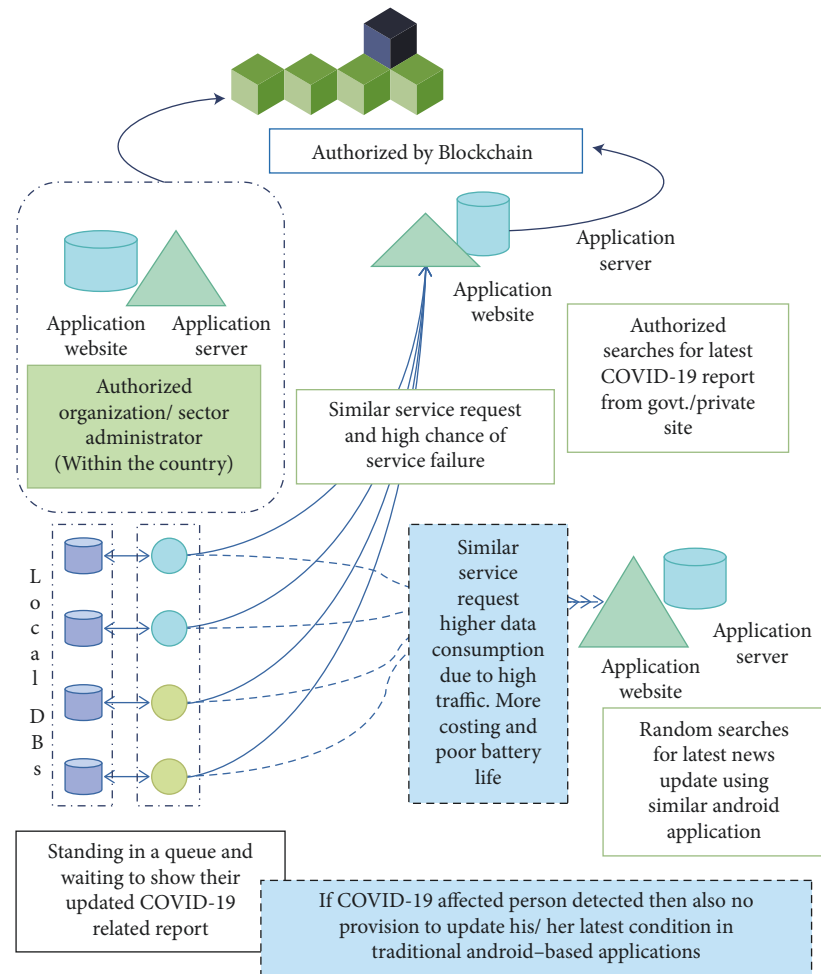
Figure 2: Request for in-country service avail.

extra quality of service (QoS) criteria [14]. We focused on two contemporary instances: admission into public meetings by people and customs checks.

(iii) Case 1: Figure 1 was added to the mix. Waiting in line to display their updated COVID-19 linked report, this gathering can expose people to infectious illnesses more seriously. An Android application was created to prevent this, although it has some security flaws. As a result, service failure is more likely when people in the queue/group make similar service requests. Due to increasing traffic, similar service requests can result in higher data usage. As a result, there is an increase in cost and a decrease in battery life. Figure 2 shows request for in-country service avail.

In this situation, the affiliations to which the user wishes to get access and the report supplier authorization/administrator each have their application website and application server (within the same country). As a result, we may delegate soul authority to a particular association/sector to scan every incomer, validate their provided report/information via direct access to that administrative website, and

update the individual's most recent health clearance without requiring any human interaction. Hemayah provides this precise digital platform, which aids in the reduction of paper printed copy transfer during social assemblies.

(ii) Case 2: it is expanded into Figure 3 (request for outside-country service avail) waiting in line to show their updated COVID-19-related report in a country checkpoint after arriving from another country.

For storing and verifying proposals, a centralized system is also employed. As a result, there is a risk of data privacy, as data can be altered with or hacked. KSA is the authorized institution administrator. To monitor COVID-19, we also require a blockchain-based contactless notification system. The cloud is used to back up all of your data.

The major contributions are as follows:

(1) A blockchain-based decentralized system is proposed to get a better and contactless notification for COVID-19 contamination.

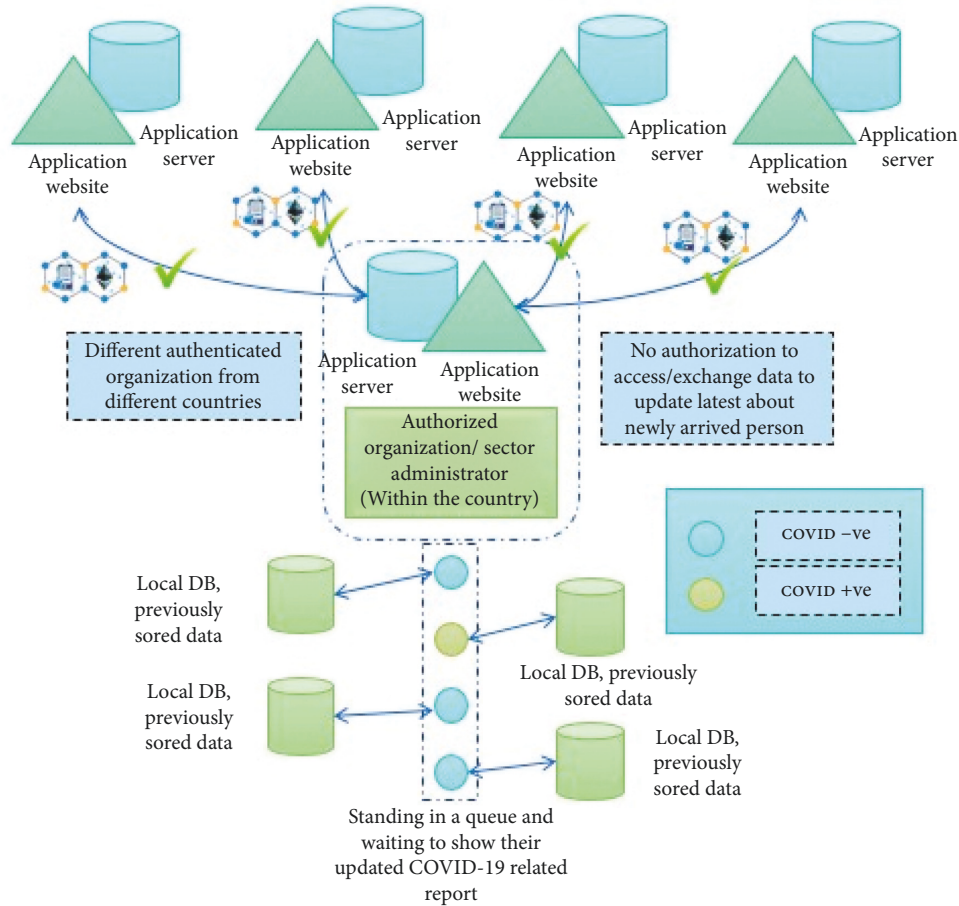(2) A secure system order is used for escalation customer confidentiality, safety, and clearness.

FIGURE 3: Request for outside-country service avail.

(3) Encryption and decryption methods were also incorporated to generate both key pairs.

(4) Bluetooth is used for connecting one user to another user and generating a spontaneous and speed notification system.

1.2. Organization of Paper. The roadmap of this paper is mentioned in this section. Section 2 defines the background study of this present context. Section 3 formulizes our proposed system. Section 4 represents the simulation process along with evaluating scheme performance or outcome. Section 5 presents the result and discussion for this work. The last part of our work represents the conclusion for this paper

2. Related Work

MIT, Apple, and Google all have contact tracing-related products and initiatives. On the other hand, their remedies are either a centralized database incorporated into the system or insufficient data confidentiality for consumers. Such designs are unable to fulfill the demands of user privacy [15]. The smart contract ensures that operations are carried out consistently and that a consistent result is obtained in terms of data security. One study describes a trading platform for computer resources based on a smart contract-based edge computing network. This approach employs a tree-structured smart contract group similar to ours. However, their implementation focuses on matching users and completing resource trade. The goal of smart contracts, on the other hand, is to keep track of the infection state of sites. Some existing research uses differential privacy (DP) and completed their work [16]. Several publications employ DP algorithms on the Internet of Technology facts managing; however, DP approaches will yield a pretty precise outcome with impurity in it. This feature will not go to work with the property of decentralized technology like blockchain [17, 18]. While keeping information, the subsequent node should test the integrity of the preceding block's contents and cannot accept variances [19–21]. However, exploring how these two topics cross in the study might be fascinating. Table 1 represents a comparative analysis of different verification approaches with their advantages and disadvantages. Table 2 represents a descriptive discussion of decentralized blockchain approaches with their advantages and disadvantages.

Proposed technology can trace users' visits to other venues and their personal experiences with each other. When a user comes to know about the contaminated report, the proposed system will notify another person not to come in the major contacts either directly or indirectly and offer

TABLE 1: Verification approaches with their features.

Verification approaches	Benefit	Starfish
Fingerprint-based verification	More secure than other approaches and highly convincing	High-cost and difficult to implement and manage
Verification using hardware or software	More secure than the verification process using data or information	High threat of compromising sensitive data, entire data will be lost, one's terminal mislaid
Verification using information	Nominal cost with limited resources	Centralized control, prone to vulnerability
Others	Mantation higher safety, compact deception threat	High-cost and difficult to implement and manage

TABLE 2: Benefit and disadvantage of decentralized System.

Parameter	Benefit	Disadvantage
Within decentralize network	Immutability	High cost
	Clearness	Making possible forks
	Privacy	Complicated
	Trestles environment	Respectively slow
Database	Distributed	No centralized control

important information for the same. Lastly, the system tries to recognize that person who may contact unknowingly and get contaminated.

2.1. End-to-End Tracking. Contacting trustworthy persons while using wireless technology can be possible in proposed smartphone-based method, which also uploads personal details to distributed, trustless blockchain systems. Wireless technology like Bluetooth can detect another present just approximately 4 to 8 meters. As a result, when the patient's smartphone receives Bluetooth signals, there are others around. When a person registers himself as contaminated, our system broadcasts their contamination situation to other customers, alerting them to their health condition; maybe they are in close interaction with this sick customer. Although viruses may adhere to water vapor and propagate via the aerosol, and users may be affected by other persons nearby, tracking the direct contact recorded by Bluetooth is critical. As a result, submitting customers' connection records will assist them in tracking the virus's invasion route and determining the likelihood of acquisition. Figure 4 represents the user logs on details to the corresponding site and records information in the blockchain database.

3. Health Tracing Service

3.1. Inflammation Possibility. As per WTO medical staff manual, healthy people can be infected both intrinsically and extrinsically, with the direct interaction being close person-to-person contact and the indirect interaction. The infection persisting on the object's external spreads the patient infecting healthy individuals after reaching the surface. As a result, the computer would assess the participant based on feature data collected from geographical tracking and individual contact tracings, such as the duration of interaction time among patients, the distance between patients, and the items in public spaces' risk from these aspects.

3.2. Infection Notice. After calculating the likelihood of contamination for this patient, the alerting function refers him a warning notification message, reminding him to either prepare for disease ahead of time or seek medical care before his health condition worsens. Whenever a client claims that they are contaminated, the proposed framework will publish their simulated individuality to other clients. The customers who get the warning notification can ask the native database to determine whether they have an infection or not by contacting directly or indirectly with the sick person, and the transmission risk will be calculated.

3.3. Tracing User Visited Locations. In a typical case, the customer may frequently meet numerous people in public locations in a single day, like workplaces, cafeterias, malls, or clubs; thus she may utilize the provided interaction tracking facility to upload her staying data, which she wants to include. Figure 4 shows the user logs on to the site and make the bunch of records and information in the blockchain-based database.

It informs our system about the time and place. The visitation data will be kept in the distributed blockchain system. Users may also verify the infection status before visiting to guarantee their protection. When a customer tested COVID-19 positive, a set of smart contracts incorporated in the proposed framework are responsible for updating the contamination condition of the spaces with modes of conveyance that the user visited or used, depending on their visit data.

4. Proposed Method

In this part, we have described and enlightened the proposed blockchain-based risk notification system with all components starting from the standpoint and different layers present in the system and the connections within it. Figure 5 defines the proposed blockchain-based architecture for contactless monitoring.
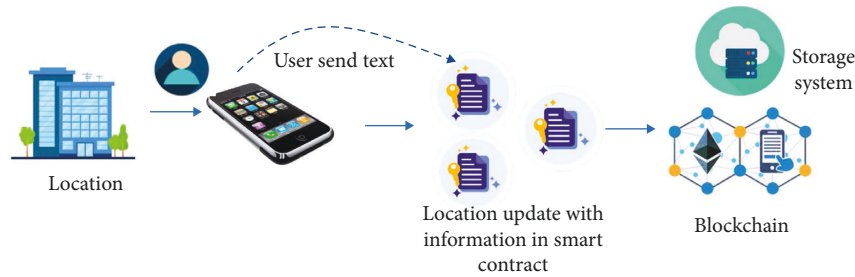
FIGURE 4: The user logs on to the site and records information in the blockchain database.
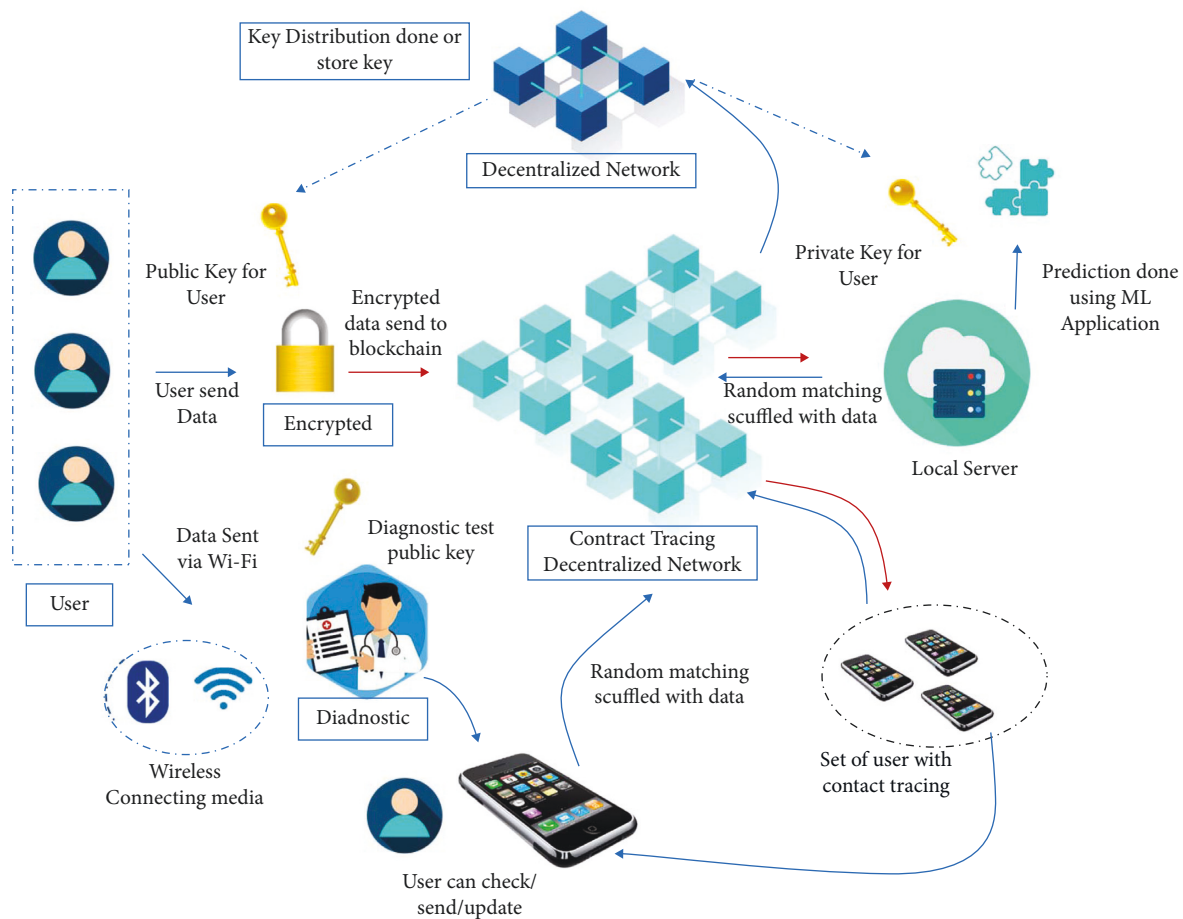
FIGURE 5: Proposed blockchain-based architecture for contactless monitoring.

4.1. System Architecture. Users may utilize our four-layer trace and notification system to track individual Bluetooth connections, registration positions, also contamination question conditions with other patients on the applied decentralized platform. Figure 6 depicts different layers: patient communication layer, remote facility layer, service provided by SM layer, and record-keeping layer are the layers that make up the user interface. This system offers two main tracing and alerting services: Bluetooth-based individual contact tracking and position-based contact tracking. The data created by these two services are kept in distributed blockchain databases, and both services are built on the public blockchain. The smart contracts in the third tier

coordinate the position-based contact tracking, while the wireless contact trace is handled by the next layer. Figure 6 represents the work flow diagram of proposed contactless monitoring.

4.2. Patient Communication Layer. Customer C and position P are both entities in the user interaction layer. Users are persons who have Bluetooth-enabled phones and fall into one of two categories of health: healthy or unhealthy. Both of you are infected; users who are not affected and those who are infected. In the second tier, users access cell phone services and update their health status regarding the medical
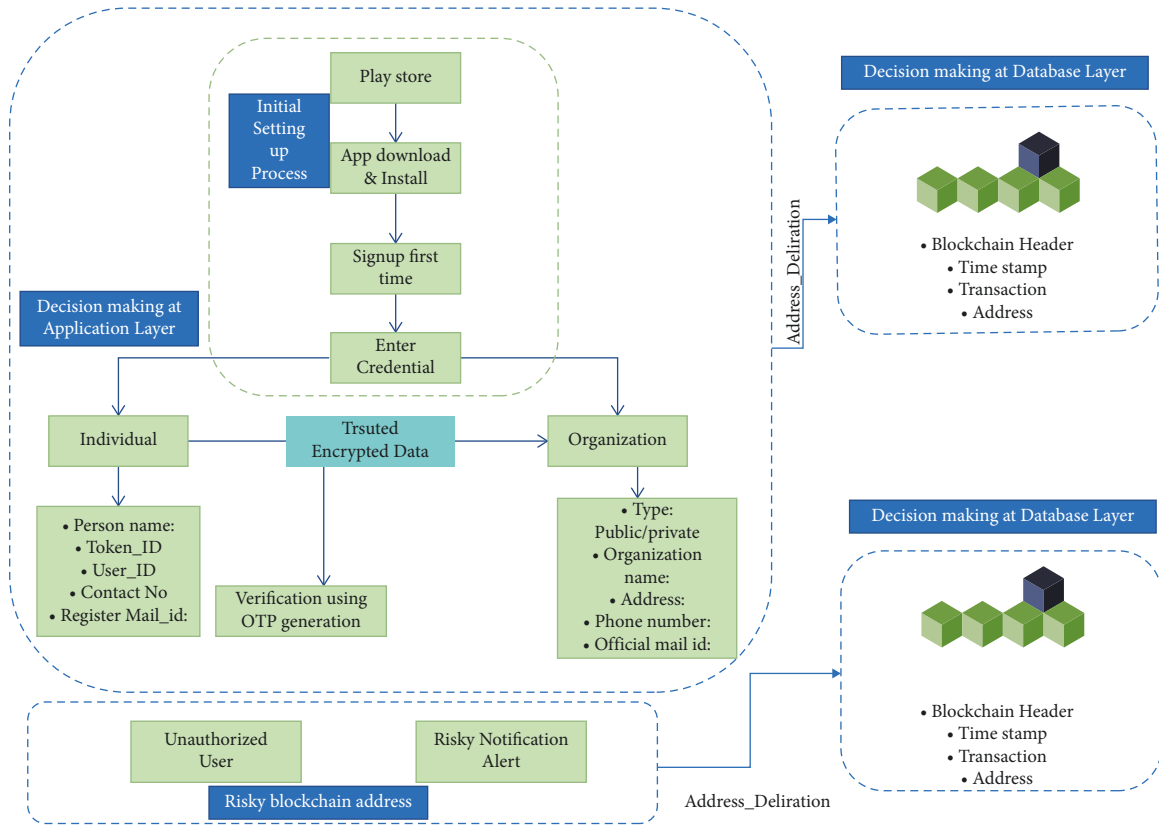
Figure 6: Proposed flow work for contactless monitoring.

assessments. We take it for granted that users constantly update our system with accurate information about their infection condition. A position P is a communal venue or mode of transport used by people in their everyday lives, such as workplaces, restaurants, stadiums, buses, and even aircraft. Uninfected position U_p normal and infected destination I_p infected are the two status kinds for position P. If this place P was visited by an infected user I_p infected, the system would record it as P contaminated.

4.3. Remote Facility Layer.

Our system's primary handler, the mobile service Layer, communicates directly with the other three levels. In this layer, the remote facility $Cell_p$ is our planned mobile phone application. The remote facility layer, in collaboration with different layers, such as an edge layer for delivering service to users, contains two major aspects: interaction tracking based on wireless or position and fitness tracking basis of information from the public blockchain.

4.4. Service Provided by SM Layer.

Our system's second core is the smart contract service layer. The remote facility layer processes the check-in request rechecking created by the user visiting position P and forwards it to this smart contract facility layer, where the smart contract group manages it. The smart contract group ties contracts together based on the organizational structure scheme. The SM dedicated for the state level is SCont_state at the top of the hierarchy, followed

through the county SCont_county Contract, the town SCont_city, and lastly, the minor unit location SCont_pos. $SCont\_city$ manages smart contracts based on location town contracts, SCont_county manages district contracts, and States SCont_state manages county-level contracts.

Every agreement or smart contract may only inherit from one superior contract, and it cannot be a part of two excellent contracts simultaneously. One of these three states must be present at each site: $\{E_{status}, Af_{status}, Neg_{status}\}$ and the smart contract that goes with it. Contract location dynamically records the infection status of position P. This place P is deemed infected by this customer C infected if an infected customer I_c infected visits it or if a user who has seen it reports that he is affected. The position P is regarded as a Neg_{status} only if it has been cleansed or fourteen days after being contaminated. The subsequent requests will reduce the smart contract SCont_pos operation costs while maintaining the correctness of the position P status record. Requirements cause the smart contract SCont_pos to check and update the infection state of position P. Otherwise, the SM SCont_pos will not vigorously detect the contamination condition of position P. This approach guarantees that customers obtain the most up-to-date location status for their requests while eliminating smart contract activities.

4.5. Record-Keeping Layer.

In the record-keeping layer, we have deployed a distributed blockchain database DB. Every customer and compute block in this system may be synced to

(1) Initiation for setup
(2) System setup for Mobile Application installation and get the credential
(3) Check Login credential working or not
(4) If yes
(a) .Then end
(5) Else repeat line 2
(6) Generate User_id_temp with *geo* location
(7) Apply for verification and validation
(8) Once validate users get User_id
(9) If get error
(a) Then apply line 8
(10) Update user device to the network
(11) Get device_pair_id ready to connect with others via Bluetooth
(12) User will broadcast User_id
(13) Users can connect multiple times but need to match *a dd ress_i d*
(14) Start Testing by Miner
(15))req_sample from the user and identify COVID-19 in the lab
(16))if,req_sample == POV
(a) Then
(b) reg_id user details and generate new id
(c) Key_pairs is generated by the applied method
(d) .Provide treatment by the health unit
(e) .Find any Local_match nearest to the user
(f) .Generate alert_warning and broadcast it to the author
(g) Update contaminated info blockchain
(17) Else declare re_sample == NOV
(a) Update user info into blockchain
(18) End
(19) Only Updated and users can access the data while using keys
(20) Gov. can only check the numbers of COVID tested req_sample == POV to confirm the user's confidentiality

ALGORITHM 1: Proposed blockchain-based secured data sharing algorithm.

TABLE 3: Overall comparison of existing work with proposed work.

Paper name	Decentralized	Authentication of user	Data confidentiality	Availability	Tractability	Integrity
Azzaoui [3]	Yes	Yes	Yes	No	No	No
Sharma et al. [4]	Yes	Yes	No	No	No	Yes
Kim et al. [2]	Yes	Yes	Yes	No	No	Yes
Abouyoussef et al. [5]	Yes	No	Yes	No	No	No
Dhaliwal et al. [12]	No	No	Yes	Yes	No	No
Gupta et al. [18]	No	Yes	Yes	Yes	Yes	No
Proposed work	Yes	Yes	Yes	Yes	Yes	Yes

receive a comprehensive database consistent with all others. Typically centralized databases hold all data in a single data server center, whereas conventional distributed records store information in numerous data server centers; however, each storage system may not contain entire worldwide information. Database systems need an essential block to execute input and keep the output of operations in the database. In contrast, a blockchain-based database never requires a central module because all users may query the same database locally for consistency.

The blockchain database in our system will hold all transaction processing, such as customers' Bluetooth commerce data, registration info for the frequented position, and changes in the user's general medical status, except for position-based contact tracking, which requires SM to upload, update, and keep contamination report condition in the DB. For other services like tracking facilities, position-based contact tracking, wireless contact tracking, and e-health tracking facilities, customers can ask questions to the decentralized database unswervingly for private contacts and staying data.

5. Result Analysis

We create a working demo and test its work in the following tests, which employ the Poisson distribution equation to replicate users' daily contact and check-in actions. The average cost of submission requests and the overall cost of

```
1    pragma solidity >=0.4.22 <0.7.0;
2
3    contract SmartContSubscription {
4        uint256 subm;
5
6        constructor(uint256 subm) public {
7            monthlyCost = subm;
8        }
9
10       function makePayment() payable public {
11
12       }
13   }
```

FIGURE 7: Example of pragma.
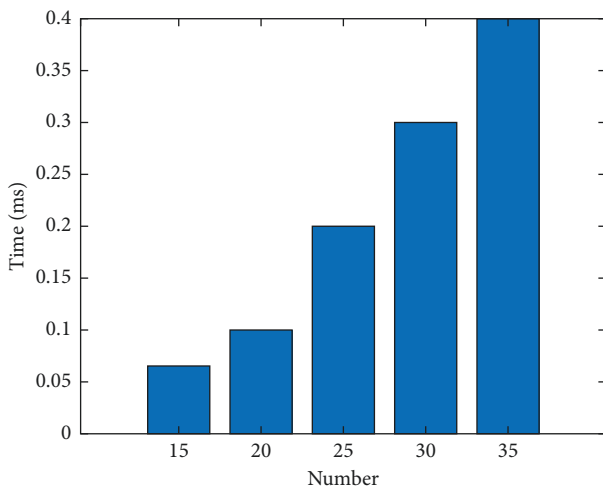
FIGURE 8: Time to create a block.

FIGURE 9: Time to validate a block. Calculate overhead in the system. The expenses of interaction between remote facility and patients and the operational expenses of smart contracts are quantified by Ethereum gas.

operating the proposed prototype framework are the studies' subjects. We begin by setting the stage for the tests. The service's security and adaptability are next evaluated and analyzed. The proposed system may set up and create benchmarks in the future to assess while the actual dataset becomes accessible.

Implementation of the System Experiments is carried out using an HP with Windows 10 operating system. This computer features a 2.3 GHz Intel i3 processor and eight gigabytes of RAM. The SM set is established and implemented using the Solidity programming language, and it is implemented on a sample Ethereum blockchain modeled using Ganache software. The script for data analysis is then written in Python [22]. Table 3 defines the overall comparison of existing work with proposed work. A sample code is displayed in Figure 7.

To calculate the average submission cost, we calculate the average gas cost of all requests and the standard deviation on

the average cost of fifteen iterations of tests using three measures of arranged smart contracts and five different numbers of submissions ranging from one hundred to six hundred. The average request gas consumption is lowered by a factor of five from two hundred thousand Wei to four hundred thousand Wei. The variance of request cost is lowered by five times as the number of requests increases. The actual overhead is relatively minimal, even though the gas volume and deviation in Figures 8 and 9 are rather large. We understand that the lowest gas unit in the Ethereum system is the Wei and that one ether equals 1011 Wei.

It shows that as the number of applications rises from 50 to 200 and the contract rises from 15 to 25, the system's total gas usage rises linearly, taking into account the case of the same number of applications with different figures of
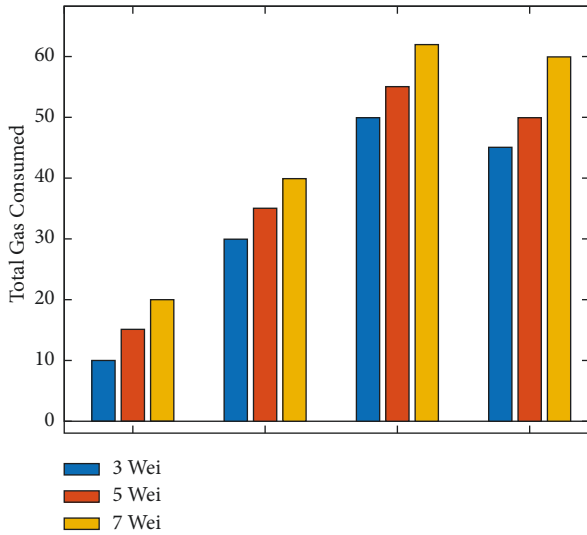
FIGURE 10: The amount of gas used by the remote facility, smart contracts, and consumers combined.
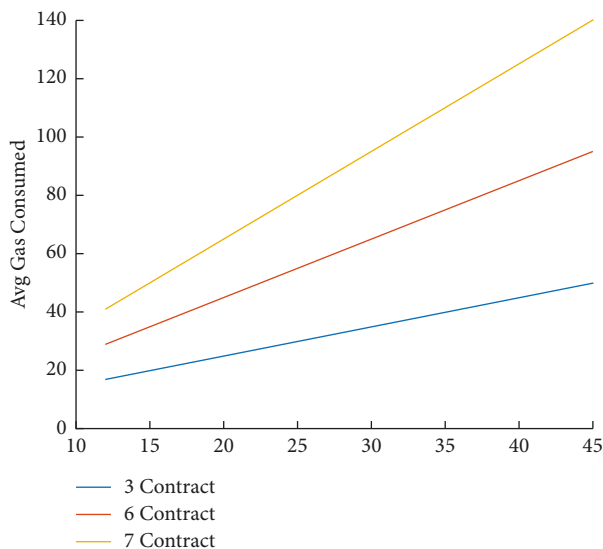
FIGURE 11: The average gas consumption.

contracts, as well as the case of the equal number of agreements with varying numbers of requests. A comparison is also demonstrated in Figure 10 of gas consumption by remote facility, smart contracts, and consumers combined.

Our suggested scheme has high stability and scalability based on the three measures [23]. The demand cost, which is the most significant overfit in the framework functioning, has been steadily approaching a lower threshold as the number of requests and contracts has increase. Lastly, Figure 11 shows an average gas consummation for the entire system.

6. Conclusions

In this work, we propose a tracking and alerting framework based on blockchain and smart contracts that offer three types of services: position-based contact tracking, wireless tracking, and smart contract-based tracking. Solutions for health tracing our technology can track a customer's travel and interaction record, as well as reminding them of previous infections they may have had. The health tracking program also allows users to evaluate their chances of becoming sick. Customers can securely transmit their visit data and health condition to the blockchain network to secure their confidentiality. Users may also utilize a massive set of arbitrary physical addresses generated by wireless technology as a provisional identity to preserve their anonymity even more.

Furthermore, the set of smart contracts was integrated into the framework to keep the contamination condition of each and every place. It executes the equivalent order of check-in procedures to guarantee that each patient receives the location's contamination findings consistently. We also simulate user contact with the proposed prototype organization before assessing its performance, including gas consumption, operating constancy, and request handling speed. Our system offers high scalability and stability in a simulated environment. We plan to have actual data regarding customer contact data to assess our technology in the forthcoming.

Data Availability

The data used to support the findings of this study are included within the article.

Conflicts of Interest

The authors declare that they have no conflicts of interest.

Acknowledgments

References

[1] D. C. Nguyen, M. Ding, P. N. Pathirana, and A. Seneviratne, "Blockchain and AI-based solutions to combat coronavirus (COVID-19)-like epidemics: a survey," *IEEE Access*, vol. 9, no. 2021, pp. 95730–95753, 2021.

[2] H.-W. Kim and Y.-S. Jeong, "Secure authentication-management human-centric scheme for trusting personal resource information on mobile cloud computing with blockchain," *Human-centric Computing and Information Sciences*, vol. 8, no. 1, pp. 11–13, 2018.

[3] A. E. L. Azzaoui, T. W. Kim, Y. Pan, and J. H. Park, "A quantum approximate optimization algorithm based on blockchain heuristic approach for scalable and secure smart logistics systems," *Human-centric Computing and Information Sciences*, vol. 11, 2021.

[4] A. Sharma, S. Bahl, A. K. Bagha, M. Javaid, D. K. Shukla, and A. Haleem, "Blockchain technology and its applications to

combat COVID-19 pandemic," *Research on Biomedical Engineering*, vol. 38, no. 1, pp. 173–180, 2020.

[5] M. Abouyoussef, S. Bhatia, P. Chaudhary, S. Sharma, and M. Ismail, "Blockchain-enabled online diagnostic platform of suspected patients of COVID-19 like pandemics," *IEEE Internet of Things Magazine*, vol. 4, no. 4, pp. 94–99, 2021.

[6] A. K. Das, B. Bera, D. Giri, and D Giri, "AI and blockchain-based cloud-assisted secure vaccine distribution and tracking in IoMT-enabled COVID-19 environment," *IEEE Internet of Things Magazine*, vol. 4, no. 2, pp. 26–32, 2021.

[7] M. Shuaib, N. Hafizah Hassan, S. Usman et al., "Identity model for blockchain-based land registry system: a comparison," *Wireless Communications and Mobile Computing*, vol. 2022, pp. 1–17, Article ID 5670714, 2022.

[8] Y. Kim and J. Park, "Hybrid decentralized PBFT blockchain framework for OpenStack message queue," *Human-centric Computing and Information Sciences*, vol. 10, no. 1, pp. 31–12, 2020.

[9] K. Dev, S. A. Khowaja, A. S. Bist, V. Saini, and S. Bhatia, "Triage of potential COVID-19 patients from chest X-ray images using hierarchical convolutional networks," *Neural Computing & Applications*, pp. 1–16, 2021.

[10] P. Zhai, Y. Ding, X. Wu, J. Long, Y. Zhong, and Y. Li, "The epidemiology, diagnosis and treatment of COVID-19," *International Journal of Antimicrobial Agents*, vol. 55, no. 5, Article ID 105955, 2020.

[11] R. Guha and S. Narayana, "A blockchain-based cyber attack detection scheme for decentralized Internet of things using software-defined network," *Software: Practice and Experience*, vol. 51, no. 7, pp. 1540–1556, 2021.

[12] P. Dhaliwal, P. Kumar, and P. Chaudhary, "An approach for concept drifting streams: early dynamic weighted majority," *Procedia Computer Science*, vol. 167, pp. 2653–2661, 2020.

[13] Y. Xiong, H. K. S. Lam, A. Kumar, E. W. T. Ngai, C. Xiu, and X. Wang, "The mitigating role of blockchain-enabled supply chains during the COVID-19 pandemic," *International Journal of Operations & Production Management*, vol. 41, no. 9, pp. 1495–1521, 2021.

[14] L. Ricci, D. D. F. Maesa, A. Favenza, and E. Ferro, "Blockchains for covid-19 contact tracing and vaccine support: a systematic review," *IEEE Access*, vol. 9, no. 2021, pp. 37936–37950, 2021.

[15] S. Bhatia, A. K. Dubey, R. Chhikara, P. Chaudhary, and A. Kumar, *Intelligent Healthcare*, Springer International Publishing, Berlin, Germany, 2021.

[16] M. H. Kassab, V. V. G. Neto, G. Destefanis, and T. Malas, "Could blockchain help with COVID-19 crisis?" *It Professional*, vol. 23, no. 4, pp. 44–50, 2021.

[17] W. Alkhader, K. Salah, A. Sleptchenko, R. Jayaraman, I. Yaqoob, and M. Omar, "Blockchain-based decentralized digital manufacturing and supply for COVID-19 medical devices and supplies," *IEEE Access*, vol. 9, no. 2021, pp. 137923–137940, 2021.

[18] R. Gupta, P. Pandey, S. K. Chaudhary, and S. K. Pal, "Technological and analytical review of contact tracing apps for COVID-19 management," *Journal of Location Based Services*, vol. 15, no. 3, pp. 198–237, 2021.

[19] M. Khalid Imam Rahmani, F. Taranum, R. Nikhat, M. Rashid Farooqi, and M. Arshad Khan, "Automatic real-time medical mask detection using deep learning to fight COVID-19," *Computer Systems Science and Engineering*, vol. 42, no. 3, pp. 1181–1198, 2022.

[20] G. F. Frederico, "Towards a supply chain 4.0 on the post-COVID-19 pandemic: a conceptual and strategic discussion for more resilient supply chains," *Rajagiri Management Journal*, vol. 15, no. 2, pp. 94–104, 2021.

[21] T. P. Mashamba-Thompson and E. D. Crayton, "Blockchain and artificial intelligence technology for novel coronavirus disease-19 self-testing," *Diagnostics*, vol. 10, no. 4, p. 198, 2020.

[22] P. Gandhi, S. Bhatia, and K. Dev, Eds., *Data Driven Decision Making Using Analytics*, CRC Press, Florida, USA, 2021.

[23] S. Basheer, S. B. Bhatia, and S. B. Sakri, "Computational modeling of dementia prediction using deep neural network: analysis on OASIS dataset," *IEEE Access*, vol. 9, pp. 42449–42462, 2021.

WILEY | Hindawi

Research Article

A New Nonlinear Controller Design for a TCP/AQM Network Based on Modified Active Disturbance Rejection Control

Anwer S. Aljuboury,[1,2] **Subhi R. M. Zeebaree,**[3] **Firas Abedi,**[4] **Zahraa Sabah Hashim,**[5] **Rami Q. Malik,**[6] **Ibraheem Kasim Ibraheem,**[7] **and Ahmed Alkhayyat** ⓘ[8]

[1]*Continuing Education Center, Mustansiriyah University, Baghdad, Iraq*
[2]*Information Technology Unit, Hilla University College, Babylon, Iraq*
[3]*Energy Department, Technical College of Engineering, Duhok Polytechnic University, Duhok, Iraq*
[4]*Department of Mathematics, College of Education, Al-Zahraa University for Women, Karbala, Iraq*
[5]*Department of Electrical Engineering, College of Engineering, University of Baghdad, Baghdad, 10001, Iraq*
[6]*Department of Medical Instrumentation Techniques Engineering, Al-Mustaqbal University College, Hillah, 51001, Iraq*
[7]*Department of Computer Engineering Techniques, Al-Rasheed University College, Baghdad, 10001, Iraq*
[8]*College of Technical Engineering, The Islamic University, Najaf, Iraq*

Correspondence should be addressed to Ahmed Alkhayyat; ahmedalkhayyat85@iunajaf.edu.iq

The main aim of this study was to address the problem of congestion in TCP nonlinear systems in the presence of mismatched exogenous disturbances. To achieve this problem, two methods are proposed: the first is active queuing management, based on two proposed controllers, an NLPID and STC-SM, while the second is the application of active queuing management-based anti-disturbance techniques such as active disturbance rejection control (ADRC) and the nonlinear disturbance observer (NLDO). The proposed ADRC consists of a new NLPID and a new super-twisting sliding mode controller (STC-SM), which functions as a novel NLSEF, and a proposed NLESO estimates the applied disturbance and cancels it in a responsive manner. A new tracking differentiator with a novel function is also used to generate a smooth and accurate reference signal and derivative. The NLDO is proposed to estimate the disturbance and combine this with the control signal of the designed nonlinear controller as a way to compensate for the disturbance. The simulation results for the proposed scheme (ADRC) as applied to a nonlinear model of the TCP network are thus found to provide smoother and more accurate tracking of the desired value, with high robustness against applied disturbance, as compared to the other schemes introduced in this study. The proposed scheme also shows a noticeable improvement in terms of the utilized performance indices and the OPI.

1. Introduction

The requirements for quick, high-speed, and reliable communication have become more intense with recent increases in the number of Internet users. To achieve the necessary reliable communication between the server and the client, TCP is thus widely used. TCP offers a connection-oriented packet switching method that provides a reliable, bidirectional connection between two endpoints; however, although TCP is more reliable than UDP, any significant increase in TCP flow may cause serious congestion in the

router, which will reduce network communication quality. A network congestion control method must thus be utilized, and there are two main types of congestion control. The first is source-based TCP management, such as Sack, New Reno, and Vegas, while the second is router-based active queuing management (AQM). Issues with global synchronization caused by the first method mean, however, that it is the second method that has been most widely utilized, which has attracted the attention of most researchers [1].

Initially, AQM was proposed by [2] in a form known as random early detection; after that, Misra provided an

analytical model for TCP/AQM in [3] using differential equations and fluid flow theory. AQM forms a method that actively drops the packet in the router buffer before it is full, ensuring that queuing length is always monitored: when congestion occurs, the queuing length becomes greater than the desired value, and the AQM uses this as an indication of congestion. At such times, the AQM provides effective, reliable, efficient, and fair communication between sender and receiver in the TCP network [1, 4].

AQM based on advanced control theory is now widely used, and it has thus attracted the attention of several researchers seeking to deal with the problem of congestion in TCP networks by achieving the desired trajectory of queuing length. The author in [1] presented the use of integral backstepping as an AQM for a multi-route TCP/AQM model as a way to reduce congestion, while in [5], the author proposed three controllers, H_∞, PSO-PID, and ACO-PID, as AQMs to reduce the effects of disturbance and uncertainty and to track the desired set point. In [6], the author introduced an AQM-based novel PD controller for both single and multiple bottleneck routers as a way to adjust the queuing length to the desired set point under small oscillations. The author in [7] designed a nonlinear disturbance observer with a backstepping controller to form a nonlinear TCP network system, while the author in [8] presented a backstepping controller that adopted a minimax approach to control congestion and avoid the influence of applied disturbance. In [9], the author introduced another controller, which utilized a combination of H_∞ theory and integral backstepping, to a nonlinear model of the TCP network system to control the congestion occurring in the network. The author in [10] further proposed the use of a PD controller as an AQM and linear disturbance observer (DOB), with a smith predictor (SP) and the linearized model of the TCP network used to avoid congestion in the TCP network and to eliminate the influence of or compensate for the time delay effect. A further finite time backstepping controller was proposed in [11], with the nonlinear model of the TCP network system encouraged to reach the desired value in a finite time; the author in [12] also proposed a self-tuning rate and queuing-based PI controller (SQR-PI) with a single/multiple bottleneck router model to control queuing length by estimating the rate of traffic and using this alongside a PI controller to map congestion levels and to dramatically reduce the probability of losing packets. A combination of finite time control, backstepping technique, prescribed performance, and fuzzy logic was then presented in [13] as a way to deal with applied disturbance and achieve queuing length in a finite time.

Although all the studies noted above provide robust controller techniques for a TCP network, several studies used the linearized model of the TCP network, while others considered the round trip time (RTT) as a constant. Further, no recent research has used the disturbance/uncertainty rejection technique, also known as active disturbance rejection control (ADRC). The ADRC is a powerful method, first proposed by [14], for dealing with the problem of exogenous disturbance, uncertainty, and unknown perturbations that may affect linear and nonlinear systems, whether SISO or MIMO. At present, while the ADRC is widely used in different fields, as introduced in [15–17], the effectiveness of the proposed methods as compared to the conventional one is unknown. Motivated by this survey, the researchers in this study used a modified version of the conventional ADRC technique as an AQM in this study.

The main aim of this study was to design an accurate control technique that can control congestion in the TCP nonlinear system and thus handle nonlinearity, disturbance, and uncertainty effects. A modified ADRC is thus proposed as an AQM in the time-delayed TCP network nonlinear model. The proposed method also contains two new controllers, NLPID and STC-SM, which are proposed as new NLSEFs, while a new fractional power nonlinear extended state observer is also proposed. Additionally, a new tracking differentiator is proposed using the sigmoid function, with three parts combined to form a modified ADRC that provides smooth, accurate, and excellent results. The parameters of the proposed controller, proposed NLESO, and the tracking differentiator were thus tuned using a genetic algorithm as an optimization technique [18], while a new multi-objective performance index was used in the minimization process. This includes the absolute of the control signals, the square of the control signals, the integral time absolute error, the integral time square error, and the mean square error.

The rest of this study is organized as follows: Section 2 presents the modelling of the TCP network, and then, the problem statement is illustrated in Section 3. Section 4 presents the design of the proposed ADRC, while Section 5 presents the design and convergence of NLDO, along with closed-loop stability analysis. Section 6 then illustrates the simulation results and offers a discussion of these simulations. Finally, Section 7 presents the conclusion of this study.

2. TCP/AQM Mathematical Models

Using fluid flow theory, the nonlinear model of a TCP network can be described using the following nonlinear differential equations with time-varying delays [19], assuming a single bottleneck router network topology as shown in Figure 1.

$$
\begin{cases}
\dot{W}(t) = \dfrac{1}{R(t)} - \dfrac{W(t)W(t - R(t))}{R(t)R(t - R(t))} p(t - R(t)), \\[4mm]
\dot{q}(t) = \dfrac{N(t)}{R(t)} W(t) - C(t) + d(t),
\end{cases}
\tag{1}
$$

$$
\begin{cases}
R(t) = \dfrac{q(t)}{C(t)} + \tau_p, \\[4mm]
R(t - R(t)) = \dfrac{q((t - R(t)))}{C(t)} + \tau_p,
\end{cases}
\tag{2}
$$

where $W(t)$ represents the average window size of the TCP network, $q(t)$ represents the average queuing length at the router, $R(t)$ is the round trip time, $C(t)$ is the link capacity, $N(t)$ is the number of TCP sessions, τ_p is the propagation
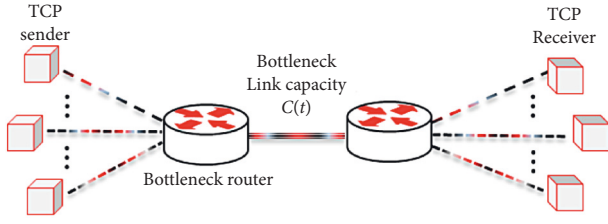
FIGURE 1: TCP network topology.

delay, and $p(t - R(t))$ is the probability of a packet marking that represents the AQM control strategy; additionally, $d(t)$ is the exogenous disturbance, denoted by the UDP unresponsive flows.

As this model incorporates time-varying delays, if $C(t)$ and $N(t)$ can be assumed to be constant (fixed) within a period of time, then $C(t) = C$ and $N(t) = N$ [19].

$$\begin{cases} p(t - R(t)) = u_0, \\ u = \aleph(u_0), \end{cases} \tag{3}$$

where $\aleph = \varepsilon + \varepsilon \tan h(u_0/\varepsilon)$ to ensure $u \in [0, 1]$, and ε is a positive tuning parameter. Thus, equation (1) can be re-written as follows:

$$\begin{cases} \dot{W}(t) = \dfrac{1}{R(t)} - \dfrac{W(t)W(t - R(t))}{R(t)R(t - R(t))}u, \\[2mm] \dot{q}(t) = \dfrac{N}{R(t)}W(t) - C + d(t). \end{cases} \tag{4}$$

The dynamic behavior of the window size in equation (1) is described by "addition increase multiplication decrease" [3]. The first term of $\dot{W}(t)$, which is $1/R(t)$, means that the window size increases by one for every round trip time ($R(t)$), while the second term, which is $W(t)W(t - R(t))/R(t)R(t - R(t))$, means that the window size is halved when congestion occurs, and the packet is lost. The first term of $\dot{q}(t)$, which is $N/R(t)W(t)$, thus refers to a newly arriving queuing packet. As the UDP shares the same link and channel with the TCP, the probability of losing a packet increases as the UDP continues sending packet even where congestion occurs: UDP unresponsive flow is thus considered to represent exogenous disturbance, $d(t)$.

3. Problem Statement

Let $x_1(t) = q(t) x_2(t) = N/R(t)W(t)$.

Remark 1. The model in equation (4) is different than the model introduced in [19], with the $\tan h(\cdot)$ function used as a limit function, with ε as a tuning parameter, rather than the sat $(\cdot)$ function as a way to solve the problem of the sharp edge. In addition, the effect of both the disturbance and the

time-varying delay is considered in this model, to approximately reflect the real behavior of the TCP network.

Based on the parameters from Remark 1, the equations for the TCP/AQM network can be represented as follows:

$$\begin{cases} \dot{x}_1(t) = x_2(t) + d(t), \\ \dot{x}_2(t) = f(\dot{x}_1, x_2, N, R(t), C, d(t)) + g_1(x)u, \\ y(t) = x(t), \end{cases} \tag{5}$$

where

$$f(x_1, x_2, N, R(t), C) = \frac{N}{R^2(t)} - \frac{x_2(t)\dot{x}_1(t)}{R(t)C},$$

$$g_1(x) = -\frac{x_2(t) + C}{2N}\left[(x_2(t) - R(t)) + C\right], \tag{6}$$

where $x = \{x_1, x_2\} \in \mathbb{R}^2$, representing the queuing length and the window size, respectively, $y(t) = x_1(t) \in \mathbb{R}$ is the measured output, and u is the control input, which is designed to stabilize and minimize the probability of packet loss to achieve the desired queuing length and reduce or avoid congestion when the exogenous disturbance $d(t)$ and parameter uncertainty are applied to the TCP/AQM network.

4. The Proposed ADRC Design

The ADRC is one of the most effective anti-disturbance methods, and it was first proposed by [14] in the late 1980s. The effectiveness of the ADRC is due to its ability to actively estimate disturbance, thus providing fast-tracking and accurate control. The design of the ADRC depends on its relative degree, and in this section, the design of the proposed ADRC, which consist of two options, a nonlinear controller and a tracking differentiator, and two schemes supporting the proposed nonlinear ESO, is introduced and examined.

4.1. The Proposed Tracking Differentiator. The tracking differentiator is that part of the ADRC used to generate the reference signal and the reference signal derivative, which must therefore offer a tuned and efficient response. The dynamic equation of the proposed tracking differentiator is thus given as

$$\begin{cases} \dot{r}_1(t) = r_2(t), \\[3mm] \dot{r}_2(t) = -a_1 R^2\left(\dfrac{(r_1(t) - r(t)) + 2(r_1(t) - r(t))^3}{1 + \left|(r_1(t) - r(t)) + 2(r_1(t) - r(t))^3\right|}\right) \\[5mm] -a_2 R r_2(t), \end{cases} \tag{7}$$

where $r_1(t)$ is the desired trajectory and $r_2(t)$ is its derivative and R, a_1, and a_2 are positive tuning parameters. It is worth noting that the function used in this equation (i.e., $((r_1(t) - r(t)) + 2(r_1(t) - r(t))^3/1 + |(r_1(t) - r(t)) + 2(r_1(t) - r(t))^3|))$ was introduced in [20] in the form "*Rational functions and absolute value*" as a replacement for the function used in [14].

4.2. Proposed Nonlinear Controllers.

In this subsection, the nonlinear controllers used in this study are introduced and defined:

(i) The first controller is the NLPID, which can be expressed as follows:

$$
\begin{cases}
u_1 = \dfrac{k_1}{1 + \exp(e^2)} |e|^{\alpha_1} \operatorname{sign}(e), \\[3mm]
u_2 = \dfrac{k_2}{1 + \exp(\dot{e}^2)} |\dot{e}|^{\alpha_2} \operatorname{sign}(\dot{e}), \\[3mm]
u_3 = \dfrac{k_3}{1 + \exp(\int e^2 dt)} \left| \int e dt \right|^{\alpha_3} \operatorname{sign}\left(\int e dt \right),
\end{cases} \tag{8}
$$

$$
u_{0_{\text{NLPID}}} = u_1 + u_2 + u_3. \tag{9}
$$

(ii) The second controller is the proposed super-twisting sliding mode controller (STC-SM), expressed as

$$
\begin{cases}
\varsigma = \kappa e + \dot{e}, \\[2mm]
u_{0_{\text{STC-SM}}} = \kappa |\varsigma|^p \operatorname{sign}(\varsigma) + \xi \tan h\left(\dfrac{\varsigma}{\delta}\right),
\end{cases} \tag{10}
$$

where $(k_1, k_2, k_3, \alpha_1, \alpha_2, \alpha_3, \kappa, \xi, p, \delta)$ are the shared controller tuning parameters, ς is the sliding surface, and $e = r_1 - z_1$ and $\dot{e}$ are the reference error and its derivative.

4.3. The Proposed Nonlinear Extended State Observer.

The nonlinear ESO is an improved nonlinear version of the linear ESO shown previously to effectively estimate

disturbances in specific cases. The proposed NLESO is a modified version of the NLESO proposed by [21], and the mathematical representation of the first scheme of the modified NLESO is expressed as

$$
\begin{cases}
\dot{z}_1(t) = z_2(t) + \beta_1 \hat{e}_1(t), \\
\dot{z}_2(t) = z_3(t) + \beta_2 \hat{e}_2(t) + b_0 u(t), \\
\dot{z}_3(t) = \beta_3 \hat{e}_3(t).
\end{cases} \tag{11}
$$

For the nonlinear function,

$$
\begin{cases}
\hat{e}_1(t) = \operatorname{sign}(e_1(t)) |e_1(t)|^a + e_1(t), \\
\hat{e}_2(t) = \operatorname{sign}(e_1(t)) |e_1(t)|^{2a-1} + e_1(t), \\
\hat{e}_3(t) = \operatorname{sign}(e_1(t)) |e_1(t)|^{3a-2} + e_1(t),
\end{cases} \tag{12}
$$

where β_1, β_2, and β_3 are the observer gain, z_1 and z_2 are the estimated state, z_3 is the estimated total disturbance, and $0.67 < a < 1$ is a positive tuning parameter. Another scheme for NLESO is also proposed and used in this study. The mathematical representation of the second scheme for a modified NLESO can be expressed as follows:

$$
\begin{cases}
\dot{z}_1(t) = z_2(t) + \beta_1 \hat{e}_1(t), \\
\dot{z}_2(t) = z_3(t) + \beta_2 \hat{e}_2(t) + b_0 u(t), \\
\dot{z}_3(t) = \beta_3 \hat{e}_3(t),
\end{cases} \tag{13}
$$

where $\hat{e}_i(t), i \in \{1, 2, 3\}$ is expressed as follows:

$$
\begin{cases}
\hat{e}_1(t) = \operatorname{sign}(e_1(t)) |e_1(t)|^a + A e_1(t), \\
\hat{e}_2(t) = \operatorname{sign}(e_1(t)) |e_1(t)|^{a/2} + A e_1(t), \\
\hat{e}_3(t) = \operatorname{sign}(e_1(t)) |e_1(t)|^{a/4} + A e_1(t),
\end{cases} \tag{14}
$$

where $e_1(t) = q(t) - z_1(t)$, $e_1(t)$ is the estimation error, $z_1(t)$ is the estimation state of q, $\hat{e}_1(t), \hat{e}_2(t)$, and $\hat{e}_3(t)$ are the nonlinear functions, a is a tuning parameter that should be less than 1, and $\mathscr{A}$ is another tuning parameter.

The complete diagrams of both the proposed controllers and the proposed ADRC with the TCP/AQM nonlinear model are shown in Figures 2 and 3. In this study, the tracking differentiator is used instead of the ordinary derivative as a way to access both the error and its derivative: thus, equations (7), (8), and (10) can be rewritten as follows.

(i) The tracking differentiator is as follows:

$$
\begin{cases}
\dot{\tilde{e}}_1(t) = \tilde{e}_2(t), \dot{\tilde{e}}_2(t) = -a_1 R^2 \left(\dfrac{(\tilde{e}_1(t) - \tilde{e}(t)) + 2(\tilde{e}_1(t) - \tilde{e}(t))^3}{1 + \left| (\tilde{e}_1(t) - \tilde{e}(t)) + 2(\tilde{e}_1(t) - \tilde{e}(t))^3 \right|} \right) - a_2 R \tilde{e}_2(t).
\end{cases} \tag{15}
$$

(ii) The NLPID controller is as follows:
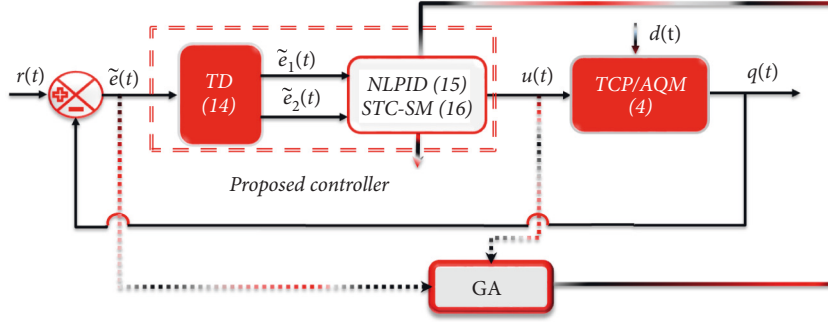
FIGURE 2: Completed diagram of the TCP/AQM based on the proposed controllers.
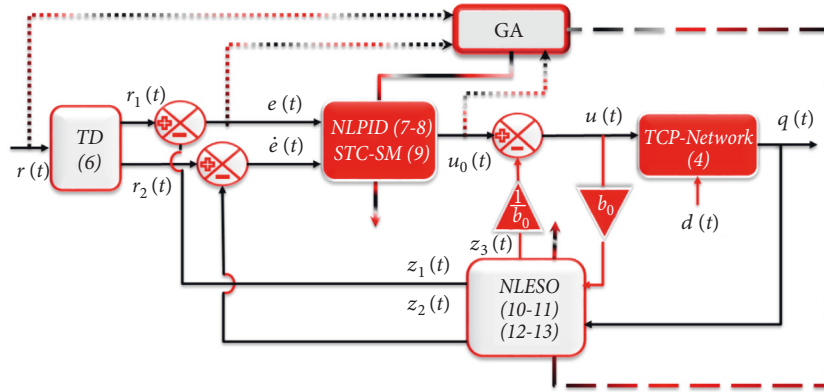
FIGURE 3: Completed diagram of the TCP/AQM based on the proposed ADRC.

$$\begin{cases} u_1 = \dfrac{k_1}{1 + \exp(\tilde{e}_1^2)} |\tilde{e}_1|^{\alpha_1} \mathrm{sign}(\tilde{e}_1), \\[4mm] u_2 = \dfrac{k_2}{1 + \exp(\tilde{e}_2^2)} |\tilde{e}_2|^{\alpha_2} \mathrm{sign}(\tilde{e}_2), \\[4mm] u_3 = \dfrac{k}{1 + \exp(\int \tilde{e}_1^2)} |\tilde{e}_1|^{\alpha_3} \mathrm{sign}\left(\int \tilde{e}_1 \mathrm{d}t\right), \\[4mm] u_{0_{\mathrm{NLPD}}} = u_1 + u_2 + u_3. \end{cases} \quad (16)$$

(iii) The STC-SM controller is as follows:

$$\begin{cases} \varsigma = \kappa \tilde{e}_1 + \tilde{e}_2, \\[3mm] u_{0_{\mathrm{STC\text{-}SM}}} = \kappa |\varsigma|^a \mathrm{sign}(\varsigma) + \xi \tan h\left(\dfrac{\varsigma}{\delta}\right), \end{cases} \quad (17)$$

where $\tilde{e}_1$ and $\tilde{e}_2$ are the tracking error and its derivative and $\tilde{e}(t) = r(t) - q(t)$.

As mentioned previously, the design of the ADRC depends on the relative degree of the system, and as the TCP network is a SISO system, with a single input $u(t)$ and single output $q(t)$, the relative degree of the TCP/AQM network is thus $\rho = 2$.

5. The Proposed Nonlinear Disturbance Observer (NLDO) Design

The disturbance observer is one of the anti-disturbance techniques presented in [22], which can be linear or nonlinear; in this work, the nonlinear disturbance observer is thus presented, which is designed to estimate external disturbance, such as an unknown load, and the changes and UDP unresponsive flow are calculated so that the estimated value can be employed to compensate for the influence of the disturbance.

The NLDO can be expressed as follows [22]:

$$\begin{cases} \dot{\mathscr{Z}} = -l(x)\mathscr{G}_2(x)Z - l(x)[\mathscr{G}_2(x)P(x) + \mathscr{F}(x) + \mathscr{G}_1(x)u], \\[3mm] \hat{d} = P(x) + Z, \end{cases}$$

$$(18)$$

where $\hat{d}$ and $\mathscr{Z}$ are the estimated disturbance and the internal state of the nonlinear observer, respectively, and $P(x)$ is a nonlinear function to be designed, while $\ell(x)$ is the nonlinear observer gain where $x \in \{x_1, x_2\}$. To ensure that the NLDO is asymptotically stable, the nonlinear function $P(x)$ must be designed in such a way as to force the NLDO to be asymptotically stable.

5.1. Convergence of the Proposed NLDO. To prove the effectiveness of the designed NLDO with the TCP network, an inclusive analysis was done using a Lyapunov stability approach [23].

As shown, equation (4) cannot fit the form of equation (18) due to the system in equation (4) having input in one channel and a disturbance in the other. To convert the system from a mismatched to a matched one, the following procedure must thus be applied:

Let $x_1(t) = q(t) x_2(t) = (N/R(t))W(t)$ so that

$$
\begin{cases}
\dot{x}_1(t) = x_2(t) - C + d(t), \\[4pt]
\dot{x}_2(t) = \dfrac{N}{R^2(t)} - \dfrac{x_2(t)\dot{x}_1(t)}{R(t)C} \\[8pt]
\qquad\quad - \dfrac{x_2(t) + C}{2N}\left[(x_2(t) - R(t)) + C\right]u(t), \\[8pt]
y(t) = x_1(t).
\end{cases}
\tag{19}
$$

For simplicity, $\phi(t - t_0) = \phi(t)$ is assumed; equation (19) can thus be rewritten as

$$
\begin{cases}
\dot{x}_1(t) = x_2(t) - C + d(t), \\
\dot{x}_2(t) = m_1 - m_2 x_2(t)u, \\
y(t) = x_1(t),
\end{cases}
\tag{20}
$$

where $m_1 = (N/R^2(t)) - (x_2(t)\dot{x}_1(t)/R(t)C)$ and $m_2 = -((x_2(t) + C)^2/2N)$.

Equation (21) can then be transformed into the following form:

$$
\begin{cases}
\dot{x}_1(t) = \mathbb{F}_1(x_1, x_2) + bd(t), \\
\dot{x}_2(t) = \mathbb{F}_2(x_1, x_2) + b_2 u(t), \\
y = x_1(t).
\end{cases}
\tag{21}
$$

Differentiating the first equation of equation (21) yields

$$
\ddot{x}_1 = \frac{\partial \mathbb{F}_1(x_1, x_2)}{\partial x_1}\dot{x}_1 + \frac{\partial \mathbb{F}_1(x_1, x_2)}{\partial x_2}\dot{x}_2 + b_1\dot{d}(t),
\tag{22}
$$

while substituting equations (21) into (22) produces

$$
\begin{aligned}
\ddot{x}_1 = {} & \frac{\partial \mathbb{F}_1(x_1, x_2)}{\partial x_1}\left[\mathbb{F}_1(x_1, x_2) + b_1 d(t)\right] \\
& + \frac{\partial \mathbb{F}_1(x_1, x_2)}{\partial x_2}\left[\mathbb{F}_2(x_1, x_2) + b_2 u(t)\right] + b_1\dot{d}(t),
\end{aligned}
\tag{23}
$$

Rearranging equation (23) gives

$$
\ddot{x}_1 = \frac{\partial \mathbb{F}_1(x_1, x_2)}{\partial x_1}\mathbb{F}_1(x_1, x_2) + \frac{\partial \mathbb{F}_1(x_1, x_2)}{\partial x_2}\mathbb{F}_2(x_1, x_2) + \frac{\partial \mathbb{F}_1(x_1, x_2)}{\partial x_2}b_2 u(t) + \frac{\partial \mathbb{F}_1(x_1, x_2)}{\partial x_1}b_1 d(t) + b_1\dot{d}(t),
$$

$$
\ddot{x}_1 = \frac{\partial \mathbb{F}_1(x_1, x_2)}{\partial x_1}\mathbb{F}_1(x_1, x_2) + \frac{\partial \mathbb{F}_1(x_1, x_2)}{\partial x_2}\mathbb{F}_2(x_1, x_2) + b_2\frac{\partial \mathbb{F}_1(x_1, x_2)}{\partial x_2}\left[u(t) + \frac{\partial \mathbb{F}_1(x_1, x_2)/\partial x_1 b_1 d(t) + b_1\dot{d}(t)}{\partial \mathbb{F}_1(x_1, x_2)/\partial x_2 b_2}\right].
\tag{24}
$$

Then,

$$
\ddot{x}_1 = \widehat{\mathbb{F}}(x_1, x_2) + \widehat{b}(u + \mathbb{D}),
\tag{25}
$$

where

$$
\begin{aligned}
\widehat{\mathbb{F}}(x_1, x_2) = {} & \frac{\partial \mathbb{F}_1(x_1, x_2)}{\partial x_1}\mathbb{F}_1(x_1, x_2) \\
& + \frac{\partial \mathbb{F}_1(x_1, x_2)}{\partial x_2}\mathbb{F}_2(x_1, x_2), \\
\widehat{b} = {} & b_2\frac{\partial \mathbb{F}_1(x_1, x_2)}{\partial x_2}, \\
d = {} & \frac{\partial \mathbb{F}_1(x_1, x_2)/\partial x_1 b_1 d(t) + b_1\dot{d}(t)}{(\partial \mathbb{F}_1(x_1, x_2)/\partial x_2)b_2}.
\end{aligned}
\tag{26}
$$

Let $x_1(t) = x_1(t)$ and $x_2(t) = \dot{x}_1(t)$; this allows equation (20) to be rewritten as

$$
\begin{cases}
\dot{x}_1(t) = x_2(t), \\
\dot{x}_2(t) = \widehat{\mathbb{F}}(x_1, x_2, x_2) + \widehat{b}(u + d), \\
y(t) = x_1(t).
\end{cases}
\tag{27}
$$

where $x = \{x_1(t), x_2(t)\} \in \mathbb{R}^2, \widehat{\mathbb{F}}(x_1, x_2, x_2)$ is the matched nonlinear function, and $Y(t) \in \mathbb{R}$ is the output of the system.

Remark 2. As seen from equation (27), $\widehat{\mathbb{F}}$ depends on x_2; thus, to find an expression for x_2, the first equation of (19) can be used, and the x_2 thus found substituted into equation (27) to transform the system in the term $(x_1(t), x_2(t))$. $x_2(t) = \dot{x}_1(t) + C - d(t) \longrightarrow x_2(t) = x_2(t) + C - d(t)$. This means that equation (27) can be rewritten as

$$
\begin{cases}
\dot{x}_1(t) = x_2(t), \\
\dot{x}_2(t) = \widehat{\mathbb{F}}(x_1, x_2, C, d(t)) + \widehat{b}(u + D), \\
y(t) = x_1(t).
\end{cases}
\tag{28}
$$

Adding $\pm b_0 u$ to the second equation of (28) yields

$$
\begin{cases}
\dot{x}_1(t) = x_2(t), \\
\dot{x}_2(t) = \mathsf{F} + b_0 u, \\
y(t) = x_1(t),
\end{cases}
\tag{29}
$$

where $\mathsf{F} = \widehat{\mathbb{F}}(x_1, x_2, C, d(t)) + \widehat{b}D + (\widehat{b} - b_0)u$.

Theorem 1. *Assuming a TCP network as given in equation (28), the proposed NLDO will be asymptotically stable if $P(\mathbb{X})$*
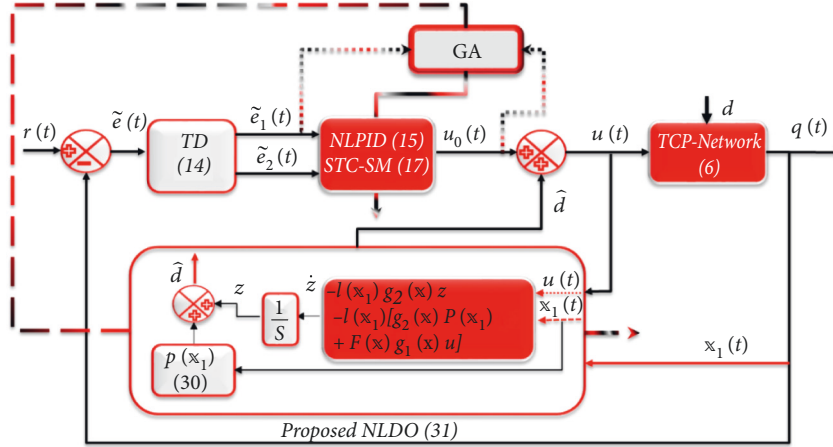
FIGURE 4: Completed diagram of TCP/AQM based on the proposed NLDO.

is designed appropriately. An appropriate nonlinear function $P(\mathbb{X})$ is proposed as

$$\begin{cases} P(x) = k + kx, \\ l(x) = \dfrac{\partial P(x)}{\partial x}, \end{cases} \tag{30}$$

where $x = x_1 \in \mathbb{R}h$ is a positive tuning parameter.

Proof. Assuming a system as given in equation (28), the proposed NLDO can be expressed as follows:

$$\begin{cases} \dot{\mathcal{Z}} = -l(x_1)g_2(x)Z - l(x_1)\big[g_2(x)P(x_1) + \hat{\mathbb{F}}(x) + g_1(x)u\big], \\ \hat{d} = P(x_1) + Z. \end{cases} \tag{31}$$

Differentiating $\hat{d}$ gives

$$\dot{\hat{d}} = \dot{P}(x_1) + \dot{\mathcal{Z}}. \tag{32}$$

Differentiating the first equation of (30) yields

$$\dot{P}(x_1) = \frac{dP}{dx_1} = hx_1. \tag{33}$$

Substituting equation (33) into the first equation of (31) creates

$$\dot{\hat{d}} = h\dot{x}_1 - \ell(x)g_2(x)\mathcal{Z} - g_2(x)P(x)\ell(x) \\ - \ell(x)\hat{\mathbb{F}}(x)\ell(x) - \ell(x)g_1(x)u. \tag{34}$$

Simplifying equation (34) yields

$$\dot{\hat{d}} = hg_2(x)d(t) - hg_2(x)\mathcal{Z} - hg_2(x)P(x). \tag{35}$$

Substituting $\hat{d} = P(x) + \mathcal{Z}$ into equation (35) gives

$$\dot{\hat{d}} = hg_2(x)[d(t) - \hat{d}(t)], \tag{36}$$

where $d(t) - \hat{d}(t) = e_d$ represents the disturbance observer error, $d(t) = D$ is the applied exogenous disturbance, and $\hat{d}(t)$ is the estimated disturbance.

$$e_d = d(t) - \hat{d}(t). \tag{37}$$

Differentiating equation (37) allows the error dynamics to be expressed as

$$\dot{e}_d = \dot{d}(t) - \dot{\hat{d}}(t). \tag{38}$$

Assuming a constant disturbance, $\dot{d}(t) = 0$, the dynamic of the disturbance observer error can thus be given as

$$\dot{e}_d = -hg_2(x)e_d. \tag{39}$$

□

Remark 3. The NLDO is asymptotically stable if the estimated error converges to zero as $t \longrightarrow \infty$. To achieve this, a Lyapunov stability approach can be utilized [23].

Taking the Lyapunov function $V_{\text{NLDO}} = (1/2)e_d^T e_d$,

$$\dot{V}_{\text{NLDO}} = e_d^T \dot{e}_d,$$
$$\dot{V}_{\text{NLDO}} = -e_d^T[hg_2(x)e_d], \tag{40}$$
$$\dot{V}_{\text{NLDO}} < -hg_2(x)e_d^2.$$

The system in equation (30) is thus asymptotically stable when the following conditions are satisfied:

(i) V_{NLDO} is positive definite, $V_{\text{NLDO}}(e_d) > 0$ for $e_d \neq 0$
(ii) $\dot{V}_{\text{NLDO}}(e_d) < 0$ for $e_i \neq 0$

Thus, the NLDO is asymptotically stable if $hg_2(\mathbb{X}) > 0$, $h > 0$.

The complete diagram of the proposed NLDO with TCP network nonlinear model is shown in Figure 4.

5.2. Closed-Loop Stability. The overall stability analysis of the proposed ADRC with a TCP network nonlinear model is presented in this subsection. The ESO in the ADRC converts the system into a chain of integrators; however, the TCP network given in equation (7) cannot be converted into a chain of integrators due to the mismatch in the disturbance. To redress this, the TCP network given in equation (7) must be transformed from a mismatched system into matched one, as noted previously in equation (30).

Assuming that $\mathbb{L} = \mathsf{F} = x_3(t)$, equation (30) can be rewritten as

$$
\begin{cases}
\dot{x}_1(t) = x_2(t), \\
\dot{x}_2(t) = x_3(t) + b_0 u, \\
\dot{x}_3(t) = \dot{\mathbb{L}}, \\
y(t) = \dot{x}_1(t),
\end{cases}
\tag{41}
$$

where $x_3(t)$ and $\dot{\mathbb{L}}$ represent the total disturbance and its derivative, respectively, and b_0 is a rough approximation of $\widehat{b}$ within the range of $\pm 50\%$ [14].

Assumption 1 (see [15]). The total disturbance $\mathbb{L}$ should satisfy the following conditions:

(i) $\mathbb{L}$ and $\dot{\mathbb{L}}$ are bounded as
    $\sup_{0 \le t \le \infty} \mathbb{L} \le c_1$ and $\sup_{0 \le t \le \infty} \dot{\mathbb{L}} \le c_2$

(ii) $\mathbb{L}$ and $\dot{\mathbb{L}}$ are constant at the steady state such that
    $\lim_{t \to \infty} \mathbb{L} = c_3$ and $\lim_{t \to \infty} \dot{\mathbb{L}} \le 0$
    where $c_1 c_2$ and c_3 are positive constants.

Theorem 2. *Suppose an n order system with relative degree* $\rho \, (\rho \le n)$ *is given as*

$$
\begin{cases}
\dot{x}_1(t) = f_1(x), \\
\vdots, \\
\dot{x}_\rho(t) = f_\rho(x) + b(u + d), \\
y = x.
\end{cases}
\tag{42}
$$

where $x \in \{x_1, x_1, \ldots x_{\rho-1}\}$, *and* $f_1, \ldots, f_\rho$ *are the system nonlinear functions.*

According to equation (42), equation (30) can thus be represented as a chain of integrators in the form as follows:

$$
\begin{cases}
\dot{x}_1(t) = \dot{x}_2(t), \\
\vdots \\
\dot{x}_\rho(t) = x_{\rho+1}(t) + b_0 u, \\
\dot{x}_{\rho+1}(t) = \dot{\mathbb{L}}, \\
y(t) = x_1(t),
\end{cases}
\tag{43}
$$

where $x_{\rho+1}(t)$ is the generalized disturbance.

If Assumption 1 is satisfied, then the system described by equation (43) is asymptotically stable when the estimated error of the proposed NLESO, as seen in equations (13) and (14) and expressed in the form $e_i = x_i - z_i, i \in \{1, 2, \ldots, \rho + 1\}$, approaches zero as $t \longrightarrow \infty$.

Proof. Let the estimated error e_i be

$$
e_i = x_i - z_i,
\tag{44}
$$

where $i \in \{1, 2, \ldots, \rho + 1\}$, ρ is the relative degree of the system, e_i is the estimated error, and z_i is the estimated state of x_i.

$$
\begin{cases}
e_1 = x_1 - z_1, \\
e_2 = x_2 - z_2, \\
e_\rho = x_\rho - z_\rho, \\
e_{\rho+1} = x_{\rho+1} - z_{\rho+1}.
\end{cases}
\tag{45}
$$

Differentiating equation (45) produces

$$
\begin{cases}
\dot{e}_1 = \dot{x}_1 - \dot{z}_1, \\
\dot{e}_2 = \dot{x}_2 - \dot{z}_2, \\
\vdots \\
\dot{e}_\rho = \dot{x}_\rho - \dot{z}_\rho, \\
\dot{e}_{\rho+1} = \dot{x}_{\rho+1} - \dot{z}_{\rho+1}.
\end{cases}
\tag{46}
$$

Substituting (43) into (46) gives

$$
\begin{cases}
\dot{e}_1 = x_2 - z_2 - \beta_1 \widehat{e}_1, \\
\dot{e}_2 = \dot{x}_3 - z_3 - \beta_2 \widehat{e}_2, \\
\vdots \\
\dot{e}_\rho = x_{\rho+1} + b_0 u - z_{\rho+1} - b_0 u - \beta_\rho \widehat{e}_\rho, \\
\dot{e}_{\rho+1} = \dot{\mathbb{L}} - \beta_{\rho+1} \widehat{e}_{\rho+1}.
\end{cases}
\tag{47}
$$

Simplifying equation (47) yields

$$
\begin{cases}
\dot{e}_1 = e_2 - \beta_1 \widehat{e}_1, \\
\dot{e}_2 = e_3 - \beta_2 \widehat{e}_2, \\
\dot{e}_\rho = e_{\rho+1} - \beta_\rho \widehat{e}_\rho, \\
\dot{e}_{\rho+1} = \dot{\mathbb{L}} - \beta_{\rho+1} \widehat{e}_{\rho+1}.
\end{cases}
\tag{48}
$$

Expressing equation (48) in matrix form gives

$$
\dot{e} = A_0 e + A_d \dot{\mathbb{L}}.
\tag{49}
$$

Assume $\hat{e}_1 = K_1(e_1), \ldots, \hat{e}_\rho = K_\rho(e_1)$ and $\hat{e}_{\rho+1} = K_{\rho+1}(e_1)$.

Then,

$$A_0 = \begin{bmatrix} -\beta_1 K_1(e_1) & 1 & \cdots & 0 & 0 \\ -\beta_2 K_2(e_1) & 0 & \ddots & 0 & 0 \\ -\beta_\rho K_\rho(e_1) & \vdots & \cdots & \vdots & \vdots \\ \vdots & & 0 & \cdots & 0 & 1 \\ -\beta_\rho K_{\rho+1}(e_1) & 0 & \cdots & 0 & 0 \end{bmatrix},$$

$$A_d = \begin{bmatrix} 0 \\ \vdots \\ 0 \\ 1 \end{bmatrix},$$

$$\dot{e} = \begin{bmatrix} \dot{e}_1 & \cdots & \dot{e}_{\rho+1} \end{bmatrix},$$

$$e = \begin{bmatrix} \dot{e}_1 & \cdots & \dot{e}_{\rho+1} \end{bmatrix}.$$

(50)

The NLESO is asymptotically stable if the estimated error converges to zero as $t \longrightarrow \infty$. To check this, the Lyapunov stability can be used [23]. Taking the Lyapunov function $V_{\text{NLESO}} = 1/2 e^T e$ gives $\dot{V}_{\text{NLESO}} = e^T \dot{e}$.

For the TCP network, the relative degree $\rho = 2$; hence,

$$\dot{V}_{\text{NLESO}} = \begin{bmatrix} e_1 & e_2 & e_3 \end{bmatrix} \begin{bmatrix} -\beta_1 K_1(e_1) & 1 & 0 \\ -\beta_2 K_2(e_1) & 0 & 1 \\ -\beta_3 K_3(e_1) & 0 & 0 \end{bmatrix} \begin{bmatrix} e_1 \\ e_2 \\ e_3 \end{bmatrix} + \dot{\mathbb{L}}. \quad (51)$$

According to Assumption 1, $\dot{\mathbb{L}}$ converges to zero as $t \longrightarrow \infty$, so that the quadric form $\dot{V}_{\text{NLESO}} = e^T Q \dot{e}$ is asymptotically stable if Q is a negative definite matrix, and thus, the system as a whole is asymptotically stable. To check whether the matrix Q_i is negative definite or not, the Routh stability criteria can be utilized. This first requires computing the characteristic equation for matrix Q:

$$|\lambda I - Q| = 0,$$

$$\begin{vmatrix} \lambda + \beta_1 K_1(e_1) & -1 & 0 \\ \beta_2 K_2(e_1) & \lambda & -1 \\ \beta_3 K_3(e_1) & 0 & \lambda \end{vmatrix} = 0. \quad (52)$$

$\lambda^3 + \beta_1 K_1(e_1)\lambda^2 + \beta_2 K_2(e_1)\lambda + \beta_3 K_3(e_1) = 0$; using the Routh stability criteria thus yields

$$\begin{array}{lll} \lambda^3 & 1 & \beta_2 K_2(e_1) \\[2mm] \lambda^2 & \beta_1 K_1(e_1) & \beta_3 K_3(e_1) \\[2mm] \lambda^1 & \dfrac{\beta_1 K_1(e_1)\beta_2 K_2(e_1) - \beta_3 K_3(e_1)}{\beta_1 K_1(e_1)} = c_1 & 0 \\[4mm] \lambda^0 & \dfrac{\beta_3 K_3(e_1) c_1}{c_1} = \beta_3 K_3(e_1) & 0 \end{array}, \quad (53)$$

$$\beta_1 K_1(e_1)\beta_2 K_2(e_1) - \beta_3 K_3(e_1) > 0, \beta_1 K_1(e_1) < \frac{\beta_2 K_2(e_1)}{\beta_3 K_3(e_1)}, \beta_3 K_3(e_1) > 0, \beta_3 > 0.$$

Q is thus negative definite if the observer gain $\beta_1, \beta_2, \beta_3 > 0$, which also leads to the NLESO being asymptotically stable. Generally, the error dynamics of the closed-loop system can be written as

$$\begin{cases} \tilde{e}_1 = r - z_1, \\ \tilde{e}_2 = \dot{r} - z_2, \\ \vdots \\ \tilde{e}_\rho = r^{\rho-1} - z_\rho. \end{cases} \quad (54)$$

Differentiating equation (54) gives

$$\left\{ \dot{\tilde{e}}_1 = \dot{r} - z_1, \dot{\tilde{e}}_2 = \ddot{r} - z_2, \ \vdots \ , \dot{\tilde{e}}_\rho = r^\rho - z_\rho. \right. \quad (55)$$

Simplifying equation (55) yields

$$\left\{ \dot{\tilde{e}}_1 = \tilde{e}_2, \dot{\tilde{e}}_2 = \tilde{e}_3, \ \vdots \ , \dot{\tilde{e}}_\rho = -z_{\rho+1} - b_0 u. \right. \quad (56)$$

$\square$

Assumption 2. The tracking differentiator in equation (7) tracks the reference signal with only a very small error, which thus approaches zero with $r^\rho = 0$.

$$\lim_{t \longrightarrow \infty} \left| r_{1,\ldots,\rho} - r^{\rho-1} \right| = 0. \tag{57}$$

Assumption 3. The NLESO in equations (12) to (15) estimates the states of the nonlinear system completely.

$$\lim_{t \longrightarrow \infty} e_{1,2,\ldots,\rho+1} = 0. \tag{58}$$

Theorem 3. *Given the nonlinear system in (43) and the tracking differentiator given in (7) in conjunction with the NLPID given in (8) and (9) and the NLESO presented in (12) to (15), based on Assumptions 2 and 3, the closed-loop system is stable if* $\left\{ \mathscr{K}_1(\tilde{e}_1)\tilde{e}_1, \mathscr{K}_2(\tilde{e}_2)\tilde{e}_2 \right\}$ *is chosen in such a way that the Q matrix is negative definite and satisfies the characteristic equation* $\lambda^2 + \mathscr{K}_2'\lambda + \mathscr{K}_1 = 0$, *which is Hurwitz.*

Proof. Taking $u = u_0 - (z_{\rho+1}/b_0)$, (56) can be rewritten as

$$\begin{cases} \dot{\tilde{e}}_1 = \tilde{e}_2, \\ \\ \dot{\tilde{e}}_2 = \tilde{e}_3, \\ \\ \vdots \\ \\ \dot{\tilde{e}}_\rho = -z_{\rho+1} - b_0 \left[u_0 - \dfrac{z_{\rho+1}}{b_0} \right], \end{cases} \tag{59}$$

$$\begin{cases} \dot{\tilde{e}}_1 = \tilde{e}_2, \\ \dot{\tilde{e}}_2 = \tilde{e}_3, \\ \vdots \\ \dot{\tilde{e}}_\rho = -z_{\rho+1} - b_0 u_0 + z_{\rho+1}. \end{cases} \tag{60}$$

Simplifying (60) gives

$$\begin{cases} \dot{\tilde{e}}_1 = \tilde{e}_2, \\ \\ \dot{\tilde{e}}_2 = \tilde{e}_3, \\ \\ \vdots \\ \\ \dot{\tilde{e}}_\rho = -b_0 u_0, \end{cases} \tag{61}$$

$$\begin{cases} \dot{\tilde{e}}_1 = \tilde{e}_2, \\ \dot{\tilde{e}}_2 = \tilde{e}_3, \\ \vdots \\ \dot{\tilde{e}}_\rho = -b_0 \left[u_1(\tilde{e}_1) + \cdots\cdots + u_\rho(\tilde{e}_\rho) \right]. \end{cases} \tag{62} \qquad \square$$

Assumption 4. Assume $\mathscr{K}_i(\tilde{e}_i) = (k_i/1 + \exp(\tilde{e}_i^2))i \in \{1, 2 \ldots\ldots, \rho+1\}$ and that $\alpha_1, \alpha_2, \ldots, \alpha_\rho$ approaches unity:

based on these assumptions, the term $|\mathbb{S}|\text{sign}(\mathbb{S})$ in equation (8) is approximately equal to $\mathbb{S}$.

Based on Assumption 4, equation (62) can thus be rewritten as

$$\begin{cases} \dot{\tilde{e}}_1 = \tilde{e}_2, \\ \\ \dot{\tilde{e}}_2 = \tilde{e}_3, \\ \\ \vdots \\ \\ \dot{\tilde{e}}_\rho = -b_0 \left[\mathscr{K}_1(\tilde{e}_1)\tilde{e}_1 + \cdots + \mathscr{K}_\rho(\tilde{e}_\rho)\tilde{e}_\rho \right]. \end{cases} \tag{63}$$

Expressing equation (63) in matrix form gives

$$\dot{\tilde{e}} = A_{C_{\text{NLPID}}} \tilde{e}, \tag{64}$$

where

$$A_{C_{\text{NLPID}}} = \begin{bmatrix} 0 & 1 & \cdots & 0 & 0 \\ 0 & 0 & \cdots & 0 & 0 \\ \vdots & \vdots & \ddots & \vdots & \vdots \\ 0 & 0 & \cdots & 0 & 1 \\ -\mathscr{K}_1 & -\mathscr{K}_2 & \cdots & -\mathscr{K}_{\rho-1} & -\mathscr{K}_\rho \end{bmatrix}, \tilde{e} = \begin{bmatrix} \tilde{e}_1 \\ \tilde{e}_2 \\ \vdots \\ \tilde{e}_{\rho-1} \\ \tilde{e}_\rho \end{bmatrix},$$

$\mathscr{K}_i = b_0 \mathscr{K}_i(\tilde{e}_i)$, $i \in \{1, 2, \ldots, \rho+1\}$.

A Lyapunov function can be used to check the stability of the closed-loop system: $V_{cl} = 1/2\tilde{e}^T\tilde{e}$. Then, $\dot{V}_{cl} = \tilde{e}^T\dot{\tilde{e}}$.

$$\dot{V}_{cl} = \left[\tilde{e}_1, \tilde{e}_2, \ldots, \tilde{e}_\rho \right] \begin{bmatrix} 0 & 1 & \cdots & 0 & 0 \\ 0 & 0 & \cdots & 0 & 0 \\ \vdots & \vdots & \ddots & \vdots & \vdots \\ 0 & 0 & \cdots & 0 & 1 \\ -\mathscr{K}_1 & -\mathscr{K}_2 & \cdots & -\mathscr{K}_{\rho-1} & -\mathscr{K}_\rho \end{bmatrix} \begin{bmatrix} \dot{\tilde{e}}_1 \\ \dot{\tilde{e}}_2 \\ \vdots \\ \dot{\tilde{e}}_\rho \end{bmatrix}. \tag{65}$$

The quadric form $\dot{V}_{cl} = \tilde{e}^T Q \dot{\tilde{e}}$ is stable if Q is a negative semi-definite matrix, at which point the system is stable.

Finding the characteristic equation for matrix Q using the Routh stability criteria allows a check on the negative definiteness of matrix Q,

$$|\lambda I - Q| = 0 - \begin{vmatrix} \lambda & \cdots & 0 \\ 0 & \cdots & 0 \\ \vdots & \ddots & \vdots \\ 0 & \cdots & \lambda \end{vmatrix}$$

$$\begin{bmatrix} 0 & 1 & \cdots & 0 & 0 \\ 0 & 0 & \cdots & 0 & 0 \\ \vdots & \vdots & \ddots & \vdots & \vdots \\ 0 & 0 & \cdots & 0 & 1 \\ -\mathscr{K}_1 & -\mathscr{K}_2 & \cdots & -\mathscr{K}_{\rho-1} & -\mathscr{K}_\rho \end{bmatrix},$$

$$\lambda^\rho + \mathscr{K}_\rho \lambda^{\rho-1} + \cdots + \mathscr{K}_2'\lambda + \mathscr{K}_1' = 0. \tag{66}$$

Table 1: TCP network model parameters.

Parameter	Description	Value	Unit
$q(t)_{des}$	The desire queuing length	200	packets
$N(t)$	Load factor	100	unitless
$C(t)$	Link capacity	3750	packets/sec
τ_p	The propagation delay	0.195	Sec

Table 2: Descriptions and mathematical representations of the performance indices.

Performance index (PI)	Description	Mathematical representation
ITAE	Integral time absolute error	$\int_0^{t_f} t|e(t)|\mathrm{d}t$
IAU	Integral absolute of the control signal	$\int_0^{f} |u(t)|\mathrm{d}t$
ISU	Integral square of the control signal	$\int_0^{f} u(t)^2\mathrm{d}t$
IAE	Integral square error	$\int_0^{t_f} e(t)^2\mathrm{d}t$
ISE	Integral absolute error	$\int_0^{t_f} |e(t)|\mathrm{d}t$
MSE	Mean square error	$(1/T)\int_0^{t_f} e(t)^2\mathrm{d}t$

Table 3: LPID parameters.

Controller	Parameter	Value	Parameter	Value
LPID	k_p	0.025000	k_i	0.015000
	k_d	0.010000	δ	3.039957

For $\rho = 2$,

$$\lambda^2 + \mathscr{K}_2'\lambda + \mathscr{K}_1' = 0,$$

$$\begin{array}{ccc} \lambda^2 & 1 & \mathscr{K}_1' \\ \lambda^1 & \mathscr{K}_2' & 0 \\ \lambda^0 & \dfrac{\mathscr{K}_1'\mathscr{K}_2'}{\mathscr{K}_2'} & \lambda^2 \end{array}, \tag{67}$$

$$\mathscr{K}_2' > 0, \frac{\mathscr{K}_1'\mathscr{K}_2' - 0}{\mathscr{K}_2'} > 0 \Rightarrow \mathscr{K}_1'\mathscr{K}_2' > 0 \Rightarrow \mathscr{K}_1' > 0.$$

The system is thus stable if the nonlinear function gains $\mathscr{K}_1'$ and $\mathscr{K}_2'$ satisfy the conditions mentioned above.

6. Simulation Results

The TCP network nonlinear model and the proposed controllers, the modified ADRC, and the proposed NLDO were designed and simulated using a MATLAB/Simulink environment. In addition, the parameters of all schemes mentioned previously and those proposed were tuned using a genetic algorithm (GA) [18]. Finally, the multi-objective performance index was utilized to investigate the performance and accuracy of the designed and proposed schemes. The TCP network model parameters are listed in Table 1, while the multi-objective performance index (OPI) is given as follows:

Table 4: NLPID parameters.

Controller	Parameter	Value	Parameter	Value
NLPID	k_1	0.562500	k_2	3.147000
	α_1	0.895600	α_2	0.779600
	k_3	7.193000	α_3	0.548450
TD	R	24.680000	a_2	7.842000
	a_1	2.912000	δ	10.326000

Table 5: STC-SM parameters.

Controller	Parameter	Value	Parameter	Value
STC-SM	κ	0.146000	ξ	0.000200
	p	0.954500	δ	0.426500
TD	R	6.190000	a_2	9.703000
	a_1	2.501000	—	—

$$\mathrm{OPI} = w_1 * \frac{\mathrm{ITAE}}{\mathscr{N}_1} + w_2 * \frac{\mathrm{IAU}}{\mathscr{N}_2} + w_3 * \frac{\mathrm{ISU}}{\mathscr{N}_3} + w_4 * \frac{\mathrm{ISE}}{\mathscr{N}_4}$$
$$+ w_5 * \frac{\mathrm{IAE}}{\mathscr{N}_5} + w_6 * \frac{\mathrm{MSE}}{\mathscr{N}_6}, \tag{68}$$

where $w_1, w_2, \ldots, w_6$ are the weighting factors that satisfy $w_1 + w_2 + \cdots + w_6 = 1$. These are thus set to $w_1 = 0.3$, $w_2 = 0.2$, $w_3 = 0.1$, $w_4 = 0.2$, $w_5 = 0.1$, and $w_6 = 0.1$, with $\mathscr{N}_1, \mathscr{N}_2, \ldots, \mathscr{N}_6$ as the nominal values of the individual objective functions, with values set to $\mathscr{N}_1 = 772$, $\mathscr{N}_2 = 1000$, $\mathscr{N}_3 = 20$, $\mathscr{N}_4 = 86014.936857$, $\mathscr{N}_5 = 260$, and $\mathscr{N}_6 = 860$.
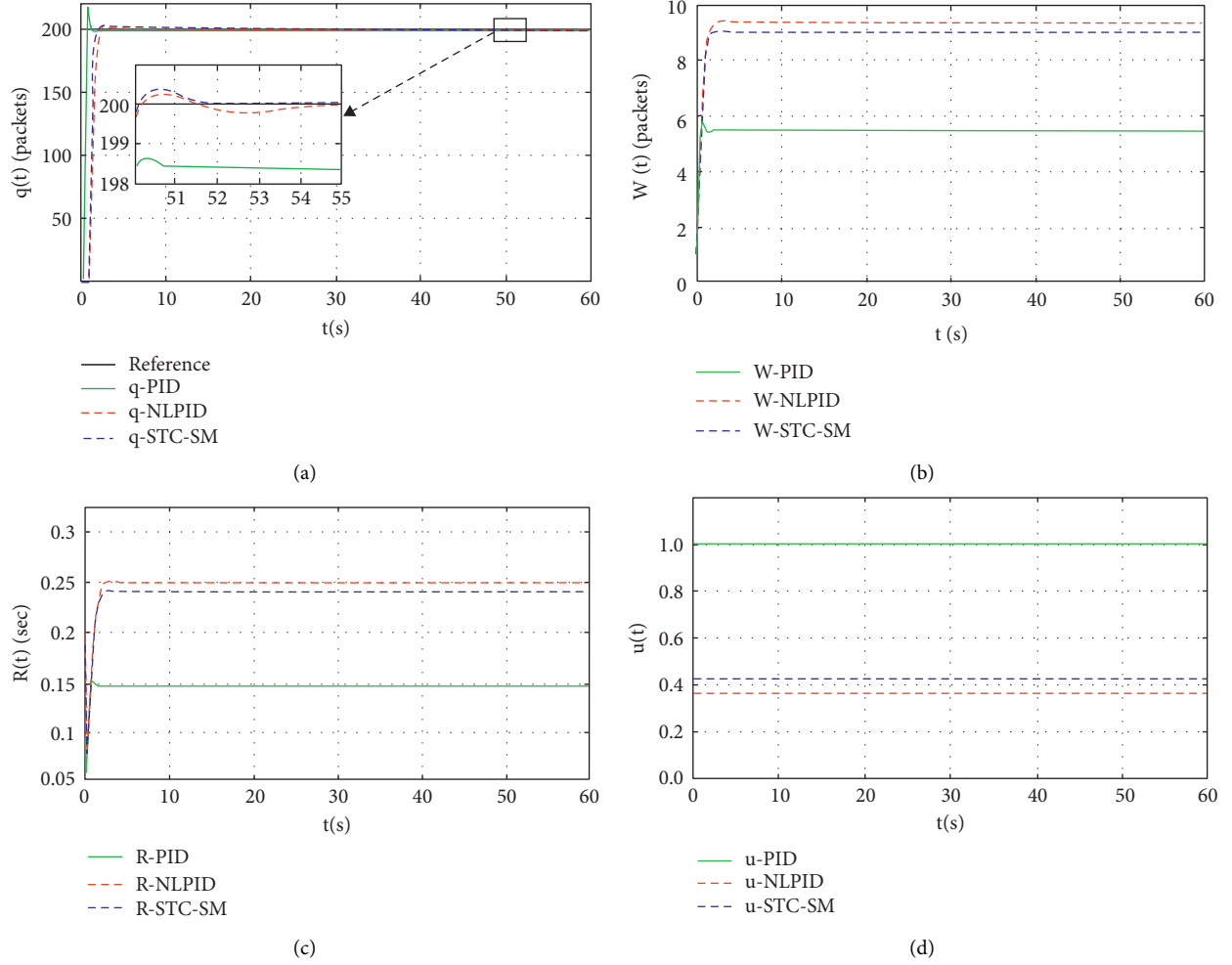
(a)

(b)

(c)

(d)

FIGURE 5: The output response when the disturbance is applied at $t = 50$ s. (a) The average queuing length $q(t)$. (b) The window size $W(t)$. (c) The round trip time $R(t)$ (d). The probability of losing packets $u(t)$. The performance index values are shown in Table 6. As demonstrated, the proposed controllers (NLPID and STC-SM) show noticeable improvements in OPI of 63.7363% and 72.52524%, respectively. The proposed controllers thus demonstrate effectiveness based on smooth response and minimized OPI.

TABLE 6: Performance indices.

PI	LPID	NLPID	STC-SM
ITAE	609.745670	544.413440	424.866163
IAU	5233.023924	544.539821	112.530207
ISU	132.195167	2.694587	0.184691
IAE	323.637549	301.475409	273.064131
ISE	53979.519643	48988.720573	44771.045158
MSE	4065.828712	1632.413215	1491.870882
OPI	2.078752	0.753616	0.571132

TABLE 7: LADRC parameters.

ADRC parts	Parameter	Value	Parameter	Value
LPID	k_p	10.237000	k_i	1.015000
	k_d	10.237000	δ	10.326000
TD	R	100	—	—
LESO	ω_0	10.326000	b_0	−69505.943979

The mathematical representations of the performance indices used are presented more clearly in Table 2.

$$u_{0_{PID}} = k_p e + k_i \int_0^T e \, dt + k_d \frac{de}{dt}, \qquad (69)$$

where $k_p, k_i,$ and k_d are the proportional, integral, and derivative gains, respectively. The parameters of the LPID, NLPID, and STC-SM controllers are listed in full in Tables 3–5.

6.1. Simulation Using the Proposed Controllers. In this subsection, the simulation results from using the proposed controllers only are introduced. The obtained results are then compared with the LPID, which can be expressed as follows:

The simulation results using only controllers within the TCP network nonlinear model under the presence of an exogenous disturbance (UDP flow) are shown in Figure 5. Figure 5(a) shows the output response for queuing length: here, the queuing length reaches the desired or steady-state

TABLE 8: NLPID-ADRC parameters.

ADRC parts	Parameter	Value	Parameter	Value
NLPID	k_1	3.842000	k_2	3.386000
	α_1	0.998900	α_2	0.905400
	k_3	0.339800	α_3	0.043300
TD	R	11.150000	a_2	9.656000
	a_1	0.391000	δ	0.365300
NLESO	ω_0	50.335000	b_0	−4283.212200
	a_1	0.269550	$\mathscr{A}$	7.043000

TABLE 9: STC-ADRC parameters.

ADRC parts	Parameter	Value	Parameter	Value
STC-SM	κ	0.000200	ξ	0.000100
	p	0.300500	δ	0.586600
TD	R	49.340000	a_2	1.950000
	a_1	5.210000	—	—
NLESO	ω_0	56.334000	b_0	−1061.793374
	a_1	0.997100	—	—

TABLE 10: NLDO parameters.

	Parameter	Value	Parameter	Value
NLPID	k_1	0.059000	k_2	0.013400
	α_1	0.071600	α_2	0.441500
	k_3	0.417750	α_3	0.784600
TD	R	95.030000	a_2	9.573000
	a_1	6.030000	δ	0.383700
NLDO	h	4.049500	—	—

value at about 3.61 s under both the NLPID and the STC-SM, while in the LPID, the queuing length did not reach the desired value despite coming close to it. In addition, when applying a disturbance of 5 at a time 50 s after starting the simulation, the proposed controllers (NLPID and STC-SM) show greater robustness against the resulting disturbance, with STC-SM showing an overshoot of 0.2% of the steady-state value for about 1 s before moving back to the steady-state value and NLPID showing an overshoot and under-shoot of 0.15% and 0.1%, respectively, of the steady state for about 4 s before returning to the steady-state value. The LPID is clearly more significantly affected by the applied disturbance; however, Figures 5(b) and 5(c) show the output response of the window size and the round trip time, while Figure 5(d) shows the control signal. As these indicate, comparing the performance of the LPID, NLPID, and the STC-SM shows that the NLPID and STC-SM give better responses with minimum packet loss, while the LPID packet loss rate is at maximum, exceeding the predefined limits of packet loss: LPID is thus clearly weakest at handling both complexity and delay in TCP networks.

6.2. Simulation with Anti-Disturbance Methods. In this subsection, the simulation results of the anti-disturbance methods (modified ADRC and NLDO) are introduced. The results of the proposed methods are also compared with linear ADRC (LADRC) that utilizes a conventional TD as proposed by [14], the linear ESO (LESO), and the LPID. The dynamics of the conventional TD and LESO are thus given as follows:

(i) For conventional TD [14],

$$\begin{cases} \dot{r}_1(t) = r_2(t), \\ \dot{r}_2(t) = -\text{Rsign}\left(r_1(t) - r(t) + \frac{r_2(t)\left|r_2(t)\right|}{2R}\right), \end{cases} \tag{70}$$

where $r_1(t)$ is the desired trajectory and $r_2(t)$ is its derivative. R is an application that depends on the other parameters [14].

(ii) For LESO,

$$\begin{cases} \dot{z}_1(t) = z_2(t) + \beta_1(e_1), \\ \dot{z}_2(t) = z_3(t) + \beta_2(e_1) + b_0 u(t), \\ \dot{z}_3(t) = \beta_3(e_1). \end{cases} \tag{71}$$

The parameters of the proposed methods and the LADRC are listed in Tables 7–10.

A step function of $5u(t - 50)$ was applied to the system as an exogenous disturbance. The simulation results when applying a UDP data flow as an exogenous disturbance to the
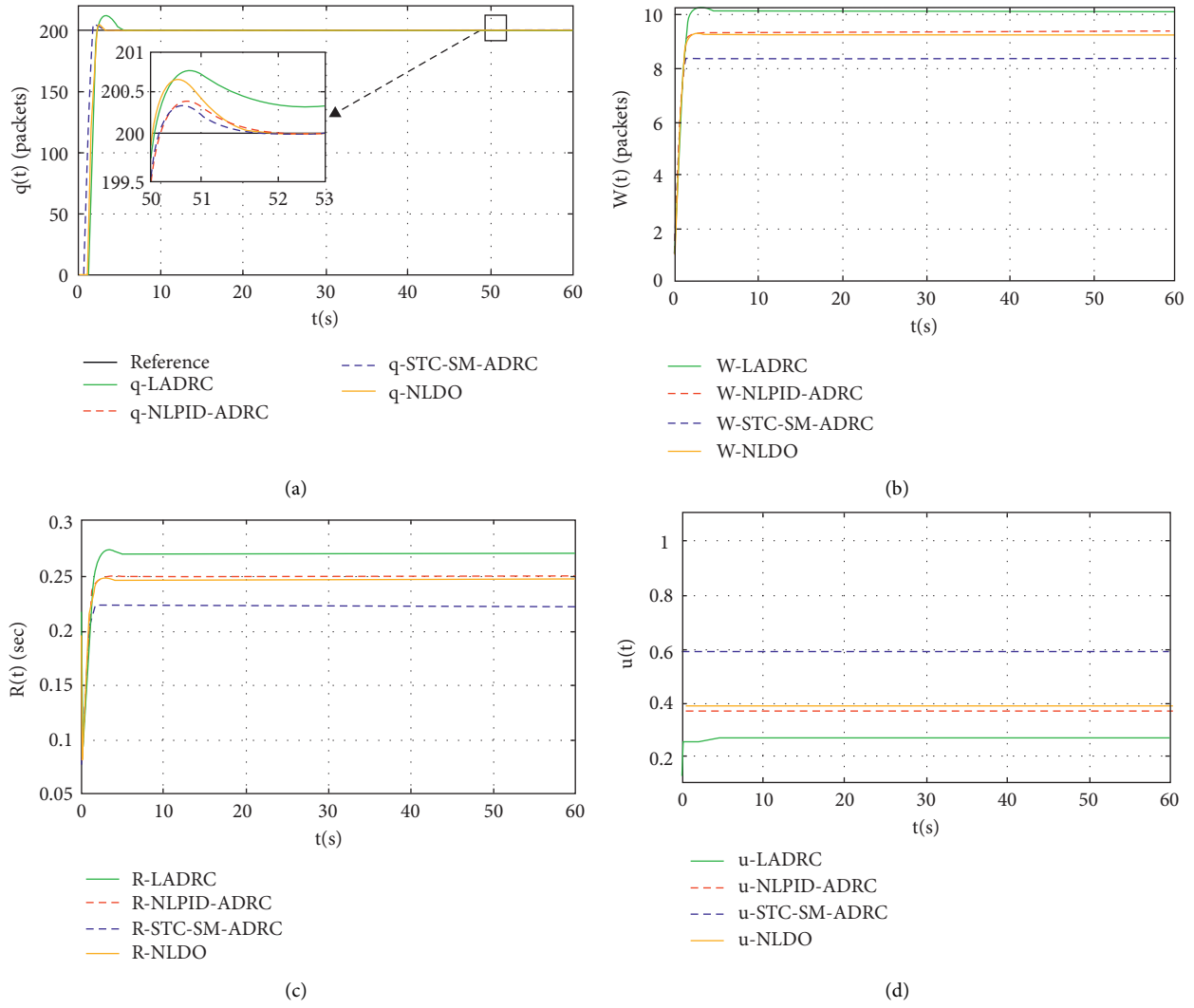
(a)

(b)

(c)

(d)

FIGURE 6: The output response when the disturbance is applied at $t = 50$ s. (a) The average queuing length $q(t)$. (b) The window size $W(t)$. (c) The round trip time $R(t)$ (d). The probability of losing packets $u(t)$.
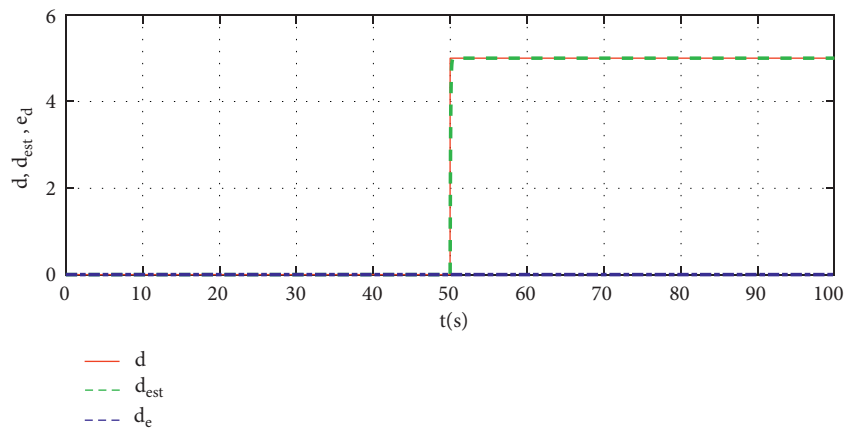

FIGURE 7: The applied disturbance $d(t)$, the estimated disturbance $\widehat{d}(t)$, and the disturbance error e_d.

TABLE 11: Performance indices.

PI	LADRC	NLDO	NLPID-ADRC	STC-SM-ADRC
ITAE	492.215585	275.662813	269.542633	209.239930
IAU	754.090790	71.626049	1.560232	0.315629
ISU	1.897476	0.019749	0.011761	0.000003
IAE	354.656276	278.636823	285.147109	221.044196
ISE	58172.631469	47530.946990	48837.954709	37063.347796
MSE	1938.441568	1583.836954	1627.389361	1235.033249
OPI	0.848649	0.523400	0.5176	0.396178

TCP network nonlinear model with the anti-disturbance methods (ADRC and NLDO) are shown in Figures 6 and 7. As shown in Figures 6(a)–6(c), the proposed methods (NLPID-ADRC and STC-ADRC) show excellent performance in terms of tracking the desired value and attenuating the disturbance as compared with the LADRC and NLDO options. Moreover, both NLPID-ADRC and STC-SM-ADRC reach a steady state in less than 2 s that lasts for about 1.5 s and 1.9 s, respectively, with movement back to the steady-state value after overshoots of 0.15% and 0.2% of the steady-state value. The NLDO lasted about 2.5 s before returning to the steady-state value after an overshoot of 0.35%. Finally, the LADRC is shown to be the weakest method in terms of disturbance attenuation as compared to the other methods. Figure 6(d) shows the control signal, which makes it clear that nearly all the presented methods show only small packet loss. Figure 7 shows the applied disturbance, the estimated disturbance, and the disturbance observer error, demonstrating that the proposed NLDO can perfectly estimate the applied disturbance.

The performance index values are shown in Table 11. The proposed controllers NLPID and STC-SM show noticeable improvement in OPI of 39.00894% and 53.30579%, respectively, in addition to improvements across all performance indices. Based on this, the proposed methods (NLPID-ADRC and STC-SM-ADRC) are thus shown to have improved accuracy and effectiveness based on smooth response and minimized OPI.

7. Conclusion

In this study, the time-delayed TCP network nonlinear model was utilized to design an accurate AQM using the ADRC approach to deal with the congestion problem and mismatched disturbances by stabilizing the nonlinear system. Two methods to achieve the main aim of this work were thus proposed in this study. A new NLPID and a new STC-SM were proposed to control and reduce congestion in the TCP network and stabilize the nonlinear system, and then, an NLDO was proposed to handle the problem of mismatched exogenous disturbance. Finally, a modified ADRC, consisting of the new NLPID and the new STC-SM as controller and tracking differentiator, respectively, was proposed to control congestion in the TCP network and to stabilize the nonlinear system as well as eliminating and rejecting the disturbance applied to the nonlinear system. The simulation results support the effectiveness of the modified ADRC in terms of congestion reduction and disturbance rejection. The modified ADRC was shown to provide a better performance, with smooth responses and minimum OPI, as compared to all the other methods introduced in this study. Moreover, the closed-loop stability and the convergence of NLESO were confirmed. Further studies related to this work could include using another optimization technique to tune the parameters of the modified ADRC.

Data Availability

All data are included within the manuscript.

Conflicts of Interest

The authors declare that there are no conflicts of interest.

References

[1] L. Ma, X. Liu, H. Wang, and X. Deng, "Congestion tracking control for multi-router TCP/AQM network based on integral backstepping," *Computer Networks*, vol. 175, Article ID 107278, 2020.

[2] S. Floyd and V. Jacobson, "Random early detection gateways for congestion avoidance," *IEEE/ACM Transactions on Networking*, vol. 1, no. 4, pp. 397–413, 1993.

[3] V. Misra, W. B. Gong, and D. Towsley, "Fluid-based analysis of a network of AQM routers supporting TCP flows with an application to RED," in *Proceedings of the 19th IEEE International Conference on SIGCOMM*, pp. 151–160, New York, NY, USA, August 2000.

[4] R. A. Hotchi, *Active queue management based on control-theoretic approaches for diversified communication services*, A Thesis for the Degree of Ph.D, Graduate School of Science and Technology Keio University, Tokyo, Japan, 2021.

[5] H. I. Ali and K. S. Khalid, "Swarm intelligence based robust active queue management design for congestion control in TCP network," *IEEJ Transactions on Electrical and Electronic Engineering*, vol. 11, no. 3, pp. 308–324, 2016.

[6] S. K. Bisoy and P. K. Pattnaik, "Design of feedback controller for TCP/AQM networks," *Engineering Science and Technology, an International Journal*, vol. 20, no. 1, pp. 116–132, 2017.

[7] M. N. Lin, T. Ren, H. W. Yuan, and M. Li, "The congestion control for TCP network based on input/output saturation," in *Proceedings of the 2017 29th Chinese Control and Decision Conference*, pp. 1166–1171, Chongqing, China, May 2017.

[8] Y. Jing, Z. Li, and G. Dimirovski, "Minimax based congestion control for TCP network systems with UDP flows," *MATEC Web of Conferences*, vol. 210, 2018.

[9] Y. Liu, X. Liu, Y. Jing, Z. Zhang, and X. Chen, "Congestion tracking control for uncertain TCP/AQM network based on integral backstepping," *ISA Transactions*, vol. 89, pp. 131–138, 2019.

[10] R. Hotchi, H. Chibana, T. Iwai, and R. Kubo, "Active queue management supporting TCP flows using disturbance observer and smith predictor," *IEEE Access*, vol. 8, Article ID 173413, 2020.

[11] K. Wang, X. Liu, and Y. Jing, "Command filtered finite-time control for nonlinear systems with state constraints and its application to TCP network," *Information Sciences*, vol. 550, pp. 189–206, 2021.

[12] S. K. Bisoy, P. K. Pattnaik, M. Sain, and D. U. Jeong, "A self-tuning congestion tracking control for TCP/AQM network for single and multiple bottleneck topology," *IEEE Access*, vol. 9, Article ID 27735, 2021.

[13] J. Shen, Y. Jing, and T. Ren, "Adaptive finite time congestion tracking control for TCP/AQM system with input-saturation," *International Journal of Systems Science*, vol. 53, no. 2, pp. 253–264, 2021.

[14] J. Han, "From PID to active disturbance rejection control," *IEEE Transactions on Industrial Electronics*, vol. 56, no. 3, pp. 900–906, 2009.

[15] A. A. Najm and I. K. Ibraheem, "Altitude and attitude stabilization of UAV quadrotor system using improved active disturbance rejection control," *Arabian Journal for Science and Engineering*, vol. 45, no. 3, pp. 1985–1999, 2020.

[16] W. R. A. Adheem and I. K. Ibraheem, "An improved active disturbance rejection control for a differential drive mobile robot with mismatched disturbances and uncertainties", systems and control," 2018, https://arxiv.org/abs/1805.12170.

[17] A. J. Humaidi and I. K. Ibraheem, "Speed control of permanent magnet DC motor with friction and measurement noise using novel nonlinear extended state observer-based anti-disturbance control," *Energies*, vol. 12, no. 9, p. 1651, 2019.

[18] A. Najm, I. Ibraheem, A. Azar, and A. Humaidi, "Genetic optimization-based consensus control of multi-agent 6-DoF UAV system," *Sensors*, vol. 20, no. 12, p. 3576, 2020.

[19] A. P Piña and D. M Aguilar, "Stability analysis of PD AQM control for delay models of TCP networks," *International Journal of Control*, vol. 95, no. 5, pp. 1279–1289, 2020.

[20] W. R. A. Adheem, I. K. Ibraheem, A. J. Humaidi et al., "Design and analysis of a novel generalized continuous tracking differentiator," *Ain Shams Engineering Journal*, vol. 23, Article ID 101656, 2021.

[21] B. Z. Guo and Z. l. Zhao, "On the convergence of an extended state observer for nonlinear systems with uncertainty," *Systems & Control Letters*, vol. 60, no. 6, pp. 420–430, 2011.

[22] S. Li, J. Yang, W. H. Chen, and X. Chen, *Disturbance Observer-Based Control Methods and Applications*, CRC Press Taylor & Francis Group, Boca Raton, FL, USA, 2014.

[23] K. H. Khalil, *Nonlinear Control*, Pearson Education, London, UK, 2015.

WILEY | Hindawi

Research Article

End-to-End Semantic Leaf Segmentation Framework for Plants Disease Classification

Khalil Khan (ID),[1,2] **Rehan Ullah Khan** (ID),[3] **Waleed Albattah** (ID),[3] **and Ali Mustafa Qamar** (ID)[4]

[1]*Department of Information Technology and Computer Science, Pak-Austria Fachhochschule,*
 Institute of Applied Sciences and Technology, Haripur 22620, Pakistan
[2]*Faculty of Computer Sciences and Information Technology, Superior University, Lahore 54660, Pakistan*
[3]*Department of Information Technology, College of Computer, Qassim University, Buraydah, Saudi Arabia*
[4]*Department of Computer Science, College of Computer, Qassim University, Buraydah, Saudi Arabia*

Correspondence should be addressed to Rehan Ullah Khan; re.khan@qu.edu.sa

Pernicious insects and plant diseases threaten the food science and agriculture sector. Therefore, diagnosis and detection of such diseases are essential. Plant disease detection and classification is a much-developed research area due to enormous development in machine learning (ML). Over the last ten years, computer vision researchers proposed different algorithms for plant disease identification using ML. This paper proposes an end-to-end semantic leaf segmentation model for plant disease identification. Our model uses a deep convolutional neural network based on semantic segmentation (SS). The proposed algorithm highlights diseased and healthy parts and allows the classification of ten different diseases affecting a specific plant leaf. The model successfully highlights the foreground (leaf) and background (nonleaf) regions through SS, identifying regions as healthy and diseased parts. As the semantic label is provided by the proposed method for each pixel, the information about how much area of a specific leaf is affected due to a disease is also estimated. We use tomato plant leaves as a test case in our work. We test the proposed CNN-based model on the publicly available database, PlantVillage. Along with PlantVillage, we also collected a dataset of twenty thousand images and tested our framework on it. Our proposed model obtained an average accuracy of 97.6%, which shows substantial improvement in performance on the same dataset compared to previous results.

1. Introduction

The plants' diseases in crops and fruits have adverse effects on agriculture production. If these diseases are not identified and treated on time, an increase in food insecurity can occur. Some particular crops, such as wheat, rice, and maize are vital for ensuring the food supply as well as agriculture production. Early warnings and some forecasting are very effective prevention in controlling plants' diseases. Forecasting and prevention play an essential role in adequately managing agricultural production. However, until now, visual observations of producers are the only approach for various plants' disease identification in mostly rural areas, specifically in less developed countries. Continuous monitoring of experts is needed, which might be prohibitively very expensive in large farms.

Similarly, to contact experts' farmers may have to travel large distances, which also makes the consultation expensive and time consuming. We argue that this conventional approach is not practical for large farming areas looking into the demands of the crops in the production industry. Therefore, automatic plant disease recognition and classification are still crucial topics in computer vision (CV).

Diseases seriously affect the health of every living organism, including plants and animals. The state-of-the-art (S.O.A) algorithms in the CV and ML domains have enabled us to identify diseases beyond human accuracy. Interestingly, the CV and ML algorithms can be applied to all domains, including plants and humans, with almost no difference in implementation. Modern technology enables human society to generate sufficient food to fulfill the human population's requirements. Conversely, numerous factors

still affect food safety, including plant diseases, climate change, and the decline of pollinators. Plant diseases are the primary danger to food safety. At the same time, the deficiency of essential infrastructure makes it hard to identify these diseases in many parts of the world quickly. With the latest developments in CV algorithms, the ML paradigm paves its way for agile and on-spot disease diagnosis.

Plant diseases not taken seriously have caused a decline in agricultural productivity in several countries worldwide. The disease symptoms have a detrimental effect on crop growth, restraining yields and rendering agricultural goods unsuitable to be consumed. Therefore, their early detection, modeling, and recognition are essential. This article explores the modeling, detection, and recognition of plant diseases that involve appearance-based analysis and can be captured and modeled using ML. Since the leaves of plants provide expressive appearance-based modeling, from modeling perspectives, our interest is inclined towards disease detection in tomato plants using deep learning (DL).

Determining the health quality of a plant is essential. Several models have been created to deter the loss of crops to pests and diseases. Plant disease symptoms are usually noticeable when the leaves change color or shape. Traditionally, the identification of pests and diseases was done using the naked eye and was supported by agronomic organizations. Presently, detection of plant diseases and pests can be done through machine vision. Plant disease identification using ML is not a new research field. CV experts have reported many good papers worth mentioning in [1–6]. The extensive penetration of smartphones, high-density cameras, and high-performance processors have made it possible for diseases to be detected by automated image recognition.

This paper proposes an end-to-end (E2E) segmentation model for plant disease identification and classification. The model uses semantic leaf segmentation (SLS) using an optimized CNN. By successfully highlighting the foreground and background regions, the proposed model classifies them into healthy and disease parts. The proposed model encodes the high-density maps and classifies tomato plant leaves into ten different categories of various diseases. Our model outperforms previous approaches in an evaluation setup on the PlantVillage database. The significant contributions of the proposed work are as follows:

(i) A new CNN-based algorithm for plants' disease recognition and classification has been presented in the paper. ML and DL experts have already proposed numerous methods for plants disease recognition; the novelty of our model is providing information about each pixel of a leaf image, which tells if a pixel belongs to a diseased or healthy part.

(ii) Second, we contributed a new dataset for tomato leaves disease classification. We collected these images from the Internet. These images are labeled

manually as healthy and diseased images. The database will be available after the publication of the proposed work for research purposes.

(iii) The proposed model also provides information regarding how much leaf area is affected by a specific disease. Most of the previous ML-based approaches do not provide this information. Along with predicting the diseased and healthy part, information regarding how much leaf area is affected by a specific disease is also provided.

The presentation of the remaining paper is arranged as follows. In Section 2, we discuss previous research work on the topic. Both conventional ML and DL-based methods are discussed in this part. The proposed CNN-based method is discussed in Section 3. Section 4 presents the experimental setup, obtained results, and comparison of obtained results with previous results. Finally, the conclusion is presented in Section 5 with some promising future directions.

2. Related Work

Plant diseases typically affect the growth of crops in all stages of development and sometimes may lead to the death of the plant. Plant diseases affect food security globally and affect small subsistence farmers who depend on their crops for food and livelihood. Therefore, determining the health quality of a plant is very important. Several models have been created to deter the loss of crops to pests and diseases. Traditionally, the identification of pests and diseases was done using the naked eye and was supported by agronomic organizations. Plant disease identification using ML is a well-researched area. CV experts have reported many good papers on the topic [1–9].

In meticulous agriculture, the subdivision of crops in agricultural images is vital. Various techniques have been deployed for the segmentation process, such as SS. The SS marks the multiple features in an image into semantically meaningful items and classifies each item into a class. For example, the various classes can be leaf, stalk, or flower in plants. Several studies have used different SS techniques to identify plants from nonplants. For example, Sodjinou et al. [10] suggest a method grounded on the mixture of SS and K-means for detecting weed from images. K-means algorithm is used for categorizing things that belong to similar groups. The proposed technique provided a more accurate segmentation of weeds and plants from the study results. Several approaches were used by Miao et al. [11] to semantically segment hyperspectral images of sorghum plants, such as manual pixel annotation and classifying each of the pixels as either nonplant or plant. The scholars further classified the plant as belonging to either a panicle, leaf, or stalk of the sorghum plant. They could separate the plant pixels from the background, only that they could not classify to what organ the plant pixel belonged. In another study, Li et al. [12] used the region-based segmentation to detect crops

from the images derived from a natural field. They used the method to detect cotton specifically. The model was successful as it could even detect the boll opening stage of the cotton plant.

While identifying a plant from a nonplant can be an easy task using SS, identifying plant diseases through an image is tough since plants are complex environments. Through the developmental stages of crops, their flowers, fruits, and leaves change constantly. During the day, solar radiation affects plants' spectral response, so their appearance also changes slightly. Additionally, different shapes, layouts, and colors of plant diseases make them difficult to recognize. Regardless, several successful techniques improve detection methods for diseases in plants, both in a controlled environment and in natural conditions.

Chen et al. [13] proposed using BLSNet to recognize the rice bacterial leaf streak in rice and segmentation based on UNet network. Rice bacterial leaf streak (BLS) is a threatening disease usually found in rice leaves. BLS affects the yield and quality of rice. BLSNet used a large-scale extraction and an attention mechanism to increase the precision of segmentation of the lesion.

One technique that has been widely successful in identifying plant diseases is SS through CNN. The layers of CNN can be viewed as corresponding filters that are directly taken from the input data. CNNs bring out a hierarchy of visual images adjusted for a precise task. The accuracy of CNNs in detecting objects such as plant diseases and image organization has made incredible growth over time [14]. The CNN-based classification network implementation is the most regularly used pattern in categorizing plant diseases and pests, owing to CNN's strong feature extraction capability. Zabawa et al. [15] used SS using convolutional neural networks to extract phenotypic traits in grapevine berries.

According to Bhatt et al. [16], CNN-based methods have been used to achieve extraordinary results in supervised image segmentation of leaves. Usually, the methods used work under fully controlled conditions, whereas the deep CNN models are built on various changing parameters. However, the images would have different backgrounds, lighting conditions, obstructions, and overlapping in an environmental setting. In various stages of growth, plants do have a reasonable amount of variation. The authors propose unsupervised machine learning algorithms to segment the leaves images to make it possible to be applied to various crops and regions. Afterward, the specific segments are then assessed for their texture, size, and color to measure any change, such as the presence of a pest or disease.

Unsupervised feature learning, with fully convolutional networks (FCN) followed by conditional random fields, makes it possible to segment images into an optimal number of clusters devoid of any prior training. The real-time performance of this technique allows easy distribution of devices such as cameras and mobile phones in the fields. In addition, Shao et al. [17] propose using localization and DL-based method to recognize dense rice images. The proposed model can be used to determine rice diseases. The results from the study show that better results can be obtained compared to conventional ML methods. The SS method

grounded on deep CNNs can also identify crops from the compound and natural field environments [18]. According to Martins et al. [19], it can also detect tree canopies in an urban setting.

The SS method based on DL demonstrates great precision in remote sensing categorization as well, and it necessitates vast sets of data in controlled learning [20]. The simple notion of DL is using a neural network for analyzing information and learning image feature. In their study of estimating sorghum panicles, Malambo et al. [21] applied an image analysis method founded on a SegNet framework. Sorghum panicles are critical phenotypic data in the improvement of sorghum crops. The study results demonstrated that DL combined with SS shows excellent precision with large data. On the other hand, Pena et al. [22] suggest using data fusion to enrich images used in remote sensing.

In very recent works [23–26], plant disease recognition models have been improved for better results and performance. Manjula et al. [24] have used ResNet-50 architecture, a variant of the Resnet model that has 48 convolution layers. The accuracy of the developed system is around 97-98%. Chen et al. [25] have improved the plant disease-recognition model based on the original YOLOv5 network model, which accurately identified plant diseases under natural conditions. Hassan and Maji [26] have proposed a novel deep learning model based on the inception layer and residual connection. They used Depthwise separable convolution to reduce the number of parameters, which led the model to achieve higher accuracy.

3. Materials and Methods

3.1. Dataset Description and Data Annotation. The typical DL-based methods require sufficient data for the training phase. In contrast, conventional ML can also be trained on limited data scenarios. One of the main drawbacks of DL techniques is requiring a large amount of data. In this research work, we used an already available dataset and also collected our own database. We use two kinds of data in our experiments, the details of which are provided next.

PlantVillage database [27]: The PlantVillage database is publicly available for downloading and research purposes. It is an open-access repository having more than 54K images. PlantVillage is a large dataset with various plants' leaves and related materials collection. Most of the data in this database are collected in controlled laboratory conditions. Exposure to the real-time scenario is significantly less in the PlantVillage database. Therefore, most researchers using only PlantVillage database get nearly perfect results. The database includes images of 14 crops, including grape, corn, tomato, and soybean. The database consists of 10 folders, one for healthy leaves and the remaining for nine different kinds of diseases listed in Tables 1 and 2. We use a subset of images for the tomato plant. Our subset consists of around 16012 images of plant leaves collected from tomato plants. The total number of classes in these images is limited to ten only. Nine classes are of various diseases for tomato plant leaves, whereas one class is for healthy leaves. We keep the resolution of each image as *250 x 250* pixels. Some sample images of the database used are shown in Figure 1.

Table 1: Number-wise distribution of the PlantVillage database.

Disease	Number of images
Bacterial spot (BS)	2127
Late blight (LB)	1909
Two-spotted spider mite (TSSM)	1676
Yellow leaf curl virus (YLCV)	5357
Leaf mold (LM)	952
Target spot (TS)	1404
Early blight (EB)	1000
Tomato mosaic virus (TMV)	373
Septoria leaf spot (SLS)	1771

Table 2: TomatoDB images and different diseases' statistics.

Disease	Number of images in TomatoDB
EB	2250
LB	1800
TMV	2190
HL	1600
LM	2000
YLCV	1802
BS	2380
SLS	2100
TS	2270
SM	2340
Total	20732

We use all images of the tomato plant contained in the PlantVillage. The diseased leaf images vary from 373 to 5357, as clear from Table 1. The total number of healthy images for tomatoes in PlantVillage is 1591. It is clear from Table 1 that all the ten classes in the dataset are not balanced as far as the number of images is concerned. On the one hand, the minimum value is 373, with a maximum of 5357. We use data augmentation methods to balance all classes, including adjusting the contrast, flipping images vertically and horizontally, and changing brightness levels.

TomatoDB: since images in the PlantVillage are simple and less challenging, comparatively good results are reported in the literature. To assess the framework's performance more precisely, we also tested our model on a collection of images we had taken from the Internet. Our own collected dataset consists of more than 20000 images taken from tomato plant leaves. We collected these images from the Internet. While image collection, real-time scenarios, and more challenging conditions have been considered. The database TomatoDB will be available to the research community after the publication of the proposed research article. All ten classes are equally considered while collecting the database.

For SLS, correctly labeled leaf data for each pixel is needed. This ground truth data are created through annotation. We annotated these images manually using the interface we developed. This labeling involves selecting the areas of interest, random sketch application, adjustment of contrast and brightness, and assigning a label. Such kind of manual labeling is prone to errors. No automatic tool is used in such labeling. The labeling is highly dependent on the

subjective perception of the human doing this labeling process. Hence, chances of error exist while providing an exact label to every pixel.

Images setup for experiments: The model we presented in this paper is applicable and valid to any plant disease with some visible symptoms. However, manual labeling will be needed to create an SS framework for training purposes. As a test case, we select a tomato plant with ten classes. However, since images in the PlantVillage dataset are not exposed to light and other variations, we collected some images (20000) from the Internet. Some tomato leaves images we collected from the Internet are shown in Figure 2. We use a combination of PlantVillage dataset images and our own collected data set. We split the dataset into the ratio of 80 to 20, a commonly used strategy for training and testing DL-based models. Some of the authors also adopt 5-fold or 10-fold cross validation. We set 80% data for training and 10% for validation to know the model overfitting problem. We resize each image in PlantVillage and TomatoDB to a size of *250 x250* before training and testing. The following section discusses all the hyperparameters of the deep CNN-based model.

3.2. Deep Model Learning. The performance of the visual recognition tasks is improved with the introduction of DL-based methods [28–33]. The proposed paper addresses leaf disease recognition and classification using deep CNNs. We utilize the concept of SLS in the proposed research.

Convolution layer: This layer plays a vital role in the features extraction stage. The CovL is an essential component of the CNN model. The layers consist of a set of learnable filters. These terms are also known as kernels [34]. In this convolution process, the filter with a specific size slides over the image and is convolved with pixel values of the target image. The dot product is computed between kernel and input image pixels producing a feature map.

ReLU: We use ReLU as activation function. This function plays a crucial role in converting the input signal from a specific network node to the output signal. The resultant signal obtained a form as shown in equation.

$$f(F) = \max(0, F_j). \tag{1}$$

Pooling layer: The pooling layer follows the CovL. The output from the CovL is given to the pooling layer. ML experts use three pooling strategies: random pooling, maximum pooling (MPL), and average pooling. We, in the proposed work, adapted MPL. The MPL achieved spatial invariance by reducing the feature map size obtained previously from CovL [35]. In this strategy, the max operation is applied to the feature map when the feature map is passed through MPL. This operation can be performed as described by :

$$MPL_j = \max(F_i). \tag{2}$$

Classification: we use the SoftMax classifier for classification. The pooling layers provide a feature vector to the

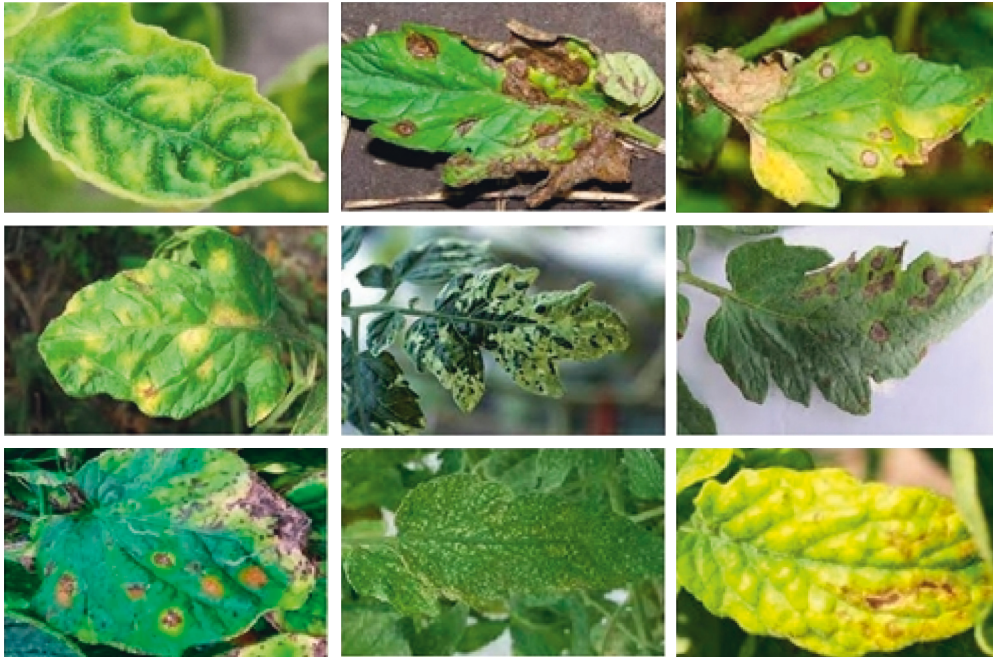FIGURE 1: Sample images from PlantVillage database.

FIGURE 2: Some images of the leaves from the TomatoDB dataset.

SoftMax in the output layer. In the output layer, a function that appears is the activation function for a multiclass classification problem. The activation function calculates a vector having a real number (k) and performs the normalization task. The normalization converts input values into vectors consisting of probability values in the range 0 to 1. The Softmax returns each class probability value, having the maximum probability value as the target class [36].

Adam: It is a standard optimizer that computes individual adaptive learning rates for each parameter [37]. The exponential decaying average of previous gradients n_t is used by this optimizer.

The proposed framework is presented in Figure 3.

Tables 3 and 4 summarize various parameters in the proposed CNN framework. As an activation function, we use ReLU. For constructing CNN-based model, we use three

FIGURE 3: SLS-based leaf disease identification model.

layers containing CovL, MPL, and FCL. The details of these layers with feature map description, kernel size, and stride are summarized in Table 3. The feature extractor extracts the features from the images of the leaves, including healthy and affected leaves. More description of the feature extraction part is in Figure 4. Features variation is handled by stage 1. Certain environmental factors produce scaling variations in images. These receptive fields overcome all the variations. Each field has sixteen filters. Stage 1 output is given to stage

TABLE 3: CovL and MPL parameters' setting.

Type of layer	Size of stride	Feature map	Size of kernel	Output size
Input	—	—	—	250×250
CovL1	2	96	5×5	124×124
MPL1	2	96	3×3	62×62
CovL2	2	256	5×5	30×30
MPL2	2	256	3×3	15×15
CovL3	2	316	5×5	12×12
MPL3	2	316	3×3	6×6
CovL4	2	512	5×5	4×4
MPL4	2	512	3×3	2×2

TABLE 4: Deep CNN parameters' settings.

Parameters	Values
Number of epochs	500
Activation function	ReLU
Momentum	0.99
Batch size	150
Base learning rate	0.0001
Drop our rate	0.40

2. We use the 2×2 kernel in MPL in stage 2. Each layer of ConvL is followed by ReLU. We place a special pyramid (SPD) between CovL and FCL. In stage 3, output from SPD is given to FCL. Both stages 3 and 4 extract desired features. More details about deep CNN parameters are presented in Tables 3 and 4 and Figure 4.

Data including both training images and ground truth are given to the framework. The density map is predicted in density estimation (DE), taking supervision from the ground truth data. We combined the segmentation map and DE map, feeding the results to the CovL. Loss is added to the algorithm (Dice Coefficient) in the SS section. Additionally, we add Euclidean distance loss for optimizing the estimated density maps.

3.3. CNN Optimization. A complete illustration of how hyperparameters are tuned and optimization is performed is presented in this subsection. Overfitting is a severe problem faced mainly by ML models. We use the methodology as suggested and used in [38] to tackle this problem. We use a combination of four different loss functions. We use the Euclidean distance for better optimization. The obtained segmentation density map can be written as shown in (3) and (4)

$$\text{Loss}_{\text{int}} = \frac{1}{2M} \sum_{k=1}^{M} \widehat{p}_k - P_{k2}^2. \tag{3}$$

$$\text{Loss}_{\text{den}} = \frac{1}{2M} \sum_{k=1}^{M} \widehat{P}_k - P_{k2}^2. \tag{4}$$

In (3), $\widehat{p}$ shows the estimated density in the supervision process. Similarly, $\widehat{P}_k$ represents the estimated density, and

P_k represents the ground truth density value. Similarly, M represents the pixel numbers in the GT density map.

We also introduce a loss in the SS part of the framework. The loss in the framework is due to the dice coefficient. The dice coefficient is two times the overlap area between the predicted segmentation and true values. The result is then divided by the total pixels in the ground truth and the original image. The range of the dice coefficient is between 0 and 1. We use another special loss function, called cross-entropy loss, which we represent as

$$\text{Loss}_{X-\text{entropy}} = -\frac{1}{Q} \sum_{b=1}^{Q} \sum_{c=1}^{C} x_c^b \log(x^b). \tag{5}$$

In (5), the symbol Q represents the total sample, and C shows the number of classes used. Similarly, the ground truth class is shown by x_c^b, whereas the estimated output is represented by x^b. The final weighted loss function is represented by :

$$W.L = \text{Loss}_{\text{int}} + \text{Loss}_{\text{den}} + \lambda \text{Loss}_{X-\text{entropy}}. \tag{6}$$

In (6), the value of λ was 0.3.

4. Results and Discussion

4.1. Performance Evaluation Measures. We use different evaluation measures, including precision (P_r), recall (R_c), accuracy (A_{cc}), F-measure (F_m), and confusion matrix (C_{mat}). Most of these measures are defined with some terms called false positive (FP), true positive (TP), true negative (TN), and false-negative (FN). P_r is lower if the number of FPs is more. The R_c measures the correct prediction (positive only) by calculating the proportion of the number of TPs to the total sample (TP + FN). The range of both P_r and R_c is between 0 and 1. The F_m assesses the performance of the model by calculating the weighted harmonic mean between P_r and R_c. Mathematically, all the evaluation measures are defined in equations (7)–(10):

$$P_r = \frac{(\text{TP})}{(\text{TP}) + (\text{FP})}. \tag{7}$$

$$R_c = \frac{(\text{TP})}{(\text{TP}) + (\text{FN})}. \tag{8}$$

$$F_m = 2 * \frac{(\text{Precision}) x (\text{Recall})}{(\text{Precision}) + (\text{Recall})}. \tag{9}$$

$$A_{cc} = \frac{(\text{TP} + \text{TN})}{(\text{TP} + \text{TN} + \text{FP} + \text{FN})}. \tag{10}$$

4.2. Experimental Setup. We perform our experiments with an Intel i7 workstation and employ NVIDIA GPU 840 graphics card. We perform all our experimental work with Tensor-flow, Keras, and *Python*. The number of epochs we use is 500, having a batch size of 150. We use the base learning rate as 0.0001 and the dropout rate as 0.4. We use two datasets for experimental work: including PlantVillage
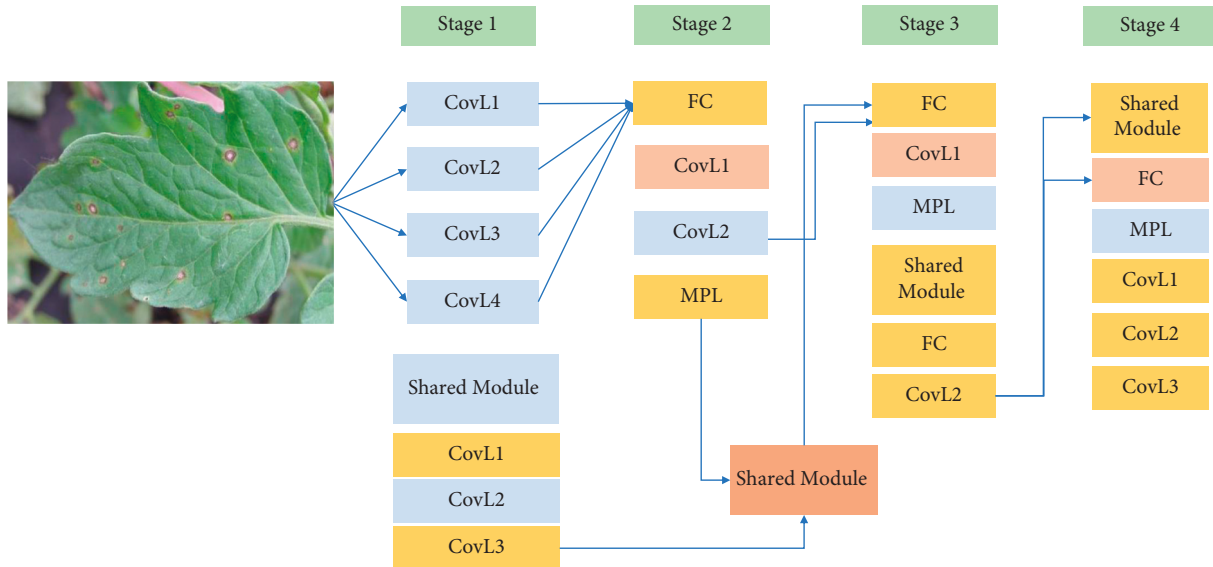
FIGURE 4: Proposed feature extractor module.

and our own collected database. The PlantVillage consists of more than 16K images, and our own database consists of more than 20K images. We combined both datasets and performed our experiments in the ratio of training to testing as 80 to 20.

4.3. Limitations of the Proposed Work.

The numerical solutions and results reported in this paper show that a good performance is achieved by the proposed method; however, our proposed algorithm still has limitations. It is a fact that the research community has concerns about using DL architectures. All DL-based methods are complex and require inputs at several stages. Researchers using these techniques rely on a trial and error strategy. To summarize, these methods are time consuming and very well engineered. However, it is also confirmed that the only choice CV experts have for any CV-based task is DL methods. We use the idea of SLS in our proposed work. Ground truth data are needed for the training and testing phases to implement this model. In order to create the ground truth data, manual labeling is required. Since a single person does all this manual labeling, errors are expected most of the time in labeling. We also did this labeling manually through humans, which is a weakness of our proposed method.

4.4. Reported Results and Its Discussion.

Some conclusions that emerge from the results and experiments are summarized in the following paragraphs.

(i) Plant disease classification and identification using ML is not a new research area for CV and ML experts. The state-of-the-art reports many good papers on this topic. Due to diverse applications in agriculture, researchers explored this field sufficiently. However, we notice less emphasis, particularly on interclass disease identification. Researchers mainly focus on a single plant disease

recognition, whereas our proposed work focuses on tomato plant disease classification with ten classes.

(ii) Initially, we run the whole experimental setup for a maximum of 14 epochs (please see Figure 5). We run this setup to know how the model performance varies on training and validation databases. As clear from Figure 5, training along with validation accuracy changes very quickly up to value 6. After value 6, change occurs very slowly in the upcoming epochs. Both training and validation losses are also shown. It is clear that loss is high in the initial stages and is gradually reduced after increasing the epochs. This loss reduction clearly shows that the network is fine-tuned gradually with increasing epochs.

(iii) We use ten class disease problems in our work. The names of the classes, along with abbreviations, are shown in Table 5. We report the results for P_r, R_c, and F_m for all the ten classes. It is clear from Table 5 that near-perfect results are reported for the class BS using all three evaluation measures. Similarly, better results are reported for the classes LB, TMV, SM, and HL. The worst performance has been shown for the class EB with precision 0.93, recall 0.95, and F-measure 0.95, which also shows acceptable and good results. Our proposed method semantically segments leaf images into background and foreground. Please see some images in Figure 6, where column 1 represents the original images, column 2 ground truth, and column 3 segmentation results. After foreground estimation, each disease classification is performed. Moreover, it is also estimated how much percent of the leaf area is affected by a disease.

(iv) C_{mat} is the best choice for multiclass evaluation problems, which ML experts commonly use. It shows the corresponding percentage of the
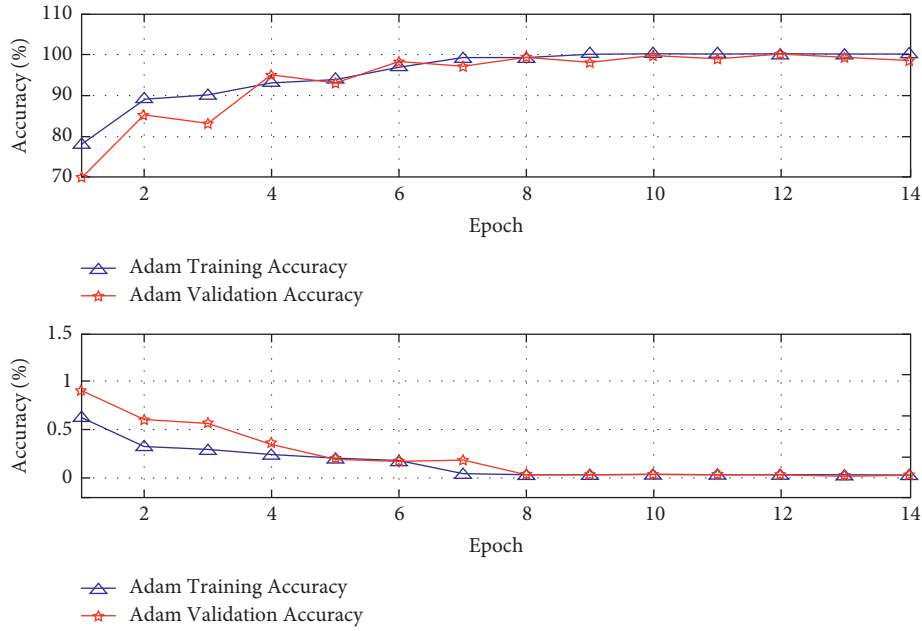
FIGURE 5: Using Adam optimizer, accuracy, and loss changing obtained using training and validation sets.

TABLE 5: Performance reported in the form of P_r, R_c, and F_m for the proposed model.

Class	Precision	Recall	F-measure
EB	0.93	0.95	0.95
LB	0.96	0.99	1.00
TMV	0.97	0.99	0.96
HL	0.96	0.97	0.97
LM	0.93	0.95	0.98
YLCV	0.94	0.93	0.96
BS	0.96	0.99	1.00
SLS	0.96	0.96	0.98
TS	0.96	0.94	0.94
SM	0.96	0.98	0.99
Mean	0.95	0.96	0.97

predicted class and true class. The C_{mat} for the reported results for the 10-class problem is demonstrated in Table 6. The results vary from 94% (lowest) to 100% (highest). The lowest results are reported for EB, whereas the highest values are reported for HL. The LM, YLCV, BS, and LB results are comparatively better, with predicted accuracy values as 99%, 98%, 98%, and 97%, respectively.

4.5. Performance Comparison with Previous Results. We compared the reported results with S.O.A. in Table 7. It is clear that the reported results are far better than previous results. The reported results and their comparison with S.O.A. are for accuracy measure only. As most of the papers reported their accuracy results, we compared our work with this metric only. We want to add that some research papers reporting results on plant disease classification using hand-crafted features show better results than DL-based methods. However, we believe a better understanding of DL methods
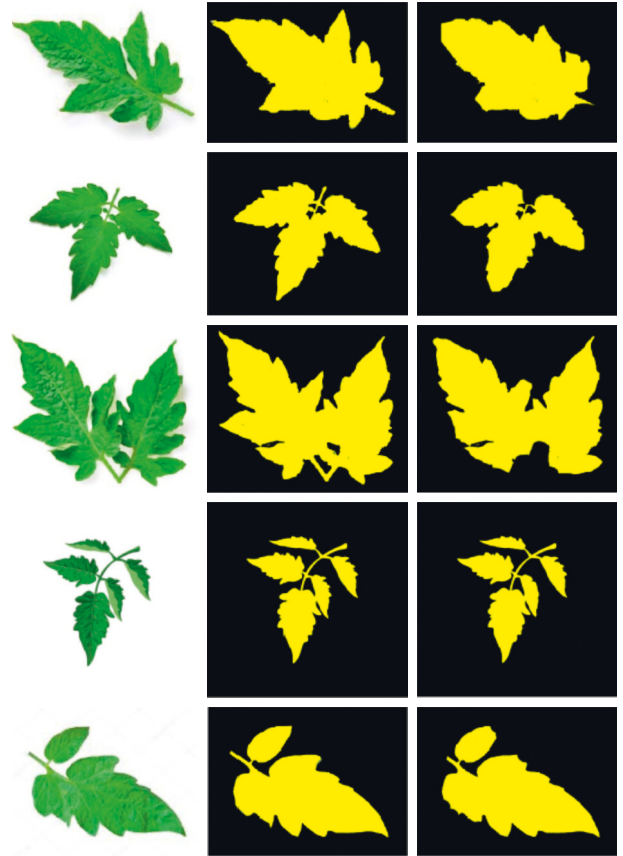

FIGURE 6: Some example images we used during our experiments: column 1 shows original images, column 2 shows ground truth data, and column 3 shows segmentation images with the proposed SLS method.

TABLE 6: Reported confusion matrix for tomato plant diseases recognition with proposed SLS-based method.

		Predicted class									
		EB	LB	TMV	HL	LM	YLCV	BS	SLS	TS	SM
	EB	**94**	1	0	0	2	1	1	1	0	0
	LB	1	**98**	0	0	0	0	0	0	1	0
	TMV	0	0	**100**	0	0	0	0	0	0	0
	HL	0	0	0	**100**	0	0	0.24	0	0	0
True class	LM	0	0	0	0	**99**	1	0	0	0	0
	YLCV	0	0	0	0	0	**98**	0	1	1	0
	BS	1	0	0	0	0	0	**98**	1	0	0
	SLS	0	0	0	0	0	1	1	**96**	1	1
	TS	0	0	0	0	0	2	1	1	**95**	1
	SM	0	0	0	0	0	0	1	1	1	**97**

TABLE 7: Reported results and their comparison with previous results.

Method used	Year	Algorithm (s)	Reported accuracy (%)
Proposed method	2022	SLS and CNNs	97.25
Abbas et al. [39]	2021	DenseNet	95.1
Agarwal et al. [40]	2020	GNN-based network	91.2
Elhassouny and Smarandache [41]	2019	MobileNet	90.3
Durmuş et al. [42]	2017	Combination of squeez net and AlexNet	95.65
Howard et al. [43]	2017	MobileNet	63.7
Szegedy et al. [44]	2016	Inception V3	63.4
Simonyan and Zisserman [45]	2014	VGG 16	77.2

is still required to address a specific task. For example, the requirement of a large amount of data is a problem DL methods face. Generally, traditional ML methods perform well on data collected in indoor scenes; however, researchers report a significant drop in performance when these methods are tested in real-time scenarios. On the contrary, DL architectures extract a higher level of abstraction from the data with much better results. Thus, the need for feature engineering is minimized to a large extent with DL algorithms.

5. Summary and Concluding Remarks

Due to diverse applications in the agriculture sector, plant disease identification using DL is an active area of research. Plant disease recognition is more challenging when the method is exposed to real-time data. However, CV researchers have shown tremendous progress in the past 5 to 10 years. Our current research provides unification and extension of our previous work reported in [7]. Our study is mainly motivated by looking into the human visual cortex to design an E2E trainable neural network architecture. We propose an E2E SS framework for plant disease identification using DL. We introduce the idea of SS for plant disease recognition. The proposed model predicts the nature of the disease of the tomato plant and tells how much area of a specific leaf is affected due to a certain disease. The model successfully classifies tomato plant leaves into ten distinct classes. We present a novel loss function that improves the model's performance on a state-of-the-art dataset. We evaluate our model with the standard dataset PlantVillage, noticing much better results than

previous results. Along with the PlantVillage database, we also collected a database of more than 20000 images and tested our framework on it. We expect more evaluation using a much better optimized DL model for plant disease recognition from the research community. In the future, we intend to analyze some more tasks to develop robust continual DL models, considering some complex combinations of the neural network along with information extraction.

Data Availability

The dataset used in this research, PlantsVillage, is available from https://www.kaggle.com/emmarex/plantdisease.

Conflicts of Interest

The authors declare no conflicts of interest.

Acknowledgments

References

[1] E. C. Too, L. Yujian, S. Njuki, and L. Yingchun, "A comparative study of fine-tuning deep learning models for plant disease identification," *Computers and Electronics in Agriculture*, vol. 161, pp. 272–279, 2019.

[2] J. G. Arnal Barbedo, "Plant disease identification from individual lesions and spots using deep learning," *Biosystems Engineering*, vol. 180, pp. 96–107, 2019.

[3] J. Chen, J. Chen, D. Zhang, Y. Sun, and Y. A. Nanehkaran, "Using deep transfer learning for image-based plant disease identification," *Computers and Electronics in Agriculture*, vol. 173, Article ID 105393, 2020.

[4] M. H. Saleem, J. Potgieter, and K. M. Mahmood Arif, "Plant disease detection and classification by deep learning," *Plants*, vol. 8, no. 11, p. 468, 2019.

[5] K. P. Ferentinos, "Deep learning models for plant disease detection and diagnosis," *Computers and Electronics in Agriculture*, vol. 145, pp. 311–318, 2018.

[6] M. H. Saleem, S. Khanchi, J. Potgieter, and K. M. Arif, "Image-based plant disease identification by deep learning meta-architectures," *Plants*, vol. 9, no. 11, p. 1451, 2020.

[7] R. U. Khan, K. Khan, W. Albattah, and A. M. Qamar, "Image-based detection of plant diseases: from classical machine learning to deep learning journey," *Wireless Communications and Mobile Computing*, vol. 202113 pages, Article ID 5541859, 2021.

[8] D. Srinivasa Rao, R. Babu Ch, V. Sravan Kiran et al., "Plant disease classification using deep bilinear CNN," *Intelligent Automation & Soft Computing*, vol. 31, no. 1, pp. 161–176, 2022.

[9] S. Nandhini and K. Ashokkumar, "An automatic plant leaf disease identification using DenseNet-121 architecture with a mutation-based henry gas solubility optimization algorithm," *Neural Computing & Applications*, vol. 34, no. 7, pp. 5513–5534, 2022.

[10] S. G. Sodjinou, V. Mohammadi, A. T. S. Mahama, and P. Gouton, "A deep semantic segmentation-based algorithm to segment crops and weeds in agronomic color images," *Information Processing in Agriculture*, 2021.

[11] C. Miao, A. Pages, Z. Xu, E. Rodene, J. Yang, and J. C. Schnable, "Semantic segmentation of Sorghum using hyperspectral data identifies genetic associations," *Plant Phenomics*, vol. 202011 pages, Article ID 4216373, 2020.

[12] Y. Li, Z. Cao, H. Lu, Y. Xiao, Y. Zhu, and A. B. Cremers, "In-field cotton detection via region-based semantic image segmentation," *Computers and Electronics in Agriculture*, vol. 127, pp. 475–486, 2016.

[13] S. Chen, K. Zhang, Y. Zhao et al., "An approach for rice bacterial leaf streak disease segmentation and disease severity estimation," *Agriculture*, vol. 11, no. 5, p. 420, 2021.

[14] S. Guo, Q. Jin, H. Wang, X. Wang, Y. Wang, and S. Xiang, "Learnable gated convolutional neural network for semantic segmentation in remote-sensing images," *Remote Sensing*, vol. 11, no. 16, p. 1922, 2019.

[15] L. Zabawa, A. Kicherer, L. Klingbeil, R. Töpfer, H. Kuhlmann, and R. Roscher, "Counting of grapevine berries in images via semantic segmentation using convolutional neural networks," *ISPRS Journal of Photogrammetry and Remote Sensing*, vol. 164, pp. 73–83, 2020.

[16] P. Bhatt, S. Sarangi, and S. Pappula, "Unsupervised image segmentation using convolutional neural networks for automated crop monitoring," in *Proceedings of the 8th International Conference on Pattern Recognition Applications and Methods (ICPRAM)*, pp. 887–893, Prague, Czech Republic, February 2019.

[17] H. Shao, R. Tang, Y. Lei, J. Mu, Y. Guan, and Y. Xiang, "Rice ear counting based on image segmentation and establishment of a dataset," *Plants*, vol. 10, no. 8, p. 1625, 2021.

[18] S. Zhuang, P. Wang, and B. Jiang, "Segmentation of green vegetation in the field using deep neural networks," in *Proceedings of the 2018 13th World Congress on Intelligent Control and Automation*, Changsha, China, July 2018.

[19] J. A. C. Martins, K. Nogueira, L. P. Osco et al., "Semantic segmentation of tree-canopy in urban environment with pixel-wise deep learning," *Remote Sensing*, vol. 13, no. 16, p. 3054, 2021.

[20] M.-D. Yang, H.-H. Tseng, Y.-C. Hsu, and H. P. Tsai, "Semantic segmentation using deep learning with vegetation indices for rice lodging identification in multi-date UAV visible images," *Remote Sensing*, vol. 12, no. 4, p. 633, 2020.

[21] L. Malambo, S. Popescu, N.-W. Ku, W. Rooney, T. Zhou, and S. Moore, "A deep learning semantic segmentation-based approach for field-level sorghum panicle counting," *Remote Sensing*, vol. 11, no. 24, p. 2939, 2019.

[22] J. Pena, Y. Tan, and W. Boonpook, "Semantic segmentation based remote sensing data fusion on crops detection," *Journal of Computer and Communications*, vol. 07, no. 07, pp. 53–64, 2019.

[23] T. S. Poornappriya and R. Gopinath, "Rice plant disease identification using artificial intelligence approaches," *International Journal of Electrical Engineering and Technology*, vol. 11, no. 10, pp. 392–402, 2022.

[24] K. Manjula, S. Spoorthi, R. Yashaswini, and D. Sharma, "Plant disease detection using deep learning," in *Proceedings of the 2nd International Conference on Data Science, Machine Learning and Applications (ICDSMLA)*, pp. 1389–1396, Singapore, April 2020.

[25] Z. Chen, R. Wu, Y. Lin et al., "Plant disease recognition model based on improved YOLOv5," *Agronomy*, vol. 12, no. 2, p. 365, 2022.

[26] S. M. Hassan and A. K. Maji, "Plant disease identification using a novel convolutional neural network," *IEEE Access*, vol. 10, pp. 5390–5401, 2022.

[27] D. P. Hughes and M. Salathé, "An open access repository of images on plant health to enable the development of mobile disease diagnostics," 2015, https://arxiv.org/abs/1511.08060.

[28] A. Voulodimos, N. Doulamis, A. Doulamis, and E. Protopapadakis, "Deep learning for computer vision: a brief review," *Computational Intelligence and Neuroscience*, vol. 201813 pages, Article ID 7068349, 2018.

[29] N. Akhtar and A. Mian, "Threat of adversarial attacks on deep learning in computer vision: a survey," *IEEE Access*, vol. 6, pp. 14410–14430, 2018.

[30] P. Pradhyumna, G. P. Shreya, and Mohana, "Graph neural network (GNN) in image and video understanding using deep learning for computer vision applications," in *Proceedings of the 2021 Second International Conference on Electronics and Sustainable Communication Systems (ICESC)*, pp. 1183–1189, Coimbatore, India, August 2021.

[31] R. K. Sinha, R. Pandey, and R. Pattnaik, "Deep learning for computer vision tasks: a review," in *Proceedings of the 2017 International Conference on Intelligent Computing and Control (I2C2)*, Coimbatore, India, June 2017.

[32] V. Rajesh, U. P. Naik, and Mohana, "Quantum Convolutional Neural Networks (QCNN) using deep learning for computer vision applications," in *Proceedings of the 2021 International Conference on Recent Trends on Electronics, Information, Communication & Technology (RTEICT)*, pp. 728–734, Bangalore, India, August 2021.

[33] N. O'Mahony, S. Campbell, A. Carvalho et al., "Deep learning vs. traditional computer vision," in *Proceedings of the Science*

and Information Conference, pp. 128–144, Las Vegas, NV, USA, April 2019.

[34] Y. Zheng, Q. Liu, E. Chen, Y. Ge, and J. L. Zhao, "Exploiting multi-channels deep convolutional neural networks for multivariate time series classification," *Frontiers of Computer Science*, vol. 10, no. 1, pp. 96–112, 2016.

[35] M. D. Zeiler and R. Fergus, "Stochastic pooling for regularization of deep convolutional neural networks," 2013, https://arxiv.org/abs/1301.3557.

[36] I. Goodfellow, Y. Bengio, and A. Courville, *Deep Learning*, MIT press, Cambridge, 2016.

[37] D. P. Kingma and J. Ba, "Adam: a method for stochastic optimization," in *Proceedings of the 3rd International Conference for Learning Representations (ICLR)*, San Diego, CA, USA, May 2015.

[38] R. Collobert and J. Weston, "A unified architecture for natural language processing: deep neural networks with multitask learning," in *Proceedings of the 25th International Conference on Machine Learning*, pp. 160–167, Helsinki, Finland, July 2008.

[39] A. Abbas, S. Jain, M. Gour, and S. Vankudothu, "Tomato plant disease detection using transfer learning with C-GAN synthetic images," *Computers and Electronics in Agriculture*, vol. 187, Article ID 106279, 2021.

[40] M. Agarwal, A. Singh, S. Arjaria, A. Sinha, and S. Gupta, "ToLeD: tomato leaf disease detection using convolution neural network," *Procedia Computer Science*, vol. 167, pp. 293–301, 2020.

[41] A. Elhassouny and F. Smarandache, "Smart mobile application to recognize tomato leaf diseases using convolutional neural networks," in *Proceedings of the 2019 International Conference of Computer Science and Renewable Energies (ICCSRE)*, pp. 1–4, Agadir, Morocco, July 2019.

[42] H. Durmus, E. O. Günes, and M. Kırcı, "Disease detection on the leaves of the tomato plants by using deep learning," in *Proceedings of the 2017 6th International Conference on AgroGeoinformatics*, pp. 1–5, Fairfax, VA, USA, August 2017.

[43] A. G. Howard, M. Zhu, B. Chen et al., "Mobilenets: efficient convolutional neural networks for mobile vision applications," 2017, https://arxiv.org/abs/1704.04861.

[44] C. Szegedy, V. Vanhoucke, S. Ioffe, J. Shlens, and Z. Wojna, "Rethinking the inception architecture for computer vision," in *Proceedings of the 2016 IEEE Conference on Computer Vision and Pattern Recognition (CVPR)*, pp. 2818–2826, Las Vegas, NV, USA, June 2016.

[45] K. Simonyan and A. Zisserman, "Very deep convolutional networks for large-scale image recognition," 2014, https://arxiv.org/abs/1409.1556.

WILEY | Hindawi

Research Article

Cooperative Scheme ToA-RSSI and Variable Anchor Positions for Sensors Localization in 2D Environments

Monji Zaidi,[1,2] **Imen Bouazzi,**[2,3] **Mohammed Usman,**[1]
Mohammed Zubair Mohammed Shamim,[1] **Ninni Singh** [ID],[4] **and Vinit Kumar Gunjan** [ID][4,5]

[1]*Department of Electrical Engineering, College of Engineering, King Khalid University, Abha, Saudi Arabia*
[2]*Electronic and Microelectronic Laboratory, Monastir University, Monastir, Tunisia*
[3]*Department of Industrial Engineering, College of Engineering, King Khalid University, Abha, Saudi Arabia*
[4]*Department of Computer Science and Engineering, CMR Institute of Technology, Hyderabad 501401, Telangana, India*
[5]*University of Science and Technology Chattogram, Chittagong, Bangladesh*

Correspondence should be addressed to Vinit Kumar Gunjan; vinit.gunjan@ustc.ac.bd

To rich good accuracy in the 2D area for wireless sensor network (WSN) nodes, a localization method has to be selected. The objective of this paper is first to select which localization technique is required (Received Signal Strength Indicator (RSSI)) or (Time of Arrival (ToA)) against anchors placement in a 2D area. Depending on whether the anchor nodes are spaced or not and inspired by the idea of using the RSSI method for small distances and the ToA method for greater distances, we will show which method should be used for the positioning process which mainly guarantees a minimal localization error. Second, a two-dimensional localization scheme for WSN which is called Combined Advantages of ToA-RSSI (CA ToA-RSSI), hereafter, ranging methods, is designed in this work, to make the accuracy better during the positioning process. Results provided through MATLAB simulations show that our new technique improves considerably the positioning accuracy compared with the traditional RSSI and ToA ranging method. The proposed scheme can be run under Line of Sight and (LOS) and Nonline of Sight (NLOS) conditions taking into account a difference in the measurement error.

1. Introduction

The current development of Micro- and Electromechanical Systems (MEMS) and computational technologies has caused the emergence of wireless sensor networks, which can be made up [1] of hundreds of thousands of nodes. Each node is able to listen to the environment, perform simple calculations, and communicate with its neighboring sensors. To deploy sensor networks, it is important to disperse the nodes in the positions of interest. This makes the network topology optimal. These networks are widely used for multitasking [2].

The majority of applications using wireless sensor networks rely on the large number of microsensors which are placed randomly; this requires fine position computation, i.e., to calculate their positions in a system with fixed coordinate. As a result, location algorithms become more than essential, not only for the functioning of the network but also to better exploit the collected data. Some sensor nodes know their own positions; these nodes are called anchors. All other nodes are located using the location references received from these anchors.

Technically, the location algorithm is the most important part of the location system. It defines the way in which the available information (distances, angles, positions of already located nodes) is manipulated so that most or all of the nodes can estimate their positions.

From the point of view of researchers' interest, much attention has been given to the location accuracy in sensor networks and to the computational efforts. The importance of the smart deployment of reference nodes is often known but rarely discussed in a study. From another side view, the

choice of the positioning method with respect to the topology of the reference nodes remains a very little discussed subject in the previous research work.

In this work, we will start first by showing the right choice to use RSSI or ToA with respect to the anchor nodes' locations. Secondly, by combining the advantage of standards RSSI and ToA ranging methods, a new scheme which is called (CA ToA-RSSI) is designed and discussed in terms of location accuracy and compared with standards RSSI and ToA techniques.

The remaining parts of this paper are organized as follows. Related works will be discussed in Section 2. The third section discusses the suitable choice (RSSI or ToA) depending on the topology of the anchors in the 2D area. RSSI and ToA error positions taking into account the topology of the anchors are shown in Section 4. The design and evaluation of a new scheme which is called CA ToA-RSSI will be detailed in Section 5. Finally, the conclusion of this work will be presented in Section 6.

2. Related Work

In the current literature, most of the positioning methods for sensor networks can be classified into two categories, as discussed in [3–6]. The most remarkable difference between these two categories is that the first category handles the physical behaviors of the arrival signal to calculate the 2D distance which separates two sensor nodes, while the second estimates nodes' locations solely on the basis of the network connectivity information.

In the range-based techniques, RSSI [7], ToA [8], (TDoA) [9], and angle of arrival (AoA) [10] are the main frequently exploited methods. However, the localization process still suffers from many weaknesses in real scenario cases. In this context, we can cite as an example that the RSSI determination of distances is strongly linked to the existing disturbances, signals interactions, and frequently switching of wireless channels, which gives rise to the incredible measurement.

ToA localization method is often affected, in indoor environments, giving rise to multipath effects, and needs the use of exact time synchronization between communicating devices, making it unsuitable for employment in high disturbance networks.

Many works have been accomplished in theoretical analysis and laboratory testing in recent years [3, 4] having the fight against noise and dynamic variations in communication channels as objectives.

Concerning the range-free positioning techniques, they have low-cost characteristics and can be implemented on hardware targets [11, 12].

In DV-Hop [13], as being a range-free technique, to estimate distances to anchors, the algorithm determines the Average Jump Progress (AJP) for each sensor node and anchor to finally deal with the multiplication of hop counts by the AJP. In an almost identical way, LAEP [14] is based on statistics to calculate the Network Expected Jump Progress (NEJP). To calculate approximately the distances and anchors to the sensor, LAEP multiplies hop counts by the

recorded EHP. This can be done under the condition that the nodes in the network obey the Poisson law, which made LAEP difficult to reach accuracy localization.

Received Signal Strength Indicator (RSSI) technology [15] can be considered a vital solution for estimating distances in sensor networks. It considers the power losses of a signal between its transmission and reception sensors as the main key to predict point-to-point distance. This loss varies depending on the distance between the two sensors; the further the sensors are (resp. Close), the greater the loss (resp. Low). This loss will then be translated into a distance.

Since they are simple and of low cost, many positioning techniques already available in the published works use RSSI to approximate the sensor coordinates [16]. To mention, but not limited to, in [17], the input signal strength to the sensor node is almost employed to determine losses due to propagation and estimate the range between two sensors using an empirical or conceptual equation of path loss [18].

Generally, the RSSI ranging method does not use complementary components and can be integrated on wireless devices with few resources since they do not need either a back and forth timing process or exact synchronization between sensors. RSSI process is challenging, and the major ambiguity lies in determining the signal level.

The precision of localization-based RSSI depends principally on how a wireless channel-based RSS model can translate reliably the real noise inferred from the fundamental signal. The RSSI schemes proposed in the existing literature generally consider that the received signal is proportionate to the direct path between the communicating sensors and that the errors caused by the fluctuations of the RSSI values follow a Gaussian distribution. However, in real cases, measurements using wireless sensors prove that the assumptions mentioned above do not reflect reality [16, 19, 20].

As aforementioned, four standard techniques are used, such as RSS, ToA, AoA, and TDoA [21–23]. Nevertheless, determining the node location is not an obvious process, for the reason that the measurements have nonlinear correspondence with the source location. From the clock synchronization side of view, the four ranging techniques have rigorous demands. Therefore, positioning an unknown sensor node is a significant challenge. In addition, these schemes cannot provide high localization accuracy. In order to conduct better the positioning system, a few combined ranging methods and some deviation negligence techniques have been proposed in [24–27].

Recently, several combined schemes that merge two types of positioning methods have been proposed. To mention, but not limited to, the idea in [28] merged RSS and AOA techniques. The paper [29] studied the node positioning problem in combined and noncombined three-dimension WSN, respectively. From the cooperative WSN side of view, it was evident to assemble RSS propagation channel modeling with its geometry relationship. Ho et al. [28] and Sun and Ho [30] proposed a combined TDOA-FDOA node localization scheme in three-dimension positioning scenarios. A simple TDOA-AOA has been proposed in [31] with two targets. The study in [31] was carried out by making

a novel geometric source position-sensor relationship, which is very simple to be conducted.

ToA (Time of Arrival) technology considers that the sensors of the network are synchronous. The distance separating two sensors is deduced from the difference between the times when the message is sent and received and the signal propagation speed. This technology is used by the GPS system (Global Positioning System) [32].

Often, authors choose the placement of anchors at random positions and discuss the network topologies based on their own empirical data. In [33, 34], the authors chose anchors in their studies randomly within the network. However, in [33], the authors mentioned that they chose a collinear set of anchor nodes in one of the examples, without supporting evidence as to why this is not a random choice.

Previous work [35] requires that reference nodes should be located ideally at the corners of the network. In this configuration, the proposal is facing a problem with a simple and single constraint and still requires that all unknown sensors should be located in the convex envelope of the anchor points, and accordingly, better positioning results are obtained when the anchors are in the corners.

In January 2011, a study [36] was done on the impact of anchor sensor coordinates, emphasizing a series of hypotheses presented. Each assumption centers on a metric that can be calculated from the anchor nodes themselves, where network designers might have other data before deploying the network or analyzing the location results.

The authors in [37, 38] proposed their localization algorithm based on RSSI data, which used the received power at the node from the reference anchor resulting in the position estimation of the unknown sensor node. In [39], the authors proposed a target positioning technique by using both ToA and RSSI input signals in the case of NLOS conditions. In the same context, the sensors' positions already calculated can be used to determine the sensors' location not yet determined, thus minimizing the number of anchors needed by the localization process [40]. To better reduce the localization error, we will propose in this present work the suitability (localization method/anchors topology) which will somehow provide a positive gain in terms of the exact position.

In this work, the localization problem of multiple sensors' nodes is considered. To improve the positioning process, a new combined ToA-RSSI positioning scheme is proposed. Firstly, we will show the importance of the proper placement of anchors nodes in improving the localization accuracy for unknown sensor nodes (USNs). Thereby, the advantage and disadvantage of ToA and RSSI will be well exposed. Secondly, a two-dimensional localization scheme for WSN which is called Combined Advantages of ToA-RSSI (CA ToA-RSSI) ranging methods will be proposed, to better improve the accuracy during the positioning process. Results provided through MATLAB simulations show that our proposed algorithm improves considerably the positioning accuracy compared with the traditional RSSI and ToA ranging method.

3. RSSI and ToA against Working Environment

3.1. Position Estimation from RSSI Measurements.
In the literature, the most used model using RSSI is based on log-normal shadowing [41–46].

$$RSS\,(dBm) = P_0 - 10n\log\left(\frac{d}{d_0}\right) + X_\sigma, \tag{1}$$

where

(i) P_0 is the received power on the receiver antenna (dBm)

(ii) d_0 is a reference distance from the transmitter (m)

(iii) n is the path loss factor that characterizes the working environment (without unit)

(iv) d is the actual distance separating two sensors antenna (m)

(v) X_σ is a Gaussian centered random variable with variance σ_{RSS}^2, which also depends on the working environment (without unit)

For IEEE 802.15.4 standard, σ_{RSS} can vary between 0.5 dB and 6 dB [47, 48] while n varies in the range [1.9, 4.75] depending on the working environment [47–52].

As a general rule, short ranges and/or visibility situations (resp. long ranges and nonvisibility) naturally give the lowest (resp. strong) values for σ_{RSS} and n. For example, in the IEEE 802.15.4 standard, if the distance between sensors is less than 8 m (resp. greater than 8 m), it gives rise to $n = 2$ (resp. $n = 3.3$). An evolution of this basic model, which takes into account the NLOS conditions, has already been proposed in [53, 54]. Other experimental parameters were also found in [55–59].

3.2. Position Estimation from ToA Measurements.
Another widely used metric for location techniques is Time of Arrival (ToA). Literally, this metric would correspond to the Time of Arrival of the transmitted signal, defined according to the receiver's local clock and relative to its own observation window. Measuring the Time of Arrival (round trip), which is more directly linked to the distance between two asynchronous devices, would require exchanging several consecutive packets at the protocol level (n-way ranging) and making an estimation of ToA for each of these packages. In the ToA technique, the distance between sensors and their required time of flight are linked by the following equation:

$$D = c \times t\left(c = 3 \times 10^8 \frac{m}{s}\right). \tag{2}$$

The IEEE 802.15.4 standard proposes the Symmetric Double-Sided Two-Way Sending (SDS-TWS) scheme for the ToA localization process [60] as depicted in Figure 1.

In the positioning scheme, the Time of Arrival technique requires the nodes of the source and the destination to transmit signals at the same time. This requirement makes the ToA process considerably restricted in practical scenarios. The IEEE 802.15.4 standard proposes the Symmetric Double-Sided Two-Way Sending (SDS-TWS) scheme for the
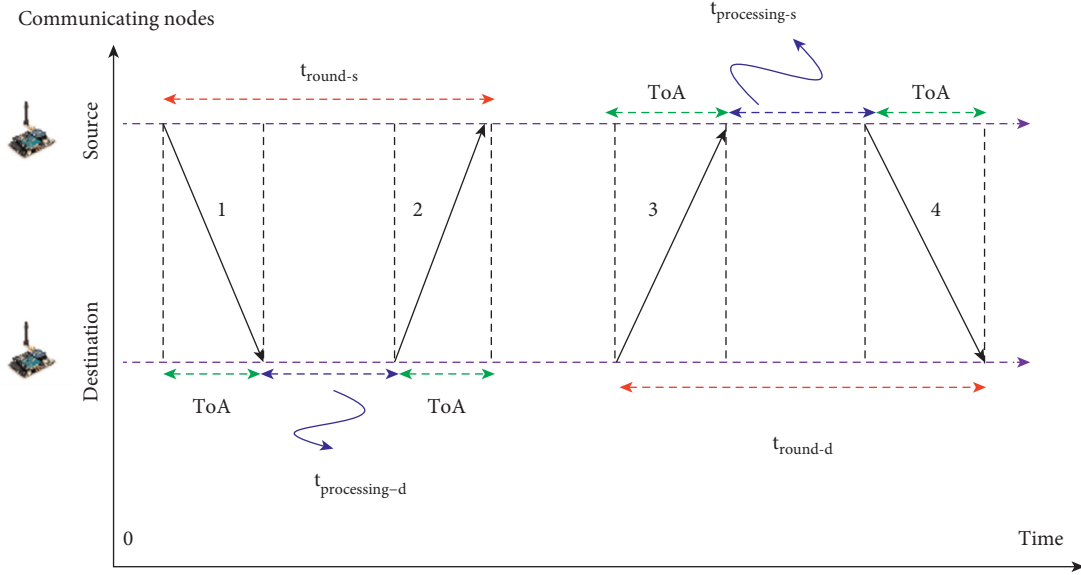
Figure 1: ToA measurement between two nodes.

ToA localization process [60]. This can offset the effect of the lag time due to the incapability to meet time synchronization on the ranging results. The SDS-TWS technique makes use of symmetrical sending and receiving to determine ToA in two ways. The specific design process is as follows. (1) In the first TWR, the source serves as a transmitter and the destination serves as a signal receiver. (2) In the second TWR, destination serves as a transmitter and source serves as a receiver. This process of sending and receiving messages can be shown in Figure 1. Thereby, a Time of Arrival (ToA), that is, the considered time measurement output can be formulated as follows:

$$ToA = \frac{t_{round-source} - t_{processing-destination} + t_{round-destination} - t_{processing-ssource}}{4}. \tag{3}$$

3.3. Ranging Accuracy versus Distance between Anchors. Based on [61], it has been concluded that the signal loss, when using the RSSI technique, varies strongly due to different parameters in various environments. When operating within a short distance, the transmission and reception of the signal essentially obey log-normal law already integrated into the design of RSSI hardware, and in that condition, the precision is then high. If the unknown sensor is at a certain distance from the reference node (anchor), the received power across the signal decreases quickly, and the positioning error will step up. On the other hand, and based on [62], it has been proven that the ToA process always needs a very precise time synchronization during the transmission/reception cycles and an offset occurs in the small distance communication, which will automatically generate a nonnegligible deviation in the sensor positioning steps. Nevertheless, when the measurement occurs at a considerable distance, it has a small error.

Starting from standard methods (ToA and RSSI), excluding their disadvantages, and keeping only their advantages, an extended algorithm will take place. In this new algorithm, RSSI and ToA algorithms will be executed alternately. To develop this algorithm, an average distance between the anchor and unknown sensors (Threshold Distance: TD) is to be fixed rigorously, and then, the extended localization process is mainly based on this new parameter TD. Roughly speaking, if the actual distance is less (res greater) than TD, then RSSI (res ToA) will be activated and vice versa.

The Distance Threshold which causes the switch from one ringing to another is determined by several simulations and it was approximately fixed to $L/2 = 10/2 = 10$ m. L is the length of the sensor network area. More than fifty simulations were done to determine the threshold distance. Results show that beyond $L/2$ RSSI is more efficient in terms of accuracy and that ToA is recommended for distances above $L/2$. The design of the new scheme which is called CA ToA-RSSI is shown in Figure 2. USN in this figure means unknown sensor node.

Four anchors in a workspace of 20 m $\times 20$ m will be the main key of this proposal, and a two-dimensional positioning process for blind nodes is then designed, which
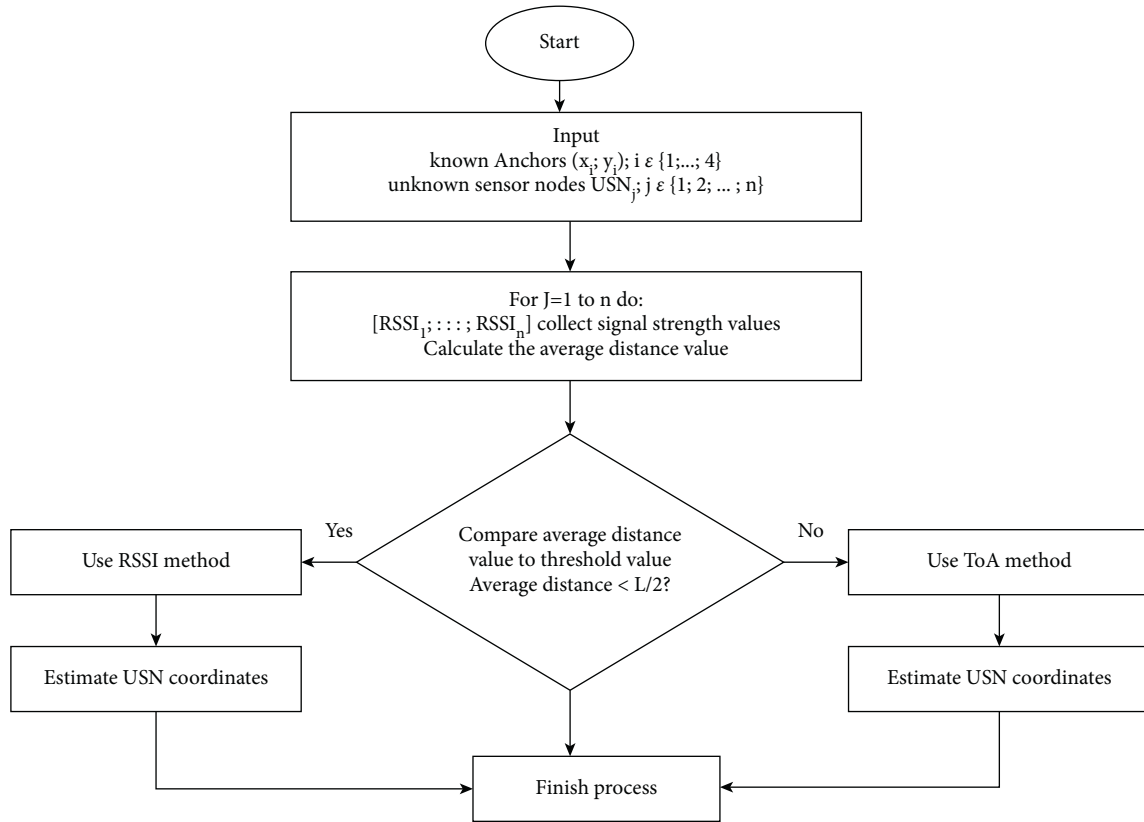
FIGURE 2: Proposed CA ToA-RSSI for coordinates estimation.

merges RSSI and ToA advantage points. The implementation phases are as follows.

3.3.1. Data Input

(i) A workspace of $20\,m \times 20\,m$ will be covered by hundred unknown sensors randomly placed

(ii) Four anchor nodes will be placed for each scenario at known positions

(iii) It is supposed that all communicating sensors have the same radius (R) of communication

3.3.2. RSSI Method

(i) Standard RSSI is executed to compute the actual distance of the required sensor from each Anchor, and (1) is used to obtain the attenuation value of the received signal

(ii) In the WSN workspace, if the actual distance between the reference node and the unknown sensor is below the Threshold Distance ($L/2$), the distance value is taken into account

3.3.3. ToA Method

(i) Standard ToA is executed to compute the actual distance of the required sensor from each Anchor extracted by (2)

(ii) In the WSN workspace, if the actual distance between the reference node and the unknown sensor is above the Threshold Distance ($L/2$) and less than R, then the actual distance value is taken into account

3.3.4. Coordinates Computations

(i) At the node localization phase and regardless of the distance calculation method (ToA or RSSI), the wireless sensor node can estimate its coordinates by the RSSI or ToA technique according to the actual distance already calculate

(ii) Finally, CA ToA-RSSI ranging method will provide the unknown sensor node coordinates much better than ToA or RSSI alone

4. Simulation and Analysis

To perform our simulations, we used MATLAB software. A choice motivated by the fact that localization can be seen as a purely geometric problem.

$20\,m \times 20\,m$ is considered a simulation scene. At the beginning of the process, 100 sensors are deployed in a two-dimensional workspace so as to cover the entire surface without knowing their coordinates.

A rectangular surface formed by the four anchors varies over the global area, thus giving rise to four scenarios as shown in Figures 3–6. The communication radius R between every two sensors is fixed to 2.5 m. The speed of light is
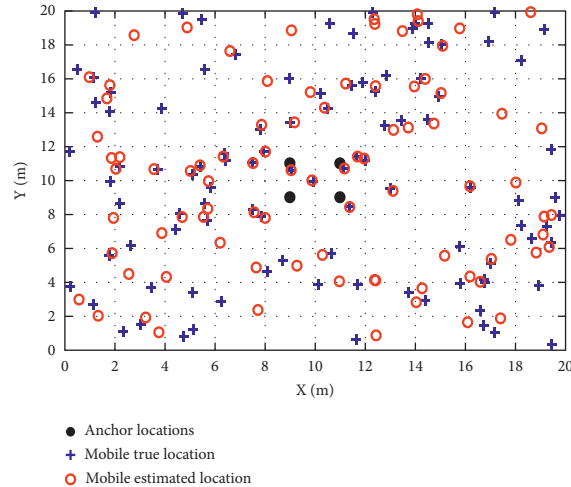
FIGURE 3: A: Locations estimation with anchors positions at (9, 9), (11, 9), (11, 11), and (9, 11).
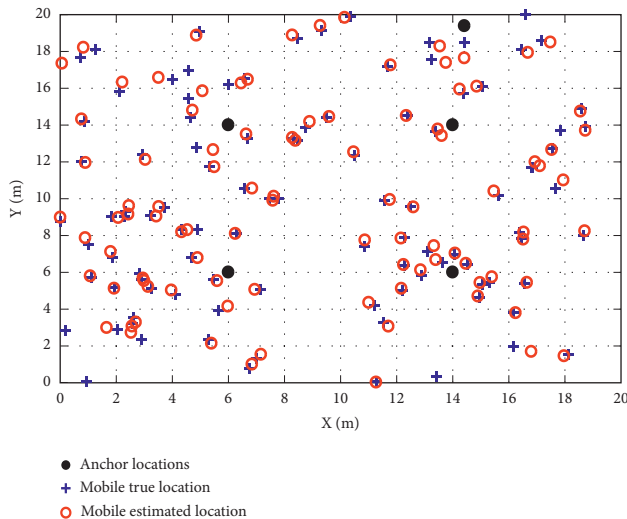

FIGURE 4: B: Locations estimation with anchors positions at (6, 6), (14, 6), (14, 14), and (6, 14).

known and is to be set to 3×10^8 m/s. The received power P_0 on the receiver antenna in this simulation is fixed to −30.

The path loss factor (n) is 1, and the Gaussian centered random variable X_σ is 2. Figure 7 shows the deployment of the unknown sensor nodes and the four anchors inside the simulation area.

All simulations' outputs are approved on 50 executions time, and then, the mean output value of all experimental tests is considered as the final result.

Simulation results allowed deducing that the metric "Area of anchors' nodes" can be a good indicator of the quality of the localization process. Based on the anchors' node location, the choice of the location (RSSI or ToA) can be retained. In total, four tests were carried out for each of the two measurements ranging (RSSI and ToA) at different anchors locations in order to find out how anchors' positions would affect the positioning error. In each simulation, the coordinates of all nodes were recorded along with the measured RSSI and ToA outputs. Table 1 gives the global

network error for each test. We note that the results provided in Table 1 are depending on the simulation parameters such as the number of nodes, number of anchors, and network size. However, anchor positioning relative to such sensors' deployment remains the general idea provided in this paper.

Standard RSSI and ToA results shown in Table 1 are provided according to the WSN two-dimensional space of 20 m × 20 m. When using RSSI ranging alone, the minimum mean location error (3.76 m) is reached at the anchors' coordinates (6, 6), (14, 6), (14, 14), and (6, 14) which correspond to Figure 4. The mean location error increases at the anchors' coordinates (9, 9), (11, 9), (11, 11), and (9, 11) which correspond to Figure 3. However, when using ToA ranging alone, minimum and maximum mean location errors abstain at anchor locations (0, 0), (20, 0), (20, 20), (0, 20), and (6, 6), (14, 6), (14, 14), and (6, 14), respectively which correspond to the Figures 3 and 4. From the existing literature point of view, the results shown in Table 1 are well matching with [61, 62].

The same scenarios (A, B, C, and D) shown in Figures 3–6 were simulated according to standard RSSI, standard ToA, and even the proposed CA ToA-RSSI.

Figure 8 shows the mean positioning errors of the three methods (standards and proposed) under the four scenarios of anchor node locations. It is approved, from Figure 8, that when using CA ToA-RSSI, a minimum error is always guaranteed. On the other hand, it is also shown that in each scenario a large localization error is generated by either standard ToA or standard RSSI. In A and D scenarios, standard ToA can estimate the coordinates of the unknown sensor node with a small error compared to standard RSSI. Opposite results are provided in scenarios B and C. However, in all scenarios, CA ToA-RSSI can estimate the coordinates of an unknown sensor node introducing the smallest error compared with standard ranging methods.

Table 2 summarizes all data and results relative to different scenarios.

Table 2 shows the overall errors obtained by each technique, namely, RSSI, ToA, and the proposed technique
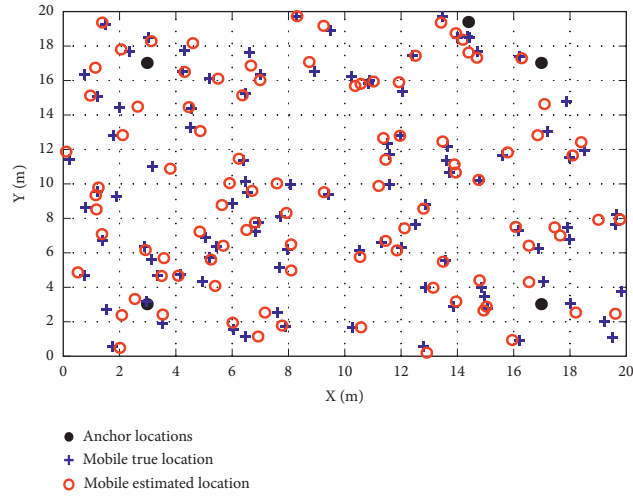
FIGURE 5: C: Locations estimation with anchors positions at (3, 3), (17, 3), (17, 17), and (3, 17).
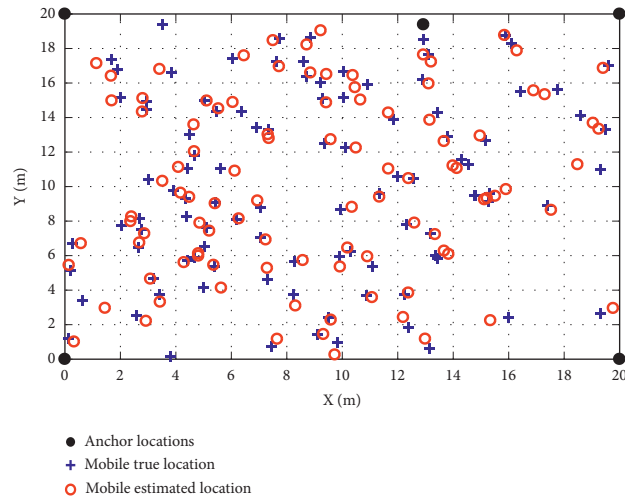

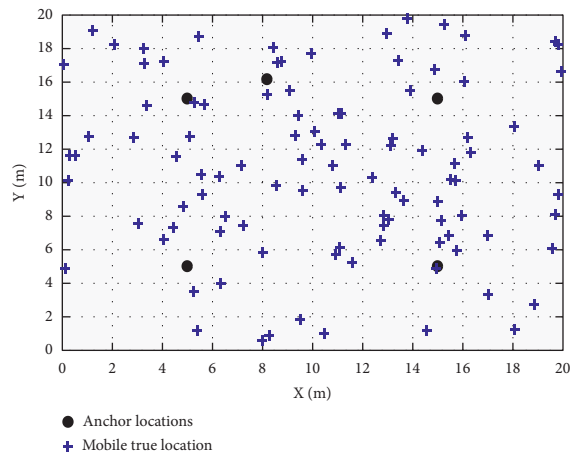FIGURE 6: D: Locations estimation with anchors positions at (0, 0), (20, 0), (20, 20), and (0, 20).

FIGURE 7: Unknown sensor nodes and anchors deployment in 20*20 m area.

TABLE 1: Basic RSSI and ToA mean error relative to anchors location.

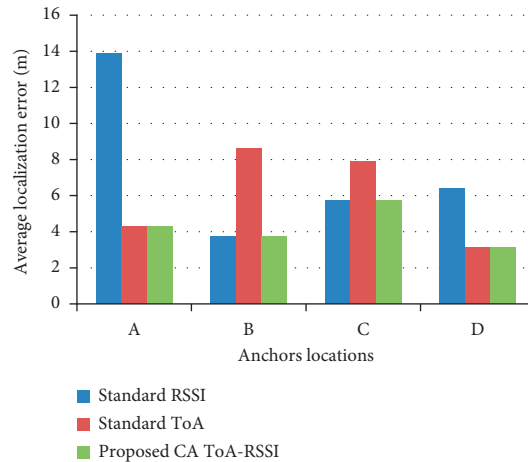| Anchors coordinates (m)	Deployed sensor nodes	Mean localization error using standard RSSI	Mean localization error using standard ToA
A: (9, 9), (11, 9), (11, 11), (9, 11)	100	13.91	4.31
B: (6 ,6), (14, 6), (14, 14), (6, 14)	100	3.76	8.62
C: (3, 3), (17, 3), (17, 17), (3, 17)	100	5.72	7.92
D: (0, 0), (20, 0), (20, 20), (0, 20)	100	6.41	3.13

FIGURE 8: Average localization error versus different ranging methods.

TABLE 2: Mean error and gain of proposed scheme versus standards ranging methods.

	RSSI	ToA	Proposed	Proposed versus RSSI gain (%)	Proposed versus ToA gain (%)
Scenario A mean error (m)	13.91	4.31	4.31	69.01	0
Scenario B mean error (m)	3.76	8.62	3.76	0	56.38
Scenario C mean error (m)	5.72	7.92	5.72	0	27.77
Scenario D mean error (m)	6.41	3.13	3.13	51.17	0
Mean of means error (m)	7.45	5.99	4.23	43.22	29.38

(CA-ToA-RSSI). If we take, for example, the first line of this table (the same principle for the other lines), RSSI, ToA, and the proposed technique (CA-ToA-RSSI) provide mean errors of 13.91 m, 4.31 m, and 4.31 m, respectively. Thereby, the percentage gain of the proposed technique (CA-ToA-RSSI) with respect to RSSI is calculated as follows.

Percentage gain = (13.91 − 4.31/13.91)× 100% = 69.01%. All other percentages are obtained in the same way. From the global side of view and by taking the average of mean errors of the four scenarios, it is clearly shown that the new extended scheme provides the highest accuracy against standard ranging methods. It can allow a significant gain of 43.22% and 29.38% compared with standard RSSI and ToA, respectively.

5. Conclusion

First, the right positioning of anchor nodes is the key to precise localization. Depending on whether the anchor nodes are spaced or not, the localization method can be selected. If the totalities of the unknown sensor nodes are far from the reference nodes (anchors), the positioning error steps up when using the RSSI ranging method; therefore, the positions of the anchors must be modified until we reach the minimum error. On the other hand, it has been proven that the ToA process provides a small error in the opposite scenarios.

Second, a new scheme is proposed that merges the advantages of RSSI and ToA techniques in this paper. The new solution drops the average location errors through the employment of the RSSI or ToA phase. To better optimize the positioning precision, four anchor nodes at different locations are introduced. The results provided by simulations are successful in producing desired objectives of the cooperative CA ToA-RSSI method and provided a better localization process. The proposed scheme can allow a significant gain of 43.22% and 29.38% compared with standard RSSI and ToA, respectively.

In our future works, we are ready to develop and design other cooperative techniques like ToA-TDoA and RSSI-

TDoA taking from their geometric advantages, thus achieving simple and effective techniques suitable for wireless nodes with limited resources.

Data Availability

Data sharing is not applicable to this article as no datasets were generated or analyzed during the current study.

Conflicts of Interest

The authors declare that they have no conflicts of interest.

Acknowledgments

References

[1] S. Tanvir, *Thèse docteur d'udg en informatique*, Université De Grenoble, Saint-Martin-d'Hères, France, 2010.

[2] B. D. H. Liu, L. Zhang, L. Duan, and G. Huang, "S-mrl distributed localization algorithm for wireless sensor networks," in *Proceedings of the 4th International Conference on Wireless Communications, Networking and Mobile Computing*, pp. 1–4, Alian, China, October 2008.

[3] X. Liu, J. Yin, S. Zhang, B. Ding, S. Guo, and K. Wang, "Rangebased localization for sparse 3-D sensor networks," *IEEE Internet of Things Journal*, vol. 6, no. 1, pp. 753–764, 2019.

[4] S. Han, Z. Gong, W. Meng, C. Li, D. Zhang, and W. Tang, "Automatic precision control positioning for wireless sensor network," *IEEE Sensors Journal*, vol. 16, no. 7, pp. 2140–2150, 2016.

[5] S. Phoemphon, C. So-In, and N. Leelathakul, "Fuzzy weighted centroid localization with virtual node approximation in wireless sensor networks," *IEEE Internet of Things Journal*, vol. 5, no. 6, pp. 4728–4752, 2018.

[6] S. Zaidi, A. El Assaf, S. Affes, and N. Kandil, "Accurate rangefree localization in multi-hop wireless sensor networks," *IEEE Transactions on Communications*, vol. 64, no. 9, pp. 3886–3900, 2016.

[7] L. Chen, K. Yang, and X. Wang, "Robust cooperative Wi-Fi fingerprintbased indoor localization," *IEEE Internet of Things Journal*, vol. 3, no. 6, pp. 1406–1417, 2016.

[8] N. Patwari, J. N. Ash, S. Kyperountas, A. O. Hero, R. L. Moses, and N. S. Correal, "Locating the nodes: cooperative localization in wireless sensor networks," *IEEE Signal Processing Magazine*, vol. 22, no. 4, pp. 54–69, 2005.

[9] S. Misra, G. Xue, and A. Shrivastava, "Robust localization in wireless sensor networks through the revocation of malicious anchors," in *Proceedings of the in IEEE Int. Conf. Commun*, pp. 3057–3062, Glasgow, U.K, June 2007.

[10] Y. Wang and K. C. Ho, "Unified near-field and far-field localization for AOA and hybrid AOA-TDOA positionings," *IEEE Transactions on Wireless Communications*, vol. 17, no. 2, pp. 1242–1254, 2018.

[11] T. He, C. Huang, B. M. Blum, J. A. Stankovic, and T. Abdelzaher, "Range-free localization schemes for large scale sensor networks," in *Proceedings of the 9th Annu. Int. Conf. Mobile Comput*, pp. 81–95, San Diego, CA, USA, Septmber 2003.

[12] A. El Assaf, S. Zaidi, S. Affes, and N. Kandil, "Robust ANNs-based WSN localization in the presence of anisotropic signal attenuation," *IEEE Wireless Commun, Lett.* vol. 5, no. 5, pp. 504–507, 2016.

[13] D. Niculescu and B. Nath, "Ad hoc positioning system (APS)," in *Proceedings of the IEEE Global Telecommun. Conf*, pp. 2926–2931, San Antonio, TX, USA, November 2001.

[14] Y. Wang, X. Wang, D. Wang, and D. P. Agrawal, "Range-free localization using expected hop progress in wireless sensor networks," *IEEE Transactions on Parallel and Distributed Systems*, vol. 20, no. 10, pp. 1540–1552, Oct. 2009.

[15] P. Bahl and V. N. Padmanabhan, "RADAR: an in-building rf based user location and tracking system," in *Proceedings of the IEEE INFOCOM*, Tel Aviv, Israel, March 2000.

[16] P. Pivato, L. Palopoli, and D. Petri, "Accuracy of RSS-based centroid localization algorithms in an indoor environment," *IEEE Transactions on Instrumentation and Measurement*, vol. 60, no. 10, pp. 3451–3460, Oct. 2011.

[17] P. Bahl and V. N. Padmanabhan, "RADAR: an in-building RF-based user location and tracking system," in *Proceedings of the 19th Annu. Joint Conf. IEEE Comput. Commun. Societies*, vol. 2, pp. 775–784, Tel Aviv, Israel, March 2000.

[18] O. G. Adewumi, K. Djouani, and A. M. Kurien, "RSSI based indoor and outdoor distance estimation for localization in WSN," in *Proceedings of the in 2013 IEEE International Conference on Industrial Technology (ICIT)*, pp. 1534–1539, Cape Town, South Africa, February 2013.

[19] G. Zhou, T. He, S. Krishnamurthy, and J. A. Stankovic, "Models and solutions for radio irregularity in wireless sensor networks," *ACM Transactions on Sensor Networks*, vol. 2, no. 2, pp. 221–262, 2006.

[20] Q. Jiang, Y. Ma, K. Liu, and Z. Dou, "A probabilistic radio map construction scheme for crowdsourcing-based fingerprinting localization," *IEEE Sensors Journal*, vol. 16, no. 10, pp. 3764–3774, 2016.

[21] Y. I. Wu, H. Wang, and X. Zheng, "WSN localization using RSS in three dimensional space—a geometric method with closed-form solution," *IEEE Sensors Journal*, vol. 16, no. 11, pp. 4397–4404, 2016.

[22] W. Wei, X. Jin-Yu, and Z. Zhong-Liang, "A new NLOS error mitigation algorithm in location estimation," *IEEE Transactions on Vehicular Technology*, vol. 54, no. 6, pp. 2048–2053, 2005.

[23] H. Xiong, S. Wang, S. Gong, M. Peng, J. Shi, and J. Tang, "Improved synchronisation algorithm based on reconstructed correlation function for BOC modulation in satellite navigation and positioning system," *IET Communications*, vol. 12, no. 6, pp. 743–750, 2018.

[24] A. Bahillo, S. Mazuelas, R. M. Lorenzo et al., "Hybrid RSS-RTT localization scheme for indoor wireless networks," *EURASIP Journal on Applied Signal Processing*, vol. 2010, no. 1, pp. 126082–126112, 2010.

[25] M. R. Gholami, S. Gezici, and E. G. Strom, "Improved position estimation using hybrid TW-TOA and TDOA in cooperative networks," *IEEE Transactions on Signal Processing*, vol. 60, no. 7, pp. 3770–3785, 2012.

[26] Y. Xie, Y. Wang, P. Zhu, and X. You, "Grid-search-based hybrid TOA/AOA location techniques for NLOS environments," *IEEE Communications Letters*, vol. 13, no. 4, pp. 254–256, 2009.

[27] L. Xu, Z. Li, and X. Li, "A hybrid approach using multistage collaborative calibration for wireless sensor network

localization in 3D environments," *IEEE Access*, vol. 8, pp. 130205–130223, 2020.

[28] K. C. Ho, X. Lu, and L. Kovavisaruch, "Source localization using TDOA and FDOA measurements in the presence of receiver location errors: analysis and solution," *IEEE Transactions on Signal Processing*, vol. 55, no. 2, pp. 684–696, 2007.

[29] S. Tomic, M. Beko, and R. Dinis, "3-D target localization in wireless sensor networks using RSS and AoA measurements," *IEEE Transactions on Vehicular Technology*, vol. 66, no. 4, pp. 3197–3210, 2017.

[30] M. D. Ansari, V. K. Gunjan, and E. Rashid, "On security and data integrity framework for cloud computing using tamper-proofing," in *ICCCE 2020*, pp. 1419–1427, Springer, Berlin, Germany, 2021.

[31] J. Yin, Q. Wan, S. Yang, and K. C. Ho, "A simple and accurate TDOA-AOA localization method using two stations," *IEEE Signal Processing Letters*, vol. 23, no. 1, pp. 144–148, 2016.

[32] B. Parkinson et al., *Global Positionning System: Theory and Application*, Vol. 1, American Institute of Astronomics and Aeronotics, Washington, DC, USA, 1996.

[33] Y. Shang, W. Rumi, Y. Zhang, and M. Fromherz, "Localization from connectivity in sensor networks," *IEEE Transactions on Parallel and Distributed Systems*, vol. 15, no. 11, pp. 961–974, 2004.

[34] G. SuryaNarayana, K. Kolli, M. D. Ansari, and V. K. Gunjan, "A traditional analysis for efficient data mining with integrated association mining into regression techniques," in *Proceedings of the ICCCE 2020*, pp. 1393–1404, Springer, Berlin, Germany, 2021.

[35] L. Doherty, K. S. J. Pister, and L. El Ghaoui, "Convex position estimation in wireless sensor networks," in *Proceedings of the IEEE INFOCOM*, pp. 1655–1663, Anchorage, AK, USA, Apirl 2001.

[36] B. Tatham and T. Kunz, "Anchor node placement for localization in wireless sensor networks," in *Proceedings of the Ottawa-Carleton Institute for Electrical and Computer Engineering*, Shanghai, China, November 2011.

[37] K. Langendoen and N. Reijers, "Distributed localization in wireless sensor networks: a quantitative comparison," *Computer Networks*, vol. 43, no. 4, pp. 499–518, 2003.

[38] Y. Zhao, J. Xu, and J. Jiang, "RSSI based localization with mobile anchor for wireless sensor networks," in *Proceedings of the in 2017 International Conference on Geo-Spatial Knowledge and Intelligence*, pp. 176–187, Chiang Mai, -ailand, Chiang Mai, Thailand, June 2018.

[39] E. Rashid, M. D. Ansari, V. K. Gunjan, and M. Khan, "Enhancement in teaching quality methodology by predicting attendance using machine learning technique," in *Modern Approaches in Machine Learning and Cognitive Science: A Walkthrough*, pp. 227–235, Springer, Berlin, Germany, 2020.

[40] P. Singh, A. Khosla, A. Kumar, and M. Khosla, "Computational intelligence based localization of moving target nodes using single anchor node in wireless sensor networks," *Telecommunication Systems*, vol. 69, no. 3, pp. 397–411, 2018.

[41] H. Cho, M. Kang, J. Park, B. Park, and H. Kim, "Performance analysis of location estimation algorithm in zigbee networks using received signal strength," in *Proceedings of the 21st International Conference on Advanced Information Networkinmg and Applications Workshops (AINAW'07)*, Falls, ON, Canada, May 2007.

[42] D. Lymberopoulos, Q. Lindsey, and A. Savvides, "An empirical characterisation of radio signal strength variability in 3-D IEEE 802.15.4 network using monopole antennas," *Lecture Notes in Computer Science*, vol. 3868, 2006.

[43] F. Bouchereau and D. Brady, "Bound on range-solution degradation using RSSI measurements," in *Proceedings of the IEEE International Conference*, Paris, France, June 2004.

[44] F. Shaik, A. Kumar Sharma, S. Musthak Ahmed, V. Kumar Gunjan, and C. Naik, "An improved model for analysis of diabetic retinopathy related imagery," *Indian Journal of Science and Technology*, vol. 9, p. 44, 2016.

[45] N. Patwari, A. O. Hero, M. Perkins, N. S. Correal, and R. J. O'Dea, "Relative location estimation in wireless sensor networks," *IEEE Transactions on Signal Processing*, vol. 51, no. 8, pp. 2137–2148, 2003.

[46] W. Chen and X. Meng, "A cooperative localization scheme for zigbee based wireless sensor networks," in *Proceedings of the 14th IEEE International Conference*, Singapore, September 2006.

[47] V. K. Gunjan, P. S. Prasad, and S. Mukherjee, "Biometric template protection scheme-cancelable biometrics," in *Proceedings of the ICCCE 2019*, pp. 405–411, Springer, Berlin, Germany, 2020.

[48] C. Singh and N. J. Ahuja, "Bug model based intelligent recommender system with exclusive curriculum sequencing for learner-centric tutoring," *I*, vol. 14, no. 4, pp. 1–25, 2019.

[49] IEEE Std 802.15.4a-2007, *PART 15.4: Wireless Medium Access Control (MAC) and Physical Layer (PHY) Specifications for Low-Rate Wireless Personal Area Networks (LRPANs)*, Standards Association, Kovaipudur, Tamil Nadu, 2006.

[50] G. J. M. Janssen and R. Prasad, "Propagation measurements in an indoor radio environment at 2.4GHz, 4.75GHz and 11.5 GHz," in *Proceedings of the IEEE VTC'92*, vol. 2, pp. 617–620, Denver, May 1992.

[51] E. Walker, H.-J. Zepernick, and T. Wysocki, "Fading measurements at 2.4GHz for the indoor radio propagation channel," in *Proceedings of the in Proc. International Zurich Seminar on Broadband Communications, Accessing, Transmission, Networking '98*, pp. 171–176, Zurich, Switzerland, February, 1998.

[52] R. Akl, D. Tummala, and X. Li, "Indoor propagation modeling at 2.4GHz for IEEE 802.11 networks," in *Proceedings of the in Proc. IASTED International Multi-Conference on Wireless and Optical Communications*, Banff, Canada, January 2006.

[53] N. Singh, A. Kumar, and N. J. Ahuja, "Implementation and evaluation of personalized intelligent tutoring system," *International Journal of Innovative Technology and Exploring Engineering*, vol. 8, no. 6C, pp. 46–55, 2019.

[54] A. J. Zargar, N. Singh, G. Rathee, and A. K. Singh, ". Image data-deduplication using the block truncation coding technique," in *Proceedings of the In 2015 International Conference on Futuristic Trends on Computational Analysis and Knowledge Management (ABLAZE)*, pp. 154–158, IEEE, Greater Noida, India, February 2015.

[55] R. Ouni, M. Zaidi, M. Alsabaan, W. Abdul, and A. Amr, "Mobile geolocation techniques for indoor environment monitoring" KSII transactions on internet and information systems," vol. 14, no. 3, 2020.

[56] Z. Monji, O. Ridha, J. Bhar, and T. Rached, "A novel positioning technique with low complexity in wireless lan: hardware implementation," in *Proceedings of the World Congress on Engineering*, London, U.K, July 2011.

[57] B. Mishra, N. Singh, and R. Singh, "Master-slave group based model for co-ordinator selection, an improvement of bully algorithm," in *Proceedings of the In 2014 International Conference on Parallel, Distributed and Grid Computin*, Solan, India, December 2014.

[58] L. Wang, M. J. Er, and S. Zhang, "A kernel extreme learning machines algorithm for node localization in wireless sensor networks," *IEEE Communications Letters*, vol. 24, no. 7, pp. 14433–1436, 2020.

[59] M. Zhou, Y. Li, Y. Wang, Q. Pu, X. Yang, and W. Nie, "Device-to-device cooperative positioning via matrix completion and anchor selection," *IEEE Internet of Things Journal*, vol. 9, no. 7, pp. 5461–5473, 2022.

[60] N. Singh, N. J. Ahuja, and A. Kumar, "A novel architecture for learner-centric curriculum sequencing in adaptive intelligent tutoring system," *Journal of Cases on Information Technology*, vol. 20, no. 3, pp. 1–20, 2018.

[61] N. Singh and N. J. Ahuja, "Empirical analysis of explicating the tacit knowledge background, challenges and experimental findings," *International Journal of Innovative Technology and Exploring Engineering*, vol. 8, no. 10, pp. 4559–4568, 2019.

[62] S. Wu, S. Zhang, and D. Huang, "A TOA-based localization algorithm with simultaneous NLOS mitigation and synchronization error elimination," *IEEE Sensors Letters*, vol. 3, no. 3, pp. 1–4, 2019.

WILEY | Hindawi

Research Article

Multiobjectives for Optimal Geographic Routing in IoT Health Care System

K. Aravind and Praveen Kumar Reddy Maddikunta [ID]

School of Information Technology and Engineering, Vellore Institute of Technology, Vellore, India

Correspondence should be addressed to Praveen Kumar Reddy Maddikunta; praveenkumarreddy@vit.ac.in

In numerous internet of things (IoT) appliances, messages might require to be distributed to certain specified nodes or objects with the multicast transmission. "The multicast routing protocol can be divided into nongeographic based and geographic based." As locations of device are roughly extracted by GPS devices, geographic-oriented multicast routing schemes were chosen, because it induces lesser overheads. Nevertheless, the extant geographic-oriented routing models are found to have particular disadvantages. After the advent of the IoT systems for remote healthcare, medical services can be rapidly provided to patients in rural areas. The IoT network encapsulates flexible sensors in the environment to collect environmental information. This gathered sensor information is sent to the nursing stations for timely medical assistance. The IoT network is wireless, which leads to security breaches. Therefore, there is a necessity to have a secured data transmission in the context of healthcare. Hence, this study intends to propose a novel optimal route selection model in IoT healthcare by deploying optimized ANFIS. Here, the optimal routes for medical data are selected using a new self-adaptive jellyfish search optimizer (SA-JSO) that is the enhanced edition of the extant JSO model. Accordingly, the optimal route selection for medical data is performed under the consideration of "energy, distance, delay, overhead, trust, quality of service (QoS), and security (high risk, low risk, and medium risk)." In the end, the performances of adopted work are compared and proved over other extant schemes.

1. Introduction

The WSNs are introduced in IoT and act a significant role to give a wider range of appliances via sensors, like environmental monitoring, smart homes, traffic supervision, and smart grids [1]. A WSN includes sinks/receivers and various distributed SNs that collaboratively gather and convey data to carry out various missions [2]. Being built on WSNs, offering consistent data deliverance is generally expected for IoT-oriented appliances. This appliance needs WSNs to offer reliable data deliverance that is considered as the crucial aspect of data transmission. Nevertheless, depending upon the diverse wireless media, WSNs are vulnerable to signal fading or interferences that might considerably reduce the QoS [3–5]. As a result, supporting consistent data deliverance turns out to be a demanding crisis in WSNs.

Recently, the IoT networks provide a lot of advantages in the medical field for providing timely assistance to patients even during the pandemic period. In healthcare, the IoT and cloud resources are wholly utilized, and hence, they are said to be the fundamental aspects of the healthcare context [6]. In between the computational resource, medical equipment, and medical data transmissions from the cloud environment to the cloud computing, the connection is supported by the standard protocols in the cloud environment. Since the cloud platform is open access, there is a huge chance for security breaches to take place. Therefore, there is a necessity to develop an efficient and secured data routing model for reliable data transmissions.

In recent times, a proficient method to meet the conditions of data reliability is deploying (opportunistic) geographic routing that does not portray the routing paths before the transmission of data [7]. In comparing over

multipath routing, geographic routing proffers enhanced performances since no further interferences or signal contentions subsist among nodes [8]. Being a conventional routing model, geographic routing was a striking option regarding the dynamic wireless link, as it does not require maintaining routes from source to sinks [9].

Thereby, the amalgamation of "opportunistic routing and geographic routing is known as geographic opportunistic routing" [10, 11]. Conventional "geographic opportunistic routing" models achieved higher reliability over wireless links. Nevertheless, they endure from DoS attacks [12]. Malevolent attackers might consciously transmit a larger count of illogical data, intending to misuse the resources and to interrupt the normal functions of the network. The IoT, smart sensors, and mobile wearable devices are assisting in the development of healthcare systems that are more pervasive, smarter, faster, and easier to use. Security, on the other hand, is a big worry for the IoT, with access control being one of the major issues. With these systems increasing scale and presence, a crucial concern is how to administer policies in a scalable and adaptable manner. Table 1 describes the abbreviations used in this study.

The major contributions of the adopted methodology are given below:

(i) An optimized ANFIS system is deployed to select the most optimal routes for data transmission in the context of healthcare.

(ii) A new self-adaptive jellyfish search model is introduced for optimizing the membership function of ANFIS.

The remaining of this study is arranged as follows: the second section reviews this topic. Section 3 tells about the system model of the developed EEG protocol. Sections 4 and 5 depict about description of multiobjective and optimized ANFIS for data routing via the SA-JSO model. In addition, Section 6 portrays about the deployed steps of the proposed EEG routing protocol. The results and conclusions are given in Sections 7 and 8.

2. Literature Review

2.1. Related Works. In 2017, Huang et al. [13] proposed an EMGR for achieving EER. EMGR employed an "energy-aware multicast tree," created by source and destination nodes depending upon the energy, for guiding multicast message deliverance. Accordingly, the nodes were adaptively selected for conserving energy. Simulated and analytic resultants demonstrated that the developed model achieved enhanced performances regarding lower complexity, energy utilization, and overhead.

In 2020, Naghibi and Hamid et al. [14] suggested a technique for dividing the network into certain cells in a geographic way and applied 2 mobile sinks for collecting the information sensed by cell nodes. Depending upon the communiqué among mobile sinks and cells, the cells were separated into 2 classes: "SCCs and MCCs." When sinks were motionless, SCCs transmit data to sinks in a direct manner; however, MCCs applied the adopted EGRPM model to transmit data to sinks.

In 2020, Hameed et al. [4] proposed an EEG routing model for focusing upon energy utilization and throughput of SNs. The adopted model applied the MSE approach to resolving the sensor localization issue. In addition, routing overhead was minimized by limiting the SN to sustain single neighbor data. The adopted model reduced the energy holes in the network by efficiently evaluating the energy utilization amid SNs.

In 2019, Lyu et al. [15] proposed a SelGOR model for defending against the DoS attack and for satisfying the needs of reliability and authenticity in WSNs. By examining SSI, SelGOR leveraged an SSI-oriented trust scheme for improving the effectiveness of data freedom. Moreover, SelGOR ensured data reliability by generating an entropy-oriented model and was capable of isolating DoS attackers and reducing the cost.

In 2021, Banyal et al. [16] have suggested a new method for segmenting the network topology depending upon the node's characteristics. This model was accomplished by means of "intelligent transmission." The HiLSeR's suggested model was deployed for packet routing. For "topology sectionalization and routing decision-making, hierarchical learning, a multidimensional data conduct-oriented soft clustering paradigm," was deployed. By performing experimentation, the efficiency of the proposed model was evaluated over other models. For demonstrating the enhanced efficiency, diverse parameters like "Energy Unit per Message, Dead node Percentage, Overhead Ratio, Average Latency, and Success Ratio" were computed.

In 2019, Thangaramya et al. [17] suggested a novel "Neuro-Fuzzy Rule-Based Cluster Formation and Routing Protocol" for proficient routing of data in IoT-oriented WSN appliances. The adopted scheme has provided considerably superior network efficiency regarding "energy consumption, packet distribution ratio, latency, and network life span," which was proved to form the outcomes.

In 2021, Pingale and Shinde [18] have suggested a novel routing scheme for optimizing network lifetime by means of the SFG model. The projected "SFG algorithm" had elected the most excellent routes by merging the SFO and GWO schemes. The simulation of IoT initially appeared, along with the execution of multipath routing in IoT. The SFG model has chosen the optimal routes among the multipath obtainable for routing depending upon "context awareness, network lifetime, residual energy, trust, and latency."

In 2019, Dhumane & Prasad [19] have adopted a "multiobjective FGSA" for electing the optimal CH in an IoT network for EER protocol. The EER in IoT was attained by exploiting FGSA to find out the finest CH. The CH node in MOFGSA was selected depending upon the fitness appraisal of numerous criteria, together with "distance, latency, connection lifetime, and energy." MATLAB execution was used to assess the simulated outcomes.

2.2. Review. Table 2 shows the review on EEG in IoT-WSN. Initially, EMGR was implemented, which provides high PDR, less overhead, and less complexity; however, wastage of resources should be concerned more. The uses of the

TABLE 1: Nomenclature.

Abbreviation	Description
ANFIS	Adaptive neuro-fuzzy inference system
DoS	Denial of service
EMGR	Energy-efficient multicast geographic routing protocol
EER	Energy-efficient routing
EEG	Energy-efficient geographic
FGSA	Fractional gravitational search algorithm
GPS	Global positioning system
GWO	Gray wolf optimizer
IoT	Internet of things
MOFGSA	Multiobjective FGSA
MCCs	Multihop communication cells
MSE	Mean square error
PDR	Packet delivery ratio
SFG	Sunflower-based GWO
SNs	Sensor nodes
SelGOR	Selective authentication-based geographic opportunistic routing
SSI	Statistic state information
SCCs	Single-hop communication cells
SA-JSO	Self-adaptive jellyfish search optimizer
SFO	Sun flower optimization
QoS	Quality of service
WSN	Wireless sensor network

TABLE 2: Review on conventional routing protocol in WSN.

Ref. no.	Proposed model	Pros	Cons
1	EMGR	(i) High PDR (ii) Minimal overhead (iii) Less complexity	(i) Wastage of resources should be concerned more
2	EGRPM	(i) Maximizes life span (ii) Minimizes delay	(i) No consideration of overhead
3	ECMSE	(i) Higher energy utilization (ii) Improved throughput (iii) Higher PDR	(i) Network interference issues are not deliberated
4	SelGOR	(i) High reliability (ii) Lower computational cost	(i) Delay performance is not good
5	HiLSeR	(i) High throughput (ii) Enhances PDR	(i) Low PDR (ii) High end-to-end delay.
6	"Neuro-Fuzzy Rule-Based Cluster Formation and Routing Protocol"	(i) Higher energy utilization (ii) Improved network life span (iii) Higher PDR	(i) High computational complexity (ii) Higher delay (iii) Higher end-to-end delay
7	SFG	(i) Reducing data overflow (ii) Lower bandwidth usage	(i) Less convergence rate
8	FGSA	(i) Increased residual energy (ii) Maximum network energy	(i) Lower count of alive nodes

EGRPM algorithm are to have a higher life span and lower delay, but the overhead is high. Furthermore, the ECMSE model was implemented, which enhanced PDR and improved throughput. However, network interference issues are not deliberated. Similarly, the use of SelGOR resulted in lower computational cost and high reliability. However, delayed performance is not good. The uses of the HiLSeR algorithm are to have higher network energy, maximum alive nodes, lower latency, and lower traffic volume, but the PDR is lower. Furthermore, in [17], an efficient distance-dependent "Neuro-Fuzzy Rule-Based Cluster Formation and Routing Protocol" was implemented, which expanded network lifetime and improved PDR. However, the delay is higher and the complexity is also high. In addition, the SFG algorithm is introduced, which has a reduced number of dead nodes, higher latency, and prolonged network life span.

In addition, the convergence rate is smaller, and the run time is longer. The FGSA algorithm is proposed, which offers increased energy performance, higher network throughput, less energy usage, and maximum network life; however, it requires "extending the EER protocols in WSNs to mobile networks."

3. System Model of Developed IoT Protocol

In 1987, the first healthcare model was developed in the Picker Institute by the Picker/Commonwealth program. This has paved the way for the development of the patient-centered care services (PCCs) that are being commonly utilized on these days. The major intention behind the PCCs is to provide medical needs to the needy. After the advent of wearable sensors, healthcare services based on IoT networks are gaining huge attention among the research industry. In the normal IoT-based data transmission, the data from the source (patient) to the destination (healthcare center) take place via the lowest hop count and the shortest distance. Even though this model ensures link quality and reliable transmission, the delay in the data transmission became an unavoidable issue. This leads to delay medical services, and hence, the network became less reliable. Moreover, the IoT being battery-powered devices required huge costs for initialization and training. On the other hand, the unauthorized or hacker IoT nodes might hack the sensitive medical data during the data transmission, and they might make modifications to it. As a result, the precise life of the patient might be jeopardized. Therefore, there is a necessary route to secure the medical data from source to destination via the IoTs.

4. Deployed Steps of Proposed Medical Data Routing Protocol: An Overview

The optimal data routing for routing the medical data amid the set of "source node(S) and destination node (D)" with minimal energy utilization is said to be a major challenge in IoT-WSN. The adopted scheme attempted to triumph over this confrontation by developing a novel EEG routing model. The process taking place in the developed work is as follows:

(i) The adopted scheme develops a novel medical data routing model depending upon sixfold objective functions (energy, distance, delay, overhead, QoS, and trust).

(ii) Throughout medical data routing, the majority of optimal routes are chosen by optimized ANFIS, wherein the membership functions are optimized.

(iii) The optimal route is selected via the SA-JSO model that considers multiobjective functions. The architecture of this work is exposed in Figure 1.

4.1. An Illustration. The architectural representation of the IoT healthcare system is manifested in Figure 2. The model encapsulates the WBANs and a broader telemedicine system. This model serves hundreds or thousands of individual users.

Let there be two COVI-19 patients *User 1 and User 2*, who have been admitted to a remote healthcare location away from the hospital. Since it is being an epidemic situation, there are not enough medical resources. Therefore, the patients *User 1 and User 2* need to be continuously monitored by the doctors. These patients are embedded with numerous body sensor nodes in the user's belt, an ankle, a knee, or the trunk for monitoring their heart rate, blood pressure, and oxygen saturation as well. Each of the nodes is capable of undergoing operations such as "sampling, processing, and communication." The coordinator (C), who has greater energy and computing power, coordinates the whole network on one individual for each user. It gathers data from sensor nodes located on or within the human body. There is no personal server, such as a PDA or a PC, in this IoT healthcare system. It has the potential to lower each user's spending. Using multiple hop routing, the gathered data of the coordinator is sent to the access gateway (AG) via other coordinators. The multihop routing protocol is utilized for safe communication between IoT devices. Before building a new network or integrating an existing one, the routing protocol allows IoT devices to authenticate. To improve the security of the communication, multilayer parameters are used for authentication. AG may be connected to a hospital server and a wired or wireless network appliance. To synchronize nodes in the network, the AG and coordinators send out periodic beacon packets. The AG also uses the internet to send the data to the medical server. If a user leaves the communication range (i.e., there is no other user nearby), the coordinator begins locally buffering data. The route link is restored when the user returns. Sensor and event data are automatically uploaded by the coordinator. The localization strategy is utilized since the users' location information is also important in the IoT healthcare system. There are a few reference nodes (RNs) in the vicinity. They are GPS enabled or preprogrammed with the location of nodes. The signal of RNs and the localization method may be used by coordinators to determine their own positions. As depicted in the projected model, the secured path for data transmission takes based on the defined sixfold objective: highest energy, lowest distance, lowest delay, lowest overhead, highest QoS, and highest trust. A prominent role is being played by these parameters during the selection of the most prominent next-hop nodes for data transmission. The optimized ANFIS model finds the majority of optimal routes, and among the available next-hop paths that satisfy the sixfold objectives (i. e., highest energy, lowest distance, lowest delay, lowest overhead, highest QoS, and highest trust), the optimal one is selected with the newly projected SA-JSO model.

The medical services can be provided when the medical professional has analyzed the patient's information. The medical server keeps track of the users' personal information and their health data. The uncomplicated ailment is diagnosed by an expert method. If the patient's condition is critical, hospital specialists can determine a diagnosis based on the patient's information. Experts from all around the
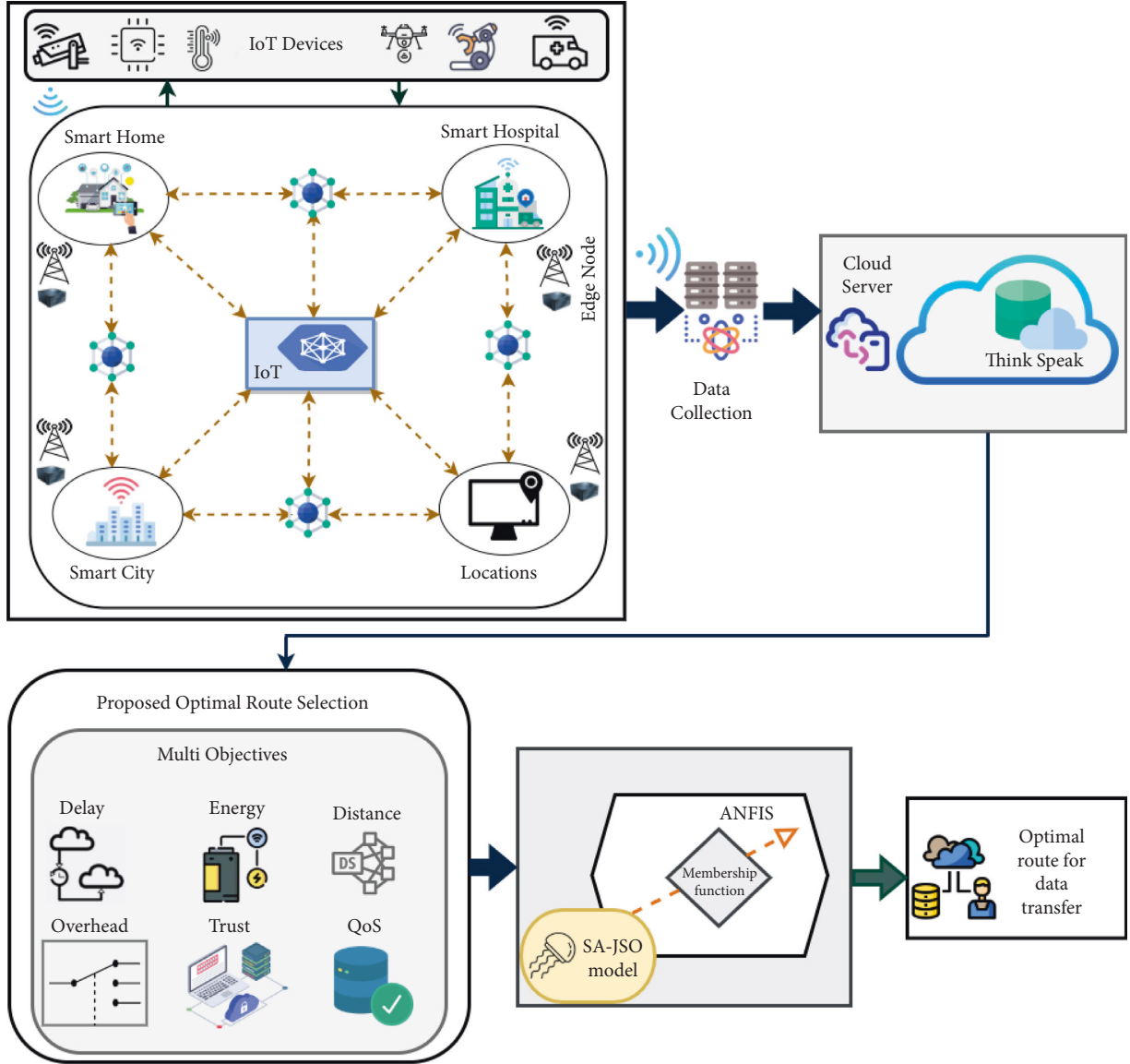
FIGURE 1: Architecture of the proposed routing model.

world can consult or collaborate over the internet. If the patient needs an ambulance in an emergency, the system can transmit the request to the nearest ambulance that is already on its way. Figure 3 shows an illustration of the communication topology of IoT healthcare systems.

5. Description of Multiobjectives

"The main objective of this study is to discover the most optimum route or path for routing the medical data that meet the specific criteria as expressed in equation (1)," wherein f^{energy}, f^{dist}, f^{delay}, f^{ohead}, f^{trust}, and f^{QoS} refer to fitness function related to energy, distance, delay, overhead, trust (direct and indirect direct), and QoS factor, respectively.

$$\text{Ob} = \min\left(\frac{1}{f^{\text{energy}}} + f^{\text{dist}} + f^{\text{delay}} + f^{\text{ohead}} + f^{\text{trust}} + f^{\text{QoS}}\right). \quad (1)$$

5.1. *Energy*. Energy is the vital factor that decides the network life span. The battery cannot be re-energized as there is no source of power. Nevertheless, transmitting data to BS requires extra energy. In equation (2), $E(\rho_l)$ signifies the energy of lth hop, and di signifies the count of hops for multihop routing.

$$\text{Energy} = \frac{1}{\text{d}i}\sum_{l=1}^{\text{d}i} E(\rho_l). \quad (2)$$

"The energy consumed during communication $E(P_l)$ is in the form of energy required for transmitting packets E_{TX}, receiving the packet E_{RX}, at idle state E_1, and energy cost E_{ST}."

$$f^{\text{energy}} = E_{\text{TX}} + E_{\text{RX}} + E_1 + E_{\text{ST}}. \quad (3)$$

The energy consumed during the packet transmission E_{TX} is mathematically shown as per equation (4).
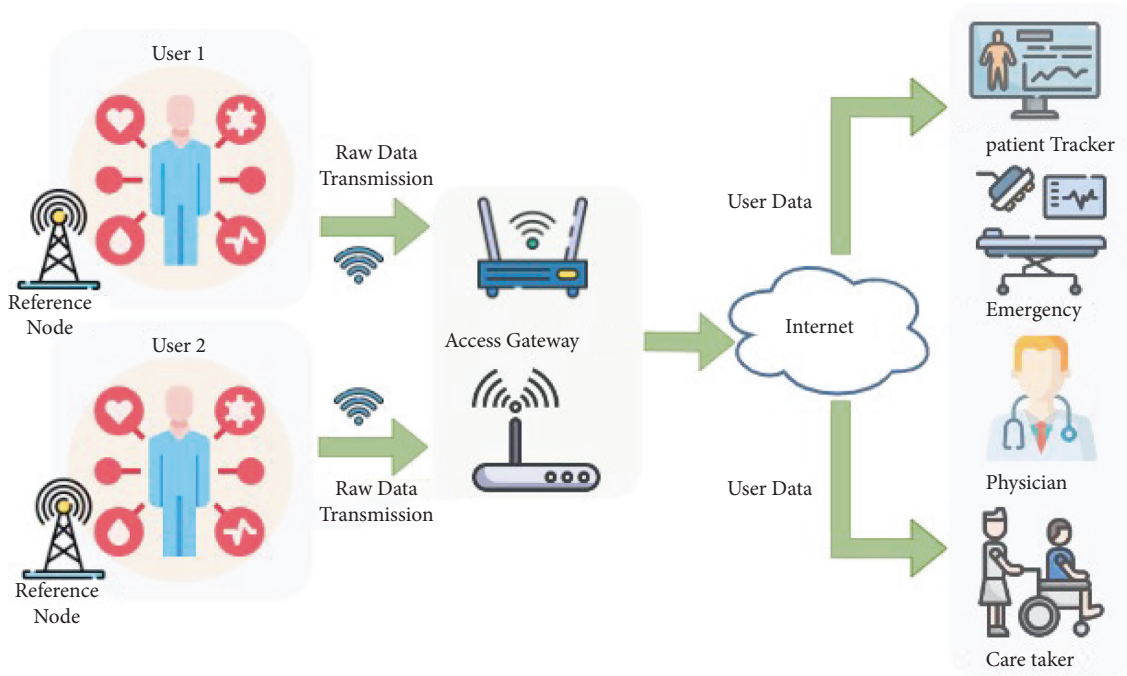
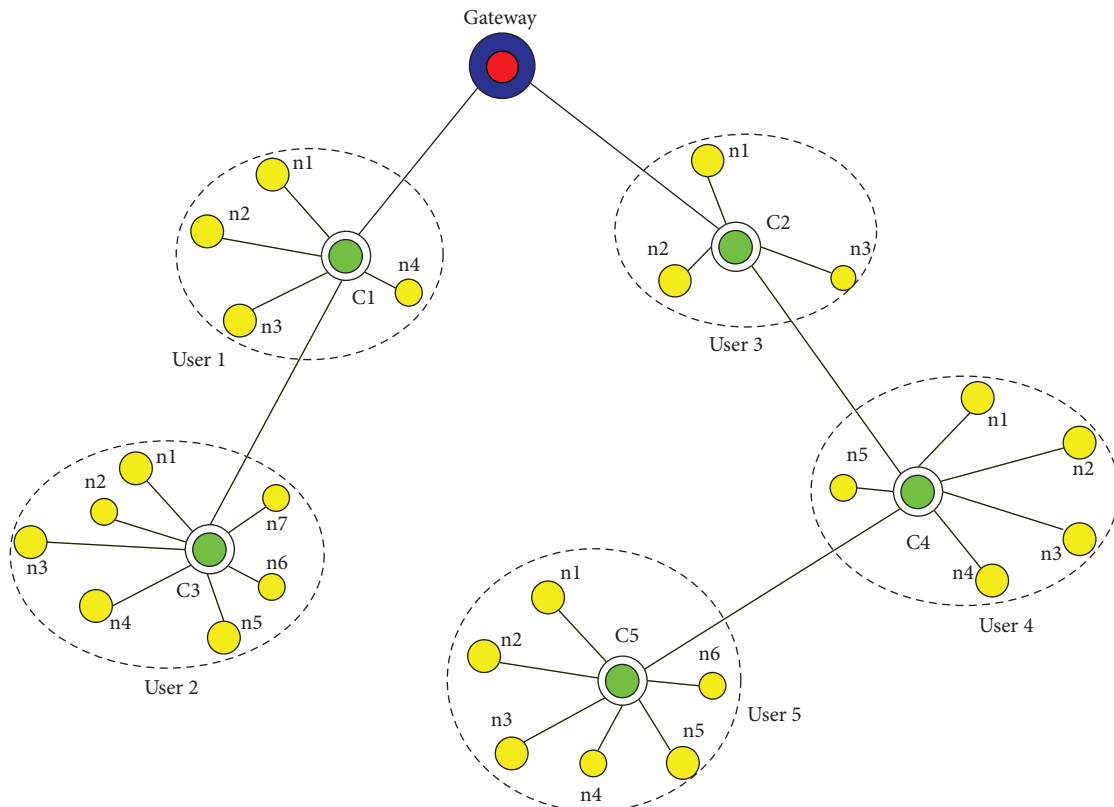Figure 2: Architecture of the IoT healthcare system: an overview.

Figure 3: The communication topology of IoT healthcare systems: an illustration.

$$E_{TX}(M: e) = \begin{cases} E_{ete} * M + E_{fr} * M * e^2, \text{if } e < e_0 \\ E_{ete} * M + E_{pr} * M * e^2, \text{if } e \geq e_0 \end{cases}. \quad (4)$$

Here, $E_{TX}(M: e)$ signifies energy necessary to convey M bytes of packets over e^{th} distance, and E_{ete} signifies electronic energy as described in equation (5)." Also, E_{agg} signifies "energy utilization during data collection." Equation (6) signifies the total energy needed for M packets at distance Di. Equation (7) signifies the threshold energy e_0.

$$E_{ete} = E_{TX} + E_{agg}. \quad (5)$$

$$E_{agg} = E_{fr}e^2. \quad (6)$$

$$e_0 = \sqrt{\frac{E_{fr}}{E_{pr}}}. \quad (7)$$

Accordingly, E_{pr} signifies y "power amplifier energy" and E_{fr} signifies energy essential to employ a free-space system.

5.2. Delay.
Delay is a significant QoS constraint for forwarding data. "It is known as the hope ratio necessary for the total number of routing nodes in the network" and is shown in equation (8), wherein d signifies the traveled distance.

$$f^{delay} = \frac{d}{speed}. \quad (8)$$

5.3. Distance.
The distance ($f^{distance}$) amid nodes is a vital factor in portraying the network's lifetime. The fitness for $f^{distance}$ is shown by equation (9), wherein v signifies node's speed and t signifies time.

$$f^{distance} = v \times t. \quad (9)$$

5.4. Trust Model.
All network hops include a higher trust degree that might be deployed for assessing the trust level among the respective nodes and hops nearby it. There are 2 types of trust model: (i) direct trust and (ii) indirect trust, which are shown in equation (9).

$$f^{trust} = \left\{ T^D + T^I \right\}. \quad (10)$$

(i) Direct trust (T^D): "The direct trust is known as local trust, and it presents the trust value as an agent to determine the familiarities with the target agent." It is formulated as in equation (12), where $B_{v_1,v_2}(t)$ correctly signifies forwarded packet count by node v_2 to v_1 at time t. In addition, $C_{v_1,v_2}(t)$ signifies packet count transferred by node v_2 from v_1 at time t.

$$T^D(t) = \frac{B_{v_1,v_2}(t)}{C_{v_1,v_2}(t)}. \quad (11)$$

(ii) Indirect trust (T^I): "It is determined from the knowledge obtained through other hops. The

knowledge of other hops helps in deciding each transaction." It is formulated as in equation (13), wherein q signifies the nearest node count.

$$T^I(t) = \frac{1}{q} \sum_{n=1}^{q} T^D(t) \quad (12)$$

5.5. QoS.
The QoS is the procedure for managing the network resources to reduce network jitter, latency, and packet loss. The fitness function related to QoS f^{QoS} is mathematically formulated as in equation (14), wherein R signifies node security.

$$f^{QoS} = \text{mean}(R). \quad (13)$$

5.6. Overhead.
In sensor networks, the reception and transmission of packets add overhead, and thus, it is essential for communication. Header length and message monitoring must be reduced, as they could raise connectivity costs. The increasing count of routing packets swapped throughout the simulation is termed as routing overhead. The fitness regarding overhead is signified by f^{ohead}.

6. Optimized ANFIS for Data Routing via SA-JSO Model

6.1. ANFIS Model.
In this work, ANFIS is deployed for optimal route selection for routing the medical data. It usually contains five layers that are described as follows.

At the initial (fuzzy) layer, the membership degrees of all linguistic variables are computed. For instance, if only 2 membership functions (MF) are there for every input X and Y, the output of fuzzy layer is attained as in equations (15) and (16), wherein μG_i and μF_i correspondingly signify membership function of X and Y.

$$U_i^1 = \mu G_i(X), \quad i = 1, 2 \ldots n. \quad (14)$$

$$U_i^1 = \mu F_i(Y), \quad i = 1, 2 \ldots n. \quad (15)$$

Second layer: Here, the "AND part in the if-then rules" is employed in the fuzzy system. "If-then fuzzy rules in ANFIS" are described below, wherein n signifies rule count, and p_i, q_i, and ra_i signify constraints, which are illustrated throughout the training phase.

"Rule I: If X is G_i and Y is F_i, then $u_i = p_iX + q_iY + ra_i$, $i = 1, 2, \ldots, n$."

The output of the second layer is attained as shown in equation (16).

$$U_i^2 = w_i = \mu G_i(X) \times \mu F_i(Y), \quad i = 1, 2, \ldots, n. \quad (16)$$

Third layer: At this layer (normalized layer), the weights computed at the prior layer are normalized by equation (17).

$$U_i^3 = \overline{w}_i = \frac{w_i}{\sum_{i=1}^{n} w_i}, \quad i = 1, 2...n. \qquad (17)$$

Fourth layer: The system output is affected by every node by multiplying its standard weight in "fuzzy if-then rules" as shown in equation (18).

$$U_i^4 = \overline{w}_i u_i = \overline{w}_i (p_i X + q_i Y + \mathrm{ra}_i), \quad i = 1, 2, \dots, n. \qquad (18)$$

Fifth layer: At last, at the 5th layer, every input signal to the layer is combined and this is said to be the output of the system as shown in equation (19).

$$U_i^5 = \sum_{i=1}^{n} \overline{w}_i u_i, \quad i = 1, 2, \dots, n. \qquad (19)$$

In this work, the membership function denoted by μ is fine-tuned using the SA-JSO model.

6.2. Proposed SA-JSO Model. In this work, the membership functions denoted by (μ) are optimally chosen via the SA-JSO scheme. Figure 4 shows the representation for membership functions of ANFIS that are given as input for optimization, wherein wn represents the entire count of membership functions.

Even though the conventional JSO [20] model contains a variety of enhancements, it suffers from specific limitations. Hence, certain modifications are needed and a new algorithm is developed. Generally, self-improvement is established to be capable in conventional optimization schemes. The steps followed in the proposed SA-JSO are as follows.

The JSO encompasses 3 rules: "(1) jellyfish either follow the ocean current or move inside the jellyfish swarm, and a mechanism called "time control" governs the switching between these types of motions. (2) Jellyfish move in the ocean to search for food. They are more attracted to positions where the quantity of available food is greater. (3) The quantity of food found is determined by the location and the objective function."

Ocean current: It includes numerous nutrients; as a result, the jellyfish are fascinated by it. The orientation of ocean current ($\overrightarrow{\mathrm{Trend}}$) is modeled as shown in equation (20), wherein L^* refers to the location of the present best jellyfish in a swarm; μ refers to the average value of every jellyfish location.

$$(\overrightarrow{\mathrm{Trend}}) = L^* - 3 \times \mathrm{ra}(0, 1) \times \mu. \qquad (20)$$

Thus, the updated location of every jellyfish is specified as in equation (21), wherein $L_i(\mathrm{it})$ refers to the location of ith jellyfish at the time it.

$$L_i(\mathrm{it} + 1) = L_i(\mathrm{it}) + \mathrm{ra}(0, 1) \times \overrightarrow{\mathrm{Trend}}. \qquad (21)$$

Jellyfish swarm: A larger group of jellyfish is known as a swarm, wherein the jellyfish travel about their own positions (passive movement, type P) or a new position (active movement, type S). While the swarm was produced, the majority of jellyfish reveal P type of motion. Based upon time, they gradually show type S movement. Type P is the movement of jellyfish around their own locations. Conventionally, the updated locality of every jellyfish is computed based upon its position; however, as per the developed SA-JSO model, the location is updated based upon pseudorandom scalar integer ($\mathrm{ra}_i([1, 2])$) as shown in equation (22). In equation (23), $L_{\mathrm{best}}(\mathrm{it})$ refers to the location of jellyfish and $\mathrm{ra}_i([1, 2])$ allows exploring the whole neighborhood of the best jellyfish, it lies among 1 and 2, and lb and ub correspondingly refer to lower and upper bound of searching space.

$$L_i(\mathrm{it} + 1) = L_{\mathrm{best}}(\mathrm{it}) + (-1)^{\mathrm{ra}_i([1,2])} \times \mathrm{ra}(0, 1) \times (\mathrm{ub} - \mathrm{lb}). \qquad (22)$$

In addition, the proposed SA-JSO model includes an adaptive convergence strategy as modeled in equation (23).

$$L_i(\mathrm{it} + 1) = L_{\mathrm{best}}(\mathrm{it}) + \mathrm{ran}^* \left(\overrightarrow{L}_{\mathrm{rand}\,1}(\mathrm{it}) - \overrightarrow{L}_{\mathrm{rand}\,2}(\mathrm{it}) \right) \\ + (1 - \mathrm{rand})^* \left(L^* - \overrightarrow{L}_{\mathrm{rand}\,3}(\mathrm{it}) \right). \qquad (23)$$

In equation (23), $\mathrm{rand}\,1$, $\mathrm{rand}\,2$, and $\mathrm{rand}\,3$ refer to the indices of 3 solutions randomly picked from the populations and ran refers to control constraint that lies among 0 and 1.

Moreover, the time control mechanism is introduced for regulating the movement of jellyfish that deploys threshold constant c_{th} and time control function $c(\mathrm{it})$. Here, $c(\mathrm{it})$ is computed as in equation (24), where $\mathrm{it}_{\mathrm{max}}$ signifies maximal iteration. Algorithm 1 explains implemented SA-JSO model.

$$c(\mathrm{it}) = \left| \left(1 - \frac{\mathrm{it}}{\mathrm{it}_{\mathrm{max}}} \right) \times (2 \times \mathrm{ra}(0, 1) - 1) \right|. \qquad (24)$$

7. Application

The principal areas of IoT applications are healthcare, the environment, smart cities, and commercial, industrial, and infrastructural fields. IoT can be defined as generating daily information from an object and transferring it to another one. Consequently, enabling communication between objects makes the range of IoT applications extensive, variable, and unlimited. Hence, the developed ANFIS + SA-JSO model can be used to find the location of nodes in prior and forward the data packets toward the destination. At the same time, the developed method can also be used in different applications with different cases as shown in Table 3.

In healthcare programs, objects collect information about patients and send it to remote nursing stations using communication networks, especially the internet. Analysis of information in nursing stations can lead to timely treatment for patients and can also prevent potential risks for patients. Given that some patients may be in critical condition, the rapid and reliable transfer of data to the nursing station can avoid death. Patient data transfer from a remote point to a clinic or hospital, integration of medical devices, and the possibility of data exchange between them improve medical experiments in providing care. It also
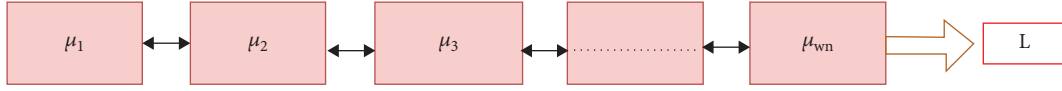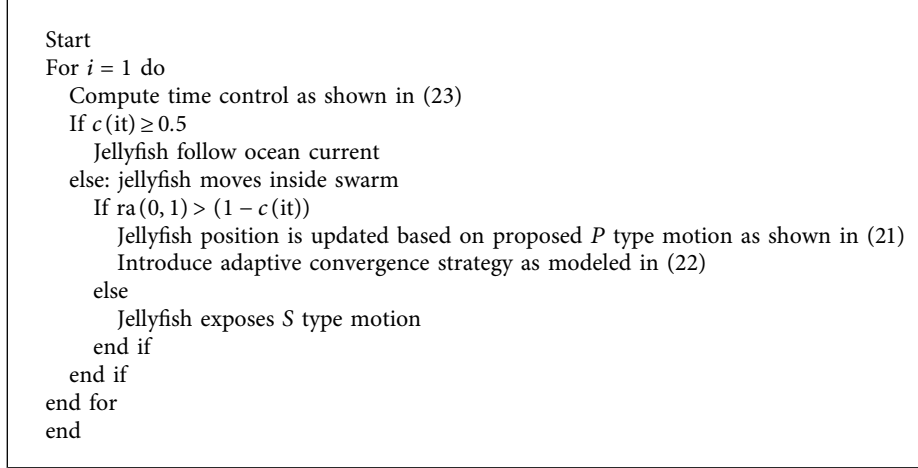
FIGURE 4: Solution encoding.

```
Start
For i = 1 do
    Compute time control as shown in (23)
    If c (it) ≥ 0.5
        Jellyfish follow ocean current
    else: jellyfish moves inside swarm
        If ra (0, 1) > (1 − c (it))
            Jellyfish position is updated based on proposed P type motion as shown in (21)
            Introduce adaptive convergence strategy as modeled in (22)
        else
            Jellyfish exposes S type motion
        end if
    end if
end for
end
```

ALGORITHM 1: Implemented SA-JSO model.

promotes interaction between physicians about the effect of the drug, management and controlling various connecting devices, the possibility of medically transmitting IoT information by physicians, accurate diagnosis of other health problems and control patterns (heart rate, temperature, blood pressure, and blood sugar levels in the body and gastrointestinal tract), the possibility of transmission, and the information used by the physician to process and perform the appropriate medical activity.

8. Results and Discussion

8.1. Simulation Procedure. The suggested EER protocol in the IoT healthcare data routing model was implemented in MATLAB. The data that support the findings of this study are openly available in the UCI repository at https://archive.ics.uci.edu/ml/datasets/heart+disease [21] reference number. "There are 76 attributes in this database, but all published studies only use a subset of 14 of them. The Cleveland database, in particular, is the only one that has been used by machine learning researchers yet. The 'goal' field indicates whether or not the patient has cardiac disease. It has an integer value ranging from 0 (no presence) to 4. Experiments with the Cleveland database have concentrated on simply attempting to distinguish presence (values 1, 2, 3, and 4) from absence (value 0)." The analysis was performed for two groups: group 1 (long-distance data transfer, i.e., end-to-end) and group 2 (short-distance data transfer (40% of distance), and the simulation parameters considered for the developed scheme are shown in Table 4. Every evaluation is performed by correspondingly setting the node counts at 100, 250, 750, and 1,000. Accordingly, an assessment of the proposed scheme was performed over the existing models such as ANFIS + MFO, [22] ANFIS + SLnO [23]ANFIS + DA

[24], ANFIS + JSO, and Fuzzy + HHO, [25] regarding "convergence analysis, fitness, life span, PDR, residual energy, and statistical evaluation."

The IoT-WSN for routing the medical data is simulated in an area of 100 m× 100 m, and the node speed is predetermined as 2 m/sec. The network is modeled in form of a "graph $G(V, E)$, with N counts of nodes denoted as $V = \{v_1, v_2, \ldots v_n\}$ and m counts of edges $E = \{e_1, e_2, \ldots .e_m\}$." The network is considered as a homogeneous one, wherein every node carries equivalent sensing area and processing power as well. During node deployment, every node is assumed to include a similar energy level. When a node is employed, they are regarded as static and then every node in the communiqué range transmits a HELLO message together with the node ID. The symmetric form of communiqué occurs amid the SNs while they are in the communiqué range R. The communiqué may be asymmetric or symmetric. For symmetric communiqué, the node v_1 arrives v_2, and v_2 arrives v_1 as well. If the distance between v_1 and v_2 is lesser than R, then they both directly converse with one another. If distance between v_1 and v_2 is superior to R, nevertheless, there are no ways for them to directly commune. The only cause following the drain of the node is its energy exhaustion.

8.2. Statistical Analysis. The statistical analysis of the implemented ANFIS + SA-JSO model over other traditional models for varied metrics is shown in Tables 5 and 6 for 2 groups. "As meta-heuristic schemes are stochastic in nature, every algorithm is executed for the number of times to attain the statistic of the objective function." The adopted ANFIS + SA-JSO model demonstrates the superior outcomes when evaluated over conventional schemes such as

TABLE 3: IoT healthcare applications.

Focus area	Applications	Device
Disease management system	IoT healthcare service providers	Independent handheld devices and smartphones
Synthesis method for e-health to ensure high availability	New structure for e-health	In connection with the patient's body

ANFIS + MFO, ANFIS + SLnO, ANFIS + DA, Fuzzy + HHO, and ANFIS + JSO models. From Table 5, the proposed ANFIS + SA-JSO model under the median case scenario attained superior values over certain distinguished schemes. In certain scenarios, the conventional schemes have exhibited better values; however, the cost function of the developed model has accomplished optimal values, and therefore, this variation can be considered negligible. Likewise, better results have been obtained by the proposed work for group 2 in specific scenarios. Thus, the improvement of the proposed NIS + SA-JSO model over the other conventional methods is proved.

8.3. Convergence Analysis. Figures 5 and 6 describe the analysis of the adopted ANFIS + SA-JSO scheme over traditional schemes such as MFO, SLnO, DA, and JSO for group 1 and group 2 scenarios. Here, analysis is performed by fixing the node counts for 4 variations such as 100, 250, 750, and 1,000, respectively. The evaluation is performed by adjusting the iterations from 0, 5, 10, 15, 20, 25, and 30 to 35, respectively. The resultants attained for group 1 by fixing node counts at 100, 250, 750, and 1,000 are shown in Figure 6. On observing the analysis outcomes, the proposed ANFIS + SA-JSO model has attained minimal values for all node counts when compared to the existing schemes. Initially, from iteration 0 to iteration 5, the cost values are found to be higher for proposed and evaluated models; however, as the iteration count increases, better outputs are attained. That is, from iteration 5 to 30, the cost values go on reducing for proposed and compared models; nevertheless, the adopted ANFIS + SA-JSO scheme exhibits least values when compared to the existing ones for both group 1 and group 2. Moreover, it can be noticed that subsequent to the proposed approach, the JSO approach has attained better outcomes than MFO, SLnO, and DA models for both group 1 and group 2. Predominantly, the adopted scheme is converged better for node count of 1,000 for group 1, i.e., the presented approach has accomplished a least-cost value (almost 0.01) since it is enhanced via the ANFIS + SA-JSO optimization theory. Thus, the overall evaluation shows the enhancement of the presented model with the optimization-assisted ANFIS technique. The optimized membership function of ANFIS has thus ensured better efficacy to attain optimal geographic routing for routing the medical data depending upon the defined multiobjectives.

8.4. Analysis of Network Life Span. The life span of the network is said to be a major aspect of WSN that is directly accountable for increasing the network's endurance. The lifetime extension of the network is the most important

TABLE 4: Simulation parameters.

Channel type	Wireless
Antenna	Omni antenna
Dimension X	100 m
Dimension Y	100 m
Total simulation time	10 s
Number of nodes	50, 100, 150, 200

confront of the WSN. The majority of the existing works have established novel schemes to prevail over this confront; however, they did not offer much satisfactory outputs. Thereby, this work focused on achieving the best routing network with lower energy utilization, and this is clear from the obtained outcomes as exposed in Figure 7. In considering group 1, the network life span is highly amplified for all variations in the node count. Particularly, at node variations of 500 and 800, the suggested model has attained a higher life span of the network (around 3), whereas at node variations of 100 and 1,000, the suggested model has attained a network life span with the value of 2 for group 1. At node count = 200, the life span of the ANFIS + SA-JSO is much better than ANFIS + MFO, ANFIS + SLnO, ANFIS + DA, and ANFIS + JSO, respectively. Therefore, the ANFIS + SA-JSO model is definitely the first rate for EEG routing, since it has achieved the chief goal of lifetime growth.

8.5. Analysis of Fitness. The resultants acquired regarding fitness for group 1 and group 2 scenarios are revealed in Figure 8. As per equation (1), the fitness (considering energy, distance, delay, overhead, and trust (direct and indirect direct and QoS factor)) of the developed model should be minimal, thereby ensuring better data transmission. Here, on noticing the resultants, the developed ANFIS + SA-JSO has accomplished minimal fitness for all node variations for both group1 and group 2 scenarios. On examining the resultants from group 1, when the count of nodes = 100, the ANFIS + SA-JSO has accomplished the optimal fitness value around 0, whereas, at other node variations, the ANFIS + SA-JSO model has accomplished relatively higher values of 10, 10, and 10 in that order.

Likewise, on observing the resultants from group 2, when the count of nodes = 100, the ANFIS + SA-JSO has acquired the optimal fitness value around 0, while, at other node variations, the ANFIS + SA-JSO model has acquired comparatively higher values of 10, 10, and 15 in that order. Also, for group 2, the developed model has achieved the least value of 15 at node variation of 200, whereas the existing models such as ANFIS + SLnO, ANFIS + DA, ANFIS + JSO, and ANFIS + MFO, and Fuzzy + HHO have acquired relatively higher values of 700, 700, 700, 100, and 50 in that

TABLE 5: Statistical analysis for adopted model over existing models for group 1 scenario.

Measures	ANFIS + SLnO	ANFIS + DA	ANFIS + JS	ANFIS + MFO	Fuzzy + HHO [38]	ANFIS + SA-JSO
Median	11.028	44.033	11.028	5.2934	25.672	5.2934
Worst	1988.4	2295.5	440.46	1049.9	94.783	61.553
Best	546.34	728.29	146.71	286.01	53.193	36.609
Mean	92.949	286.78	67.669	44.414	46.159	39.795
Std	963.32	1058.5	198.59	509.61	29.792	23.517

TABLE 6: Statistical analysis for adopted model over existing models for group 2 scenario.

Measures	ANFIS + SLnO	ANFIS + DA	ANFIS + JS	ANFIS + MFO	Fuzzy + HHO [38]	ANFIS + SA-JSO
Worst	3.368	77.616	3.368	3.368	20.32	3.368
Best	1882.8	1887.3	1887.3	3578.1	96.458	102.58
Median	498.51	657.48	594.06	922.35	42.099	53.468
Mean	53.965	332.49	242.76	53.965	25.809	53.965
Std	923.5	828.85	871.87	1770.9	36.378	48.128
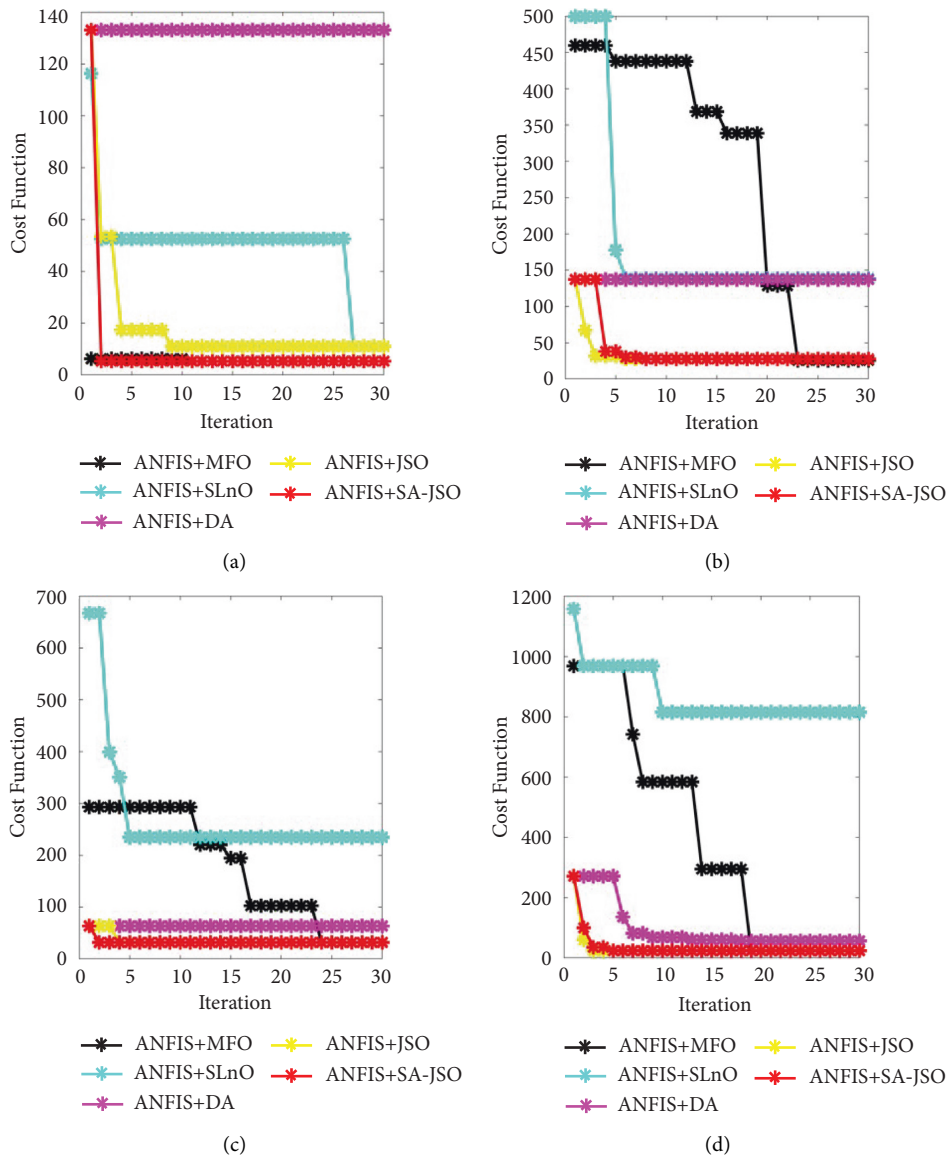
FIGURE 5: Convergence analysis of developed approach over compared approaches regarding group 1 scenario by fixing counts of nodes as (a) 100, (b) 250 (c) 750, and (d) 1,000.
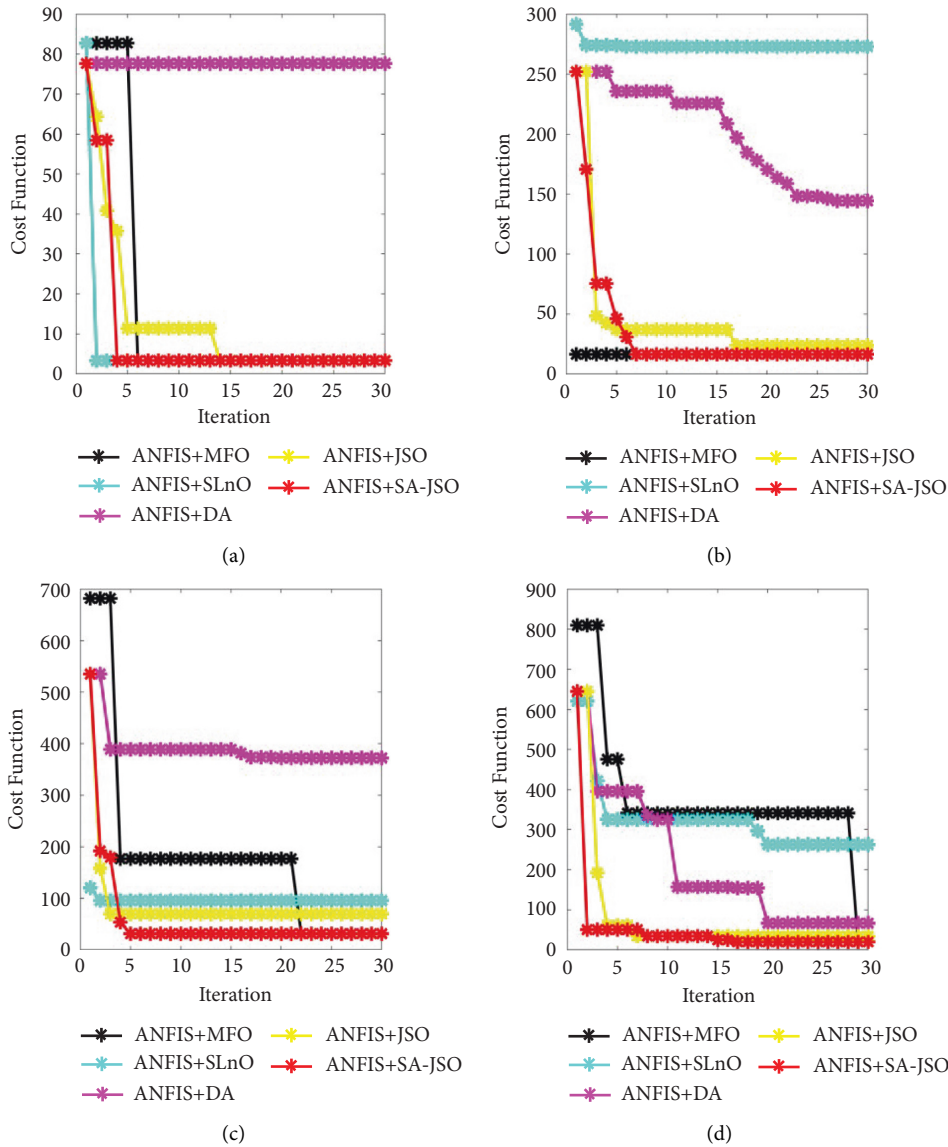
(a)

(b)

(c)

(d)

Figure 6: Convergence analysis of developed approach over compared approaches regarding group 2 scenario by fixing counts of nodes as (a) 100, (b) 250 (c) 750, and (d) 1,000.

order. Thus, the improvement of the developed model regarding fitness was established from the results.

8.6. Residual Energy.

The remaining energy left after transmitting and receiving medical data is known as residual energy. The network with high residual energy has the maximum network life span, and as a result, the reliability will be higher for data transmission. Figure 9 shows the resultants acquired for group 1 and group 2 scenarios regarding residual energy. Here, analysis is performed for varied node variations such as 100, 250, 750, and 1,000. For both group 1 and group 2 scenarios, the residual energy is found to be higher for all node variations. Moreover, the Fuzzy + HHO has acquired the nearby values as that of the developed ANFIS + SA-JSO scheme for both scenarios; however, the developed approach has acquired much superior values than the Fuzzy + HHO scheme, thus proving the supremacy of the adopted optimization-assisted ANFIS model. In particular, for the group 2 scenario, the developed approach at node count of 200 has exhibited a higher value of 98, which is better than the existing ones. Hence, from the overall assessment, it is apparent that the ANFIS + SA-JSO model had achieved the top residual energy.
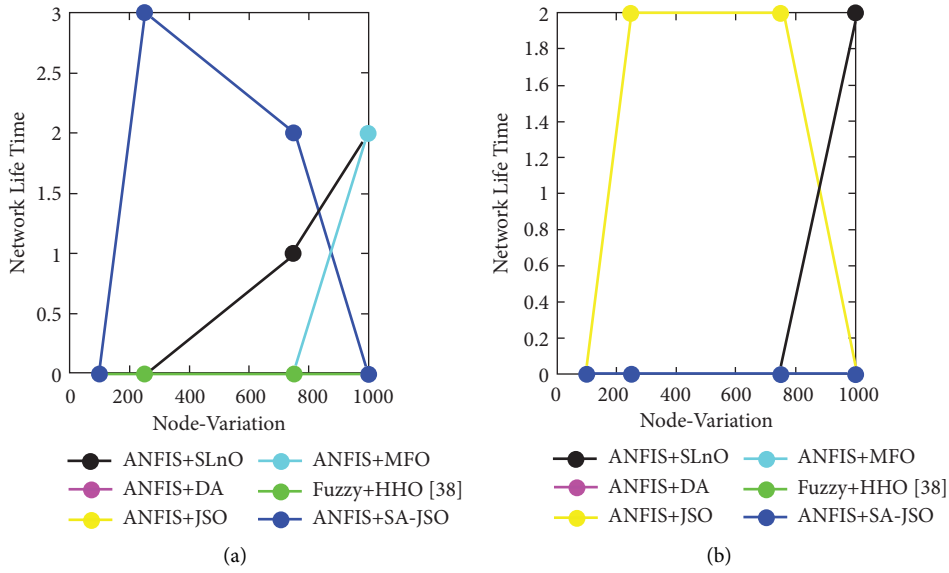
FIGURE 7: Analysis of the life span of developed approach over compared approaches regarding (a) group 1 and (b) group 2.
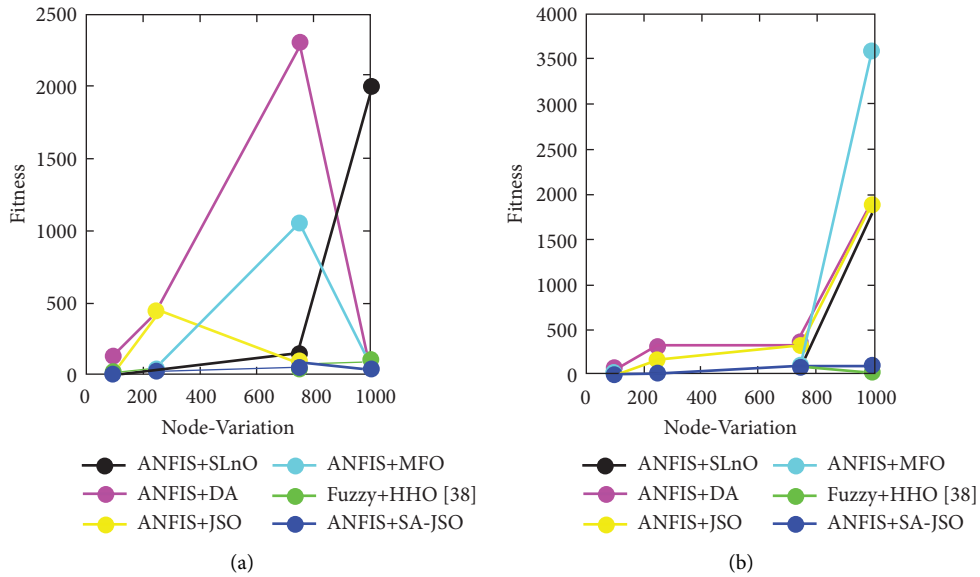

FIGURE 8: Analysis of PDR for developed approach over compared approaches regarding (a) group 1 and (b) group 2.
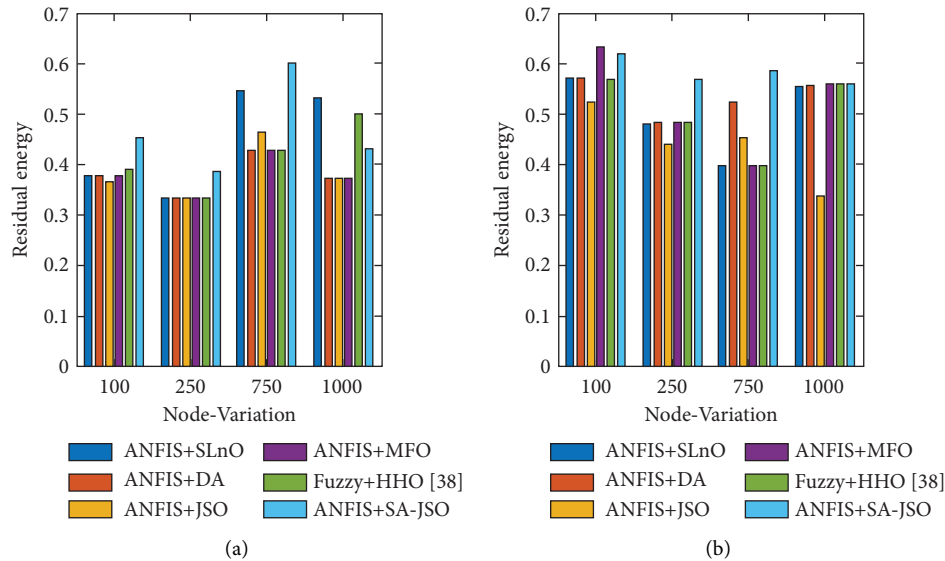
Figure 9: Analysis of residual energy for developed approach over compared approaches regarding (a) group 1 and (b) group.

9. Conclusions

A novel medical data routing protocol was developed in this research work depending upon the defined multiobjective functions. Throughout the routing, the most optimal routes were chosen by optimized ANFIS, in which the membership functions were optimized. The optimal route selection considered energy, distance, delay, overhead, QoS, and trust. Here, the ANFIS + SA-JSO model was deployed for optimization. On observing the analysis outcomes, the proposed ANFIS + SA-JSO model has attained minimal values for all node counts when compared to the existing schemes. Initially, from iteration 0 to iteration 5, the cost values were found to be higher for proposed and evaluated models; however, as the iteration count increased, better outputs were attained. That is, from iteration 5 to 30, the cost values go on reducing for proposed and compared models; nevertheless, the adopted ANFIS + SA-JSO scheme exhibited least values when compared to the existing ones for both group 1 and group 2. Also, for both group 1 and group 2 scenarios, the residual energy was found to be higher for all node variations. Moreover, the Fuzzy + HHO has acquired the nearby values as that of the developed ANFIS + SA-JSO scheme for both scenarios; however, the developed approach has acquired much superior values than the Fuzzy + HHO scheme, thus proving the supremacy of the adopted optimization-assisted ANFIS model. As a result, the adopted routing model for medical data transmission was recommended as a suitable one. In the future, this work may take into account the time parameter, and it would also be fascinating to apply our strategy to networks with heterogeneous propagation properties.

Data Availability

No data were used to support this study.

Conflicts of Interest

The authors declare that they have no conflicts of interest.

References

[1] C. Iwendi, T. R. Gadekallu, K. Lakshmanna, A. K. Bashir, and M. J. Piran, "A metaheuristic Optimization approach for energy efficiency inthe IoT networks," *Software: Practice and Experience*, vol. 51, 2020.

[2] M. Alazab, K. Lakshmanna, T. R. G, Q.-V. Pham, and P. K. Reddy Maddikunta, "Multi-objective cluster head selection using fitness averaged rider optimization algorithm for IoT networks in smart cities," *Sustainable Energy Technologies and Assessments*, vol. 43, p. 100973, Article ID 100973, 2021.

[3] S. P. R.M., P. K. R. Maddikunta, S. Koppu, T. R. Gadekallu, C. L. Chowdhary, and M. Alazab, "An effective feature engineering for DNN using hybrid PCA-GWO for intrusion detection in IoMT architecture," *Computer Communications*, vol. 160, pp. 139–149, 1 July 2020.

[4] A. R. Hameed, S. u Islam, M. Raza, and H. A. Khattak, "Towards energy and performance-aware geographic routing for IoT-enabled sensor networks," *Computers & Electrical Engineering*, vol. 85, p. 106643, Article ID 106643, 2020.

[5] L. Zhang, Z. Zhang, W. Wang, Z. Jin, Y. Su, and H. Chen, "Research on a covert communication model realized by using smart contracts in blockchain environment," *IEEE Systems Journal*, pp. 1–12, 2021.

[6] S. Maddikunta, Quoc-Viet Phamb, P. K. Reddy Maddikunta et al., "Deep learning and medical image processing for coronavirus (COVID-19) pandemic: a survey," *Sustainable Cities and Society*, vol. 65, p. 102589, Article ID 102589, 2021.

[7] K. Dev, R. K. Poluru, R. L. Kumar, P. K. R. Maddikunta, and S. A. Khowaja, "Optimal radius for enhanced lifetime in IoT using hybridization of rider and grey wolf optimization," *IEEE Transactions on Green Communications and Networking*, vol. 5, no. 2, pp. 635–644, June 2021.

[8] J. W. Lin, P. R. Chelliah, M. C. Hsu, and J. X. Hou, "Efficient fault-tolerant routing in IoT wireless sensor networks based on bipartite-flow graph modeling," *IEEE Access*, vol. 7, pp. 14022–14034, 2019.

[9] T. A. Al-Janabi and H. S. Al-Raweshidy, "A centralized routing protocol with a scheduled mobile sink-based AI for large scale I-IoT," *IEEE Sensors Journal*, vol. 18, no. 24, pp. 10248–10261, 2018.

[10] T. Mick, R. Tourani, and S. Misra, "LASeR: lightweight Authentication and secured routing for NDN IoT in smart cities," *IEEE Internet of Things Journal*, vol. 5, no. 2, pp. 755–764, April 2018.

[11] R. K. Lenka and A. K. Z. S. D. N. V. R. M. R. S. S. Rath, "Building scalable cyber-physical-social networking infrastructure using IoT and low power sensors," *IEEE Access*, vol. 6, pp. 30162–30173, 2018.

[12] Q. Zhang, M. Jiang, Z. Feng, W. Li, W. Zhang, and M. Pan, "IoT enabled UAV: network architecture and routing algorithm," *IEEE Internet of Things Journal*, vol. 6, no. 2, pp. 3727–3742, April 2019.

[13] H. Huang, J. Zhang, X. Zhang, B. Yi, F. Fan, and Q. Li, "EMGR: energy-efficient multicast geographic routing in wireless sensor networks," *Computer Networks*, vol. 129, pp. 51–63, 2017.

[14] M. Naghibi and H. Barati, "EGRPM: energy efficient geographic routing protocol based on mobile sink in wireless sensor networks," *Sustainable Computing: Informatics and Systems*, vol. 25, p. 100377, Article ID 100377, 2020.

[15] C. Lyu, X. Zhang, Z. Liu, and C. H. Chi, "Selective authentication based geographic opportunistic routing in wireless sensor networks for Internet of Things against DoS attacks," *IEEE Access*, vol. 7, pp. 31068–31082, 2019.

[16] S. Banyal, K. K. Bharadwaj, J. Joel, and P. C. Rodrigues, "HiLSeR: hierarchical learningbased sectionalised routing paradigm for pervasive communication and Resource efficiency in opportunistic IoT network," *Sustainable Computing: Informatics and Systems*, vol. 30, 2021.

[17] K. Thangaramya, K. Kulothungan, and A. Kannan, "Energy aware cluster and neuro-fuzzy based routing algorithm for wireless sensor networks in IoT," *Computer Networks*, vol. 115, 2019.

[18] R. P. P. S. N. Shinde, "Multi-objective sunflower based grey wolf optimization algorithm for multipath routing in IoT network," *Wireless Personal Communications*, 2021.

[19] A. V. Dhumane and R. S. Prasad, "Multi-objective fractional gravitational search algorithm for energy efficient routing in IoT," *Wireless Networks*, vol. 25, no. 1, pp. 399–413, 2019.

[20] J.-S. Chou and D.-N. Truong, "A nove metaheuristic optimizer inspired by behavior of jellyfish in ocean," *Applied Mathematics and Computation*, vol. 389, 2020.

[21] https://archive.ics.uci.edu/ml/datasets/heart+disease.

[22] S. Mirjalili, "Moth-flame optimization algorithm: a novel nature-inspired heuristic paradigm," *Knowledge-Based Systems*, vol. 89, pp. 228–249, November 2015.

[23] R. Masadeh, A. Sharieh, and B. Sharieh, "Sea lion optimization algorithm," *International Journal of Advanced Computer Science and Applications*, vol. 10, no. 5, pp. 388–395, 2019.

[24] M. Jafari and M. H. Bayati Chaleshtari, "Using dragonfly algorithm for optimization of orthotropic infinite plates with a quasi-triangular cut-out," *European Journal of Mechanics - A: Solids*, vol. 66, pp. 1–14, 2017.

[25] A. A. Heidari, S. Mirjalili, H. Faris, I. Aljarah, M. Mafarja, and H. Chen, "Harris hawks optimization: algorithm and applications," *Future Generation Computer Systems*, vol. 97, pp. 849–872, 2019.

WILEY | Hindawi

Research Article

Analyzing Interdisciplinary Research Using Co-Authorship Networks

Mati Ullah,[1] Abdul Shahid [ID],[1] Irfan ud Din [ID],[1] Muhammad Roman [ID],[1] Muhammad Assam,[2] Muhammad Fayaz [ID],[3] Yazeed Ghadi [ID],[4] and Hanan Aljuaid[5]

[1]*Institute of Computing, Kohat University of Science & Technology, Kohat 26000, Pakistan*
[2]*Department of Software Engineering, University of Science and Technology Bannu, Bannu, Khyber-Pakhtunkhwa, Pakistan*
[3]*Department of Computer Science, University of Central Asia, Naryn, Kyrgyzstan*
[4]*Department of Computer Science, Software Engineering, Al Ain University, Al Jimi, UAE*
[5]*Computer Sciences Department, College of Computer and Information Sciences,*
 Princess Nourah Bint Abdulrahman University (PNU), P .O. Box 84428, Riyadh 11671, Saudi Arabia

Correspondence should be addressed to Muhammad Fayaz; muhammad.fayaz@ucentralasia.org

With the advancement of scientific collaboration in the 20th century, researchers started collaborating in many research areas. Researchers and scientists no longer remain solitary individuals; instead, they collaborate to advance fundamental understandings of research topics. Various bibliometric methods are used to quantify the scientific collaboration among researchers and scientific communities. Among these different bibliometric methods, the co-authorship method is one of the most verifiable methods to quantify or analyze scientific collaboration. In this research, the initial study has been conducted to analyze interdisciplinary research (IDR) activities in the computer science domain. The ACM has classified the computer science fields. We selected the Journal of Universal Computer Science (J.UCS) for experimentation purposes. The J.UCS is the first Journal of Computer Science that addresses a complete ACM topic. Using J.UCS data, the co-authorship network of the researcher up to the 2nd level was developed. Then the co-authorship network was analyzed to find interdisciplinary among scientific communities. Additionally, the results are also visualized to comprehend the interdisciplinary among the ACM categories. A whole working web-based system has been developed, and a forced directed graph technique has been implemented to understand IDR trends in ACM categories. Finally, the IDR values between the categories are computed to quantify the collaboration trends among the ACM categories. It was found that "Artificial Intelligence" and "Information Storage and Retrieval", "Natural Language Processing and Information Storage and Retrieval", and "Human-Computer Interface" and "Database Applications" were found the most overlapping areas by acquiring an IDR score of 0.879, 0.711, and 0.663, respectively.

1. Introduction

The pattern of scientific collaboration has been increasing since the end of the 20th century [1]. Scientists are working in collaboration to address various problems, such as social, political, economic, and technological issues. The collaboration among researchers builds up a communication network where they share thoughts assets and convey new learning [2]. This scientific collaboration aids in the improvement of research findings and the expansion of research quality and variety on a particular subject [3]. On the other side, an interdisciplinary collaboration includes incorporating knowledge from multiple disciplines. Participants usually originate from diverse fields and collaborate on knowledge gained from the corresponding domains to create new knowledge. Different research support programs and science policies are increasingly paying attention toward interdisciplinary research collaboration [4].

There has been abundance of literature that addresses interdisciplinary and associated concepts. Many researchers believe interdisciplinary research positively affects information creation and creativity [5, 6]. Interdisciplinary is now

fueled by several funding instruments at the national [7], international [8], and university levels. These projects seek to enable independent researchers to collaborate to foster interdisciplinarity. Interdisciplinary research (IDR) has evolved into a wide range of brushes to demonstrate a wide range of research strategies and practices [2]. Research policies and support programs are increasingly focused on IDR, claiming that more and more research initiatives are interdisciplinary [9]. Borut et al. [10] have quantified interdisciplinarity collaboration among the country's researchers. They have used the co-authorship of researchers to quantify interdisciplinarity in research communities [10]. The co-author network is their collaboration with other researchers through their publications. Co-authors network is already used in many applications such as conflict of interest [11], knowledge diffusion [12], creating a social network of the researcher [13], and finding experts [14]. Karlovcec et al. used a graph of project collaboration and co-authorship to investigate interdisciplinarity in scientific fields and their evolution [15]. One of the essential applications of co-author networks is collaborator finding. Hence, a co-author network is an important measure used in many applications, and it is easy to compute a co-author network.

In this research, we developed, built, and deployed a co-authorship network-based solution to investigate the IDR trend in the computer science field. We developed a system to prepare and handle the J.UCS dataset, which contains over 1200 research publications published by over 2500 authors in a range of ACM categories. To study the expanding IDR patterns, we created 1st and 2nd level co-authorship networks. These trials assisted us in answering questions such as what are the most common categories of 1st-level co-authorship networks where IDR activities are carried out on a regular basis, and what are the most common categories of 2nd level co-authorship networks in which IDR activities are regularly performed? These results are discussed in detail in the Result section.

2. Related Work

Bibliometric techniques permit researchers to put together their findings concerning collected bibliographic data created by researchers working in the area and express their findings through writing, citations, and collaboration. When this information is compiled and examined, bits of knowledge into the social networks, it is possible to advance the "field's structure and topical concerns." Bibliometric techniques including bibliographic coupling cocitation analysis create underlying pictures of scientific fields using bibliographic data from publication databases. They add objectivity to the evaluation of scientific literature and can be used to differentiate between implicit research networks. For example, there are "invisible colleges" under the surface that are not formally related but having same research interests as each other. These organizations have similar scientific priorities and keep in touch through seminars, staff correspondence, and private summer schools. The "authors" judgments on the subject matter, methods, and the importance of other "authors" work are reflected in the

images cited from the study fields, which have been added over time [16].

These bibliographic methods have two main applications: results estimation and scientific visualization [17]. Performance analysis aims to evaluate the effectiveness of individual and organizational research and publication efforts. On the other hand, scientific visualization seeks to explain the nature and complexities of scientific areas. If the researcher's goal is to review a particular line of study, this insight on structure and growth may be helpful. The Bibliography method adds methodological rigor to the subjective assessment of the literature. In the review paper, they can include proof of logically derived categories.

We briefly describe the five most popular bibliographic methods in the section below. Citation analysis and cocitation analysis are the first two approaches or processes that use citation data to create measurements of effect and relations. Co-authorship data are used to assess collaboration in co-authorship research. On the other hand, the co-word study looks for links between ideas and theories that appear in document titles, keywords, or abstracts. Table 1 summarizes bibliometric methods, along with their strengths and weaknesses.

2.1. Bibliometric Methods

2.1.1. Citations. The top N list of the most cited research, author, or journal in the field of interest is typically provided by most bibliographic studies in citation analysis of research fields. Citations are used to determine the degree of impact. It is considered significant if an article is most often cited. The author references a paper relevant to his work, so this suggestion is based on that assumption. Citation review may provide information about the relative importance of publications, but it cannot understand researchers' networks [18].

2.1.2. Cocitation. Another bibliometric method, cocitation, measures how many papers are cited simultaneously in the same article. This indicator reflects the influence and impact of thematic networks and authors. However, in the final analysis, the methods of cocitation represent the responses and reactions of the scientific community to the research results. The cocitation clusters provide a complementary description of similar and related research topics and related studies measured by citations. It may also be possible to map and identify the researcher's community within a specific network. Such clusters also show how fields and subfields evolve [3].

2.1.3. Coanalysis. Co-word is a content analysis technique that builds relationships and makes the conceptual structure of the domain by using words in documents. The underlying idea behind this method is that the frequent cooccurrence of words in a document indicates a close relationship among the concepts behind words.

TABLE 1: Summary of bibliometric methods.

#	Methods	Description	Units of analysis	Strengths	Limitations
1	Citation	Citation rates evaluate the impact of documents, authors, or journals	Author document journal	Important work in the field can quickly be found	Since newer articles have little time to be referenced, citation count as a metric of impact is weighted against older publications
2	Cocitation	Connect journals, documents, and authors, based on joint presence in the reference list	Author document journal	The most widely used and validated bibliometric tool for linking authors, articles, and journals is cocitation. It is considered reliable. It filters the most important works.	Since it is conducted on cited papers, cocitation is not ideal for mapping research fronts. Since citations take time to accumulate, new publications can only be linked by knowledge base clusters. Since multiple citations are needed to map an article, it is not possible to map articles that are rarely cited.
3	Co-word	It connects keywords if they seem in a similar title, abstract, or keyword list	Word	It analyses documents based on their content. Many other methods, on the other hand, depend on metadata.	It's possible that the word will appear in multiple contexts and take on different meanings
4	Bibliographic-coupling	Connects the journals, documents, and authors based on a number of mutual references	Author document journal	.It does not need a citation to accrue. It could be used for newer publications that are not cited yet.	Can use only for a short timeframe (for the interval of five years). The most critical works are not even mentioned. Even it has trouble determining whether or not the mapped publications are relevant.
5	Co-author	When two or more authors collaborate on a document, it connects both	Author	It produces the social structure of fields and can provide an indication of collaboration	Author name disambiguation issues arise in the co-authorship network

Other methods indirectly connect the documents through coauthorships or citations, while in the case of co-word analysis, it constructs similarity measures by using the actual content of the papers. The network of themes and their relationships, which reflect the field's conceptual space, is the product of a co-word analysis. Co-word analysis may apply to entire documents, abstracts, keywords, and paper titles. However, the accuracy of the co-word analysis results depends on multiple aspects, such as the quality of keywords, the complexity of the statistical methods used for analysis, and the scope of the database used [3].

There are two possible reasons for the concern when using just the keywords for a co-word analysis. The first explanation is that often the journal's bibliographic data do not contain keywords. The second is that depending solely on keywords undergoes an indexer effect. The chart's validity depends on whether the indexer collects all the specific facets of the text. The alternative to this issue is to use entire texts or abstracts, but this indicates noise in the data as algorithms have difficulty separating the importance of terms in vast corpora of text [18].

2.1.4. Bibliographic Coupling. Bibliographic coupling is ignored, and the process is years older than cocitation [18]. Bibliographic coupling tests the compatibility between the two texts by using mutual references. Furthermore, if bibliographies overlapped in the two papers, the greater their relationship would be. Between the two articles, the number

of references remained static over time, as the number of references stayed unchanged throughout the paper. However, cocitation-based affinity grows with citation trends. When citation ways shift, bibliographical coupling works well within a short timeframe [19]. The distinction between bibliographic coupling and cocitation is that a bibliographic coupling relation is formed by the paper's authors also in focus. In contrast, a cocitation connection is established by the scholar citing the works under consideration.

When two documents are heavily cocited, it suggests that each paper is highly cited independently [20]. This demonstrates that documentation chosen based on cocitation thresholds is more valuable from the researcher's perspective when quoting them. However, since bibliographic coupling cannot be used in this manner, identifying essential documents within many documents is a difficult challenge when doing bibliographic coupling. Otherwise, the bibliographic coupling is beneficial for scientific mapping boundaries and new areas lacking citation evidence or smaller subfields where cocitation analysis cannot generate accurate relations [21, 22]. In Figure 1, the distinction between bibliographic coupling and cocitation analysis is visually depicted.

2.1.5. Co-Authorship. The co-authorship measures scientific interaction and relationships amongst networks, teams, institutions, and countries. The joint publication results from a collaboration between organizations and representatives from different countries participating in a research
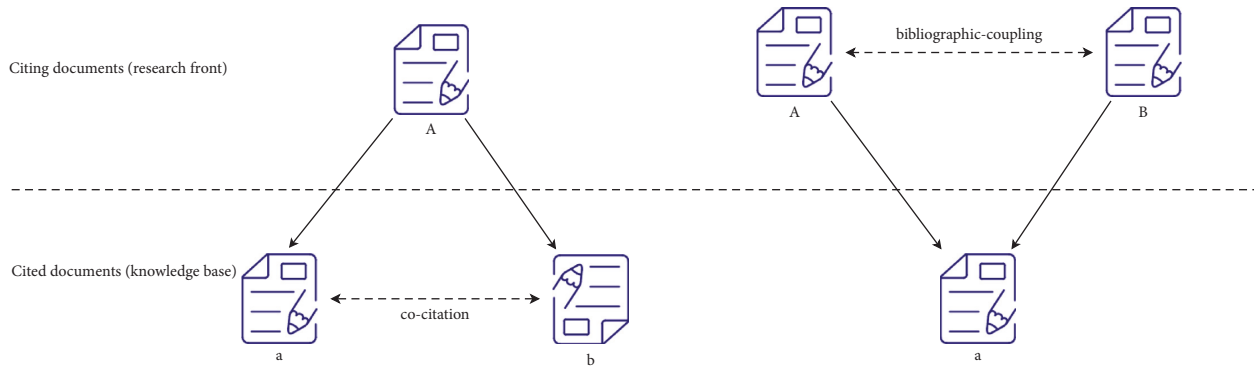
Figure 1: Bibliographic coupling and co-citation analysis.

program. Such research establishes relationships between teams (scientists, laboratories, institutes, and countries) to produce a scientific article. Co-authorship can identify, measure, and display the number of links established by individual contributors. Thus, co-authorship can be used to indicate these relationships. Following this principle, you can construct a matrix where each cell shows the number of cosignatures between the author (or authors) displayed in the rows and the author (or authors) indicated in the column. This indicator can identify key research partners and describe scientific networks descriptions [3]. Coauthorship is a credible metaphor for scientific collaboration among the various bibliometric methods discussed above. The coauthorship network has many uses, and scholars have used it in their research studies. Macro and micro features of massive co-authorship networks using SNA techniques are investigated in [23]. The dynamics and evolution of co-authorship networks were studied in [4], which followed up on "Newman's 2001 work." Since then, co-authorship networks have been widely researched in various ways in both the natural and social sciences [24].

Taskn et al. [25] analyzed co-authored astrobiology papers and also analyzed journal references. By studying topological configurations of co-authorship networks, Pavlov et al. [14] discovered essential functional knowledge characteristics of the characteristics of scientific collaboration. A systematic model of cumulative benefit in terms of preferential attachment as the guiding force of co-authorship was investigated by Barabasi and Albert [26]. They noticed a common property across several large networks: the scale-free power-law distribution is followed by the node degrees of each network. The effects of scale-free distributions have been extensively used to explain scientific co-authorship networks.

Morel et al. [27] used a graph of project collaboration and coauthorship to investigate interdisciplinary scientific fields and their evolution. Porter [28] stared into the impact of collaborative research in the academic finance literature and discovered that it could result in high-impact articles even though it was found that interdisciplinary collaborations have a higher potential for fostering research outcomes. When two authors collaborate on a study, this is known as co-authorship. It is one of the most visible and well-documented forms of scientific collaboration. By

analyzing co-authorship networks using bibliometric methods, almost every aspect of scientific collaboration networks can be reliably tracked. These networks of collaborations (co-authorship) reveal research teams, as well as factors that influence the impact or output of collaborations. According to our research requirements, we have found co-authorship network methodology to be the best and most reliable method to implement in our research methodology.

Co-authorship is among the most effective methods of scientific collaboration among the various bibliographic methods mentioned above. The co-author has many applications, and many researchers have used them in their research studies. Porter et al. [28] investigated large co-author networks' macro and micro characteristics using SNA methods. Co-author networks have since been extensively studied in various ways in both the natural and social sciences. Taskn et al. [29] reviewed journal references and co-authored publications in the field of astrobiology. By studying the topological configurations of the coauthor network, Huang et al. [30] discovered essential practical knowledge features of the research collaboration method. In co-authorship, Abramo et al. [31] established small-world systems. The accepted model of cumulative benefits in terms of preferential attachment as a guiding force for co-authorship was studied by Hennemann et al. [24]. They discovered a common property of large networks and each node degree followed a scalable power less distribution. Scientific co-author networks have been analyzed thoroughly using the results of scale-less distributions. Qin et al. [32] investigated interdisciplinary research fields and their growth using the project partnership and co-authorship graph. Figg et al. [33] studied the effects of collaborative research in academic finance and discovered that collaboration results in high-impact articles.

On the other hand, interdisciplinary collaboration has been shown to have the ability to increase research outcomes. According to the study, when two authors work on research, they are known as co-authors, having the most concrete and well-documented form of research cooperation. By analyzing co-"authors" networks using bibliometric techniques, almost any component of scientific collaboration networks can be accurately examined. These collaboration networks (co-authorship) show the impact of co-authorship, research teams, and collaboration output.

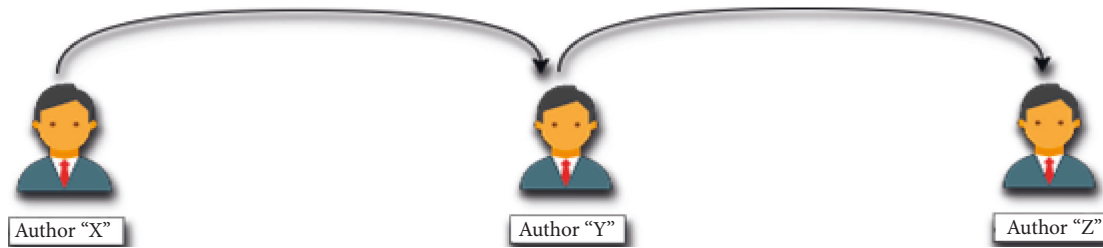Figure 2: The link of an author X with 1st-level co-author Y.

Figure 3: The link of an author X with 2nd level co-author Z.

According to our research requirements, we have concluded that the co-authorship network methodology is the best suited and most reliable method for implementing our research methodology. A co-authorship network could have various levels, as explained in the previous chapter. In our research, we have used a co-authorship network up to the second level described in the next section.

2.2. Levels of Co-Authorship Network. Co-authorship is viewed as a valid indicator for scientific collaboration in research publications. Since the 1960s, using co-authorship to assess research collaboration has been a hot topic. Research collaboration may accumulate numerous assistances for researchers to give scientific credibility from bringing different talents together [8]. One of the most concrete and well-known methods of scientific collaboration is co-authorship. Almost any component of research collaboration networks can be accurately traced by studying co-authorship networks. Co-authorship is a form of collaboration where two or more authors publish a paper, and these authors are connected to form a co-authorship network [9].

Thousands of authors can be linked together in co-authorship networks, with the best example being the "Paul Erdos" network, which has over 500 co-authors. An author who has published with Erdos has an Erdos number of 1. Those who have published with Erdos as a co-author have an Erdos number of 2, and so on in the "Paul Erdos" network [19]. However, this reveals that in a co-authorship network, there are many levels of co-authors.

2.2.1. First Level Co-Author. As previously mentioned, there are various levels of co-authors in a co-authorship network. Consider the following scenario: author X has co-authored a research paper with another author, Y, and Y is the first level co-author of X. The concept of a first-level co-author is clearly explained in Figure 2.

2.2.2. Second Level Co-Author. In the second level co-author, we can consider a scenario in which author X has published a research paper with another author Y. As explained above, author Y is at the 1st-level. However, if author Y has published a research paper with another author, Z, then author Z will be the 2nd level co-author of X. Figure 3 clarifies the current second-level co-author scenario.

Due to the advantages and availability of bibliometric data, co-authorship measures interdisciplinary, as co-authorship is commonly used as a metaphor for collaboration in science.

3. Proposed Methodology

The suggested approach is discussed in this section. Figure 4 illustrates the architecture of the current methodology. It consists of several steps, such as dataset selection of research articles, extraction of research publications, and formation of co-authorship networks that will be analyzed to quantify interdisciplinary scientific communities. However, the section is divided into subsections in detail for further clarification.

3.1. ACM Classification. The Association for Computing Machinery (ACM) is the world's largest computing society, putting together experts, scholars, and educators to exchange expertise, promote debate, and solve the field's challenges. ACM has over 100,000 participants all over the world. ACM provides opportunities for career development and professional networking to support the professional growth of its members. The ACM classification scheme is polyhierarchical, containing the list of topics available from topic A to topic M. The topics from A to K are ACM's classification and its subclassification, while other two topics were added to reveal the growth of the computer science discipline. The complete list of topics is given in Table 2.
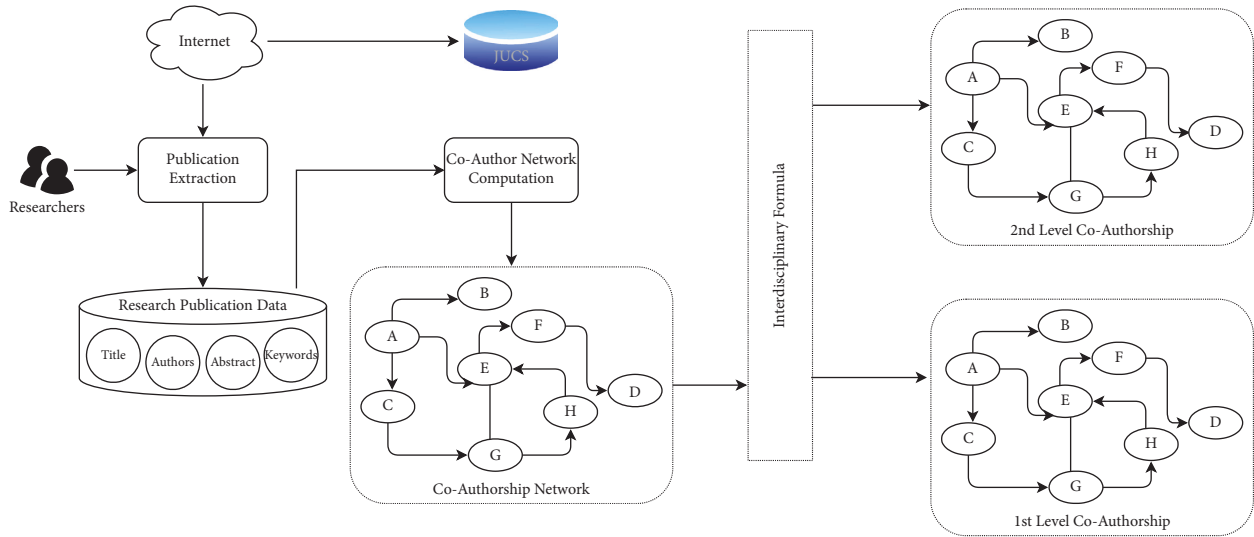
FIGURE 4: Publication information aggregation framework.

TABLE 2: Thirteen Categories following ACM classification (https://www.jucs.org/jucs_info/acm_categories).

Topic A-General Literature	Topic H-Information System
Topic B-hardware	Topic I-computing methodology
Topic C-computer system organization	Topic J-computer applications
Topic D-software	Topic K-computer milieux
Topic E-data theory	Topic L-science and technology of learning
Topic F-theory of computation	Topic M-knowledge management
Topic G-mathematics of computer	

3.2. Comprehensive Dataset Selection.

The dataset collection criteria for our proposed approach are as follows: (1) we required a large enough dataset to complete our research. The chosen dataset should cover a broad range of topics; (2) the second primary criterion for our dataset was that it should enable us to access the metadata of numerous authors' research articles and information about the authors' publication records and co-authors' information. We choose the dataset from the (J.UCS) journal of Universal Computer Science to satisfy these criteria. J.UCS is the first Journal of Computer Science that addresses various topics, where authors from different backgrounds and domains publish their research.

So, the J.UCS dataset will help us comprehensively explore our proposed research. The dataset of J.UCS is denoted at the top of Figure 4.

3.3. Extraction of Metadata.

Metadata of research papers is another source that the researchers use. Metadata is defined as data about the data. In the research articles context, the metadata could be the author, keywords, paper title, and ACM topics (if any). We believe that metadata could be divided into two categories: the traditional metadata, including the data about research articles. The second type of metadata is acquired from bookmarking and social tagging. The user could annotate the data using online services like CiteULike, which contains research articles, references, and bookmarks.

Metadata techniques have some limitations because they are usually dataset-dependent and cannot be generalized; for example, metadata of one type in a dataset may not exist in another dataset. Generally, the title of a paper, author, and publication information are available in each dataset. But, sometimes, this information is too little to compute the relatedness between the research articles. Occasionally, the free availability of metadata is not possible. In this type of situation, the metadata is automatically extracted.

Our database contains various tables, like papers and categories shown in Figure 5. Each paper in the relationship can have more than one category; therefore, we have added a third relation called "papers categories" as a join table. These tables contain metadata about papers, authors, categories, and subcategories. Our first step consists of extracting the metadata of papers, authors, categories, and subcategories using a crawler. The crawler, developed in PHP, crawls the pages of JUCS through a service. It looks for a specified structure of the content of the web page, containing the paper metadata and pdf contents. We directly store the media contents to their relevant tables in the database, whereas the pdf files are further converted to XML as it is nearly impossible to read the sections of a pdf document, explained in the next section.

3.3.1. Extraction of Authors.

The author information was extracted from XML formats of the paper containing the author's name and first- and second-level author's
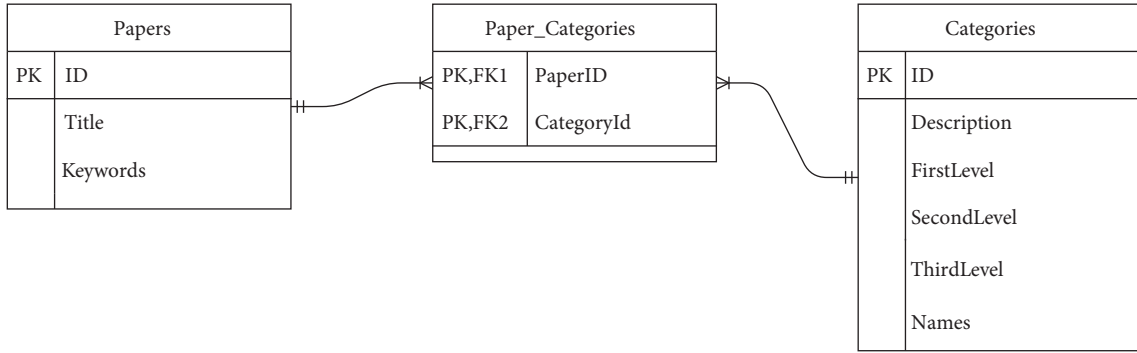
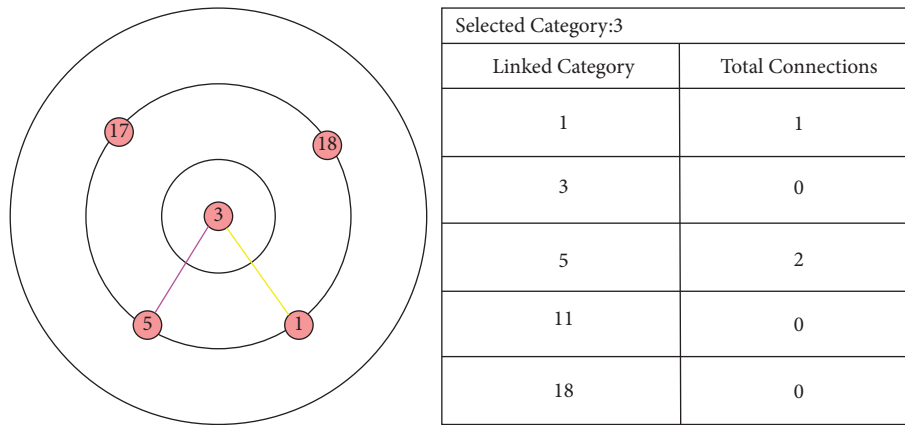FIGURE 5: Pictorial presentation of a list of three tables.

FIGURE 6: A screencast of force-directed graph.

information. We have converted the pdf format of papers to XML because it is nearly impossible to extract the author's information from pdf files. A separate author's table has been formed in our database. The table contains the author's id, author's name, and his co-author's information.

3.3.2. Extraction of Papers. The information regarding papers has been extracted from XML files and stored in organized form in a separate table. The paper table contains the paper's id, title, keyword, and the abstract. Paper information is also metadata that must be extracted as part of the researcher's publication record. Figure 6 has highlighted the papers table containing the papers' information.

3.3.3. Extraction of Papers Categories. The metadata in our database also contain the categorized information. Thirteen categories have 420 subcategories in the database following the ACM classification scheme. We created a category table that includes information about the list of categories in our database. We also created a paper-category table that indicates the specific category of paper in which the article resides. The category information of a paper is extracted from the paper-categories table. How our database has metadata containing the complete information of papers, authors, articles, and categories is summarized. This

metadata helps us in building co-authorship networks of different categories.

3.4. Building Co-Authorship Network. The co-authorship network explains how authors have been associated with each other from various fields of research based on their published articles. The network is considered one of the most credible and concrete methods for describing the author's collaborations [8]. A co-authorship network can extract any research component by studying the links among various network nodes [9]. The Paul Erdos network is one of the examples, with over 500 co-author nodes in the network [19]. The network shows all the authors who have worked directly or indirectly with the Hungarian mathematician Paul Erdos, who wrote many research articles in mathematics. The network is based on Erdos number, which describes the collaboration with Paul Erdos. If an author has published an article with Erdos as a co-author, the assigned Erdos number is 1. Authors who have an association with the co-authors of Erdos are assigned Erdos number 2, and so on. The authors with more publications with the same Erdos number are given preference while fetching the n number of collaborations. This illustrates that in a co-authorship network, there are several levels of co-authors. As explained in the literature review section, we have constructed a co-authorship network up to the 2nd level.
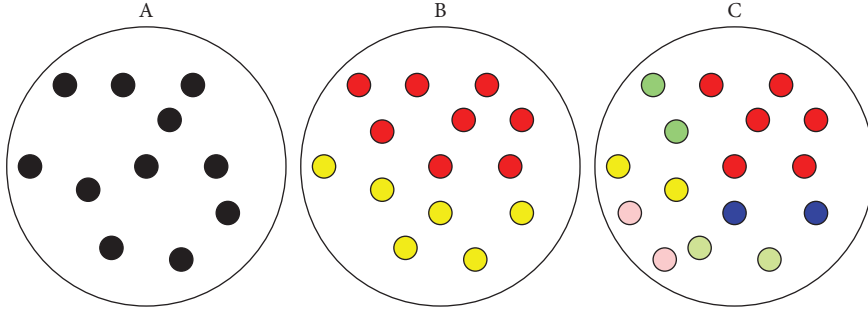
Figure 7: Groups of researchers bellowing to various categories represented by colors.

3.5. System Development. System development was our main focus for the completion of our methodology and for achieving our research goal. We had to construct co-authorship networks of authors belonging to different categories and then analyze the interdisciplinary nature of each category with other categories. To accomplish our goal, we have used the tool Visual studio 2019. Visual studio is an open-source IDE used to develop web apps, mobile apps, and computer programs. We used the ASP.net language, and the framework used in development was MVC. We have also created a database, and the formation of the database is done using MySQL.

Using the J.UCS dataset, we have constructed co-authorship networks of researchers belonging to any category up to the 2nd level. Two categories are considered to be connected by an edge if the researcher of one category has co-authored at least one paper with another researcher of any other category. However, the co-authorship networks amongst different categories are set to form scientific communities.

In our database, thirteen different categories have a total of 421 subcategories. These categories follow the ACM classification. Each researcher registered in a database has assigned a number from 1 to n, where n is equal to 421, the last category of our dataset.

The number assigned to any researcher indicates the category to which an author belongs. Some of the top categories are general literature, hardware, computer system organization, software, data theory, Theory of Computation, information system, computing methodology, computer applications, computer milieux, Science and Technology of Learning, and knowledge management.

To measure the interdisciplinary of each community C formed among a group of categories, we use the ACM classification scheme described above. The n-component vector IC has been allocated, with each component reflecting the fraction of researchers in one of the "n" categories. (1) defines the interdisciplinary amongst different categories in scientific communities:

$$IRC(C) = \beta \sqrt{1 - \sum_{i=1}^{n} Xi^2}. \tag{1}$$

Here, the ith component of IC is $[\![Xi]\!]^2$ and $\beta = [1 − (1/n)] − 0.5$, which is the normalization constant that ensures that $0 \leq IDR(C) \leq 1$. Rendering to equation (1) the IDR(C) =

0 if $[\![Xi]\!]^2 = 1$ for any n components (in this case, all the other components are 0). If the value of n is equal to 7, the $[\![Xi]\!]^2$ is 1/7, then the interdisciplinary IDR(C) is 1.

Researchers belonging to various groups are illustrated in different colors in Figure 7. There are seven categories, represented by Xi, where I = 1, 2, 3, . . ., and 7. Each category is represented by different color denoted as $n = 7$ in Equation 1. In A, all the researchers belong to the same category or work in the same research area X1. The n-component vector will be IC = (1, 0, 0, 0, 0, 0, 0), as well as the community's interdisciplinary, according to equation (1), is IDR(C) = 0.

In community B, the researchers belong to two different research areas X1 and X5. So, the n-component vector will be IC = (1/2, 0, 0, 0, 1/2, 0, 0), and the interdisciplinary of such a community is, according to equation (1), is IDR(C) = 0.88. In community C, all the researchers work in different research areas from X1 to X7. So, the n-component vector will be IC = (1/7, 1/7, 1/7, 1/7, 1/7, 1/7, 1/7), and such a community's interdisciplinary, according to equation (1), is IDR(C) = 1.

Similarly, we have analyzed the interdisciplinary of all categories in our database with other categories up to the 2nd level. We made a co-authorship network of each category up to the 2nd level. For visualization purposes, we have used some visualization libraries that show the co-authorship network of the categories is visualized, as shown in Figure 8.

3.6. Visualization. The visual presentation of co-authorship networks of categories was also important; we used several visual libraries. There are two different graphs of our visualization process and both show the categories' relatedness, but one of the graphs has more information about the connection(s).

3.6.1. Force-Directed Graph. The force-directed graph shows the relatedness of categories and, compared to the category graph, the force-directed graph shows a table that has two columns and contains the information of linked categories and the total number of connections of authors amongst different categories. As shown in Figure 6, the force-directed graph also presents the list of categories in our database.

3.6.2. Categories Graph. The category graph, shown in Figure 9, represents the categories' network information, showing the links amongst categories. The category graph
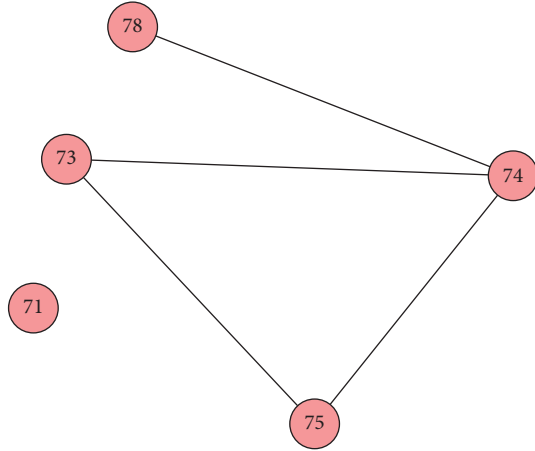
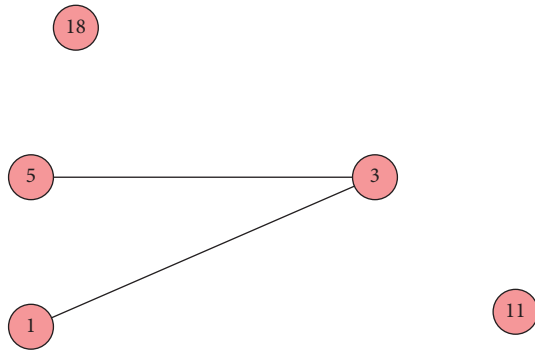FIGURE 8: Co-authorship network of five different categories.

FIGURE 9: A screencast of category graph.

does not contain any information about the connection of authors amongst categories.

4. Results

This section contains the complete results and information about many categories and subcategories, paper(s) per subcategories. It also clarifies the results at different levels of the co-authorship network amongst authors. The strong bond between any two categories depends upon how many authors of one category are linked with the authors of another category. We have further analyzed the interdisciplinary value of categories in a community.

Table 3 defines the information regarding the whole scenario of our database. The table provides information about categories and subcategories. The table also provides the number of authors in a particular category and the papers in each category.

The Pie Chart in Figure 10 shows the number of categories starting from A to *M*, which are 13 and subcategories that are 421 in number. The different colors show the total number of categories. At the same time, the subcategories are represented in the form of a percentage.

4.1. Results of Co-Authorship Network at First Level. Our dataset contains four hundred categories, including

TABLE 3: List of categories, sub-categories, authors, and paper per categories.

| Categories	Number of sub-categories	Authors per category	Papers per category
General literature	5	168	80
Hardware	56	410	144
Computer system organization	29	771	300
Software	48	2567	1018
Data theory	08	271	106
Theory of computation	27	1539	809
Mathematics of computer	24	423	211
Information system	43	3370	1270
Computing methodology	75	1706	626
Computer applications	10	484	186
Computer milieux	43	1040	425
Science and technology of learning	42	103	33
Knowledge management	11	73	26
Total:	421	12,925	5,234
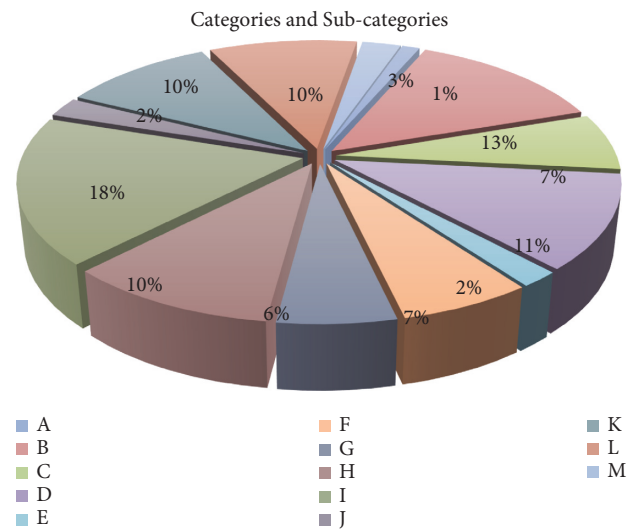
FIGURE 10: A pie chart of categories and subcategories.

subcategories. Twenty-one categories follow the ACM classification scheme as explained in the previous section. We have selected ten different subcategories to form a co-authorship network at first level to analyze interdisciplinarily, as shown in Figure 11. The subcategories include arithmetic and logic structure, control structure performance analysis and design aids, reliability, testing, fault tolerance, design styles, design, network architecture design, visual programming, management of computing and information systems, and storage management. The combination of linking subcategories will create a mesh connecting
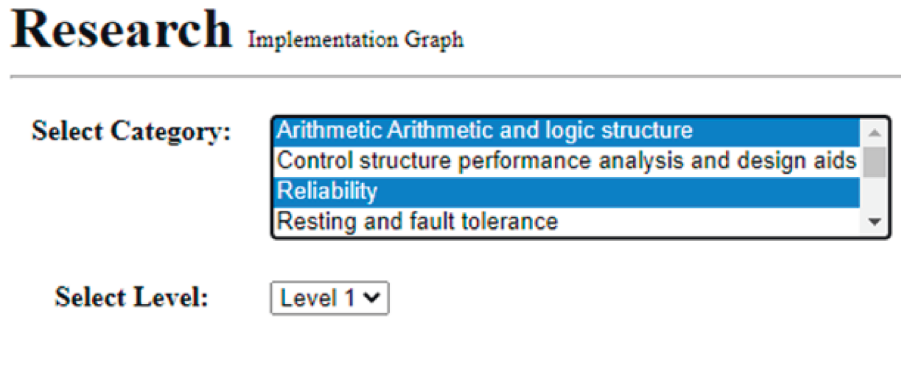
FIGURE 11: A screencast of selecting ten categories from the list of 421 subcategories to form a co-authorship network at the first level.
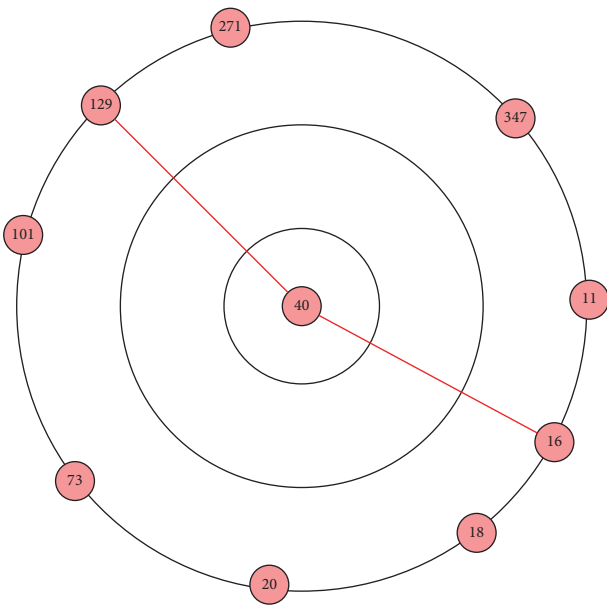

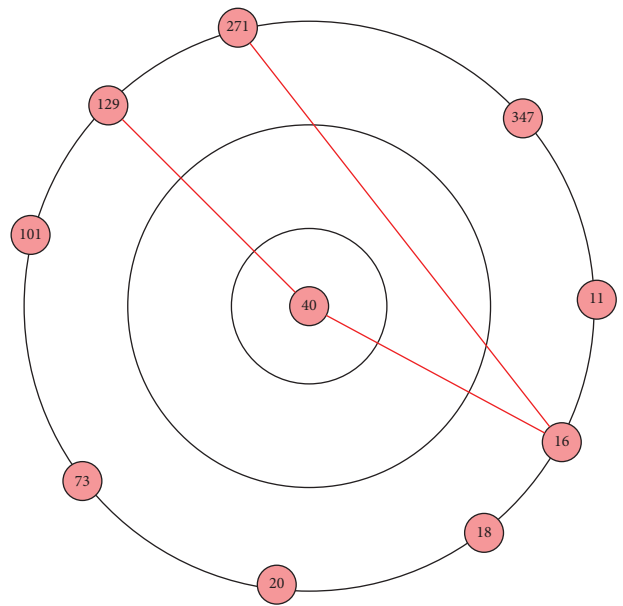
FIGURE 12: A screencast of force-directed graph.

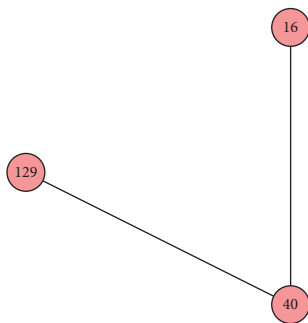FIGURE 14: A screencast of the force-directed graph.

FIGURE 13: A screencast of category graph.

TABLE 4: Connected categories represented in the directed graph at the 1st-level co-authorship network.

Selected category: 40	
Linked category	Total connections
11, 18, 20, 40, 73, 101, 129, 271, 347	0
16, 129	1

TABLE 5: Connected categories represented in the directed graph at 2nd-level co-authorship network.

Selected category: 40	
Linked category	Total connections
11, 18, 20, 40, 73, 101, 271, 347	0
16	5
129	2

each subcategory with every other subcategory; therefore, we have selected only ten subcategories. The pictorial presentations of the force-directed graph and category graph have been shown in Figures 12 and 13, respectively, describing the co-authorship network formed at the first level amongst these categories.

4.1.1. Force-Directed Graph Results. Fore directed graph is a particular type of graph in which nodes have forces applied to them. The connected nodes pull towards one another
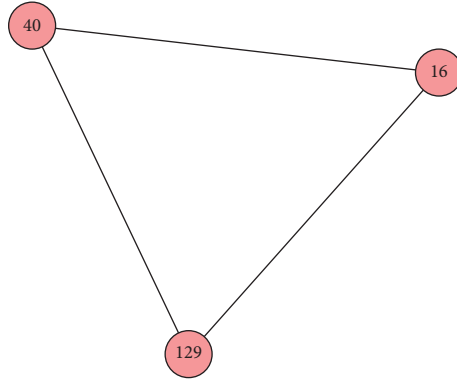
FIGURE 15: A screencast of the category graph.

TABLE 6: List of categories, sub-categories, authors, and paper per categories.

S.No	Categories from description	Categories to description	Connections	Interdisciplinarity value
1	Artificial intelligence	Information storage and retrieval	49	0.879
2	Natural language processing	Information storage and retrieval	33	0.711
3	System	Coding tools and techniques	30	0.679
4	Human-computer interface	Database applications	29	0.663
5	Logic design	Language constructs and technique	25	0.611
6	Robotics	Software engineering	21	0.572
7	Programming languages and software	Processor architectures	20	0.56
8	Computer-communication networks	Object oriented programming	18	0.543
9	System and information theory	Content analysis and indexing	16	0.521
10	Game-based learning	Software architecture	15	0.513

while nodes that are not similar repel each other. As a result, it will group nodes identical to each other based on the co-authorship, in our case. Figure 12, based on Table 4, is a force-directed graph showing the first level co-authorship network amongst ten different subcategories, where subcategory id 40 in the categories list has a connection and is linked with subcategory id 139 and 16. This means that only these three sub-categories have co-authored papers among the ten different subcategories. The table shown below represents the linked categories and total connections. The rest of the subcategories have not published a single paper with each other.

The column of total connections in the above table represents the number of co-authored papers amongst subcategories. The subcategory id # 40 has co-authored a paper only with subcategory id # 16 and subcategory id # 129. In contrast, the rest of the subcategories are unconnected because none of the remaining subcategories have co-authored a single paper with subcategory id # 40.

4.1.2. Category Graph Results. The Category graph in Figure 13 shows only the connected subcategories, leaving the other unconnected subcategories. The connection between these subcategories indicates that the authors from these three subcategories have co-authored paper(s).

4.2. Result of Co-Authorship Network at Second Level. The same ten different subcategories from the list of four hundred and twenty subcategories are selected to form a co-authorship network at the 2nd level. The results are shown in Figure 11.

4.2.1. Force-Directed Graph Results. The force-directed graph in Figure 14 shows that category 40 is connected with categories 129 and 16, but in the second level co-authorship network, the total connection column in Table 5 shows that the authors of these categories have published more than one paper with each other.

4.2.2. Category Graph Results. The category graph only shows the related categories. Figure 15 is a co-authorship network up to the 2nd level that indicates a subcategory's connectivity with the other ten subcategories selected in the network.

We have found and shown in Table 6 the top 10 most collaborating subcategories among the group of all 421 subcategories in our database. The ten subcategories shown in the table have the highest number of connections with a specific category that indicate their scientific collaboration, as well as mark the most collaborating subcategories in a scientific community. Furthermore, the interdisciplinary values between the subcategories have been analyzed and shown in Table 6.

When examining subcategory collaboration, it was discovered that subcategories with the strongest association or the most significant number of connections had key term correlations, having the highest number of correlations among the words of these categories. As an
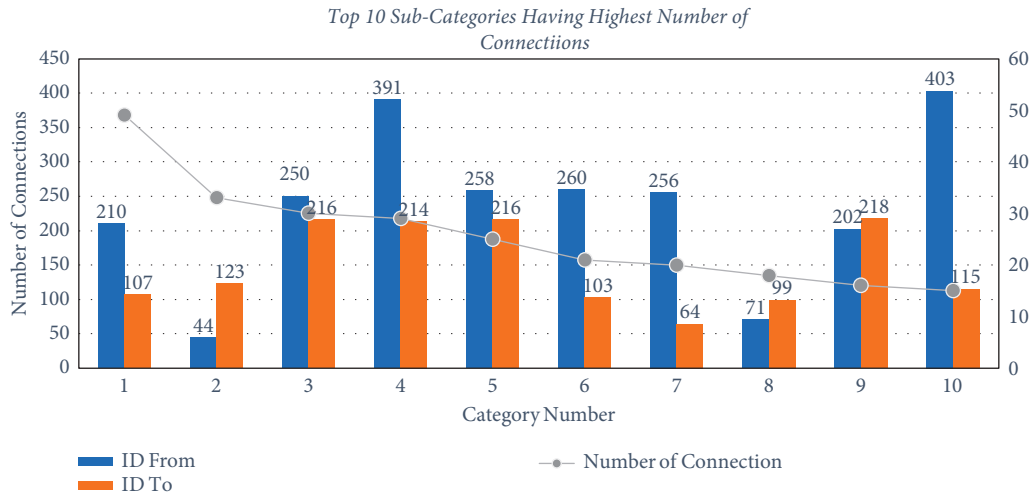
FIGURE 16: Graph of ten sub-categories having the highest number of connections.

example, the subcategory Artificial Intelligence has a close relationship with the subcategory information storage and retrieval because Artificial Intelligence has the most connections with information storage and retrieval relative to other subcategories in the co-authorship network. The same holds for all subcategories with the most links to the specific subcategory. Figure 16 displays the number of connections for each of the subcategories. It clearly shows the number of times a category is used as the source and destination.

Various methods in literature have performed the IDR analysis, but our technique has used the co-authorship network for performing IDR analysis in terms of authors' relationships from multiple disciplines.

5. Conclusion

Scientific collaboration is a dire need of today's research. Interdisciplinary collaboration is very common, and researchers from other disciplines collaborate to solve complex issues whose solutions go beyond a particular category or domain.

In this research, we designed, developed, and deployed a co-authorship network-based solution to analyze the trend of IDR in the computer science domain. We developed a system that prepared and processed the J.UCS dataset in this research. The dataset was persisted in MySQL. The dataset comprised more than 1200 research articles published in various ACM categories by authors of more than 2500. This dataset enables us to perform the experiments to answer the following research questions: Are there any IDR activities going on in various computer science fields? What are the most common categories w.r.t 1st-level co-authorship network where IDR activities are frequently conducted? and What are the most common categories w.r.t 2nd level co-authorship network where IDR activities are frequently conducted? Finally, the directed graph visualization is implemented to quickly understand the IDR activities in the computer science domain.

The growing trend of scientific collaboration has opened new avenues of research. This research may help us to understand what special training is needed for new researchers in any area. What are the different areas affecting each other? So, this kind of information can help us to design curricula for specific programs. Finally, this research may help us make a wise decision for allocating resources. In this research, we have used the J.UCS dataset related to the computer science field. In the future, it would be interesting to conduct a study that can analyze interdisciplinary phenomena among different disciplines like physical sciences, numerical sciences, and social sciences using a dataset covering a wide area of scientific disciplines.

Data Availability

The dataset was taken from the open-access journal (Journal of Universal Computer Science) https://www.jucs.org/.

Conflicts of Interest

The authors declare that they have no conflicts of interest.

References

[1] F. J. Acedo, C. Barroso, C. Casanueva, and J. L. Galan, "Co-authorship in management and organizational studies: an empirical and network analysis," *Journal of Management Studies*, vol. 43, no. 5, pp. 957–983, 2006.

[2] B. P. Fonseca, R. B. Sampaio, M. V. Fonseca, and F. Zicker, "Co-authorship network analysis in health research: method and potential use," *Health Research Policy and Systems*, vol. 14, no. 1, pp. 34–10, 2016.

[3] L. Aldieri, M. Kotsemir, and C. P. Vinci, "The impact of research collaboration on academic performance: an empirical analysis for some European countries," *Socio-Economic Planning Sciences*, vol. 62, pp. 13–30, 2018.

[4] A. L. Razera, M. R. Errera, E. D. Dos Santos, L. A. Isoldi, and L. A. O. Rocha, "Constructal network OF scientific publications, CO-authorship and citations," *Proc Roman Acad Ser A-Math Phys Tech Sci Inform Sci*, vol. 18, pp. 105–110, 2018.

[5] S. Kumar, "Co-authorship networks: a review of the literature," *Aslib Journal of Information Management*, 2015.

[6] Y. Chen, C. Ding, J. Hu, R. Chen, P. Hui, and X. Fu, "Building and analyzing a global co-authorship network using google scholar data," in *Proceedings of the 26th International Conference on World Wide Web Companion*, pp. 1219–1224, Perth, Australia, April 2017.

[7] M. Pavlov and R. Ichise, "Finding experts by link prediction in co-authorship networks," *FEWS*, vol. 290, pp. 42–55, 2007.

[8] S. Hennemann, "Hierarchies in the science and technology system of China-System reforms and their consequences for knowledge flows," *Geographische Zeitschrift*, vol. 98, no. 3, pp. 155–174, 2010.

[9] C. M. Morel, S. J. Serruya, G. O. Penna, and R. Guimarães, "Co-authorship network analysis: a powerful tool for strategic planning of research, development and capacity building programs on neglected diseases," *PLoS Neglected Tropical Diseases*, vol. 3, no. 8, p. e501, 2009.

[10] A. L. Porter, D. J. Roessner, and A. E. Heberger, "How interdisciplinary is a given body of research?" *Research Evaluation*, vol. 17, no. 4, pp. 273–282, 2008.

[11] I. Rafols and M. Meyer, "Diversity measures and network centralities as indicators of interdisciplinarity: case studies in bionanoscience," *Proceedings of ISSI*, vol. 2, pp. 631–637, 2007.

[12] M.-H. Huang and Y.-W. Chang, "A study of interdisciplinaryin information science: using direct citation and co-authorship analysis," *Journal of Information Science*, vol. 37, no. 4, pp. 369–378, 2011.

[13] G. Abramo, C. A. D'Angelo, and F. Di Costa, "Identifying interdisciplinarythrough the disciplinary classification of co-authors of scientific publications," *Journal of the American Society for Information Science and Technology*, vol. 63, no. 11, pp. 2206–2222, 2012.

[14] J. Qin, F. W. Lancaster, and B. Allen, "Types and levels of collaboration in interdisciplinary research in the sciences," *Journal of the American Society for Information Science*, vol. 48, no. 10, pp. 893–916, 1997.

[15] J. W. Grossman, "Paul Erdős: The Master of Collaboration," *The Mathematics of Paul Erdős II*, Springer, Manhattan, NY, USA, pp. 489–496, 2013.

[16] A. H. Marino, K. A. Suda-Blake, and K. R. Fulton, "Innovative Collaboration Formation: The National Academies Keck Futures Initiative," *Strategies for Team Science Success*, Springer, Manhattan, NY, USA, pp. 241–250, 2019.

[17] W. D. Figg, L. Dunn, D. J. Liewehr et al., "Scientific collaboration results in higher citation rates of published articles," *Pharmacotherapy: The Journal of Human Pharmacology and Drug Therapy*, vol. 26, no. 6, pp. 759–767, 2006.

[18] Z. Taşkın and A. U. Aydinoglu, "Collaborative interdisciplinary astrobiology research: a bibliometric study of the NASA Astrobiology Institute," *Scientometrics*, vol. 103, no. 3, pp. 1003–1022, 2015.

[19] G. Baker, R. Gibbons, and K. J. Murphy, "Subjective performance measures in optimal incentive contracts," *Quarterly Journal of Economics*, vol. 109, no. 4, pp. 1125–1156, 1994.

[20] A. Yegros-Yegros, I. Rafols, and P. D'Este, "Does interdisciplinary research lead to higher citation impact? The different effect of proximal and distal interdisciplinarity," *PloS one*, vol. 10, no. 8, Article ID e0135095, 2015.

[21] H. Small, "Co-citation in the scientific literature: a new measure of the relationship between two documents," *Journal of the American Society for Information Science*, vol. 24, no. 4, pp. 265–269, 1973.

[22] A. M. Khan, A. Shahid, M. T. Afzal, F. Nazar, F. S. Alotaibi, and K. H. Alyoubi, "SwICS: section-wise in-text citation score," *IEEE Access*, vol. 7, pp. 137090–137102, 2019.

[23] B. Lepori, P. Van Den Besselaar, M. Dinges et al., "Comparing the evolution of national research policies: what patterns of change?" *Science and Public Policy*, vol. 34, no. 6, pp. 372–388, 2007.

[24] M. Bruce, L. Daly, and N. Towers, "Lean or agile: a solution for supply chain management in the textiles and clothing industry," *International Journal of Operations & Production Management*, 2004.

[25] T. Braun and A. Schubert, "A quantitative view on the coming of age of interdisciplinaryin the science," *Scientometrics*, vol. 58, no. 1, pp. 183–189, 2003.

[26] B. Lužar, Z. Levnajić, J. Povh, and M. Perc, "Community structure and the evolution of interdisciplinaryin Slovenia's scientific collaboration network," *Plos one*, vol. 9, no. 4, Article ID e94429, 2014.

[27] B. Aleman-Meza, L. Ding, M. Nagarajan, and C. Ramakrishnan, "Semantic analytics on social networks: experiences in addressing the problem of conflict of interest detection," in *Proceedings of the 15th international conference on World Wide Web*, pp. 407–416, Scotland, UK, May 2006.

[28] I. Molotov, V. Agapov, V. Titenko et al., "International scientific optical network for space debris research," *Advances in Space Research*, vol. 41, no. 7, pp. 1022–1028, 2008.

[29] M. Karlovčec and D. Mladenić, "Interdisciplinaryof scientific fields and its evolution based on graph of project collaboration and co-authoring," *Scientometrics*, vol. 102, no. 1, pp. 433–454, 2015.

[30] A. L. Barabâsi, H. Jeong, Z. Néda, E. Ravasz, A. Schubert, and T. Vicsek, "Evolution of the social network of scientific collaborations," *Physica A: Statistical Mechanics and Its Applications*, vol. 311, no. 3-4, pp. 590–614, 2002.

[31] I. Zupic and T. Čater, "Bibliometric methods in management and organization," *Organizational Research Methods*, vol. 18, no. 3, pp. 429–472, 2015.

[32] M. J. Cobo, A. G. López-Herrera, E. Herrera-Viedma, and F. Herrera, "Science mapping software tools: review, analysis, and cooperative study among tools," *Journal of the American Society for Information Science and Technology*, vol. 62, no. 7, pp. 1382–1402, 2011.

[33] B. Jarneving, "A comparison of two bibliometric methods for mapping of the research front," *Scientometrics*, vol. 65, no. 2, pp. 245–263, 2005.

WILEY | Hindawi

Research Article

Perimeter Degree Technique for the Reduction of Routing Congestion during Placement in Physical Design of VLSI Circuits

Kuruva Lakshmanna (ID),[1] **Fahimuddin Shaik** (ID),[2] **Vinit Kumar Gunjan**,[3] **Ninni Singh**,[3] **Gautam Kumar**,[4] **and R. Mahammad Shafi** (ID)[5]

[1]*Department of Information Technology, Vellore Institute of Technology, Vellore, India*
[2]*Department of Electronics & Communications Engineering, Annamacharya Institute of Technology & Science, Rajampet, India*
[3]*Department of Computer Science & Engineering, CMR Institute of Technology, Hyderabad, India*
[4]*Department of Computer Science & Engineering, CMR Engineering College, Hyderabad, India*
[5]*Department of Electrical and Computer Engineering, College of Engineering and Technology, Tepi Campus, MIZAN-TEPI University, Tepi, Ethiopia*

Correspondence should be addressed to R. Mahammad Shafi; mahammadshafi.r@mtu.edu.et

When used in conjunction with the current floorplan and the optimization technique in circuit design engineering, this research allows for the evaluation of design parameters that can be used to reduce congestion during integrated circuit fabrication. Testing the multiple alternative consequences of IC design will be extremely beneficial in this situation, as will be demonstrated further below. If the importance of placement and routing congestion concerns is underappreciated, the IC implementation may experience significant nonlinear problems throughout the process as a result of the underappreciation of placement and routing congestion concerns. The use of standard optimization techniques in integrated circuit design is not the most effective strategy when it comes to precisely estimating nonlinear aspects in the design of integrated circuits. To this end, advanced tools such as Xilinx VIVADO and the ICC2 have been developed, in addition to the ICC1 and VIRTUOSO, to explore for computations and recover the actual parameters that are required to design optimal placement and routing for well-organized and ordered physical design. Furthermore, this work employs the perimeter degree technique (PDT) to measure routing congestion in both horizontal and vertical directions for a silicon chip region and then applies the technique to lower the density of superfluous routing (DSR) (PDT). Recently, a metaheuristic approach to computation has increased in favor, particularly in the last two decades. It is a classic graph theory problem, and it is also a common topic in the field of optimization. However, it does not provide correct information about where and how nodes should be put, despite its popularity. Consequently, in conjunction with the optimized floorplan data, the optimized model created by the Improved Harmonic Search Optimization algorithm undergoes testing and investigation in order to estimate the amount of congestion that occurs during the routing process in VLSI circuit design and to minimize the amount of congestion that occurs.

1. Introduction

However, there are several limitations to Significant Level Synthesis that must be taken into consideration. Significant Level Synthesis is swiftly becoming the industry standard for the VLSI approach. One of the challenges that needs to be solved is congestion throughout the steering cycle of bespoke chips and FPGA-based designs. The steering block is not incorporated in the VLSI plan, despite the fact that it is an openly stated idea elsewhere. Even though it has been a concern in the past with normal HDL-based designs, it has reached a level of severity that is unprecedented [1] in an instance of Considerable-Level Synthesis. Because of this, the most effective course of action is to anticipate the block issue as early in the planning phase as is reasonably possible before it occurs. The implementation of a blocking method

leaves the computerized switch with only a limited number of routing alternatives in the event of a failure. SLS, while fast becoming the industry standard for the VLSI strategy, has a number of disadvantages that must be considered. Concerns about congestion in steering cycles for bespoke chips and FPGA-based designs, among other things, are being raised by the industry. It is not typical in other designs to have a steering block, but the VLSI architecture does not have one. Previously, it had been a difficulty for classic HDL-based designs, but with Considerable-Level Synthesis, the severity of the problem has increased significantly [1]. Rather than waiting until the last minute, it is preferable to plan for the problem at a higher level rather than at the lowest one. As a result of the stringent time limits imposed by blocked nets and computerized switchbacks, the computerized switch is left with few options for routing a blockage plan when dealing with a blockage. Recently, it has been shown that steering blocks can cause robotized steering measure spans to get corrupted and diminish the yield of final results and induce director cycle discontent in plans where there is a significant amount of steering congestion. Despite the availability of cutting-edge EDA instruments, they are unable to completely mitigate the negative impact on the shoot caused by the expansion in the multidimensional nature of computerized plans and the scaling of innovation that occurs as a result of the presence of a directing block during the production.

The use of High-Level Synthesis (HLS) by architects and equipment makers has gained in popularity in recent years, particularly among the former. The most advanced EDA streams have likewise solidified HLS-based planning methodologies, elevating them to the top of their respective categories. High-level dialects such as C++, SystemC, and OpenCL (Open Computing Language) are examples of high-level dialects that can be recognized by a computerized cycle and turned into an RTL plan, which may then be used in electronic circuit design. This method can then be completed by the use of a field-programmable gate array (FPGA). FPGAs have limited resources in terms of logic cells and interconnects, which are used to design power supplies, clocks, and signal nets, and these resources are consumed quickly as the number of logic cells and interconnects increases.

When asset utilization is significant or the plan is particularly sophisticated, an inblock is created in the plan usage stream throughout the steering cycle, which must be resolved in order for the plan to be executed successfully. When this steering block is activated, it allows the rails to be skipped, and it is responsible for guiding the vehicle. On rare occasions, the equipment may even become inoperable, resulting in the failure of the overall plan and the disruption of the utilization cycle as a result. This will result in more complex decision-making procedures and longer planning cycles being implemented as a result of the current scenario. Directed-block messages and reports contain just information on the blocked cells and congestion windows, and they do not contain any other information about the network. In order to remedy the issue, the author must first determine which piece of the substantial level code is causing

this steering block. Unfortunately, there is no easy-to-find relationship that can guide him or her through this process. However, despite the fact that these ambiguous netlabels may be seen in RTL representations of the plan, there is no clear connection between them and the sophisticated rules that govern the formation of these nets.

For the most part, we are willing to work on creating a link between the HLS code and the Computational Logic Blocks located on the real-time chip area in order to approximate congestion for the streamline that shows the means by using the recommended IHS method and the ICCII tool, which is currently in the process of being developed. Because the Dataflow approach could only handle a small number of macroblocks at a time, it was slower and could not forecast congestion in both the horizontal and vertical directions, as the Flyline method did. The acronym ICC stands for Integrated Circuit Compiler, and it is a sophisticated VLSI CAD tool that generates simulation results with corresponding input files and provides detailed information about the density of congestion by various methods, which is useful for optimum placement of macroblocks and relatively short-length routing among the blocks. The optimal architecture of a benchmark circuit developed from the IHSAlgorithm is used as a significant input for the ICC tool in this research; in this study, the ICC tool receives independent inputs from the number of macroblocks and their corresponding pins made available in the architecture. In the course of the scheduled stream, data created by a large number of apparatuses is collected, and the outcome is a correlation between the increased level of code on the chip area and the number of windows that are blocked. The use of this simulated data allows us to predict routing congestion among compute blocks and their pins, which helps us to anticipate the area where we might be able to obtain a higher density of routing channels on the chip and reduce obstruction using various obstruction approaches. When processing blocks and the pins that connect them are analyzed, it becomes possible to establish whether there is routing congestion between them.

Wiring is used to produce the clock and signal nets, which are then connected together to form a classic standard cell layout. Each of them makes use of the same network resources as the others. In a typical design, as the number of cells increases, the rivalry for desired routing resources becomes much fiercer. This is due to the fact that the electrical characteristics of metal wires do not scale well with an increase in the number of cells. A rise in routing congestion, as well as a decline in the overall quality of design work performed, resulted as a result of these developments. The majority of traditional design techniques begin with the synthesis of the power supply and clock networks before moving on to the synthesis of the signal routing networks and so on. Despite the fact that power supplies and clock networks do not perform any logical operations, they are crucial in supplying power and timing support to the circuitry that does. In the process of building the power supply network, the design's current requirements, the supply voltage's permissible noise limits, and the electromigration constraints are all taken into consideration. It is the usage of

an uneven grid that has been used in the design of this network. In accordance with standard operating practice, all routing resources are normally available before any development of a power supply network can be completed, let alone begin. A more flexible routing scheme for clock nets can be implemented after the power supply grid as a result of the fact that the power supply grid consumes some of the available routing resources. When it comes to synchronization, the clocks that are used to synchronize the sequential elements of the design must meet stringent requirements for signal integrity and skew, among other things, in order to perform properly. In order to meet their higher latency and skew requirements, high-end systems typically make use of clocking technologies such as grids. When it comes to mainstream designs, grids are often implemented as trees in order to meet more stringent criteria. Clock wires are usually protected or spaced apart to avoid the clock waveform from being affected by signals on neighboring lines, which can cause errors. Routing resources, on the other hand, are required in order to achieve both shielding and spacing. The signal nets are the last to be routed after the power supply and clock wires have been routed, and they can only make use of the routing capabilities that have been left over after the previous routing procedures. Congestion in the routing protocols of these networks can cause severe performance degradation. Apart from evaluating congestion, it is possible to use the method provided in this research to analyze the decrease in chip size and operation time for various design types, in addition to evaluating congestion.

When inserting macroblocks, the IHS method is used to maximize chip area and routing wire length by minimizing the number of routing wires. It was decided to combine the Particle Swarm Optimization Algorithm with the Harmony Search Algorithm in order to produce the IHSAlgorithm. The IHS Algorithm is the outcome of combining Harmony Search (HS) with Particle Swarm Optimization approaches to get optimal performance. Combining the Harmony Search (HS) algorithm with the Particle Swarm Optimization (PSO) algorithm is accomplished through the use of a forward-cascading technique. It was decided to merge HS and PSO because their separate best results were so similar. Even though PSO has a slower convergence rate than HS, it is capable of producing answers that are nearly as good as those given by the latter. The Improved Harmony Search (IHS) Algorithm is presented for use in VLSI Physical Design Automation Floorplanning in order to obtain the required performance while maintaining the required speed and accuracy. In addition to causing death and injury, traffic congestion has the potential to cause a wide range of other catastrophes. As a result of this decision, the overall performance of the design, for example, may be compromised in some way. If the design is not followed to the letter, it is possible that lower working conditions exist. In the sections that follow, you will find in-depth examinations of each of the themes listed.

Because wire delays are no longer straightforward in modern process technologies, increased net delays on essential channels may cause a design to fail to fulfill its frequency goal as a result of increased net delays on important paths. A sudden increase in latency time on a network is frequently caused by unanticipated routing congestion that was not anticipated beforehand. Congestion is one of the many elements that can have an impact on net delay in a variety of different ways. The use of more robust metal layers in network routing will almost likely result in an increase in network latency as the number of metal layers used grows. In order to avoid congested areas, it may be necessary to introduce a detour into the network's routing system, which will be sent to the rest of the network. Because of this detour, both the net and the driver will be significantly delayed as a result of the delay.

Making a large number of vias in order to identify the shortest way across (or complete thorough routing in) an extremely densely populated area may result in a significant increase in the total network delay as a result. Due to the fact that the wire route is located in a region with a high population density, it may be more susceptible to interconnect crosstalk, resulting in greater variations in net delay fluctuations. A more sophisticated and effective simulation tool was used throughout the course of this project in order to evaluate and estimate the required parameters. Input files for the ICC tool include the Optimized BMCArchitecture from IHSAlgorithm, which is included in the ICC tool's output files. The IHSAlgorithm creates an architecture that requires the least amount of chip area and the shortest routing wire length possible with 1500 iterations.

When routing long or time-critical nets, global routers that are driven by timing will aim to route them on the lower resistive levels, where the reduced wire delays can compensate for the via stack penalty, rather than on the higher resistive layers, as opposed to the higher resistive layers. Lower layers with more damage resistance may be necessary for some of the vital nets that are routed later on as a result of the presence of other (perhaps crucial) nets that occupied those desired layers in the previous configuration. The routing of crucial nets may be placed on lower layers of the network design, which may result in time violations on paths that pass through these nets being triggered by growing delays on paths that pass through these nets. It is possible that detours to avoid congested places will lead both the net and its driver to be delayed, causing both of them to be late for their appointments. In spite of the fact that the latency of an unbuffered network increases in a quadratic fashion as the network's length increases, even when employing a simple (lumped parasitic) delay model.

2. Review of Literature

In this study, the goal was to devise a strategy for increasing the responsiveness of directors to location requests. As a result of this technique's situational and guiding coadvancements [2], it is possible to cope with diversity, contamination, and imperfection in a methodical manner. When identifying concerns connected to blocks, planners can use the methodologies described in [3] to narrow their search. Large-scale layout, as well as block dissection and analysis, are all possible with this technique. According to the paper, three areas were specially mentioned: the

automated era of the information highway format, enhanced coordination of planning, and force enhancements. It is necessary to combine numerous upper layers in order to fit a design. There is a graphical user interface for blend and effect measurement with lithography awareness. The implications of merging group and arrangement requirements on succession pair portrayal are discussed in this work, which results in a significant reduction in the arrangement space and a significant boost in computing speed. Scientists were investigating both time-saving and traditional methods of allocating level shifter districts [4, 5] while working on the project's design stage. They fail to take into account the fact that clock-network swapping contributes to more than 30% of total strength, which is significant. Several approaches have been taken to solve the issue of increasing the absolute unique force in place for large-scale integrated circuit systems, and new methodologies and methods have been established [5, 6]. An approach known as circular pressing trees, which is a floorplan visualizing technique that may be utilized to solve the full-scale problem, has also been discussed in detail. This design strategy allows for the placement of CLBs in turns or around chip restrictions, depending on the requirements. Longer wires are produced as a result of streamlining large-scale directions, and steering congestion is reduced as a result of the reduction in steering congestion. Using plan space analysis of low-power adders, we were able to carry out a comparative study of physical format and come up with some interesting results. The evaluation of the Location and Route Streams of Aware Synthesis is carried out and the result is created. Considering large-scale blended size arrangements, [7] examines an intriguing computation that is based on a heuristic in order to arrive at a convincing conclusion. Four steps must be completed in order for the procedure to be successful: assembling the items into blocks, predicting where the blocks will be placed on a floor, and increasing the wire length for good transport. Streaming [8] is able to solve some of the challenges that have been experienced by utilizing wire length advancement in conjunction with large-scale blended measured circuit design. The focus of future research should be on routability and full-scale augmentation of arrangement for advanced circuit designs based on location, time, force, and warm-determined augmentation of arrangement, as well as full-scale augmentation of arrangement. In this study, the ways of robotized floor arranging are investigated, which is critical for the achievement of effective plan space research in order to be successful. There are also some proposals for increasing the usefulness of the present floor planning tools [9], which are discussed in more detail below. The implementation of the numerous improvements that can be made on broad plan areas can be facilitated through the use of an integrated change framework [10]. Cloning and altering the register situation and retiming the register are all accomplished with entire concentration and dedication. The introduction of a new revolution power to deal with the problem of full-scale direction in a conspicuous blended size condition is necessary when dealing with the problem. A cross potential model is also offered in order to develop the turn opportunity when in a position [1]. Combination tactics

are presented in [11] for reducing wire delay for a substantially reconfigurable processor in the center of spot and course instruments, as well as an updated synthesizer, in order to reduce wire delay for a substantially reconfigurable processor in the center of spot and course instruments, as well as an updated synthesizer (HLS). In part because of the wire delay [11], it has been possible to reduce the expanded amalgamation time by a significant amount. In [12], a module position instrument is created by coordinating the computations of two key powers, which are, respectively, the KK and the FR, resulting in a module position instrument. The cover between standard cells has been removed using an adjustable and powerful blended size legitimization conspiracy, which we developed. Ultimately, a technique known as sliding-window-based cell trading is utilized to reduce the length of the wire after everything has been said and done [13]. Using a unique enlarged imperative chart, it is illustrated in [14] that it is possible to reduce division that has previously been preset or pushed on full-scale cells. According to our findings, one of the disconnection choices would be beneficial in minimizing the quantity of datapath exchanging that was causing overhead in terms of deferral, force, and zone; therefore, it was applied. A disengagement technique that makes use of inventory gates to reduce the costs associated with detaching hardware from a system is discussed in [15] in order to reduce the costs involved with detaching hardware from a system. An approach to designing and producing three-dimensional integrated circuits that takes into account the building elements of the circuit architecture is described in [16]. After taking into consideration the outcomes of the research, it will be important to put this model to the test in order to see how well it works. With the help of the TSV region and the congested mindful layout, a variety of techniques to evaluate findings can be put into practice.

In cases where there are a significant number of elements that can be ordered, floorplanning [17] techniques can be utilized to efficiently organize the required blocks. In this floorplanning, the methodologies used are linked to situational solutions in a planned stream, which answers the layout challenge by providing an answer to it. In addition, circuit designers that demand complete manual control over their circuit designs can benefit from these techniques. It is necessary to utilize a subjective discovery standard cell placer first in order to identify the primary problem, and then the floor planner is employed in order to remove the cover from the standard cell. Wire lengths have been cut by half, or even by 10%, in some situations, in order to save money. In [18], Rent's criteria for determining interconnection power consumption were applied to determine interconnection power consumption. When compared to area streamlined circuits, power consumption is reduced by 72.9 percent overall, with 44.4 percent zone overhead. When compared to area streamlined circuits, power consumption is reduced by 56.0 percent overall, with 44.4 percent zone overhead. Using a model for exact postpones inquiry in large-scale cell location calculation, it is possible to meet the needs of route deferred traffic. It is able to provide superior outcomes in terms of route latency because of the iterative

and consistent character of the technique. Using a delicate full-scale scenario in conjunction with a resynthesis strategy for optimizing region and timing, this novel chip design technique [19] has been developed. Among the three advances described in [20] are early floor planning, design-driven rationale mix, and postdesign resynthesis, to name a few. It is being researched to see if these two calculations can be merged into a single piece of equipment. When the data were compared to the existing scholarly stance gadget [21], the results were mind-blowing. According to [22], the absolute wire length and area of the following floorplan are governed by the following design.

Through the use of cell inflation techniques, it is possible to reduce the pin density in congested areas by increasing the "virtual" size of cells. This enables fewer cells to be put into congested areas, resulting in a lower pin density. Despite the fact that designers have long deployed tactics that are similar to design automation, design automation was the first to propose them [23, 24]. Despite the fact that it is in the context of programmable metal gate arrays. Following that, they were grouped in a normal cell-based arrangement and displayed one after the other in a gallery setting. The use of cell inflation was found to be effective in alleviating congestion in a simulated annealing environment. One of the most significant discoveries in this study is the use of a monotonically rising function of congestion as a target for placement improvement. c is the difference between routing demand and supply at any given location as specified in terms of routing tracks per unit area, and it is this difference that serves as the basis for the objective function that they utilize. An additional contribution was the development of an expression for the impact of padded cell moves on congested networks, which was based on the net bounding box model [25]. This enables them to calculate the exact amount of space required by each cell. When it comes to determining how much inflation each particular cell requires, however, more empirical procedures are employed. In this work, cell inflation is incorporated into a quadratic placement mechanism that resembles a Gordian knot. With the star model, it is possible to predict congestion for the two-pin Steiner segment. Congestion in each division is determined by taking into consideration the calculated routing demand and the available routing supply for that division (after routing blockages are taken into account). At the completion of the partitioning iterations, this congestion estimation is performed for the first time to determine how much congestion exists. During the previous k partitioning iterations, the congested partitions' cells have been empirically enlarged, and the quadratic placement procedure has been performed using the inflated cell sizes. During greedy congestion optimization, congested cells are shifted to sparse partitions via a series of ripple moves, which are performed in succession. Rather than using a curved path to transport cells, a straight line is formed from the most congested global placement bin to the least congested one. Cells are eagerly transferred to subsequent bins along the line, beginning with the most congested. Straight-line trajectory generation and cell movement are carried out several times before the final legalization is activated. All components of congestion-driven placement are summarized in one diagram. [BR03] describes the Bonn Place quadratic placement method, which makes use of cell inflation. This page goes into great detail about how much inflation is required for each cell in the body. Create Steiner topologies for the interpartition networks at any point during the placement process, and distribute them probabilistically over all possible two-bending ("LZ") routes. In order to accomplish this, Steiner topologies for the interpartition networks can be created at any time throughout the placement process [26, 27]. The pin density of cells within a partition is used to estimate network congestion produced by an intrapartition network partition in order to approximate network congestion caused by an intrapartition network partition. Comparing the accuracy of the heuristic placement approach to the quadratic placement method, which makes use of inflated cell sizes by rerunning the final few partitioning rounds with the inflated sizes, the heuristic placement method is superior. Instead of employing inflated cell sizes, local repartitioning shifts cells from dense partitions (which are represented by inflated cell sizes) to sparse neighboring partitions in the same region as the original partition (which is represented by normal cell sizes). The fact that BonnPlace employs a similar repartitioning technique after each quadrisectioning loop eliminates the need to be concerned about incompatibility problems. As a result of this partitioning stage, all two-two windows in congestion in their respective windows result in an alphabetical listing of all two-two windows with at least one congested partition in their respective windows. Combining the wire length and the maximum congestion of a window, we can build the repartitioning goal function, which is then optimized to provide the best results. Whenever the partitions of a window are accepted for acceptance, the sort keys of the partitions are also modified to reflect the acceptance. A concise summary of the entire congestion-driven placement process can be achieved by employing this technique.

3. Methodology

Synthesis is a transactional technique for transforming an HDL coded design module into a netlist, which is a description of the connectivity of a digital circuit; it consists of a list of the electronic components in a circuit as well as the connecting nodes. The synthesis technique is used extensively in this work to determine the highest possibilities of an IC design with optimum congestion. The design compiling software used in this study is the ICC tool; the input files provided to this tool are a BMCArchitecture with optimal placement, the number of macroblocks in architecture, and the number of pins associated with the blocks.

We hope to reduce routing density (routing congestion) in high-density and recursive places on the chip in both horizontal and vertical directions by utilizing the Pin Density Technique in conjunction with the ICC tool during the placement and routing stage of VLSI Physical Design Automation.

(i) The amount of interbin nets that exist within a bin that has at least one pin should be taken into consideration when determining the perimeter degree of the bin.

(ii) The presence of pins within the bin on two different nets, $n2$ and $n4$, which are also connected to cells outside of the bin is permissible. $N2$ and $n4$ are examples of such nets.

(iii) Its circumference is equal to $2(W + H)$, and there are two nets on either side of the bin to keep the contents contained. Because the center bin is so small, it has the smallest feasible perimeter degree of $1/(W + H)$.

(iv) Flyover nets and intrabin nets (such as n1 in our example) are not included in this statistic, which means that they are not taken into account when calculating the overall efficiency (such as net $n3$).

(v) It follows as a result of this that congestion induced by short local networks is completely ignored, and only a fraction of global congestion is represented.

(vi) Because it captures projected congestion along the exterior of the bin rather than within it, it differs from the pin density metric in that it catches predicted congestion along its perimeter rather than within it.

(vii) Through the use of Rent's rule, a relatively efficient approximation can be obtained for this measure. When inserting, the perimeter degree was used to help reduce traffic congestion.

The main goal of the proposed work is to identify regions of high dense and recursive routing in chip areas in both horizontal and vertical directions and try to minimize routing density (routing congestion) by using Pin Density Technique along with the ICC tool in VLSI Physical Design Automation placement and routing stage.

4. Simulation Results

Input, which is the design that was used to complete the floorplan using the Improved Harmonic Search Optimize technique, is applied after architecture, which is the final floorplan created using the Improved Harmonic Search Optimize technique, and the tool accepts it as input and arranges it, which is the final floorplan created using Improved Harmonic Search Optimize technique (see Figures 1 and 2).

The values of H routing and V routing represent the total number of nodes among the macroblocks where the greatest cross-path routing occurs during the Global Routing phenomena. In accordance with tool standard methods, the pin positions and cell sizes of blocks. In addition to modeling the tool, each macroblock or CLB (computational logic block) on each of the macros' faces and the number of accessible pins for each of the macros' faces are reported (see Figure 3).

A blue box surrounds each macro or computational logic block (CLB) pin, while green rectangles and square boxes
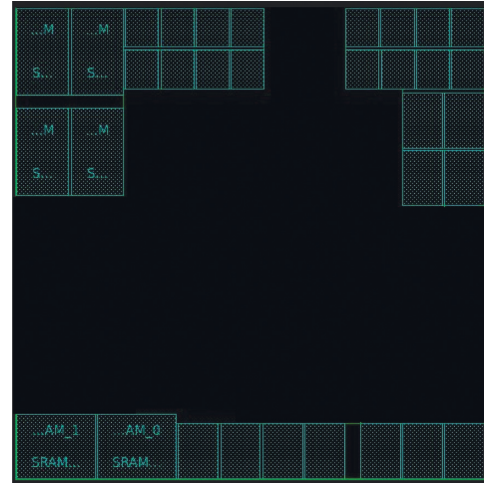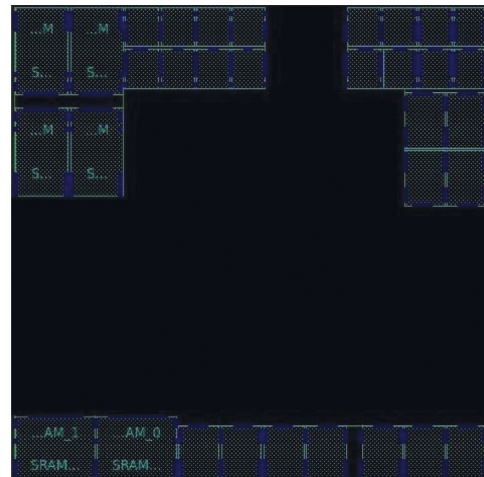

FIGURE 1: Simulated architecture.

FIGURE 2: Simulated architecture with pins.

encircle the necessary blocks. In order to properly allocate chip space and pins to blocks, the tool uses a predetermined approach that is integrated into the design process. The "report congestion" command causes the program to generate a report for the BMCircuit as a result of the command. A visual representation of an initial report on congestion incorporates architectural characteristics. The estimation of horizontal and vertical routing resources, as well as the assessment of total routing resources, are revealed in the postsimulation findings. The program also provides overflow totals for H-Routing and V-Routing, as well as maximum overflow for both directories, as well as the same predictions for Global Routing Congestion.

In addition to moving macroblocks and computational logic block (CLB) faces around, we can also add pins to the faces of the blocks using this tool. This request results in the construction of the graphic shown above, which illustrates an estimation of congestion as well as the distribution of on-chip density through the use of various colors to depict the estimation of congestion and distribution of on-chip density (see Figure 4).

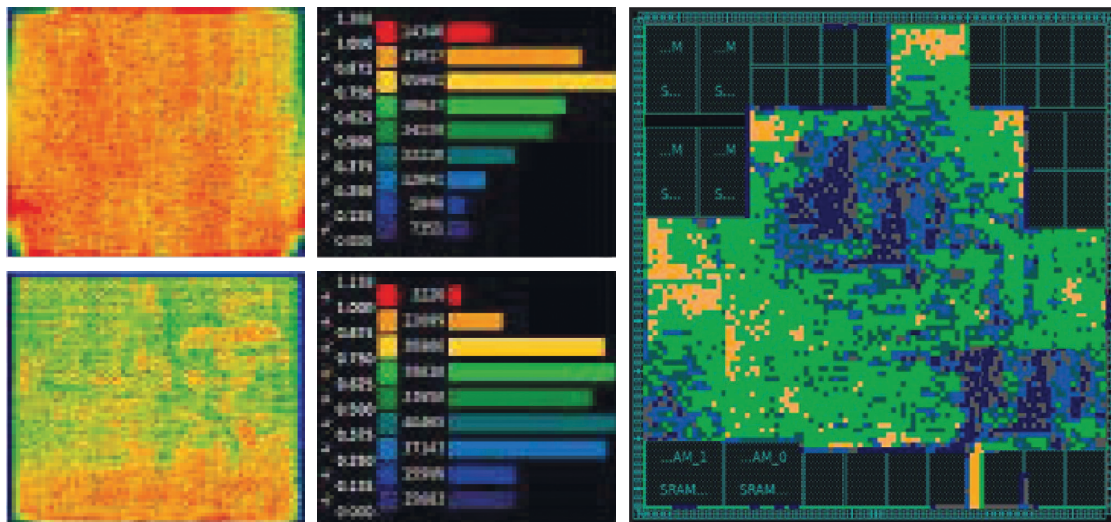FIGURE 3: Initial part of the simulation report for the optimized benchmark.

FIGURE 4: Congestion distribution on chip area.

Congestion is symbolized by four different colors, each of which represents a different level of congested traffic flow. Pink represents less congestion, blue suggests moderate congested conditions, yellow indicates severe congested conditions, and red denotes the most severe congested conditions, according to the color scale. The pins and locations that are the most congested at any given time are depicted in the figure. The IC design process becomes increasingly congested as a result of the use of this technique (CLBs). ICC II presents a technique to reduce congestion in a single design by utilizing the Perimeter Degree Congestion Technique, which is implemented in ICC II. Following the placement of blocks, we may receive a congestion report for the corresponding BMCircuit with the attainment of the H-Routing value of 20421, also attaining a V-Routing value of 18524, and a total overflow attained in the entire process is of 38945, as seen in the image below. Following the release of the BMCircuit Global Routing Congestion report, the overall overflow congestion value was 15798, which is 4.89 percent for the horizontal direction and 2.98 percent for the vertical direction, with a total overflow of 15798 (see Figure 5).

In order to alleviate this congestion, according to the first simulation results, the Perimeter Degree Congestion Approach and the Cell Spacing Congestion Technique are the only approaches that may be used. ICC II's "report congestion" command has an option called "Perimeter Degree" that you can use if you want to relieve congestion by making only minor changes to the position of blocks in your program (see Figure 6).

Simulation results demonstrate that a BMCircuit with an H-Routing value of 521, a V-Routing value of 2584, and a total overflow of 3105 is less congested than a BMCircuit with an H-Routing value of 521, a V-Routing value of 2584, and a total overflow of 3105. According to the BMCircuit Global Routing Congestion report, the network is experiencing 0.22 percent horizontal congestion and 0.09 percent vertical congestion, for the attainment of a total overflow congestion value of 0.56 percent. H-Routing value of 515, V-Routing value of 2132, and the total amount of overflow attained of 2647 indicate that the network is experiencing 0.22 percent horizontal and 0.09 percent vertical congestion (see Figure 7).

A BMCircuit with H-Routing values of 614 and V-Routing values of 3039, as well as a total overflow of 3653, is used in this simulation report to demonstrate how congestion might be minimized. There were a total of 3115 overflows, accounting for 0.22 percent of overall overflow congestion in the horizontal direction and 1.9 percent in the vertical direction, for a total of 0.56 percent of overall overflow congestion in the horizontal direction, according to the Global Routing Congestion report for BMCircuit.

Figure 5: Simulation report before Perimeter Degree Congestion Technique.

Figure 6: The postsimulation results, which show a significant reduction in the design and related simulation report congestion.
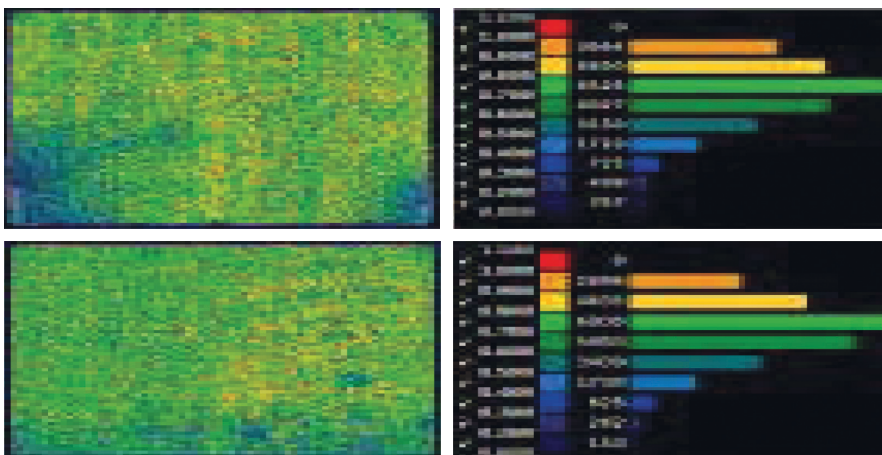

Figure 7: Simulation report after Perimeter Degree Congestion Technique.

5. Comparative Analysis

The Pin Density Technique differs from previous strategies in that it allows the pin count to be adjusted in accordance with desired architecture limits. It has also been shown to be more effective than other techniques for reducing congestion. Dataflow analysis and fly line analysis were used to compare the simulation results of our suggested congestion technique; a table comprising overflow attributes in the H and V directions, as well as total overflow and maximum

TABLE 1: Parametric Comparison of the Proposed and existing methods in the field.

| | Existing techniques | | Proposed technique |
	Maze routing analysis	Density analysis	Perimeter degree technique (PDT)
H- overflow	9	218	515
V -overflow	219	250	2132
Total amount of overflow	178	344	2647
Maximum amount of overflow (1GRC)	22	22	28

TABLE 2: Statistical Comparison of several metrics before and after the proposed congestion (PDT) estimation technique was used.

Parameters	Before perimeter degree technique (PDT)	After perimeter degree technique
H Routing	20421	521
V Routing	18524	2584
Both directions	38945	3105
Maximum overflow in the H Routing	127	4
Maximum overflow in the V Routing	309	1
Maximum overflow in the both directions	309	4
GRC based overflow values in the H Routing	9812	515
GRC based overflow values in the V Routing	5986	2132
GRC based overflow values in both directions	15798	2647
Percentage of GRC based overflow values in H Routing	3.62	0.21
Percentage of GRC based overflow values in V Routing	2.02	0.88
Percentage of GRC based overflow values in both directions	3.62	0.42
Maximum GRC based overflow value in H Routing	1	8
Maximum GRC based overflow value in V Routing	0	28
Maximum GRC based overflow value in both directions	1	28

overflow per unit Global Routing Congestion, was created. When it comes to anticipating congestion in the chip region, there are two approaches to consider: the PDT approach and the Global Routing Congestion strategy. The PDT Congestion approach is used to estimate congestion in the chip area (GRC).

The technique displays the accomplishment of the objectives in a comparative manner, based on the data in Table 1. According to the findings of a table, the recommended technique produces the best results.

The simulation results for the optimized standard BMCircuit obtained using the suggested congestion estimate approach for the optimized standard BMCircuit are displayed in the table's tabular column, which is displayed in the next section. According to the simulation results, when H Routing and V Routing are combined, there is a significant improvement in the approximation of congestion, as well as in the maximum amount of overflow in the H Routing, the maximum amount of overflow in the V Routing, the percentage of GRC based overflow in the H routing, the percentage of GRC based overflow in the V Routing, the GRC based overflow in the H Routing, and the maximum GRC based overflow (refer Table 2). This combination of traits enabled us to establish the feasibility of our proposed study utilizing a technically and statistically cutting-edge technique, which will be valuable for future experiments and evaluations in this field in the years to come.

In order to make their relevance evident, the results of simulating an optimized BMC with and without the PDT Congestion Technique are shown in Table 2 to the right of the text.

6. Conclusion and Future Scope

An in-depth method for calculating and minimizing congestion in VLSI Physical Design Automation, as well as optimization of placement area and routing wire length, is described in this study. By incorporating the proposed Perimeter Degree Congestion Technique (PDCT) into an integrated circuit design, it surpasses existing techniques for forecasting and mitigating congestion density in the H- and V-direction, such as fly line analysis and Dataflow analysis, in terms of performance. Logic communication between macros or Computational Logic Blocks can be achieved through the use of PDT (Programmable Data Transfer) (CLBs). In order to perform this operation, the integrated circuit (IC) tools that were used have proven to be complicated, as well as having user-friendly interfaces that contain a huge number of colorful technical elements while not overlooking even the most fundamental of qualities. The Perimeter Degree Congestion Technique is used to alleviate congestion in places that are logically congested, such as urban areas (PDT). As part of the experimentation, the method under consideration has supplied a standardization for the use of logic procedures in order to perceive the intended aims of the task, which has been useful in the future. In addition, it has been demonstrated to be cost-effective in a variety of ways when used in conjunction with the congestion control process, which is a positive step forward. While the Dataflow approach could only handle a small number of macroblocks and took longer to anticipate congestion, the Flyline technique was more accurate but was unable to estimate congestion in both horizontal and vertical

directions at the same time, whereas the Dataflow method could. Numerous studies have proved the usefulness of this technique in terms of, among other things, lowering wire length, area, and power consumption during the design of integrated circuits. The usage of the perimeter degree technique, which is highly recommended, can help to achieve these reductions in energy consumption. The proposed approach gives better results, but a few additional improvements to the process flow and operational processes can help to avoid the requirement for the development of more complex approaches that can deliver answers in a shorter period of time. In order to accomplish this, a more in-depth study on a wide range of unique characteristics of the integrated circuit design circuit sector can be conducted. Additionally, the suggested method may be used to analyze chip area and operation time reductions for various architectures in addition to evaluating congestion for various architectures.

Data Availability

The processed data are available upon request from the corresponding author.

Conflicts of Interest

The authors declare that they have no conflicts of interest.

References

[1] S. M. Ahmed, B. Kovela, and V. K. Gunjan, "IoT based automatic plant watering system through soil moisture sensing-A technique to support farmers' cultivation in rural India," in *Advances in Cybernetics, Cognition, and Machine Learning for Communication Technologies*, pp. 259–268, Springer, Singapore, 2020.

[2] I. Ratkovi, O. Palomar, M. Stani, O. Unsal, A. Cristal, and M. Valero, "Physical vs. physically-aware estimation flow: case study of design space exploration of adders," in *Proceedings of the IEEE Computer Society*, Tampa, FL, USA, July, 2014.

[3] S. Karimullah and Dr. D. Vishnuvardhan, "Experimental Analysis of Optimization Techniques for Placement and Routing in Asic Design," *ICDSMLA 2019*, vol. 601, Springer Nature Singapore Pte Ltd, Singapore, 2020.

[4] IC Compiler, *Implementation User Guide Version J-2014.09-SP4*, March 2015.

[5] K. Golshan, *Physical Design Essentials*, Springer Science Business Media, LLC, Heidelberg, Germany, 2016.

[6] S. Karimullah and D. Vishnu Vardhan, "Iterative Analysis of Optimization Algorithms for Placement and Routing in Asic Design," *ICDSMLA 2019*, Vol. 601, Springer Nature Singapore Pte Ltd, Singapore, 2020.

[7] S. Karimullah, D. Vishnu Vardhan, and S. J. Basha, "Floorplanning for Placement of Modulesin VLSI Physical Design Using HarmonySearch Technique," *ICDSMLA 2019*, Vol. 601, Springer Nature Singapore Pte Ltd, Singapore, 2020.

[8] Yi-F. Chen, C.-C. Huang, C.-H. Chiou, Y.-W. Chang, and C.-J. Wang, Routability-driven blockage-aware macro placement," in *Proceedings of the 51st Annual Design Automation Conference*, pp. 1–6, San Francisco, CA, USA, June 2014.

[9] S. Karimullah and Dr. D. A. Vishnuvardhan, *A Review Paper on Optimization of Placement and Routing Techniques"at NC'e-TIMES # 1.0 IN2018*, pp. 2395–1303, IJET ISSN, 2018.

[10] J. Z. Yan, V. Natarajan, and C. Chu, "Handling Complexities in Modern Large-Scale Mixed-Size Placement," in *Proceedings of the 46th Annual Design Automation Conference*, pp. 436–441, NY, USA, July, 2009.

[11] J. Shin, J. A. Darringer, G. Luo et al., "Floorplanning Challenges in Early Chip Planning," in *Proceedings of the 2011 IEEE International SOC Conference*, pp. 388–393, IEEE, Taipei, Taiwan, September 2011.

[12] P. S. Prasad, B. Sunitha Devi, M. Janga Reddy, and V. K. Gunjan, "A survey of fingerprint recognition systems and their applications," in *International Conference on Communications and Cyber Physical Engineering 2018*, pp. 513–520, Springer, Singapore, 2018.

[13] S. Karimullah and D. Vishnuvardhan, "Simulation of optimized architecture for the estimation of congestion during placement and routing," *Design Engineering*, pp. 755–764, 2021.

[14] B. Mokhlesabadifarahani and V. K. Gunjan, *EMG Signals Characterization in Three States of Contraction by Fuzzy Network and Feature Extraction*, Springer, Heidelberg, Germany, 2015.

[15] M. Samaranayake, H. Ji, and J. Ainscough, "Module placement based on hierarchical force directed approach," in *Proceedings of the International Conference on Signals, Circuits and Systems*, pp. 1–6, IEEE, Medenine, Tunisia, November 2009.

[16] M. D. Ansari, V. K. Gunjan, and E. Rashid, "On security and data integrity framework for cloud computing using tamper-proofing," in *ICCCE 2020*, pp. 1419–1427, Springer, Singapore, 2021.

[17] M. Thenappan, T. Senthil Arasu, K. M. Sreekanth, and R. S. Guzar, "An overlap removal algorithm for macrocell placement in VLSI layouts," in *Proceedings of the International Conference on Computing: Theory and Applications (ICCTA'07)*, March 2007.

[18] K. Prasanna and M. Seetha, "A doubleton pattern mining approach for discovering colossal patterns from biological dataset," *International Journal of Computer Application*, vol. 119, no. 21, pp. 41–47, 2015.

[19] M. Usman, M. Wajid, M. Z. Shamim, M. D. Ansari, and V. K. Gunjan, "Threshold detection scheme based on parametric distribution fitting for optical fiber channels," *Recent Advances in Computer Science and Communications*, vol. 14, no. 2, pp. 409–415, 2021.

[20] S. N. Adya and I. L. Markov, "consistent placement of MacroBlock using floorplanning and StandardCell placement"" in *Proceedings of the 2002 international symposium on Physical design*, Del Mar, CA, USA, Apri, 2002.

[21] Z. Lin and N. K. Jha, "Interconnect-aware High-Level Synthesis for Low Power," in *Proceedings of the 2002 IEEE/ACM international conference on Computer-aided design*, pp. 110–117, IEEE, San Jose, CA, USA, November 2002.

[22] A. J. Zargar, N. Singh, G. Rathee, and A. K. Singh, "Image data-deduplication using the block truncation coding technique," in *Proceedings of the 2015 International Conference on Futuristic Trends on Computational Analysis and Knowledge Management (ABLAZE)*, pp. 154–158, IEEE, Greater Noida, India, February 2015.

[23] S. Pinge, K. N. Rajeev, and M. Chrzanowska-Jeske, "Fast Floorplanning with Placement Constraints," in *Proceedings of*

the *2013 IEEE 4th Latin American Symposium on Circuits and Systems (LASCAS)*, IEEE, Cusco, Peru, February 2013.

[24] S. Iyengar and L. Shrinivasn, "Power, Performance and Area Optimization of I/O Design," in *Proceedings of the International Conference on Inventive Research in Computing Applications (ICIRCA 2018)*, Coimbatore, India, July 2018.

[25] J.-M. Lin, W.-Y Cheng, C.-L. Lee, C. Richard, and J. Hsu, "Voltage Island-Driven Floorplanning Considering Level Shifter Placement," in *Proceedings of the 17th Asia and South Pacific Design Automation Conference*, pp. 443–448, IEEE, Sydney, NSW, Australia, January 2012.

[26] S. Karimullah and D. V. Vardhan, "Pin density technique for congestion estimation and reduction of optimized design during placement and routing," *Applied Nanoscience*, pp. 1–10, 2022.

[27] S. Karimullah, S. J. Basha, P. Guruvyshnavi, K. Sathish Kumar Reddy, and B. Navyatha, "A Genetic Algorithm with Fixed Open Approach for Placements and Routings," *ICCCE 2020*, Vol. 698, Springer Nature Singapore Pte Ltd, Singapore, 2020.